# Developing 1,2,3,4-tetrahydro-*5H*-aryl[1,4]diazepin-5-ones and Related Scaffolds as Poly-(ADP-ribosyl) Polymerase (PARP) Inhibitors and Exploring Their Targeted Polypharmacology with Kinases

Kiaya M. Sulier

Thesis submitted to the faculty of Virginia Polytechnic Institute and State University in partial fulfillment of the requirements for the degree of

Master in Science
In
Chemistry

Jatinder S. Josan, (Chair)
Paul R. Carlier
David G. I. Kingston
Joseph S. Merola

May 10, 2017
Blacksburg, Virginia

**Keywords:** Poly-(ADP-Ribosyl) Polymerase (PARP), cyclin-dependent kinase 1 (CDK1), triple negative breast cancer (TNBC), benzodiazepines, isoform specific inhibitors

Copyright © 2017 Kiaya Sulier

**Developing 1,2,3,4-tetrahydro-*5H*-aryl[1,4]diazepin-5-ones and Related Scaffolds as Poly-(ADP-ribosyl) Polymerase (PARP) Inhibitors and Exploring Their Targeted Polypharmacology with Kinases**

Kiaya M. Sulier

Abstract

Poly-(ADP-ribsoyl) Polymerases (PARPs) are a superfamily of enzymes comprised of 17 known isoforms. PARP inhibitors (PARPi) have shown success in clinical trials for the treatment of homologous recombination-deficient cancers. Though proven effective initially, tumors treated with PARPi eventually develop resistance. Combinatorial therapeutics targeting PARP and other pathways that may re-sensitize tumors to PARP inhibition, including PI3K/AKT/mTor pathway, and cell-cycle checkpoints (such as CDKs, CHK, and Wee) are being tested. In this context, the synthetic lethality of cyclin-dependent kinase 1 (CDK1) and PARP1 is known.

Evaluation of PARP1 and CDK1 pharmacophores led to the development of the tetrahydro-arylazepinone (TAAP) scaffold as a potential dual PARP1/CDK1 inhibitor. We screened a handful of TAAP analogs against PARP1 in a cell-free assay that identified the low micromolar PARP1 inhibitor 1,2,3,4-tetrahydro-5*H*-benzo[*e*][1,4]-diazepin-5-one (TBAP), which served as the lead compound. The analogous 1,2,3,4-tetrahydro-5*H*-pyrido[2,3-*e*][1,4]-diazepin-5-one (TPAP) series showed a similar bioactivity profile. Satisfyingly, the $N^1$-benzyl TPAP analogue showed activity in the low nanomolar range. The TAAP series (i.e., 6/7-membered scaffold) unfortunately lacked CDK1 inhibitory activity.

Finally, many PARPi's show poor isoform-selectivity. The development of isoform-selective PARPi can clarify the specific function of each PARP isoform and may reduce the adverse side effects shown by PARPi. A handful of TAAP analogs were screened against 13 PARP isoforms, where some compounds demonstrated exquisite PARP1/2 selectivity. Concurrently, we

discovered an inhibitor for PARP11, an isoform that lacks any known synthetic ligand. Future directions are suggested towards fine-tuning the structure-activity relationship of TAAP-isoform selective PARPi as well as developing a dual PARP1/CDK1 inhibitor.

**Developing 1,2,3,4-tetrahydro-*5H*-aryl[1,4]diazepin-5-ones and Related Scaffolds as Poly-(ADP-ribosyl) Polymerase (PARP) Inhibitors and Exploring Their Targeted Polypharmacology with Kinases**

Kiaya M. Sulier

General Audience Abstract

The aim of this work is to explore the therapeutic potential of poly-(ADP-ribosyl) polymerase inhibitors (PARPi) for the treatment of ovarian and breast cancer, specifically triple negative breast cancer. Poly-(ADP-ribsoyl) Polymerases (PARPs) are a superfamily of enzymes comprised of 17 known isoforms. Currently, there are three FDA approved PARPi - olaparib, rucaparib, and niraparib; however, these PARPi demonstrate non-selectivity amongst the PARP isoforms. Further, tumors have been shown to develop resistance to PARPi. Herein, we explored the 1,2,3,4-tetrahydro-5*H*-aryl[1,4]diazepin-5-one scaffold as a potential PARP1/2-selective inhibitor and its possibility for targeted pharmacology with other kinases.

## Acknowledgements

First, I would like to express my gratitude to my advisor, Dr. Jatinder Josan. Though it was never easy, he never gave up on me, always supported my decisions, and always took the extra stride to better my well-being and career. Through this long journey, we became a team. Dr. Josan is not only a research advisor, but also became a mentor, a life coach, and a friend, and for that, I am forever grateful. I would also like to thank Dr. Paul Carlier, Dr. David Kingston, and Dr. Joseph Merola, for serving on my committee, taking the time to talk about research and sharing their knowledge, and for all the advice given beyond chemistry and research.

Secondly, I would like to thank my friends and family for their support throughout graduate school. I know without their support and understanding I would not be here today. I would also like to give special thanks to Christine DuChane and Matthew Vincent for proofreading my Master's thesis countless times. I would also like to thank my group members for their support, discussions on research, and their enjoyable company, making long hours in the lab and Saturday group meetings tolerable. Lastly, I would like to thank the Virginia Tech Chemistry department for this educational opportunity and financial support.

I would like to dedicate this work to Nathanael Burklin Fox and the Fox family, and Brandon Lee Meerscheidt and the Meerscheidt family.

**Table of Contents**

**Chapter 1: Targeted Polypharmacology of PARP1 with Kinases in Triple Negative Breast Cancer**

1.1 Synthetic Lethality: An Overview……..1

1.2 BRCAness ……3

1.3 Poly-(ADP-ribosyl) Polymerase 1/2 and Inhibitors……...….3

1.4 Synthetic Lethality and Triple Negative Breast Cancer……..5

1.5 Resistance to PARP Inhibitors and the Involvement of Kinases…….6

1.6 Cyclin-Dependent Kinase 1 and Inhibitors……7

1.7 Rationale and Design of a Multifunctional Ligand……...10

1.8 References……14

**Chapter 2: Probing the Tetrahydro-arylazepineone A/B Ring Scaffold for PARP Isoform-Specific Inhibition and Dual Inhibition with CDKs**

2.1 Introduction……..18

2.2 Initial Exploration of the A/B Ring Scaffold……...…18

*2.2.1 Design*…….18

*2.2.2 Synthesis*……..19

*2.2.3 Results*…….20

2.3 TAAP Derivatives and $IC_{50}$ Determinations…….22

*2.3.1 The Amide TBAP Derivatives*……..22

*2.3.2 The Sulfonamide TBAP Derivatives*…….24

*2.3.3 The TPAP Derivatives*…….25

2.4 PARP Isoform Selectivity……29

2.5 TAAP Atropisomerism……32

2.6 Dual inhibition with CDKs……...37

2.7 Summary……..38

2.8 Experimental……40

2.9 References……53

**Chapter 3: Synthetic Methodology for the Benzoazepine-dione Scaffold**

3.1 Introduction……..……55

3.2 Polyphosphoric Acid (PPA) Cyclization…….……56

3.3 The Minisci Reaction……56
3.4 Lithium-Halogen Exchange……59
3.5 The Schmidt Reaction……..60
3.6 Summary……..……64
3.7 Experimental……66
3.8 References……75
**Chapter 4: Future Perspectives**
4.1 A Brief Overview……..…78
4.2 Targeted Polypharmacology of PARP with Kinases……....79
*4.2.1 PARP1 and CDK1*……...…79
*4.2.2 PARP and Other Kinases*……..…79
*4.2.3 PARP and Chalcones*……...80
*4.2.4 PARP Trapping and Isoform-selective Inhibitors*……...…….81
4.3 References……84

**Appendices**
Appendix A: Abbreviations
Appendix B: Inventory of compounds
Appendix C: Schmidt Reaction Conditions
Appendix D: Nuclear Magnetic Resonance (NMR) Spectra
Appendix E: High-Resolution Mass Spectra (MS)
Appendix F: High-Performance Liquid Chromatograms (HPLC)
Appendix G: X-ray Crystallography
Appendix H: Geometry Optimizations
Appendix I: PARP1 assay– Tips and Tricks
Appendix J: Dose-Response Curves
Appendix K: BPS Biosciences Procedures and Data

## Chapter 1: Targeted Polypharmacology of PARP1 with Kinases in Triple Negative Breast Cancer

### 1.1 Synthetic Lethality: An Overview

An emerging, alternative cancer therapy, *synthetic lethality*, defines the genetic interaction between two genes where the loss of one gene function leaves a viable cell, while the loss of two gene functions becomes lethal (**Figure 1.1**).[1-3] The term synthetic lethality derives from the Greek word, *synthetickó* or *syntithénai*, meaning "placed together" or "to put together".[4] The discovery of synthetic lethality occurred in 1922 by Calvin Bridges in *Drosophila;*[5] however, the term was coined in 1946 by Theodore Dobzhansky, who recognized the same phenomenon with his genetic studies of *Drosophile pseudoobscura*.[6]

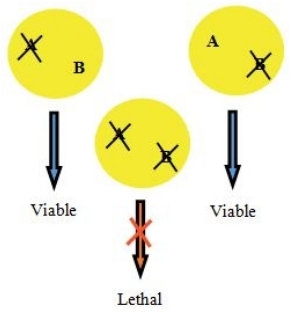



**Figure 1.1. Illustration of synthetic lethality.** One cell lacks the functionality of gene A, but leaves a viable cell. Another cell lacks the functionality of gene B, but leaves a viable cell. Lacking the functionality of both genes leads to cell death.

The basis of this therapeutic approach requires the two genes to contribute to the same essential cellular process. While one genetic or epigenetic aberration may previously exist in the cancer cell that does not affect the viability, the introduction of a second alteration could result in complete abolition of an essential cellular function, leading to apoptosis and cell death.[1] Utilizing a genetic mutation strongly associated with a specific cancer while mimicking a second mutation through pharmacological means could yield therapeutic selectivity for the cancer cells. Since the healthy cells lack the carcinogenic mutation and the pharmacological inhibition may only sicken or arrest the healthy cells, the cancer cells undergo selective death while avoiding the destruction of healthy cells, a side effect of contemporary chemotherapies.

Following the discovery of synthetic lethality, abundant yeast model studies helped to elucidate many synthetically lethal gene pairs. These fundamental studies aided in determining protein-protein interactions and unraveling cellular functions.[7-9] At the turn of the century, synthetically lethal studies conducted with mammalian cells helped in establishing its utility for pharmacological targeting in cancer cells. In 2005, Bryant et al. and Farmer et al. simultaneously discovered that utilizing a non-essential DNA repair protein mutation in conjunction with protein inhibition could provide a selective cancer therapy without the use of an external DNA-damaging agent.[2,3] Their work stemmed from consideration of the synthetically lethal interaction between the ***br****east* ***c****ancer* ***a****ssociated* gene (BRCA) and poly(ADP-ribose) polymerase (PARP1).

BRCA and PARP1 both contribute to the DNA repair process. The repair of double strand breaks in DNA relies on BRCA, which repairs these breaks by the homologous recombination process (HR). PARP1 aids the repair of single strand breaks in DNA by the base excision repair (BER) process; lacking BER, single strand breaks eventually lead to double strand breaks during replication, thus making cells reliant on HR and sensitive to HR perturbation. The inhibition of both DNA repair pathways by treating HR-deficient cells (BRCA-/-) with PARP1 inhibitors results in persistent collapsed replication forks with ultimately lethal outcomes. This seminal discovery, summarized in **Figure 1.2**, exploited the increased sensitivity of BRCA1/2 deficient cells to

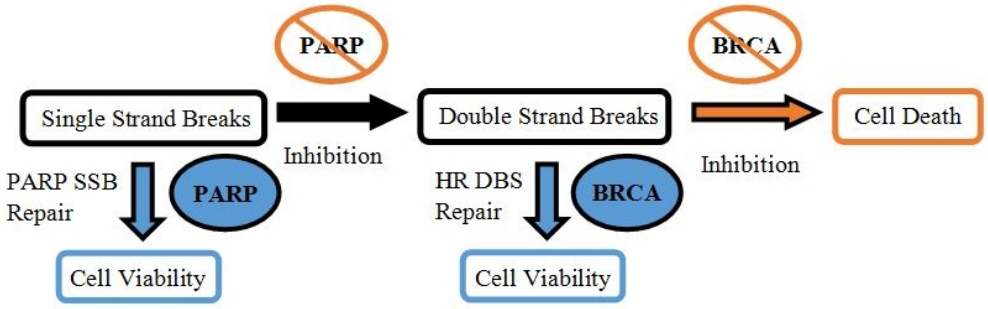



**Figure 1.2. Visual representation of the synthetically lethal interaction between PARP and BRCA.** SSB: single strand breaks; DBS: double strand breaks.

PARP1 inhibition[2,3] and led to the further exploration of this synthetically lethal interaction for clinical drug development.

### 1.2 BRCAness

BRCAness characterizes the extension of synthetic lethality beyond the BRCA mutation.[10] The enhanced sensitivity of PARP1 inhibition relies on the homologous recombination deficiency resulting from BRCA mutation; therefore, any cell deficient in homologous recombination could display an enhanced sensitivity to PARP1 inhibition.[3] Additionally, many metastatic tumors overexpress the genes involved in DNA repair pathways and deregulate the cell cycle.[11] Consequently, the development of a new, synthetically lethal target with PARP1 inhibition requires an overexpressed or overactivated enzyme involved in the homologous recombination pathway. The inhibition of this enzyme could cause the cells to execute homologous recombination insufficiently, leading to "*BRCAness*".[10]

### 1.3 Poly-(ADP-ribosyl) Polymerase 1/2 (PARP1/2)

Among the 17 known PARPs, PARP1 is the most studied isoform. PARP plays an essential role in the cleavage of nicotinamide adenine dinucleotide ($NAD^+$) to produce ADP-ribose and nicotinamide, which acts as a mild inhibitor for this process. The discovery of nicotinamide's inhibitory activity provided the first basic scaffold for PARP inhibitors, which led to the first class of benzamide analog inhibitors. Despite the initial success, these compounds only inhibited PARP in millimolar concentrations, which rendered them impractical for therapeutic purposes.[12]

Many of the reported PARP inhibitors, including the PARP inhibitors in clinical trials, show little to no PARP isoform selectivity. PARP inhibitors classified as "PARP", "PARP1", "PARP2", or "PARP1/2" often have not been screened against all the PARP isoforms, and while some reports

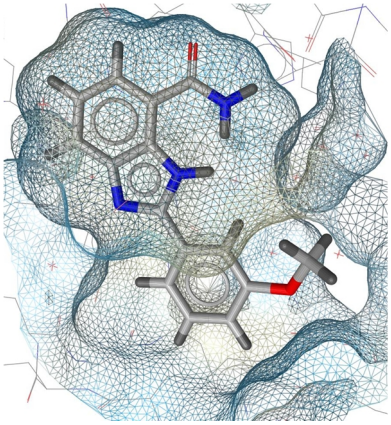


**Figure 1.3. PARP crystal structure.** PARP1 bound with a benzimidazole inhibitor (PDB: 1EFY).

screen against 3–5 PARP isoforms, rarely are all PARP isoforms screened. Due to the clinical successes of PARP inhibitors, the need for isoform selective PARP inhibitors is increasing. Isoform selective inhibitors would help determine which observed effects, therapeutic and/or adverse, are from specific enzymatic inhibition or a result of pan-PARP inhibition.[13] PARPs are highly conserved in the ADP-ribosyltransferase (ART) domain, but beyond the ART domain, their structures diversify, which differentiates their function. PARP1–4 play a role in genomic integrity, while another subset of PARPs, PARP5A and PARP5B (tankyrases, TNKS), are crucial in telomere replication. The last classification of PARPs is the mono-ADP-ribosyltransferase family, which includes PARP6–16.[13,14]

The ligand bound crystal structure of PARP1 complexed with a benzimidazole inhibitor (**Figure 1.3**) provides crucial structural information concerning the catalytic site and basic scaffold for PARP inhibitors. Analysis of this crystal structure indicates that an amide group, a common

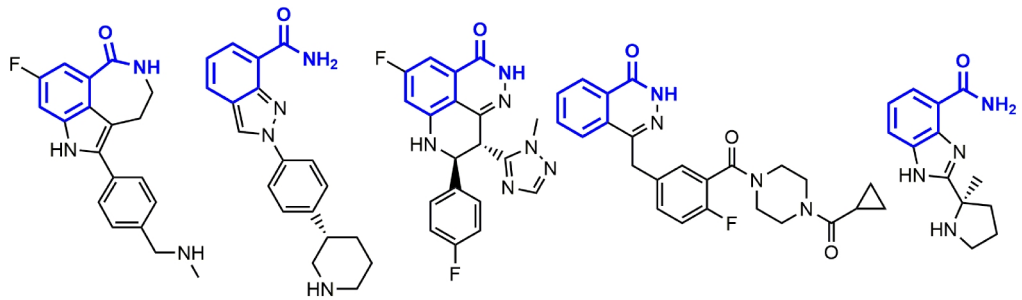



**Figure 1.4. PARP inhibitors in clinical trials.** The nicotinamide pharmacophore is highlighted in blue. Rucaparib is undergoing several clinical trials for ovarian cancer, undergoing phase II clinical trials for BRCA mutated TNBC, and is FDA approved for BRCA mutated relapsed ovarian cancer; Niraparib is undergoing clinical trials for various carcinomas, undergoing phase I clinical trials for TNBC, and is FDA approved for recurrent ovarian cancer; Talazoparib is undergoing clinical trials for various carcinomas, but also is undergoing phase I clinical trials for TNBC and BRCA mutated solid tumors and phase III clinical trials for BRCA mutated metastatic breast cancer; Olaparib is undergoing several clinical trials for various carcinomas and is FDA approved for BRCA1/2 mutated platinum-sensitive relapsed ovarian cancer; Veliparib is undergoing several clinical trials for various carcinomas, but also is undergoing pilot studies with metastatic TNBC.

feature of almost all PARP inhibitors, provides several necessary hydrogen bonds to the serine and glycine residues in the catalytic domain of PARP1, resulting in strong binding and potency. In some PARP inhibitors, the incorporation of the amide group into a six or seven-membered ring reduces the entropic cost of amide binding by providing a structural orientation favorable for hydrogen bonding. **Figure 1.4** illustrates the nicotinamide pharmacophore in PARP inhibitors from recent pre-clinical and clinical studies.[12,15,16]

1.4 Synthetic Lethality and Triple Negative Breast Cancer

The BRCA gene mutation, described as the deficiency in BRCA expression, is commonly found in gene expression profiles of triple negative breast cancer (TNBC).[17] TNBC is a recently coined term that defines the estrogen receptor (ER) negative, progesterone receptor (PR) negative, human epithelial growth factor receptor (HER2) negative phenotype,[18] and this phenotype is represented by 12–24% of breast and ovarian cancer patients.[17-19]

TNBC diagnosis usually reveals a progressed stage and/or high-grade tumors, giving TNBC an aggressive reputation.[17] The available endocrine therapies and therapies targeting HER2 proved ineffective for TNBC patients, while common chemotherapy proved dichotomous.[18] Chemotherapy improves the health of 22% of the TNBC population, of which 94% survive the first three years after diagnosis. However, the survival rate for chemo-insensitive patients drops to 68% for the first three years after diagnosis.[18] Though those who receive chemotherapy in the early stages of TNBC respond better than the patients treated for other types of breast cancer, TNBC commonly develops chemoresistance resulting in tumor progression and metastatic spreading.[20]

Exploiting the enhanced PARP1 sensitivity in HR-deficient cells could lead to an effective synthetically lethal therapy for BRCA-deficient patients. The combination of DNA-damaging agents with PARP1 inhibitors in early clinical trials of BRCA mutated tumors (TNBC included)

correlated with an increase in the rate of tumor regression, progression-free survival (PFS), and overall survival (OS).[18] PARP inhibitors display synergism with DNA-damaging agents, such as cisplatin, with approximately threefold higher efficacy in BRCA deficient cells than DNA-damaging agents do alone.[3] Although the majority of TNBC patients feature BRCA deficient tumors, only 5% of overall breast tumors display the BRCA deficiency, thereby, restricting the percent patient coverage and the utility of PARP1 inhibition as a target therapy.[21,22] Implementing analogous logic, *BRCAness* would establish a viable therapy for the entire TNBC patient population, for example, by targeting an overexpressed enzyme related to HR or the DNA repair pathways (**Section 1.2**).

1.5 Resistance to PARP Inhibitors and the Involvement of Kinases

The preclinical efficacy of PARP inhibitors brought a great deal of excitement to the field of breast cancer therapeutics. Although PARP inhibitors are showing success in clinical trials for various carcinomas (**Figure 1.4**), BRCA deficient tumors treated with PARP inhibitors eventually develop PARP resistance pathways, including genetic reversion of the BRCA mutation that can lead to full recovery of HR defects; increased activity of the BRCA hypomorphic alleles and upregulation of proteins associated with DNA-end resection,[23] both of which lead to partial HR recovery;[24] and P-glycoprotein-mediated drug efflux. The most concerning resistance pathway, and the one that is observed in human tumors, is the genetic reversion pathway, which likely proceeds via development of a second mutation that restores HR by either correcting or bypassing the original mutation.[24] Though the full mechanistic understanding of these pathways is not yet known, the search for methods to circumvent PARP resistance is ongoing. Although mouse models show that tumors can extrude olaparib via P-glycoprotein mediated drug efflux, PARP inhibitors that are poorly recognized by P-glycoproteins are already available (i.e., veliparib). Reversion

pathways related to hypomorphic alleles and DNA-end resection only partially restore HR; therefore, tumors exhibiting resistance via one of these pathways may retain responsiveness to other therapies.

Combinatorial therapies with inhibitors that target the phosphoinositide-kinase, protein kinase B, and mTor (PI3K/Akt/mTor) pathway, cell-cycle checkpoints (such as CDKs, CHK, and Wee), or other targets that may sensitize tumors to PARP inhibition may circumvent resistance pathways.[24] It is important to note that the severity of HR-deficiency varies from patient to patient, so choosing the right patients for PARP inhibitors is valuable in avoiding potential PARP resistance; unfortunately, biological markers that accurately identify patients best suited for treatment with PARP inhibitors are still unknown.

1.6 Cyclin-dependent kinase 1 (CDK1)

Cyclin-dependent kinases (CDKs) initiate cell proliferation and actively participate in each checkpoint of the cell cycle.[25] The activation of CDKs' catalytic cycles involves a binding interaction between the kinases and various subunits (cyclins), yielding a holoenzyme complex.[26,27] Commonly, specific CDK-cyclin complexes lack carcinogenic mutations; however, the amplified levels of CDKs and cyclins strongly associate with human malignancies. Because amplification of these CDK-cyclin complexes results in uncontrolled proliferation, specific inhibition of CDKs could provide a viable target for cancer therapeutics.[25]

Of the thirteen discovered CDKs, CDK1, 2, 4 and 6 take part in the direct regulation of the cell cycle.[27] CDK1 participates in the checkpoint kinase 1 (CHK1) pathway in the DNA synthesis (S) and second gap (G2) phase in the cell cycle. CDK1 aids DNA repair and prevents the cells from entering the mitosis (M) phase until DNA integrity is restored; if restoration fails, cell death follows.[25] CDK1 associates with the subunits cyclin A and cyclin B at different phases of the cell

cycle. The CDK1/cyclin A complex participates in the G2 phase, in which cell growth continues, and regulates entry into mitosis. The CDK1/cyclin B complex manages the G2/M transition and aids the mitotic state.[26,28,29]

In addition to the active participation of CDK1 in the G2 phase and G2/M transition, CDK1 phosphorylates BRCA1, which allows the gene to prepare the DNA damaged sites for repair in HR. Consequently, the BRCA1 mediated S phase checkpoint relies on the functionality of CDK1, rendering suppression of CDK1 function as an attractive target for synthetic lethality.[22,30] Ultimately, the inhibition of this kinase cripples the cell's DNA repair ability causing cell cycle arrest and a higher affinity for apoptosis, vital enzymatic characteristics for cancer therapeutics.[28] CDK1 overactivation associates with cancers of the breast, bladder, colon, ovary, lung, vulva, prostate[25] and skin,[31] as well as lymphomas and osteosarcomas. Thus, the intricate role of CDK1 vis-à-vis BRCA1 function means concurrent CDK1 and PARP1 inhibition could cause synthetic lethality in TNBC as well as in other potential carcinomas.[25] Indeed, a recent report convincingly highlights the utility of this synthetic lethal pair in non-small cell lung cancer, and possibly others (**Section 1.7**).

The three-dimensional structures of CDKs encompass a binding pocket suitable for adenosine triphosphate (ATP) with a high degree of homology between all the kinases. These protein kinases transfer the terminal phosphate from ATP to the hydroxyl group of a tyrosine, serine or threonine residue on various kinases. Initially, the highly conserved ATP binding domain brought concerns of selectivity for the design of a specific CDK inhibitor, but the discovery of the specific epidermal growth factor tyrosine kinase inhibitor, Iressa, reduced these concerns and encouraged the further investigation of kinase-selective inhibitors.[26]

Endicott and Noble et al. and Cano et al. recently published the first and only X-ray crystallographic structures of CDK1.[32,33] Endicott and Nobel et al. show that the interacting residues in the ligand-bound X-ray crystal structure of CDK1 (PDB: 4Y72) and the analogous ligand-bound X-ray crystal structure of CDK2 (PDB: 2VTP) are "identical or highly conserved".[33] Since ligand-bound CDK1 X-ray crystal structures are limited, extrapolation from the HMD-bound CDK2 X-ray crystal structure (**Figure 1.5**) provided valuable information regarding the conserved catalytic site. CDK1 and CDK2 share approximately 64% sequence homology, offering CDK2 as an appropriate template for CDK1.[26,32,33]

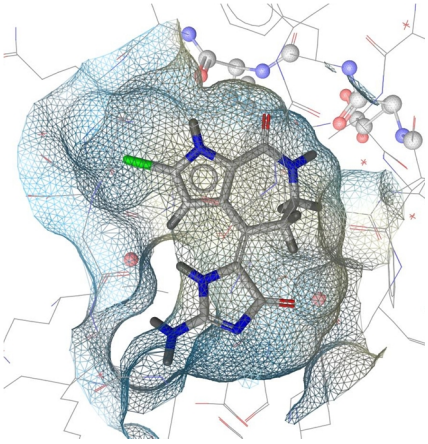


**Figure 1.5. Crystal structure of CDK2 bound with hymenialdisine (PDB: IDM2).**

The homology-modeled structure of CDK1, confirmed with the recent X-ray crystal structures, suggests a large hydrophobic pocket, categorized into two differently sized sub-pockets. CDK1 inhibitors can extend hydrophobic side chains into these two pockets, affirmatively contributing to the binding affinity. In addition, functional groups interacting with the hydrogen bond donating and accepting moieties lining the CDK1 pocket enhance the binding affinity.[26,28] Finally, docking studies for the CDK1/cyclin B complex indicate a hydrophobic pocket gatekeeper, which allows a water molecule to enter the catalytic site and provides an additional hydrogen bonding source.[28] Although CDK1 and CDK2 are highly conserved proteins, CDK1 shows a greater degree of flexibility and exploiting the plasticity of CDK1 may be the key to selective targeting.[33]

The first potent CDK inhibitor to enter clinical trials, flavopiridol (**Figure 1.6**), acts as a competitive CDK1 inhibitor and a non-selective inhibitor of several other CDKs. The evolution of selective CDK1 inhibitors followed shortly after the discovery of flavopiridol; current CDK1

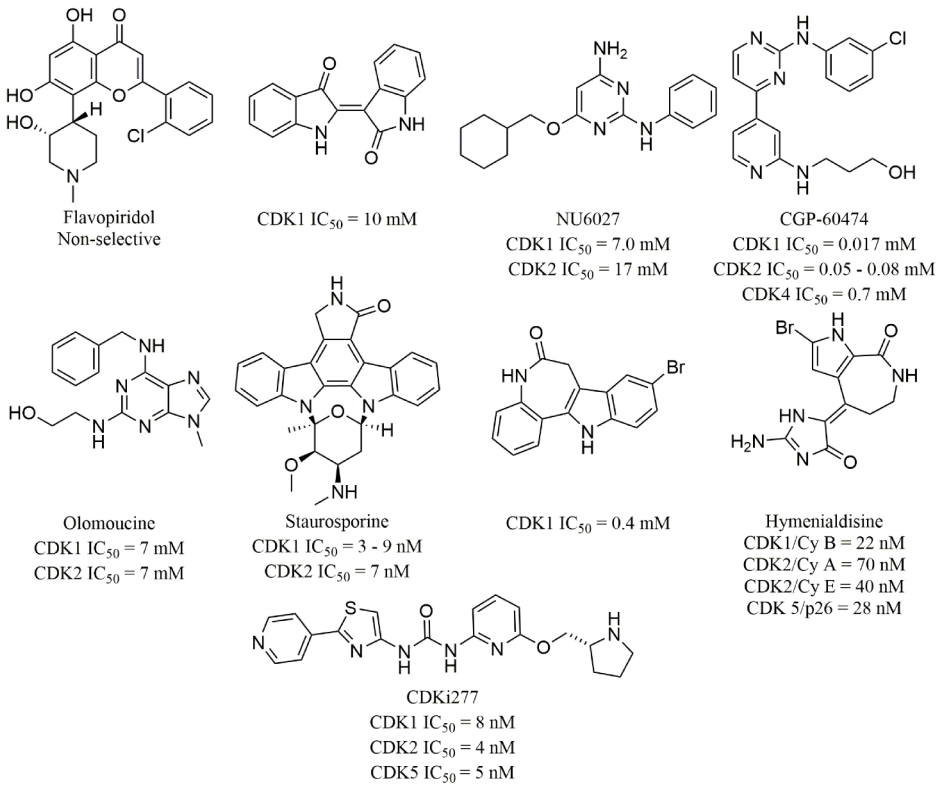



**Figure 1.6. Common CDK inhibitors and their reported $IC_{50}$ values.**

inhibitors ordinarily display high potency but low selectivity for CDK1, as is typical for most ATP-pocket binders. Selective CDK1 inhibitors support the inferred structural information regarding the CDK1 binding pocket, particularly, the importance of a hydrogen-bonding moiety as an essential component for binding.[28,34]

1.7 Rationale and Design of a Multifunctional Ligand

The 2011 studies on PARP inhibition in conjunction with compromised CDK1 activity supports the viability of a synthetically lethal strategy for BRCA-wild-type cancer cells. When compared to cells with normal levels of CDK1, Johnson et al. found the depletion of CDK1 in non-small-cell-lung cancer cells results in an 80% reduction in homologous recombination.[30] Additionally, exposing normal cells with normal CDK1 activity to the PARP inhibitor, AG14361, resulted in DNA damage repaired by HR. PARP inhibition in conjunction with CDK1-depleted activity displayed hypersensitivity to PARP inhibition and showed no further sensitization in the

originally BRCA deficient cells. The lack of further sensitization in the initially BRCA deficient cells support the hypothesis that the sensitivity of PARP inhibition directly correlates to the abrogation of BRCA1 function.[30]

Johnson exploited these *in vitro* findings and showed that mice bearing human non-small-lung carcinoma xenografts treated with the CDK1 inhibitor, AG024322, and PARP inhibitor, AG014699, displayed delayed tumor growth with 60% tumor volume reduction after thirteen days. After three weeks of treatment, mice treated with the CDK inhibitor or PARP inhibitor alone displayed considerable tumor growth, while mice treated with both the CDK inhibitor and PARP inhibitor maintained reduced tumor volume. The Kaplan-Meier curve showed the median survival of mice treated with both inhibitors increased by 86% and by 70% when compared to those treated with either inhibitor alone. Consequently, this study illustrates the potential expansion of the synthetically lethal pair, BRCA deficiency and PARP inhibition, as an effective cancer therapy beyond BRCA deficient tumors, as the inhibition, or depletion, of CDK1 resulted in HR deficient and PARP hypersensitive cancer cells.[30]

The redundancy of CDK1 and CDK2 may influence the effectiveness of PARP/CDK inhibition. CDK2 participates in a similar checkpoint pathway upstream of CDK1 by preventing the cells from entering the S phase of the cell cycle.[25] However, the sole depletion of CDK2 does not result in a reduction of homologous recombination, lead to cell death in conjunction with PARP inhibition or sensitize PARP inhibition. In some instances, like DNA-end resection in HR, CDK2 can compensate for CDK1 and decrease the effectiveness of CDK1 inhibition; thus, concomitant inhibition of CDK1 and CDK2 would likely deliver the most effective cancer therapeutic.[30]

The binding pockets of CDK and PARP lack sequence homology and are suitable for ATP binding and for $NAD^+$ binding, respectively. Further investigation of CDK1/2 and PARP1/2

inhibitor scaffolds indicates basic structural similarities in some known inhibitors (for comparison, rucaparib/hymenialdisine in **Figure 1.4** and **Figure 1.6**, respectively), which would imply some degree of pharmacophoric similarity. Thus, we explored the design and syntheses of isoform-selective PARP inhibitors and a multifunctional agent that could target both CDK1 and PARP1. Similarities between some of the CDK and PARP inhibitors provided us an initial template for the drug design of a multifunctional agent. The CDK inhibitor hymenialdisine (HMD) (**Figure 1.6**) and the PARP inhibitor rucaparib (**Figure 1.4**) show pre-clinical and clinical efficacy in many cancers[12,35] and, therefore, provided the starting scaffold for the multifunctional agent.

A thorough analysis of the binding pockets of both CDK and PARP suggested the viability of a multifunctional agent responsible for both CDK1 and PARP1 inhibition. Both binding domains share the necessity of the hydrogen-bonding moiety, as well as common pharmacophore cores. The structural requirements of CDK and PARP inhibitors, illustrated in **Figure 1.7**, provide affirmative data for the HMD/rucaparib-type scaffold. Visually represented, the CDK2 catalytic cleft contains glutamic acid and leucine residues. The amide groups within these residues form two or three specific hydrogen bonds, which are necessary for binding, with HMD (ring **B** in **Figure 1.7**, *left panel*). The bulky scaffold oriented outward of the catalytic cleft (represented as the light blue sphere in **Figure 1.7**) has the potential to interact with the lysine residue lining the cleft, or other polar side chains, which may provide selectivity for CDK1 inhibition. In addition to these moieties, substituting the HMD exocyclic primary amine on ring C

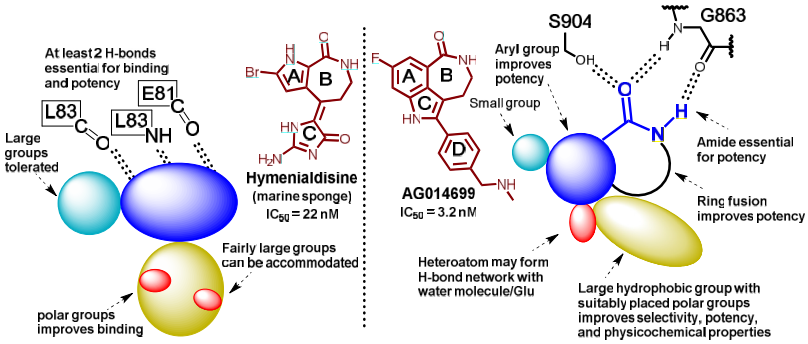



**Figure 1.7. Visual representation of the structural requirements of CDK1/2 (*left panel*) and PARP1 inhibitors (*right panel*).**

with a small, polar group could enhance binding; however, introducing large or bulky substituents will likely decrease the binding affinity. Thus, ensuring the presence of a small polar group on the C ring will promote proper binding in the CDK1/2 catalytic cleft.[36]

In a similar fashion to CDK1 inhibitors, PARP inhibition requires hydrogen bonding from not only the amide group of the ligand, rucaparib, but also the serine and glycine residues in the catalytic domain (ring **B** in **Figure 1.7**, *right panel*). Fusion of the arylamide moiety with another ring enhances the configurational preference for the bin ding domain and increases the inhibitory potency. The **A** ring in rucaparib features a fluoro-substituent that fits into a tight, small pocket formed by alanine and lysine. The glutamate residue that lines the C ring in rucaparib (**Figure 1.7**) can form a hydrogen bond with the heteroatom allowing an increase in potency when oriented correctly. Finally, rucaparib and related analogs feature a large hydrophobic substituent that fits within the adenine-ribose binding site. Reported modifications of this hydrophobic substituent increased the solubility and potency for PARP inhibitors.[37]

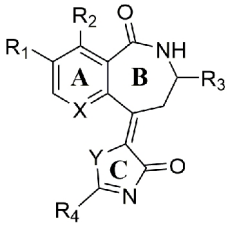


**Figure 1.8. TAAP scaffold.**

Utilizing the available knowledge about CDK and PARP inhibitors, a ligand that inhibits both targets could circumvent PARP resistance pathways and provide a therapy with minimal off-target side effects. Thus, the design of a **1,2,3,4-tetrahydro-arylazepinone** (**TAAP**) (**Figure 1.8**) core, which amalgamates common features of both these known ligands, could bind to both the proteins. In **Chapter 2**, we synthesized and geometrically analyzed several TAAP derivatives in order to understand the inhibitory potential of TAAP ligands for PARP isoforms and CDK1.

1.8 References


(1) Chan, D. A.; Giaccia, A. J. Harnessing synthetic lethal interactions in anticancer drug discovery. *Nat. Rev. Drug Discov.* **2011**, *10*, 351.

(2) Bryant, H. E.; Schultz, N.; Thomas, H. D.; Parker, K. M.; Flower, D.; Lopez, E.; Kyle, S.; Meuth, M.; Curtin, N. J.; Helleday, T. Specific killing of BRCA2-deficient tumours with inhibitors of poly(ADP-ribose) polymerase. *Nature* **2005**, *434*, 913.

(3) Farmer, H.; McCabe, N.; Lord, C. J.; Tutt, A. N. J.; Johnson, D. A.; Richardson, T. B.; Santarosa, M.; Dillon, K. J.; Hickson, I.; Knights, C.; Martin, N. M. B.; Jackson, S. P.; Smith, G. C. M.; Ashworth, A. Targeting the DNA repair defect in BRCA mutant cells as a therapeutic strategy. *Nature* **2005**, *434*, 917.

(4) Dictionary.com. www.dictionary.reference.com/browse/synthetic (accessed 10/25/2014).

(5) Bridges, C. B. The origin of variations in sexual and sex-limited characters. *Amer. Nat.* **1922**, *56*, 51.

(6) Dobzhansky, T. Genetics of natural populations. XIII. Recombination and variability in populations of *Drosophila pseudoobscura*. *Genetics* **1946**, *31*, 269.

(7) Thomas, J. H. Thinking about genetic redundancy. *Trends Genet.* **1993**, *9*, 395.

(8) Avery, L.; Wasserman, S. Ordering gene function: the interpretation of epistasis in regulatory hierarchies. *Trends Genet.* **1992**, *8*, 312.

(9) Guarente, L. Synthetic enhancement in gene interaction: a genetic tool come of age. *Trends Genet.* **1993**, *9*, 362.

(10) Lupo, B.; Trusolino, L. Inhibition of poly(ADP-ribosyl)ation in cancer: old and new paradigms revisited. *BBA - Rev. Cancer* **2014**, *1846*, 201.

(11) Kauffmann, A.; Rosselli, F.; Lazar, V.; Winnepenninckx, V.; Mansuet-Lupo, A.; Dessen, P.; van den Oord, J. J.; Spatz, A.; Sarasin, A. High expression of DNA repair pathways is associated with metastasis in melanoma patients. *Oncogene* **2007**, *27*, 565.

(12) Curtin, N. J.; Szabo, C. Therapeutic applications of PARP inhibitors: anticancer therapy and beyond. *Mol. Aspects Med.* **2013**, *34*, 1217.

(13) Thorsell, A.-G.; Ekblad, T.; Karlberg, T.; Löw, M.; Pinto, A. F.; Trésaugues, L.; Moche, M.; Cohen, M. S.; Schüler, H. Structural basis for potency and promiscuity in poly(ADP-ribose) polymerase (PARP) and tankyrase inhibitors. *J. Med. Chem.* **2017**, *60*, 1262.

(14) Riffell, J. L.; Lord, C. J.; Ashworth, A. Tankyrase-targeted therapeutics: expanding opportunities in the PARP family. *Nat. Rev. Drug Discov.* **2012**, *11*, 923.

(15) Jenner, Z. B.; Sood, A. K.; Coleman, R. L. Evaluation of rucaparib and companion diagnostics in the PARP inhibitor landscape for recurrent ovarian cancer therapy. *Future Oncology* **2016**, *12*, 1439.

(16) U.S. National Institutes of Health. www.clinicaltrials.gov (accessed 10/11/2016).

(17) Seong, M.-W.; Kim, K. H.; Chung, I. Y.; Kang, E.; Lee, J. W.; Park, S. K.; Lee, M. H.; Lee, J. E.; Noh, D.-Y.; Son, B. H.; Park, H.-L.; Cho, S. I.; Park, S. S.; Korean, H. B. C. S. G.; Kim, S.-W. A multi-institutional study on the association between BRCA1/BRCA2 mutational status and triple-negative breast cancer in familial breast cancer patients. *Breast Cancer Res. Treat.* **2014**, *146*, 63.

(18) Foulkes, W. D.; Smith, I. E.; Reis-Filho, J. S. Triple-negative breast cancer. *N. Engl. J. Med.* **2010**, *363*, 1938.

(19) Rummel, S.; Varner, E.; Shriver, C. D.; Ellsworth, R. E. Evaluation of BRCA1 mutations in an unselected patient population with triple-negative breast cancer. *Breast Cancer Res. Treat.* **2013**, *137*, 119.

(20) Opyrchal, M.; Salisbury, J. L.; Iankov, I.; Goetz, M. P.; McCubrey, J.; Gambino, M. W.; Malatino, L.; Puccia, G.; Ingle, J. N.; Galanis, E.; D'Assoro, A. B. Inhibition of Cdk2 kinase activity selectively targets the CD44(+)/CD24(-)/Low stem-like subpopulation and restores chemosensitivity of SUM149PT triple-negative breast cancer cells. *Int. J. Oncol.* **2014**, *45*, 1193.

(21) Pruthi, S.; Gostout, B. S.; Lindor, N. M. Identification and management of women with BRCA mutations or hereditary predisposition for breast and ovarian cancer. *Mayo Clin. Proc.* **2010**, *85*, 1111.

(22) Xia, Q.; Cai, Y.; Peng, R.; Wu, G.; Shi, Y.; Jiang, W. The CDK1 inhibitor RO3306 improves the response of BRCA-proficient breast cancer cells to PARP inhibition. *Int. J. Oncol.* **2014**, *44*, 735.

(23) Liu, T.; Huang, J. DNA end resection: Facts and mechanisms. *Genomics, Proteomics Bioinf.* **2016**, *14*, 126.

(24) Bouwman, P.; Jonkers, J. Molecular pathways: how can BRCA-mutated tumors become resistant to PARP inhibitors? *Clin. Cancer Res.* **2014**, *20*, 540.

(25) Lapenna, S.; Giordano, A. Cell cycle kinases as therapeutic targets for cancer. *Nat. Rev. Drug Discov.* **2009**, *8*, 547.

(26) Hardcastle, I. R.; Golding, B. T.; Griffin, R. J. Designing inhibitors of cyclin-dependent kinases. *Ann. Rev. Pharmacol. Toxicol.* **2002**, *42*, 325.

(27) Dai, Y.; Grant, S. Small molecule inhibitors targeting cyclin-dependent kinases as anticancer agents. *Curr. Oncol. Rep.* **2004**, *6*, 123.

(28) Wang, Q.; Su, L.; Liu, N.; Zhang, L.; Xu, W.; Fang, H. Cyclin dependent kinase 1 inhibitors: a review of recent progress. *Curr. Med. Chem.* **2011**, *18*, 2025.

(29) Rzymski, T.; Zarebski, A.; Dreas, A.; Osowska, K.; Kucwaj, K.; Fogt, J.; Cholody, M.; Galezowski, M.; Czardybon, W.; Horvath, R.; Wilkik, K.; Milik, M.; Brozoka, K. Substituted tricyclic benzimidazoles as kinase inhibitors. *WO/2014/072435*.

(30) Johnson, N.; Li, Y. C.; Walton, Z. E.; Cheng, K. A.; Li, D.; Rodig, S. J.; Moreau, L. A.; Unitt, C.; Bronson, R. T.; Thomas, H. D.; Newell, D. R.; D'Andrea, A. D.; Curtin, N. J.; Wong, K. K.; Shapiro, G. I. Compromised CDK1 activity sensitizes BRCA-proficient cancers to PARP inhibition. *Nat. Med.* **2011**, *17*, 875.

(31) Georgieva, J.; Sinha, P.; Schadendorf, D. Expression of cyclins and cyclin dependent kinases in human benign and malignant melanocytic lesions. *J. Clin. Pathol.* **2001**, *54*, 229.

(32) Coxon, C. R.; Anscombe, E.; Harnor, S. J.; Martin, M. P.; Carbain, B.; Golding, B. T.; Hardcastle, I. R.; Harlow, L. K.; Korolchuk, S.; Matheson, C. J.; Newell, D. R.; Noble, M. E. M.; Sivaprakasam, M.; Tudhope, S. J.; Turner, D. M.; Wang, L. Z.; Wedge, S. R.; Wong, C.; Griffin, R. J.; Endicott, J. A.; Cano, C. Cyclin-Dependent Kinase (CDK) inhibitors: structure–activity relationships and insights into the CDK-2 selectivity of 6-substituted 2-arylaminopurines. *J. Med. Chem.* **2017**, *60*, 1746.

(33) Brown, N. R.; Korolchuk, S.; Martin, M. P.; Stanley, W. A.; Moukhametzianov, R.; Noble, M. E. M.; Endicott, J. A. CDK1 structures reveal conserved and unique features of the essential cell cycle CDK. *Nat. Commun.* **2015**, *6*, 6769.

(34) Mariaule, G.; Belmont, P. Cyclin-dependent kinase inhibitors as marketed anticancer drugs: where are we now? A short survey. *Molecules* **2014**, *19*, 14366.

(35) Tepe, J. J. Preparation of hymenialdisine derivatives and use thereof. *US20040235820A1*, 26.

(36) Wu, S. Y.; McNae, I.; Kontopidis, G.; McClue, S. J.; McInnes, C.; Stewart, K. J.; Wang, S.; Zheleva, D. I.; Marriage, H.; Lane, D. P.; Taylor, P.; Fischer, P. M.; Walkinshaw, M. D. Discovery of a novel family of CDK inhibitors with the program LIDAEUS: Structural basis for ligand-induced disordering of the activation loop. *Structure* **2003**, *11*, 399.

(37) Ferraris, D. V. Evolution of poly(ADP-ribose) polymerase-1 (PARP-1) inhibitors. From concept to clinic. *J. Med. Chem.* **2010**, *53*, 4561.

## Chapter 2: Probing the Tetrahydro-arylazepineone A/B Ring Scaffold for PARP Isoform-Specific Inhibition and Dual Inhibition with CDKs

### 2.1 Introduction

The TAAP scaffold, extrapolated from the structural similarities of hymenialdisine (HMD) and rucaparib, provided the initial design template for a multifunctional CDK/PARP inhibitor (**Figure 1.8**). We tested several compounds for preliminary validation of the TAAP platform, with emphasis placed on the **A**/**B** fused ring system and PARP1. Following this confirmation, we explored derivatizations of the lead compound in search of a more potent PARP1 inhibitor.

### 2.2 Initial Exploration of the A/B Ring Scaffold

#### *2.2.1 Design*

The first step taken to validate the multifunctional ligand hypothesis involved determining the potency of compounds similar to HMD, de-brominated HMD (**1**) and the HMD **A**/**B** ring fragment (**2**), via a PARP1 ELISA assay. The preliminary results collected from a pool of test ligands, comprised of commercially available compounds and those with slight modification to the **A**/**B** ring, guided the lead selection. The modifications to the HMD 5/7-membered ring core included aryl halides (**3**, **4** and **5**), the removal of the carbonyl (**6**) at the benzylic position (**7**), and substitution of the benzylic carbon with an oxygen (**8**) and nitrogen (**9a**) (**Figure 2.1**).

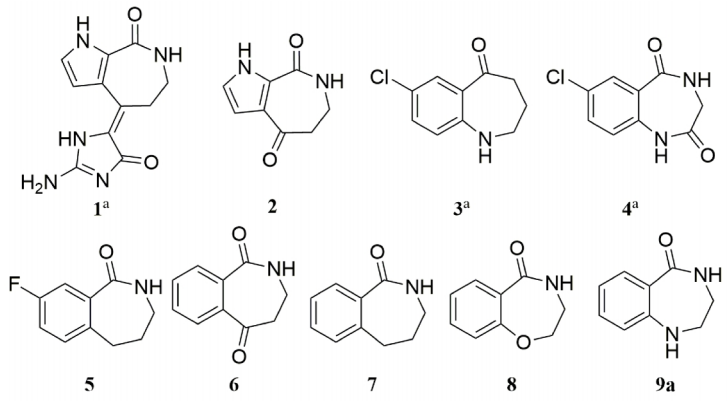
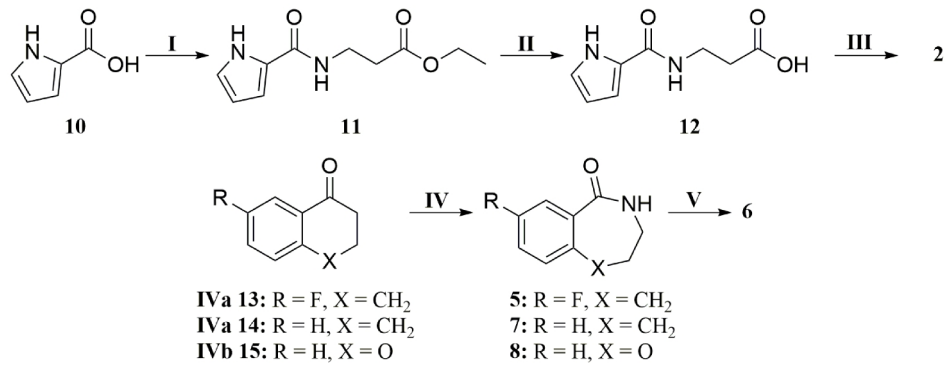



**Figure 2.1. Initial compounds probed for PARP1 inhibition.** [a]Commercial source

*2.2.2 Synthesis*

A standard literature procedure was followed for the synthesis of **2** (**Scheme 2.1**).[1] The β-alanine ethyl ester coupled to **10** using EDC and 6-Cl-HOBt yielded **11** in sufficient purity. The ester hydrolysis of **11** yielded **12** quantitatively, when condensed with polyphosphoric acid and

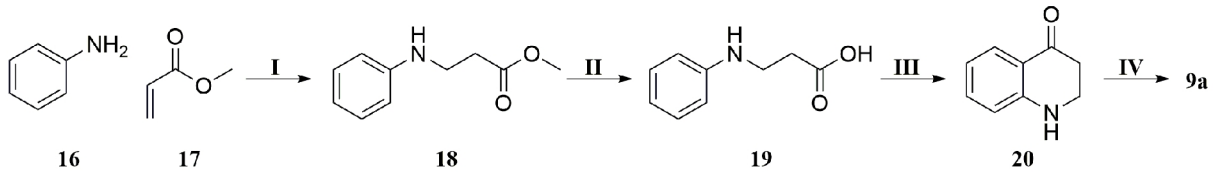



**Scheme 2.1. Synthetic overview of the initial compounds probed for PARP1.** Reagents and conditions, **I**: **10** (1.00 eq), β-Ala ethyl ester hydrochloride (1.05 eq), *N*-(3-dimethylaminopropyl)-*N'*-ethylcarbodiimide hydrochloride (EDC HCl) (1.50 eq), 1-hydroxy-6-chloro-benzotriazole (6-Cl-HOBt) (1.50 eq), 1M $KHCO_3$ (2.00 eq), dichloromethane (DCM), room temperature (RT), 18 hr (70% crude yield); **II**: LiOH (3.0 eq), water (3.0 eq), ethanol (EtOH), μW irradiation, 60°C, 1 hr (quantitative yield); **III**: polyphosphoric acid (PPA) (11% w/w), $P_2O_5$ (3.0 eq), 120°C, 18 hr (16% yield); **IVa (X = C)**: $NaN_3$ (2.0 eq), HCl, 0°C, 18 hr (**5**: 56% yield, **7**: 41% yield); **IVb (X = O)**: $NaN_3$ (2.0 eq), $H_2SO_4$, 0°C, 4 hr (60% yield); **V**: $KMnO_4$ (10.0 eq), $FeCl_3 \cdot 6\ H_2O$ (6.0 eq), acetone, −78°C→RT, 1h at RT (15% yield (0.5 mmol), 5% yield (10 mmol)).

phosphorous pentoxide yielded the cyclic compound **2** in a 16% yield. The commercially available starting materials **13–15** were ring expanded under Schmidt reaction conditions with sodium azide to yield **5**, **7**, and **8** (**Scheme 2.1**).[2] When X = O (**15**), the use of sulfuric acid proved necessary for the Schmidt reaction as the use of hydrochloric acid yielded the constitutional isomer in majority (i.e., the benzylic lactam). The benzylic oxidation of **7** (X = $CH_2$) with potassium permanganate and iron (III) chloride hexahydrate yielded **6** (15% yield (0.5 mmol), 5% (10 mmol)).[3]

The synthesis of compound **9a** (**Scheme 2.2**) derives mainly from literature reports. The initial synthetic scheme utilized microwave irradiation for reactions **I** and **II**;[4] however, the Michael addition reaction **I** with **16** and **17** produced several decomposition products, complicating the purification of **18**. The efficiency of reaction **I** significantly improved with the use of an ionic

liquid,[5] so much so that the crude product was used directly in reaction **II** to yield **19**. Polyphosphoric acid catalyzed cyclization yielded compound **20**, and Schmidt reaction conditions




**Scheme 2.2. Synthetic scheme of the TBAP scaffold (9a).** Reagents and conditions, **I:** aniline (1.0 eq), methyl acrylate (1.1 eq), triethylammonium acetate (TEAA), 50°C, 18 hr (87% crude yield); **II**: 1M NaOH, methanol, 50°C, 18 hr (82% yield); **III**: PPA (25% w/w), $P_2O_5$ (0.6 eq), 90°C, 18 hr (1.6 mmol, 90% yield, 10 mmol, 51%); **IV**: $NaN_3$ (2.0 eq), $H_2SO_4$, 0°C→RT, 4 hr (62% yield).

generated the lactam (**9a**). This scheme provides **9a** in four steps with a 36% overall yield.

*2.2.3 Results*

The initial results validated the hypothesis that derivatives of HMD will effectively bind in PARP1 (**Table 2.1**). Although the CDK1 inhibitor fragments (**1** and **2**) only exhibit moderate potency on PARP1, inhibition in the μM range supports the hypothesis that a suitable multifunctional ligand can be developed. Many of the A/B rings shown in **Figure 2.1** either lost activity or displayed modest activity on PARP1. Since many known PARP inhibitors either lack a **B** ring or contain planar **A**/**B** rings (**Figure 1.4**), the planarity of the fused rings and the amide may contribute to high potency seen in known PARP inhibitors. Further, although many of the A/B rings in **Figure 2.1** are analogous to the 6/7 membered ring core of rucaparib, the tricyclic ring system in rucaparib may enhance the planarity of the **A**/**B** ring, resulting in its high potency.

| Compound | $IC_{50}$ (μM) |
|---|---|
| **1** | 24.0 ± 5.4 |
| **2** | 17.7 ± 9.5 |
| **3** | > 60 |
| **4** | 11.3 ± 5.6 |
| **5** | > 60 |
| **6** | > 60 |
| **7** | 41.5 ± 32.7 |
| **8** | 6.5 ± 4.8 |
| **9a** | 2.5 ± 0.4[a] |

**Table 2.1. $IC_{50}$ values of initial compounds probed for PARP1 inhibition.** [a]Indicates average ± propagated error.

Replacing the pyrrole ring in **2** with a benzene ring (**6**) diminishes the potency, which discourages the validity of the TAAP scaffold. Unlike **2**, **6** contains a hydrogen (9H) oriented towards the benzylic carbonyl (1C=O), resulting in decreased amide planarity and increased ring pucker (**Figure 2.2**). Obtained from geometry optimization calculations (B3LYP/6-31G(d)), the

calculated dihedral angle of the amide (∠10C–11C–5C–4N, DA1) is −9.2° and −36.8° for **2** and **6**, respectively, and the calculated dihedral angle of the benzylic carbonyl (∠11C–10C–1C–1O, DA2) is −0.7° and −25.7° for **2** and **6**, respectively. Upon removal of the benzylic carbonyl from **6** (**7**), the calculated amide dihedral angle (DA1) increased in planarity from −36.8° to −16.9°, and the ligand **7** regains activity (41.5 μM), providing further evidence that ring pucker and amide planarity influences the PARP1 potency.

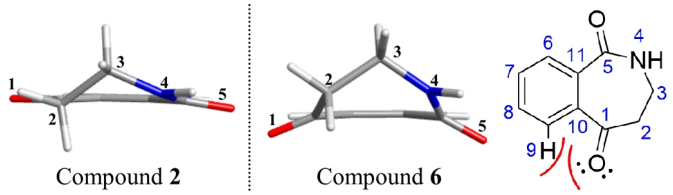



**Figure 2.2. Compound 2 and 6 illustrated to demonstrate the increased amide planarity and ring pucker.** A 2D image of 6 demonstrates the potential steric strain between the benzylic carbonyl and 9H. Image generated from geometry optimizations (B3LYP/6-31G(d)).

An electron-donating atom (N or O) in the benzylic position can participate in resonance with the aromatic ring, which may encourage a more favorable planar conformation for PARP1 inhibition; this postulate helps explain the increased activity of **4**, **8**, and **9a**. Lastly, the inactive **3** is unsurprising since the amide is essential for PARP1 binding, as previously mentioned in **Section 1.7**. Ultimately, the 1,2,3,4-tetrahydo-5*H*-benzo[*e*][1,4]-diazepin-5-one (**9**, TBAP) exhibited the best μM activity and served as the lead compound. This preliminary study highlighted the importance of geometry for the design of a potent PARP1 inhibitor. The narrow PARP1 pocket above and below the plane of any bound ligand (ATP or an inhibitor) restricts large deviations from ligand planarity (**Figure 2.3**). The rigid, planar ligands tend to bind to many PARP isoforms and are non-selective. Our latest biological evaluation appears to suggest that the TAAP flexibility and 3D topology

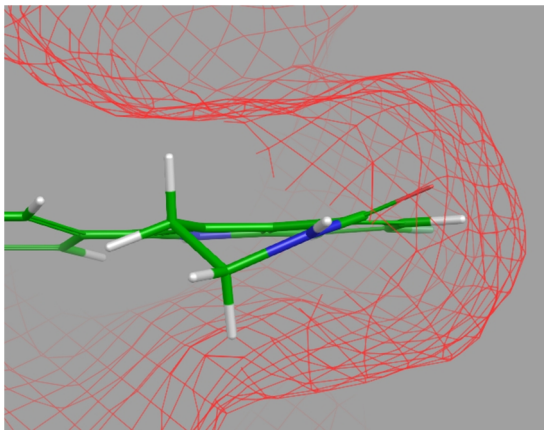


**Figure 2.3. PARP1 with rucaparib X-ray crystal structure.** The side view of the surface binding site of rucaparib crystalized with PARP1 to illustrate the space above and below the **A**/**B** ring (PBD: 4RV6).

described here can influence the PARP isoform selectivity (**Section 2.4**). Thus, if we can retain or improve the TAAP activity with further diversification, the slight non-planarity of these ligands could drive PARP isoform selectivity.

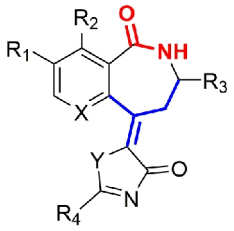


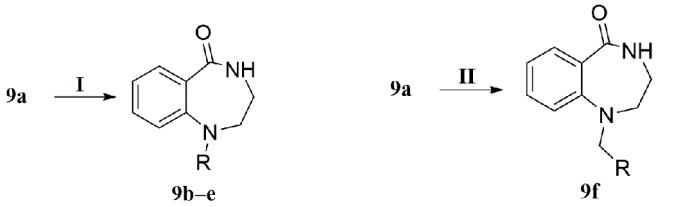

**Figure 2.4. Important pharmacophore features of the TAAP scaffold.** The amide (red) forms key hydrogen bonds with the residues lining the PARP1 and CDK1 pocket. The $sp^2$ benzylic position induces planarity of the diazepine ring.

2.3 TAAP Derivatives and $IC_{50}$ Determinations

Effective multifunctional ligand design requires tailoring the derivatives to the essential pharmacophore moieties of PARP1 and CDK1: the amide and the fused ring planarity (highlighted in red and blue, respectively, in **Figure 2.4**). Since the PARP1 X-ray crystal structure is available, the first milestone in this research is to develop a sub-micromolar PARP1 inhibitor.

*2.3.1 The Amide TBAP Derivatives*

The benzylic amine of **9a** was reacted with various acid chlorides to yield various amide derivatives (**Scheme 2.3**, compounds **9b–e**) . Despite the trivial nature of acylations, the synthesis of **9b** required several reaction condition optimizations to avoid the acylation of both the amine and the lactam. The ease of the lactam acylation hinted at increased amide $sp^3$-character and reduced amide planarity. Synthesizing the benzoyl (**9e**) and heterocyclic amides (**9c** and **9d**) allowed us to explore the **C** ring effects on PARP1 potency.

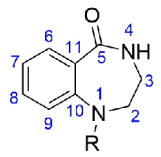



| **I** | R | Yield |
|---|---|---|
| **9b**[a] | Acetyl | 34% |
| **9c** | Furoyl | 53% |
| **9d** | α-Thenoyl | 35% |
| **9e** | Benzoyl | 71% |

| **II** | R | Yield |
|---|---|---|
| **9f** | Phenyl | 72% |

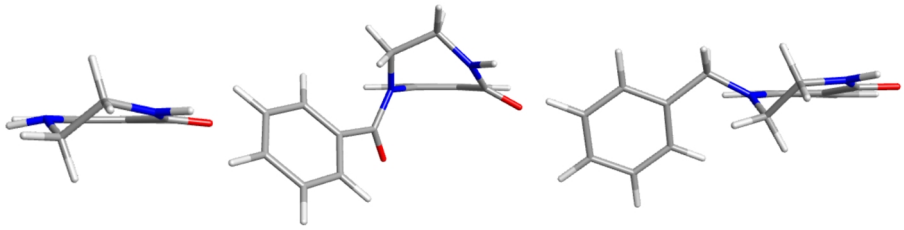
**Scheme 2.3. Overall synthetic scheme of the amide-TBAP derivatives.** Reagents and conditions, **I**: acyl chloride (1.0 eq), diisopropylethylamine (DIEA) (1.5 eq), DCM, RT, 18 hr; **II**: $K_2CO_3$ (2.0 eq), benzyl bromide (1.0 eq), $CH_3CN$, 50°C, 18 hr. [a]Alternative reagents for **9b**: acetic anhydride (1.0 eq), pyridine, RT, 18 hr. **9a** R = H

Surprisingly, the amide derivatives led to diminished PARP1 activity (**Table 2.2**). Geometry optimizations (B3LYP/6-31G(d)) of the amide TBAP derivatives (**9b**–**9e**) reveal that the newly introduced 1N-amide bond promotes even more distortion of the fused ring system. The underivatized **9a** is relatively planar with one methylene carbon and the lactam nitrogen slightly protruding from the azimuthal plane (**Figure 2.5**). Contrarily, the amide TBAP derivatives (**9b**–**9e**) show protrusion of two methylene carbons, the lactam nitrogen, and the newly synthesized amide bond (**9e** illustrated in **Figure 2.5**). The steric interactions between 9H and the amide carbonyl, discussed previously in **Figure 2.2**, could induce the diazepine **B** ring distortion. We synthesized a benzyl derivative (**9f**) in order to probe this hypothesis (**Scheme 2.3**). As shown in **Table 2.2**, **9f** displays slightly increased activity compared to its parent compound (**9a**) possibly because the benzyl ring can occupy the PARP1 hydrophobic pocket without distorting the **B** ring (**9f** in **Figure 2.5**). The decreased activities for the amide TBAP derivatives and the retention of activity for the benzyl **9f** provide evidence that parallels ligand planarity with PARP1 inhibition.




| TBAP | R | $IC_{50}$ (μM) |
|---|---|---|
| **9a** | H | 2.5 ± 0.4[a] |
| **9b** | Acetyl | >60 |
| **9c** | Furoyl | >60 |
| **9d** | α-Thenoyl | >60 |
| **9e** | Benzoyl | >60 |
| **9f** | Benzyl | 1.6 ± 0.7[a] |

**Table 2.2. TBAP derivatives (9) probed for PARP1 activity.** [a]Indicates average ± propagated error.



**9a** **9e** **9f**

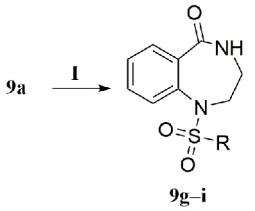
**Figure 2.5. The azimuthal plane of 9a, 9e and 9f.** Note the overall planarity of the underivatized **9a**, the significant distortion of **9e**, and overall planarity of **9f**. The benzoyl **9e** is an example of the diazepine ring distortion induced by amide derivatization. Images generated from geometry optimizations (B3LYP/6-31G(d)) using Cresset Torch.

Further investigation of the optimized geometries showed that the underivatized **9a** benzylic nitrogen (1N) adopts a trigonal planar geometry due to the resonance between the aromatic ring

and the benzylic nitrogen (**9a** in **Figure 2.5**). Alkylating the benzylic nitrogen (**9f**) still permits resonance, maintains the 1N trigonal planar geometry, and ultimately retains the PARP1 activity. In contrast, acylation of the benzylic nitrogen (**9b–9e**) distorts the 1N trigonal planar geometry due to the steric interactions between 9H and the 1N amide carbonyl. Allowing the benzylic nitrogen to assume trigonal planar geometry by introducing smaller, more flexible **C** rings may decrease the steric and bond angle strain of the diazepine **B** ring thereby maintaining the overall planarity and potentially increasing PARP1 potency. We will test this hypothesis with future derivatives containing 5-membered heterocycles and **9f** analogues (**Chapter 4**).

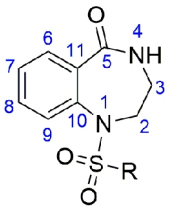
*2.3.2 The Sulfonamide TBAP Derivatives*

In addition to the amide TBAP derivatives, we synthesized and assayed a small series of sulfonamide TBAP derivatives (**Scheme 2.4**); however, the sulfonamides resulted in diminished activity as well (**Table 2.3**). Brief geometry optimization studies show that the R group can orient underneath the **A**/**B** ring plane in a "folded" conformation (**Figure 2.6**). The energy difference between the folded and extended conformations varies for each R group. While the mesyl **9g** folded and extended conformations differ in approximately 4.0 kcal/mol, the energy differences between the isomers of the vinyl **9h** and phenyl **9i** are within error of the calculations (approximately 1 kcal/mol). Geometry optimizations of the folded conformations revealed that the dihedral angle ∠11C–10C–1N–1S (DA3) for the mesyl **9g** starts to approach 90° (104.1°), indicating that the 1N-$SO_2$ bond is almost




| I | R | Yield |
|---|---|---|
| **9g** | Methyl | 2% |
| **9h**[a] | Vinyl | 12% |
| **9i** | Phenyl | 28% |

**Scheme 2.4. Overall synthetic scheme of the sulfonamide-TBAP derivatives.** Reagents and conditions, **I**: sulfonyl chloride (1.5–3.0 eq), DIEA (1.5 eq), DCM, RT, 18 hr. [a]Alternative reagents for **9h**: 2-chloroethanesulfonyl chloride (1.0 eq), triethylamine (TEA) (2.0 eq), DCM, RT 18hr.




| TBAP | R | $IC_{50}$ (μM) |
|---|---|---|
| **9g** | Methyl | >60 |
| **9h** | Vinyl | >60 |
| **9i** | Phenyl | >60 |

**Table 2.3. Sulfonamide TBAP derivatives probed for PARP1 activity.**

perpendicular to the **A**/**B** ring plane. This folded conformation significantly distorts diazepine **B** ring and increases the vertical height such that the ligand is too large for the PARP1 pocket (for the vertical illustration of the PARP1 pocket see **Figure 2.3**).

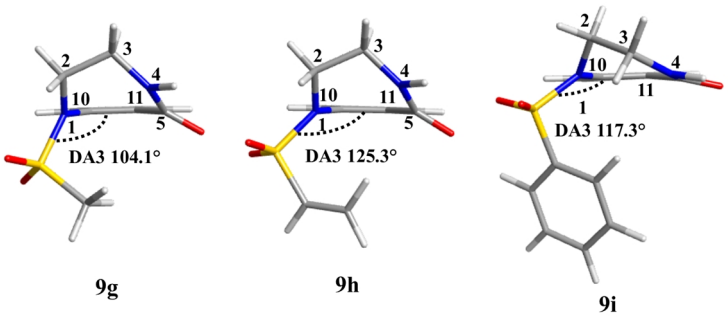



**Figure 2.6. The azimuthal plane of the sulfonamide TBAP derivatives 9g–9i.** DA3: dihedral angle ∠11C–10C–1N–1S. Images generated from geometry optimizations (B3LYP/6-31G(d)) using Cresset Torch.

We confirmed the structure of the phenyl sulfonamide **9i** with X-ray crystallography (**Figure 2.7**). The DA3 obtained from the CIF file is 98.6°, nearly a perpendicular 1N-$SO_2$ bond with respect to the **A**/**B** fused ring plane. Although the calculated DA3 from geometry optimizations is larger than the measured DA3 from the X-ray crystal structure, the relative geometry of the optimized phenyl sulfonamide **9i** resembles the geometry obtained from the X-ray crystal structure. The folded conformation of the sulfonamide TBAP derivatives helps justify the absence of PARP1 activity and provides evidence that future TBAP **9a** derivatives must contain a small, flexible **C** ring to maintain planarity and potentially increase potency.

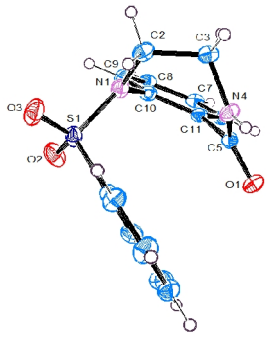
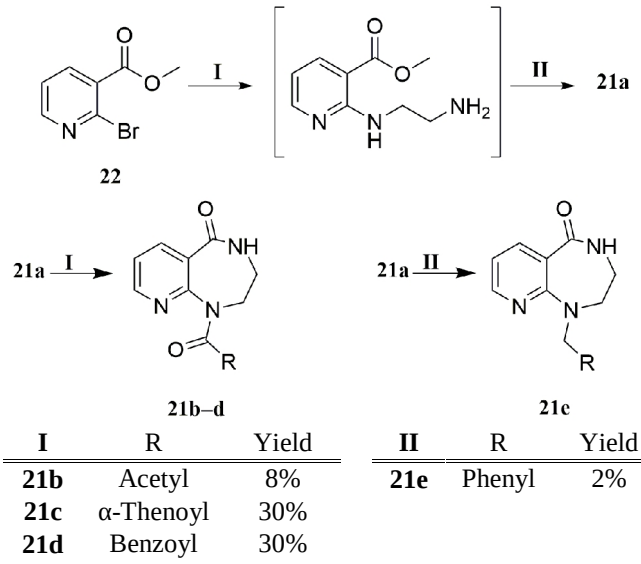



**Figure 2.7 X-ray crystal structures of the phenyl sulfonamide 9i shown as ellipsoids.** Image extracted from CIF file.

*2.3.3 The TPAP derivatives*

We synthesized and tested a series of pyrido-based compounds (X = N, TPAP, **21**, **Scheme 2.5**) to determine whether the pyridyl nitrogen could participate in hydrogen bonding to polar residues and/or a water molecule in the PARP1 pocket, and therefore, increase potency. Optimizing the synthesis of **21a** initially proved troublesome due to the high water solubility of the product and the lack of affordable, commercially available precursors. Though we pursued

several different synthetic pathways, a "one-pot" reaction proved to be an expedient strategy with a 23% isolated yield (**Scheme 2.5**). The strongly activated 2-bromo position of **22** made the synthesis of **21a** troublesome due to facile bromine substitution under acid and basic hydrolytic conditions. The initial synthetic scheme involved hydrolysis of the methyl ester, amide-coupling techniques to introduce the ethylenediamine fragment, and high temperatures/strong base to encourage the cyclization to yield the final product **21a**. In order to hydrolyze the methyl ester, hydrobromic acid in conjunction with mild reaction conditions were necessary to prevent hydroxyl substitution at the 2-bromo position. Further, the amidation of the carboxylic acid derivative **22** invariably involved substitution at the 2-bromo position. Alternative attempts to take advantage of the highly activated 2-bromo position by first substituting the bromine with ethylenediamine followed by various cyclization/ring-closing attempts also were fraught with problems. Substituting the 2-bromo position increased the water solubility of the molecule, thus making isolation and purification difficult. The culmination of these results led to the development of the "one-pot" reaction. Substitution of the 2-bromo position with ethylenediamine followed by liquid/liquid extraction yielded the intermediate in the aqueous layer (**Scheme 2.5**) while removing any organic




| I | R | Yield |
|---|---|---|
| **21b** | Acetyl | 8% |
| **21c** | α-Thenoyl | 30% |
| **21d** | Benzoyl | 30% |

| II | R | Yield |
|---|---|---|
| **21e** | Phenyl | 2% |

**Scheme 2.5 Synthetic scheme of 21a and 21a derivatives.** Reagents and conditions, **I:** ethylenediamine (1.2 eq), methanol, 50°C, 18 hr; **II:** liquid/liquid extraction followed by microwave irradiation, 110°C, 1.5 hr (23% yield); **III**: acyl chloride (1.5 eq), DIEA (1.5 eq), DCM, RT, 18 hr. **IV**: Benzyl bromide (2.0 eq), $K_2CO_3$ (2.0 eq), $CH_3CN$, microwave irradiation, 70°C, 1.5 hr.

side products. After extraction, we subjected the aqueous layer to microwave irradiation at 110°C for 90 minutes to obtain **21a** in moderate yields.

Although the pyrido-TPAP analogues replace the 9C-9H bond with a nitrogen, the lone pair on the pyridyl nitrogen could cause stereoelectronic repulsion with the lone pairs on the 1N-amide carbonyl, inducing similar steric effects as described in **Figure 2.2**. Accordingly, the pyrido-TPAP analogue **21a** exhibits similar activity to **9a** (**Table 2.4**), which agrees with the nearly identical computational models of both **9a** and **21a** (**Figure 2.8A**). This result also suggests that the pyridyl nitrogen does not participate in any additional hydrogen bonding with the water molecule or the glutamate residue lining the PARP1 pocket.




**21**

| TPAP | R | $IC_{50}$ (μM) |
|---|---|---|
| **21a** | H | 3.3 ± 0.8[a] |
| **21b** | Acetyl | 4.4 ± 1.5[a] |
| **21c** | α-Thenoyl | >60 |
| **21d** | Benzoyl | >60 |
| **21e** | Benzyl | 0.2 ± 0.1[a] |

**Table 2.4. TPAP derivatives (21) probed for PARP1 activity.** [a]Indicates average ± propagated error.

The TPAP analogues (**21a**–**21e**) generally exhibit similar geometries to the analogous TBAP derivatives (**Figure 2.8B**). Comparison of the benzoyl TBAP derivative **9e** and the benzoyl TPAP derivative **21d** revealed increased diazepine **B** ring planarity (**Figure 2.8B**). Although **21d** displays a relatively planar diazepine **B** ring, theoretically sufficient for the PARP1 binding pocket, **21d** is not active against PARP1. Since the **21d** diazepine **B** ring is more planar, the benzoyl group cannot orient in the same plane as the **A**/**B** fused ring and must orient perpendicularly to minimize steric strain; therefore, the molecule loses its *overall* planarity and activity. Surprisingly, the benzyl TPAP derivative (**21e**) displays an order of magnitude increase in activity compared to the TBAP and other TPAP derivatives. The benzyl **21e** is active in the nM range, while the TAAP derivatives are active in the μM range, including the analogous benzodiazepine **9f**. Additionally, unlike the

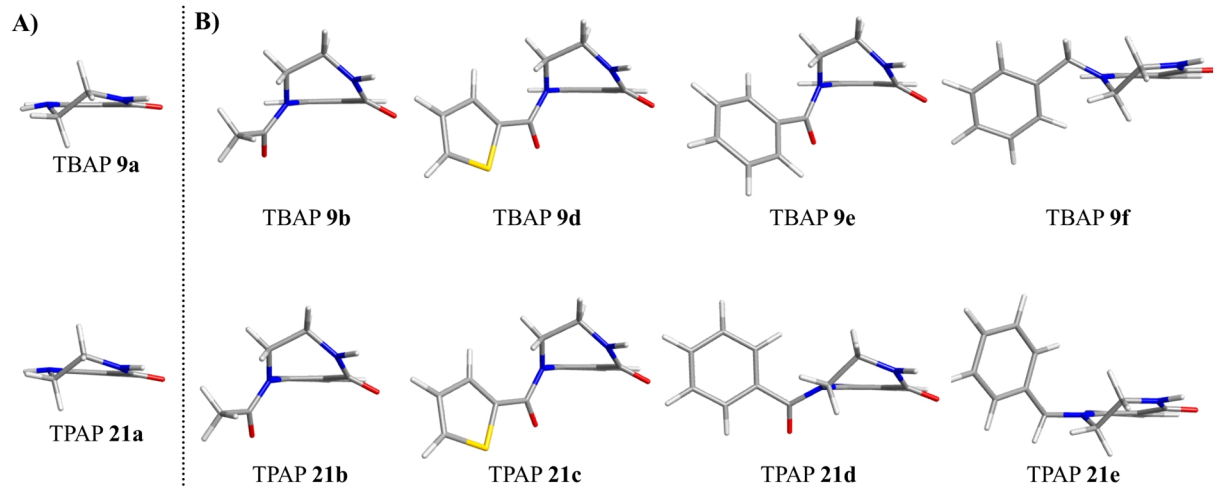



**Figure 2.8. The azimuthal plane of the analogous TPAP and TBAP derivatives.** A) TBAP **9a** and TPAP **21a**. A) The derivatized TPAP (**21b–21e**) and TBAP analogues (**9b**, **9d–9f**). Note the increased **B** ring planarity of **21d** when compared to **9e** Images generated from geometry optimizations (B3LYP/6-31G(d)) using Cresset Torch.

acetyl TBAP **9b**, **21b** still maintains its potency compared to its parent compound (**21a**) despite the conformational similarities between **9b** and **21b** (**Figure 2.8B**).

We used $^{1}$H-NMR to rationalize the differences in activity between the TBAP **9b** and TPAP **21b**. The $^{1}$H-NMR spectra show diastereotopic peaks for the methylene hydrogens in **9b** (**Figure 2.9B**), but show a triplet and quartet for the analogous methylene hydrogens in **21b** (**Figure 2.9A**); therefore, suggesting that the acetyl **21b** is more flexible than the acetyl **9b** (**Figure 2.9**). Although modeled conformations of

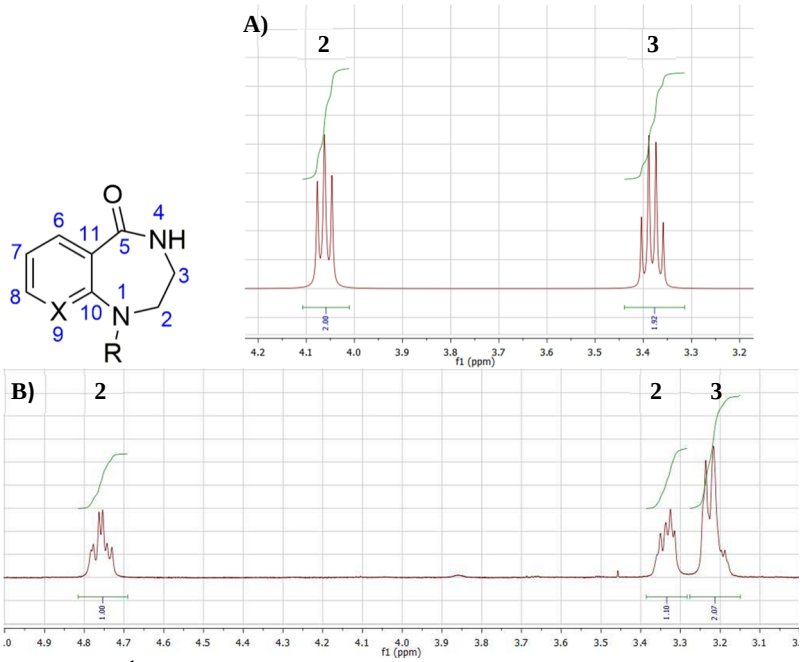



**Figure 2.9. $^{1}$H-NMR spectra of 21b (A) and 9b (B).** The NMR spectrum is zoomed to view the methylene hydrogens at the 2 and 3 positions (3 ppm–5 ppm). A) NMR spectrum of the acetylated TPAP derivative (**21b**); NMR solvent: $CDCl_3$. B) NMR spectrum of the acetylated TPAP derivative (**21b**); NMR solvent: 1,1,2,2-tetrachloroethane-$d_2$.

both acetyl derivatives are nearly identical, the inferred flexibility from $^{1}$H-NMR could explain the lack of activity for **9b** and the retention of activity for **21b**. In addition to overall molecular planarity, this result also indicates that the R group flexibility is important for proper PARP1 binding and provides additional evidence that the introduction of smaller, more flexible **C** rings could promote PARP1 binding and potentially increase potency.

Although the initial attempts to synthesize planar TAAP derivatives (i.e., TBAP and TPAP) for PARP1 inhibition proved inadequate, the knowledge gained from the active derivatives (TBAP **9a, 9f** and TPAP **21a**, **21b**, **21e**) and geometry optimizations will govern the future design of the TAAP PARP1 inhibitors. Furthermore, the X-ray crystal structure of the inactive sulfonamide **9i** confirmed the predicted folded conformation and substantiated our investigation of axial chirality in the TAAP derivatives (**Section 2.5**).

2.4 PARP Isoform Selectivity

The currently reported PARP1 vs. PARP2 selective inhibitor exhibits 89-fold selectivity with an $IC_{50}$ value of 45 nM, though $IC_{50}$ values were not determined for any other PARP isoforms.[6] The most selective PARP2 vs. PARP1 inhibitor shows 60-fold selectivity, but again, $IC_{50}$ values for any other PARP isoforms were not determined. Only one compound (ME0328) classifies as a PARP3 selective inhibitor with 7-fold selectivity over PARP1, and $IC_{50}$ values were determined for PARP2, PARP4, TNKS1 (PARP5A) and TNKS2 (PARP5B). Lastly, TNKS1/TNKS2 selective inhibitors show selectivity over PARP1, PARP2, and PARP3, when reported.[6]

Despite the lack of PARP1 activity demonstrated by much of the TAAP series, we were able to show some PARP isoform selectivity from some TAAP derivatives. Utilizing a commercial screening service,[7] we tested the TAAP analogues against PARP1, PARP2, PARP3, TNKS1, TNKS2, PARP6, PARP7, PARP8, PARP10, PARP11, PARP12, PARP14 and PARP15 in a

single-point assay and determined the percent inhibition at 10 μM. For clarity, we divided the results into three different radar plots, containing fragment-based derivatives (**Figure 2.10**), TBAP derivatives (**Figure 2.11**), and TPAP derivatives (**Figure 2.12**). The plot of A/B fragments (**Figure 2.10**) shows selectivity for **8** (orange), **9a** (green), and **21a** (gray) for PARP1/2 versus all other PARP isoforms. Interestingly, the benzo-oxazepine **8** displays selectivity for PARP2 versus PARP1, while the analogous benzodiazepine **9a** and pyridodiazepine **21a** exhibit weak, if any, PARP1 vs. PARP2 selectivity (**Figure 2.10**). $IC_{50}$ value determination of the benzo-oxazepine **8** revealed approximately 6-fold selectivity for PARP2 versus PARP1 (PARP2 $IC_{50}$ = 1.5 μM, PARP1 $IC_{50}$ = 8.7 μM). The TBAP derivatives generally demonstrate low activity over all 13 PARP isoforms (**Figure 2.11**); however, the benzyl **9f** (yellow) shows 100% inhibition of PARP2 and approximately 90% inhibition of PARP1. Albeit we anticipated the near 100% PARP1 inhibition, the complete inhibition of PARP2 is appealing for future

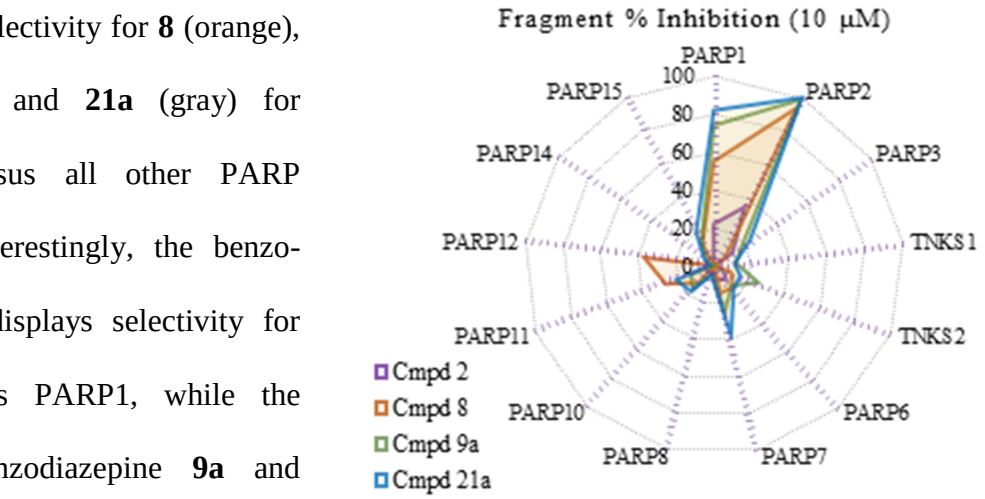



**Figure 2.10. Percent inhibition of the fragment-based derivatives from a single point assay for 13 PARP isoforms at 10 μM.** Compound **8**, **9a**, and **21a** demonstrate selectivity for PARP1/2 over all the PARP isoforms, with a slight preference in selectivity for PARP2.

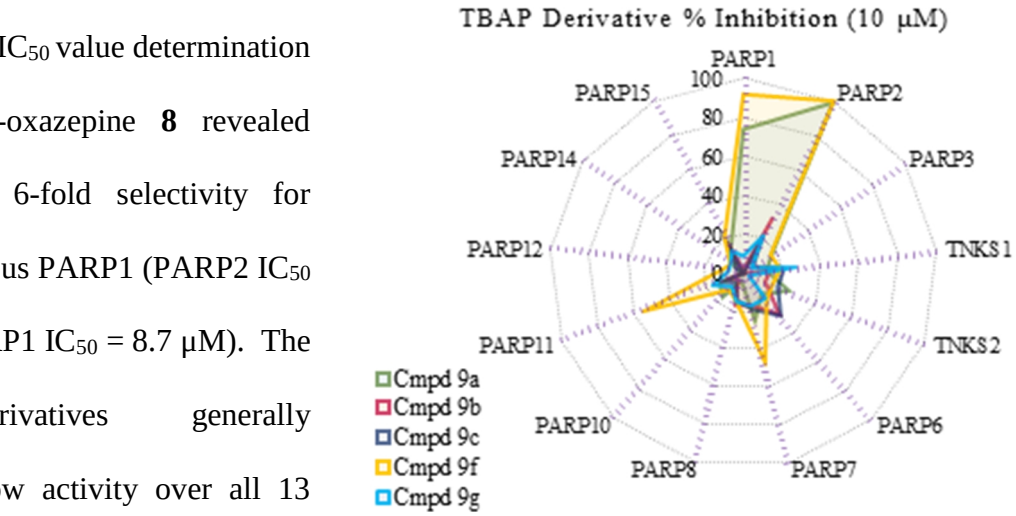



**Figure 2.11. Percent inhibition of the TBAP derivatives from a single point assay for 13 PARP isoforms at 10 μM.** Compound **9a** is included for comparison. **9f** demonstrates selectivity for PARP1/2 over all the PARP isoforms, modest activity for PARP11 and some activity for PARP7.

investigation. In addition to satisfactory PARP2 activity, **9f** is also modestly active on PARP11 (approximately 50% inhibition at 10 μM). The benzyl TPAP **21e** (purple, **Figure 2.12**) displayed 100% inhibition for PARP1 and PARP2, greater than 50% inhibition for PARP11, and modest inhibition for PARP7. Further investigation of the benzyl TPAP **21e** revealed inhibitory concentrations for PARP1, PARP2, and PARP11 (178 nM, 15.0 nM and 3.1μM, respectively). The benzyl TPAP **21e** demonstrated approximately 12-fold selectivity for PARP2 versus PARP1, which is comparable to the most potent and selective PARP2 inhibitor reported in the literature ($IC_{50}$ = 8 nM, 13-fold selectivity).[6] To the best of our knowledge, **9f** and **21e** are the only known PARP11 inhibitors. PARP11 function remains largely unexplored; hence, the benzyl TAAP derivatives could serve as a starting lead for further SAR studies and the development of selective PARP11 biological probes. Notably, the pyrido analog shows better inhibition for PARP1 and PARP11 than the benzyl benzodiazepine **9f**.

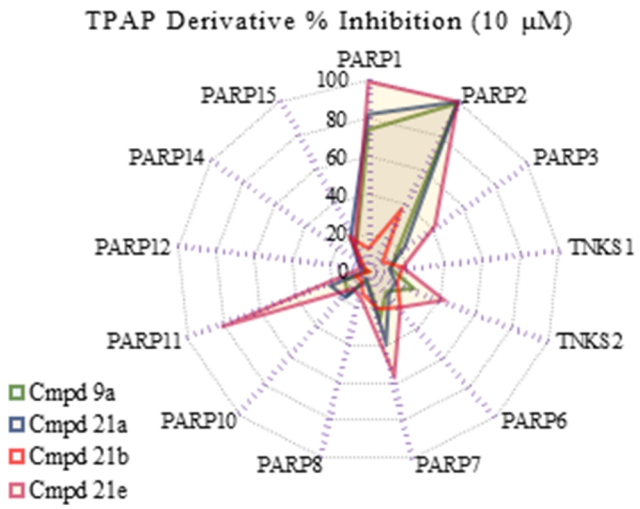



**Figure 2.12. Percent inhibition of the TBAP derivatives from a single point assay for 13 PARP isoforms at 10 μM.** Compound **9a** is included for comparison. **21e** demonstrates selectivity for PARP1/2/11 over all the PARP isoforms and modest activity for PARP7.

Albeit the active TAAP derivatives must contain some degree of planarity, the slight flexibility in the diazepine **B** ring might lead to PARP1/2 selectivity. The non-selective PARP inhibitors usually contain rigid, planar moieties, while the selective PARP inhibitors contain a flexible moiety. It is important to reiterate that the active TAAP derivatives must be planar to a degree since the PARP1 sub-pocket, where the A/B ring docks, is intolerable to significant deviations from planarity. Although we cannot make decisive conclusions about the rigidity of other PARPs

based on this preliminary study, the general TAAP selectivity for PARP1/2 is promising, and the discovery of a potential PARP11 inhibitor is encouraging.

2.5 TAAP Atropisomerism

The loss of PARP1 activity shown by the majority of the TAAP analogues encouraged the investigation of the TAAP geometry. Geometry optimizations (B3LYP/6-31G(d)) of the derivatized TBAP and TPAP analogues revealed that acylations and sulfonylations introduced a site of steric strain that subsequently caused significant distortion to the diazepine **B** ring (**Section 2.3**). In addition to the diazepine distortion, geometry optimizations also revealed that the amide TBAP and TPAP derivatives contain a chiral axis and *cis/trans*-rotamers: a chiral axis with respect to the 10C-1N bond ($A_1$, blue) and *cis/trans*-rotamers with respect to the 1N amide bond (**Figure 2.13A**). We based the *cis/trans*-rotamer assignments on priority of the substituents, thus we gave the 1N amide carbonyl higher priority than the 1N amide R group and the aryl **A** ring higher priority than the diazepine **B** ring. Thus, the *cis*-rotamer is assigned when the 1N amide carbonyl is on the same side as the aryl **A** ring, and the *trans*-rotamer is assigned when the 1N amide carbonyl is *anti* to the aryl **A** ring. Geometry optimizations of both sets of

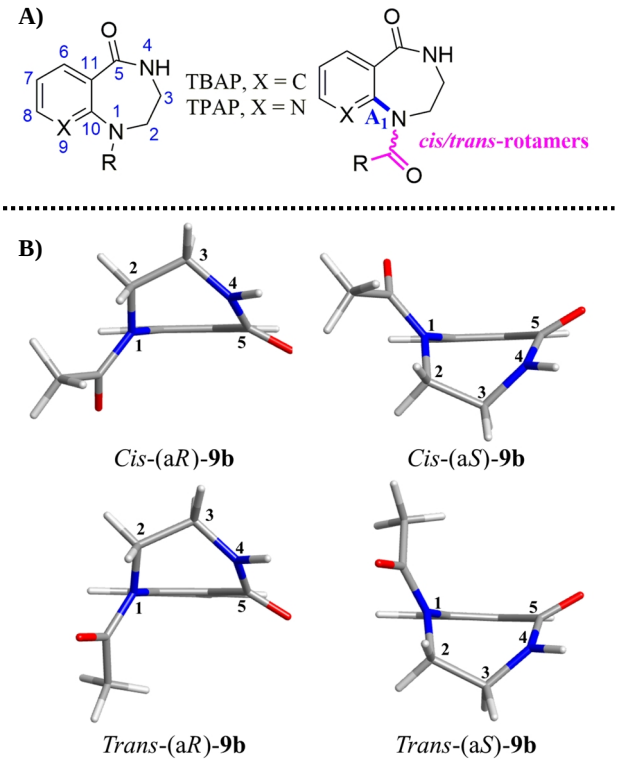



**Figure 2.13. The atropisomers of the amide TBAP and TPAP derivatives.** A) The chiral axis is highlighted in blue ($A_1$) and the *cis/trans*-rotamers in purple. B) TBAP **9b** used as an example to demonstrate the two sets of enantiomers obtained from geometry optimizations (B3LYP/6-31G(d)) using Cresset Torch.

enantiomers revealed that the *trans*-isomer is more stable than the *cis*-isomer by approximately 3-8 kcal/mol (**Figure 2.13B**).

The sulfonamide TBAP derivatives also display axial chirality with respect to the $A_1$ axis, but lack the *cis/trans*-rotamers observed with the amide TBAP and TPAP derivatives. Natsugari et al. studied *N*-benzoyl and *N*-sulfonyl-1,5-benzodiazepines for their atropisomeric and conformational properties. They could separate the (a*R*)- and (a*S*)-atropisomers, which revealed that the *N*-benzoyl and *N*-sulfonyl congeners had different conformational preferences. They describe these two conformations as "folded" (the substituent resides above or below the diazepine ring) and as "extended" (the substituent is *anti* to the diazepine ring).[8] Similarly to Natsugari's *N*-sulfonyl-1,5-benzodiazepines, the phenyl sulfonamide **9i** exclusively displays a folded conformation in the X-ray crystal structure. The X-ray crystal structure shown in **Figure 2.7** displays only one folded atropisomer (a*R*), but the crystal unit cell confirms the presence of both atropisomers (**Figure 2.14**). Although the crystal structure only provides evidence of the folded conformation, this does not necessarily preclude the existence of the extended conformation, but rather implies the folded conformation was selectively crystallized. Any further conclusions on the topic would merely be speculative given the small body of evidence currently available.

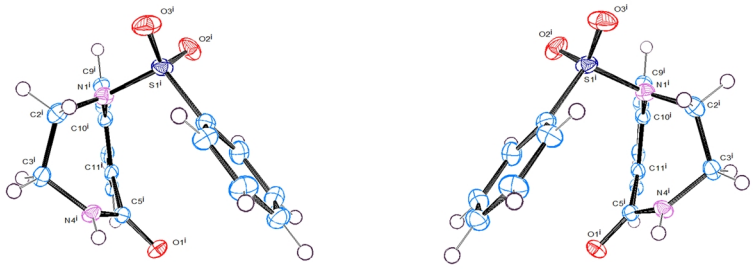


**Figure 2.14. X-ray crystal structure of the phenyl sulfonamide 9i as a racemate extracted from the CIF file.**

In addition to the geometry optimizations, $^1$H-NMR integrations also indicate the presence of atropisomers. The $^1$H-NMR spectra show broad diastereotopic signals for the amide TBAP and the **21c** TPAP methylene hydrogens, which is indicative of both an isomeric mixture and of slow

interconversion between isomers with respect to the NMR time scale. Dynamic NMR experiments resolved the diastereotopic signals, tracked the coalescence of the diastereotopic peaks, and provided the means to estimate the activation free-energy barrier to enantiomerization ($\Delta G^{\ddagger}$). Estimated from dynamic NMR, the coalescence temperature ($T_c$) in Kelvin and the difference in diastereotopic chemical shifts in Hertz ($\nu_{AB}$) give $\Delta G^{\ddagger}$ from $\Delta G^{\ddagger} = RT_c\left[23.76 + \ln\left(\frac{T_c}{k_c}\right)\right]$ where $k_c$ is the rate constant in Hertz $k_c = \left(\frac{\pi}{\sqrt{2}}\right)\nu_{AB}$.[9] Although several other $^1$H-NMR spectra indicate the presence of atropisomers, we performed dynamic NMR experiments on the benzoyl TBAP **9e**, the

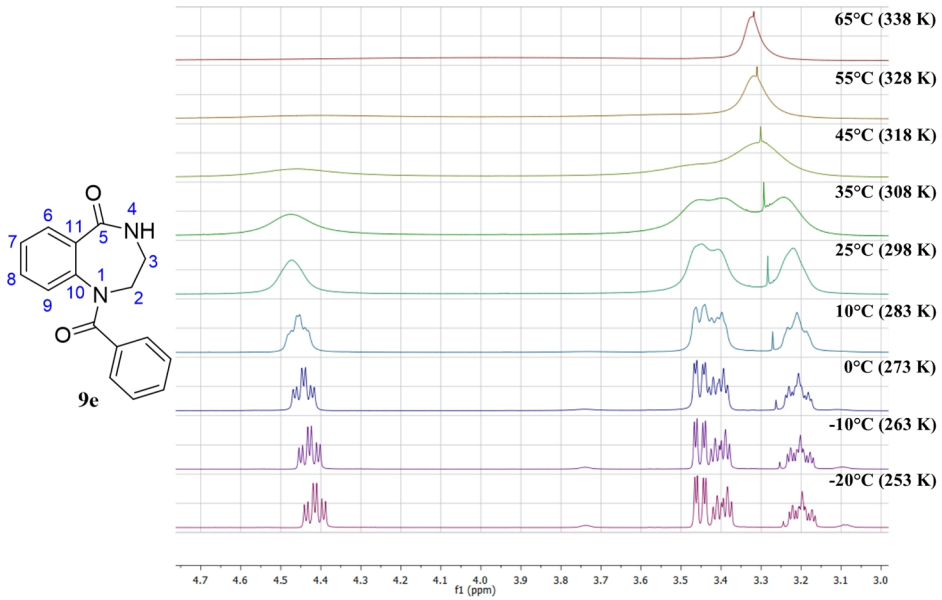



**Figure 2.15. Dynamic NMR spectra of 9e from −20°C (253 K)—65°C (338 K).** The maximum resolution of the diastereotopic peaks occurs at approximately −10°C (263 K). The coalescence of the 3C methylene hydrogens occurred at approximately 65°C (338 K), and coalescence of the 2C methylene hydrogens occurred at approximately 45°C (318 K). Solvent: $CD_3CN$

benzoyl TPAP **21d**, and the phenyl sulfonamide **9i** to assess the $\Delta G^{\ddagger}$ associated with the presence or the absence of the 9C-9H bond (TBAP and TPAP, respectively) and to assess the $\Delta G^{\ddagger}$ differences between the amide and the sulfonamide TBAP derivatives.

At room temperature, the benzoyl TBAP **9e** shows four broad signals for the 2C and 3C methylene hydrogens. Resolution of the diastereotopic peaks occurred at approximately −10°C (263 K), and the observed coalescence temperature occurred at approximately 65°C (338 K) for

the 3C methylene hydrogens and 45°C (318 K) for the 2C methylene hydrogens, estimating the $\Delta G^{\ddagger}$ at 63 kJ/mol (**Figure 2.15**).

The room temperature NMR for the benzoyl TPAP **21d** displays one broad signal that integrates to two protons (2C) and one quartet that integrates to two protons (3C). We collected

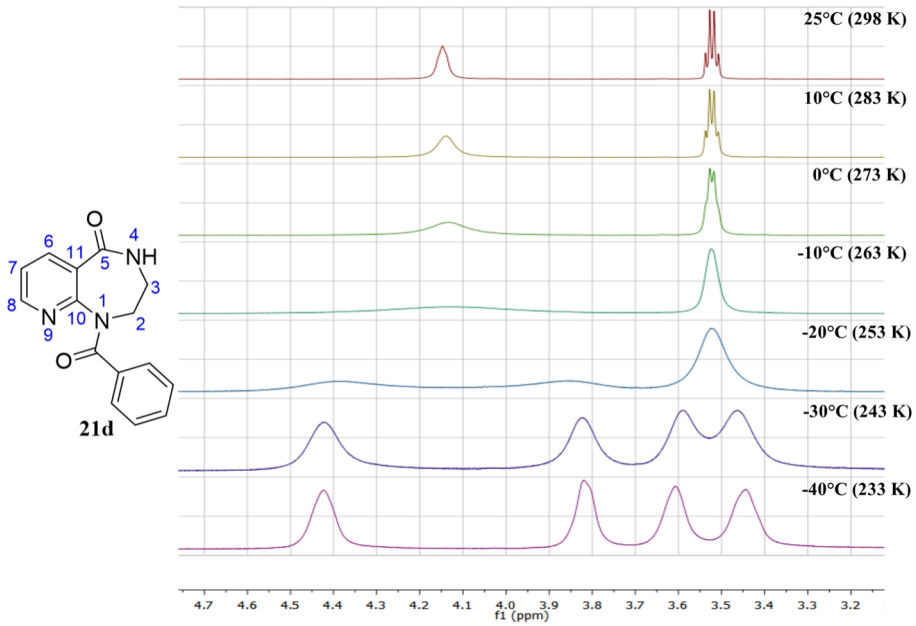



**Figure 2.16. Dynamic NMR spectra of 21d from −40°C (233 K)—25°C (298 K).** The diastereotopic peak resolution starts to occur at −40°C (233 K). The coalescence of the 3C methylene hydrogens occurred at approximately −10°C (263 K), and coalescence of the 2C methylene hydrogens occurred at approximately −20°C (253 K). Solvent: 1,1,2,2-tetrachloroethane-$d_2$

dynamic NMR spectra from room temperature to −40°C (233 K) (**Figure 2.16**). Coalescence of the 3C and 2C methylene hydrogens occurred at −10°C and −20˚C, respectively, but the diastereotopic protons were not completely resolved at the lower limit of −40˚C. Although complete resolution of the diastereotopic protons would require temperatures below −40°C, we estimated the $\Delta G^{\ddagger}$ at 50 kJ/mol. The larger $\Delta G^{\ddagger}$ observed with **9e** (63 kJ/mol) compared to **21d** (50 kJ/mol) is consistent with the hypothesis that the 9C-9H bond is a source of steric hindrance. Replacing the rigid 9C-9H bond with a more malleable lone pair reduces the $\Delta G^{\ddagger}$ such that complete resolution of the diastereotopic protons would require temperatures lower than −40°C.

Interestingly the phenyl sulfonamide **9i** shows a defined triplet and quartet for the 2C and 3C methylene hydrogens at room temperature (**Figure 2.17**). The well-defined triplet and quartet are indicative of rapid isomer interconversion at room temperature. Upon cooling to −40°C, the 3C methylene hydrogens broaden from the quartet to the coalescence peak and the 2C methylene

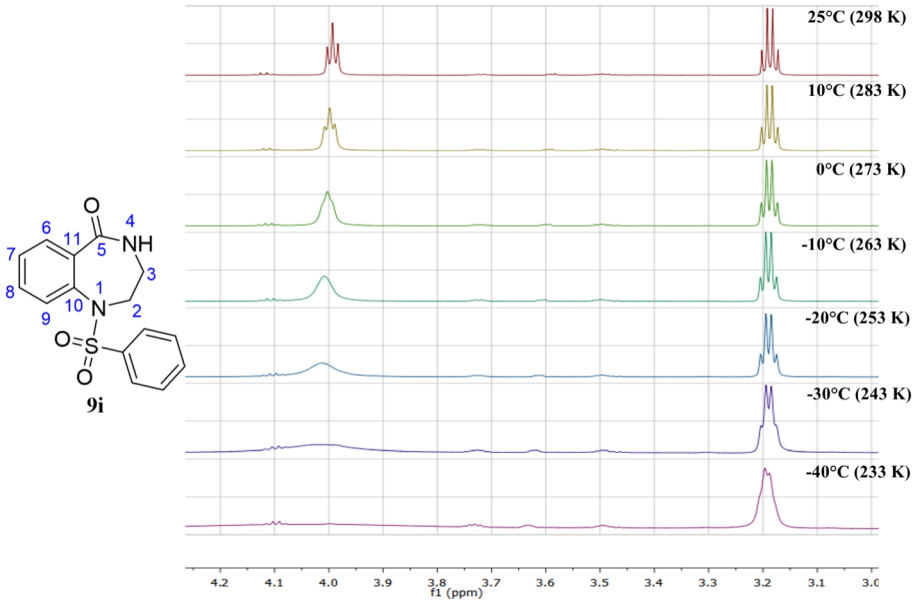



**Figure 2.17. Dynamic NMR spectra of 9i from −40°C (233 K)—25°C (298 K).** The visualization of the 2C coalescence occurs approximately at −40°C (233 K), and the coalescence for the 3C methylene hydrogens starts at −40°C (233 K). Lower temperatures are necessary in order to visual the diastereotopic peaks. Solvent: acetone-$d_6$

hydrogens begin to resolve. We were unable to approximate the $\Delta G^{\ddagger}$ since we could not resolve the **9i** diastereotopic protons.

In all three cases, the dynamic NMR studies show that the 2C methylene hydrogens coalesce at a different temperature than the 3C methylene hydrogens (**Table 2.5**), suggesting that the 2C methylene carbon rotates slower than the 3C methylene carbon. This seems trivial since the 2C methylene carbon is closer in proximity to the newly synthesized 1N amide

| Compound | -$CH_2$-[a] | $T_c$ (K) | $\nu_{AB}$ (Hertz) | $\Delta G^{\ddagger}$ (kJ/mol) |
|---|---|---|---|---|
| **9e** | 2 | 318 | 527.8 | 63 |
| **9e** | 3 | 338 | 119.6 | |
| **21d** | 2 | 253 | 361.9 | 50 |
| **21d** | 3 | 263 | 97.97 | |
| **9i** | 2 | ND | ND | - |
| **9i** | 3 | ND | ND | |

**Table 2.5. Summary of dynamic NMR experiments.** [a]Indicates the 2C methylene hydrogens and the 3C methylene hydrogens. ND: unable to determine accurately the coalescence temperature and the difference in chemical shift of the diastereotopic protons.

bond, but this also provides insight to the lactam flexibility. The large $\Delta G^{\ddagger}$ for **9e** is not surprising due to the inherent rigidity of the overall molecule and bulkiness of the benzoyl group. The anticipated $\Delta G^{\ddagger}$ decrease for the TPAP **21d** supports the notion that the pyridyl N lone pairs relieve some steric strain on the diazepine ring by decreasing steric interactions between the **A** and **C** rings. Unexpectedly, the phenyl sulfonamide interconverts so rapidly that visualization of one isomer on a NMR time scale at −40°C proved unachievable. The sulfonamide **9i** room temperature NMR suggested a lower $\Delta G^{\ddagger}$, relative to **9e** and **21d**. Although the sulfonamide folded conformation would suggest a $\Delta G^{\ddagger}$ similar to the amide derivatives and be observable on NMR time scale, it appears that the rigid amide (due to greater orbital overlap in the O-C-N bonds) poses higher steric constraints, while the sulfonamide S-N bond is more flexible allowing rapid atropisomerization.

In addition to the *N*-benzoyl and *N*-sulfonyl-1,5-bezodiazepines, Natsugari et al. has also researched the atropisomeric properties of various other benzodiazepines and their utility in biological systems. They were able to demonstrate an eutomer preference for the $GABA_A$ receptor with pyrimido[1,2-α][1,4]benzodiazepines[10] and an isomeric preference for the vaptan class of vasopressin receptors.[11] In addition, Chobanian et al. synthesized various potent, selective benzodiazepine sulfonamide bombesin receptor subtype 3 (BRS-3) agonists where they were able to modify the lead compound to stabilize the desired atropisomer, avoid isomeric interconversions, and maintain, or improve, the potency.[12] Natsugari routinely reiterates the biological importance of atropisomers and advocates further investigations of atropisomerism as many researchers overlook the latent chirality.[11] Hence, further geometric analysis of the TAAP scaffold will guide the design of future analogues to optimize their PARP1 activity (**Section 2.7**).

2.6 Dual inhibition with CDKs

The design of the TAAP scaffold encompassed key binding moieties for the inhibition of both PARP1 and CDK1. An important TAAP structural feature is overall molecular planarity, which is necessary for PARP1 and CDK1 binding. As demonstrated in **Section 2.3**, the derivatization of the **A**/**B** TAAP core via acylation and sulfonylation yields distorted, non-planar diazepine **B** rings. This **B** ring distortion likely is the source of diminished PARP1 activity, and likely for CDK1 inhibition as well. Thus, we screened all the TAAP analogues against a CMGC kinase panel of CDK1/CyclinA2, CDK2/CyclinE1, CDK3/CyclinE1, CDK5/p25, CDK5/p35, CDK6/CyclinD3, CDK9/CyclinK, and CLK3, in a single point assay at a 10 μM concentration. The preliminary results suggest that the TAAP analogous and fragments are not potent kinase inhibitors, and in some cases, the analogues showed agonistic activity. Further validation of the preliminary results is necessary to make any reliable conclusions.

2.7 Summary

The TBAP **9a** and TPAP **21a** display modest PARP1 activity in the μM range. Derivatization via acylation and sulfonylation diminished PARP1 activity, but derivatization via alkylation (**9f** and **21e**) retained or improved the PARP1 activity. Alkylating the TBAP **9a** and the TPAP **21a** with smaller, more flexible **C** rings will hopefully maintain overall planarity and increase the potency. A single-point assay revealed that the TAAP scaffold shows some selectivity for PARP1/2. Although most of the TAAP derivatives did not display optimal geometry for PARP1 inhibition, the phenyl sulfonamide **9i** X-ray crystal structure unveiled a peculiar folded conformation. Dynamic NMR studies allowed the comparison of the $\Delta G^{\ddagger}$ of the benzoyl **9e**, benzoyl **21d**, and the phenyl sulfonamide **9i** atropisomers, where **9i** displayed the lowest $\Delta G^{\ddagger}$ despite the large distance and the several intermediary “folded” and “unfolded” conformations the phenyl ring would need to acquire in order to interconvert atropisomers.

Future work analyzing the factors that influence TAAP atropisomer interconversions could provide useful insight to a potential PARP isoform atropisomer preference and provide clues to the overarching factors that govern the **A**/**B** ring planarity. In this context, computational modeling of the *cis/trans* isomerization could provide insight to the conformational preference, or lack of conformational preference, of the amide TAAP derivatives. Variable temperature NOESY experiments could verify the modeled conformations and conformational preferences. Furthermore, dynamic NMR studies of TAAP derivatives could help guide the future modifications necessary to obtain the desired geometry. Lastly, X-ray crystal structures of the previously synthesized TAAP derivatives would confirm the geometrical observations determined by computational modeling and dynamic NMR experiments.

2.8 Experimental

**Synthesis of Compound 2**

A standard literature procedure was followed.[1] Polyphosphoric acid (1.83 g) was added to a pre-dried flask and was heated to 120°C under vacuum. The mixture was evacuated and purged three times with nitrogen gas. After the third purge, phosphorous pentoxide (0.213 g, 1.50 mmol) was added to the polyphosphoric acid. Once all of the phosphorous pentoxide had dissolved, 3-(1H-pyrrole-2-carboxamido)propanoic acid (91 mg, 0.50 mmol) was added, and the reaction was stirred overnight at 120°C. The reaction was quenched with ice and then extracted with dichloromethane (5 x 20 mL). The organic layer was then dried over magnesium sulfate and evaporated under reduced pressure. The residue was recrystallized in methanol, yielding a white solid (16%). **6,7-dihydropyrrolo[2,3-c]azepine-4,8(1H,5H)-dione (2)**, $C_8H_8N_2O_2$, $^1$H NMR (400 MHz, DMSO-$d_6$) δ 12.15 (s, 1H), 8.31 (t, *J* = 5.2 Hz, 1H), 6.98 (t, *J* = 2.7 Hz, 1H), 6.55 (t, *J* = 2.6 Hz, 1H), 3.39 – 3.34 (m, 2H), 2.72 – 2.67 (m, 2H); $^{13}$C NMR (101 MHz, DMSO-$d_6$) δ 194.3, 162.2, 127.9, 123.6, 122.4, 109.5, 43.5, 36.6; mp 277–278°C; HRMS (ESI) *m/z* calcd for $(M+K)^+$ 203.0217, found 203.0204.

**Synthesis of Compound 5 & 7**

A standard literature procedure was followed.[2] The appropriate tetralone was added to pre-chilled concentrated hydrochloric acid. In small portions, sodium azide (2.0 eq) was added to the mixture, and the slurry was stirred overnight. Solid potassium carbonate was added to the reaction mixture until the mixture reached a basic pH. The basic solution was then extracted with dichloromethane (3 x). The organic layer was then dried over magnesium sulfate and evaporated under reduced pressure. The residue was purified by flash chromatography on silica gel (2:3 hexanes:ethyl acetate). **8-Fluoro-2,3,4,5-tetrahydro-1H-benzo[c]azepin-1-one (5)**, $C_{10}H_{10}FNO$,

white solid, 56% yield; $^{1}$H NMR (400 MHz, $CDCl_3$) δ 7.41 (dd, *J* = 8.9, 2.7 Hz, 1H), 7.21 – 7.00 (m, 3H), 3.13 (q, *J* = 6.5 Hz, 2H), 2.83 (t, *J* = 7.1 Hz, 2H), 2.02 (p, *J* = 6.8 Hz, 2H); $^{13}$C NMR (101 MHz, $CDCl_3$) δ 172.9 (d, $^{4}J_{CF}$ = 2.3 Hz), 161.9 (d, $^{1}J_{CF}$ = 245.7 Hz), 136.9 (d, $^{3}J_{CF}$ = 7.1 Hz), 134.2 (d, $^{4}J_{CF}$ = 3.4 Hz), 130.5 (d, $^{3}J_{CF}$ = 7.5 Hz), 118.1 (d, $^{2}J_{CF}$ = 21.3 Hz), 115.8 (d, $^{2}J_{CF}$ = 23.1 Hz), 39.6, 30.5, 29.7; mp 166–167°C; HRMS (ESI) *m/z* calcd for $(M+H)^+$ 180.0825, found 180.0817; **2,3,4,5-Tetrahydro-1H-benzo[c]azepin-1-one (7)**, $C_{10}H_{11}NO$, white solid, 42% yield; $^{1}$H NMR (400 MHz, $CDCl_3$) δ 7.70 (dd, *J* = 7.4, 1.6 Hz, 1H), 7.45 – 7.23 (m, 3H), 7.18 (ddd, *J* = 7.4, 1.4, 0.6 Hz, 1H), 3.12 (q, *J* = 6.5 Hz, 2H), 2.86 (t, *J* = 7.1 Hz, 2H), 2.01 (p, *J* = 6.8 Hz, 2H); $^{13}$C NMR (101 MHz, $CDCl_3$) δ 174.3, 138.5, 135.1, 131.3, 128.8, 128.7, 127.1, 39.7, 30.7, 30.4; mp 101.0–101.4°C; HRMS (ESI) *m/z* calcd for $(M+H)^+$ 162.0913, found 162.0910.

**Synthesis of Compound 6**

A standard literature procedure was followed.[3] 2,3,4,5-tetrahydro-1*H*-benzo[*c*]azepin-1-one (compound **7**) (81 mg, 0.50 mmol) was dissolved in acetone (3 mL) and cooled to −78°C with a dry ice/acetone bath. Once cooled, potassium permanganate (0.80 g, 5.0 mmol) was added to the reaction mixture followed by iron (III) chloride hexahydrate (0.81 g, 3.0 mmol). The reaction was stirred for two hours at −78°C then slowly warmed to room temperature. Once room temperature was reached, the reaction was stirred for an additional hour. Following completion, the reaction mixture was filtered over a pad of celite and rinsed generously with dichloromethane. The resulting dichloromethane solution was extracted with water (2 x 20 mL). The organic layer was then dried over magnesium sulfate and evaporated under reduced pressure. The residue was purified by flash chromatography on silica gel (1:1 hexanes:ethyl acetate) resulting in a white solid (15% yield). This reaction has been scaled to 10 mmol (5% yield). **3,4-dihydro-1H-benzo[c]azepine-1,5(2H)-dione (6)**, $C_{10}H_9NO_2$, $^{1}$H NMR (400 MHz, $CDCl_3$) δ 7.96 (ddd, *J* = 7.7, 1.5, 0.05 Hz, 1H), 7.80-

7.58 (m, 3H), 6.96 (br, 1H), 3.65-3.51 (m, 2H), 3.07-2.96 (m, 2H); $^{13}$C NMR (101 MHz, $CDCl_3$) δ 202.3, 171.4, 136.3, 133.0, 132.3, 132.2, 130.4, 128.7, 46.3, 37.6; mp 144–145°C; HRMS (ESI) *m/z* calcd for $(M+H)^+$ calcd 176.0712, found 176.9122.

**Synthesis of Compound 8 and 9a**

Chroman-4-one or 2,3-dihydroxyquinolin-4(1*H*)-one was dissolved in concentrated sulfuric acid (1 M) at 0°C. The sodium azide (2.0 eq) was added slowly to the reaction mixture at 0°C. Upon addition of the azide, gas evolution begins, and the reaction is complete when the gas evolution has stopped (approximately four hours). After the addition of the azide, the reaction is slowly warmed to room temperature. Upon reaction completion, the reaction mixture is diluted with water at 0°C and quenched with solid potassium bicarbonate until a basic pH is reached. The basic solution is then extracted with ethyl acetate (3 x). The organic layer was then dried over magnesium sulfate and evaporated under reduced pressure. The residue was purified by flash chromatography on silica gel (100% ethyl acetate). **3,4-dihydrobenzo[*f*][1,4]oxazepin-5(2*H*)-one (8)**, $C_9H_9NO_2$, white solid, 60% yield, $^1$H NMR (400 MHz, $CDCl_3$) δ 8.32 (s, 1H), 7.93 (ddd, *J* = 7.9, 1.8, 0.4 Hz, 1H), 7.41 (ddd, *J* = 8.2, 7.2, 1.8 Hz, 1H), 7.11 (ddd, *J* = 7.9, 7.2, 1.2 Hz, 1H), 7.01 (ddd, *J* = 8.2, 1.2, 0.4 Hz, 1H), 4.37 (t, *J* = 4.8 Hz, 2H), 3.48 (q, *J* = 4.8 Hz, 2H); $^{13}$C NMR (101 MHz, $CDCl_3$) δ 171.2, 155.4, 133.4, 131.7, 124.1, 122.9, 121.4, 73.4, 41.4; mp 118–120°C; HRMS (ESI) *m/z* calcd for $(M+H)^+$ calcd 164.0706, found 164.0703;

**1,2,3,4-tetrahydro-5*H*-benzo[e][1,4]diazepine-5-one (9a)**, $C_9H_{10}N_2O$, white solid, 62% (1.0 mmol), 49% (6.8 mmol) $^1$H NMR (400 MHz, $CDCl_3$) δ 7.97 (ddd, *J* = 8.0, 1.7, 0.4 Hz, 1H), 7.23 (ddd, *J* = 8.2, 7.0, 1.7 Hz, 1H), 6.95 (s, 1H), 6.78 (ddd, *J* = 8.1, 7.0, 1.1 Hz, 1H), 6.59 (dd, *J* = 8.2, 1.1 Hz, 1H), 3.60 – 3.56 (m, 2H), 3.53 – 3.47 (m, 2H); $^{13}$C NMR (101 MHz, $CDCl_3$) δ 172.1,

146.1, 133.2, 132.8, 118.4, 117.9, 117.7, 49.1, 42.1; mp 152–153°C; HRMS (ESI) *m/z* calcd for $(M+H)^+$ 163.0866, found 163.0860.

**Synthesis of Compound 9b**

Compound **9a** (0.047 g, 0.29 mmol) was dissolved in dichloromethane (3.0 mL) and pyridine (0.3 mL), and then cooled to 0°C. The acetyl chloride (20.7 µL, 0.29 mmol) was diluted in dichloromethane (2.0 mL) and added dropwise to the reaction mixture at 0°C. The reaction mixture was slowly warmed to room temperature and stirred for 2.5 hours. Upon completion, the reaction was extracted with 10% HCl (aqueous), water, and saturated sodium chloride. The organic layer was dried over magnesium sulfate and filtered. The remaining solution was evaporated under reduced pressure and purified by recrystallization (50:50 ethyl acetate:acetonitrile) to yield a white solid (34% yield). **1-acetyl-1,2,3,4-tetrahydro-5H-benzo[e][1,4]diazepin-5-one**, $C_{11}H_{12}N_2O_2$, $^1$H NMR (600 MHz, 1,1,2,2-tetrachloroethane-$d_2$) δ 7.77 (dd, *J* = 7.6, 1.6 Hz, 1H), 7.59 (td, *J* = 7.7, 1.7 Hz, 1H), 7.53 (td, *J* = 7.6, 1.2 Hz, 1H), 7.21 (dd, *J* = 7.8, 1.2 Hz, 1H), 4.76 (td, *J* = 13.9, 13.0, 5.6 Hz, 1H), 3.42 – 3.14 (m, 3H), 1.82 (s, 3H); $^{13}$C NMR (126 MHz, DMSO-$d_6$) δ 206.5, 169.7, 137.6, 133.8, 131. 9, 129.1, 129.0, 128.7, 49.1, 38.2, 30.7; mp 158–159°C; HRMS (ESI) *m/z* calcd for $(M+Na)^+$ 227.0791, found 227.0772.

**Synthesis of Compound 9(c-e) & 21(b-d)**

The respective aryldiazepine, **9a** or 2**1a**, (0.2–0.3 mmol) was dissolved in dichloromethane (10 mg/mL). The corresponding acyl chloride (1.0 eq) and diisopropylethylamine (2.0 eq) were added to the reaction mixture. The reaction was stirred at room temperature overnight. The reaction was diluted with dichloromethane and extracted with water (2x) followed by saturated sodium chloride (1x). The remaining organic layer was then dried over magnesium sulfate and filtered. The residue was purified by flash chromatography on silica gel (100% ethyl acetate). **1-(Furan-2-carbonyl)-**

**1,2,3,4-tetrahydro-5H-benzo[e][1,4]diazepin-5-one (9c)**, $C_{14}H_{12}N_2O_3$, white solid, 53% yield, $^1$H NMR (500 MHz, $CDCl_3$) δ 7.85 (dd, *J* = 7.6, 1.6 Hz, 1H), 7.49 (td, *J* = 7.7, 1.2 Hz, 1H), 7.42 (td, *J* = 7.7, 1.7 Hz, 1H), 7.05 (d, *J* = 7.8 Hz, 1H), 6.64 (s, 1H), 6.19 (dd, *J* = 3.5, 1.7 Hz, 1H), 5.99 (d, *J* = 3.5 Hz, 1H), 4.66 (s, 1H), 3.54–3.35 (m, 3H); $^{13}$C NMR (126 MHz, $CDCl_3$) δ 171.2, 160.7, 146.7, 144.9, 138.2, 133.0, 132.4, 130.0, 129.0, 117.0, 111.3, 51.3, 39.3; mp 246–247°C; HRMS (ESI) *m/z* calcd for $(M+H)^+$ 257.0921, found 257.0906;

**1-(Thiophene-2-carbonyl)-1,2,3,4-tetrahydro-5H-benzo[e][1,4]diazepin-5-one (9d)**, $C_{14}H_{12}N_2O_2S$, white solid, 35% yield, $^1$H NMR (500 MHz, $CDCl_3$) δ 7.86 (dd, *J* = 7.7, 1.6 Hz, 1H), 7.50 (td, *J* = 7.6, 1.2 Hz, 1H), 7.41 (td, *J* = 7.7, 1.6 Hz, 1H), 7.31 (dd, *J* = 5.0, 1.1 Hz, 1H), 7.07 (dd, *J* = 7.9, 1.1 Hz, 1H), 6.75 (dd, *J* = 4.9, 3.8 Hz, 1H), 6.64 (dd, *J* = 3.8, 1.1 Hz, 1H), 6.40 (s, 1H), 4.67 (s, 1H), 3.56 (s, 1H), 3.43 (s, 2H); $^{13}$C NMR (126 MHz, $CDCl_3$) δ 171.0, 164.3, 138.4, 137.6, 133.2, 132.6, 132.2, 131.0, 130.1, 129.8, 129.3, 127.1, 51.7, 39.5; mp 147–148°C; HRMS (ESI) *m/z* calcd for 2M*+ 544.1233, found 544.1187;

**1-Benzoyl-1,2,3,4-tetrahydro-5H-benzo[e][1,4]diazepin-5-one (9e)**, $C_{16}H_{14}N_2O_2$, white solid, 71% yield, $^1$H NMR (500 MHz, $CD_3CN$) δ 7.62 (dd, *J* = 7.6, 1.6 Hz, 1H), 7.37 – 7.04 (m, 7H), 6.89 – 6.80 (m, 2H), 4.47 (s, 1H), 3.58 – 3.08 (m, 3H); $^{13}$C NMR (126 MHz, $CD_3CN$) δ 172.0, 171.4, 139.5, 137.3, 134.6, 132.3, 130.6, 130.5, 123.0, 129.0, 129.9, 128.8, 52.0, 39.5; mp 145-146°C; HRMS (ESI) *m/z* calcd for $(M+H)^+$ 267.1128, found 267.1124;

**1-Acetyl-1,2,3,4-tetrahydro-5H-pyrido[2,3-e][1,4]diazepin-5-one (21b)**, $C_{10}H_{11}N_3O_2$, white solid, 8% yield, $^1$H NMR (500 MHz, $CDCl_3$) δ 8.27 (dd, *J* = 4.6, 1.9 Hz, 1H), 8.18 (ddd, *J* = 7.8, 1.9, 0.6 Hz, 1H), 6.79 (dd, *J* = 7.9, 4.6 Hz, 1H), 5.30 (s, 1H), 4.20 – 4.08 (m, 2H), 3.67 – 3.58 (m, 2H), 2.62 (s, 3H); $^{13}$C NMR (126 MHz, $CDCl_3$) δ 172.2, 169.9, 155.6, 153.9, 142.6, 114.7, 113.6, 46.6, 39.5, 26.8; mp 220-223°C; HRMS (ESI) *m/z* calcd for $(M+H)^+$ 206.0924, found 206.0913;

**1-(Thiophene-2-carbonyl)-1,2,3,4-tetrahydro-5H-pyrido[2,3-e][1,4]diazepin-5-one (21c)**, $C_{13}H_{11}N_3O_2S$, white solid, 30% yield, $^1$H NMR (400 MHz, DMSO-$d_6$) δ 8.59 (t, *J* = 5.9 Hz, 1H), 8.45 (dd, *J* = 4.8, 1.9 Hz, 1H), 8.12 (dd, *J* = 7.6, 1.9 Hz, 1H), 7.64 (dd, *J* = 5.0, 1.2 Hz, 1H), 7.55 (dd, *J* = 7.6, 4.8 Hz, 1H), 6.87 (dd, *J* = 5.0, 3.8 Hz, 1H), 6.42 (dd, *J* = 3.8, 1.2 Hz, 1H), 3.90 (s, 2H), 3.29 (s, 2H); $^{13}$C NMR (126 MHz, DMSO-$d_6$) δ 168.3, 163.7, 151.6, 150.1, 138.9, 138.3, 131.3, 130.5, 128.5, 127.2, 124.4, 51.8, 38.0; mp 265-267°C; HRMS (ESI) *m/z* calcd for $(M+H)^+$ 274.0645, found 274.0621;

**1-Benzoyl-1,2,3,4-tetrahydro-5H-pyrido[2,3-e][1,4]diazepin-5-one (21d)**, $C_{15}H_{13}N_3O_2$, white solid, 30% yield, $^1$H NMR (500 MHz, 1,1,2,2-tetrachloroethane-$d_2$) δ 8.21 (dd, *J* = 4.9, 1.9 Hz, 1H), 8.12 (dd, *J* = 7.6, 1.9 Hz, 1H), 7.31 – 7.23 (m, 2H), 7.21 – 7.14 (m, 4H), 7.02 – 6.68 (m, 1H), 4.15 (t, *J* = 5.9 Hz, 2H), 3.52 (q, *J* = 6.0 Hz, 2H); $^{13}$C NMR (126 MHz, 1,1,2,2-tetrachloroethane-$d_2$) δ 172.0, 169.4, 151.5, 151.1, 139.0, 135.5, 130.1, 128.0, 128.0, 126.3, 122.9, 51.7, 39.0; mp 232–233°C; HRMS (ESI) *m/z* calcd for $(M+H)^+$ 268.1081, found 268.1069.

**Synthesis of Compound 9f**

1,2,3,4-tetrahydro-5H-benzo[e][1,4]diazepin-5-one, **9a**, (50 mg, 0.31 mmol) was dissolved in acetonitrile (4 mL) and stirred with potassium carbonate (86 mg, 0.62 mmol) and benzyl bromide (52 µL, 0.47 mmol) at 50°C overnight. The resulting mixture was diluted with dichloromethane and extracted with 10% HCl (aqueous), water, and saturated sodium chloride. The organic layer was dried over magnesium sulfate and filtered. The resulting solution was evaporated under reduced pressure and purified by flash chromatography on silica gel (100% ethyl acetate) yielding a colorless oil (72%). Crystallization with dichloromethane and hexanes yields white crystals (mp 141–143°C). **1-benzyl-1,2,3,4-tetrahydro-5H-benzo[e][1,4]diazepin-5-one (9f)**, $C_{16}H_{16}N_2O$, $^1$H NMR (500 MHz, DMSO-$d_6$) δ 8.16 (d, *J* = 5.7 Hz, 1H), 7.47 (dd, *J* = 7.6, 1.7 Hz, 1H), 7.35 – 7.18

(m, 6H), 6.99 – 6.87 (m, 2H), 4.37 (s, 2H), 3.18 (m, 4H); $^{13}$C NMR (126 MHz, DMSO-$d_6$) δ 171.1, 146.7, 138.3, 131.6, 129.9, 128.5, 128.4, 127.6, 126.9, 120.4, 118.8, 57.6, 55.8, 39.1; HRMS (ESI) *m/z* calcd for $(M+H)^+$ 253.1335, found 253.1331.

**Synthesis of Compound 9g & 9i**

1,2,3,4-tetrahydro-5H-benzo[e][1,4]diazepin-5-one (20 mg, 0.12 mmol) was dissolved in dichloromethane (10 mg/mL). The appropriate sulfonyl chloride (methyl sulfonyl chloride, 28µL, 0.36 mmol; benzene sulfonyl chloride, 23 µL, 0.18 mmol) and diisopropylethylamine (25 µL, 0.18 mmol) were added to the reaction mixture, and the solution was stirred at room temperature overnight. The reaction was diluted with dichloromethane (5 mL) and extracted with 10% hydrochloric acid (5 mL). The aqueous layer was extracted again with dichloromethane (5 mL). The organic layers were combined and washed with 10% hydrochloric acid (5 mL) and brine solution (5 mL). The organic layer was then dried over magnesium sulfate and filtered. The resulting solution was evaporated under reduced pressure and purified by either prep TLC (100% ethyl acetate) or recrystallization (100% dichloromethane). **1-(Methylsulfonyl)-1,2,3,4-tetrahydro-5H-benzo[e][1,4]diazepin-5-one (9g)**, $C_{10}H_{12}N_2O_3S$, light yellow solid, 2% yield, $^1$H NMR (500 MHz, DMSO-$d_6$) δ 8.37 (t, *J* = 6.1 Hz, 1H), 7.62 – 7.56 (m, 2H), 7.55 – 7.48 (m, 1H), 7.42 – 7.37 (m, 1H), 3.78 (t, *J* = 5.9 Hz, 2H), 3.11 (q, *J* = 5.9 Hz, 2H), 2.98 (s, 3H); $^{13}$C NMR (126 MHz, DMSO-$d_6$) δ 169.9, 135.1, 134.4, 131.8, 131.0, 129.3, 128.9, 52.8, 38.7, 30.7; mp 199–200°C; HRMS (ESI) *m/z* calcd for $(M+H)^+$ 241.0641, found 241.0627;

**1-(Phenylsulfonyl)-1,2,3,4-tetrahydro-5H-benzo[e][1,4]diazepin-5-one (9i)**, $C_{15}H_{14}N_2O_3S$, off-white solid, 28% yield, $^1$H NMR (500 MHz, $CDCl_3$) δ 7.73 – 7.52 (m, 6H), 7.53 – 7.38 (m, 3H), 5.88 (t, *J* = 6.2 Hz, 1H), 3.99 (t, *J* = 5.9 Hz, 2H), 3.19 (q, *J* = 6.0 Hz, 2H); $^{13}$C NMR (126

MHz, $CDCl_3$) δ 170.4, 138.9, 134.6, 133.8, 133.1, 132.6, 132.4, 130.3, 129.4, 129.3, 127.4, 53.4, 39.7; mp 249–250°C; HRMS (ESI) *m/z* calcd for $(M+H)^+$ 303.0798, found 303.0781.

**Synthesis of Compound 9h**

1,2,3,4-tetrahydro-5H-benzo[e][1,4]diazepin-5-one (7.5 mg, 0.050 mmol) was dissolved in dichloromethane (0.75 mL) and stirred with triethylamine (7.5 µL, 0.050 mmol) and 2-chloroethanesulfonyl chloride (5.2 µL, 0.050 mmol) for 15 minutes at room temperature. After the 15-minute stir period, one additional equivalent of triethylamine was added, and the reaction was left to stir overnight. The resulting mixture was extracted with 10% hydrochloric acid (10 mL) and ethyl acetate (10 mL). The aqueous layer was extracted with ethyl acetate (2 x 10 mL), and the organic layers were combined, dried over magnesium sulfate and filtered. The resulting solution was evaporated under reduced pressure and purified by prep TLC (100% ethyl acetate) yielding a white solid (12%). **1-(vinylsulfonyl)-1,2,3,4-tetrahydro-5H-benzo[e][1,4]diazepin-5-one (9h)**, $C_{11}H_{12}N_2O_3S$, $^1$H NMR (400 MHz, DMSO-$d_6$) δ 8.29 (t, *J* = 6.0 Hz, 1H), 7.61 – 7.53 (m, 2H), 7.52 – 7.46 (m, 1H), 7.40 – 7.33 (m, 1H), 6.73 (dd, *J* = 16.4, 9.9 Hz, 1H), 6.06 – 5.99 (m, 2H), 3.72 (t, *J* = 5.9 Hz, 2H), 3.09 (q, *J* = 5.9 Hz, 2H); $^{13}$C NMR (126 MHz, DMSO-$d_6$) δ 169.6, 135.1, 134.6, 134.0, 131.7, 130.8, 129.3, 128.9, 127.7, 52.7, 38.7; mp 220–222°C; HRMS (ESI) *m/z* calcd for $(M+H)^+$ 253.0641, found 253.0630.

**Synthesis of Compound 11**

Pyrrole-2-carboxylic acid (0.600 g, 5.40 mmol) was dissolved in dichloromethane (5.40 mL). N'-ethylcarbodiimide hydrochloride (1.55 g, 8.10 mmol), followed by 1-hydroxy-6-chloro-benzotriazole (1.37 g, 8.10 mmol) were added to the reaction mixture. The reaction was stirred for 15 minutes and the solution became homogenous. After the stir period, β-alanine ethyl ester hydrochloride (0.871 g, 5.67 mmol) was added, followed by 1M potassium bicarbonate (10.0 mL).

The reaction was stirred overnight. The reaction was diluted with ethyl acetate (40 mL), and extracted with 1M potassium bicarbonate (20 mL x 2), followed by 1M hydrochloric acid (20 mL). The organic layer was then dried over magnesium sulfate and evaporated under reduced pressure. The purity of the resulting residue was sufficient for the following step, resulting in a 70% yield. **Ethyl 3-(1H-pyrrole-2-carboxamido)propanoate (11)**, $^{1}$H NMR (400 MHz, DMSO-$d_6$) δ 11.42 (s, 1H), 8.09 – 8.01 (m, 1H), 6.86 – 6.79 (m, 1H), 6.72 (ddd, *J* = 3.6, 2.5, 1.5 Hz, 1H), 6.06 (ddd, *J* = 3.6, 2.7, 2.1 Hz, 1H), 4.06 (q, *J* = 7.1 Hz, 2H), 3.42 (q, *J* = 7.1 Hz, 2H), 2.53 (t, *J* = 7.0 Hz, 2H), 1.17 (t, *J* = 7.1 Hz, 3H); $^{13}$C NMR (101 MHz, DMSO-$d_6$) δ 171.4, 160.7, 126.1, 121.3, 109.9, 108.5, 59.9, 34.8, 34.2, 14.1.

**Synthesis of Compound 12**

A standard literature procedure was followed with modification for microwave assisted synthesis.[1] Ethyl 3-(1H-pyrrole-2-carboxamido)propanoate (0.500 g, 2.38 mmol) was dissolved in ethanol (12.5 mL). Subsequently, lithium hydroxide (0.170 g, 7.13 mmol) and water (.125 mL, 7.13 mmol) were added to the reaction mixture. The reaction mixture was then split into two equal volumes into two microwave tubes. Each microwave tube was subjected to microwave irradiation at 60°C for one hour. The contents of the microwave tubes were combined and the solution was acidified with 1M HCl. The acidified solution was extracted with ethyl acetate (3 x 30 mL). The organic layer was then dried over magnesium sulfate and evaporated under reduced pressure. The purity of the resulting residue was sufficient for the following step, resulting in a quantitative yield. **3-(1H-pyrrole-2-carboxamido)propanoic acid (12)**, $^{1}$H NMR (400 MHz, DMSO-$d_6$) δ 11.41 (s, 1H), 8.03 (t, *J* = 5.6 Hz, 1H), 6.83 (td, *J* = 2.6, 1.5 Hz, 1H), 6.72 (ddd, *J* = 3.8, 2.5, 1.5 Hz, 1H), 6.06 (dt, *J* = 3.6, 2.4 Hz, 1H), 3.40 (q, *J* = 7.2 Hz, 2H), 2.47 (t, *J* = 7.2 Hz, 2H); $^{13}$C NMR (101 MHz, DMSO-$d_6$ ) δ 173.0, 160.7, 126.2, 121.2, 109.9, 108.5, 34.9, 34.2.

**Synthesis of Compound 18**

A standard literature procedure was followed.[5] Aniline (0.82 mL, 9.0 mmol) and methyl acrylate (0.82 mL, 9.0 mmol) were agitated with triethylammonium acetate (TEAA) (18 mL) at 70°C overnight. The reaction was diluted with water (200 mL) and extracted with ethyl acetate (3 x 200 mL). The aqueous layer was saved, and the TEAA was recycled for future use. The organic layer was then dried over magnesium sulfate and evaporated under reduced pressure. The purity of the resulting residue was sufficient for the following step, resulting in a brown oil (87% crude yield) At a 50.0 mmol scale, this reaction yields 88%. **Methyl 3-(phenylamino)propanoate (18)**, $^{1}$H NMR (400 MHz, $CDCl_3$) δ 7.22 – 7.16 (m, 2H), 6.73 (tt, *J* = 7.3, 1.1 Hz, 1H), 6.68 – 6.59 (m, 2H), 3.71 (s, 3H), 3.46 (t, *J* = 6.4 Hz, 2H), 2.63 (t, *J* = 6.4 Hz, 2H); $^{13}$C NMR (101 MHz, $CDCl_3$) δ 173.0, 147.7, 129.5, 117.9, 113.2, 51.9, 39.6, 33.9.

**Synthesis of Compound 19**

1 M sodium hydroxide (7.000 mL) was added to methyl 3-(phenylamino)propanoate (1.2198 g, 6.807 mmol). Methanol (7 mL) was added until the solution became homogenous, and the solution was heated to 50°C overnight. The reaction mixture was quenched with a stoichiometric amount of hydrochloric acid (1 M) and extracted with ethyl acetate (3 x 200 mL). The organic layer was then dried over magnesium sulfate and evaporated under reduced pressure yielding an orange oil. The residue was purified by flash chromatography on silica gel (80:20 ethyl acetate:hexanes) resulting in an orange oil (82% yield). At a 44.2 mmol scale, this reaction yields 77%. **3-(Phenylamino)propanoic acid (19)**, $^{1}$H NMR (500 MHz, $CDCl_3$) δ 7.78 (s, 2H), 7.20 (tt, *J* = 7.4 Hz, 2H), 6.76 (t, *J* = 7.2 Hz, 1H), 6.66 (d, *J* = 7.8 Hz, 2H), 3.48 (t, *J* = 6.3 Hz, 2H), 2.68 (t, *J* = 6.3 Hz, 2H); $^{13}$C NMR (126 MHz, $CDCl_3$) δ 178.4, 147.2, 129.5, 118.5, 113.6, 39.5, 33.8.

**Synthesis of Compound 20**

Polyphosphoric acid (8 g) and 3-(phenylamino)propanoic acid (0.26 g, 1.6 mmol) were added to a pre-dried round bottom flask. The mixture was heated with a heat gun under vacuum until stirring occurred. The mixture was allowed to cool to room temperature and purged with nitrogen gas. This process was repeated two more times, and phosphorous pentoxide (0.28 g, 1.0 mmol) was subsequently added. The reaction mixture was heated to 90°C and stirred overnight. The bright orange mixture was quenched with enough ice to sufficiently decrease the viscosity such that stirring is possible at room temperature. The solution was extracted with ethyl acetate until the organic layer lost visible fluorescence. The organic layers were combined, dried over magnesium sulfate and evaporated under reduced pressure. The residue was purified by flash chromatography on silica gel (100% ethyl acetate) resulting in a yellow oil (90% yield). At a 5.2 mmol scale, the reaction yields 51%. **2,3-Dihydroquinolin-4(1H)-one (20),** $^{1}$H NMR (500 MHz, $CDCl_3$) δ 7.84 (dd, *J* = 8.0, 1.6 Hz, 1H), 7.34 – 7.23 (m, 1H), 6.81 – 6.60 (m, 2H), 4.43 (s, 1H), 3.57 (t, *J* = 7.0 Hz, 2H), 2.70 (t, *J* = 7.0 Hz, 2H); $^{13}$C NMR (126 MHz, $CDCl_3$) δ 193.9, 152.2, 135.2, 127.8, 119.5, 118.1, 115.9, 42.4, 38.2.

**Synthesis of Compound 21a**

Methyl 2-bromonicontinate (0.22 g, 1.0 mmol) was dissolved in 2 mL of methanol and ethylenediamine (0.06 g, 1.0 mmol) was added slowly to the solution. The reaction was heated to 50°C until the starting material no longer remained (monitored by TLC). Then the reaction was diluted with ethyl acetate (20 mL) and extracted with water (50 mL) followed by another extraction with ethyl acetate (20 mL) to remove any impurities and side products. The aqueous layer was then subjected to microwave irradiation for 90 minutes at 110°C with 300 W variable power to maintain the temperature. The resulting solution was evaporated under reduced pressure and purified by recrystallization (95:5 ethyl acetate: methanol) resulting in an off-white solid (23%

yield). **1,2,3,4-tetrahydro-5H-pyrido[2,3-e][1,4]diazepin-5-one (21a)**, $C_8H_9N_3O$, $^1$H NMR (400 MHz, DMSO-$d_6$) δ 8.19 – 8.04 (m, 2H), 7.21 (s, 1H), 6.61 (dd, *J* = 7.8, 4.6 Hz, 1H), 3.42 – 3.36 (m, 2H), 3.31 – 3.24 (m, 2H); $^{13}$C NMR (101 MHz, DMSO-$d_6$) δ 168.2, 156.2, 151.9, 142.0, 111.8, 110.7, 46.4, 41.5; mp 175–177°C; HRMS (ESI) *m/z* calcd for $(M+H)^+$ 164.0818, found 164.0814.

**Synthesis of Compound 21e**

1,2,3,4-tetrahydro-5H-pyrido[2,3-e][1,4]diazepin-5-one, **21a**, (10.0 mg, 0.0613 mmol) was dissolved in acetonitrile (1.00 mL) and stirred with potassium carbonate (17.0 mg, 0.122 mmol) and benzyl bromide (15.0 µL, 0.122 mmol). The reaction was subjected to microwave irradiation at 70°C for 90 minutes with 300 W variable power to maintain the temperature. The resulting mixture was extracted with water (10 mL) and ethyl acetate (3 x 10 mL). The organic layers were combined, dried over magnesium sulfate and filtered. The resulting solution was evaporated under reduced pressure and purified by prep TLC (100% ethyl acetate) yielding a white solid (2% yield). **1-Benzyl-1,2,3,4-tetrahydro-5H-pyrido[2,3-e][1,4]diazepin-5-one (21e)**, $C_{15}H_{15}N_3O$, $^1$H NMR (500 MHz, Methanol-$d_4$) δ 8.29 (dd, *J* = 4.7, 2.0 Hz, 1H), 8.22 (dd, *J* = 7.7, 2.0 Hz, 1H), 7.35 – 7.18 (m, 6H), 6.81 (dd, *J* = 7.8, 4.6 Hz, 1H), 4.95 (s, 2H), 3.61 – 3.57 (m, 2H), 3.51 – 3.44 (m, 2H); $^{13}$C NMR (126 MHz, Methanol-$d_4$) δ 172.8, 157.0, 152.7, 143.2, 139.8, 129.5, 128.7, 128.0, 115.8, 114.6, 55.3, 55.0, 42.1; mp 200–203°C; HRMS (ESI) *m/z* calcd for $(M+H)^+$ 254.1288, found 254.1271.

**Biological Assays**

The procedure provided by the manufactuer (BPS Biosciences) for the PARP1 chemiluminesent assay was followed. Serial dilutions were made by using an “in-house” PARP buffer (50 mM Tris, 2.5 mM $MgCl_2 \cdot 6H_2O$, pH 8). Since the effective volume contribution of this buffer/compound admixture is around 10% (2.5 µL in 25 µL total well volume), the effect on assay

is minimal. The procedure provided by the manufactuer (Promega) for the CMGC kinase panel was followed (See Appendix I).

2.9 References


(1) Tepe, J. J.; Preparation of hymenialdisine derivatives and use thereof. *US20040235820A1*, 26.

(2) Darras, F. H.; Kling, B.; Heilmann, J.; Decker, M. Neuroprotective tri- and tetracyclic BChE inhibitors releasing reversible inhibitors upon carbamate transfer. *ACS Med. Chem. Lett.* **2012**, *3*, 914.

(3) Lai, S.; Lee, D. G. Lewis acid assisted permanganate oxidations. *Tetrahedron* **2002**, *58*, 9879.

(4) Amore, K. M.; Leadbeater, N. E.; Miller, T. A.; Schmink, J. R. Fast, easy, solvent-free, microwave-promoted Michael addition of anilines to α,β-unsaturated alkenes: synthesis of N-aryl functionalized β-amino esters and acids. *Tetrahedron Lett.* **2006**, *47*, 8583.

(5) Verma, K. A.; Attri, P.; Chopra, V.; Tiwari, K. R.; Chandra, R. Triethylammonium acetate (TEAA): a recyclable inexpensive ionic liquid promotes the chemoselective aza- and thia-Michael reactions. *Monatshefte für Chemie - Chemical Monthly* **2008**, *139*, 1041.

(6) Steffen, J. D.; Brody, J. R.; Armen, R. S.; Pascal, J. M. Structural implications for selective targeting of PARPs. *Frontiers in Oncology* **2013**, *3*, 301.

(7) BPSBiosciences, Inc. 6042 Cornerstone Court West, Suite B, San Diego, CA 92121 USA. http://bpsbioscience.com.

(8) Yoneda, T.; Tabata, H.; Nakagomi, J.; Tasaka, T.; Oshitari, T.; Takahashi, H.; Natsugari, H. N-Benzoyl- and N-sulfonyl-1,5-benzodiazepines: comparison of their atropisomeric and conformational properties. *J. Org. Chem.* **2014**, *79*, 5717.

(9) Boiadjiev, S. E.; Lightner, D. A. Atropisomerism in linear tetrapyrroles. *Tetrahedron* **2002**, *58*, 7411.

(10) Lee, S.; Kamide, T.; Tabata, H.; Takahashi, H.; Shiro, M.; Natsugari, H. Axial chirality and affinity at the GABA-α receptor of pyrimido[1,2-a][1,4]benzodiazepines and related compounds. *Bioorg. Med. Chem.* **2008**, *16*, 9519.

(11) Tabata, H.; Nakagomi, J.; Morizono, D.; Oshitari, T.; Takahashi, H.; Natsugari, H. Atropisomerism in the vaptan class of vasopressin receptor ligands: the active conformation recognized by the receptor. *Angew. Chem., Int. Ed.* **2011**, *50*, 3075.

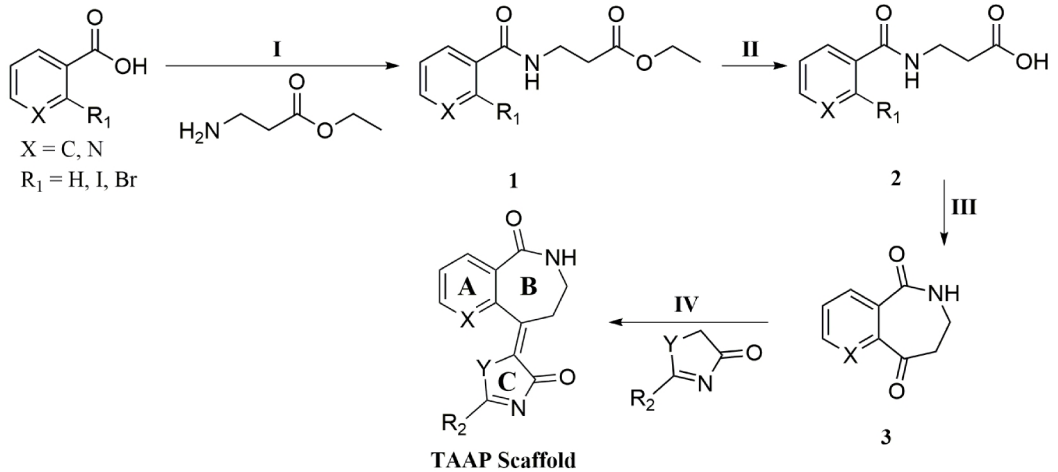
(12) Chobanian, H. R.; Guo, Y.; Liu, P.; Lanza Jr, T. J.; Chioda, M.; Chang, L.; Kelly, T. M.; Kan, Y.; Palyha, O.; Guan, X.-M.; Marsh, D. J.; Metzger, J. M.; Raustad, K.; Wang, S.-P.; Strack, A. M.; Gorski, J. N.; Miller, R.; Pang, J.; Lyons, K.; Dragovic, J.; Ning, J. G.; Schafer, W. A.;

Welch, C. J.; Gong, X.; Gao, Y.-D.; Hornak, V.; Reitman, M. L.; Nargund, R. P.; Lin, L. S. The design and synthesis of potent, selective benzodiazepine sulfonamide bombesin receptor subtype 3 (BRS-3) agonists with an increased barrier of atropisomerization. *Bioorg. Med. Chem.* **2012**, *20*, 2845.

## Chapter 3: Synthetic Methodology for the Benzoazepine-dione Scaffold

### 3.1 Introduction

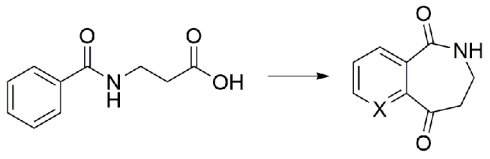
The TAAP scaffold is modeled after the natural product hymenialdisine (HMD), which was isolated from a marine sponge. HMD is active on many kinases, including CDK1 (see C**hapter 1**). Several synthetic schemes for this natural product and its analogs are reported in the literature,[1] which provided the basic synthetic scheme for the synthesis of the TAAP-based inhibitors (**Scheme 3.1**). This included the coupling of carboxylic acids with various β-amino esters (**I**), followed by base hydrolysis (**II**) to yield **2**. We explored various conditions to yield ring **B**. As reported previously, we expected the condensation of the **B** ring in the presence of titanium tetrachloride to yield various **C** ring scaffolds (**IV**).[2] This synthetic scheme is appealing for library synthesis due to the comprehensive range of commercially available starting materials and the hypothesized late-stage **C** ring modifications; however, the synthesis of **3** proved more difficult than anticipated. This chapter will discuss the various approaches taken for the synthesis of the 3,4-dihydro-arylazepine-(1,5)-dione core structure (**3**).




**Scheme 3.1. Representative synthetic scheme for the TAAP scaffold.** Reagents and conditions, **I**: *N*-(3-dimethylaminopropyl)-*N'*-ethylcarbodiimide hydrochloride (EDC HCl) (1.50 eq), 6-chloro-1-hydroxybenzotriazole (6-Cl-HOBt) (1.50 eq), 1M $KHCO_3$ (2.00 eq), DCM, RT, 18 hr, **1a**: X = C, $R_1$ = H (70% crude yield, 10 mmol), **1b**: X = N, $R_1$ = H (81% crude yield, 10 mmol); **II**: lithium hydroxide (LiOH) (3.0 eq), water (3.0 eq), EtOH (ethanol), μW irradiation, 60°C, 1 hr, **2a**: X = C, $R_1$ = H (63% yield), **2b**: X = N, $R_1$ = H (61 %yield); **III**: various conditions; **IV**: McMurry coupling. **3a**, X = C; **3b**, X = N.

## 3.2 Polyphosphoric Acid (PPA) Cyclization

Preliminary studies of the TAAP **B** ring cyclization (**3a**, X = C) with polyphosphoric acid (PPA) using the reported literature procedure[1] proved unachievable without an initial pyrrole moiety as seen in HMD (**Scheme 2.1**). Considering Friedel-Craft acylation favors electron-rich aromatic systems, the **2a** benzylic amide deactivates the ring such that nucleophilic attack is unfavorable yielding no discernible product, ultimately forcing reevaluation of this step. Alternatively, the analogous pyrrole precursor can undergo this ring closure due to the directing effect of the aromatic nitrogen and electron-rich nature of the heterocycle (see **Scheme 2.1**). We screened several PPA reaction conditions, including alternatives to PPA, to observe any detectable product for initial bioevaluation before exploring other methods (**Table 3.1**). The pyridyl (**3b**, X = N) derivative was not extensively explored with PPA due to the electron-deficient nature of pyridine. In contrast, an amine in the benzylic position yields a 6-membered cyclized product with up to a 90% yield (**Scheme 2.2**).




**2a** **3a**

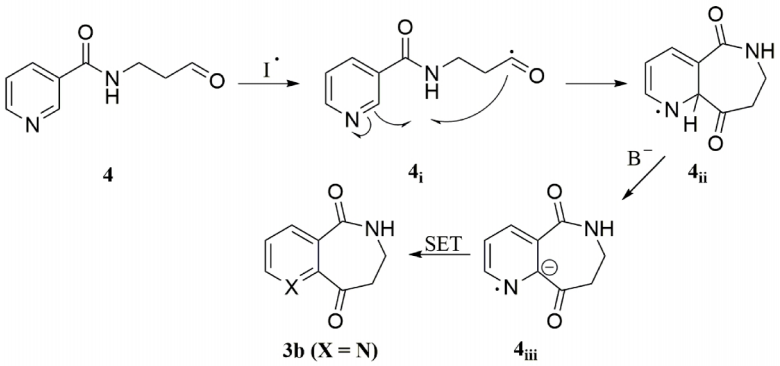
| Entry | Reagents | Solvent | Time (hr) | Temp (°C) |
|---|---|---|---|---|
| 1 | PPA (84% $P_2O_5$) | Neat | 2 | 100→RT |
| 2 | PPA (115% $H_3PO_4$) | Neat | 2 | 130→RT |
| 3 | Eaton's reagent | Neat | 3 | 110→RT |
| 4 | $P_2O_5$ (3.0 eq) | $MeSO_3H$ | 18 | 55 |
| 5 | PPA (84% $P_2O_5$) | Neat | 18 | 100 |
| 6 | PPA (84% $P_2O_5$), $P_2O_5$ (1.0 eq) | Neat | 18 | 100 |
| 7[a] | 1. $SOCl_2$, 2. $AlCl_3$ (1.2 eq) | THF | 2 | Reflux |
| 8[a] | 1. $SOCl_2$, 2. $AlCl_3$ (1.2 eq) | DCB | 2 | Reflux |

**Table 3.1. Conditions screened for PPA cyclizations (X = C).** All entries yielded no reaction, and a general procedure is located in **Section 3.7**. [a]Alternative procedure to PPA; THF: tetrahydrofuran; DCB: dichlorobenzene.

## 3.3 The Minisci Reaction

Since the PPA reaction proved fruitless (**Section 3.2**), the subsequent synthetic approach needed to accommodate the electron-deficient ring. The Minisci reaction not only favors inverse

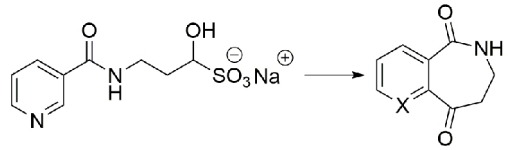
reactivity compared to that of Friedel-Craft acylation, but also uses nitrogen-based heterocycles, both useful attributes for the synthetic methodology of **3b** (X = N). The selective reduction of **2** to an aldehyde (**4**) would circumvent the need for major alterations to the original synthetic pathway (**Scheme 3.1**). The Minisci proceeds through a radical mechanism (**Scheme 3.2**)[3] in which the nitrogen heterocycle promotes radical stability. In many cases, various quinoline derivatives and aromatic aldehydes are used to provide additional radical stability as well as enhance the aromatic reactivity. We quickly discontinued our investigation of the Minisci reaction with the **4**-benzamide analogue upon finding only a single procedure reported with a nonheteroatom-containing aromatic system. This deficit in the literature is likely due to the absence of a nonheteroatom-containing aromatic system with a stable $\mathbf{4_{ii}}$ radical intermediate, which has been proven essential in the cyclization of a biphenyl substrate to the fluorenone under Minisci-type conditions.[4] Therefore, our investigation focused on the pyridyl precursor (**4**).




**Scheme 3.2. Generalized Minisci reaction mechanism from 4 to 3b (X = N).** I: radical initiator; B: base; SET: single electron transfer.

Preliminary reduction experiments with lithium tri-*tert*-butoxyaluminum hydride and **2** yielded unintentional over-reduction to the alcohol. Subsequently, we explored selective oxidation of the alcohol to the aldehyde. Ultimately, coupling nicotinic acid with 3-amino-1-propanol yielded the alcohol precursor necessary for the aldehyde synthesis. Because many of the pyridyl derivatives are water soluble, work-up conditions and chromatography purification proved troublesome. Thus, aldehyde purification required the transformation of the aldehyde to the bisulfite adduct (**5**) in order to circumvent the issue (**Table 3.2**). Commonly the bisulfite adduct is decomposed with

aqueous saturated sodium bicarbonate followed by extraction with organic solvent; however, the high water solubility of the pyridyl aldehyde (**4**) necessitated an alternative approach.[5,6] A desirable but unfortunately unsuccessful approach involved attempting a "one-pot" Minisci reaction with the bisulfite adduct **5** and in situ bisulfite decomposition (entries 4–7, **Table 3.2**).




**5** **3b, X = N**

| | **Bisulfite Decomposition** | | | | **Minisci Conditions** | | | |
|---|---|---|---|---|---|---|---|---|
| **Entry** | **Reagent** | **Solvent** | **Time (hr)** | **Temp (°C)** | **Reagents** | **Solvent** | **Time (hr)** | **Temp (°C)** |
| 1[a] | - | - | - | - | $TMSN_3$ (4.0 eq) $PhI(OCOCF_3)_2$ (4.0 eq) | Neat | 2 | RT |
| 2[b] | - | - | - | - | $K_2S_2O_8$ (2.0 eq) TBAB (30 mol %) | DCE | 1 | 80 |
| 3[c] | - | - | - | - | $FeSO_4 \cdot 7H_2O$ (0.9 eq) $H_2O_2$ (30%) (6.0 eq), conc. $H_2SO_4$ (4.0 eq) | DMSO | 1 | RT |
| 4[d] | $Ac_2O$ (2.0 eq) | MeCN | 0.25 | 110 | TBHP (70%) (3.0 eq) | MeCN | 18 | 95 |
| 5[e] | TMSCl (2.75 eq) | Neat | 1 | 60 | $PhI(OCOCF_3)_2$ (2.0 eq) | MeCN | 18 | RT |
| 6[e] | $TMSN_3$ (2.0 eq) | Neat | 1 | 60 | $PhI(OCOCF_3)_2$ (2.0 eq) | MeCN | 18 | RT |
| 7[e] | $Ac_2O$ (4.0 eq) | MeCN | 18 | 110 | $TMSN_3$ (2.0 eq) $PhI(OCOCF_3)_2$ (2.0 eq) | MeCN | 18 | RT |

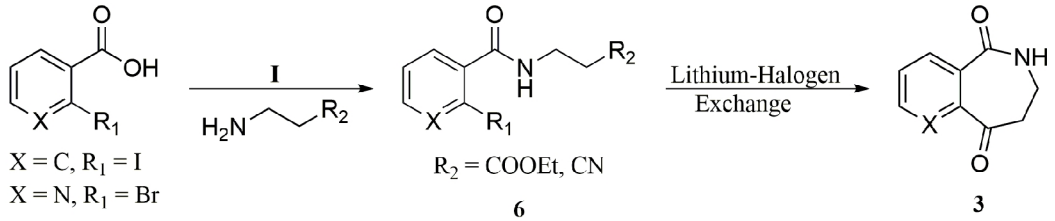
**Table 3.2. Conditions screened for the Minisci reaction (X = N).** All entries yielded complex mixtures with no desired product determined by mass spectrometry and/or NMR. The general procedures for a–e are located in **Section 3.7**. TBAB: Tetrabutylammonium bromide; $TMSN_3$: trimethylsilyl azide; $Ac_2O$: acetic anhydride; TBHP: tert-butyl hydroperoxide; TMSCl: trimethylsilyl chloride; DCE: 1,2-dichloroethane; DMSO: dimethyl sulfoxide; MeCN: acetonitrile.

Although we screened several reaction conditions, the Minisci reaction did not yield **3b** (X = N). The reported Minisci acylations typically contain polyaromatic substrates such as quinoline or highly conjugated aryl systems, which likely provides additional stability to the $\mathbf{4_{ii}}$ radical intermediate (**Scheme 3.2**). Those with a simple pyridine moiety are more commonly associated with decarboxylations, alkylations, or arylations.[7,8] Although there are reports of the Minisci reaction with aliphatic aldehydes, the aromatic substrate is always polyaromatic.[9,10] Thus, the use

of a basic pyridine moiety will likely require either an aromatic aldehyde substrate or modifications to pyridine to enhance radical stability.

3.4 Lithium-Halogen Exchange

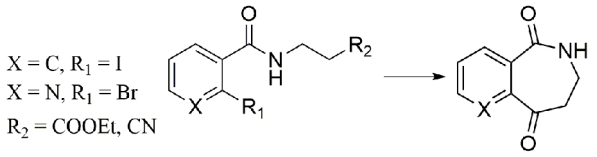
Since the aromatic ring was too electron deficient for the Friedel-Craft acylation and too unstable for the Minisci reaction, we explored lithium-halogen exchange reactions. The approach was similar to the original scheme, but instead featured a halogen-substituted carboxylic acid at the 2-position and incorporated a lithium-halogen exchange (**Scheme 3.3**). Even though this pathway required alternative starting materials that were not necessarily commercially available, this route retained the possibility for library synthesis. In addition, we were able to use previously developed procedures for the synthesis of **6**, and no longer required a hydrolysis step as seen in **Scheme 3.1**.




**Scheme 3.3. Representative synthetic scheme with lithium-halogen exchange (X = C, N).** Reagents and conditions, **I**: EDC HCl (1.50 eq), 6-Cl-HOBt (1.50 eq), 1M $KHCO_3$ (2.00 eq), DCM, RT, 18 hr, **6a**: X = C, $R_1$ = I, $R_2$ = COOEt (93% yield); **6b**: X = C, $R_1$ = I, $R_2$ = CN (73% yield); **6c**: X = N, $R_1$ = Br, $R_2$ = COOEt (40% yield); **6d**: X = N, $R_1$ = Br, $R_2$ = CN (55% yield).

All the derivatives of **6**(**a–d**) were subjected to the same lithiation procedure (entry 1, **Table 3.3**). Entry 1: **6d** primarily yielded starting material; **6a** and **6b** only yielded the hydrogen-substituted (proteo) product; **6c** yielded the proteo product in majority and various substituted products in minority. The lithiated species of **6a** and **6b** phase-separated from the THF, which perhaps is why the lithiated species did not react further to yield the product. Since the **6a** ester is prone to butylation and α-deprotonation, only **6b** was attempted in a different solvent; however, **6b** is insoluble in diethyl ether (entry 2), thus no reaction occurred. Isolation of the **6b** proteo

product confirmed a successful lithium-halogen exchange, which suggests that the nitrile group was poorly suited for nucleophilic attack, even under refluxing conditions or with a Lewis acid using **6a/6c** (entry 3). We isolated a mixture of products none of which was the desired product. Lastly, an attempt was made with a traditional Grignard procedure (entry 4), but the Grignard reagent was not synthesized successfully. Although we decided on amide protection before the lithium-halogen exchange, the observation of various substituted products (butylated, halogen, and alpha-substituted) and the need for **3** guided us to explore the Schmidt reaction that has successfully worked in our hands for the synthesis of aryl-diazepinone (TAAP) ligands (see **Chapter 2**).




**6** **3**

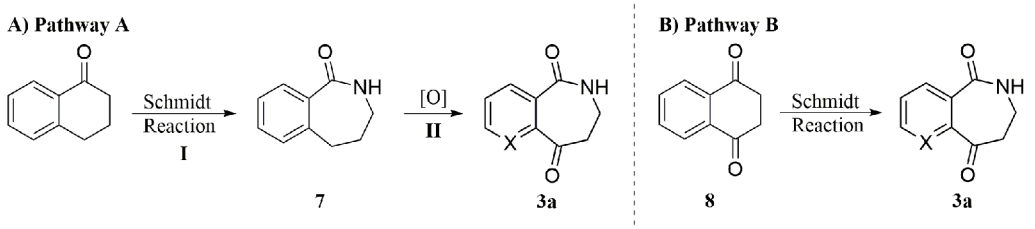
| Entry | Compound | Reagents | Solvent | Time (hr) | Temp (°C) |
|---|---|---|---|---|---|
| 1 | 6a-d | 2.5 M n-BuLi (2.1 eq) | THF | 18 | −78→RT |
| 2 | 6b | 2.5 M n-BuLi (2.1 eq) | $Et_2O$ | 1 | 0→RT* |
| 3[a] | 6a, 6c | 2.5 M n-BuLi (2.1 eq), $BF_3$ $Et_2O$ (2.0 eq) | THF | 2 | −78→RT |
| 4[b] | 6a | Mg (2 eq), $I_2$ (cat.) | THF | 1 | Reflux |

**Table 3.3. Conditions screened for metal-halogen exchange (X = C, N).** All entries yielded no desired product; for a general procedure see **Section 3.7**. **6a**: X = C, $R_1$ = I, $R_2$ = COOEt; **6b**: X = C, $R_1$ = I, $R_2$ = CN; **6c**: X = N, $R_1$ = Br, $R_2$ = COOEt; **6d**: X = N, $R_1$ = Br, $R_2$ = CN; [a,b]Alternative procedures; *Repeated under reflux conditions; THF: tetrahydrofuran; $Et_2O$: diethyl ether.

## 3.5 The Schmidt Reaction

As seen in **Chapter 2**, α-tetralone subjected to Schmidt conditions provides **7** in a 41% yield. Additionally, subjecting 2,3-dihydroquinolin-4(1*H*)-one to similar conditions affords 1,2,3,4-tetrahydro-5*H*-benzo[*e*][1,4]diazepin-5-one in a 62% yield (**Scheme 2.2**); therefore, we anticipated subjecting **8** to Schmidt reaction conditions would yield the desired product in one step

(**Scheme 3.4B**). Since **8** is not commercially available, the Schmidt reaction followed by the benzylic oxidation of **7** provides an alternative pathway to **3a** (X = C) (**Scheme 3.4A**).



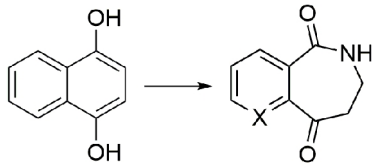

**Scheme 3.4. Representative synthetic schemes utilizing the Schmidt reaction (X = C).** Reagents and conditions, **I**: $NaN_3$ (2.0 eq), conc. HCl, 0°C→RT, 24 hr (42% yield); **II**: $FeCl_3 \cdot 6H_2O$ (3.0 eq), $KMnO_4$ (10.0 eq), acetone, −78°C→RT, 24 hr (0.5 mmol, 15% yield, 10 mmol, 5% yield); See **Section 2.7** for experimental procedures.

Both pathway A and pathway B present their own set of benefits and drawbacks. Pathway A utilizes the relatively inexpensive α-tetralone and an already published procedure for synthesizing **7**, but requires a benzylic oxidation to yield **3a**. However, in the presence of an electron-withdrawing group, benzylic oxidations are difficult to perform in high yields with (benzylic) aliphatic substrates. Pathway B would utilize a commercially unavailable starting material **8**, but literature reports on conversion of 1,4-dihydroxynaphthalene to **8** and previously performed Schmidt reactions provide evidence that pathway B could yield **3a**. Despite this, both pathways diminish the potential for library synthesis with limited analogues of α-tetralone and **8** that are both commercially available and tolerant to strong acids and azides. Since the previous approaches failed to afford **3a**, designing a synthesis with moderate overall yields and library utility became secondary to the successful synthesis of **3a**.

Darras et al. report the synthesis of **7** from α-tetralone in a 64% yield.[11] Even though we report a lower yield, others have reported yields similar to those found in **Scheme 3.4** and in **Chapter 2** (**Section 2.5**).[12,13] The reported yields increase to 52%[14] and 61%[15] upon heating concentrated hydrochloric acid overnight at 50°C. As expected, the benzylic oxidation of **7** proved difficult. Various oxidizing reagents and conditions were tried, including pyridinium chlorochromate

(PCC),[16] KBr/Oxone[17,18] and $KMnO_4/MnO_2$.[19] Ultimately, **3a** was obtained by subjecting **7** to Lewis acid assisted oxidative conditions with $KMnO_4$ and $FeCl_3 \cdot 6H_2O$[20] in low yields on a small scale (0.5 mmol, 15% yield) and lower yields when scaled up to 10 mmol (5% yield). Pathway A (**Scheme 3.4A**) was the first successful synthesis of **3a** with an overall yield of 7% on a small scale. While pathway A yielded the desired product for the bioevaluation of the **A**/**B** core, the overall yield is poor for further derivatization with ring **C**, and the reactions (**I/II, Scheme 3.4A)** present problems on a large scale. The large-scale reaction of **I** (the Schmidt reaction) is undesirable due to safety concerns, as sodium azide is explosive.

Kündig et al. reported the tautomerization of 1,4-dihydroxynaphthalene to **8** in trifluoroacetic acid (TFA);[21] utilizing their procedure, **8** was obtained in a 62% yield. Additionally, the use of trimethylsilyl azide ($TMSN_3$) with TFA could yield the desired lactam (**3a**). Since the tautomerization and Schmidt reaction utilize TFA as the solvent, we attempted to achieve tautomerization and lactamization in one-step (**Table 3.4**). Kündig et al. report maximum tautomerization once the 1,4-dihydroxynaphthalene/TFA slurry becomes homogenous (approximately 30 minutes),[21] but in these studies, a duration of three hours proved optimal for maximum tautomerization.




**3a**

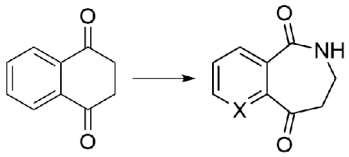
| Entry | Reagents | Solvent | Tautomerization* |
|---|---|---|---|
| 1 | $TMSN_3$ (1 eq) | TFA | 0 hr |
| 2 | $NaN_3$ (2 eq) | TFA | 3 hr |
| 3 | $NaN_3$ (2 eq) | TFA | 0 hr |
| 4[a] | $NaN_3$ (2 eq) | TFA/toluene | 3 hr |
| 5[a] | $TMSN_3$ (1 eq) | TFA/toluene | 3 hr |

**Table 3.4. Conditions screened for a "one-pot" tautomerization/Schmidt reaction (X = C).** The reaction was cooled to 0°C for the azide addition, and stirred overnight at room temperature. See **Section 3.7** for experimental procedures. Entry 1: 2% yield; [a]Alternative procedure; Tautomerization*: time allowed for tautomerization before the addition of the appropriate azide; tautomerization was done at room temperature. TFA: trifluoroacetic acid.

While entry 1 (**Table 3.4**) afforded the desired product, the reaction required extensive purification to isolate only 2% product. Initially we suspected decomposition upon work-up, but

regardless of work-up conditions, removal of the solvent led to a black residue. This residue contained multiple difficult-to-separate components, including the desired product, which led to the exploration of entries 2–5. Stirring the diol first with TFA followed by the addition of sodium azide (entry 2) afforded only tautomerization products. Entry 3 yielded only tautomerization products as the azide was insoluble in TFA. Kündig et al. mentioned the insolubility of the enol-tautomer in TFA, where evaporating the TFA reverses the tautomer equilibrium and causes the diol to precipitate; however, if the reaction is first diluted with toluene prior to TFA evaporation, the equilibrium is maintained.[21] Therefore, entries 4 and 5 were tautomerized in TFA followed by the addition of toluene and the appropriate azide. This procedure (entries 4 and 5) appeared to yield the desired product (determined by TLC and mass spectrometry), but the mixtures were too complex to isolate the product (**3a**) as a pure compound.

Since a "one-pot" synthesis utilizing 1,4-dihydroxynaphthalene provided many purification issues, the isolated keto-tautomer (**8**) was subjected to Schmidt reaction conditions (**Table 3.5**). Similarly to entry 1 (**Table 3.4)**, entry 1 in **Table 3.5** afforded the product in a 9% isolated yield. Unfortunately, the reaction purity did not improve with the keto-tautomer starting material (**8**), and the purification process proved as prohibitive as before. Interestingly, entry 2 did not yield the complex mixtures as seen previously, but four distinguishable products via TLC. Though none of the four products was the desired component, one of the products was a consistent impurity observed in all of the reaction conditions. Upon purification, we identified this impurity as a quinone analogue.




**8** **3a**

| Entry | Reagents | Solvent |
|---|---|---|
| 1 | $TMSN_3$ (1 eq) | TFA |
| 2 | $NaN_3$ (2 eq) | Conc. HCl |
| 3[a] | $TMSN_3$ (1 eq) | TFA |

**Table 3.5. Conditions screened for the Schmidt reaction utilizing the keto-tautomer (8), (X = C).** Azide addition was done at 0°C and all entries were stirred overnight at room temperature. General procedures are located in Section 3.8. Entry 1: 9% yield; [a]Oxygen and light-free reaction conditions; TFA: trifluoroacetic acid.

Alfassi and Schuler report the use of azide radicals as a source of potential aromatic oxidants,[22] and several others report oxidations similar to 1,4-dihydroxynaphthalene to yield a quinone analogue;[23-25] therefore, the 1,4-napthoquinone was suspected to derive from a radical azide mechanism. $^{1}H$ NMR and $^{13}C$ NMR suggested the other three products derive from a Diels-Alder reaction between 1,4-naphthoquinone and the 1,4-dihydroxynaphthalene, but this suspicion was not confirmed. Oxygen and/or light could generate these azide radicals, so entry 3 (**Table 3.5**) was done in an oxygen and light-free environment. Surprisingly entry 3 did not yield the desired product, rather the same products as entry 2, which suggests that radical generation could be the cause of the complex mixtures seen in **Table 3.4** and entry 1 (**Table 3.5**). Moreover, this implies that the radical generation cannot completely be attributed to oxygen or light, but rather derived from the equilibrium between hydrazoic acid and its radical.[22] Unfortunately, the determination of the reaction complexity is outside the scope of this project.

Certainly, the results of **Table 3.4** and **Table 3.5** imply that the generation of, and reactions with, the quinone analogue proceed faster than the desired Schmidt reaction. In order to determine the feasibility of reaction optimization preferring the Schmidt reaction, a brief NMR study was done with **8** and TMSCN in deuterated acetonitrile ($d_3$-MeCN). After 28 hours of agitation, the predicted product starts to form; however, **8** was still observed in large majority. A control experiment with **8** and $d_3$-MeCN was subjected to agitation to assess any potential tautomerization, and after 48 hours, no generation of the enol-tautomer was observed. This result suggests the benzylic carbonyl is susceptible to the nucleophilic attack necessary for the Schmidt reaction, but the nucleophilic attack proceeds slowly without a catalyst. Although the reactivities of TMSCN and $TMSN_3$ are not identical, the findings help further explain the previous results.

## 3.6 Summary

Albeit our initial exploration of the 3,4- dihydro-arylazepine-(1,5)-dione synthesis did not yield the desired product, the unsuccessful syntheses exacerbate the synthetic difficulties associated with the unsubstituted arylazepine-(1,5)-dione scaffold. Out of the four synthetic routes pursued, Schmidt reaction on α-tetralone followed by benzylic oxidation gave some desired product for further biological testing; however, the reactions demonstrated poor scalability and poor yields. The remaining procedures proved inadequate because of variety of reasons discussed above. Lastly, in conjunction with tautomerization, we attempted the Schmidt reaction with 1,4-dihydroxynapthalene. Unfortunately, the keto-tautomer yielded the quinone analogue, which led to several undesired products, and ultimately, complicated purifications and decreased yields. In light of the biological assay results, we will no longer pursue the synthesis and derivatization of 3,4-dihydro-arylazepine-(1,5)-dione scaffold.

3.7 Experimental

**Synthesis of Compound 1/Compound 6**

The appropriate carboxylic acid (1.0 eq) was dissolved in dichloromethane (1.0 M). N-(3-dimethylaminopropyl)-N′-ethylcarbodiimide hydrochloride (1.5 eq) followed by 6-chloro-1-hydroxybenzotriazole (1.5 eq) were added to the reaction mixture, and the reaction was stirred until homogeneity was achieved. Once homogeneous, the appropriate amine (1.05 eq) was added followed by 1M potassium bicarbonate (1.5 eq or 2.0 eq if the amine was provided as a hydrochloride salt) and the solution was stirred overnight at room temperature. The reaction was diluted with dichloromethane, and extracted with 1M potassium bicarbonate. The organic layer was then dried over magnesium sulfate and evaporated under reduced pressure. The purity of the resulting residue was sufficient for the following step unless otherwise stated. **Ethyl 3-benzamidopropanoate (1a)**, white solid, quantitative yield (1.0 mmol), 70% crude yield (10 mmol); $^{1}$H NMR (400 MHz, $CD_3OD$) δ 7.79 (dd, *J* = 8.4, 1.4 Hz, 2H), 7.59 – 7.39 (m, 3H), 4.15 (q, *J* = 7.1 Hz, 2H), 3.64 (t, *J* = 6.8 Hz, 2H), 2.65 (t, *J* = 6.8 Hz, 2H), 1.24 (t, *J* = 7.1 Hz, 3H); $^{13}$C NMR (101 MHz, $CD_3OD$) δ 173.38, 170.15, 135.50, 132.63, 129.49, 128.19, 61.65, 36.96, 34.92, 14.48;

**Ethyl 3-(nicotinamido)propanoate (1b)**, yellow oil, quantitative yield (1.0 mmol), 81% yield (10 mmol); $^{1}$H NMR (400 MHz, $CDCl_3$) δ 8.97 (s, 1H), 8.71 (dd, *J* = 4.7, 1.6 Hz, 1H), 8.09 (dt, *J* = 8.0, 2.0 Hz, 1H), 7.37 (dd, *J* = 7.9, 4.9 Hz, 1H), 7.01 (s, 1H), 4.17 (q, *J* = 7.2 Hz, 2H), 3.74 (q, *J* = 6.0 Hz, 2H), 2.65 (t, *J* = 5.9 Hz, 2H), 1.27 (t, *J* = 7.1 Hz, 3H); $^{13}$C NMR (101 MHz, $CDCl_3$) δ 172.8, 165.6, 152.1, 148.1, 135.2, 130.1, 123.5, 60.9, 35.6, 33.9, 14.2;

**Ethyl 3-(2-iodobenzamido)propanoate (6a)** white solid, (93% yield); $^{1}$H NMR (400 MHz, $CDCl_3$) δ 7.84 (dd, *J* = 7.9, 0.8 Hz, 1H), 7.41 – 7.32 (m, 2H), 7.09 (dtd, *J* = 7.9, 4.7, 0.7 Hz, 1H),

6.38 (s, 1H), 4.16 (q, *J* = 7.1 Hz, 2H), 3.72 (q, *J* = 6.5 Hz, 2H), 2.69 (t, *J* = 5.9 Hz, 2H), 1.27 (t, *J* = 7.1 Hz, 3H); $^{13}$C NMR (101 MHz, $CDCl_3$) δ 172.8, 169.5, 142.3, 139.9, 131.2, 128.3, 92.5, 61.0, 35.5, 34.0, 14.4;

**N-(2-cyanoethyl)-2-iodobenzamide (6b)** Purified by flash chromatography on silica gel (3:2 ethyl acetate:hexanes), white solid, (73% yield); $^{1}$H NMR (400 MHz, $CDCl_3$) δ 7.88 (dt, *J* = 7.8, 0.7 Hz, 1H), 7.44 – 7.35 (m, 2H), 7.13 (ddd, *J* = 8.0, 5.6, 3.6 Hz, 1H), 6.27 (s, 1H), 3.72 (q, *J* = 6.3 Hz, 2H), 2.79 (t, *J* = 6.3 Hz, 2H); $^{13}$C NMR (126 MHz, $CDCl_3$) δ 170.0, 141.3, 140.1, 131.7, 128.5, 128.4, 118.2, 92.4, 36.4, 18.5;

**Ethyl 3-(2-bromonicotinamido) propanoate (6c)** Purified by flash chromatography on silica gel (9:1 ethyl acetate:hexanes), colorless oil, (40% yield); $^{1}$H NMR (400 MHz, $CDCl_3$) δ 8.37 (dd, *J* = 4.8, 2.0 Hz, 1H), 7.81 (dd, *J* = 7.6, 2.0 Hz, 1H), 7.30 (dd, *J* = 7.6, 4.7 Hz, 1H), 6.90 (s, 1H), 4.13 (q, *J* = 7.1 Hz, 2H), 3.70 (q, *J* = 6.1 Hz, 2H), 2.65 (dd, *J* = 6.4, 5.6 Hz, 2H), 1.24 (t, *J* = 7.1 Hz, 3H); $^{13}$C NMR (101 MHz, $CDCl_3$) δ 172.5, 165.9, 151.1, 138.5, 138.3, 134.8, 122.9, 61.0, 35.6, 33.7, 14.3;

**2-Bromo-N-(2-cyanoethyl)nicotinamide (6d)** Purified by flash chromatography on silica gel (3:2 ethyl acetate:hexanes), white solid, (55% yield); $^{1}$H NMR (400 MHz, $CDCl_3$) δ 8.43 (ddd, *J* = 4.8, 2.0, 0.6 Hz, 1H), 7.88 (ddd, *J* = 7.6, 2.0, 1.0 Hz, 1H), 7.36 (ddd, *J* = 7.6, 4.8, 0.5 Hz, 1H), 6.89 (s, 1H), 3.73 (q, *J* = 6.3 Hz, 2H), 2.77 (t, *J* = 6.3 Hz, 2H); $^{13}$C NMR (101 MHz, $CDCl_3$) δ 166.4, 151.6, 138.6, 138.5, 134.0, 123.0, 118.0, 36.5, 18.3.

**Synthesis of Compound 2**

A standard literature procedure was followed with modification for microwave assisted synthesis.[1] The appropriate ester (0.500 g, 2.26 mmol) was dissolved in ethanol (3 mL), following which, lithium hydroxide (0.163 g, 6.78 mmol) and water (0.122 mL, 6.78 mmol) were added into

the microwave tube. The microwave tube was subjected to microwave irradiation at 60°C for one hour with 300 W variable power to maintain the temperature. The solution was acidified with 1 M HCl, and then extracted with dichloromethane (3 x 30 mL). The combined organic layers were dried over magnesium sulfate and evaporated under reduced pressure. The residue was purified by flash chromatography on silica gel (100% ethyl acetate). **3-Benzoamidopropanoic acid (2a)**, colorless oil, 63% yield; $^{1}$H NMR (400 MHz, $CDCl_3$) δ 7.86 – 7.62 (m, 2H), 7.57 – 7.36 (m, 3H), 6.80 (s, 1H), 3.75 (q, *J* = 6.0 Hz, 2H), 2.74 (t, *J* = 5.9 Hz, 2H); $^{13}$C NMR (101 MHz, $CDCl_3$) δ 176.6, 167.7, 134.1, 131.7, 128.6, 127.0, 35.2, 33.7.

**3-(Nicotinamido)propanoic acid (2b)**, white solid, (61% yield); $^{1}$H NMR (400 MHz, $CD_3OD$) δ 8.95 (s, 1H), 8.66 (d, *J* = 3.5 Hz, 1H), 8.22 (ddd, *J* = 8.0, 2.3, 1.6 Hz, 1H), 7.52 (ddd, *J* = 8.0, 4.9, 0.9 Hz, 1H), 3.65 (t, *J* = 6.9 Hz, 2H), 2.65 (t, *J* = 6.9 Hz, 2H); $^{13}$C NMR (101 MHz, $CD_3OD$) δ 175.2, 167.8, 152.6, 149.0, 137.0, 132.0, 125.1, 37.1, 34.5.

**General PPA Procedure**

PPA was added to a pre-dried flask and heated under vacuum followed by a nitrogen purge three times. The PPA was heated to the appropriate temperature and checked for adequate agitation. Compound **2** and $P_2O_5$ were then added to the flask under nitrogen purge. Upon the completion of the appropriate reaction time, the reaction was quenched with ice, basified with solid sodium or potassium carbonate, and extracted with organic solvent. The organic layer was then dried over magnesium sulfate and evaporated under reduced pressure.

**[a]PPA Procedure**

A general Friedel-Crafts acylation procedure was followed.[26] Thionyl chloride (10.0 eq) was added to compound **2** in a three-necked round bottom flask at 0° C. The reaction was allowed to warm to room temperature and monitored by TLC. Upon complete conversion to the acid chloride,

a gentle stream of nitrogen was used to remove the excess thionyl chloride. Dichloromethane was added to the residue and evaporated with a stream of nitrogen (3 x) to ensure all of the excess thionyl chloride had been removed. Once the acid chloride was obtained, the flask was heated with a heat gun under vacuum and purged with nitrogen gas (3 x). Aluminum trichloride (1.2 eq) and tetrahydrofuran were added to flask under inert conditions. The reaction was refluxed for two hours and quenched with dilute acid. After extraction with organic solvent, the organic layer was dried over magnesium sulfate and evaporated under reduced pressure.

**Synthesis of Compound 5**

A standard literature procedure was followed.[27] N-(3-hydroxypropyl)nicotinamide (2.00 mmol, 0.360 g) was dissolved in chloroform (2 mL). (2,2,6,6-Tetramethylpiperidin-1-yl)oxyl (0.20 mmol, 31 mg) and N-chlorosuccinimide (3.00 mmol, 0.400 g) were added to the reaction mixture followed by a mixture of 0.5 N sodium bicarbonate/0.05 N potassium carbonate (4 mL) and tetrabutylammonium chloride (0.200 mmol, 55.6 mg). The reaction was stirred vigorously at room temperature overnight. The aqueous layer was extracted with chloroform (2 x 20 mL). The organic layers were combined and washed with water until no product remained (confirmed by TLC). The water layers were evaporated under reduced pressure, and an optimized standard literature procedure was followed to generate the bisulfite adduct.[5,28] Sodium bisulfite (2.00 eq) was dissolved in minimal water, and the crude aldehyde was added. If the solution was not homogenous, additional water was added until homogeneity was achieved. Following, ethanol was added dropwise until the solution became persistently hazy. The solution was heated until homogeneous and then cooled slowly to 4°C. The precipitate was filtered and washed with cold ethanol yielding a white solid (57% yield). **1-Hydroxy-3-(nicotinamido)propane-1-sulfonate (5)**, $^{1}$H NMR (400 MHz, $D_2O$) δ 9.19 (s, 1H), 8.96 (d, *J* = 5.5 Hz, 1H), 8.89 (ddd, *J* = 8.2, 2.0, 1.4

Hz, 1H), 8.17 (ddd, *J* = 8.2, 5.8, 0.8 Hz, 1H), 4.53 (dd, *J* = 10.2, 2.9 Hz, 1H), 3.67 (ddd, *J* = 7.4, 5.9, 2.0 Hz, 2H), 2.33 (dtd, *J* = 15.3, 7.7, 2.9 Hz, 1H), 2.02 (ddt, *J* = 14.4, 10.2, 5.9 Hz, 1H); $^{13}$C NMR (101 MHz, $D_2O$) δ 164.7, 144.1, 144.1, 141.4, 133.2, 127.2, 81.6, 36.6, 30.4.

**General Minisci Procedure (*a-e)***

***a*:** A standard literature procedure was followed.[9] Compound **5** was charged in a flask with trimethylsilyl azide (4.0 eq) and [bis(trifluoroacetoxy)iodo]benzene (4.0 eq). The reaction was stirred for two hours at room temperature followed by a quench with triethylamine. Various work-up procedures were tried to isolate the product.

***b*:** A standard literature procedure was followed.[3] Compound **5** was heated to 80°C in dichloroethane with potassium persulfate (2.0 eq) and tetrabutylammonium bromide (30 mol %). The reaction was stirred for one hour and then extracted with ethyl acetate and saturated sodium bicarbonate. The organic layer was dried over magnesium sulfate and evaporated under reduced pressure.

***c*:** A modified standard literature procedure was followed.[29] Compound **5** was charged in a flask with saturated sodium bicarbonate (2.0 eq) followed by the room temperature addition of concentrated sulfuric acid (4.0 eq), iron (II) sulfate heptahydrate (0.3 eq) and dimethylsulfoxide (1 M). Subsequently, hydrogen peroxide (30%) (3.0 eq) was added dropwise to the solution. After the addition of the hydrogen peroxide, another addition of iron (II) sulfate heptahydrate (0.3 eq) was added again, and the reaction was stirred at room temperature for 30 minutes. Lastly, another addition of hydrogen peroxide (3.0 eq) and iron (II) sulfate heptahydrate (0.3 eq) were added followed by stirring for an additional 15 minutes. The reaction was quenched with aqueous sodium hydroxide (0.2 M) and extracted with diethyl ether. The organic layer was dried over magnesium sulfate and evaporated under reduced pressure.

***d*:** A modified standard literature procedure was followed.[6] Acetic anhydride (2.0 eq) and acetonitrile were added to **5** in a microwave tube and subjected to microwave irradiation at 110°C for 15 minutes with 300 W variable power to maintain the temperature. After the irradiation period, tert-butyl hydroperoxide (70%) (3.0 eq) was added, and the mixture was stirred overnight at 95°C. The resulting solution was filtered over a pad of celite, and the filtrate was subjected to various purification techniques.

***e*:** A modified literature procedure was followed.[5] Compound **5** was first decomposed into the aldehyde with either trimethylsilyl chloride (2.8 eq), trimethylsilyl azide (2.0 eq) or acetic anhydride (4.0 eq) in the desired amount of acetonitrile at either 60°C or 110°C. Once the bisulfite adduct converted to the aldehyde (monitored by TLC), the reaction was allowed to cool to room temperature followed by the addition of [bis(trifluoroacetoxy)iodo]benzene (2.0 eq), and the reaction was stirred for two hours. In the event of decomposition with acetic anhydride, trimethylsilyl azide (2.0 eq) was also added in conjunction with [bis(trifluoroacetoxy)iodo]benzene. Various work-up procedures were utilized to isolate the product.

**General Lithium-Halogen Exchange Procedure**

To a pre-dried flask purged with nitrogen atmosphere, the appropriate **6** derivative was dissolved in either tetrahydrofuran or diethyl ether then cooled down to −78°C with an acetone/dry ice bath (0°C in the case of diethyl ether). Once cooled, n-butyl lithium (2.5 M in hexanes) (2.1 eq) was added dropwise to the mixture maintaining the temperature. After the addition, the reaction was slowly warmed to room temperature and stirred overnight. The resulting solution was quenched with hydrochloric acid (1 M) and stirred vigorously at room temperature for one hour.

Afterwards, the solution was extracted with organic solvent, dried over magnesium sulfate and evaporated under reduced pressure.

**[a]Lithium-Halogen Exchange Procedure**

To a pre-dried flask purged with nitrogen atmosphere, the appropriate **6** derivative was dissolved in tetrahydrofuran and boron trifluoride etherate (2.0 eq) was added. The reaction was stirred at room temperature for 30 minutes before cooling to -78°C with an acetone/dry ice bath. Once cooled, n-butyl lithium (2.5 M in hexanes) (2.1 eq) was added dropwise to the mixture maintaining the temperature. After the addition, the reaction was slowly warmed to room temperature and stirred overnight. The resulting solution was quenched with saturated ammonium chloride and stirred vigorously at room temperature for one hour. Afterwards, the solution was extracted with organic solvent, dried over magnesium sulfate and evaporated under reduced pressure.

**[b]Magnesium-Halogen Exchange Procedure**

Rapidly wash the magnesium (2.0 mmol, 49 mg) with 1M hydrochloric acid, filter the magnesium dry, and add to a pre-dried two-neck round bottom flask. Add a catalytic amount of iodine (0.01 mmol, 3 mg), then evacuate and purge the flask with nitrogen. Under nitrogen, add anhydrous tetrahydrofuran (2.0 mL) and bring the slurry to a reflux. Dissolve the starting material (1.0 mmol, 0.35 g) in anhydrous THF (1.0 mL), and to the refluxing slurry, add the starting material/THF dropwise to the reaction mixture. The reaction was refluxed for one hour, cooled to room temperature, and stirred for an additional hour. After the stir period, no reaction had taken place (via TLC), so an additional 50 mg of magnesium was added, refluxed for an additional two hours, and stirred at room temperature overnight. After the additional stir period, the reaction still only contained starting material, and the reaction was discarded.

**Synthesis of Compound 7**

See **Section 2.8**, Compound 7

**Synthesis of Compound 3a, X = C (Scheme 3.4A)**

See **Section 2.8**, Compound 6

**Synthesis of Compound 8**

A standard literature procedure was followed.[21] 1,4-Dihydroxynaphthalene (0.80 g, 5.0 mmol) was dissolved in trifluoroacetic acid (20 mL, 0.25 M) and stirred at room temperature for 3 hours. Subsequently, toluene (4 x the reaction volume) was added and stirred well. The solvents were evaporated, and the residue was recrystallized in diethyl ether to yield off white crystalline needles (62%). **2,3-Dihydronaphthalene-1,4-dione (8)**, $^{1}$H NMR (400 MHz, $CD_3CN$) δ 7.97 (dd, *J* = 5.8, 3.3 Hz, 2H), 7.78 (dd, *J* = 5.9, 3.3 Hz, 2H), 3.04 (s, 4H); $^{13}$C NMR (126 MHz, $CD_3CN$) δ 197.1, 136.4, 135.1, 127.2, 38.1.

**General "One-pot" Tautomerization/Schmidt Reaction Procedure**

1,4-Dihydroxynaphthalene was dissolved in trifluoroacetic acid (0.25 M) and stirred for the appropriate time allotted for tautomerization at room temperature. Subsequently, the reaction was cooled to 0°C and the appropriate azide was added. After the azide addition, the reaction was gradually warmed to room temperature and stirred overnight. The solvent was evaporated and the residue was diluted with a small amount of water. Solid potassium bicarbonate was added until a basic pH was achieved. The basic solution was extracted with ethyl acetate (3 x), dried over magnesium sulfate and evaporated under reduced pressure.

**[a]"One-pot" Tautomerization/Schmidt Reaction Procedure**

1,4-Dihydroxynaphthalene was dissolved in trifluoroacetic acid (0.25 M) and stirred for 3 hours. Subsequently, toluene (4 x the reaction volume) was added and stirred well. The reaction

was then cooled to 0°C and the appropriate azide was added. After the azide addition, the reaction was gradually warmed to room temperature and stirred overnight. The solvent was evaporated and the residue was diluted with a small amount of water. Solid potassium bicarbonate was added until a basic pH was achieved. The basic solution was extracted with ethyl acetate (3 x), dried over magnesium sulfate and evaporated under reduced pressure.

**General Schmidt Reaction Procedure**

For entries 1 and 3, 2,3-dihydroquinolin-4(1H)-one (80.0 mg, 0.543 mmol) was dissolved in minimal trifluoroacetic acid (TFA) and cooled to 0°C in an ice-water bath. A 1 M solution of $TMSN_3$ (71.5 μL, 0.543 mmol) in TFA was added dropwise to the reaction through an addition funnel. Following the addition, the reaction was warmed to room temperature and stirred overnight. Solid potassium carbonate was added to the reaction mixture until it reached a basic pH. The basic solution was then extracted with ethyl acetate (3 x 20 mL). The organic layer was then dried over magnesium sulfate and evaporated under reduced pressure.

For entry 2, see **Section 2.7**, Compound 5 and 7

3.8 References


(1) Tepe, J. J.; Preparation of hymenialdisine derivatives and use thereof. *US20040235820A1*, 26.

(2) Nguyen, T. N. T.; Saleem, R. S. Z.; Luderer, M. J.; Hovde, S.; Henry, R. W.; Tepe, J. J. Radioprotection by hymenialdisine-derived Checkpoint kinase 2 inhibitors. *ACS Chem. Biol.* **2011**, *7*, 172.

(3) Siddaraju, Y.; Lamani, M.; Prabhu, K. R. A transition metal-free Minisci reaction: acylation of isoquinolines, quinolines, and quinoxaline. *J. Org. Chem.* **2014**, *79*, 3856.

(4) Shi, Z.; Glorius, F. Synthesis of fluorenones via quaternary ammonium salt-promoted intramolecular dehydrogenative arylation of aldehydes. *Chem. Sci.* **2013**, *4*, 829.

(5) Kjell, D. P.; Slattery, B. J.; Semo, M. J. A novel, nonaqueous method for regeneration of aldehydes from bisulfite adducts. *J. Org. Chem.* **1999**, *64*, 5722.

(6) Mohanty, S.; Roy, A. K.; Kumar, V. K. P.; Reddy, S. G.; Karmakar, A. C. Acetic anhydride-promoted one-pot condensation of 2,4-thiazolidinedione with bisulfite adducts of aldehydes. *Tetrahedron Lett.* **2014**, *55*, 4585.

(7) Kan, J.; Huang, S.; Lin, J.; Zhang, M.; Su, W. Silver-catalyzed arylation of (hetero)arenes by oxidative decarboxylation of aromatic carboxylic acids. *Angew. Chem., Int. Ed.* **2015**, *54*, 2199.

(8) Minisci, F.; Vismara, E.; Fontana, F.; Morini, G.; Serravalle, M.; Giordano, C. Polar effects in free-radical reactions. Rate constants in phenylation and new methods of selective alkylation of heteroaromatic bases. *J. Org. Chem.* **1986**, *51*, 4411.

(9) Matcha, K.; Antonchick, A. P. Metal-free cross-dehydrogenative coupling of heterocycles with aldehydes. *Angew. Chem., Int. Ed.* **2013**, *52*, 2082.

(10) Demırcı, S.; Göksu, S.; Boztaş, M.; Tümer, F.; Seçen, H. Synthesis of vertilecanin C and two new derivatives of aertilecanin A via nicotinic acid. *Turk. J. Chem.* **2008**, *32*, 287.

(11) Darras, F. H.; Kling, B.; Heilmann, J.; Decker, M. Neuroprotective tri- and tetracyclic BChE inhibitors releasing reversible inhibitors upon carbamate transfer. *ACS Med. Chem. Lett.* **2012**, *3*, 914.

(12) Grunewald, G. L.; Dahanukar, V. H. Synthesis of 3-alkyl-8-substituted- and 4-hydroxy-8-substituted-2,3,4,5-tetrahydro-1H-2-benzazepines. *J. Heterocycl. Chem.* **1994**, *31*, 1609.

(13) Meyers, A. I.; Hutchings, R. H. The asymmetric synthesis of 1-alkyl-2,3,4,5-tetrahydro-benzazepines and benzo[β]-1-azabicyclo[5,3,1]decanes. *Tetrahedron* **1993**, *49*, 1807.

(14) Crosby, I. T.; Shin, J. K.; Capuano, B. The application of the Schmidt reaction and Beckmann rearrangement to the synthesis of bicyclic lactams: Some mechanistic considerations. *Aust. J. Chem.* **2010**, *63*, 211.

(15) Shonberg, J.; Draper-Joyce, C.; Mistry, S. N.; Christopoulos, A.; Scammells, P. J.; Lane, J. R.; Capuano, B. Structure–activity study of N-((trans)-4-(2-(7-cyano-3,4-dihydroisoquinolin-2(1H)-yl)ethyl)cyclohexyl)-1H-indole-2-carboxamide (SB269652), a bitopic ligand that acts as a negative allosteric modulator of the dopamine D2 receptor. *J. Med. Chem.* **2015**, *58*, 5287.

(16) Parish, E. J.; Chitrakorn, S.; Wei, T.-Y. Pyridinium chlorochromate-mediated allylic and benzylic oxidation. *Synth. Commun.* **1986**, *16*, 1371.

(17) Moriyama, K.; Takemura, M.; Togo, H. Direct and selective benzylic oxidation of alkylarenes via C–H abstraction using alkali metal bromides. *Org. Lett.* **2012**, *14*, 2414.

(18) Yin, L.; Wu, J.; Xiao, J.; Cao, S. Oxidation of benzylic methylenes to ketones with Oxone–KBr in aqueous acetonitrile under transition metal free conditions. *Tetrahedron Lett.* **2012**, *53*, 4418.

(19) Shaabani, A.; Mirzaei, P.; Naderi, S.; Lee, D. G. Green oxidations. The use of potassium permanganate supported on manganese dioxide. *Tetrahedron* **2004**, *60*, 11415.

(20) Lai, S.; Lee, D. G. Lewis acid assisted permanganate oxidations. *Tetrahedron* **2002**, *58*, 9879.

(21) Kündig, E. P.; Enríquez García, A.; Lomberget, T.; Bernardinelli, G. Rediscovery, isolation, and asymmetric reduction of 1,2,3,4-tetrahydronaphthalene-1,4-dione and studies of its [$Cr(CO)_3$] complex. *Angew. Chem., Int. Ed.* **2006**, *45*, 98.

(22) Alfassi, Z. B.; Schuler, R. H. Reaction of azide radicals with aromatic compounds. Azide as a selective oxidant. *J. Phys. Chem.* **1985**, *89*, 3359.

(23) Hashmat Ali, M.; Niedbalski, M.; Bohnert, G.; Bryant, D. Silica-gel-supported ceric ammonium nitrate (CAN): a simple and efficient solid-supported reagent for oxidation of oxygenated aromatic compounds to quinones. *Synth. Commun.* **2006**, *36*, 1751.

(24) Zheng, B.; Schmidt, M. A.; Eastgate, M. D. Synergistic catalysis: Pd(II) catalyzed oxidation of 1,4-dihydroquinones in the Pd(II) catalyzed 1,4-oxidation of cyclic 1,3-dienes. *J. Org. Chem.* **2016**, *81*, 3112.

(25) Matsuno, T.; Koyama, Y.; Hiroto, S.; Kumar, J.; Kawai, T.; Shinokubo, H. Isolation of a 1,4-diketone intermediate in oxidative dimerization of 2-hydroxyanthracene and its conversion to oxahelicene. *Chem. Commun.* **2015**, *51*, 4607.

(26) Sugimori, M.; Ejima, A.; Ohsuki, S.; Uoto, K.; Mitsui, I.; Kawato, Y.; Hirota, Y.; Sato, K.; Terasawa, H. Synthesis and antitumor activity of ring A- and F-modified hexacyclic camptothecin analogues. *J. Med. Chem.* **1998**, *41*, 2308.

(27) Delfourne, E.; Kiss, R.; Corre, L. L.; Dujols, F.; Bastide, J.; Collignon, F.; Lesur, B.; Frydman, A.; Darro, F. Synthesis and in vitro antitumor activity of phenanthrolin-7-one derivatives, analogues of the marine pyridoacridine alkaloids ascididemin and meridine: Structure−activity relationship. *J. Med. Chem.* **2003**, *46*, 3536.

(28) Cong, C.; Wang, H.; Hu, Y.; Liu, C.; Ma, S.; Li, X.; Cao, J.; Ma, S. Synthesis and antibacterial activity of novel 4-O-benzimidazolyl clarithromycin derivatives. *Eur. J. Med. Chem.* **2011**, *46*, 3105.

(29) Duncton, M. A. J.; Estiarte, M. A.; Johnson, R. J.; Cox, M.; O'Mahony, D. J. R.; Edwards, W. T.; Kelly, M. G. Preparation of heteroaryloxetanes and heteroarylazetidines by use of a Minisci reaction. *J. Org. Chem.* **2009**, *74*, 6354.

## Chapter 4: Future Perspectives

### 4.1 A Brief Overview

In order to validate the TAAP scaffold for PARP1 inhibiton, we tested a series of TAAP fragment-based analogues in a cell-free assay. As discussed in **Chapter 3**, the synthesis of the 3,4-dihydro-arylazepine-1,5-dione proved to be a synthetic challenge (**Figure 4.1A**); however, the initial fragment screening showed no activity for the 3,4-dihydro-1*H*-benzo[*c*]azepine-1,5(2*H*)-dione. The fragment screening revealed the 1,2,3,4-tetrahydro-5*H*-benzo[*e*][1,4]-diazepin-5-one, TBAP, scaffold as the best PARP1 inhibitor with activity in the low μM range (**Figure 4.1B**). Further derivatization of the lead compound unvieled a small handful of PARP1 active compounds (**Figure 4.1C and 4.1D**). Though the active PARP1

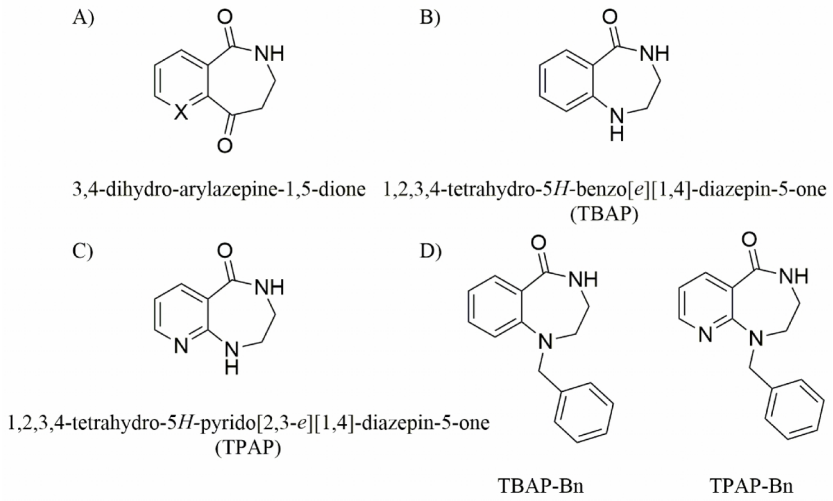



**Figure 4.1. TAAP fragments and derivatives.** A) The synthetically challenging TAAP scaffold. B) The lead TAAP scaffold, TBAP. $IC_{50}$ = 2.5 ± 0.4 μM C) TPAP: a TBAP analogue used for derivative synthesis, which provided the most potent inhibitor (TPAP-Bn). D) The benzyl TBAP and TPAP derivatives (TBAP-Bn, TPAP-Bn), which showed the best activity for PARP1.

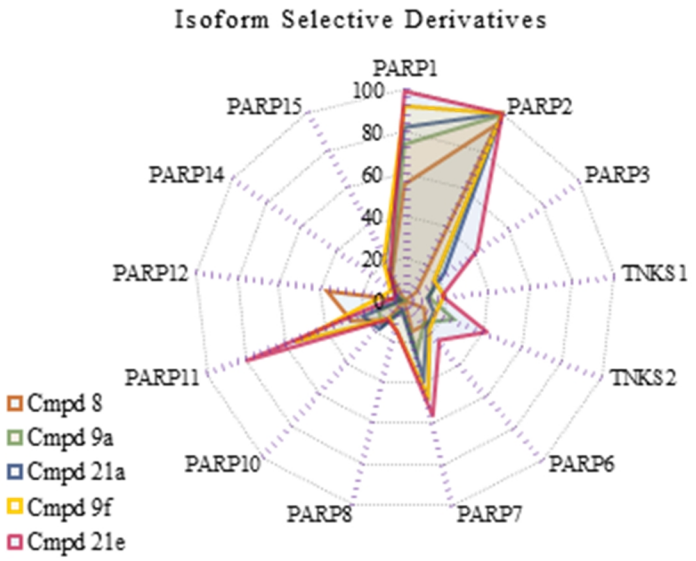


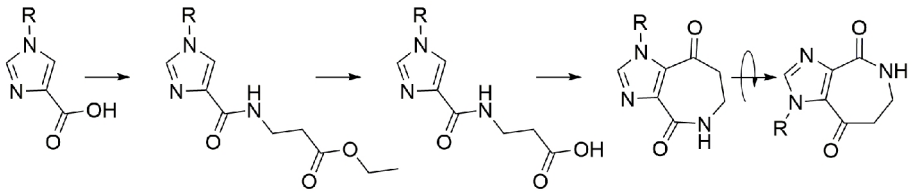

**Figure 4.2. PARP isoform selectivity for the TAAP derivatives.** Percent inhibition determined by a single point assay at 10 μM against all available PARP isoforms. Includes the TAAP derivatives that exhibited selectivity. Structures for **9a**, **21**a, **9f**, and **21e** are shown in **Figure 4.1**. Compound **8** is the oxazepine derivative of **9a**.

compounds are not active against CDK1 (**Section 2.6**), a single-point assay evaluated the percent inhibition at 10 μM of the active compounds against 13 PARP isoforms (PARP1–3, TNKS1, TNKS2, PARP6–8, PARP10–12, PARP14, PARP15) and showed that some of the active compounds against PARP1 are also active on PARP2 with selectivity for PARP1/2 (**Figure 4.2**).[1] The culmination of these results will guide our future studies of the TAAP scaffold.

## 4.2 Targeted Polypharmacology of PARP with Kinases

### *4.2.1 PARP1 and CDK1*

As shown in **Section 2.6**, the TAAP PARP1 inhibitors are not active against CDK1, as the 6/7-membered fused ring system may not be suitable for the CDK1 binding pocket. An alternative approach could include 5/7-memebered fused ring systems like HMD, but the PARP1 activity for HMD and the HMD analogues are low. The 5/7-membered fused ring system may not align appropriately for π-π stacking with the tyrosine residue lining the top of the PARP1 pocket, hence the low activity. Rather than a pyrrole-based 5/7-membered fused ring system, an imidazole-based system could increase the potency via additional hydrogen bonding with either the water molecule or the glutamate residue lining the PARP1 pocket (**Scheme 4.1**).



**Scheme 4.1. Proposed synthetic scheme for the synthesis of the imidazole analogue.** Reagents and conditions, **I**: EDC HCl (1.50 eq), 6-Cl-HOBt (1.50 eq), 1M $KHCO_3$ (2.00 eq), DCM, RT; **II**: 1M NaOH (1.0 eq), EtOH, heat; **III**: PPA, 110°C, 18 hr.

### *4.2.2 PARP and Other Kinases*

Previously, in collaboration with Dr. Hong Zheng, we tested a commercial library of more than 350 known kinase inhibitors against PARP1 in a single point assay (10 μM) and revealed moderate potency against PARP1 with a known Akt inhibitor, GSK690693 (**Figure 4.3**). The protein kinase

B (Akt) is a known target for cancer therapeutics. Akt is associated with PI3K, a targeted pathway for PARP resistance, and together are essential for the Akt/PI3K signaling cascade for survival and growth responses to extracellular signals.[2] Recently, this Akt inhibitor was screened against all PARP isoforms using BPS Biosciences commercial service, and the results are given in **Figure 4.4**.[1] The radar plot shows that the TAAP derivatives **9a** (green) and **21a** (blue) inhibit PARP2 100% at 10 μM and inhibit PARP1 greater than 50% at 10 μM, thus demonstrating selectivity towards PARP1/2; however, the Akt inhibitor (teal) shows selectivity for PARP1 versus PARP2, modest activity for TNKS2, and some activity (approximately 30% inhibition) for PARP3, PARP10, and PARP14. Although we do not fully understand how the Akt inhibitor binds to PARP1, we expect that upon derivatization we can increase the PARP1 potency while maintaining PARP1 selectivity and Akt activity. This scaffold could be developed in the future for a dual Akt/PARP inhibitor.

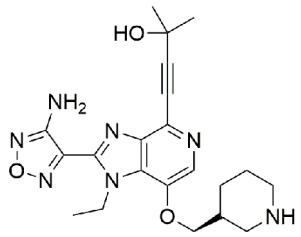



**Figure 4.3. PARP1 selective Akt inhibitor (GSK690693).** GSK690693 was tested in a single-point assay against all of the available PARP isoforms at 10 μM.

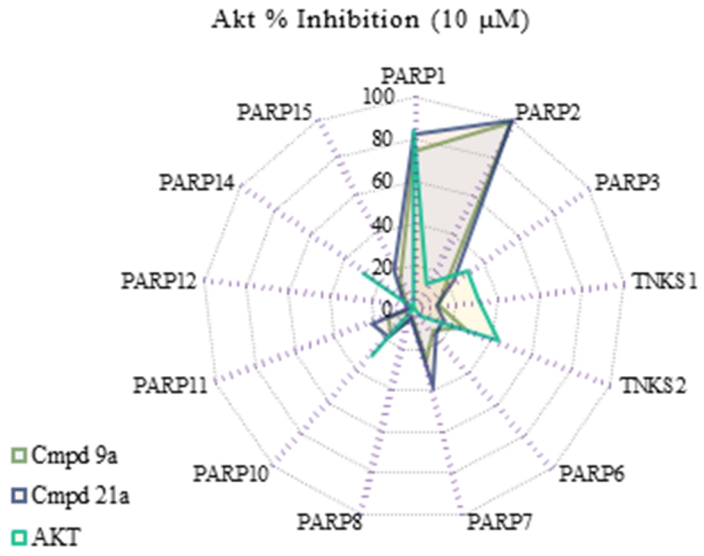



**Figure 4.4. PARP isoform selectivity for a known Akt inhibitor.** Percent inhibition determined by a single point assay at 10 μM against all available PARP isoforms. **9a** and **21a** are included for comparison.

*4.2.3 PARP and Chalcones*

In addition to the Akt inhibitor, we tested a series of chalcones (**C1–C4**) against the PARP isoforms in a single point assay (10 μM), using BPS commercial testing service, to identify isoform-selective inhibitors (**Figure 4.5**).[1] A Josan group member, Mr. Alexander Hawes,

provided the chalcones used in this assay. Although **C2–C4** displayed little to no activity against any of the PARP isoforms, **C1** (yellow) shows activity against PARP1, PARP14, and PARP15. Albeit modest activity (>10 μM), the **C1** selectivity displays a unique phenotype compared to the selectivity shown by the TAAP analogues and Akt inhibitor. Although **C1** structural modifications will be necessary to increase the inhibitory activity, these chalcones could serve as suitable scaffolds for the development of PARP selective inhibitors.

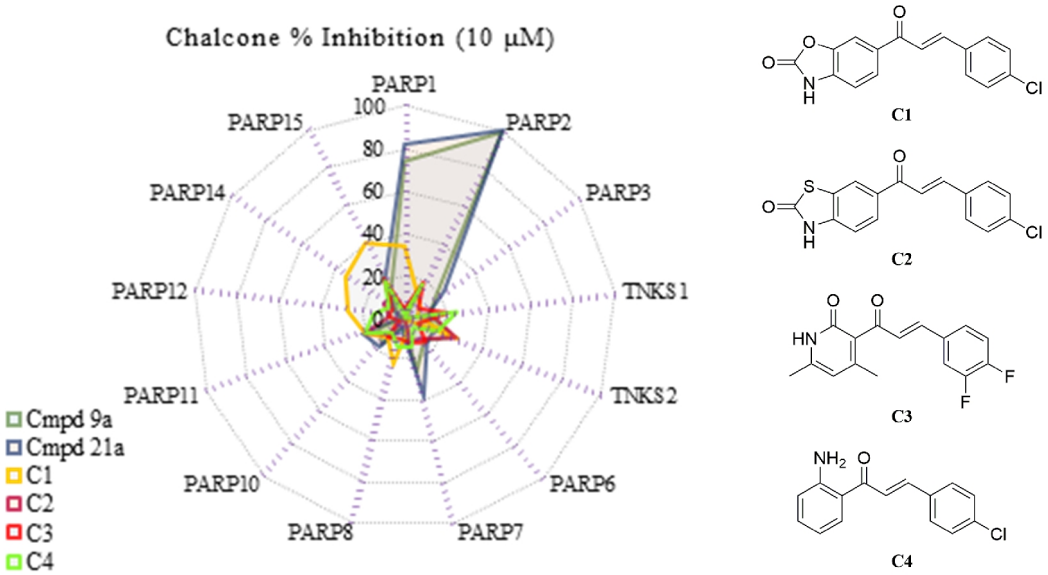



**Figure 4.5. PARP isoform selectivity for a chalcones series (C1–C4).** Percent inhibition determined by a single point assay at 10 μM against all available PARP isoforms. **9a** and **21a** are included for comparison. Chalcones synthesized by Mr. Alexander Hawes.

### *4.2.4 PARP Trapping and Isoform-selective Inhibitors*

We always assess the inhibitory potential of any PARP inhibitor with $IC_{50}$ or $EC_{50}$ values, which assesses the ligand's potency with respect to the $NAD^+$ catalytic domain. Recently, Murari et al. demonstrated that PARP inhibitors not only bind to the $NAD^+$ site, but also increase PARP-DNA binding, which is referred to as PARP trapping.[3] Despite the similar PARP1 $IC_{50}$ values of olaparib (5 nM), niraparib (3.8 nM), and veliparib (5.2 nM) (**Figure 1.4**), olaparib and niraparib are more toxic to HR-deficient cells than veliparib. Olaparib and niraparib can trap PARP1/2 at

the DNA damaged sites, which leads to increased cytotoxicity and aids in explaining their increased potency to HR-deficient cells.[3,4] The inhibitor's ability to trap the PARP-DNA complexes directly correlates to the inhibitory efficiency of HR-deficient cells. We determined the PARP1trapping efficiency of the benzyl TPAP derivative **21e**, which unfortunately does not trap PARP1 <10 μM ($IC_{50}$ = 178 nM).[1] PARPtrapping of known inhibitors tend to show higher $EC_{50}$ values when compared to the catalytic inhibitory values, so PARP1trapping of the benzyl TPAP **21e** in the μM range was expected;[1] however, since **21e** shows good selectivity for PARP2, it remains to be seen if there is any significant PARP2trapping effect. Future studies will explore the structural features of a ligand and its relationship with PARPtrapping and PARP2trapping potency.

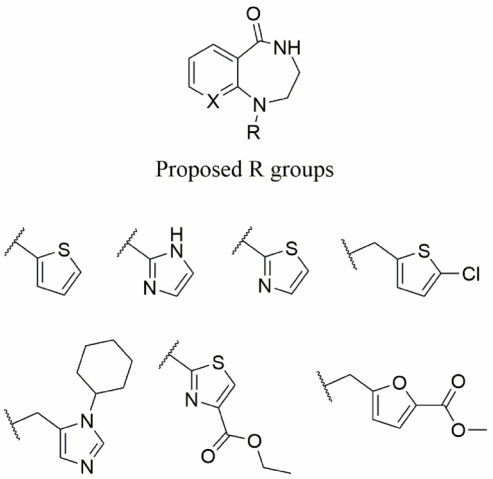


**Figure 4.6. Proposed TAAP analogues.** All proposed **C** rings are commercially available as aryl halides or alkyl halides.

In addition to evaluating the activity of the previously synthesized TAAP derivatives with PARP-DNA complexes, future work will consist of further **9a** and **21a** derivatizations. Future **9a** and **21a** derivatives will include alkylation with various aryl-based R groups, as well as the introduction of additional heteroatoms to promote hydrogen bonding with the water molecule and the glutamate residue lining the PARP1 pocket to enhance potency (**Figure 4.6**). Recently Schüler et al. explored the promiscuity in PARP inhibitors and found the more selective veliparib and niraparib interact with the carboxyl side chains lining the PARP1 and PARP2 pockets, which are not conserved in any other PARP isoform.[5] Thus, modifying the benzyl TAAP analogues at either the meta- or para-positions with basic moieties may increase potency and PARP1/2 selectivity. Potential basic substituents would include amines, azetidines, and pyrrolidines. We hope that with more

derivatives and further modifications that we can develop the TAAP scaffold into a series of PARP-selective inhibitors.

4.3 References

(1) BPSBiosciences, Inc. 6042 Cornerstone Court West, Suite B, San Diego, CA 92121 USA. http://bpsbioscience.com.

(2) Nitulescu, G. M.; Margina, D.; Juzenas, P.; Peng, Q.; Olaru, O. T.; Saloustros, E.; Fenga, C.; Spandidos, D. A.; Libra, M.; Tsatsakis, A. M. Akt inhibitors in cancer treatment: the long journey from drug discovery to clinical use (Review). *Int. J. Oncol.* **2016**, *48*, 869.

(3) Murai, J.; Huang, S.-y. N.; Das, B. B.; Renaud, A.; Zhang, Y.; Doroshow, J. H.; Ji, J.; Takeda, S.; Pommier, Y. Trapping of PARP1 and PARP2 by clinical PARP inhibitors. *Cancer Res.* **2012**, *72*, 5588.

(4) Bouwman, P.; Jonkers, J. Molecular pathways: how can BRCA-mutated tumors become resistant to PARP inhibitors? *Clin. Cancer Res.* **2014**, *20*, 540.

(5) Thorsell, A.-G.; Ekblad, T.; Karlberg, T.; Löw, M.; Pinto, A. F.; Trésaugues, L.; Moche, M.; Cohen, M. S.; Schüler, H. Structural basis for potency and promiscuity in poly(ADP-ribose) polymerase (PARP) and tankyrase inhibitors. *J. Med. Chem.* **2017**, *60*, 1262.

# APPENDIX A: ABBREVIATIONS

| | |
|---|---|
| PARP | Poly-(ADP-ribosyl) polymerase |
| PI3K | Phosphoinositide-kinase |
| Akt | Protein kinase B |
| mTor | Mechanistic target of rapamycin |
| CDK | Cyclin-dependent kinase |
| CHK | Check-point kinase |
| TAAP | Tetrahydroarylazepinone |
| TBAP | 1,2,3,4-tetrahydro-5*H*-benzo[*e*][1,4]-diazepine-5-one |
| TPAP | 1,2,3,4-tetrahydro-5*H*-pyrido[2,3-*e*][1,4]-diazepine-5-one |
| NMR | Nuclear magnetic resonance |
| BRCA | Breast cancer associated gene |
| TNBC | Triple negative breast cancer |
| PPA | Polyphosphoric acid |
| HRMS | High-resolution mass spectrometry |
| HPLC | High-performance liquid chromatography |
| DNA | Deoxyribonucleic acid |
| HR | Homologous recombination |
| BER | Base excision repair |
| $NAD^+$ | Nicotinamide adenine dinucleotide |
| ADP | Adenosine diphosphate |
| ART | ADP-ribosyltransferase |
| TNKS | Tankyrases |
| ER | Estrogen receptor |
| PR | Progesterone receptor |
| HER2 | Human epithelial growth factor receptor |
| PFS | Progression-free survival |
| OS | Overall survivial |
| S | DNA synthesis |
| G2 | Second gap |
| M | Mitosis |
| ATP | Adenosine triphosphate |
| PDB | Protein data bank |
| HMD | Hymenialdisine |
| ELISA | Enzyme-linked immunosorbent assay |
| EDC | *N*-(3-dimethylaminopropyl)-*N*'-ethylcarbodiimide |
| 6-Cl-HOBt | 1-Hydroxyl-6-chloro-benzotriazole |
| DCM | Dichloromethane |
| RT | Room temperature |
| EtOH | Ethanol |
| DA | Dihedral angle |
| TEAA | Triethylammonium acetate |
| SAR | Structure activity relationship |
| THF | Tetrahydrofuran |
| DCB | Dichlorobenzene |

| | |
|---|---|
| SET | Single electron transfer |
| TMSCl | Trimethylsilyl chloride |
| DCE | 1,2-dichloroethane |
| DMSO | Dimethyl sulfoxide |
| MeCN | Acetonitrile |
| TFA | Trifluoroacetic acid |
| $TMSN_3$ | Trimethylsilyl azide |

# APPENDIX B: INVENTORY OF COMPOUNDS

**Chapter 2**

| Compound | Amount* | Concentration/Volume | Location (Solids) | Location (Liquids) |
|---|---|---|---|---|
| 2 | 3 mg | 10 mM/500 μL | HHS 3023 | Dav 156B |
| 5 | 16 mg | 10 mM/1 mL | HHS 3023 | Dav 156B |
| 6 | 36 mg | 10 mM/400 μL | HHS 3023 | Dav 156B |
| 7 | 60 mg | 10 mM/500 μL | HHS 3023 | Dav 156B |
| 8 | 191 mg | 10 mM/700 μL | HHS 3023 | Dav 156B |
| 9a | 480 mg | 10 mM/500 μL | HHS 3023 | Dav 156B |
| 9b | 17.5 mg | 10 mM/100 μL | HHS 3023 | Dav 156B |
| 9c | 3 mg | 10 mM/200 μL | HHS 3023 | Dav 156B |
| 9d | 2 mg | 10 mM/300 μL | HHS 3023 | Dav 156B |
| 9e | 21 mg | 10 mM/700 μL | HHS 3023 | Dav 156B |
| 9f | 50 mg | 10 mM/200 μL | HHS 3023 | Dav 156B |
| 9g | 1 mg | 10mM/200 μL | HHS 3023 | Dav 156B |
| 9h | - | 10 mM/300 μL | - | Dav 156B |
| 9i | 20 mg | 10 mM/2 mL | HHS 3023 | Dav 156B |
| 21a | 6 mg | 10 mM/100 μL | HHS 3023 | Dav 156B |
| 21b | - | 10 mM/300 μL | - | Dav 156B |
| 21c | - | 10 mM/100 μL | - | Dav 156B |
| 21d | 23 mg | 10 mM/100 μL | HHS 3023 | Dav 156B |
| 21e | 1 mg | 10 mM/20 μL | HHS 3023 | Dav 156B |

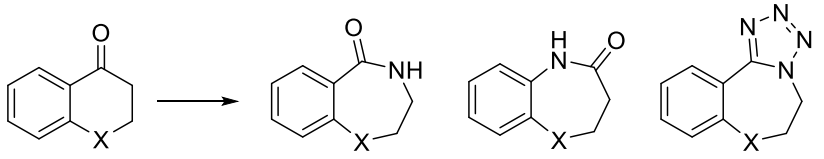
TAAP Derivatives are stored either in the HHS 3023 fridge or Dav 156B freezer (−20°C)
*Will be reweighed into amber vials with Teflon lined caps for final submission.

**Chapter 3**

| Compound | Amount | Location |
|---|---|---|
| 1a | 0.875 g | HHS 3023 |
| 1b | 0.300 g | HHS 3023 |
| 2a | 0.160 g | HHS 3023 |
| 2b | 0.050 g | HHS 3023 |
| 5 | 0.30 g | HHS 3023 |
| 6a | 0.220 g | HHS 3023 |
| 6b | 0.630 g | HHS 3023 |
| 6c | 2 mg | HHS 3023 |
| 6d | 0.165 g | HHS 3023 |
| 8 | Unstable | - |

Chapter 3 intermediates are stored in HHS 3023 in a box labeled “Chap 3 Intermediates” in Kiaya’s drawer.

# APPENDIX C: SCHMIDT REACTION CONDITIONS



**1** **2a** **2b** **2c**

| Entry | X | Scale (mmol) | Acid | Azide | 2a | 2b | 2c |
|---|---|---|---|---|---|---|---|
| 1 | N | 0.3 | TFA | $TMSN_3$ | 20% | - | V |
| 2* | N | 1.0 | TFA | $TMSN_3$ | 6% | - | - |
| 3 | $CH_2$ | 1.0 | TFA | $TMSN_3$ | 3% | 23% | - |
| 4 | N | 1.0 | HCl | $NaN_3$ | NI | ND | ND |
| 5 | $CH_2$ | 1.0 | HCl | $NaN_3$ | 39% | ND | ND |
| 6 | $CH_2$ | 10.0 | HCl | $NaN_3$ | 49% | ND | ND |
| 7 | O | 2.0 | $H_2SO_4$ | $NaN_3$ | 60% | - | - |
| 8 | N | 1.6 | $H_2SO_4$ | $NaN_3$ | 63% | 23% | - |

**Table 1.** The effect that acid and azide choice has on the Schmidt reaction product ratio. Acids: trifluoroacetic acid (TFA), concentrated hydrochloric acid, concentrated sulfuric acid. Azides: trimethylsilyl azide ($TMSN_3$), sodium azide. *Entry 2: 80% of unreacted starting material was recovered. V: variable; ND: not determined; NI: non-isolatable product.

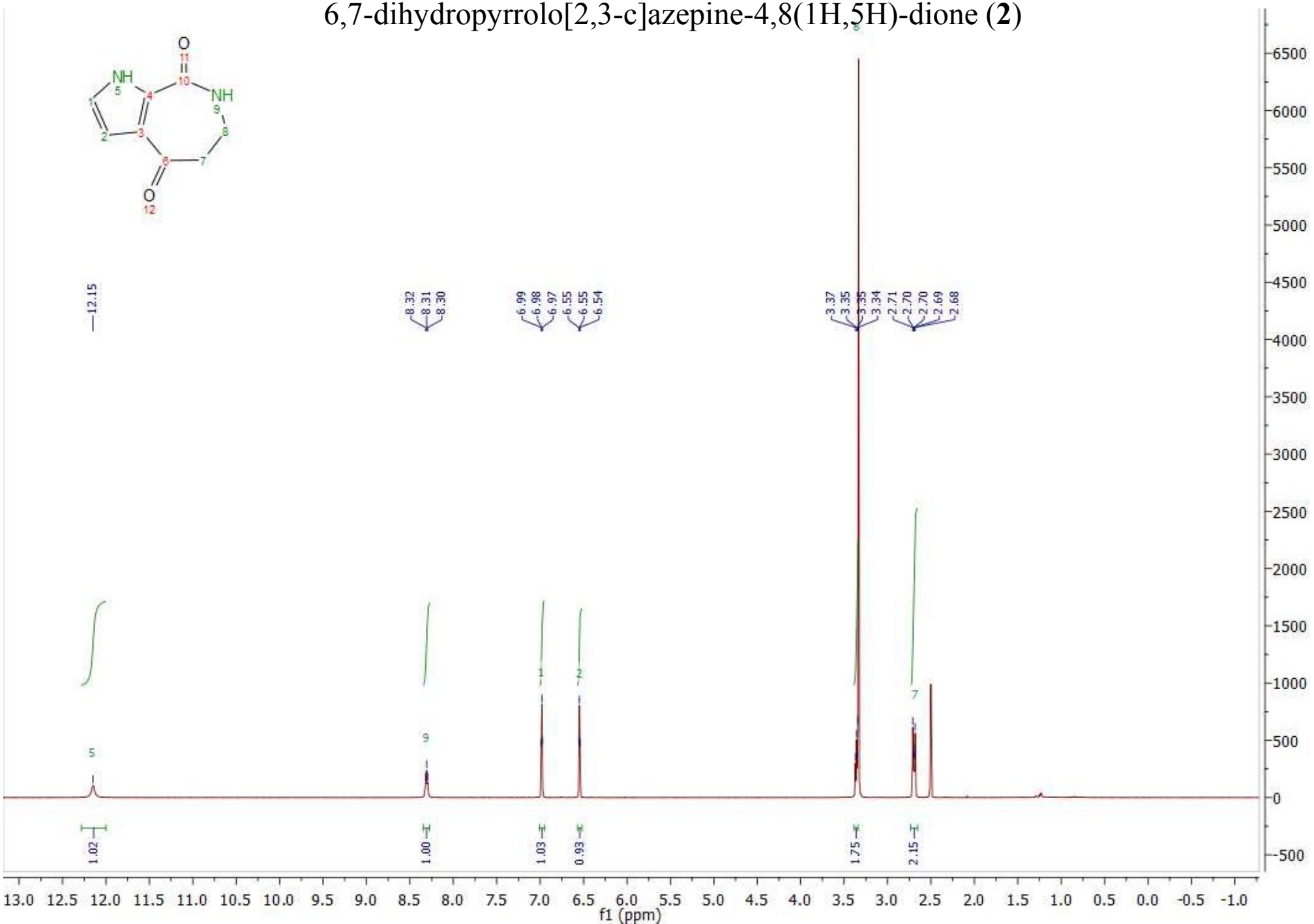
Treating **1** X = C with concentrated hydrochloric acid and sodium azide (2 eq) yielded the desired product **2a** X = C in majority without complications (entries 5 and 6); however, under the same conditions (entry 4), **1** X = N yielded the constitutional isomer of **2a** X = N (**2b**), the tetrazole **2c**, and no detectable amount of the desired product **2a** via TLC.

Initial attempts to synthesize **2a** X = N began with treating **1** X = N with TFA and $TMSN_3$ (entries 1 and 2), which yielded the desired product and various amounts of the tetrazole **2c**. The product ratio of **2a**:**2c** depended on the $TMSN_3$ rate of addition, the reaction temperature, the overall reaction concentration, the concentration of $TMSN_3$ addition, and the stoichiometry of $TMSN_3$. Two equivalents of $TMSN_3$ yielded **2c** almost exclusively, while one equivalent of $TMSN_3$ yielded majority starting material and **2a** as the major product. Since the polarity of the starting material and the product is significantly different, the starting material was easily recovered by column chromatography. When the reaction with TFA/$TMSN_3$ (1.0 eq) and **1** X = N is performed on a small scale (<1.0 mmol), the desired product **2a** was isolated in yields from 20–40%; however, when the reaction is performed on a larger scale (>1.0 mmol), the desired product **2a** was isolated in yields less than 10%. Interestingly, treating **1** X = C with TFA and $TMSN_3$ yielded **2b** in majority, **2a** in minority (entry 3). For entry 3, **2c** was visualized via TLC but was yielded in such small amounts that the tetrazole was not isolated via column chromatography. In addition, the use of concentrated sulfuric acid with sodium azide (2 eq) yielded **2a** (X = N) in majority in better yields than the TFA/$TMSN_3$ procedure and yielded the constitutional isomer **2b** (entry 8). With the same procedure, when X = O, the desired product **2a** was the only product observed (entry 7).

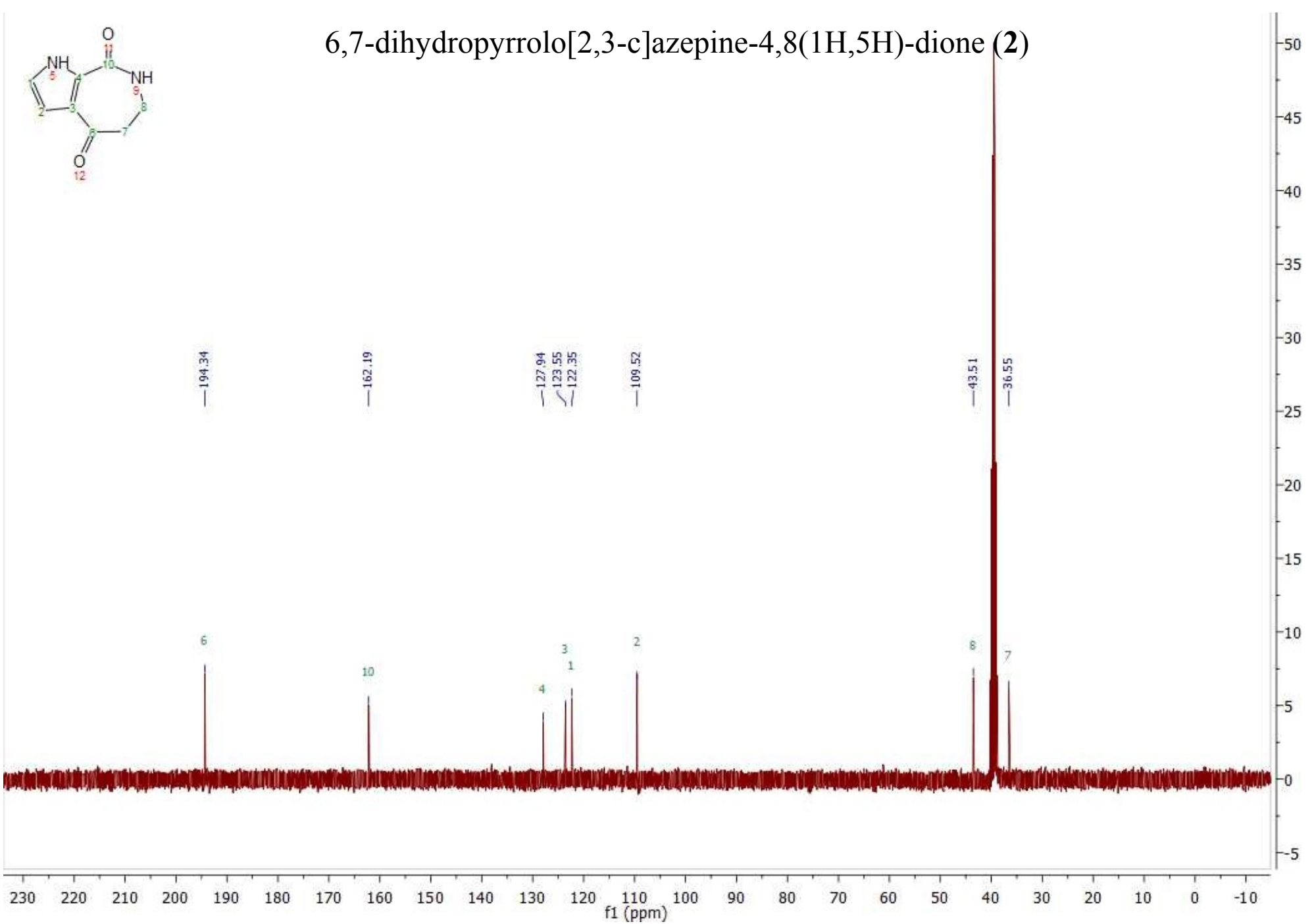
# APPENDIX D: NUCLEAR MAGNETIC RESONANCE (NMR) SPECTRA

# CHAPTER 2 SPECTRA

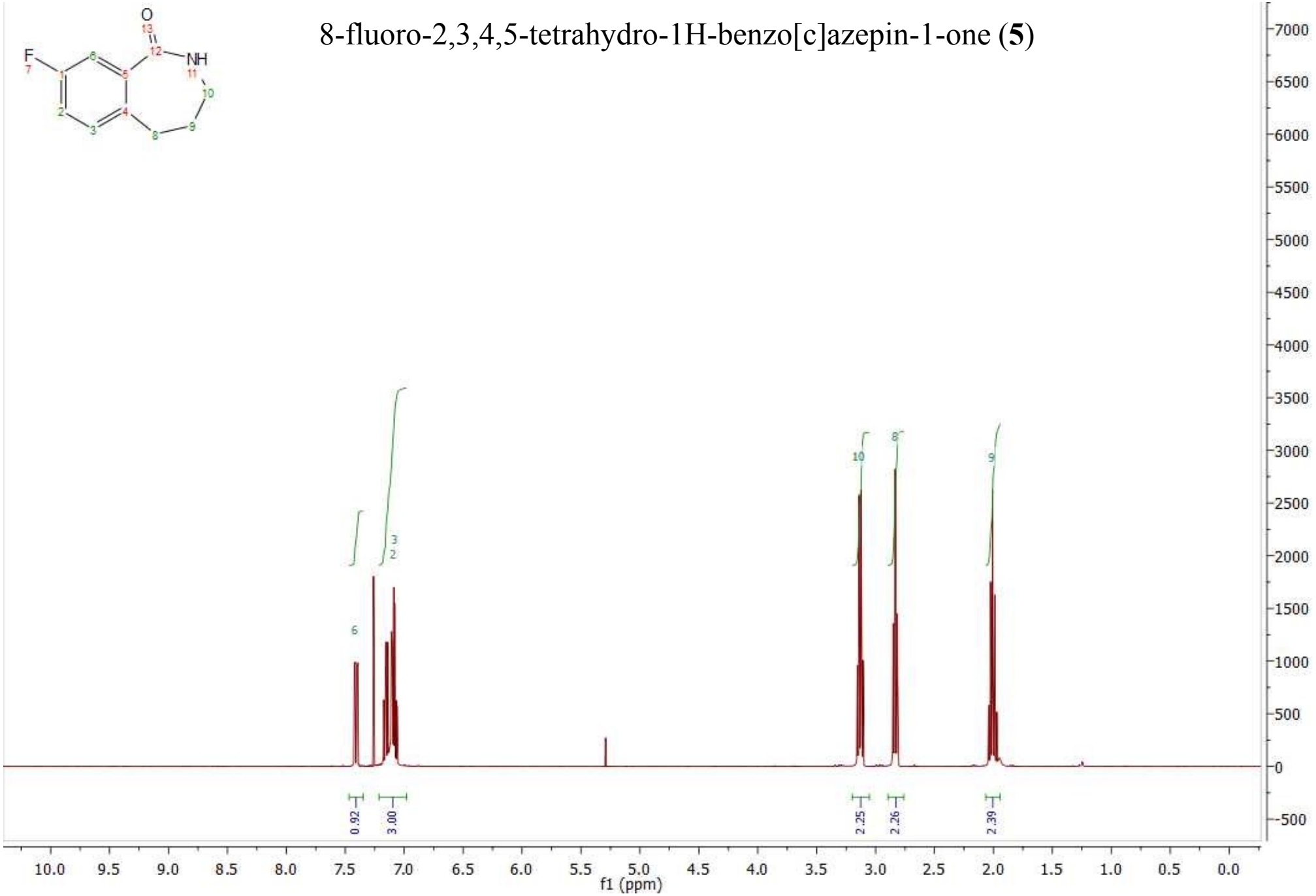
6,7-dihydropyrrolo[2,3-c]azepine-4,8(1H,5H)-dione (**2**)



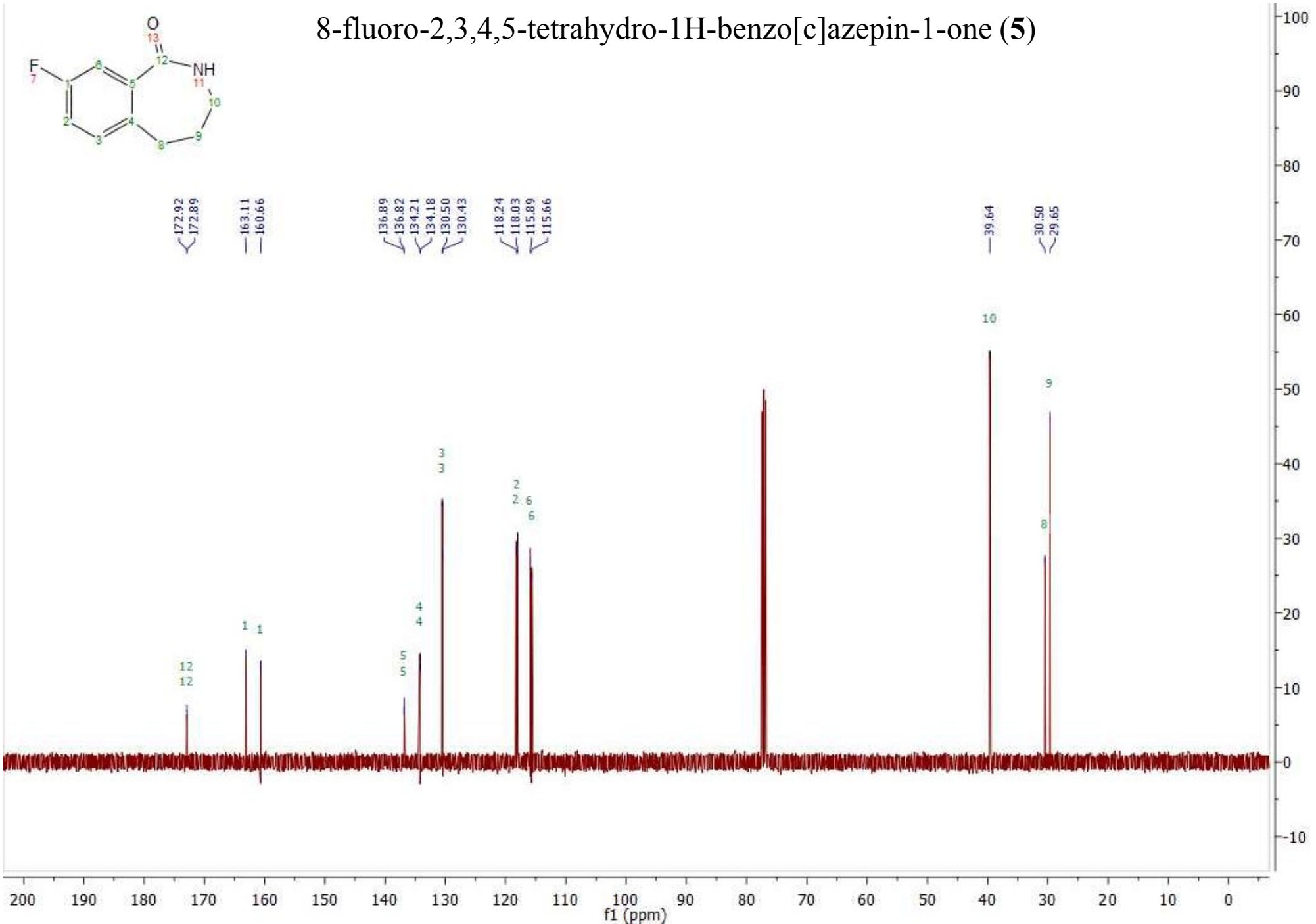
6,7-dihydropyrrolo[2,3-c]azepine-4,8(1H,5H)-dione (**2**)



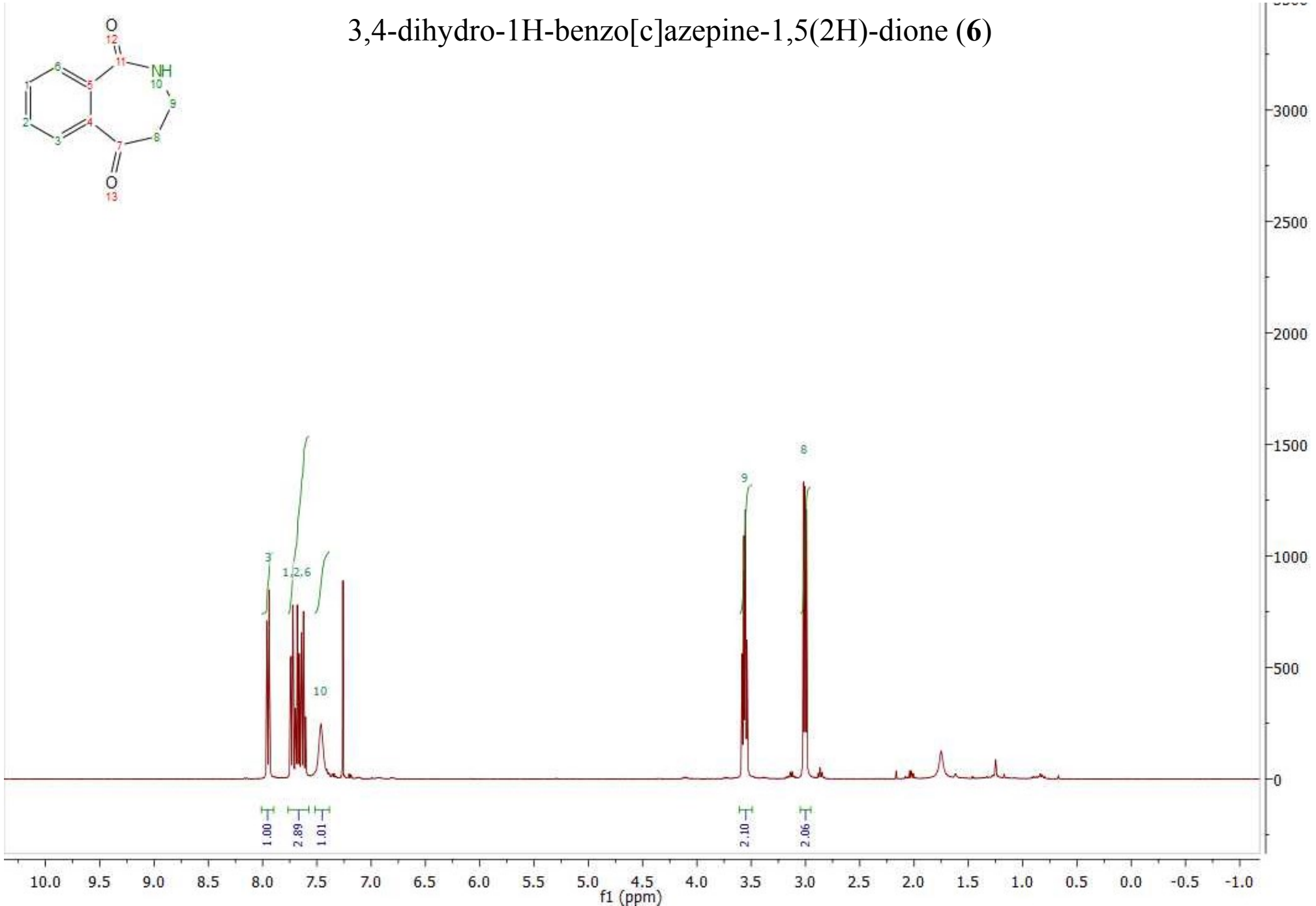
8-fluoro-2,3,4,5-tetrahydro-1H-benzo[c]azepin-1-one (**5**)



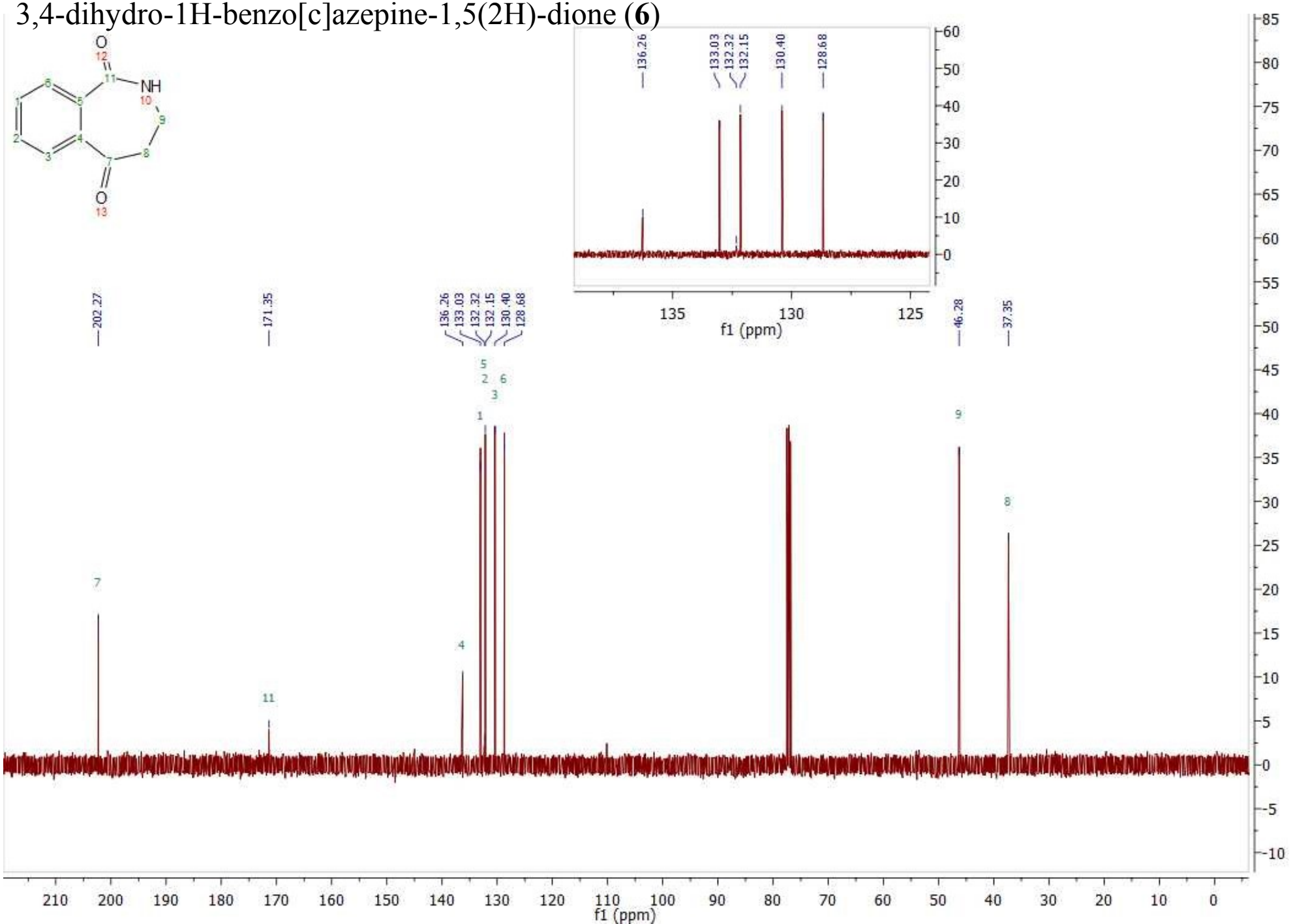
8-fluoro-2,3,4,5-tetrahydro-1H-benzo[c]azepin-1-one (**5**)



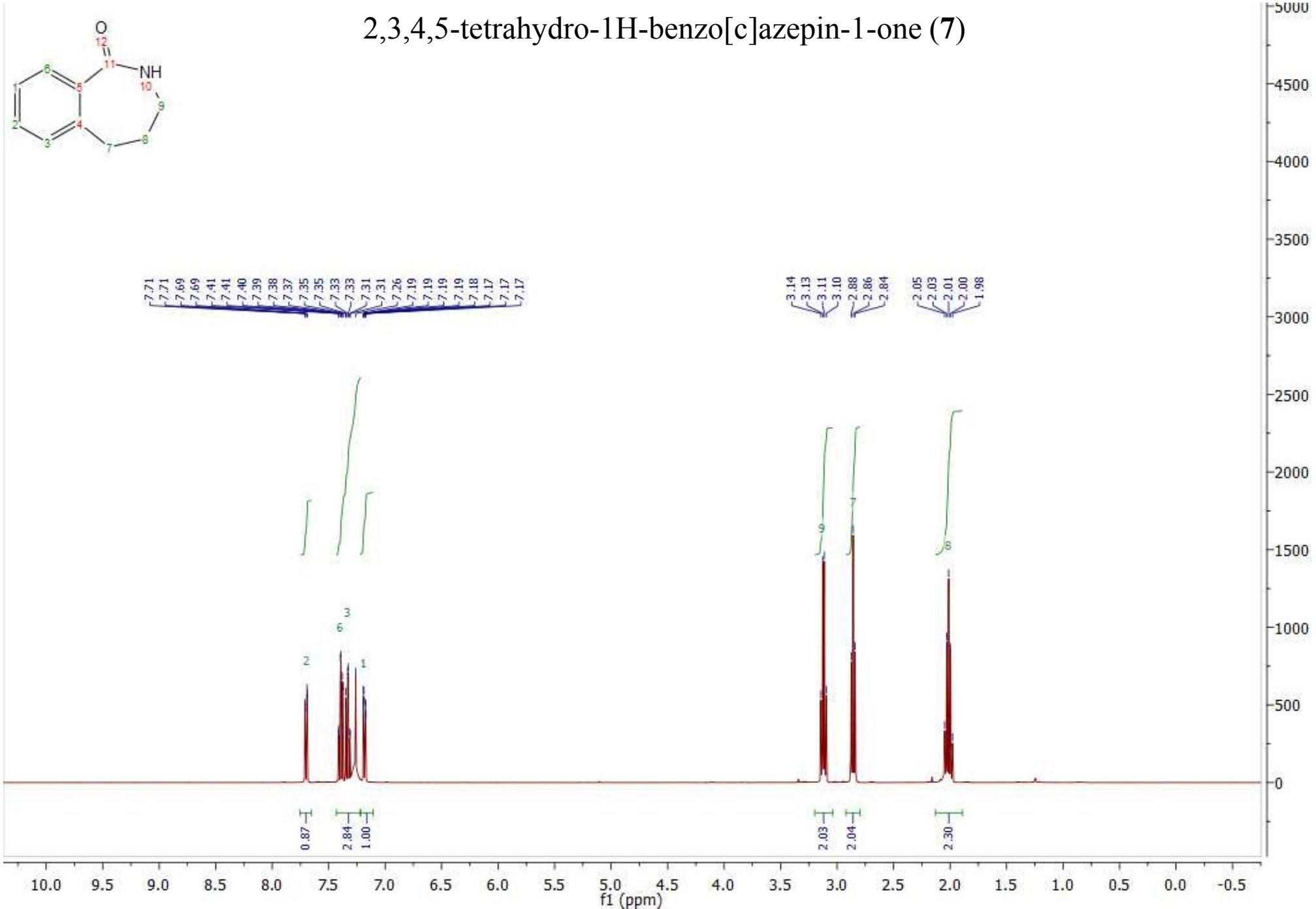
3,4-dihydro-1H-benzo[c]azepine-1,5(2H)-dione (**6**)



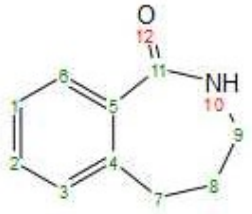
3,4-dihydro-1H-benzo[c]azepine-1,5(2H)-dione (**6**)

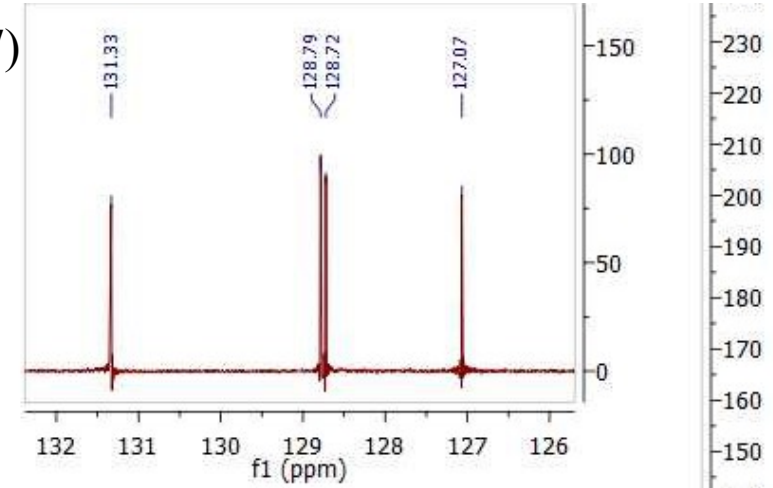


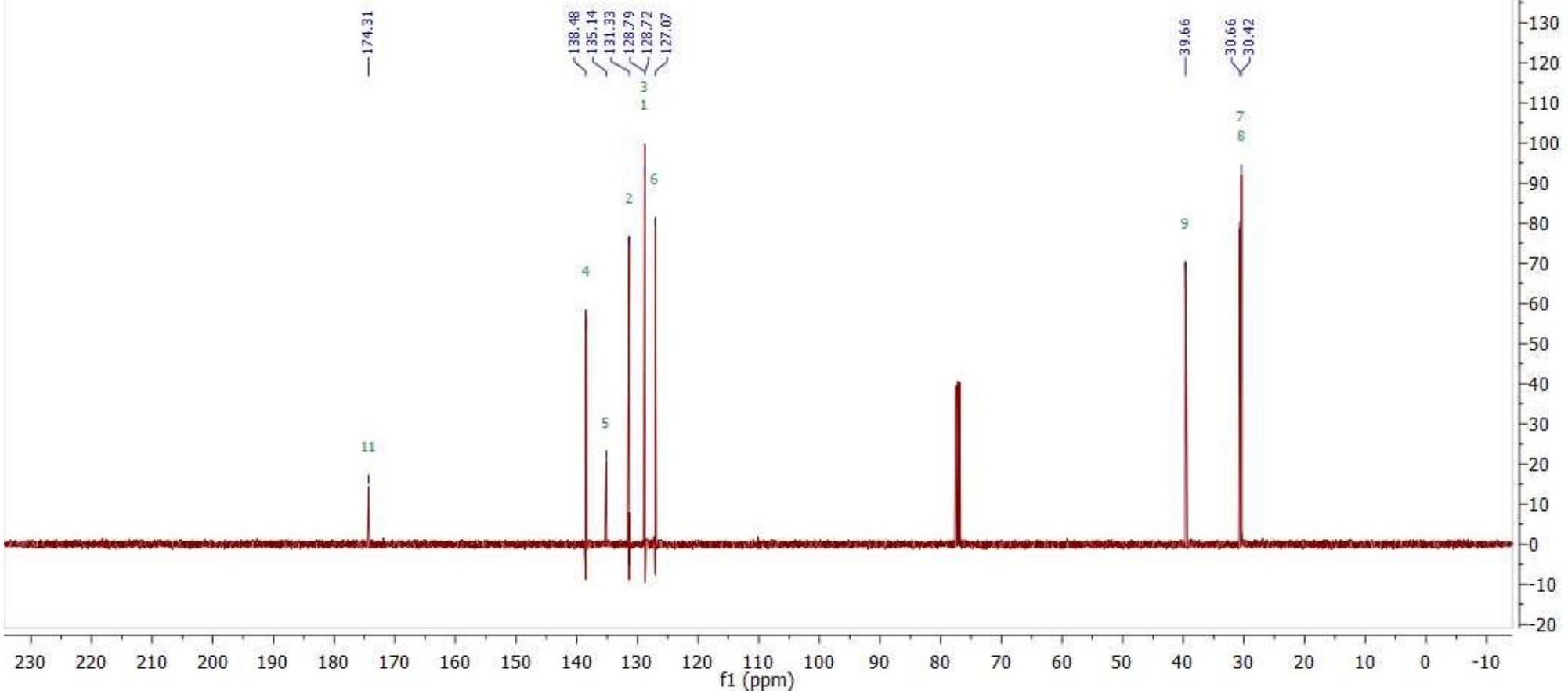
2,3,4,5-tetrahydro-1H-benzo[c]azepin-1-one (**7**)



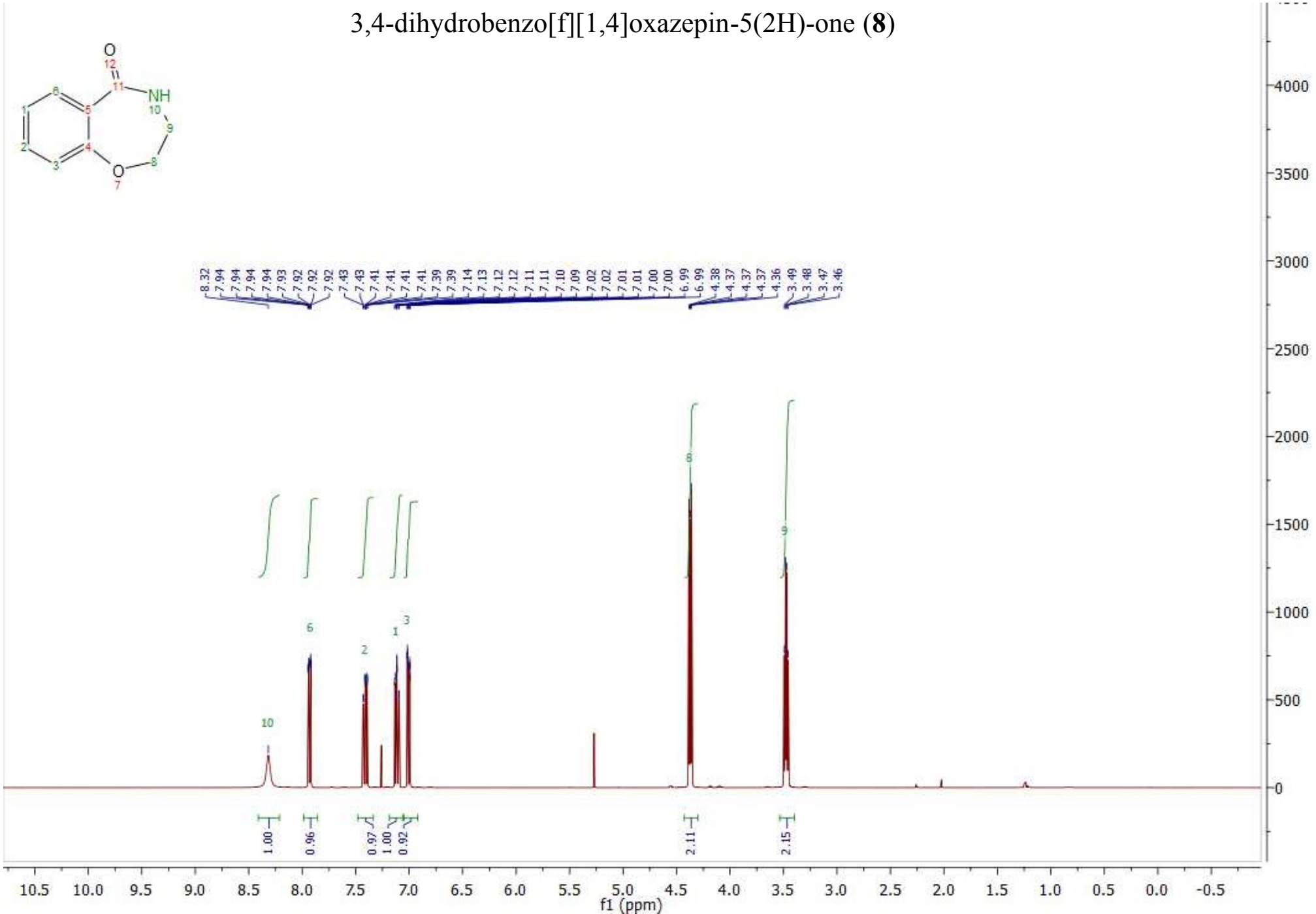
2,3,4,5-tetrahydro-1H-benzo[c]azepin-1-one (**7**)



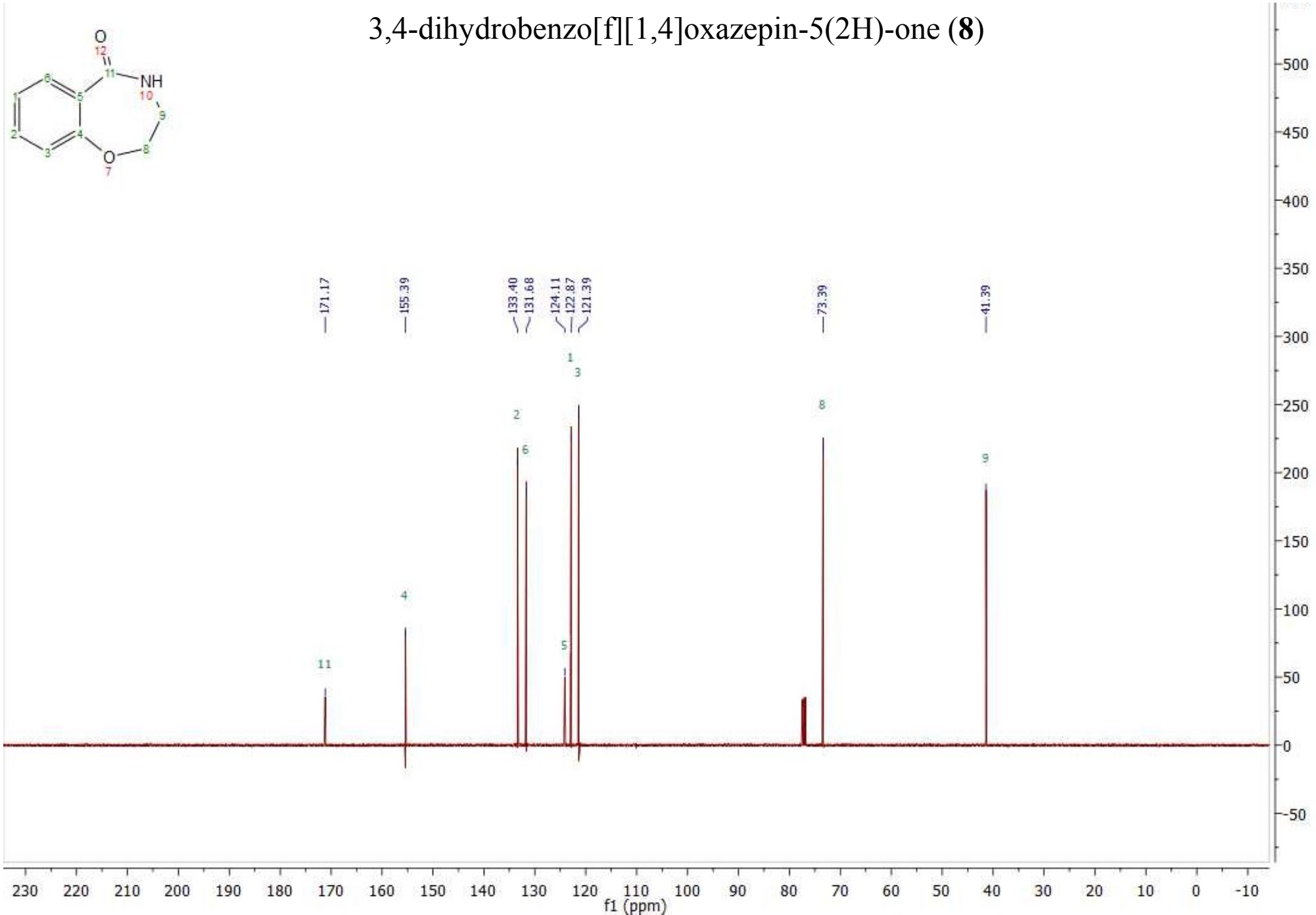



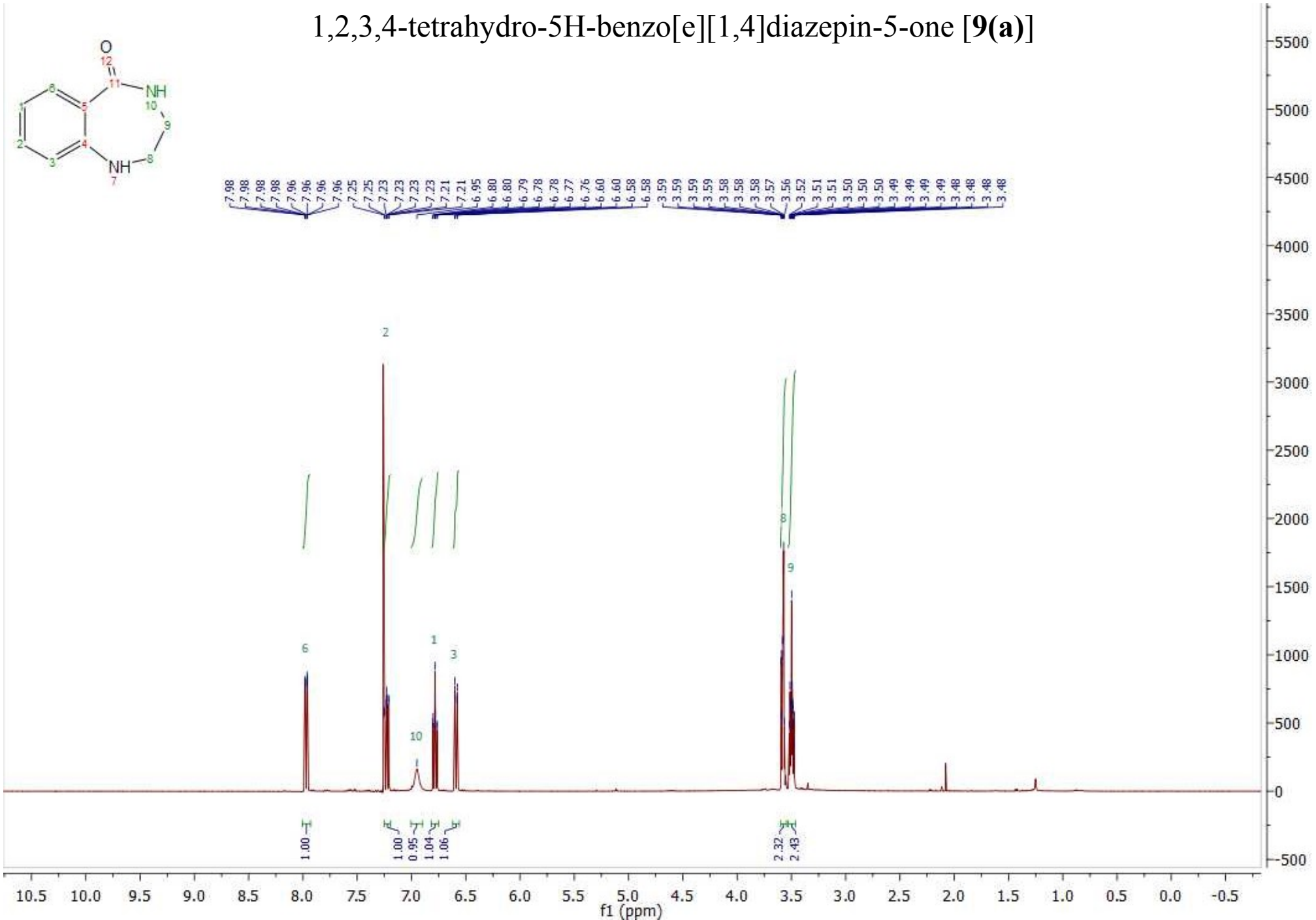
3,4-dihydrobenzo[f][1,4]oxazepin-5(2H)-one (**8**)



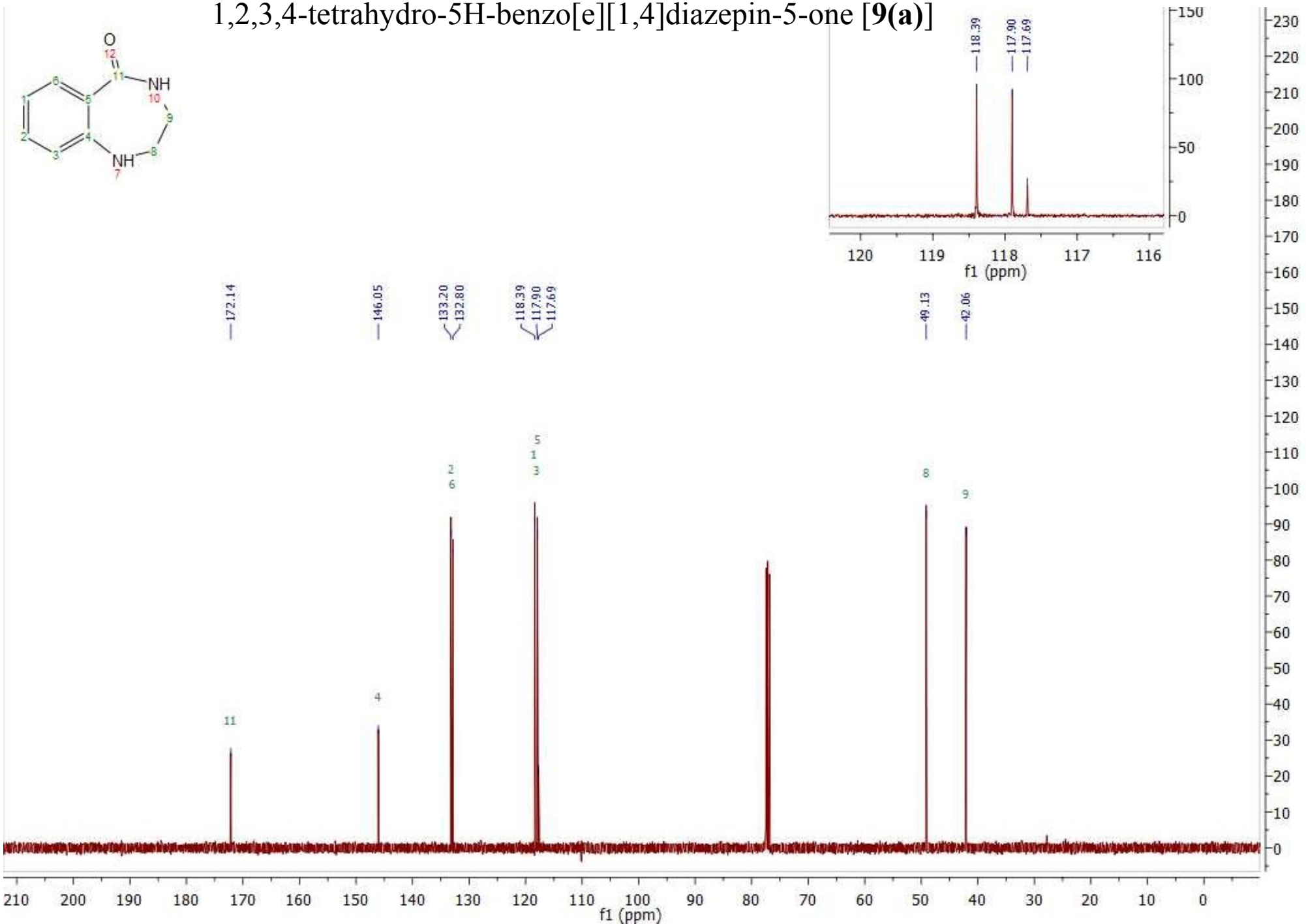
3,4-dihydrobenzo[f][1,4]oxazepin-5(2H)-one (**8**)



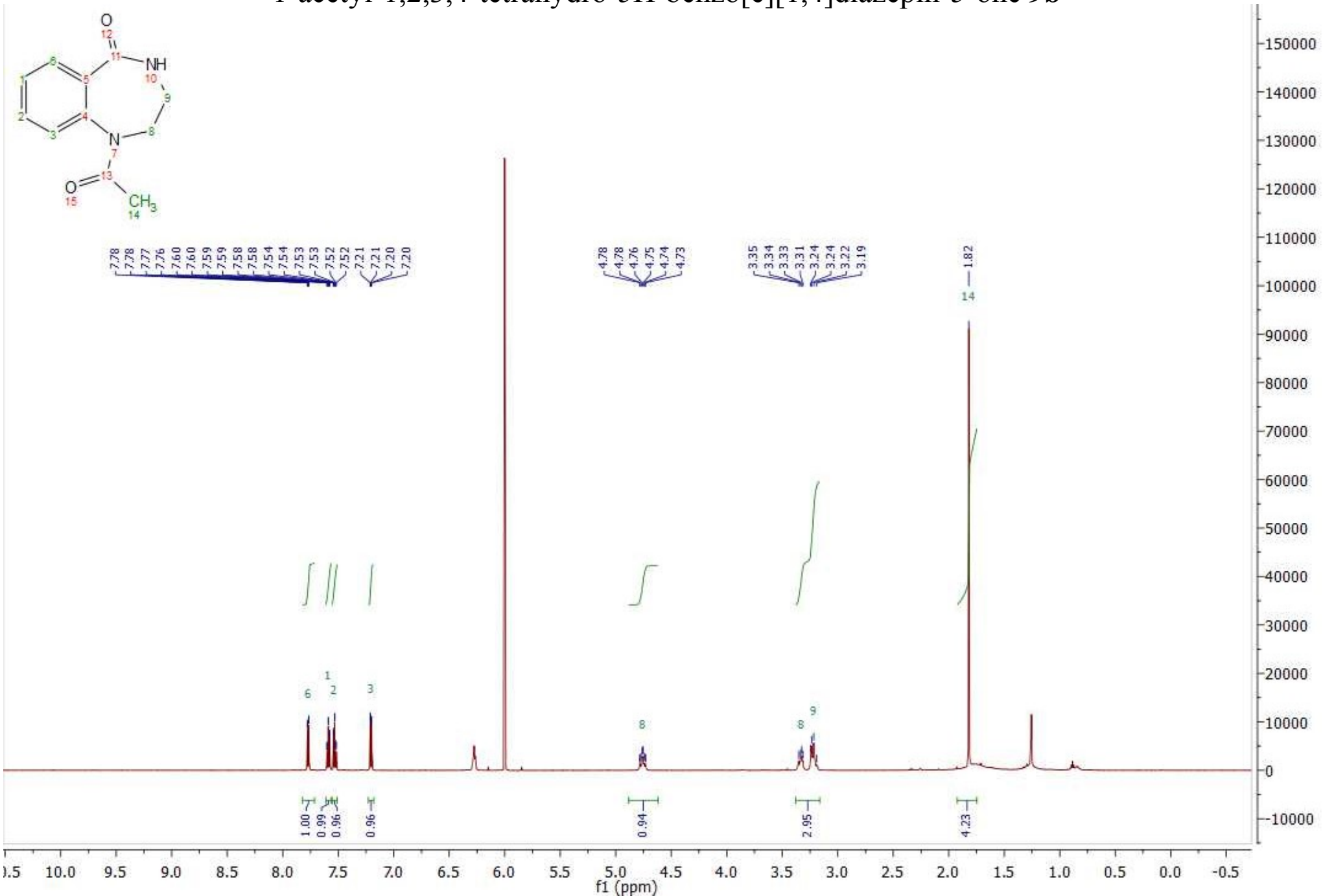
1,2,3,4-tetrahydro-5H-benzo[e][1,4]diazepin-5-one [**9(a)**]



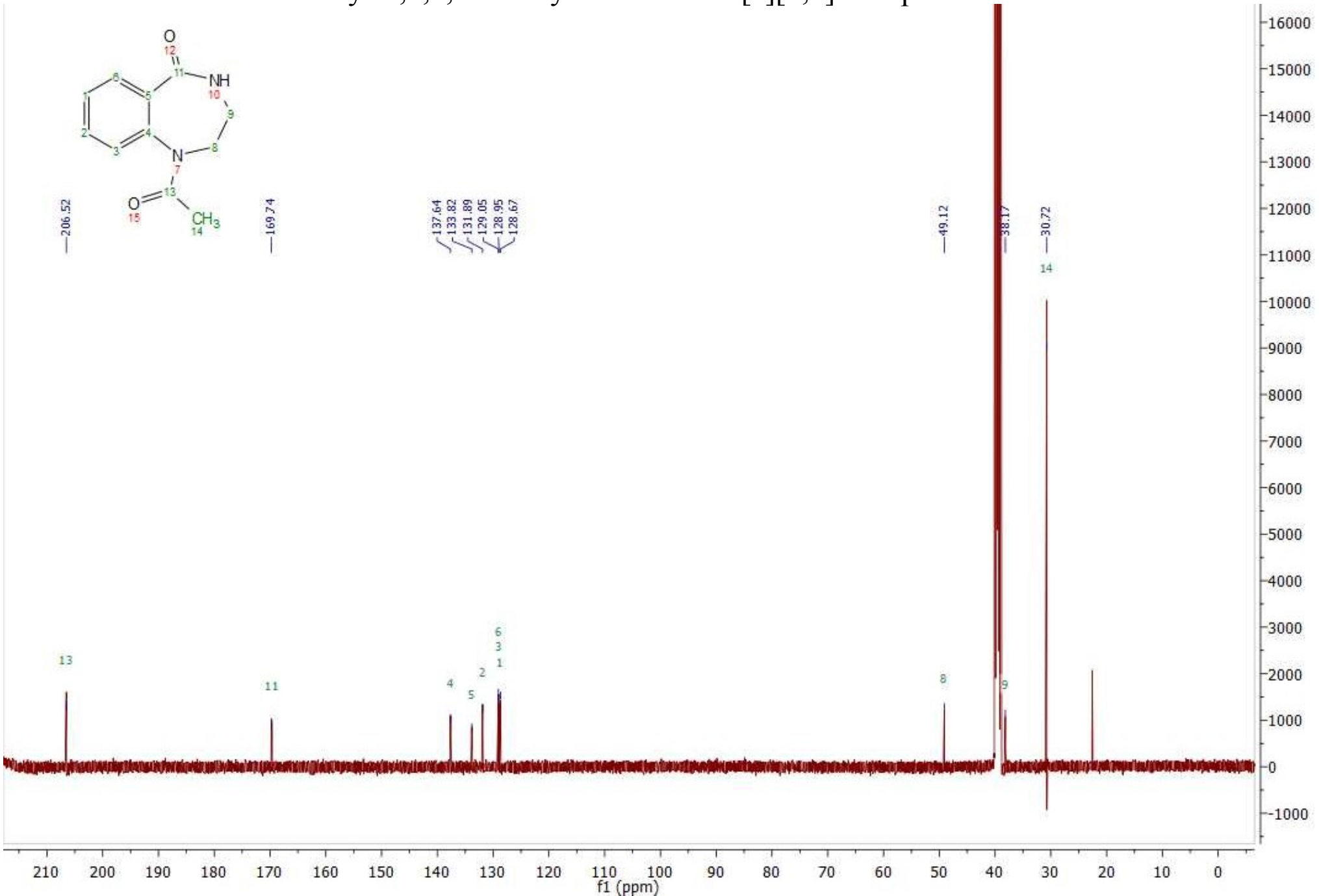
1,2,3,4-tetrahydro-5H-benzo[e][1,4]diazepin-5-one [**9(a)**]



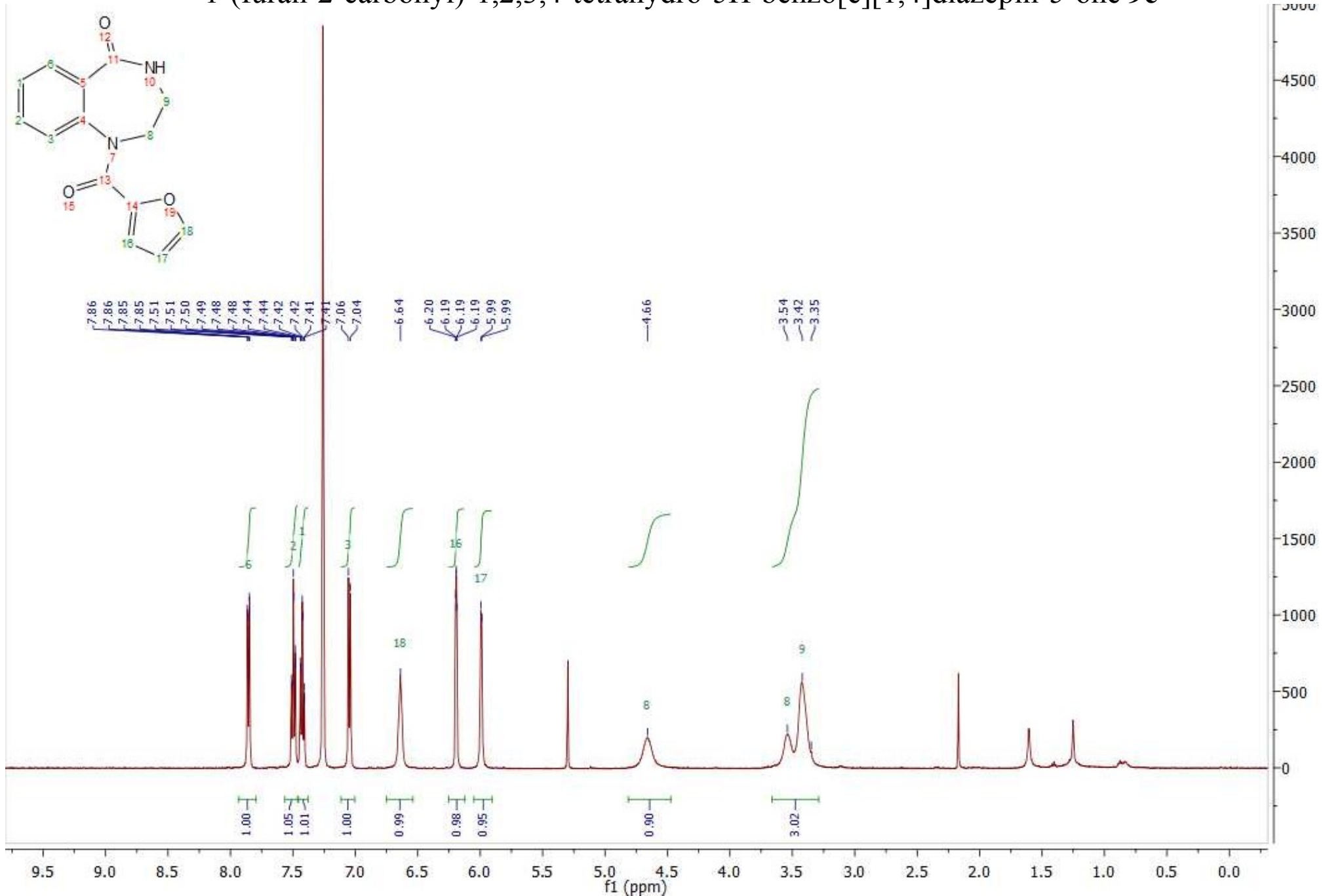
1-acetyl-1,2,3,4-tetrahydro-5H-benzo[e][1,4]diazepin-5-one **9b**



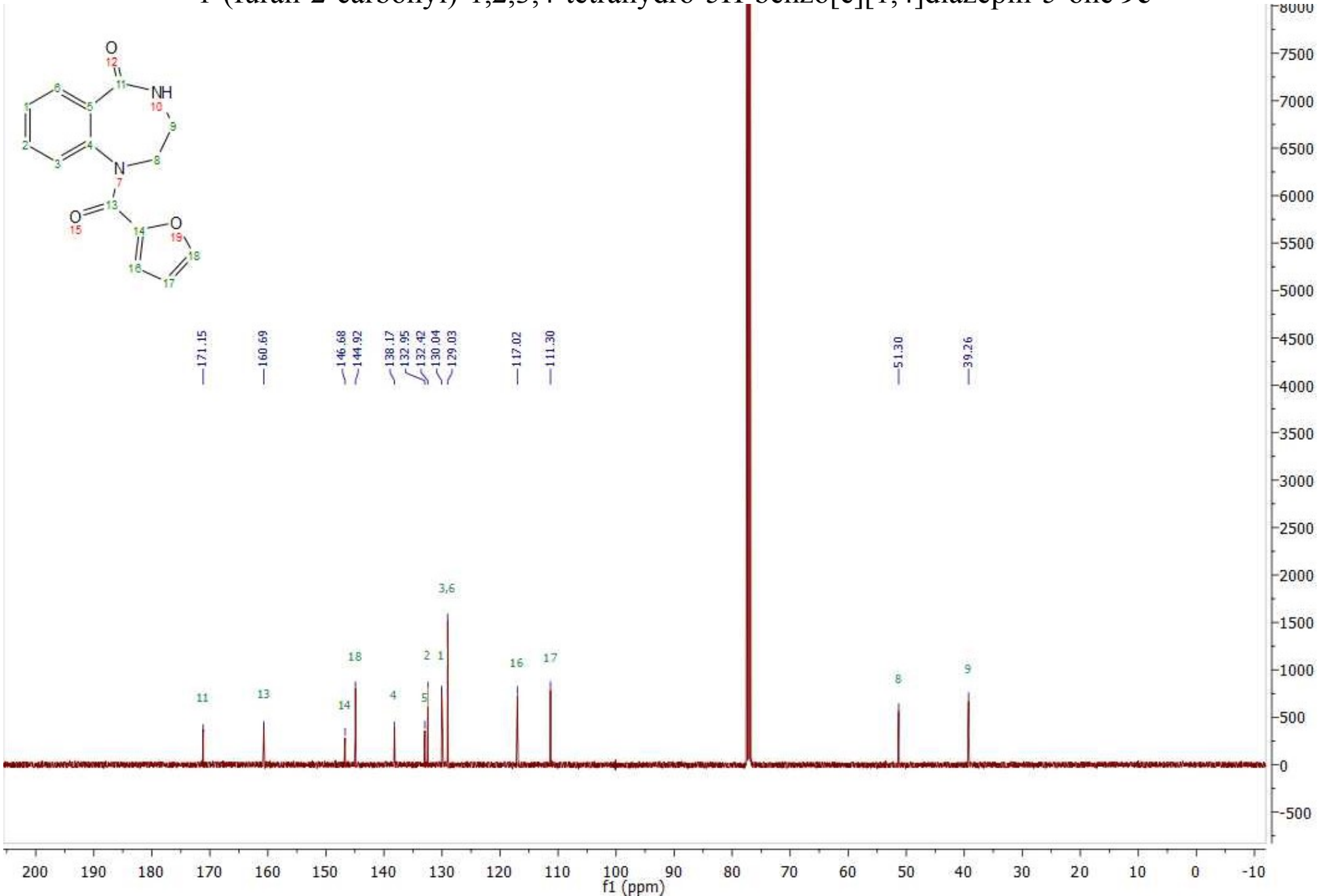
1-acetyl-1,2,3,4-tetrahydro-5H-benzo[e][1,4]diazepin-5-one **9b**



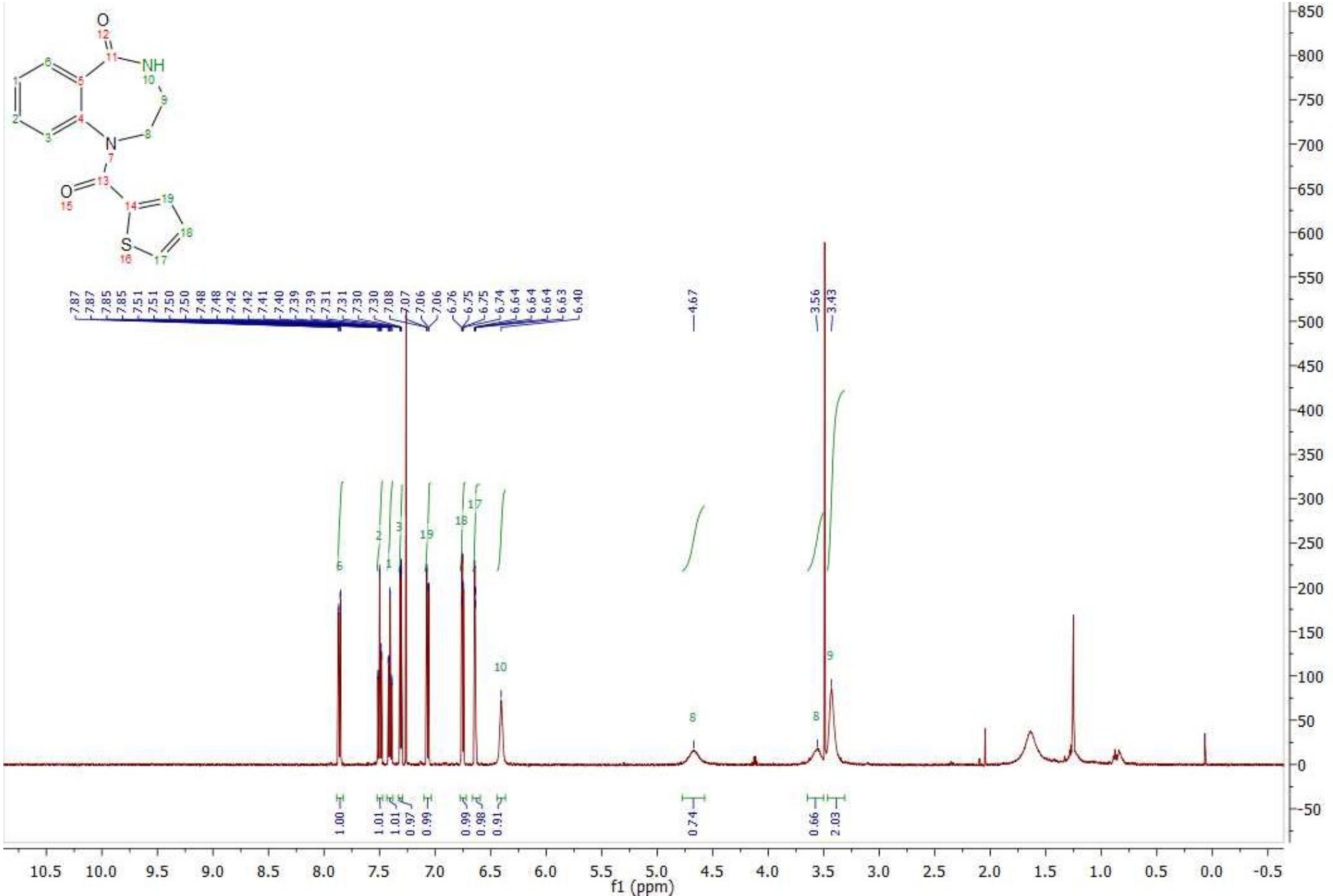
1-(furan-2-carbonyl)-1,2,3,4-tetrahydro-5H-benzo[e][1,4]diazepin-5-one **9c**



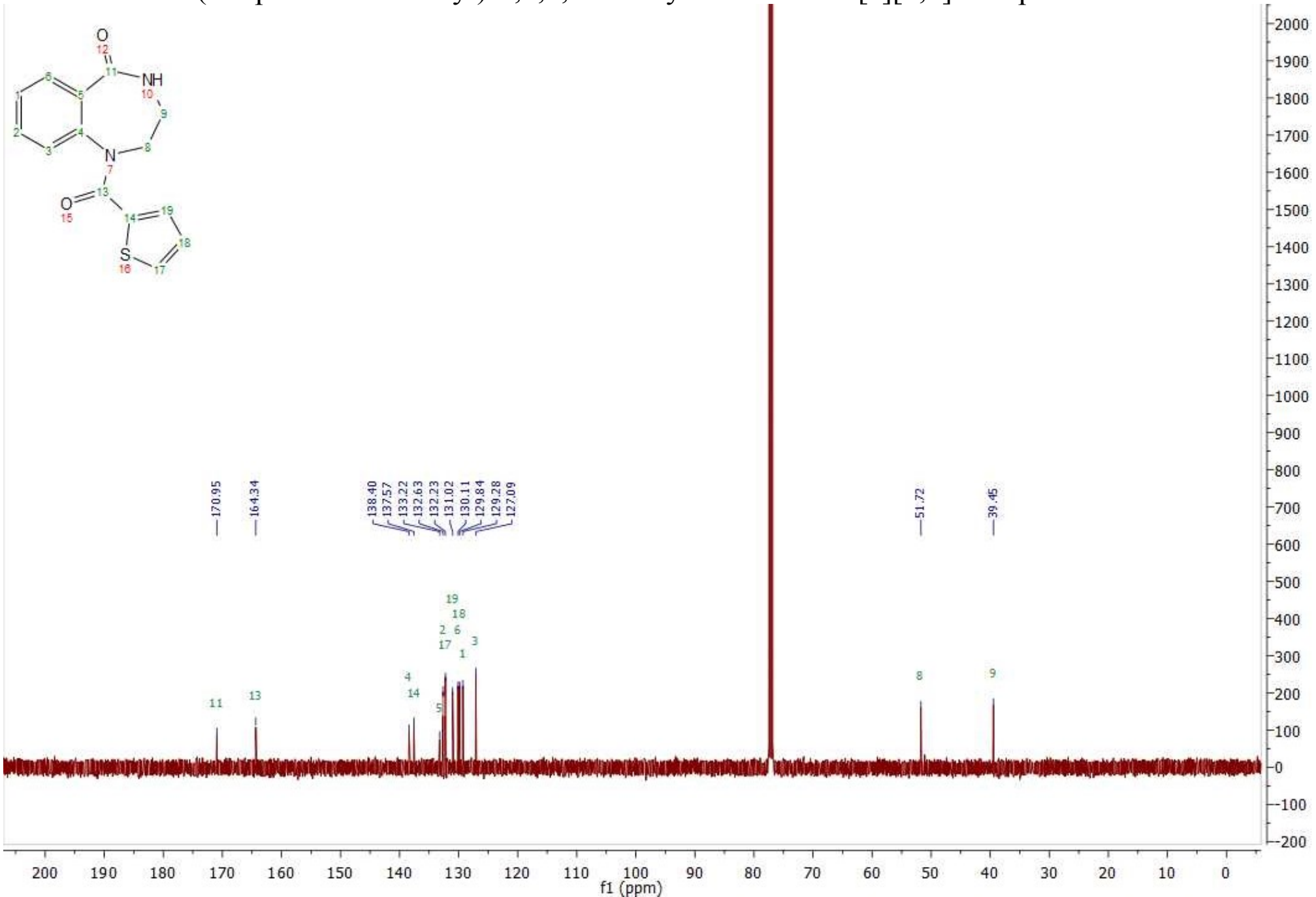
1-(furan-2-carbonyl)-1,2,3,4-tetrahydro-5H-benzo[e][1,4]diazepin-5-one **9c**



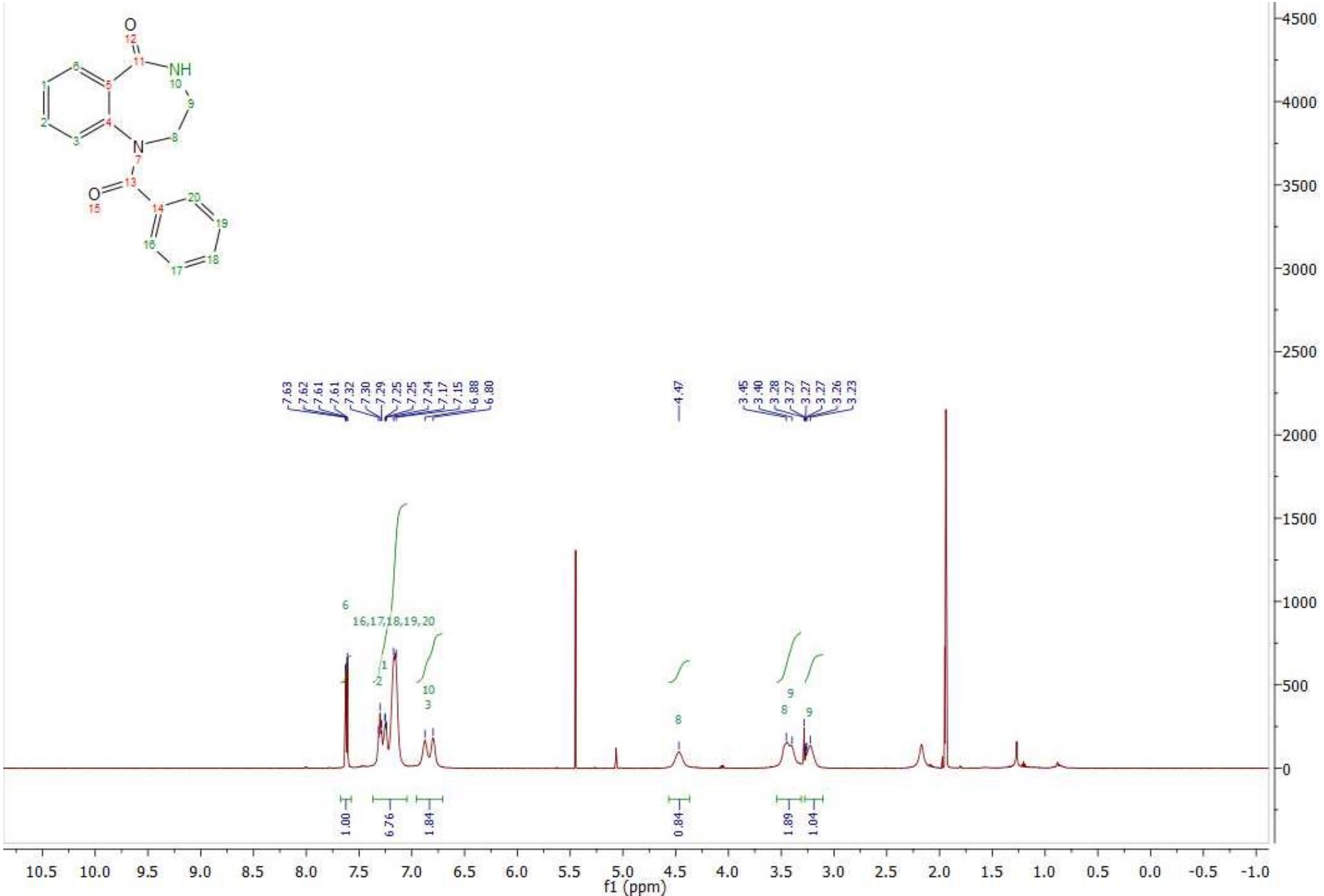
1-(thiophene-2-carbonyl)-1,2,3,4-tetrahydro-5H-benzo[e][1,4]diazepin-5-one **9d**



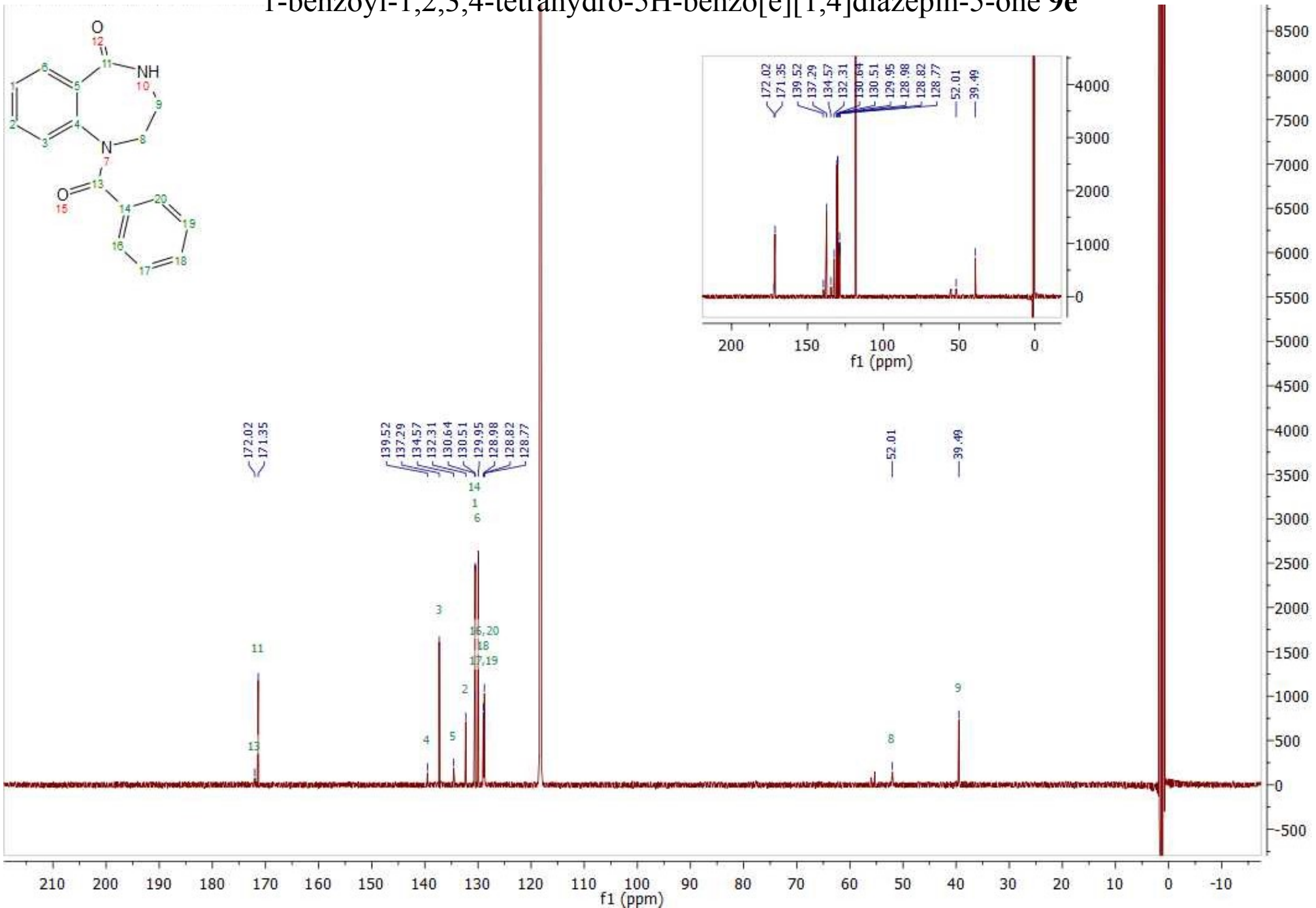
1-(thiophene-2-carbonyl)-1,2,3,4-tetrahydro-5H-benzo[e][1,4]diazepin-5-one **9d**



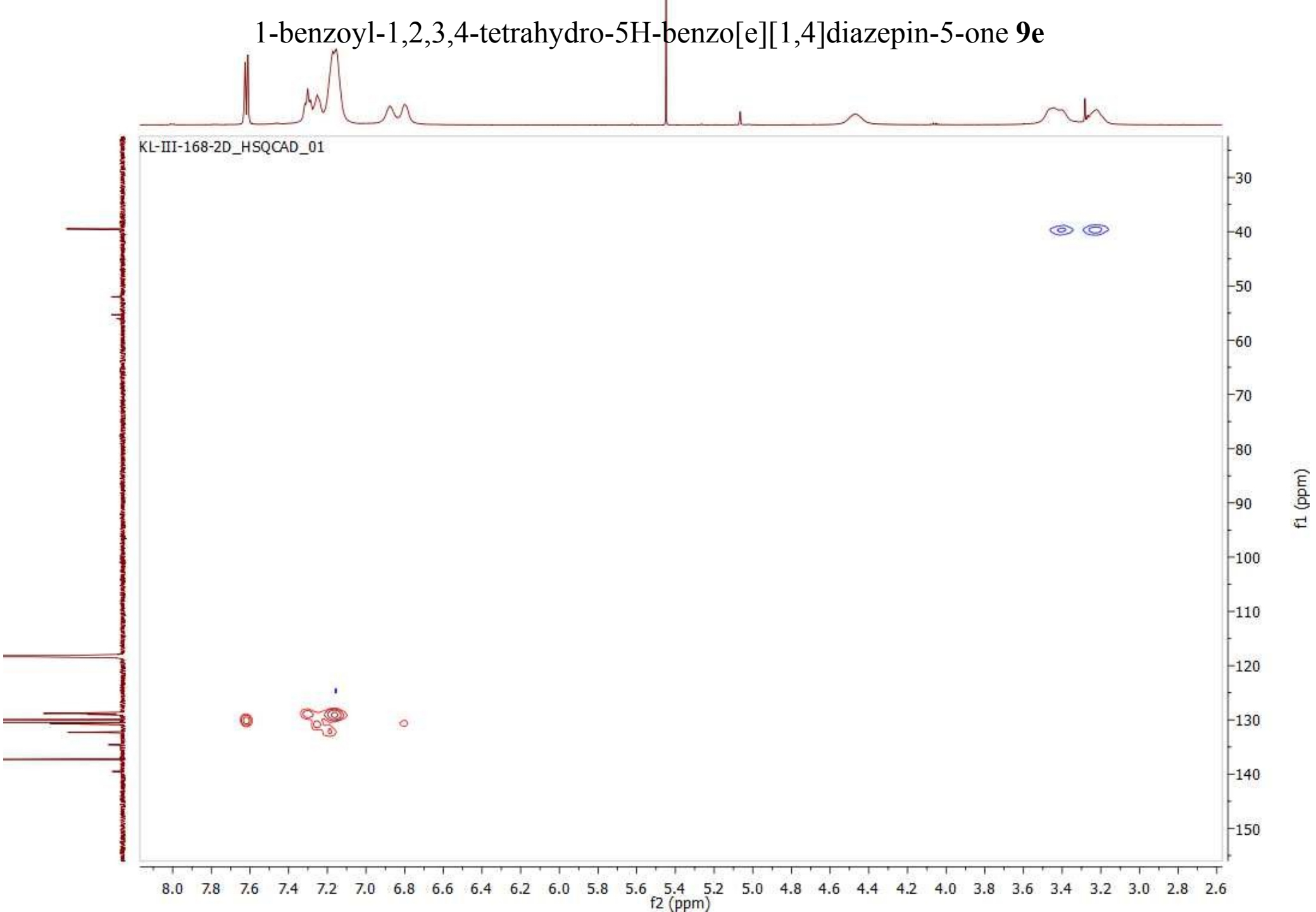
1-benzoyl-1,2,3,4-tetrahydro-5H-benzo[e][1,4]diazepin-5-one **9e**



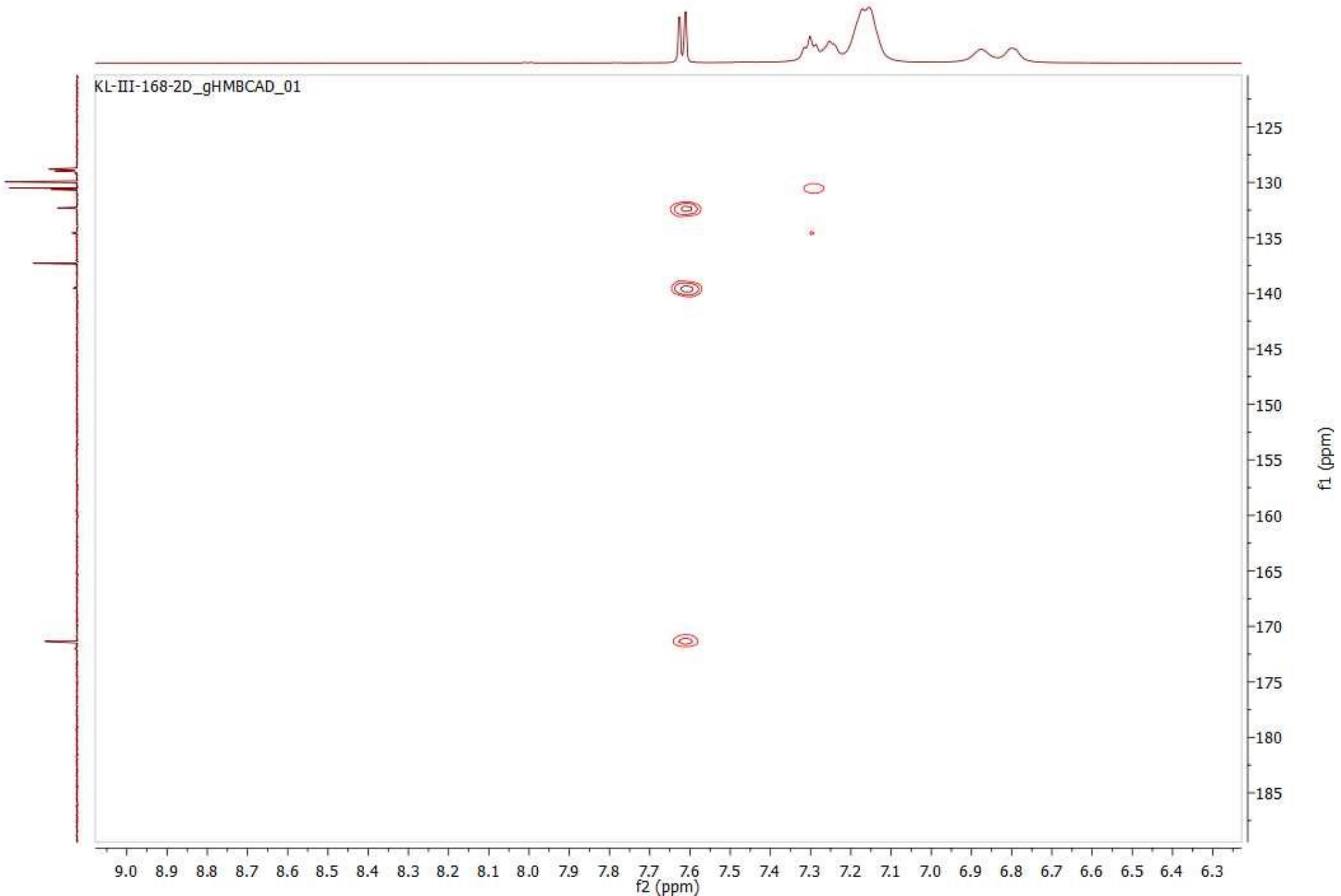
1-benzoyl-1,2,3,4-tetrahydro-5H-benzo[e][1,4]diazepin-5-one **9e**



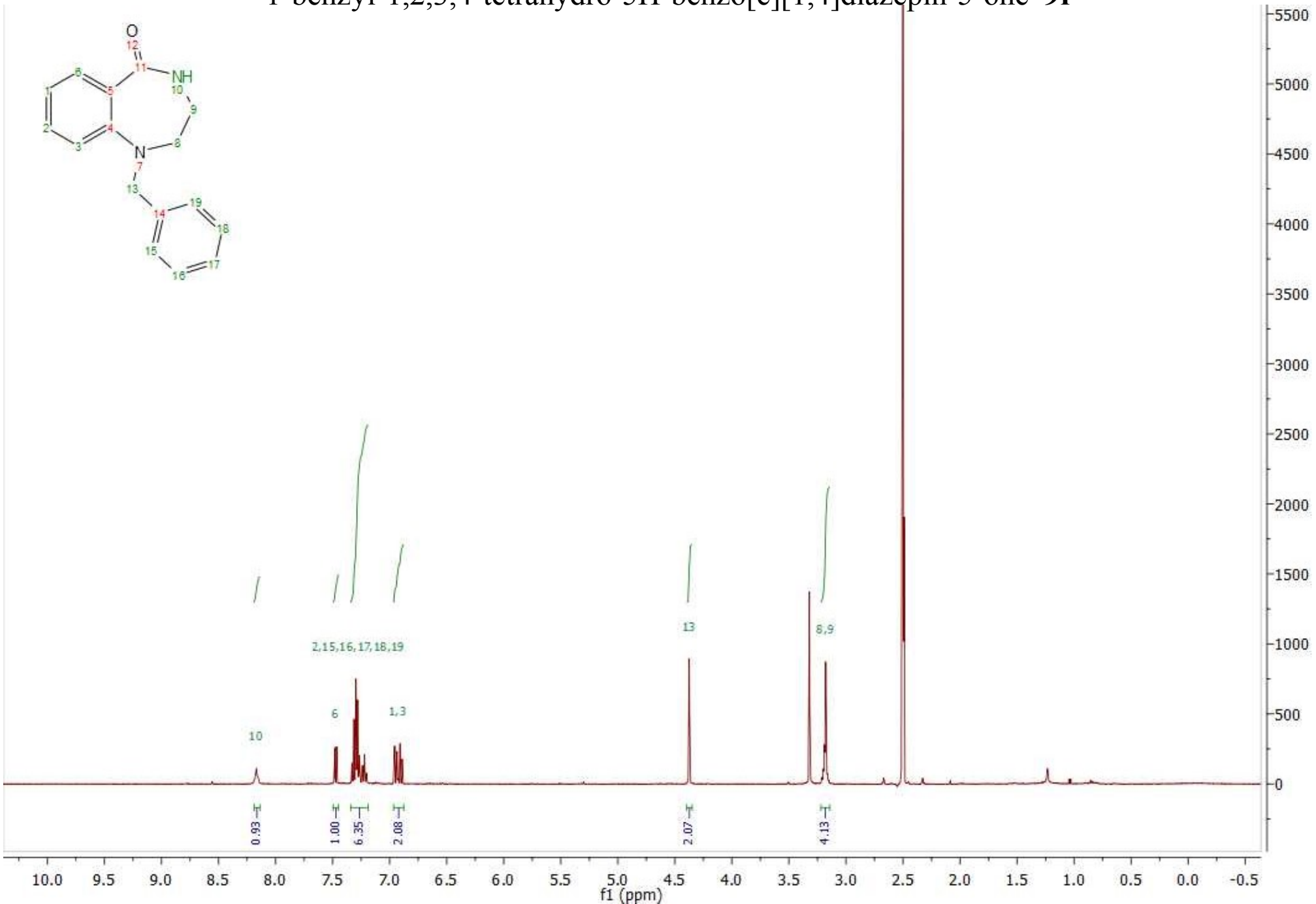
1-benzoyl-1,2,3,4-tetrahydro-5H-benzo[e][1,4]diazepin-5-one **9e**



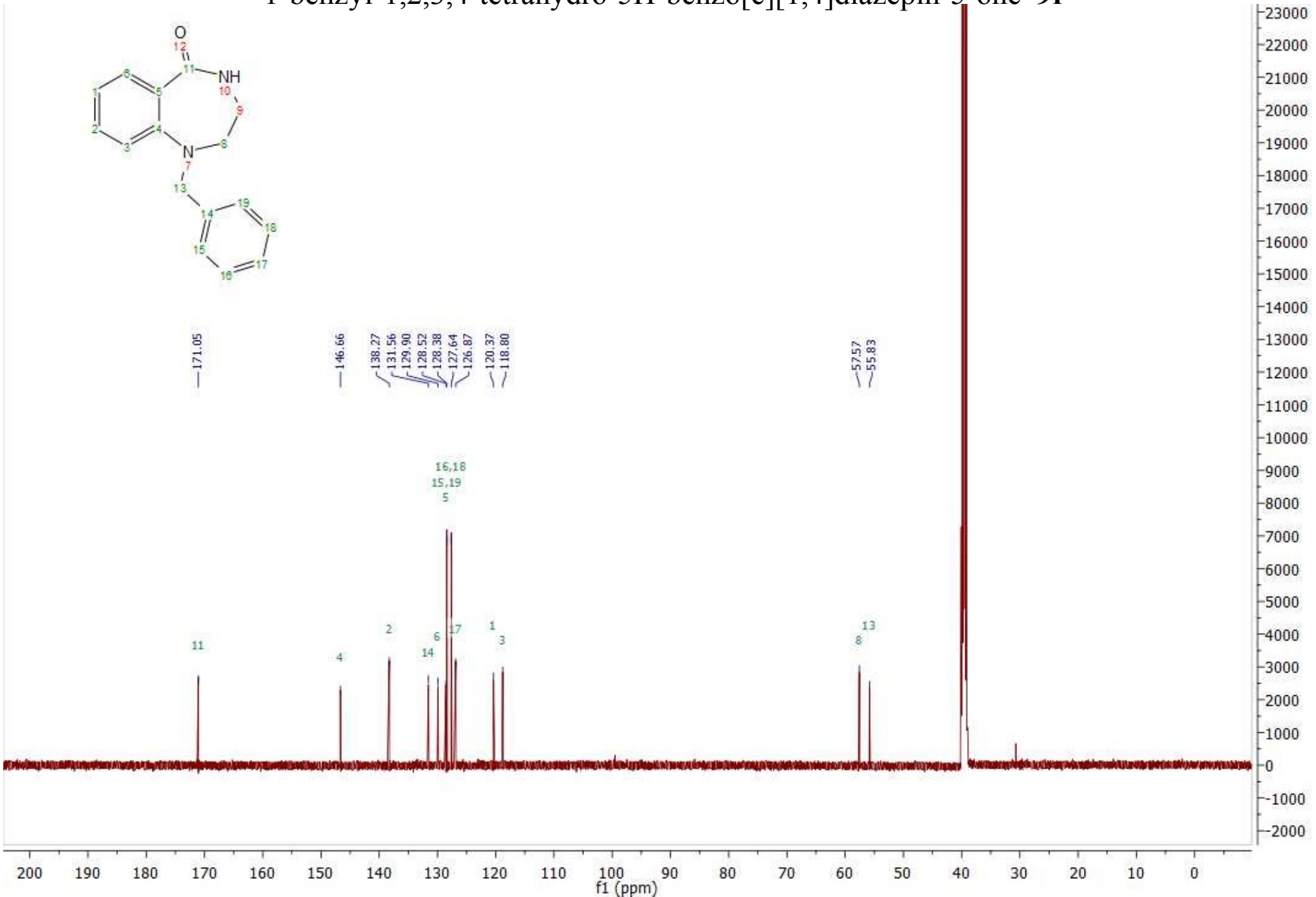
1-benzoyl-1,2,3,4-tetrahydro-5H-benzo[e][1,4]diazepin-5-one **9e**



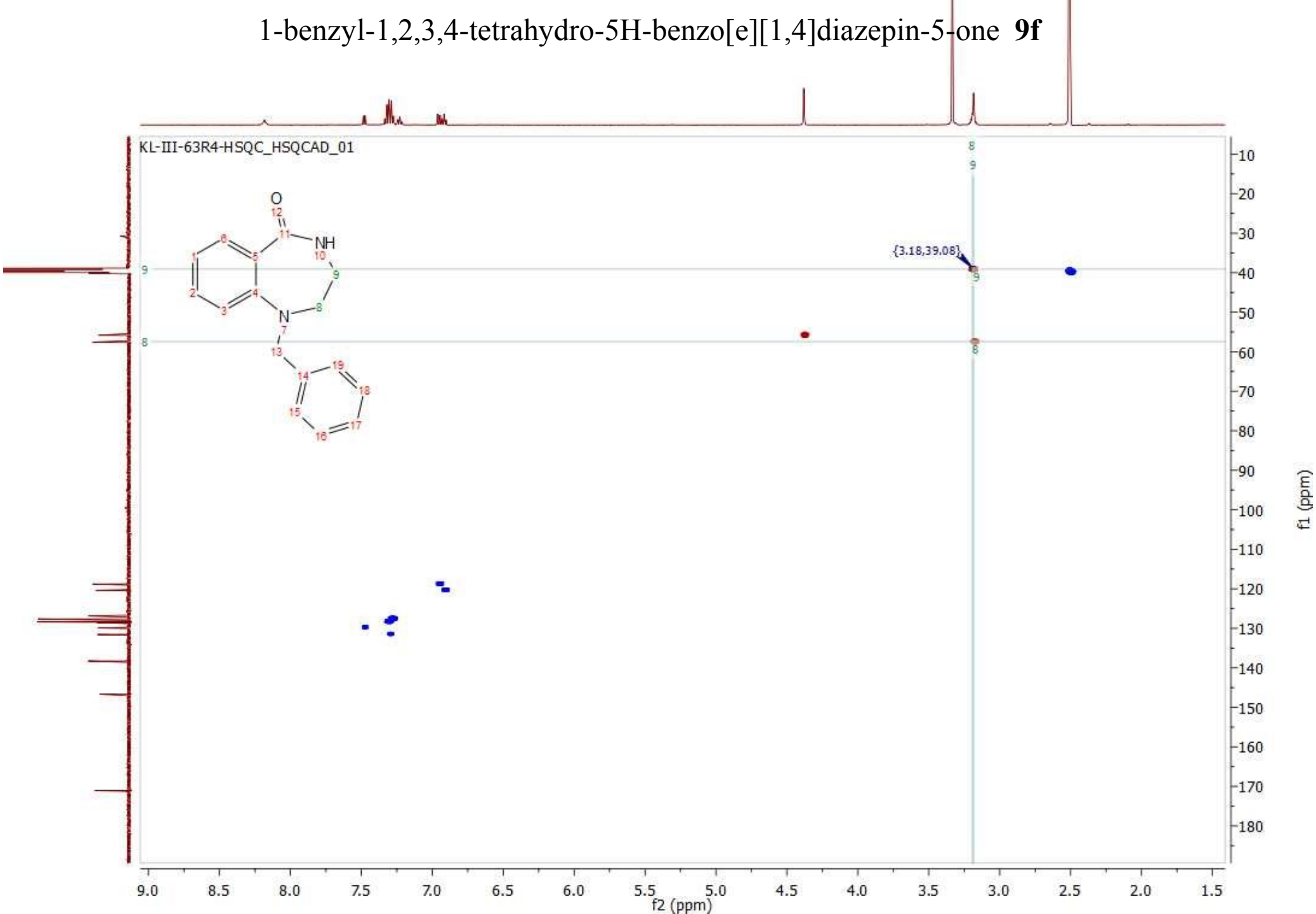
1-benzyl-1,2,3,4-tetrahydro-5H-benzo[e][1,4]diazepin-5-one **9f**



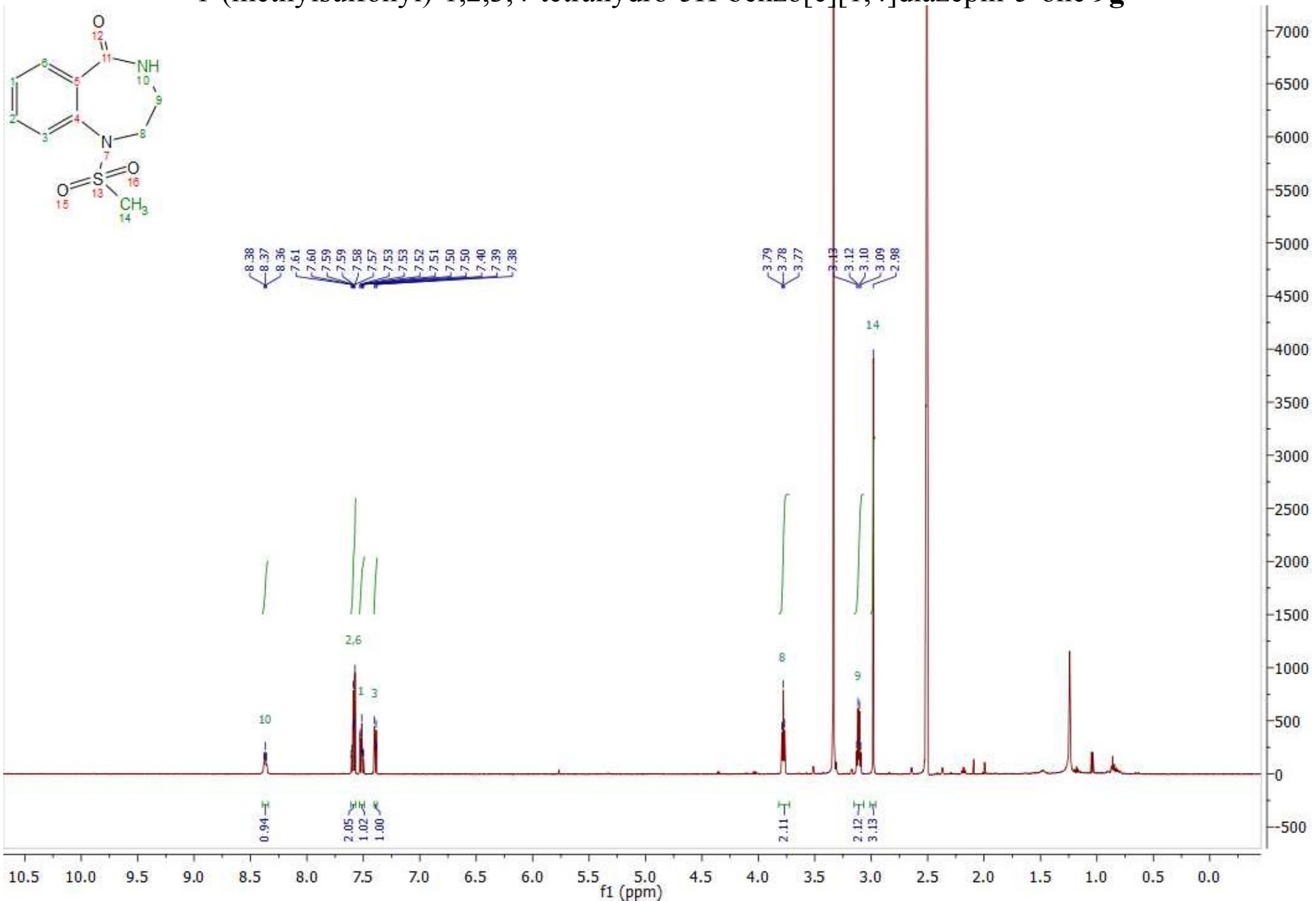
1-benzyl-1,2,3,4-tetrahydro-5H-benzo[e][1,4]diazepin-5-one **9f**



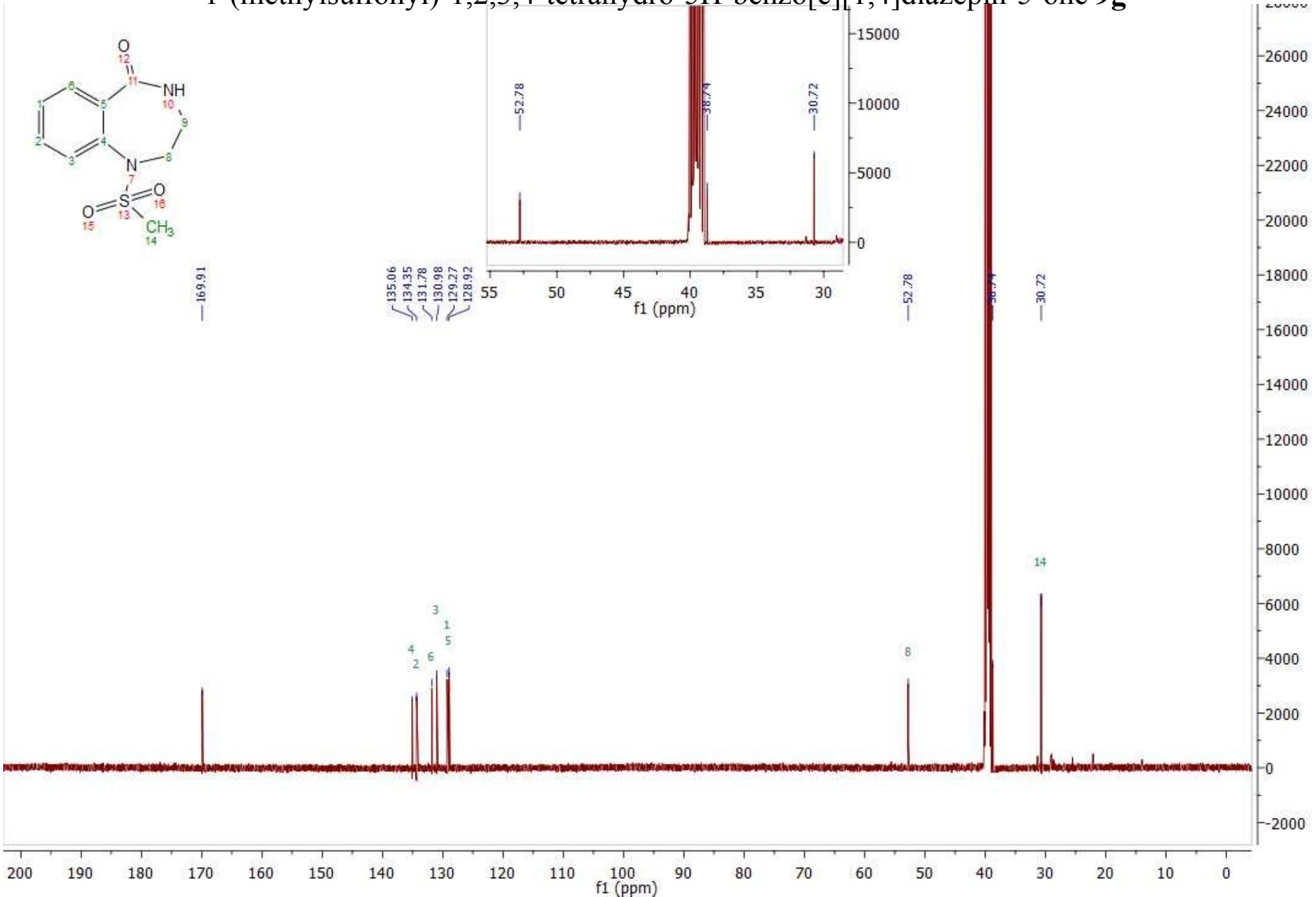
1-benzyl-1,2,3,4-tetrahydro-5H-benzo[e][1,4]diazepin-5-one **9f**



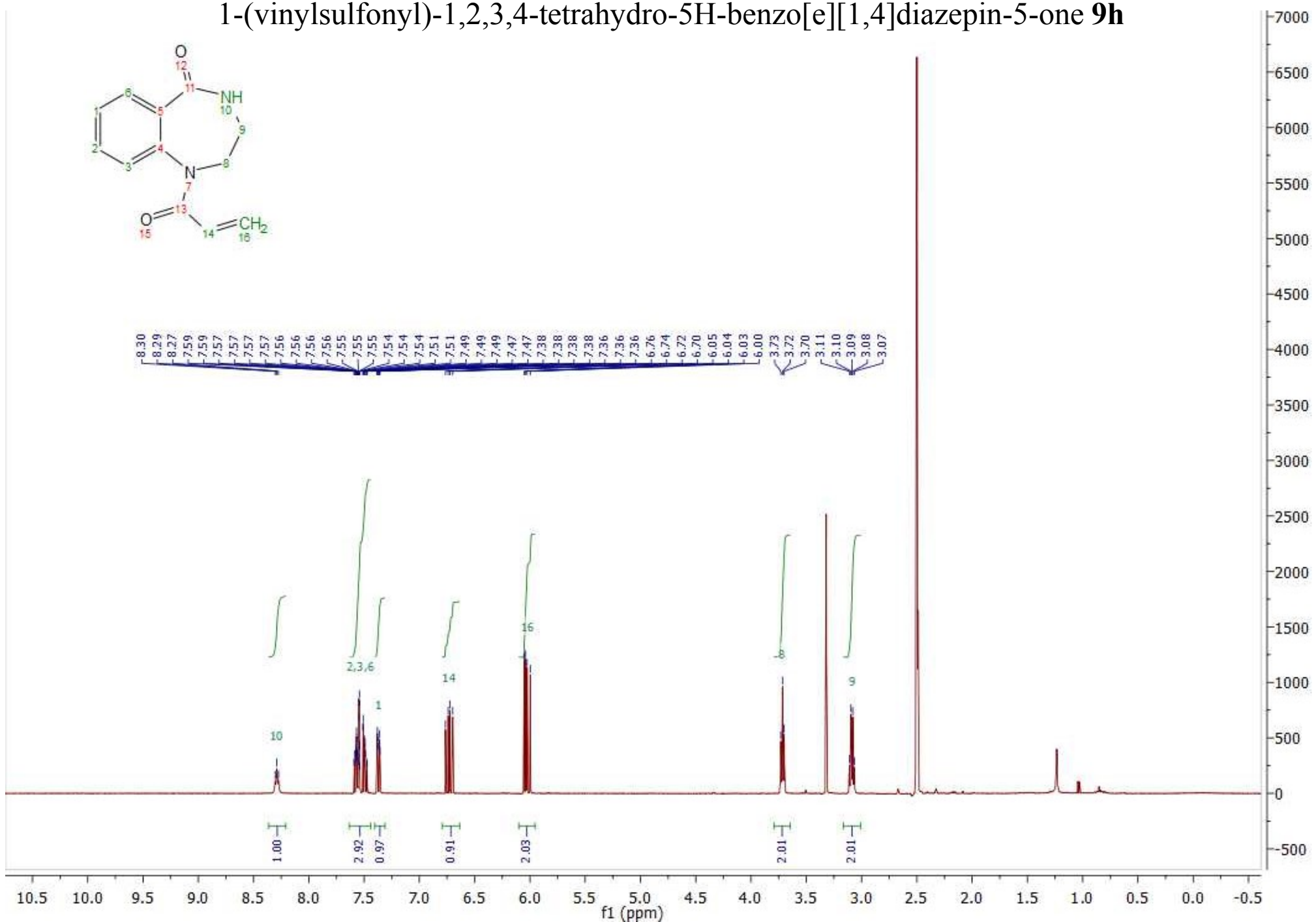
1-(methylsulfonyl)-1,2,3,4-tetrahydro-5H-benzo[e][1,4]diazepin-5-one **9g**



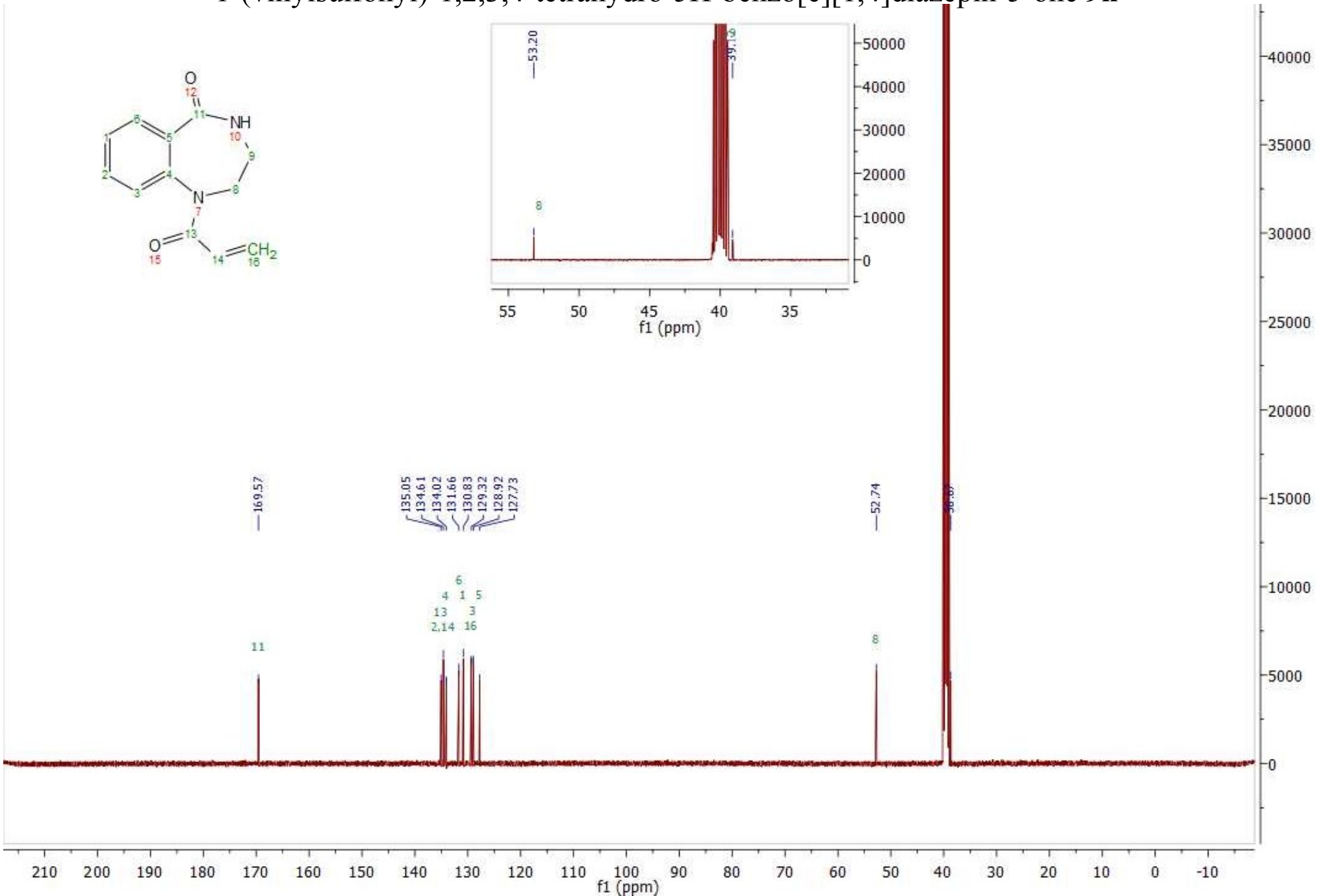
1-(methylsulfonyl)-1,2,3,4-tetrahydro-5H-benzo[e][1,4]diazepin-5-one **9g**



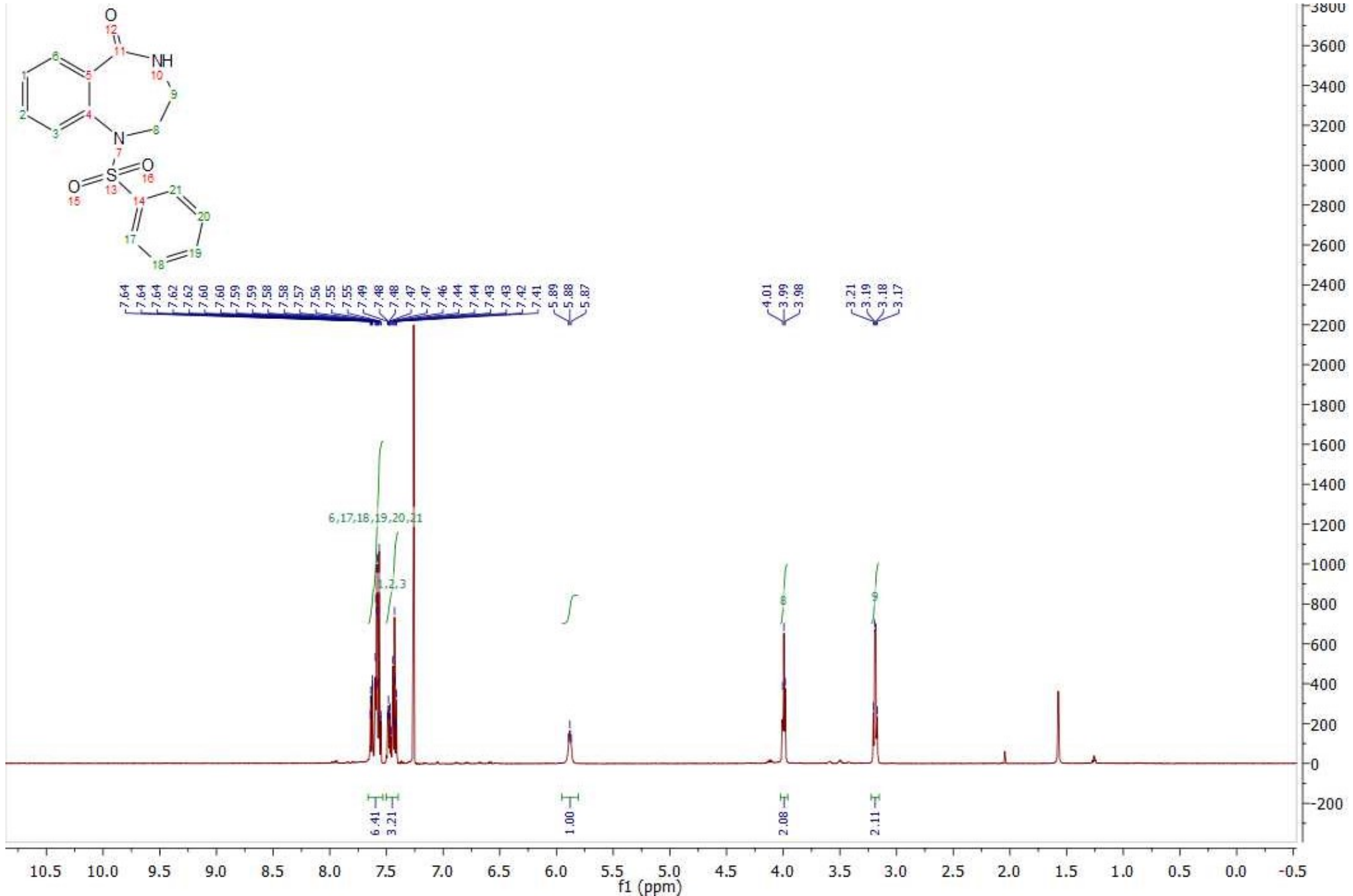
1-(vinylsulfonyl)-1,2,3,4-tetrahydro-5H-benzo[e][1,4]diazepin-5-one **9h**



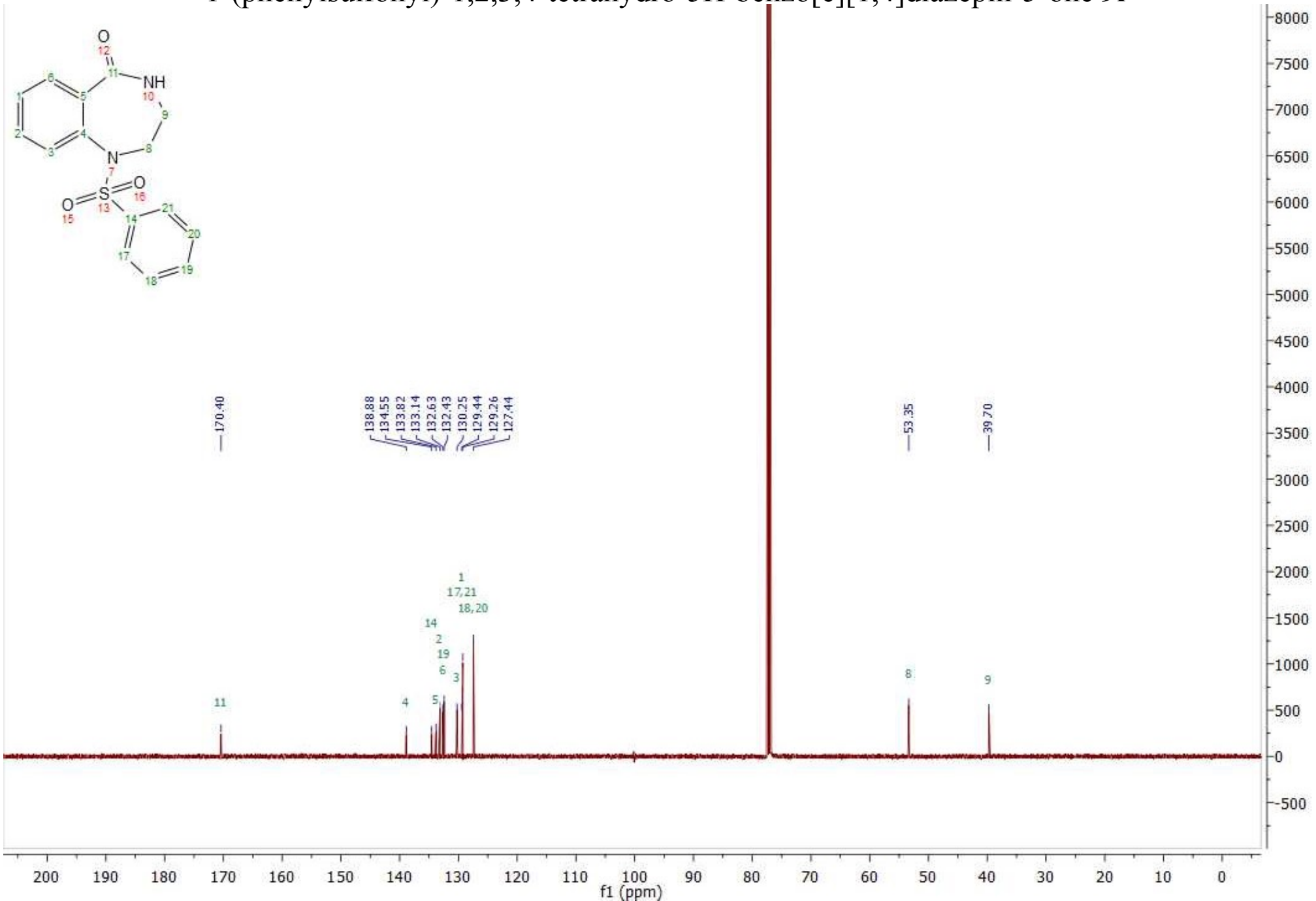
1-(vinylsulfonyl)-1,2,3,4-tetrahydro-5H-benzo[e][1,4]diazepin-5-one **9h**



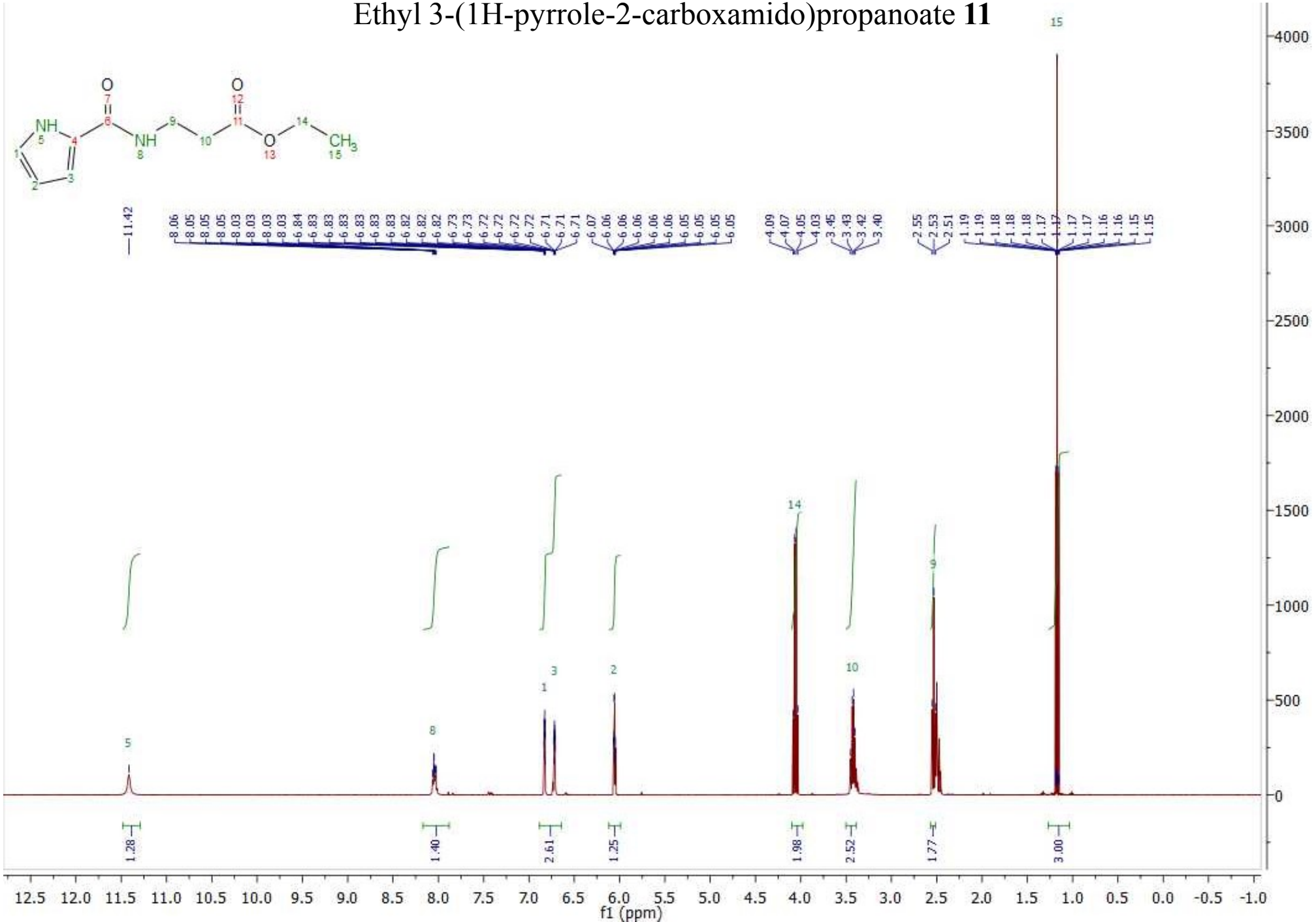
1-(phenylsulfonyl)-1,2,3,4-tetrahydro-5H-benzo[e][1,4]diazepin-5-one **9i**



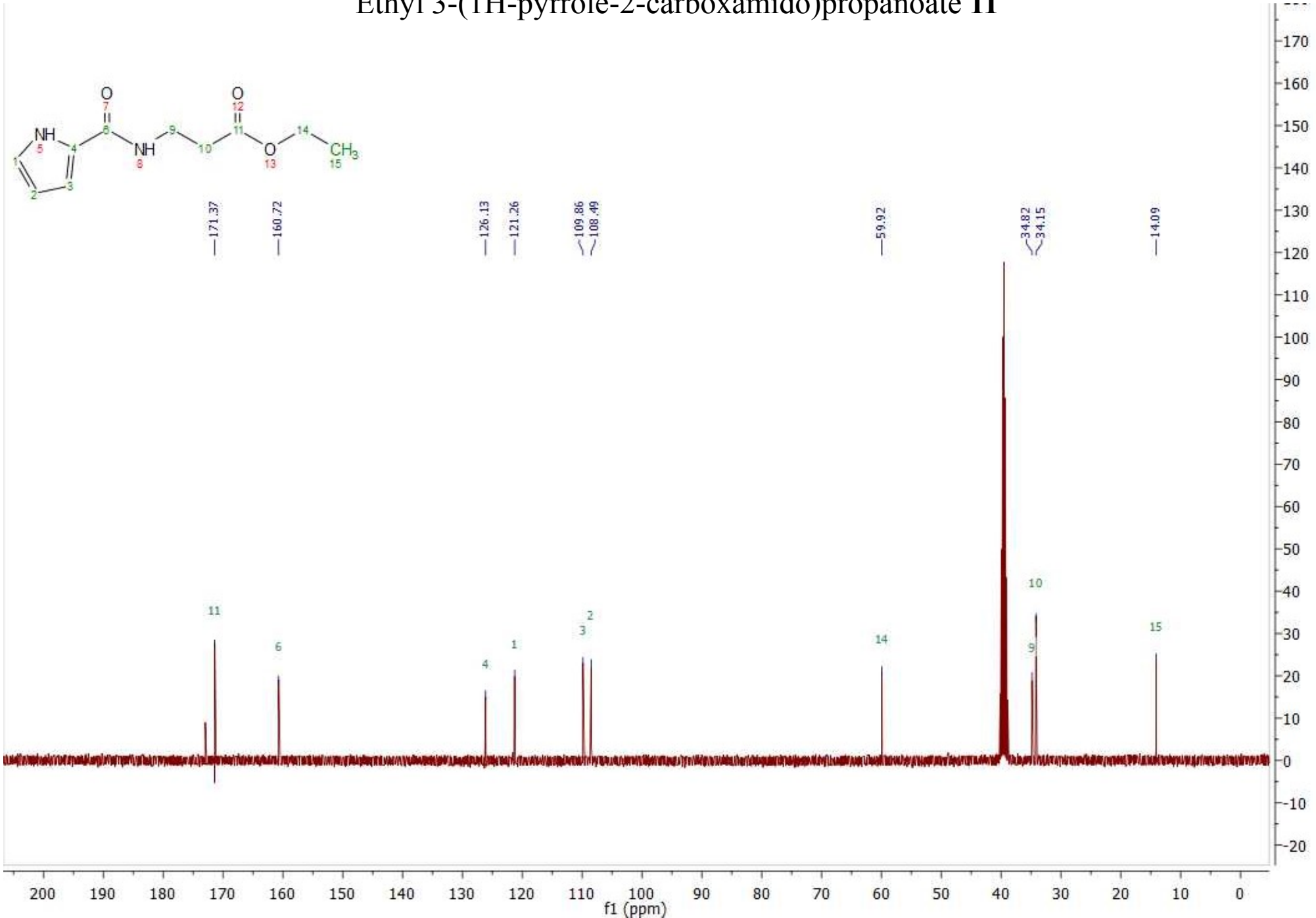
1-(phenylsulfonyl)-1,2,3,4-tetrahydro-5H-benzo[e][1,4]diazepin-5-one **9i**



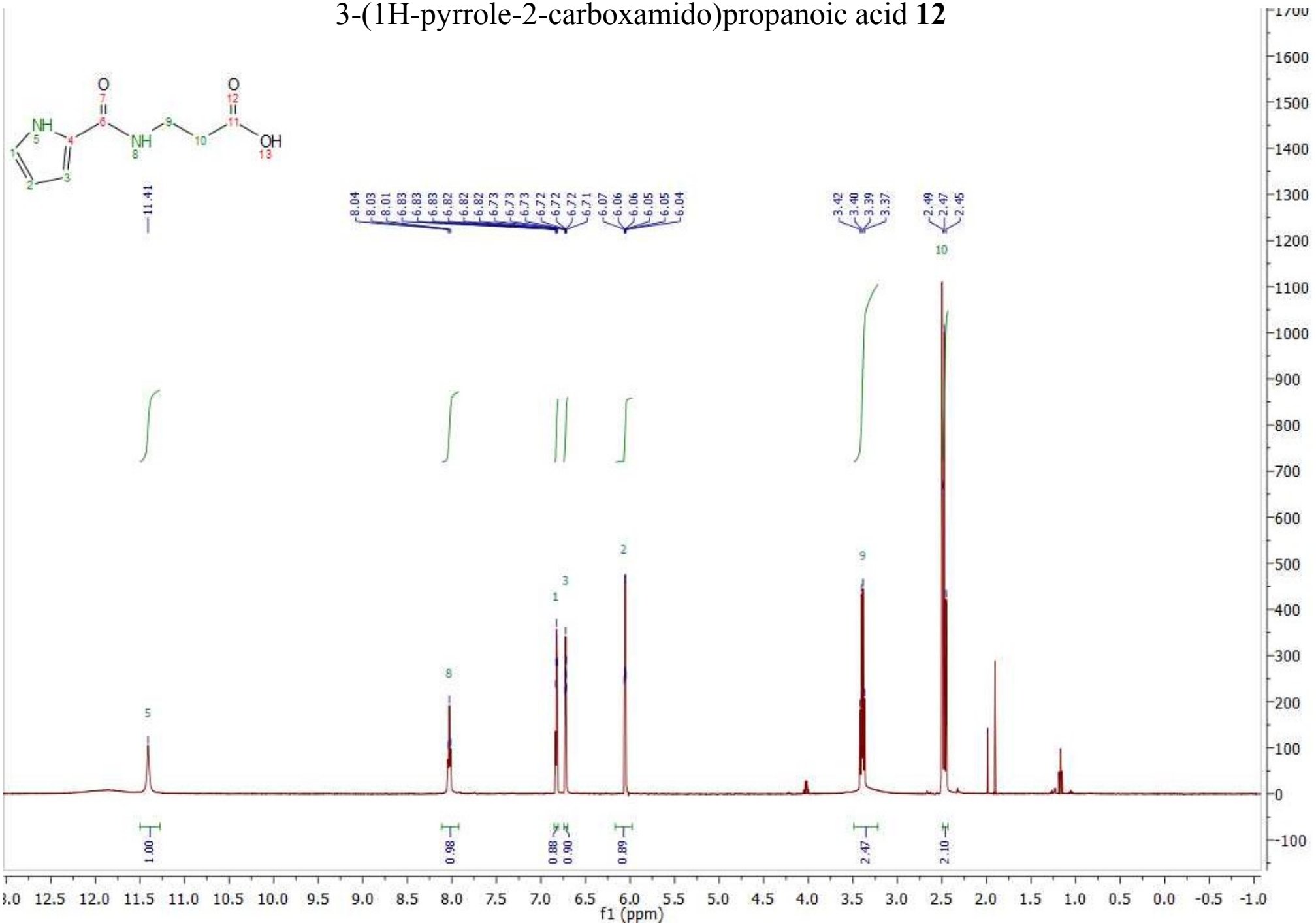
Ethyl 3-(1H-pyrrole-2-carboxamido)propanoate **11**



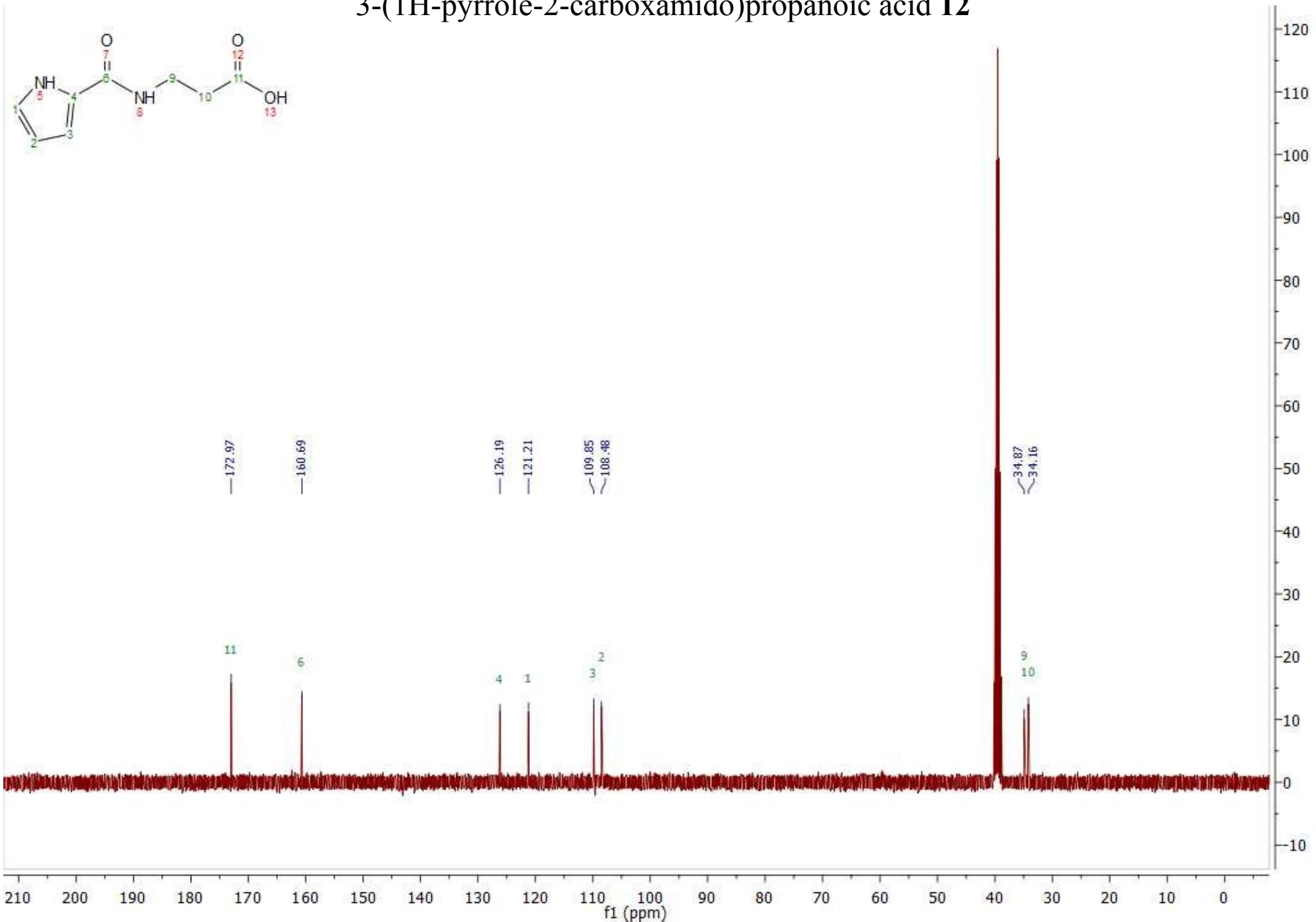
Ethyl 3-(1H-pyrrole-2-carboxamido)propanoate **11**



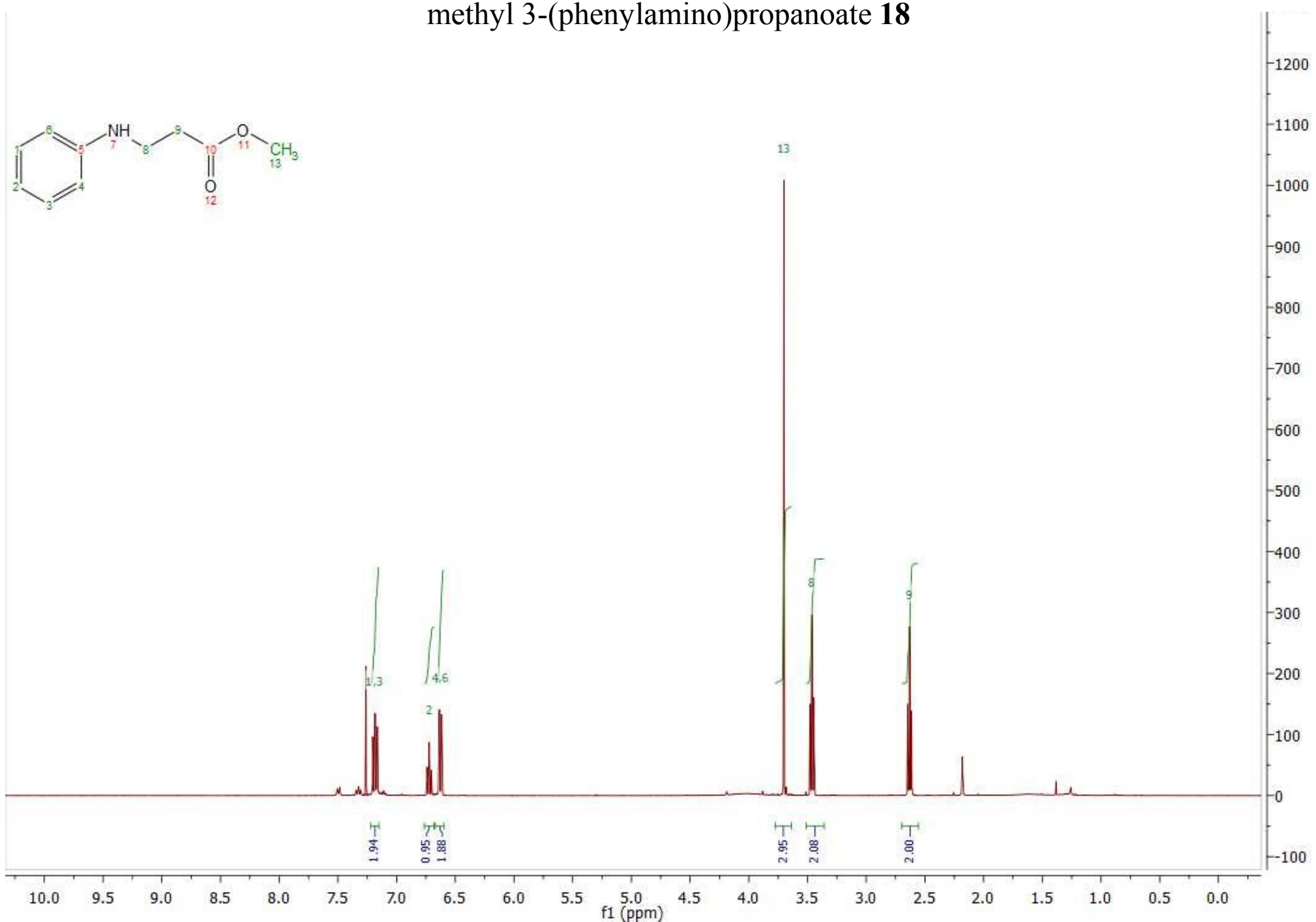
3-(1H-pyrrole-2-carboxamido)propanoic acid **12**



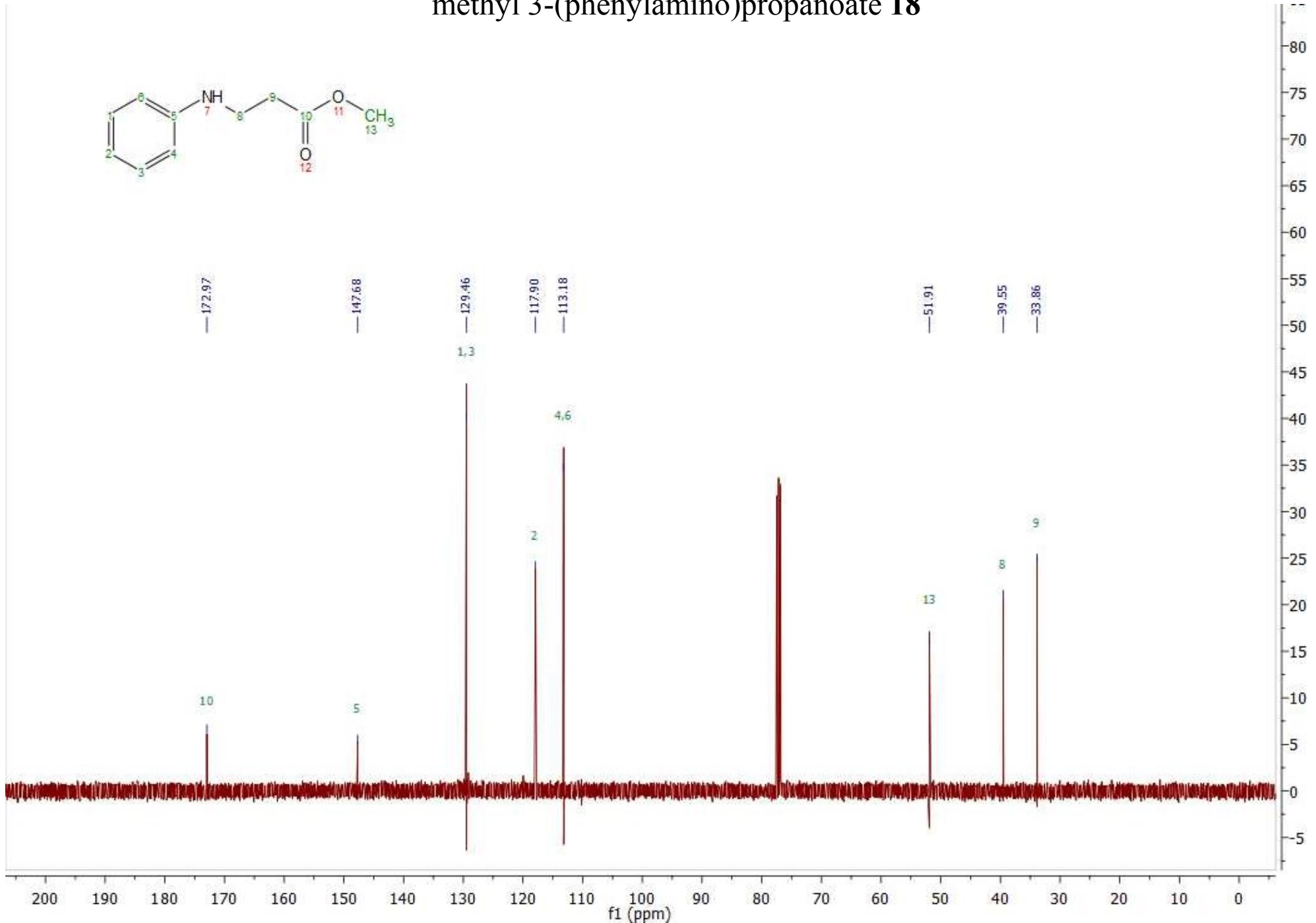
3-(1H-pyrrole-2-carboxamido)propanoic acid **12**



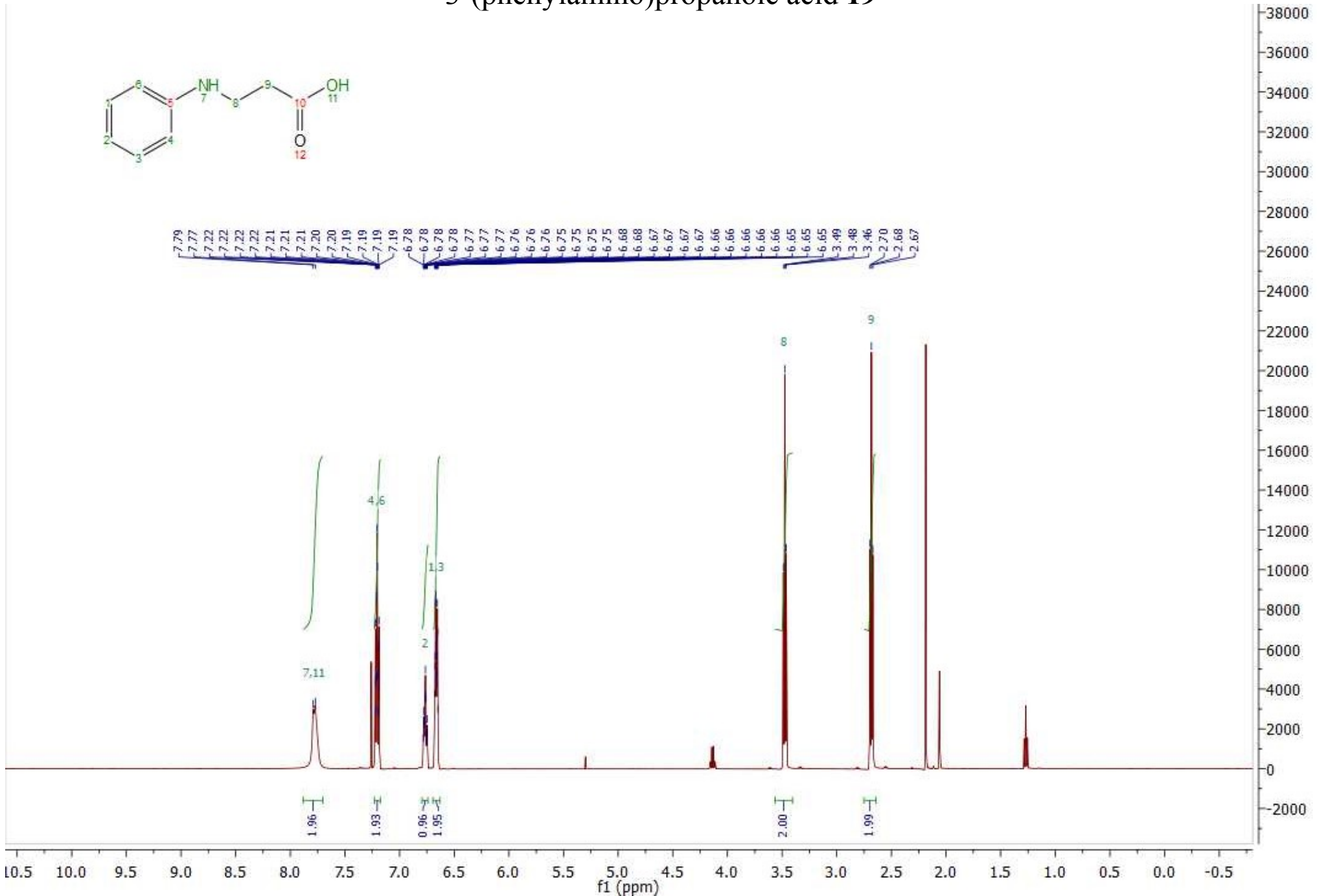
methyl 3-(phenylamino)propanoate **18**



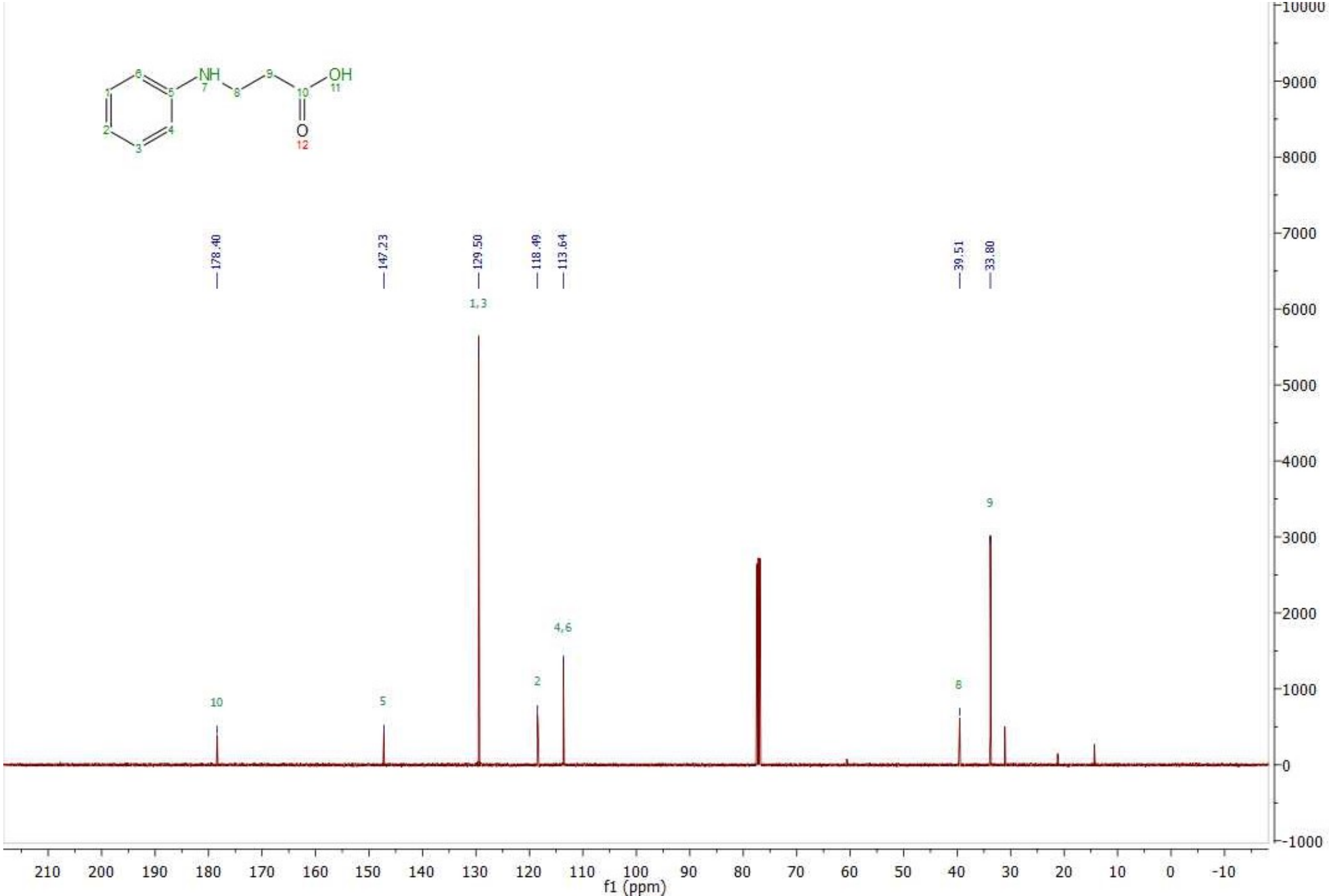
methyl 3-(phenylamino)propanoate **18**



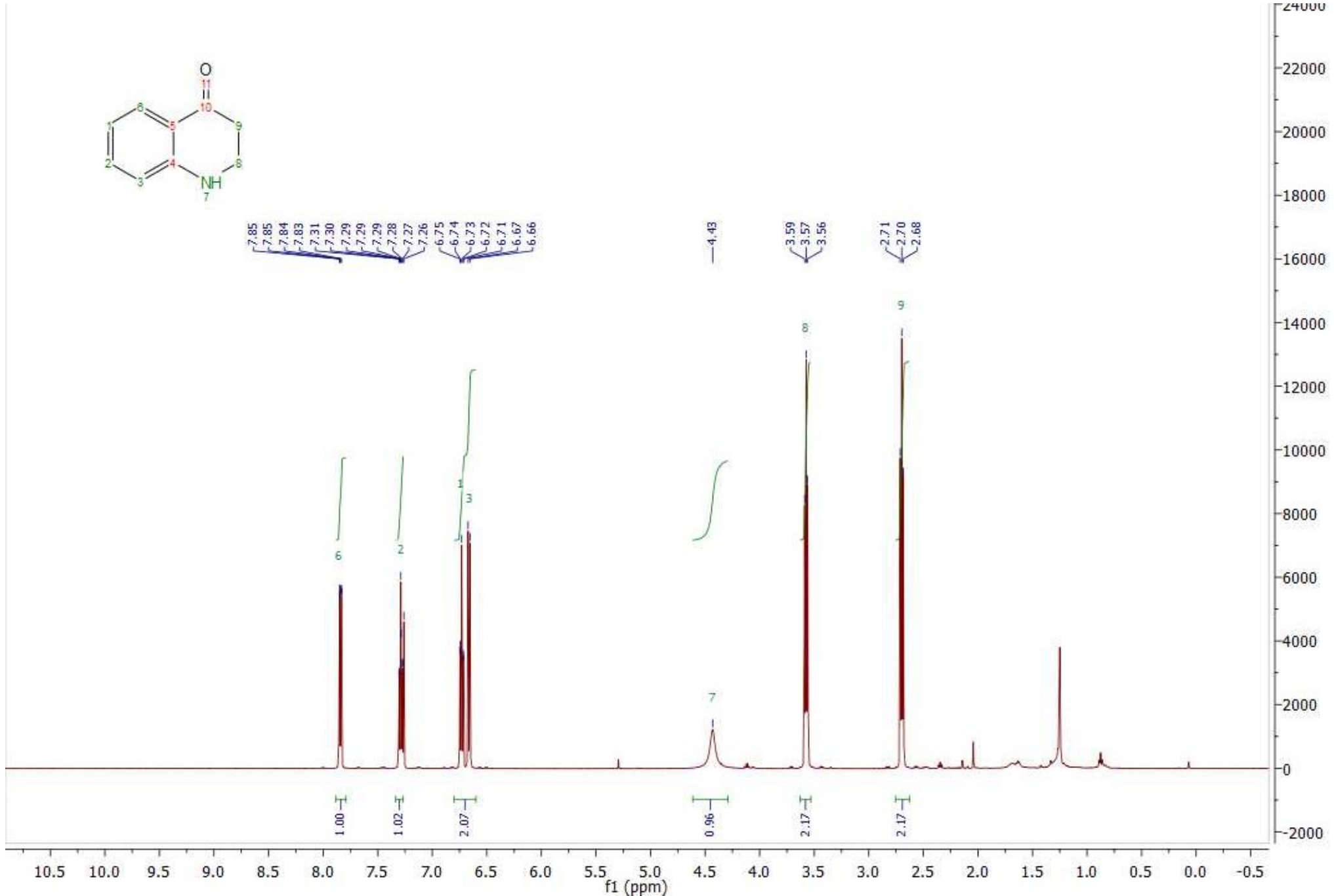
3-(phenylamino)propanoic acid **19**



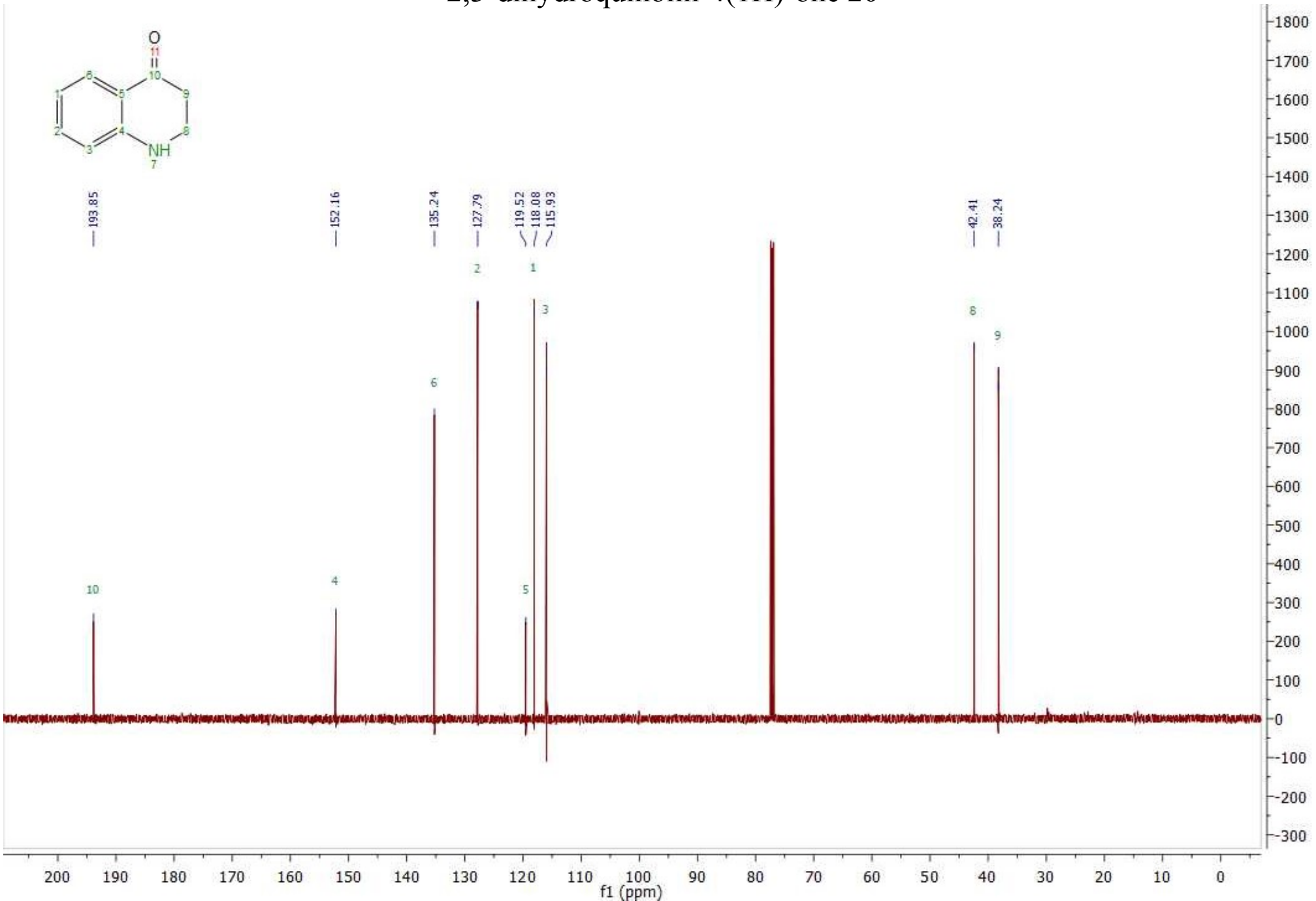
3-(phenylamino)propanoic acid **19**



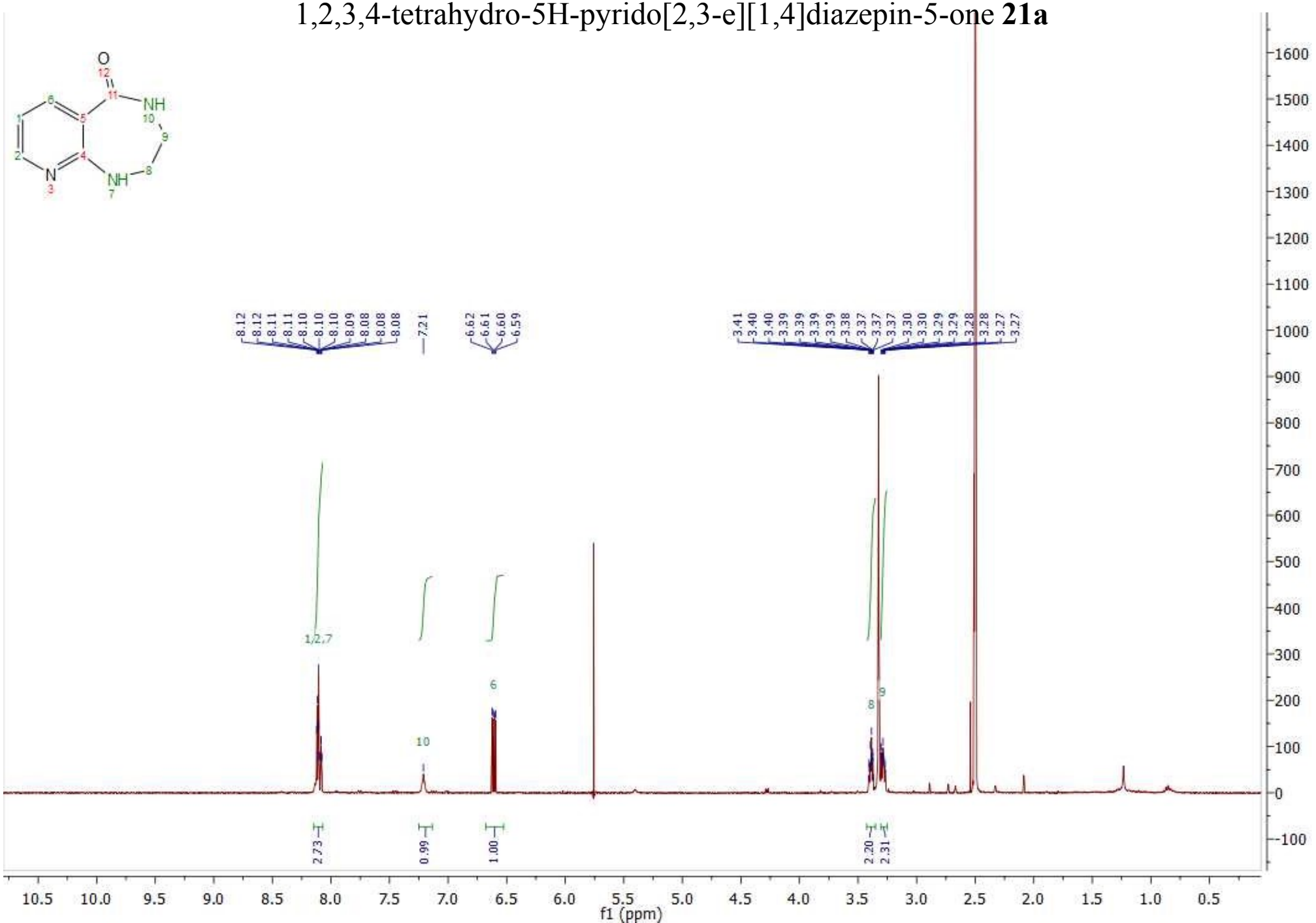
2,3-dihydroquinolin-4(1H)-one **20**



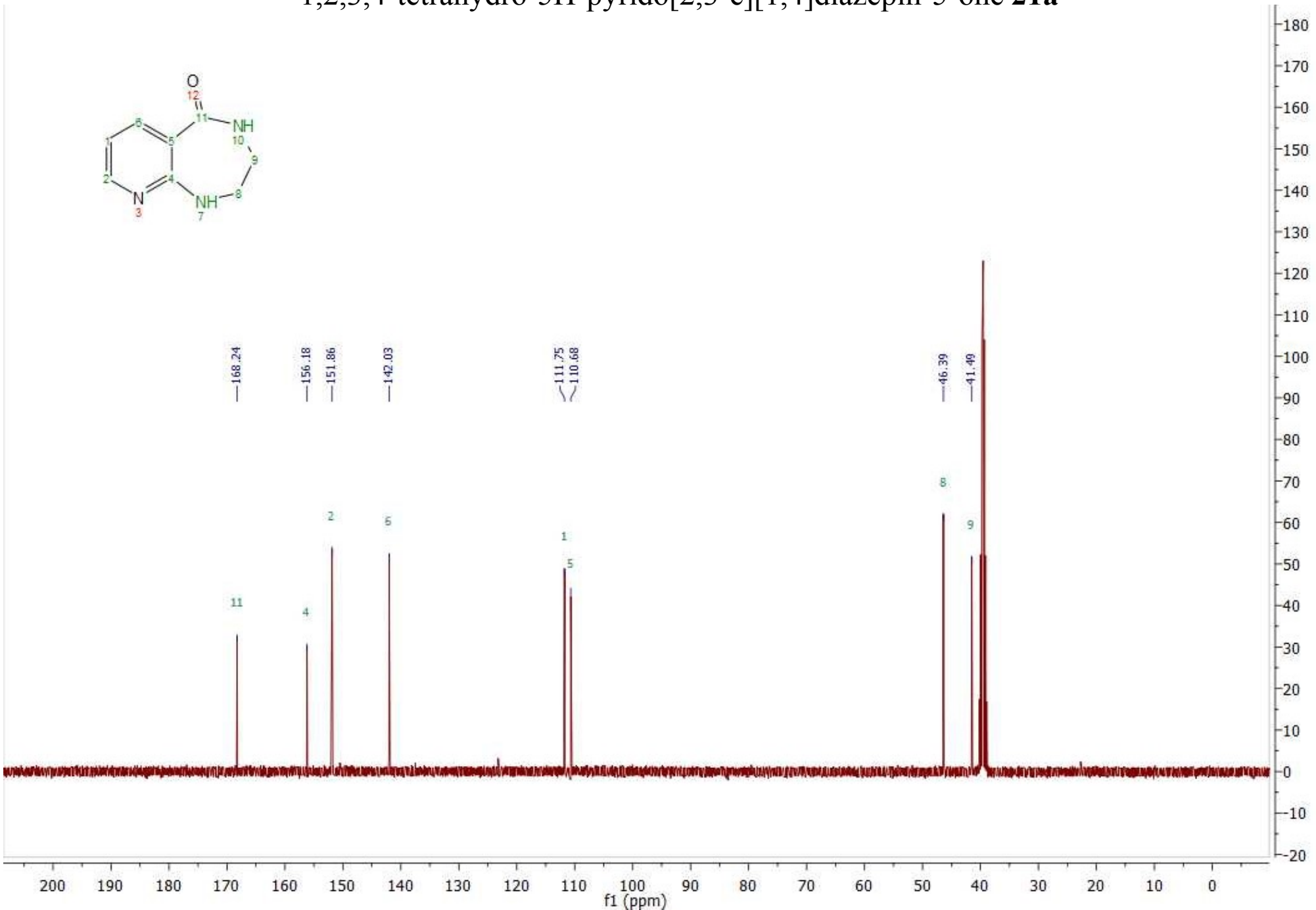
2,3-dihydroquinolin-4(1H)-one **20**



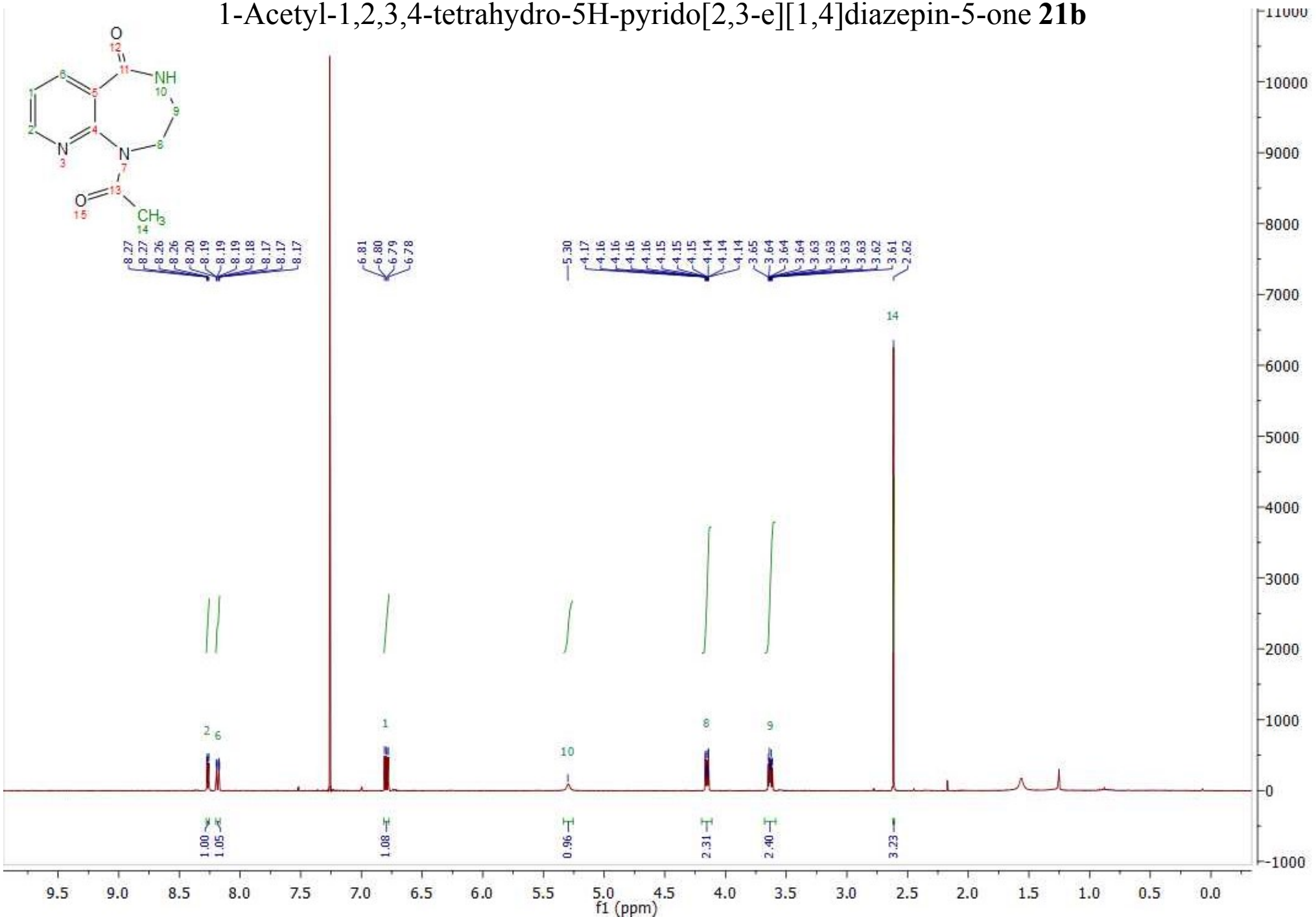
1,2,3,4-tetrahydro-5H-pyrido[2,3-e][1,4]diazepin-5-one **21a**



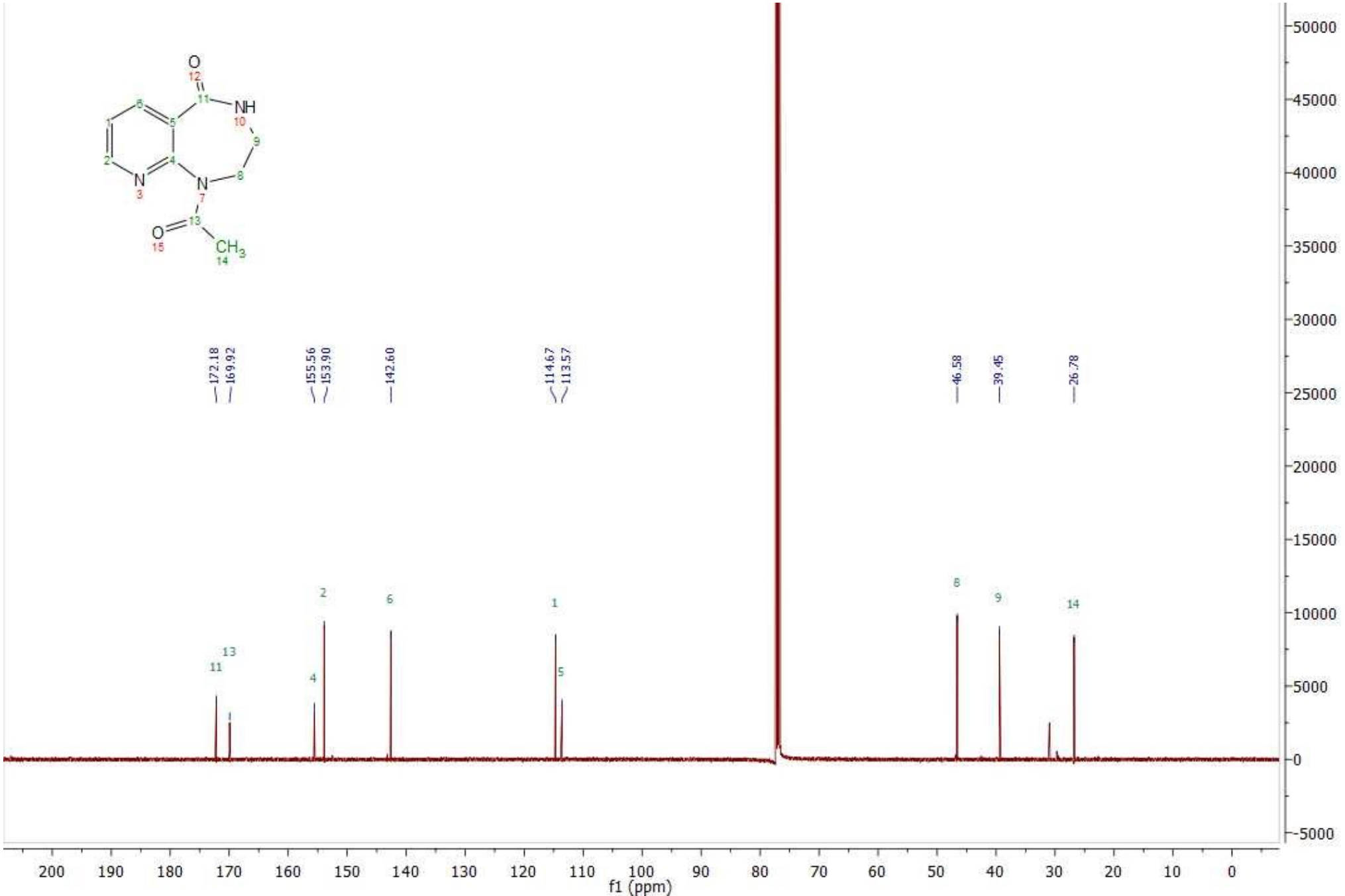
1,2,3,4-tetrahydro-5H-pyrido[2,3-e][1,4]diazepin-5-one **21a**



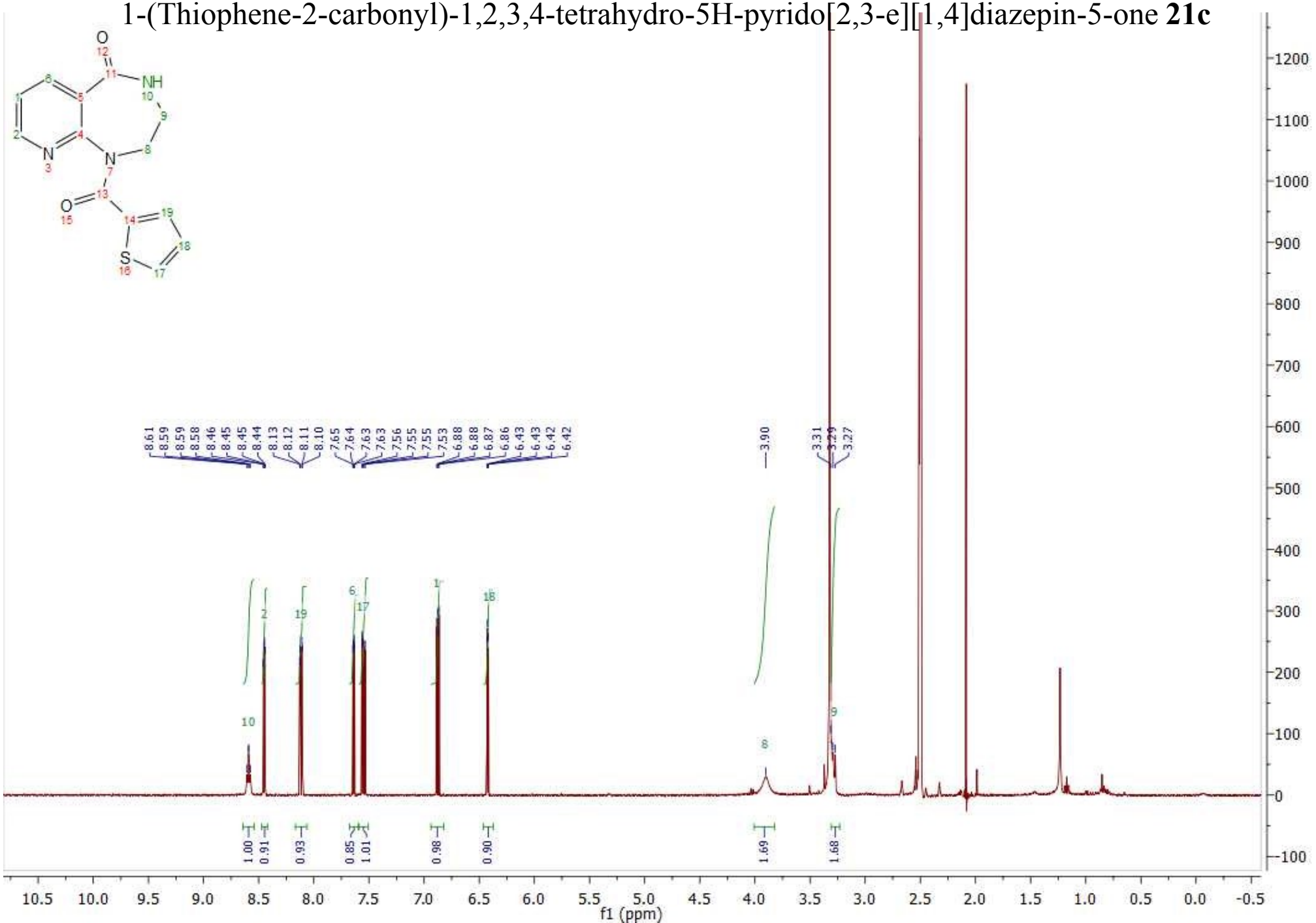
1-Acetyl-1,2,3,4-tetrahydro-5H-pyrido[2,3-e][1,4]diazepin-5-one **21b**



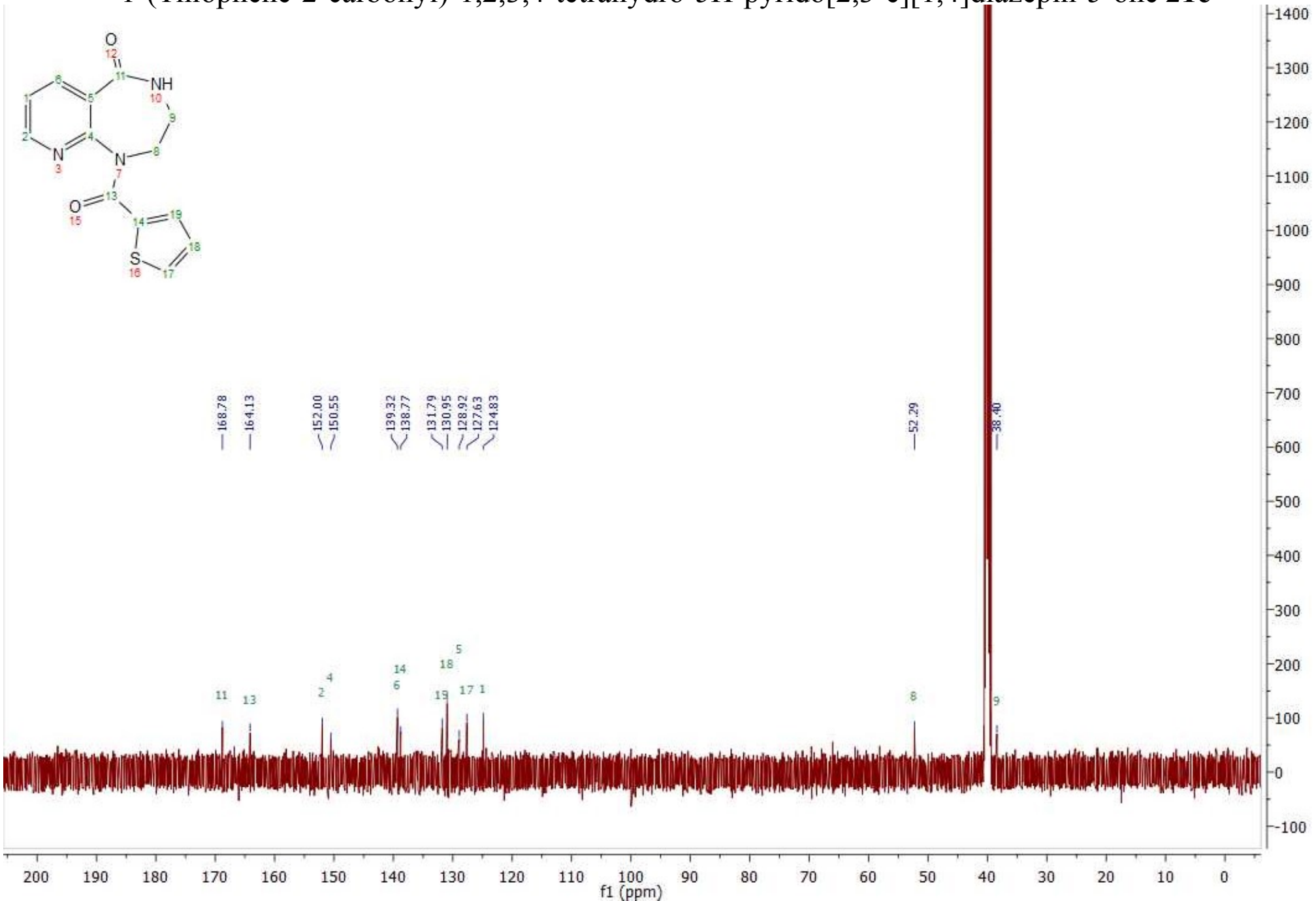
1-Acetyl-1,2,3,4-tetrahydro-5H-pyrido[2,3-e][1,4]diazepin-5-one **21b**



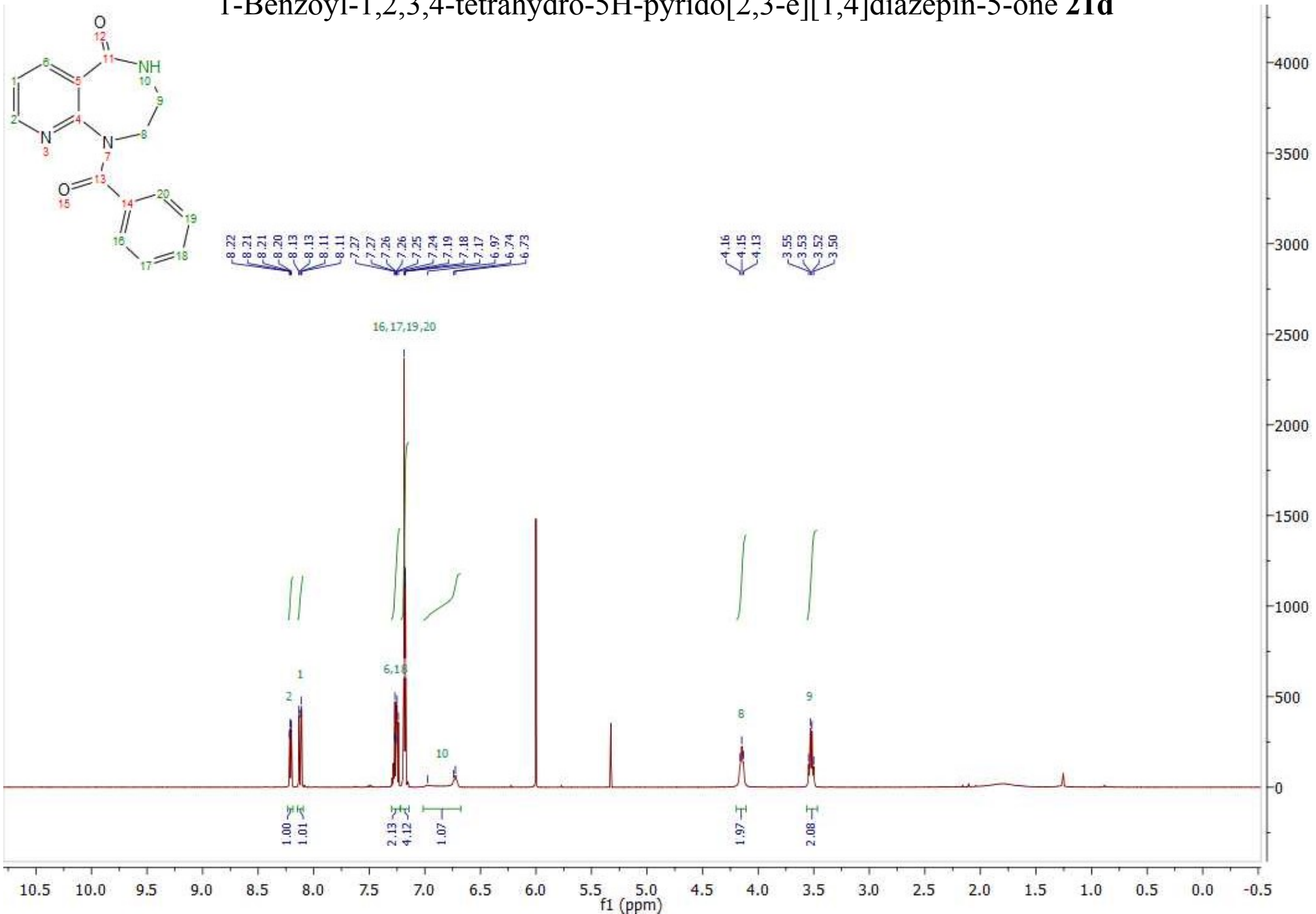
1-(Thiophene-2-carbonyl)-1,2,3,4-tetrahydro-5H-pyrido[2,3-e][1,4]diazepin-5-one **21c**



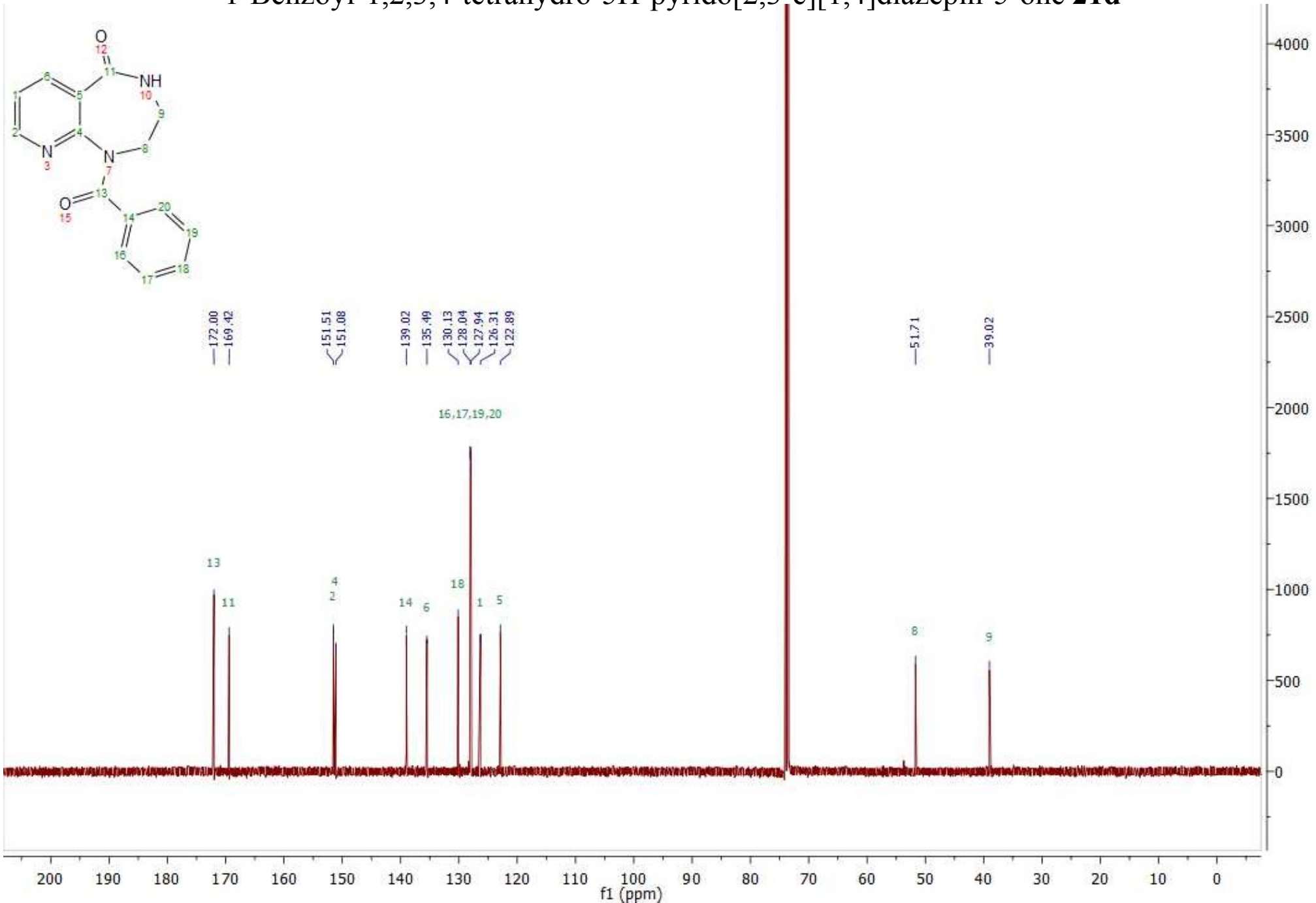
1-(Thiophene-2-carbonyl)-1,2,3,4-tetrahydro-5H-pyrido[2,3-e][1,4]diazepin-5-one **21c**



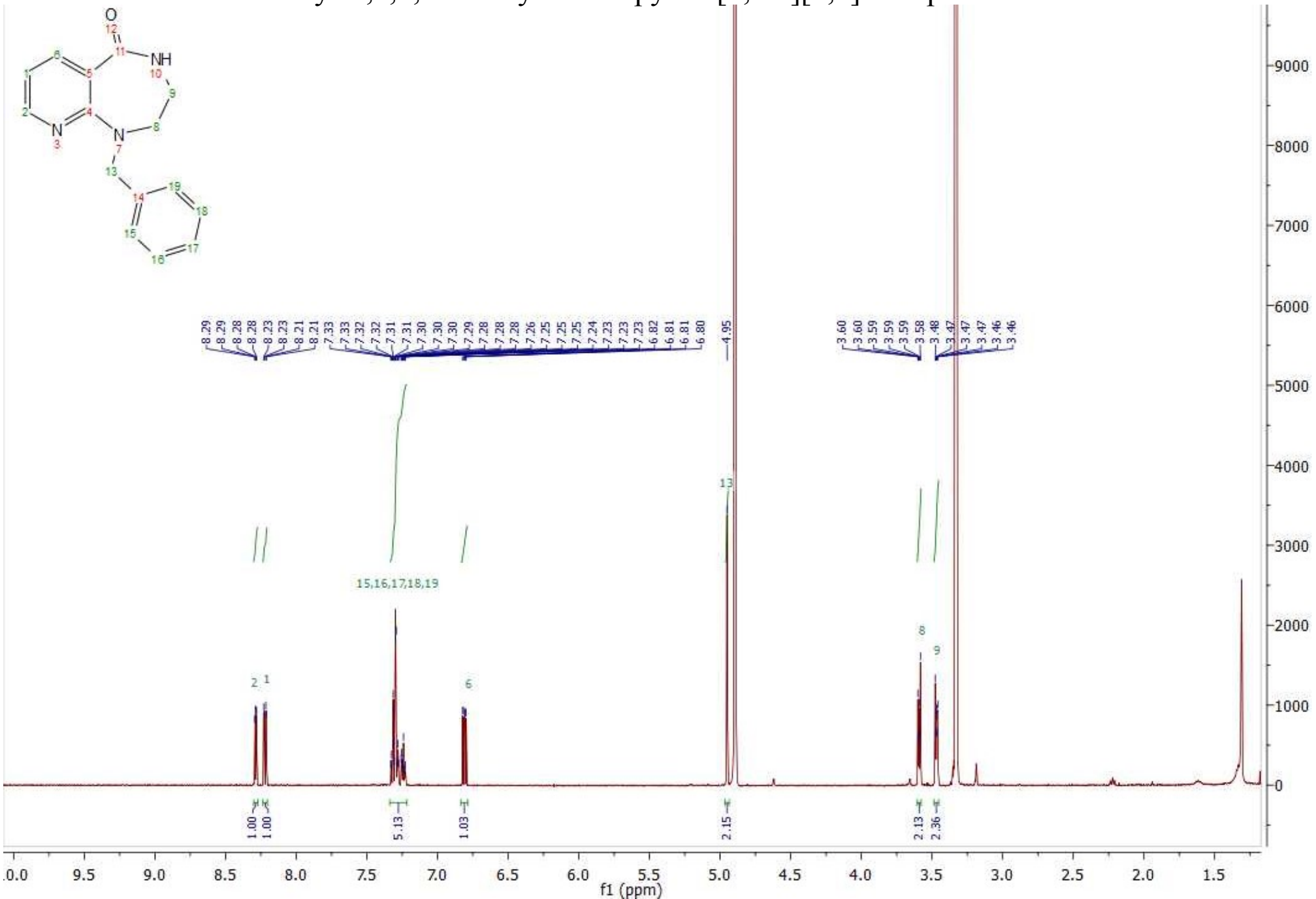
1-Benzoyl-1,2,3,4-tetrahydro-5H-pyrido[2,3-e][1,4]diazepin-5-one **21d**



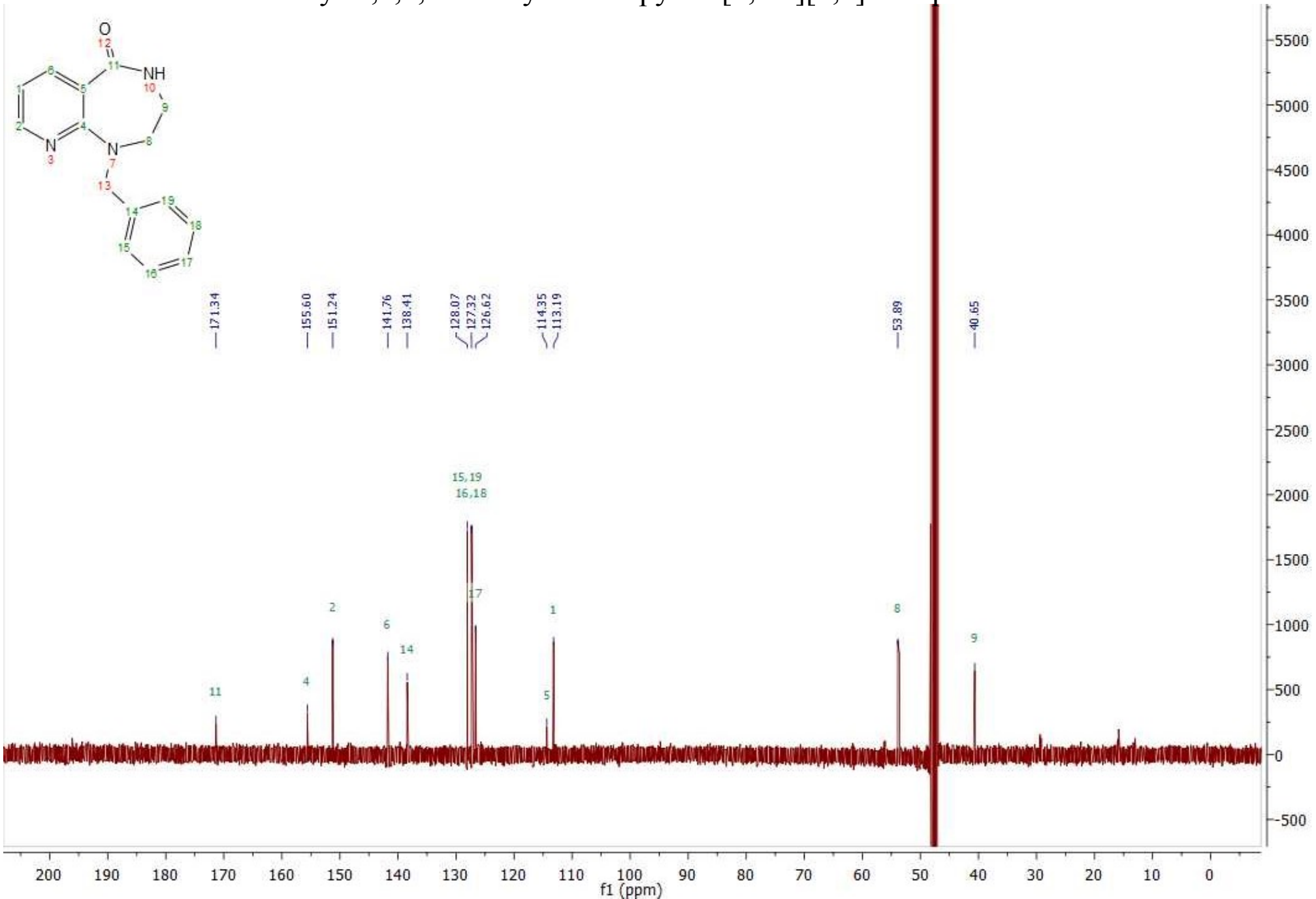
1-Benzoyl-1,2,3,4-tetrahydro-5H-pyrido[2,3-e][1,4]diazepin-5-one **21d**



1-benzyl-1,2,3,4-tetrahydro-5H-pyrido[2,3-e][1,4]diazepin-5-one **21e**

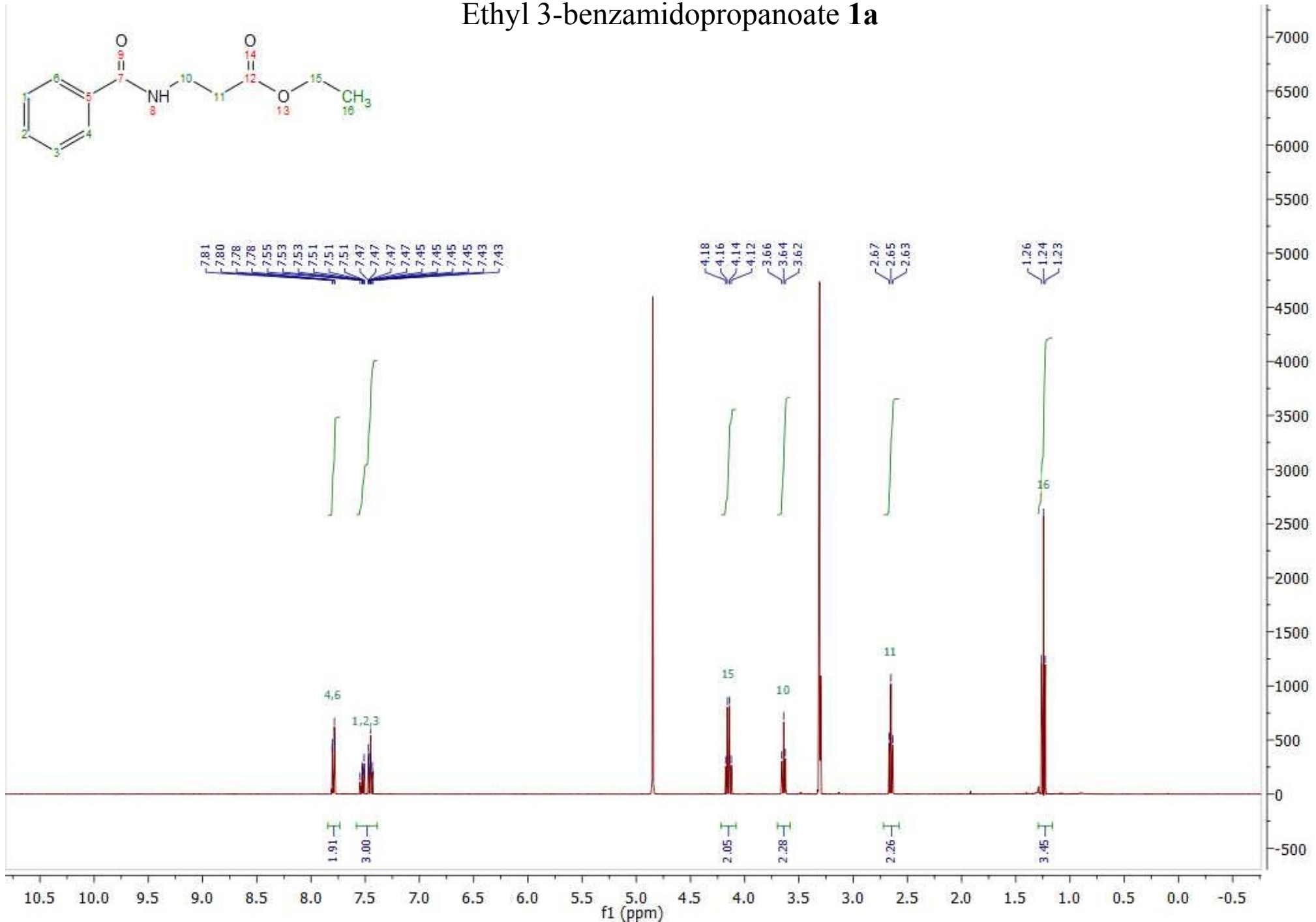


1-benzyl-1,2,3,4-tetrahydro-5H-pyrido[2,3-e][1,4]diazepin-5-one **21e**

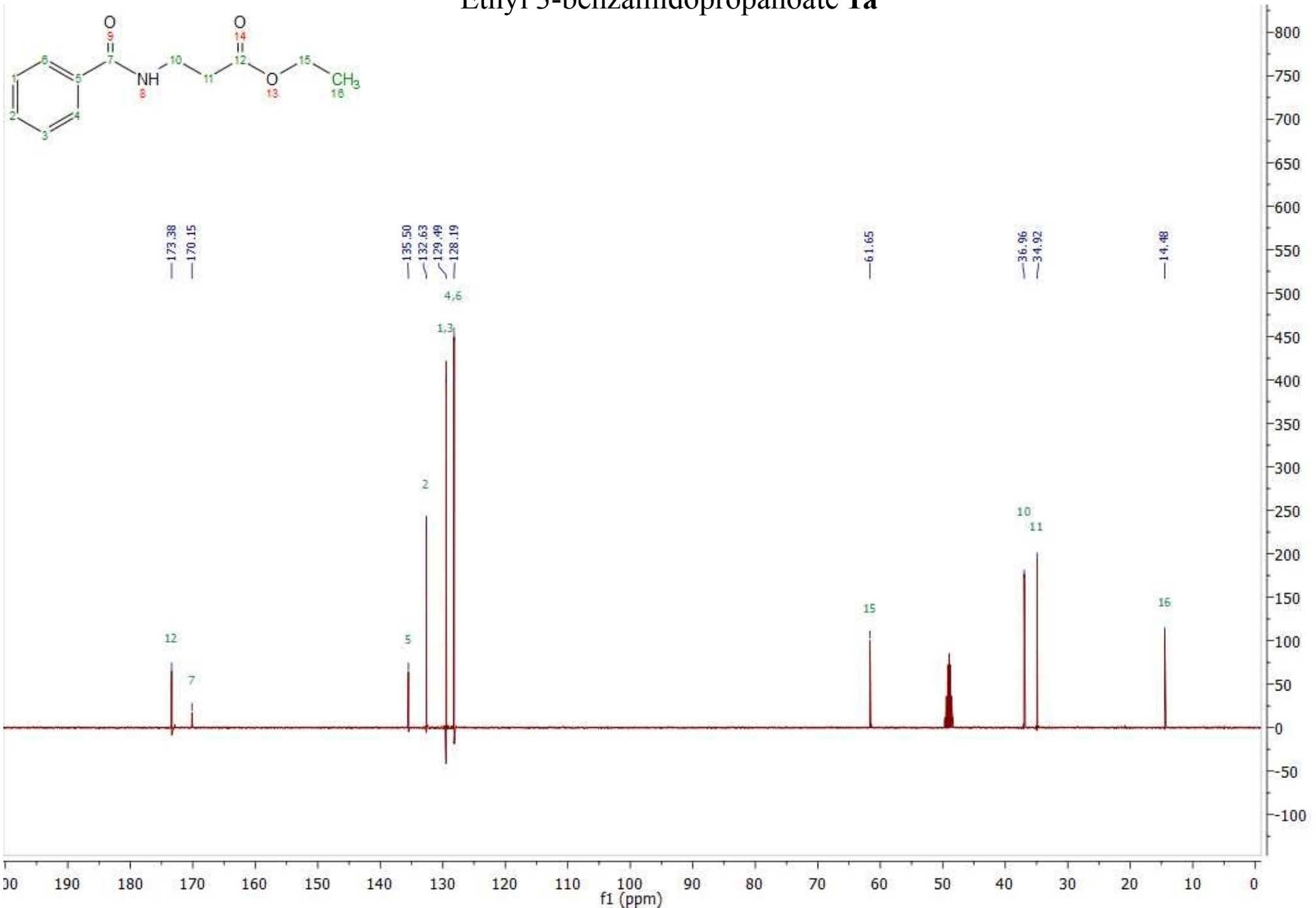


# CHAPTER 3 SPECTRA

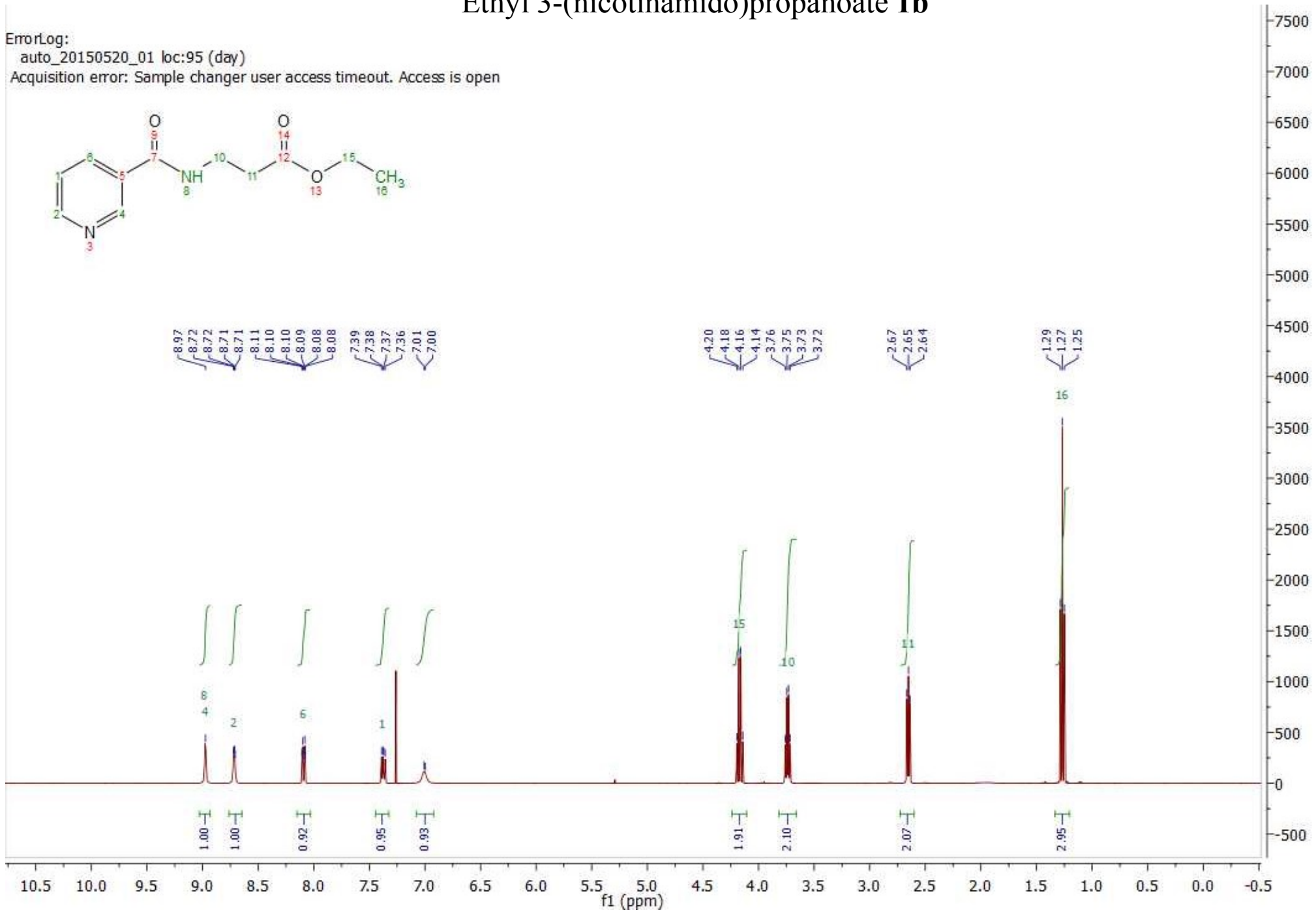
Ethyl 3-benzamidopropanoate **1a**



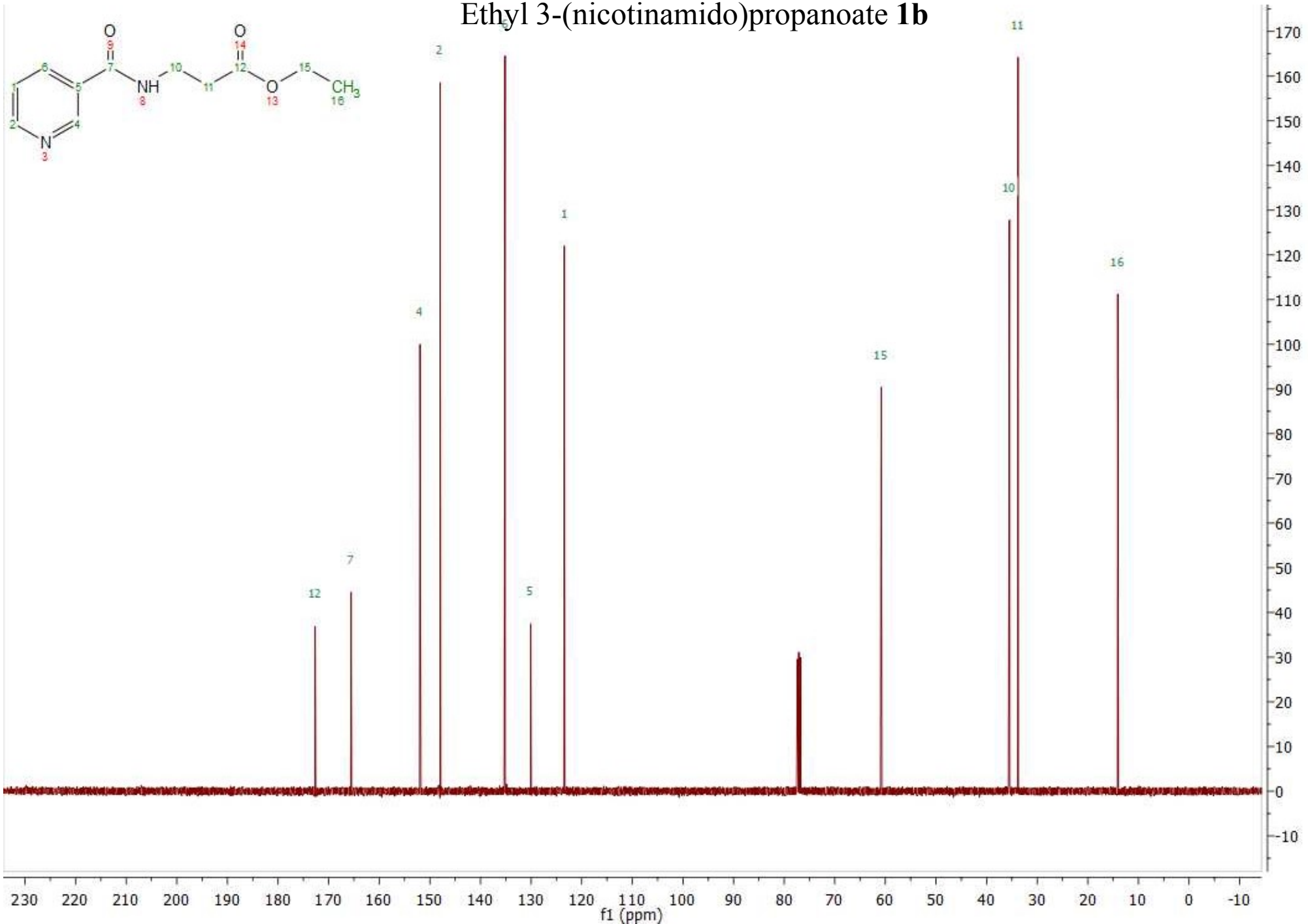
Ethyl 3-benzamidopropanoate **1a**



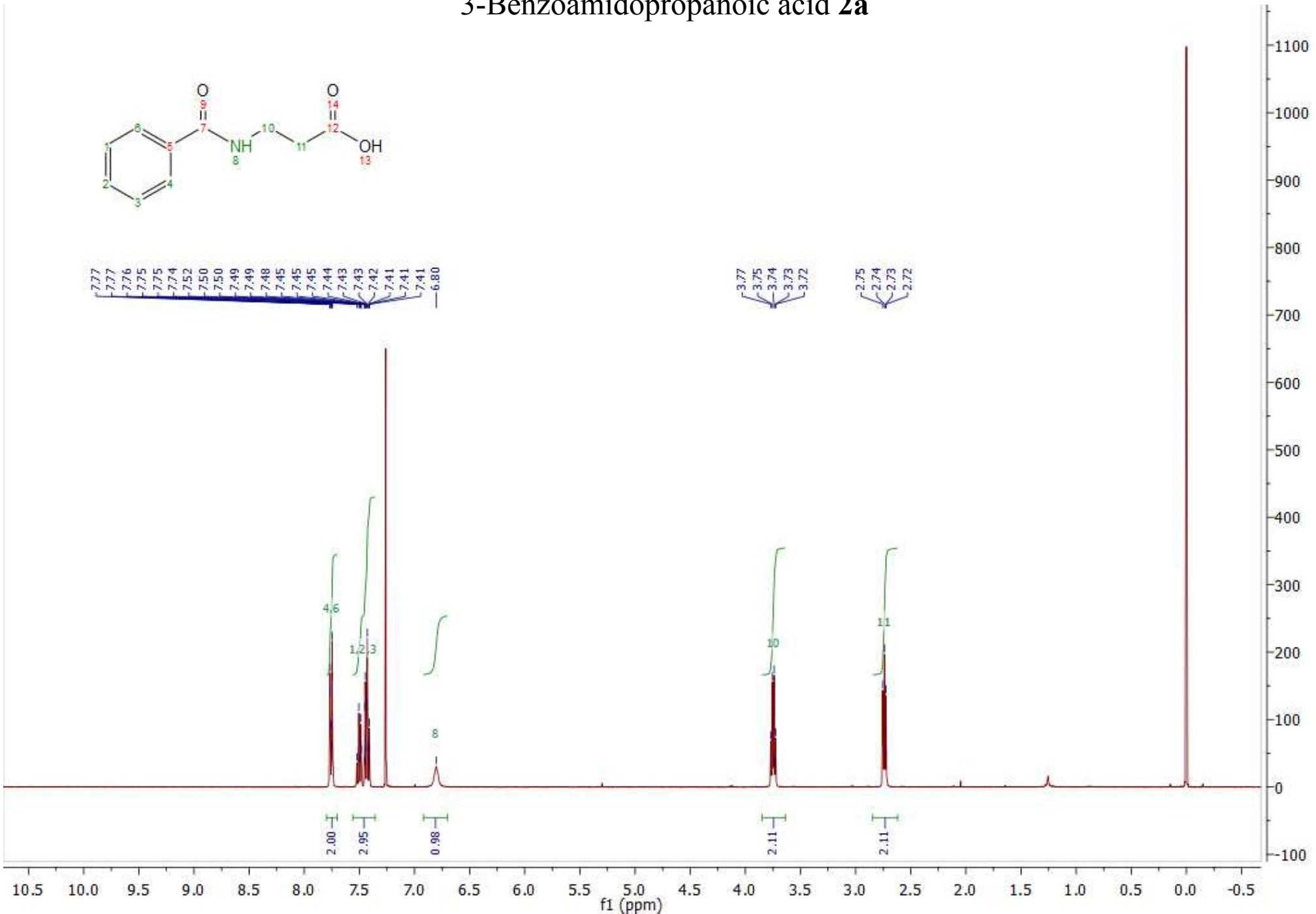
# Ethyl 3-(nicotinamido)propanoate **1b**



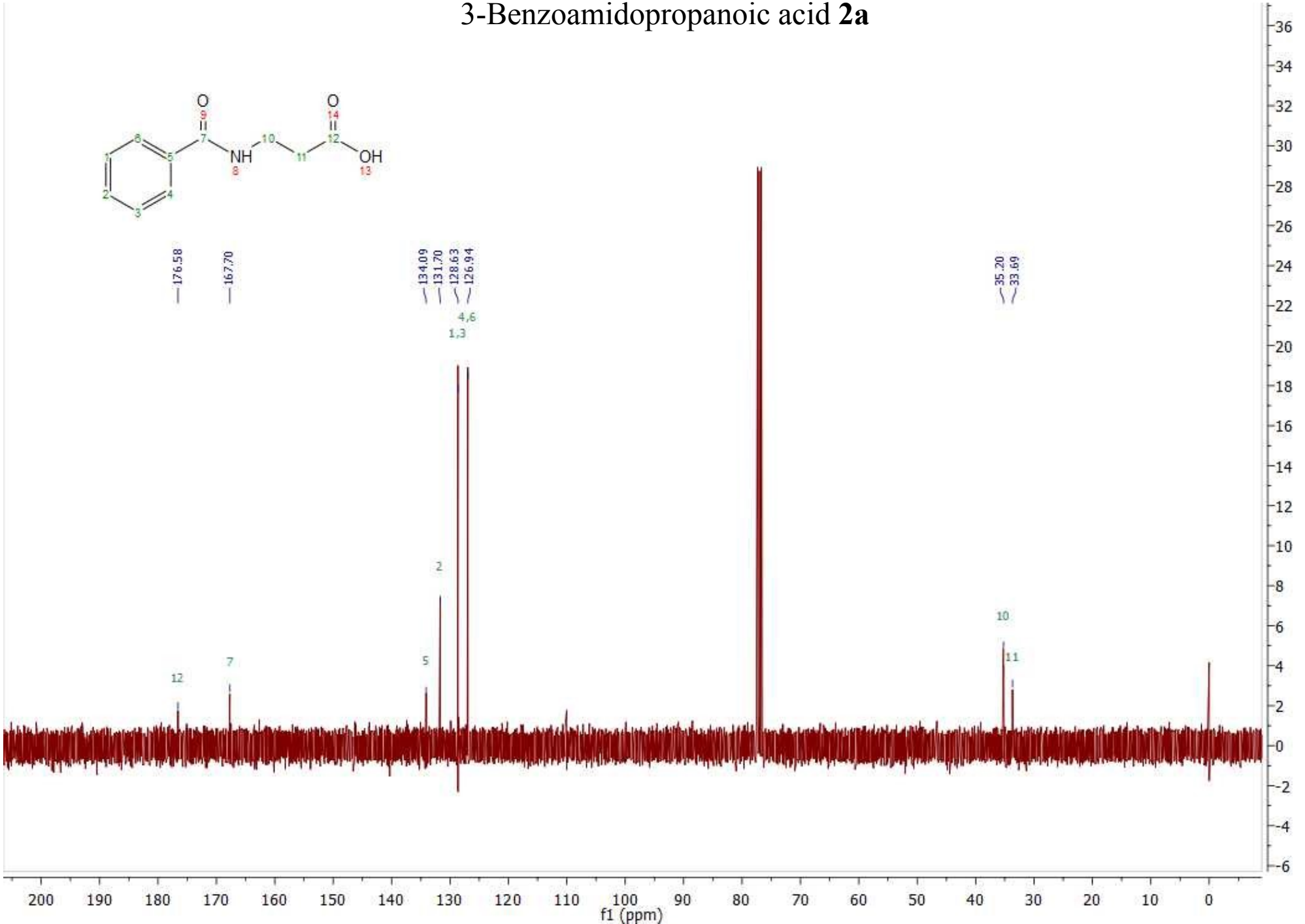
Ethyl 3-(nicotinamido)propanoate **1b**



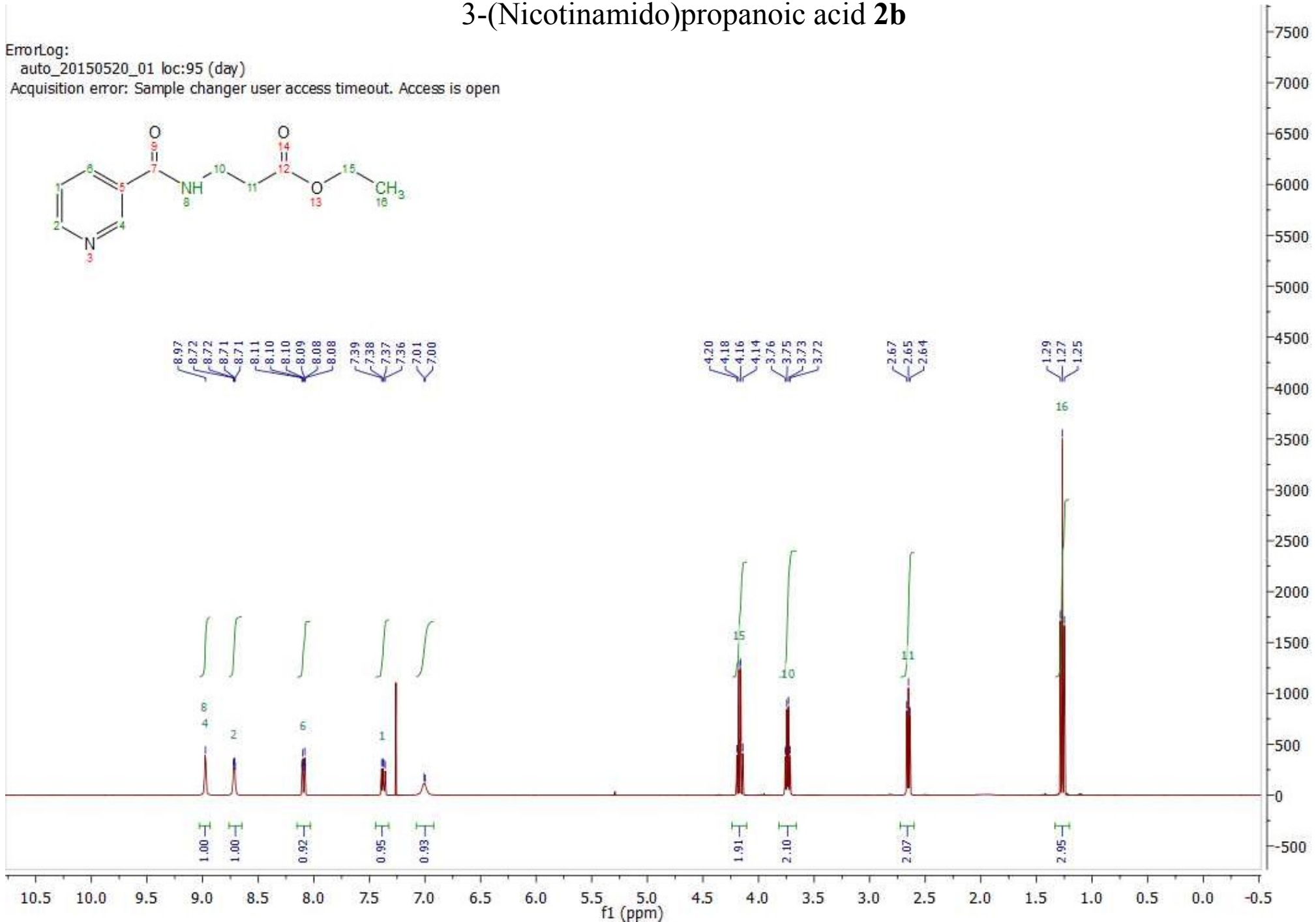
3-Benzoamidopropanoic acid **2a**



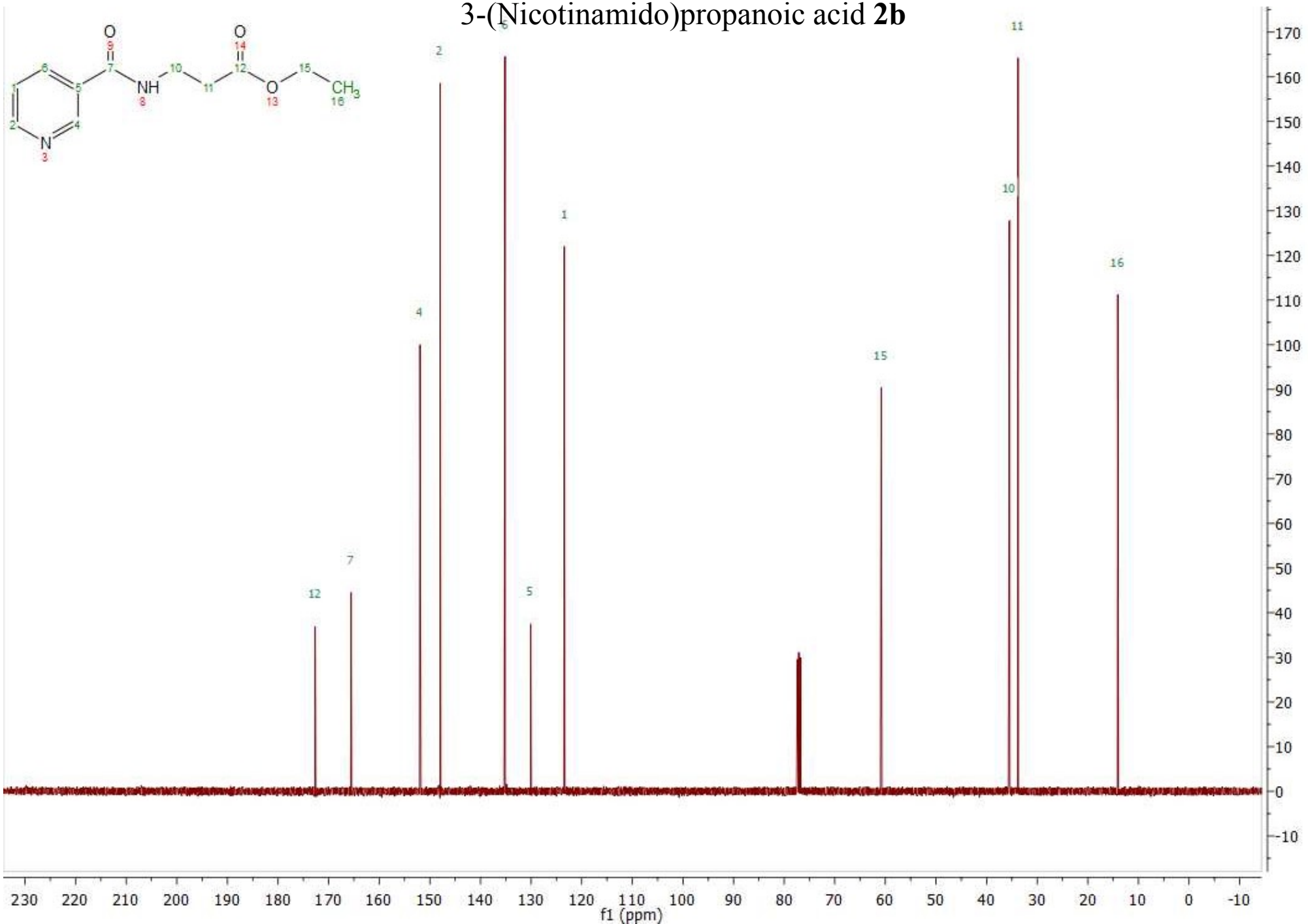
3-Benzoamidopropanoic acid **2a**



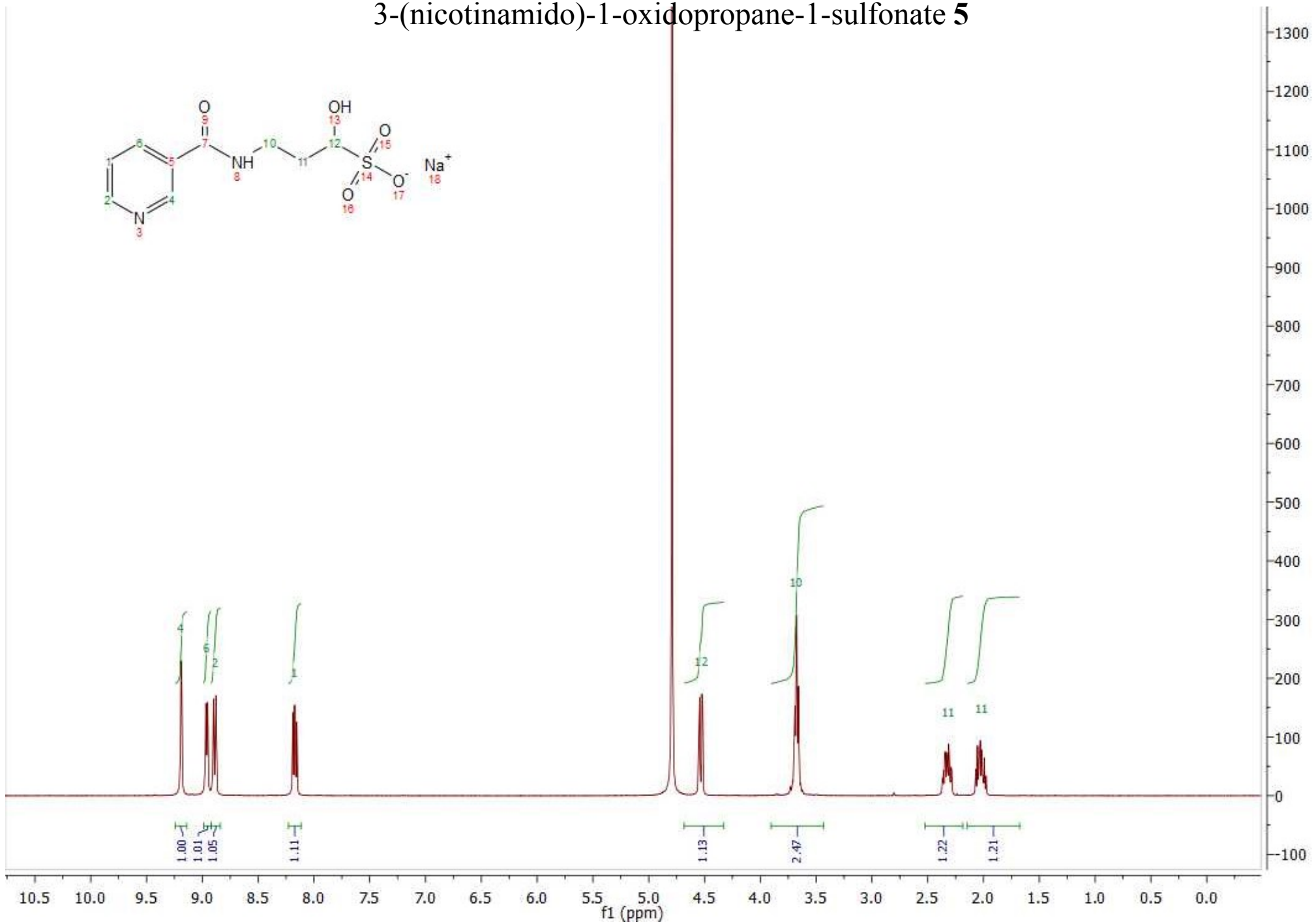
3-(Nicotinamido)propanoic acid **2b**



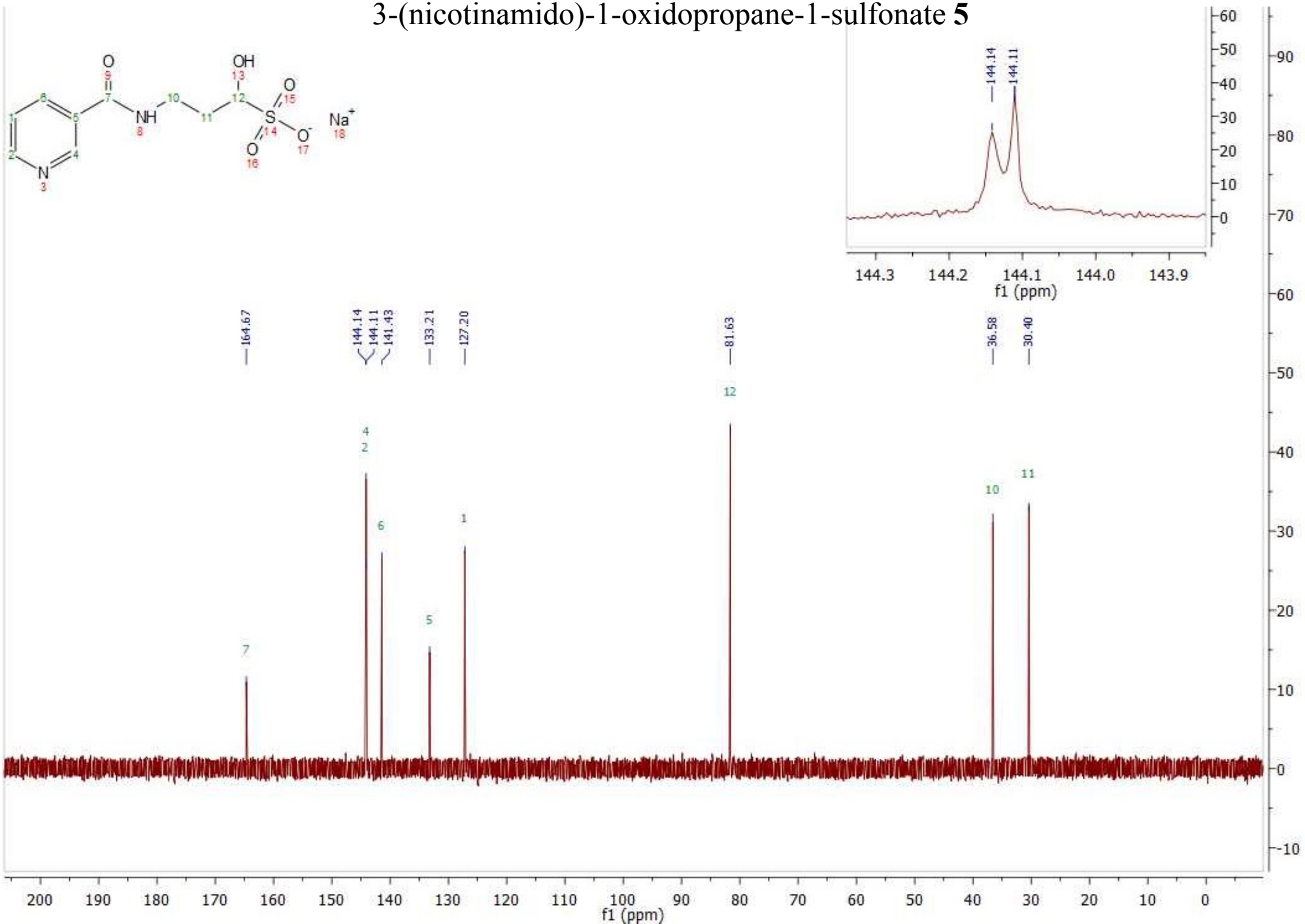
3-(Nicotinamido)propanoic acid **2b**



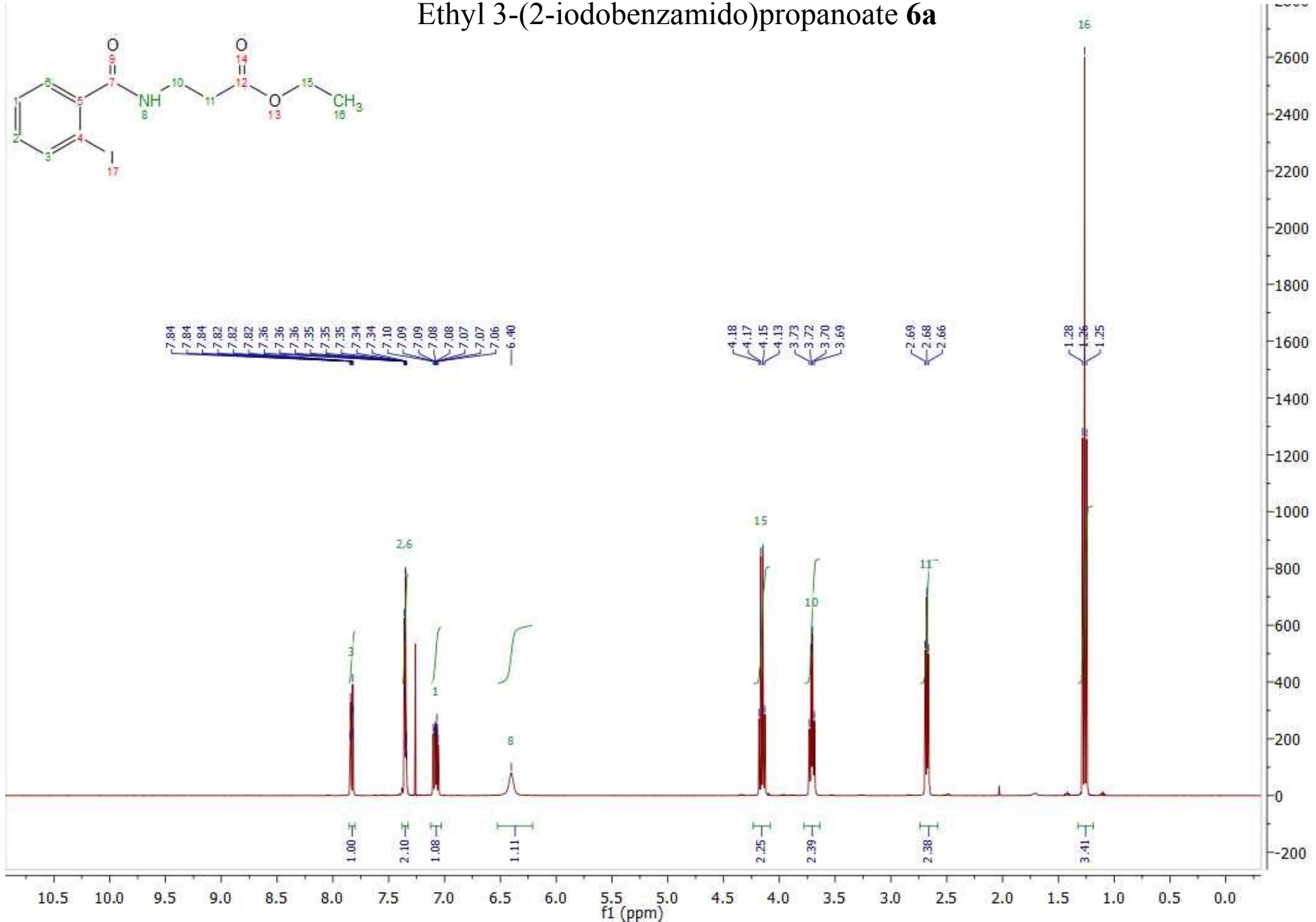
3-(nicotinamido)-1-oxidopropane-1-sulfonate **5**



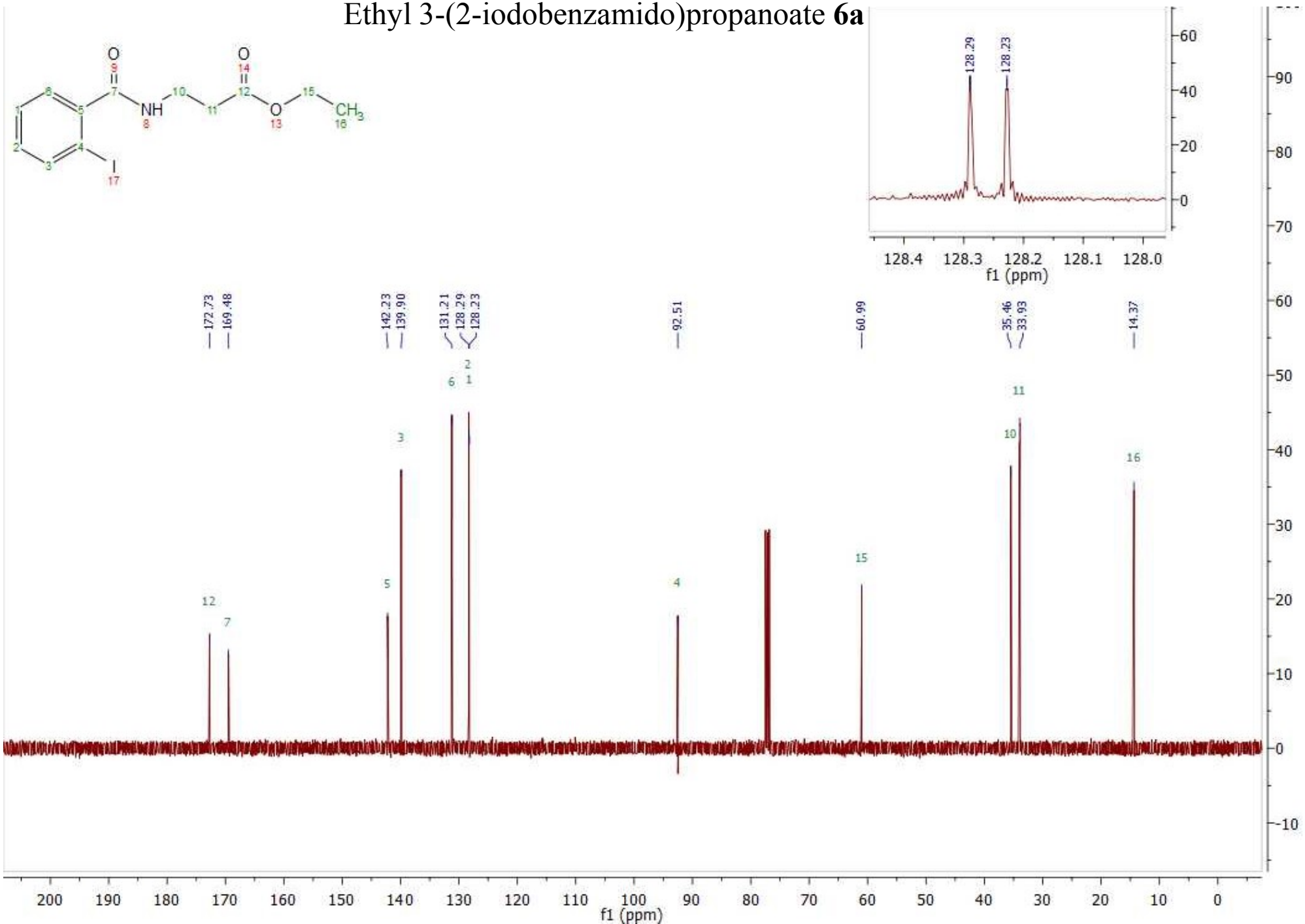
3-(nicotinamido)-1-oxidopropane-1-sulfonate **5**



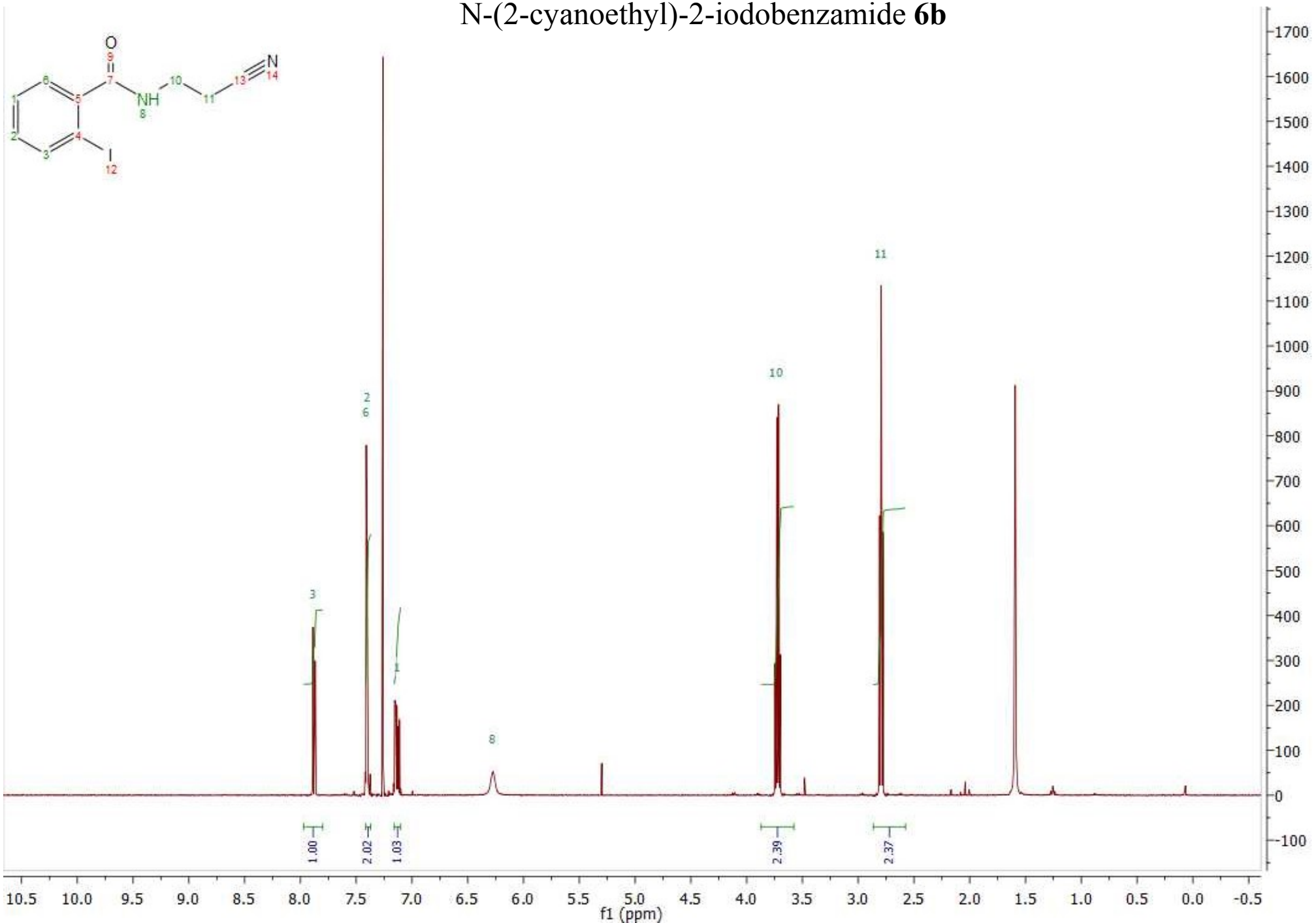
Ethyl 3-(2-iodobenzamido)propanoate **6a**



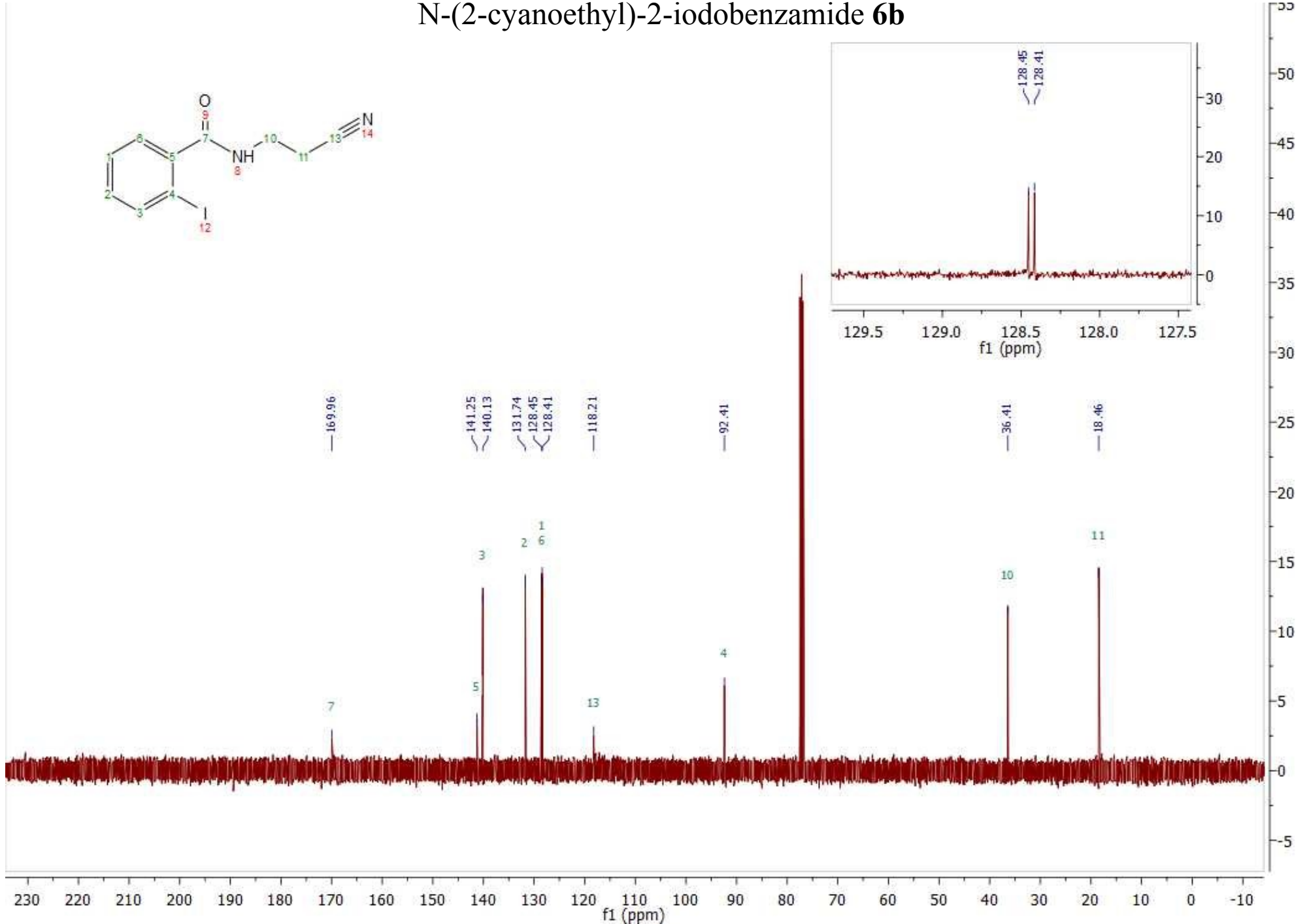
Ethyl 3-(2-iodobenzamido)propanoate **6a**



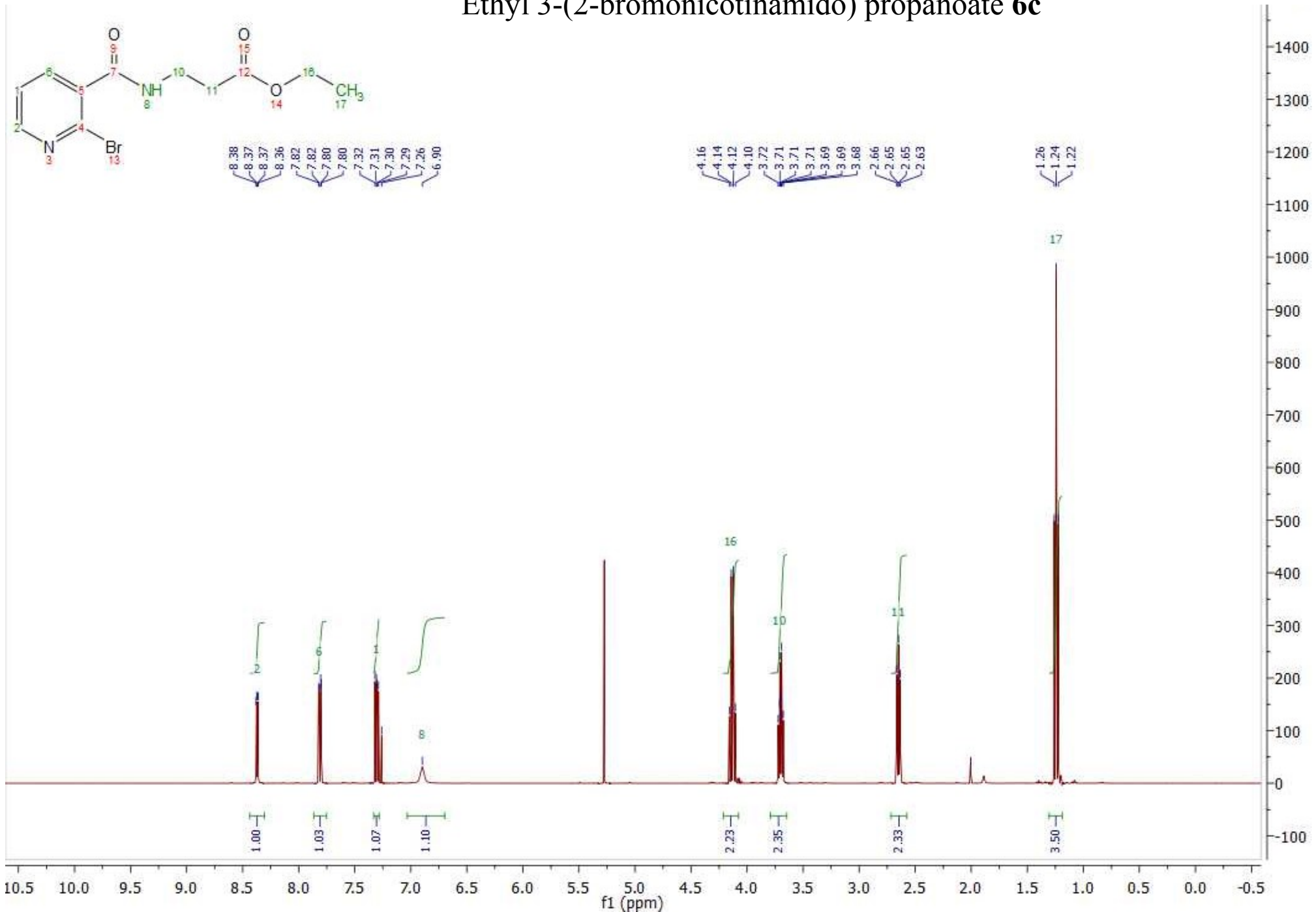
N-(2-cyanoethyl)-2-iodobenzamide **6b**



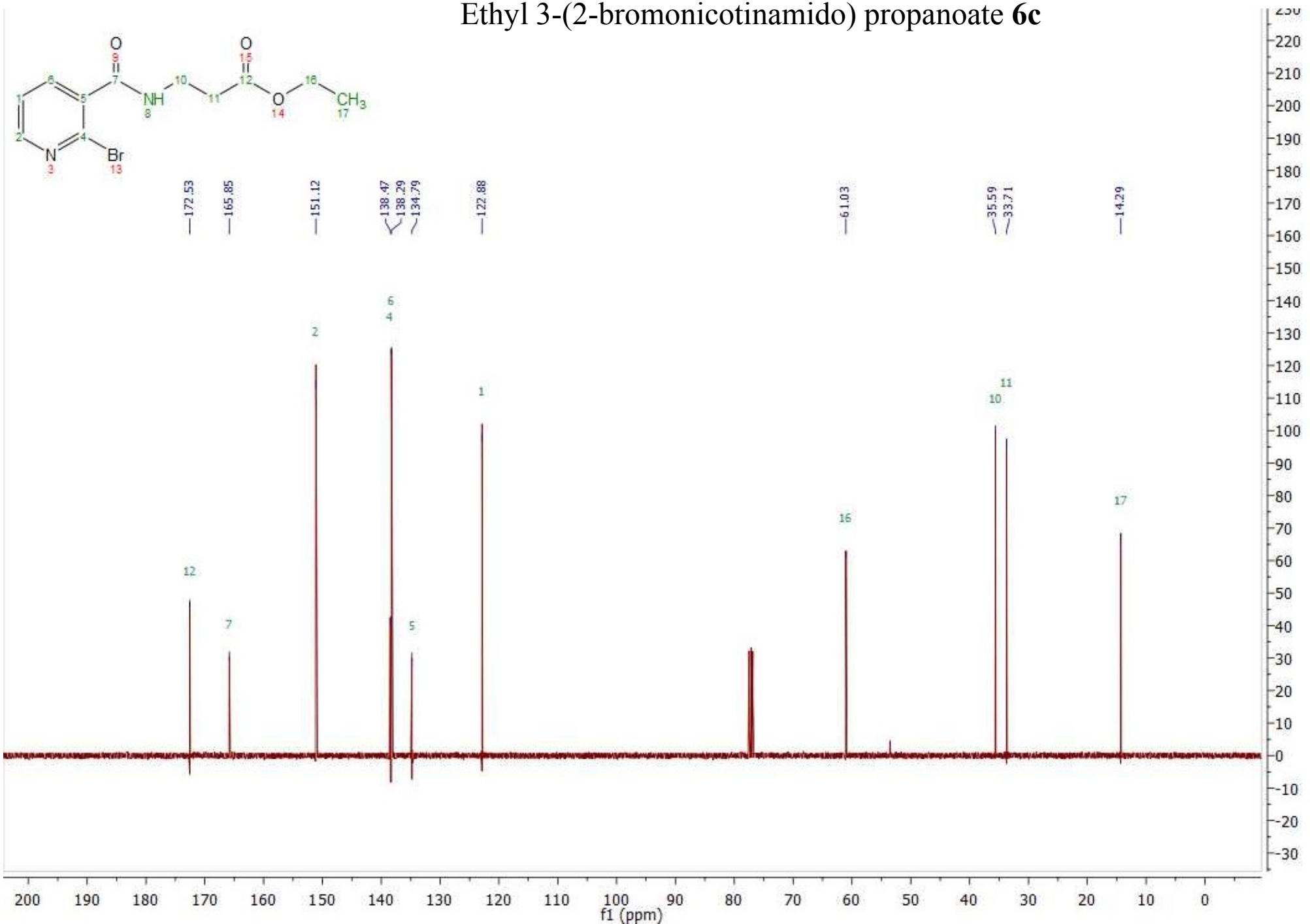
N-(2-cyanoethyl)-2-iodobenzamide **6b**



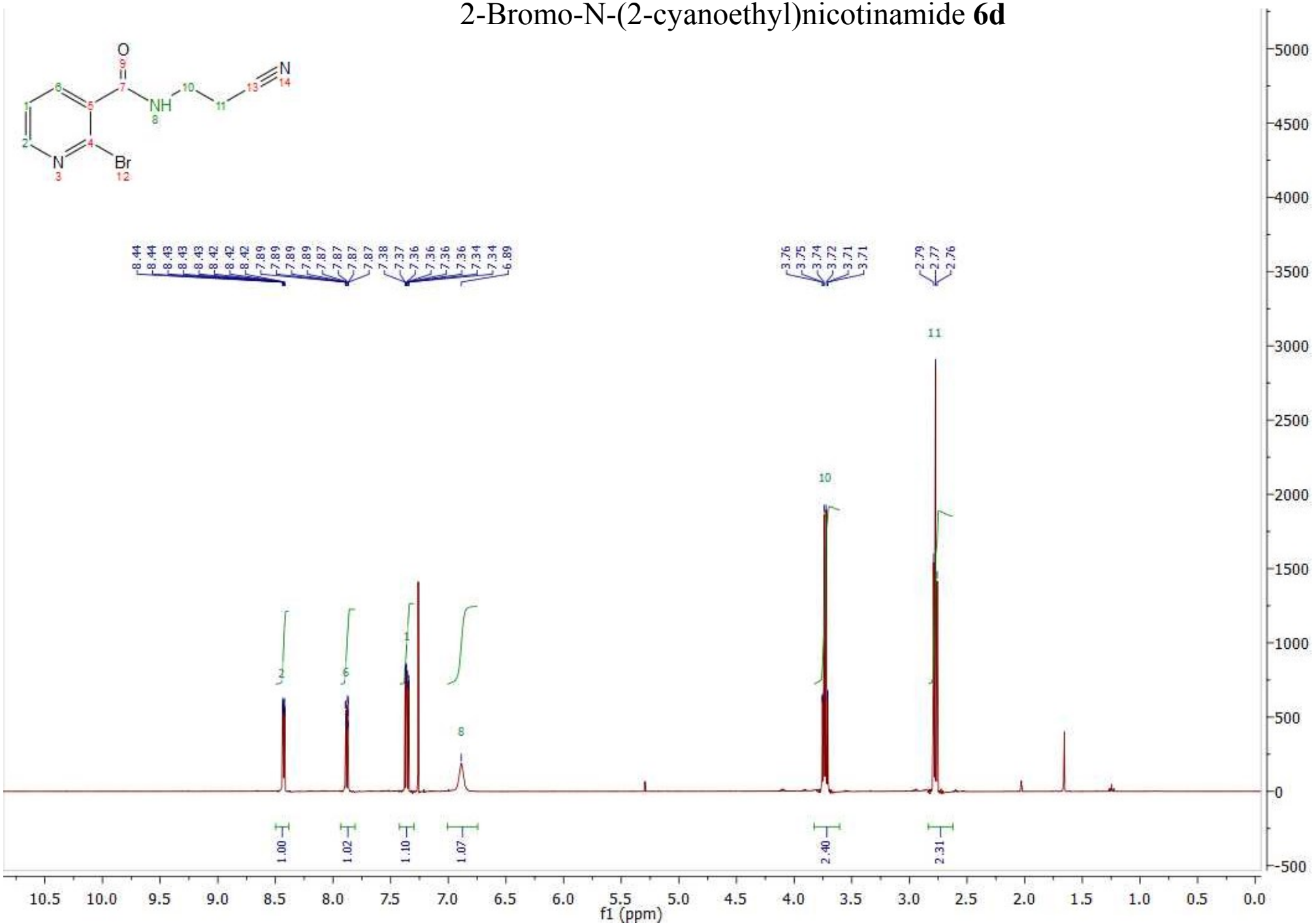
Ethyl 3-(2-bromonicotinamido) propanoate **6c**



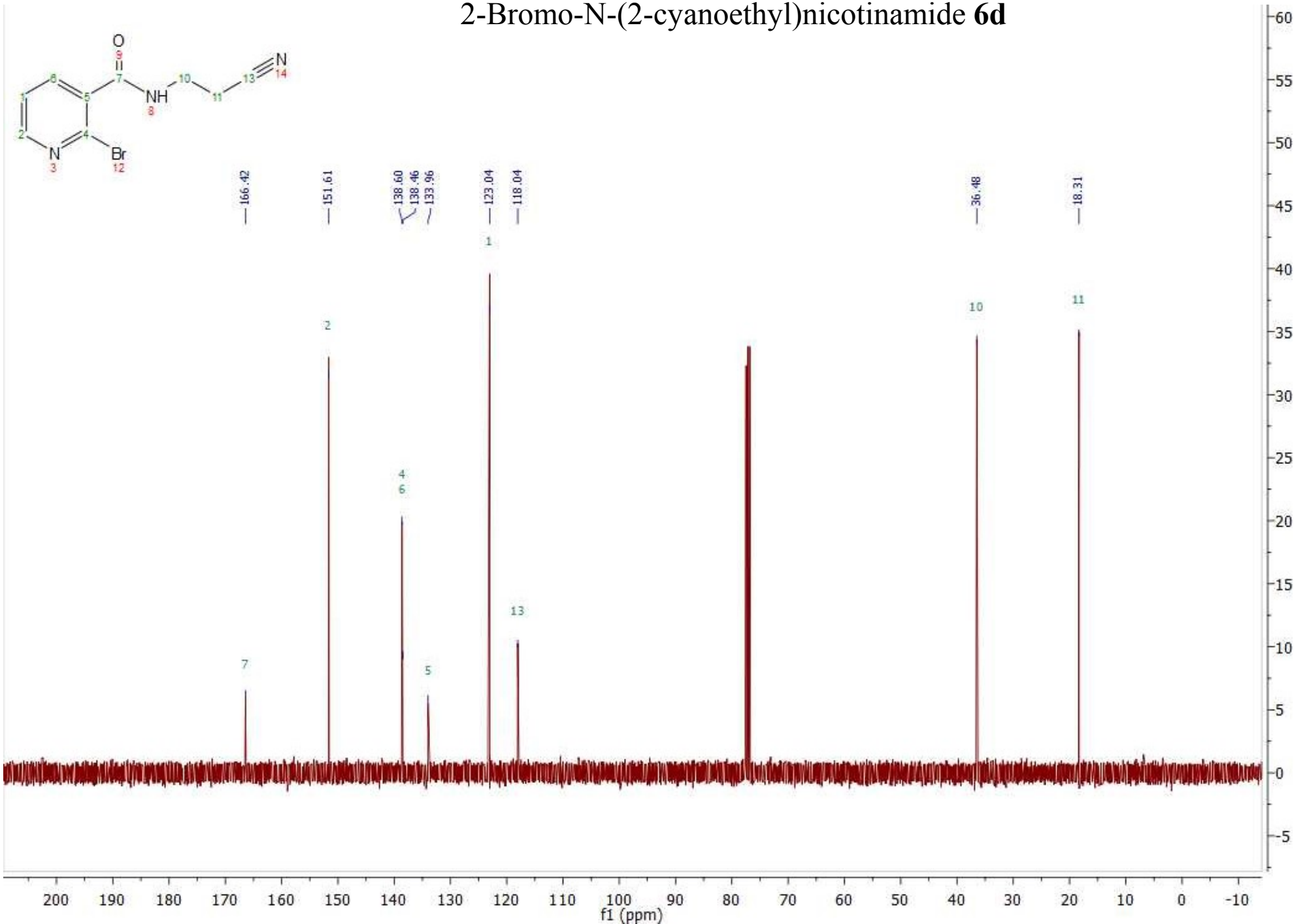
Ethyl 3-(2-bromonicotinamido) propanoate **6c**



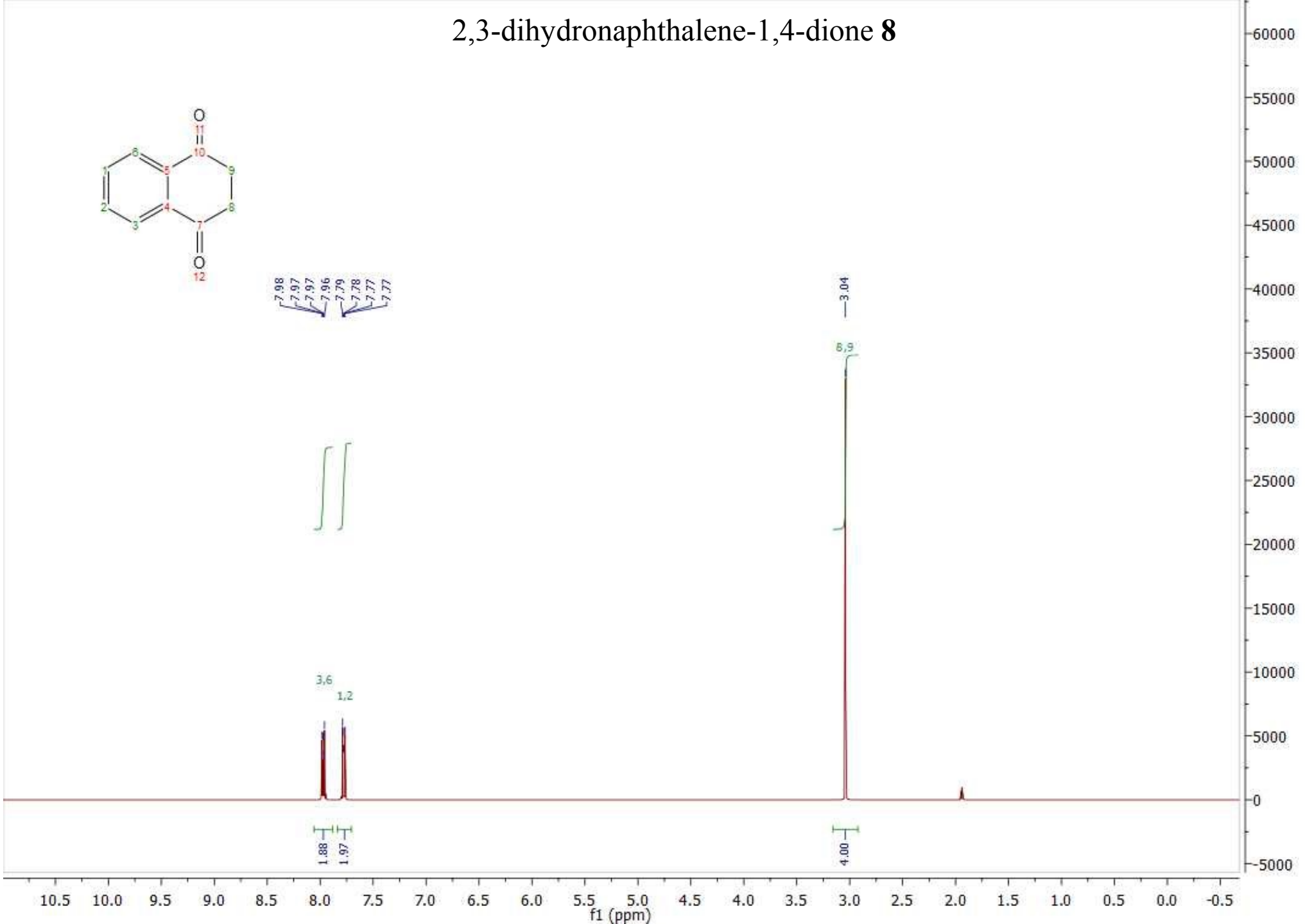
2-Bromo-N-(2-cyanoethyl)nicotinamide **6d**



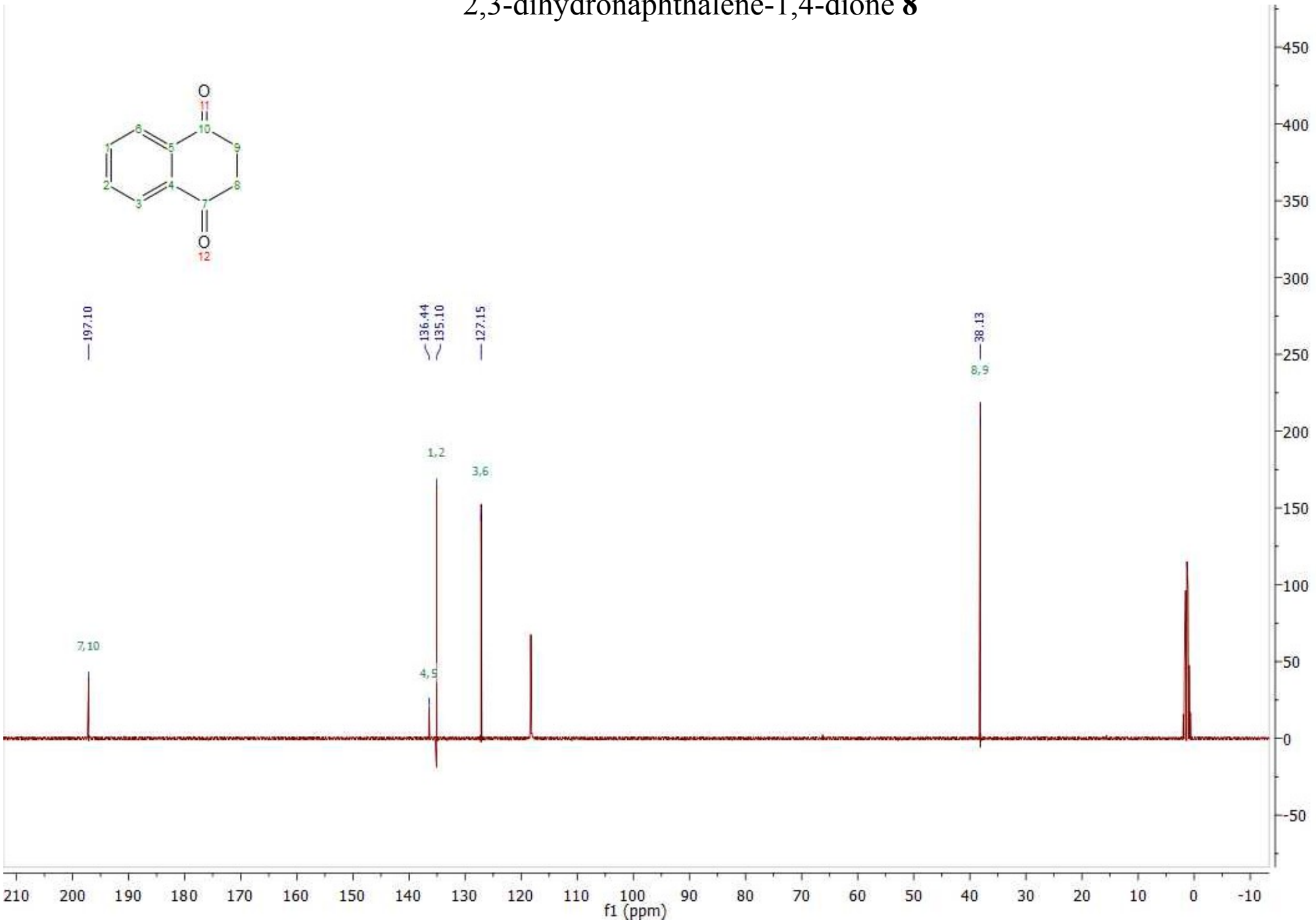
2-Bromo-N-(2-cyanoethyl)nicotinamide **6d**



2,3-dihydronaphthalene-1,4-dione **8**



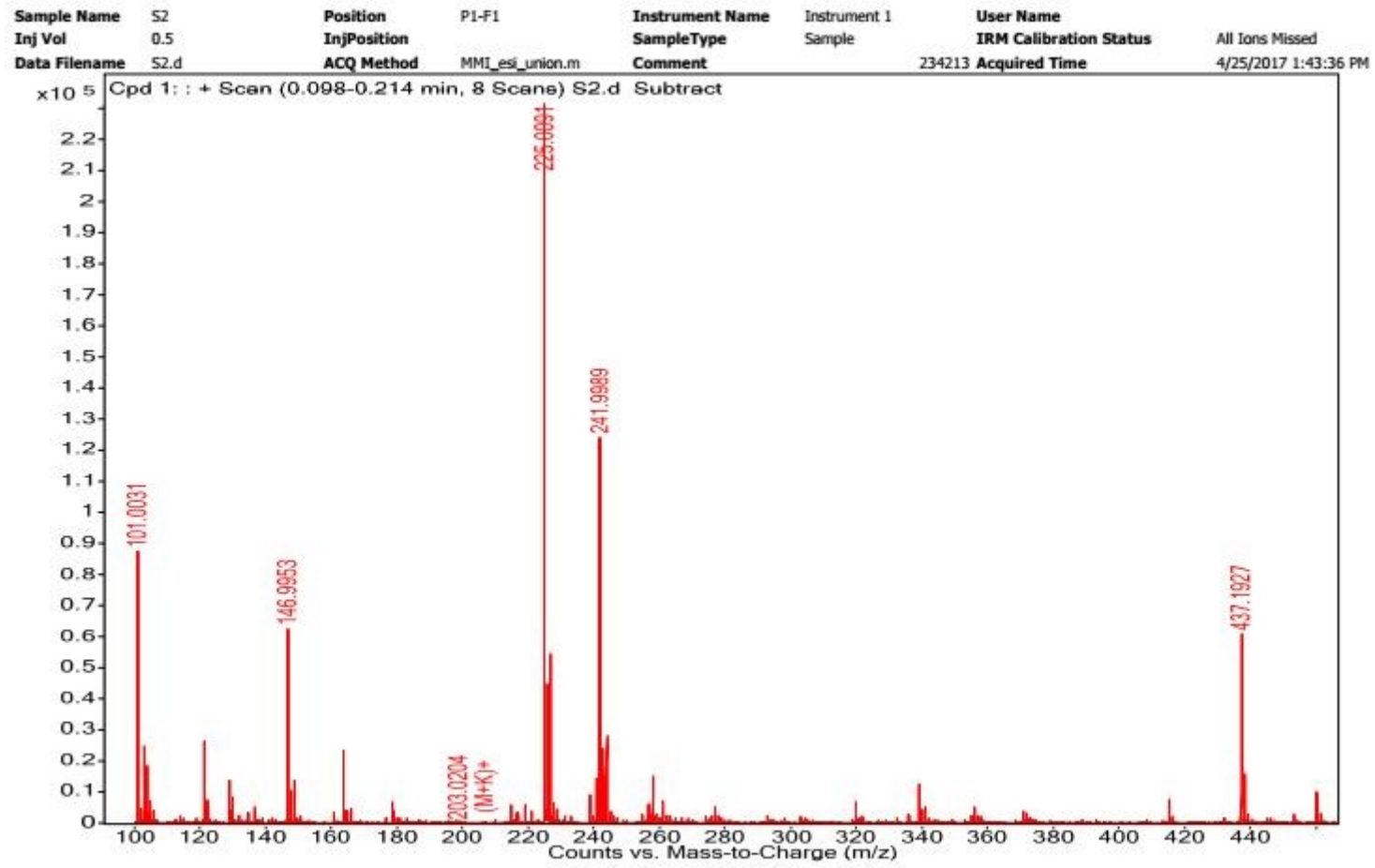
2,3-dihydronaphthalene-1,4-dione **8**



# APPENDIX E: HIGH-RESOLUTION MASS SPECTRA (MS)

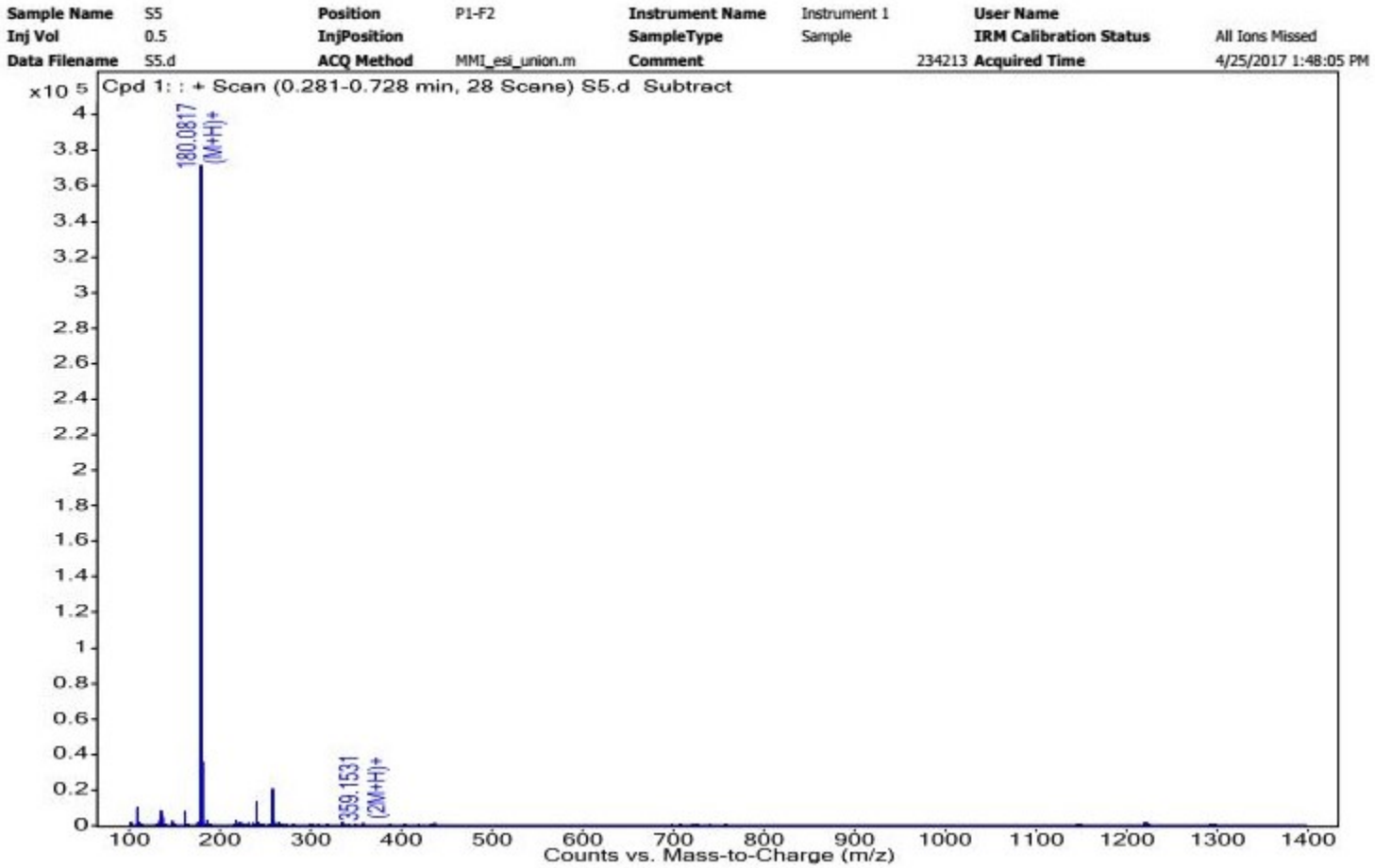
# 6,7-dihydropyrrolo[2,3-c]azepine-4,8(1H,5H)-dione ($C_8H_8N_2O_2$) **2**

HRMS (ESI) m/z calcd for (M+K)+ 203.0217, found 203.0204



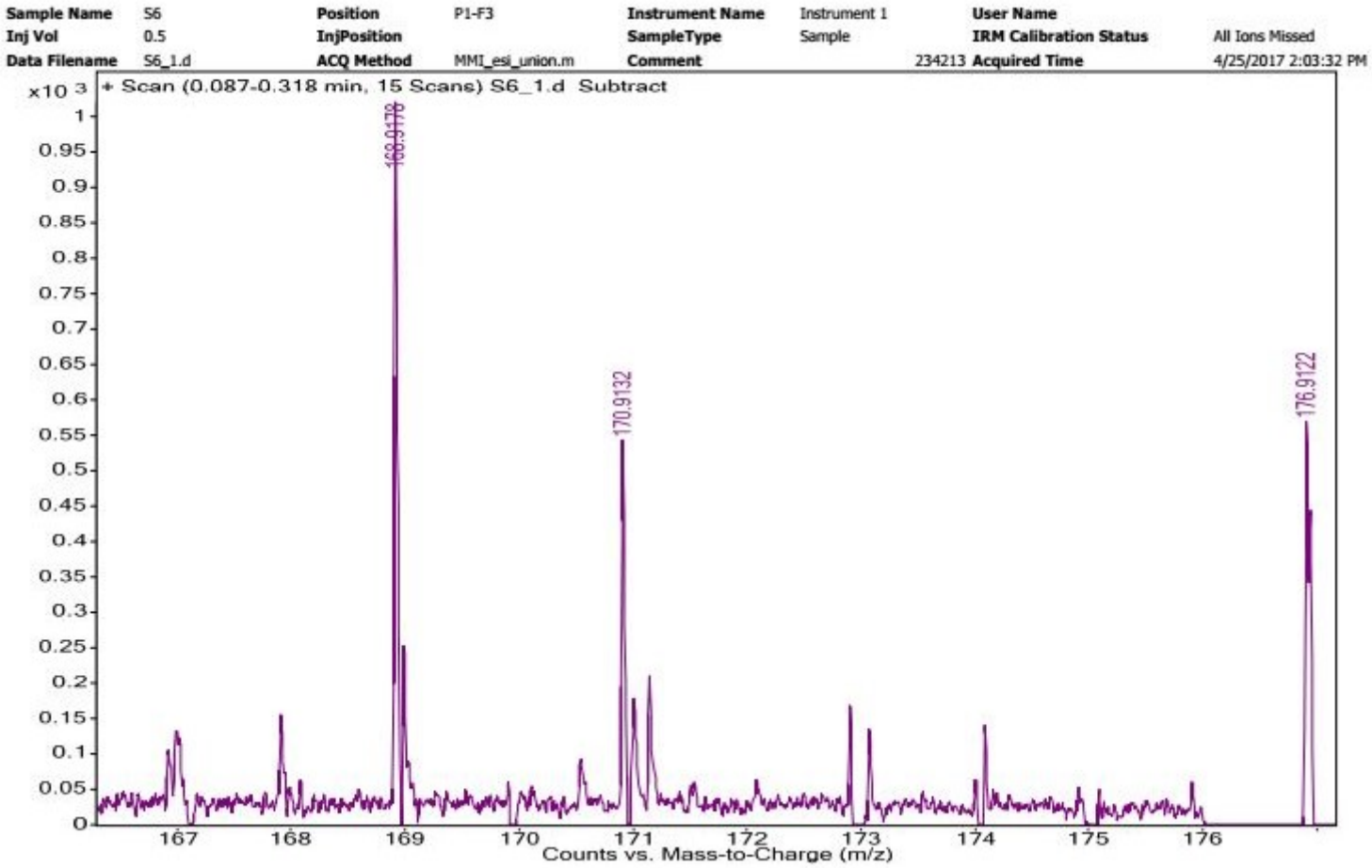
# 8-fluoro-2,3,4,5-tetrahydro-1H-benzo[c]azepin-1-one ($C_{10}H_{10}FNO$) **5**

HRMS (ESI) m/z calcd for (M+H)+ 180.0825, found 180.0817



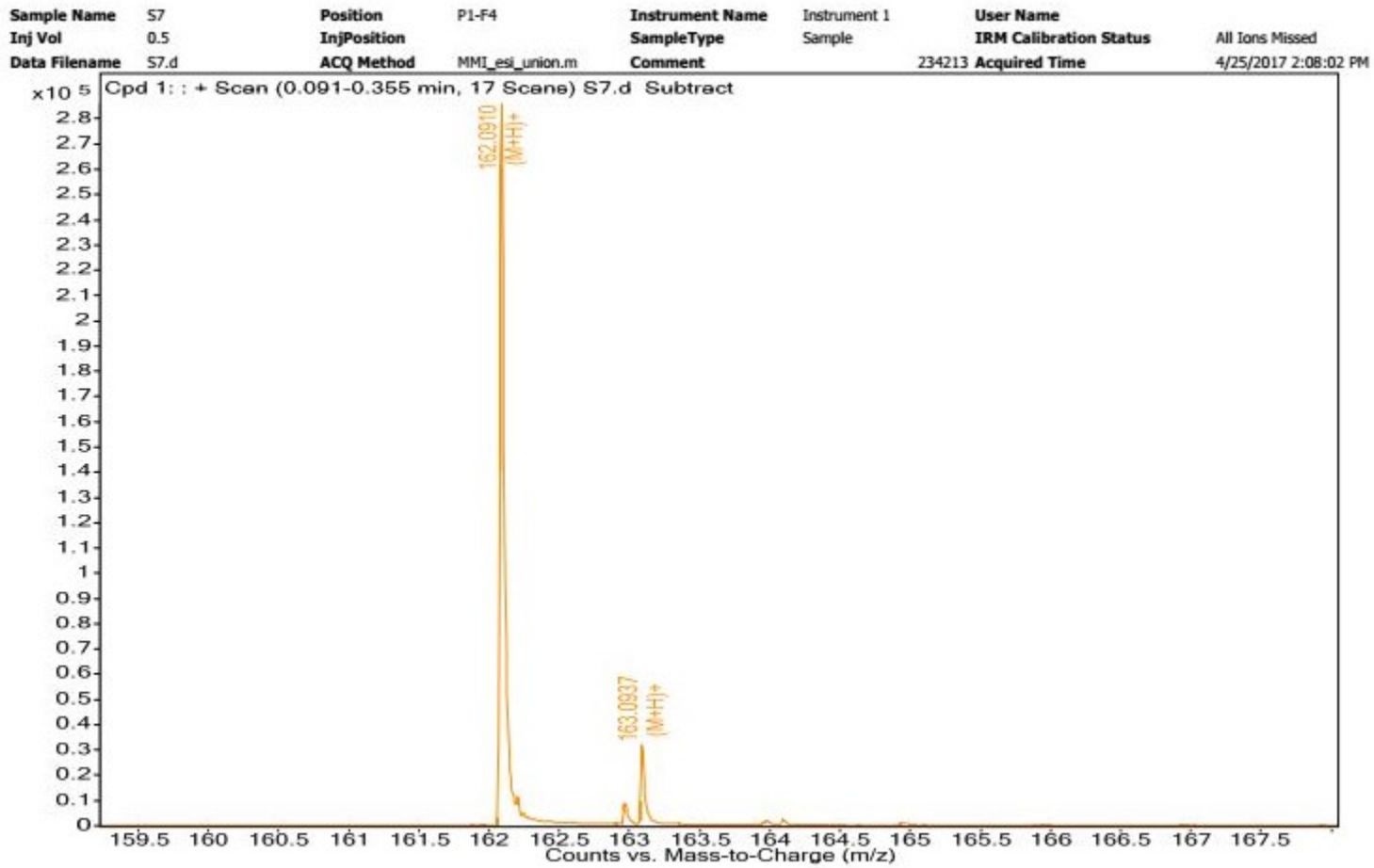
# 3,4-dihydro-1H-benzo[c]azepine-1,5(2H)-dione ($C_{10}H_9NO_2$) **6**

HRMS (ESI) m/z calcd for (M+H)+ calcd 176.0712, found 176.9122



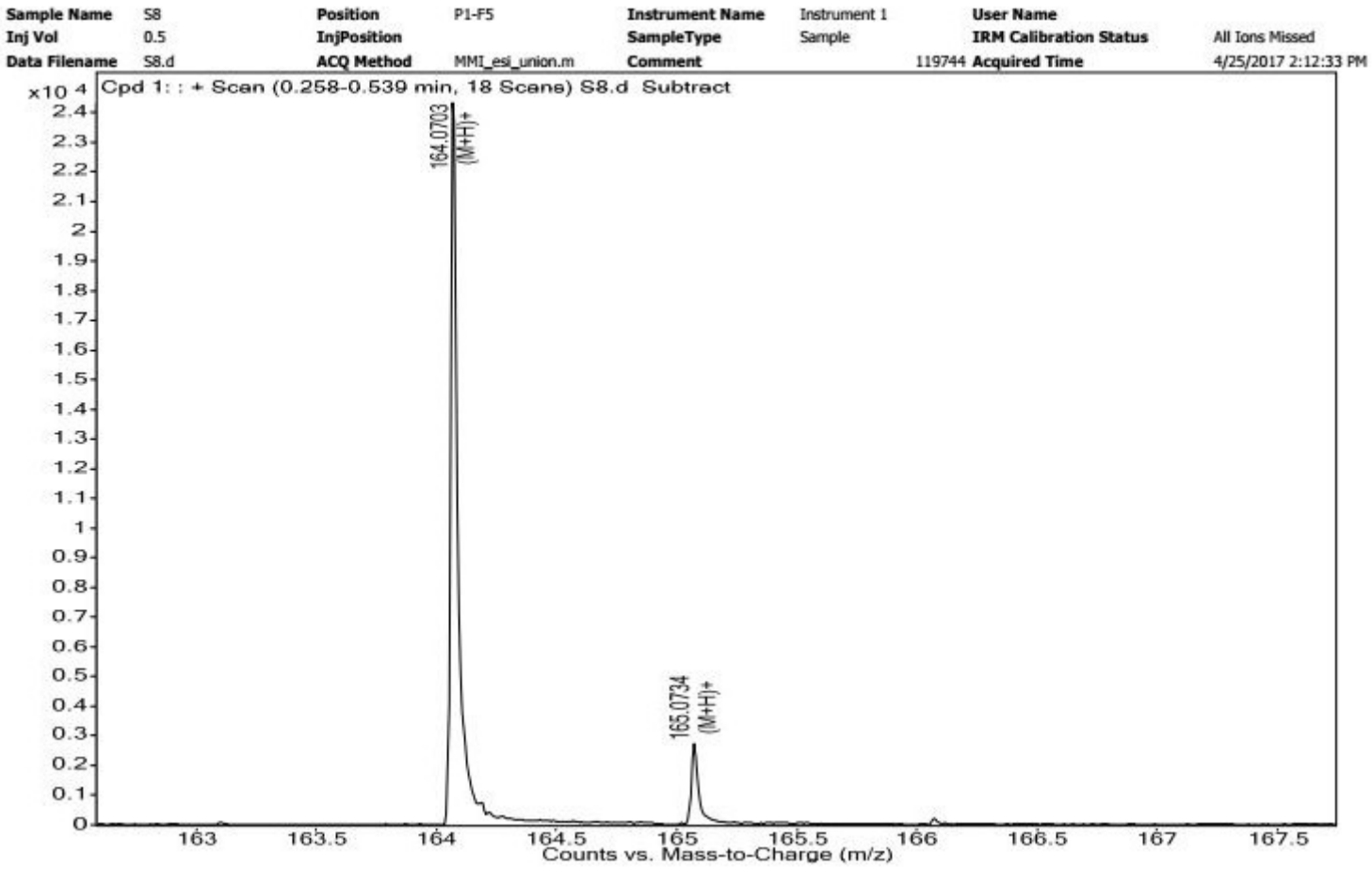
# 2,3,4,5-Tetrahydro-1H-benzo[c]azepin-1-one ($C_{10}H_{11}NO$) **7**

HRMS (ESI) m/z calcd for (M+H)+ 162.0913, found 162.0910



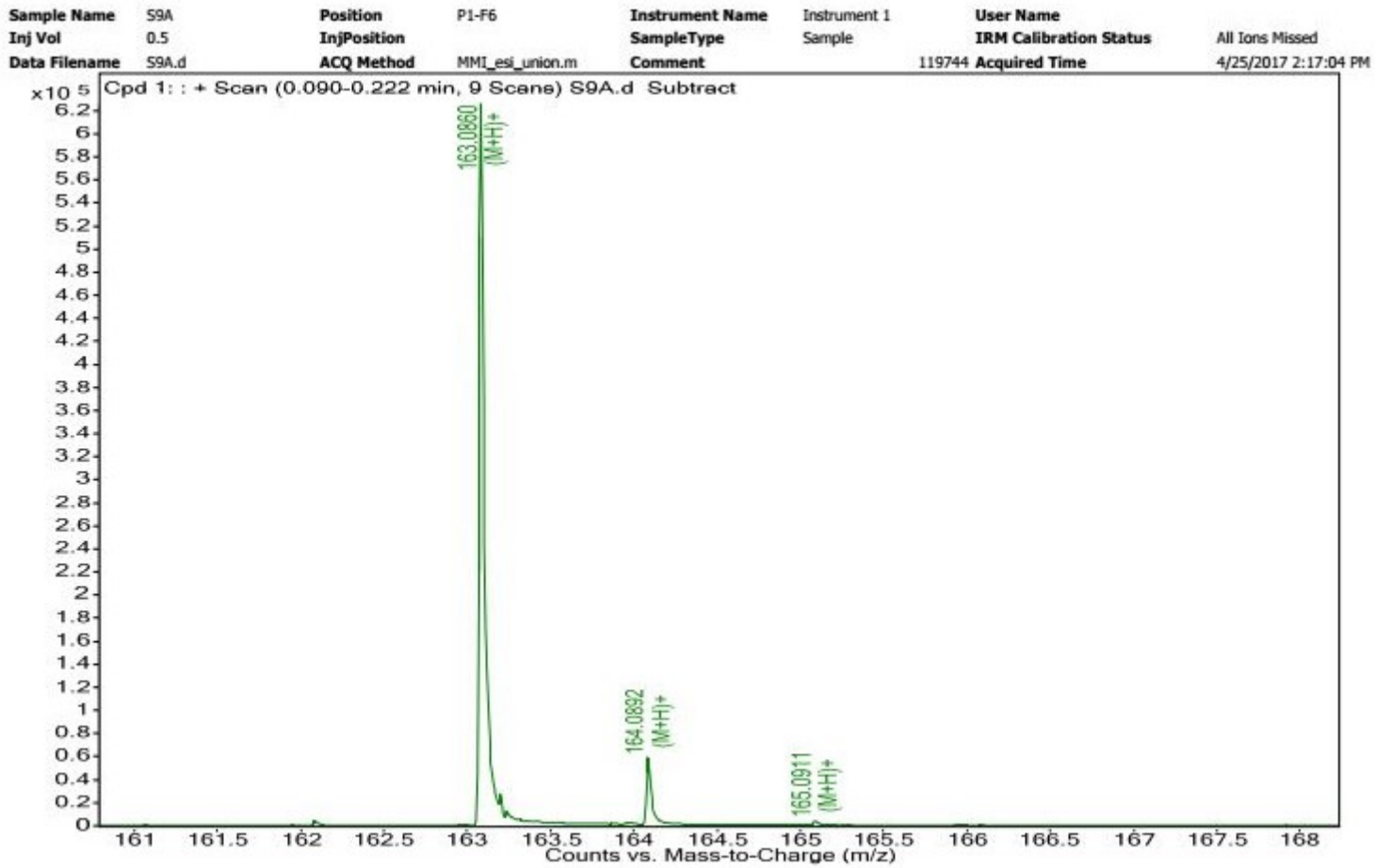
# 3,4-dihydrobenzo[f][1,4]oxazepin-5(2H)-one ($C_9H_9NO_2$) **8**

HRSM (ESI) m/z calcd for (M+H)+ calcd 164.0706, found 164.0703



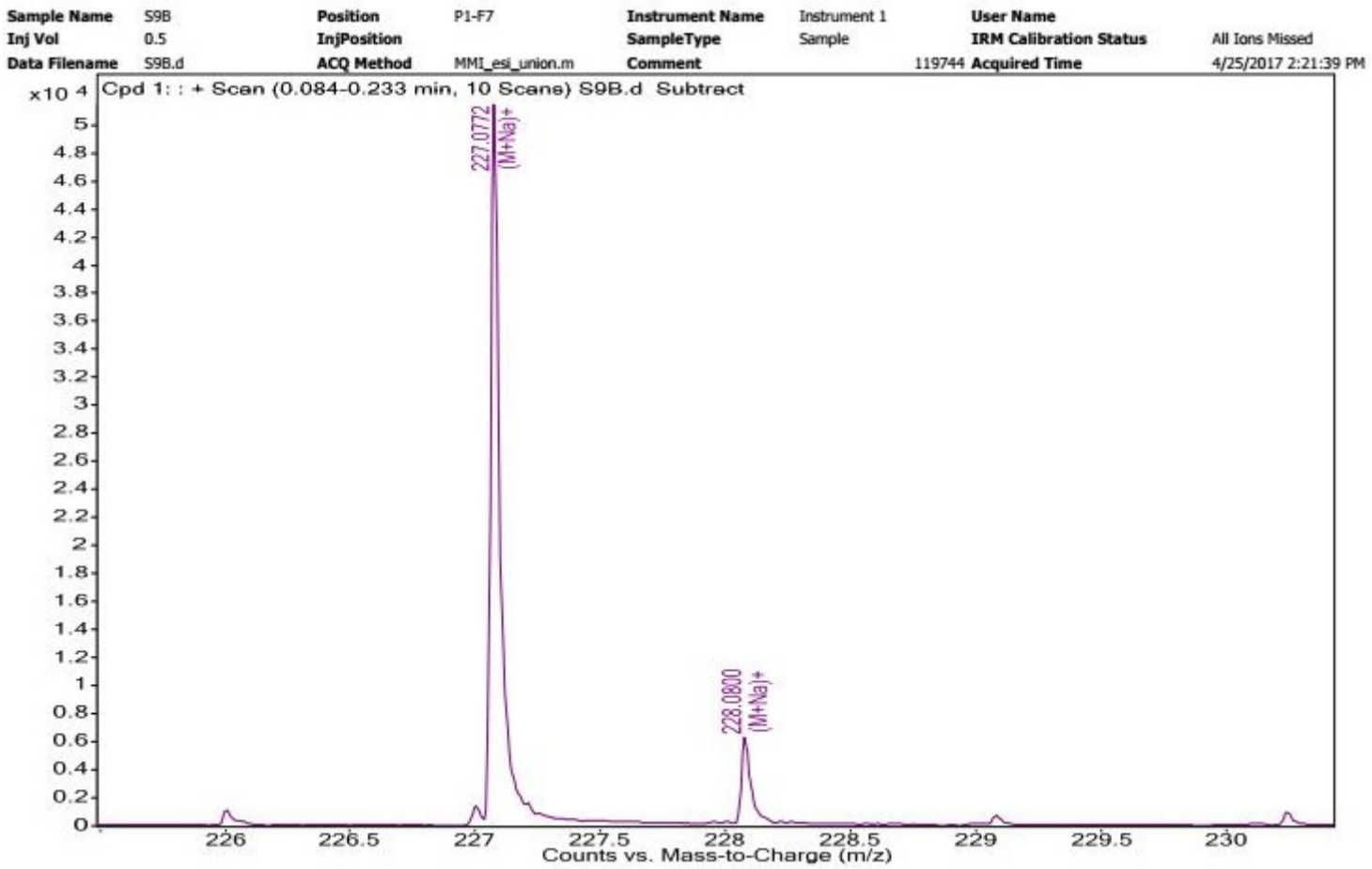
# 1,2,3,4-tetrahydro-5Hbenzo[e][1,4]diazepine-5-one ($C_9H_{10}N_2O$) **9a**

HRMS (ESI) m/z calcd for (M+H)+ 163.0866, found 163.0860



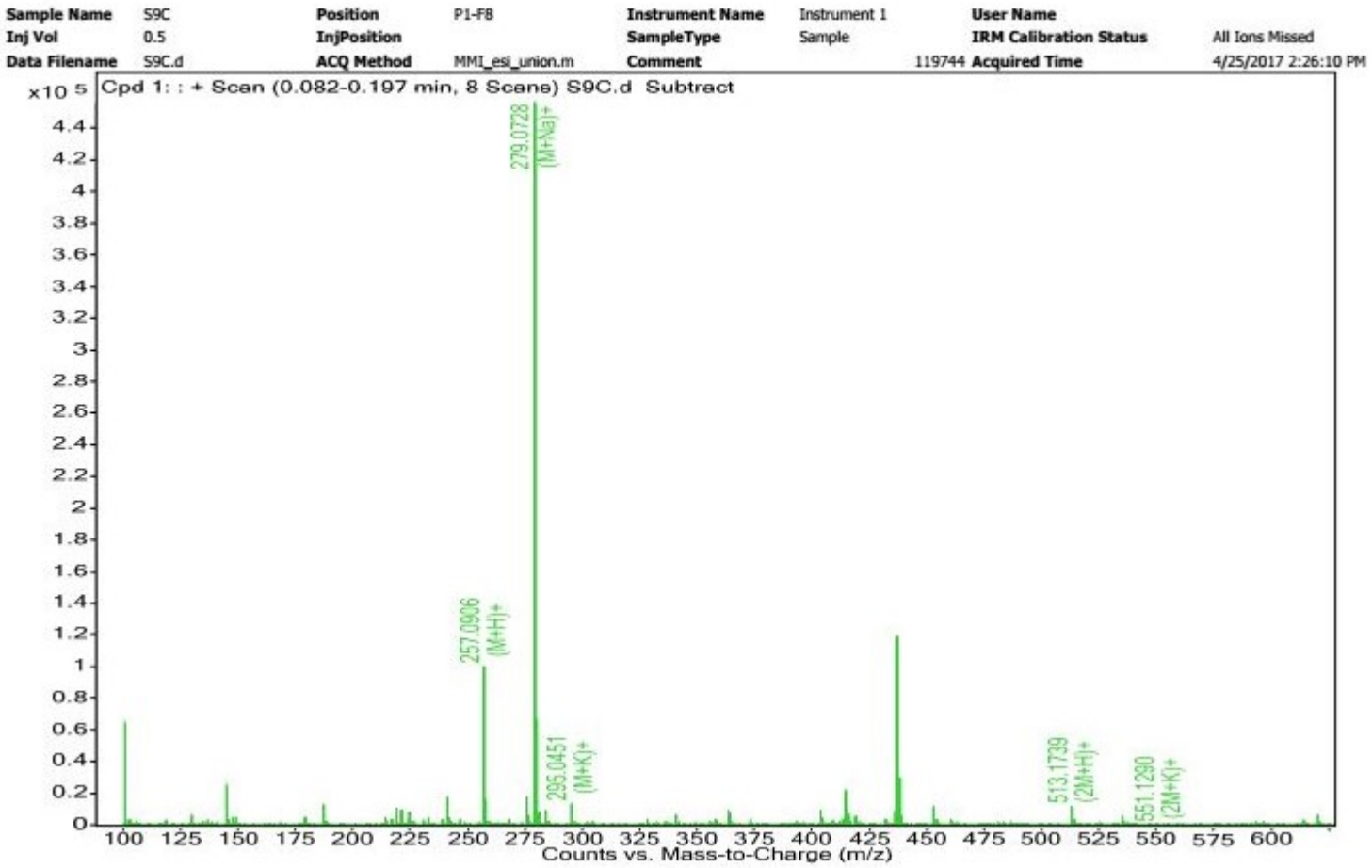
1-acetyl-1,2,3,4-tetrahydro-5H-benzo[e][1,4]diazepin-5-one ($C_{11}H_{12}N_2O_2$) **9b**

HRMS (ESI) m/z calcd for (M+Na)+ 227.0791, found 227.0772



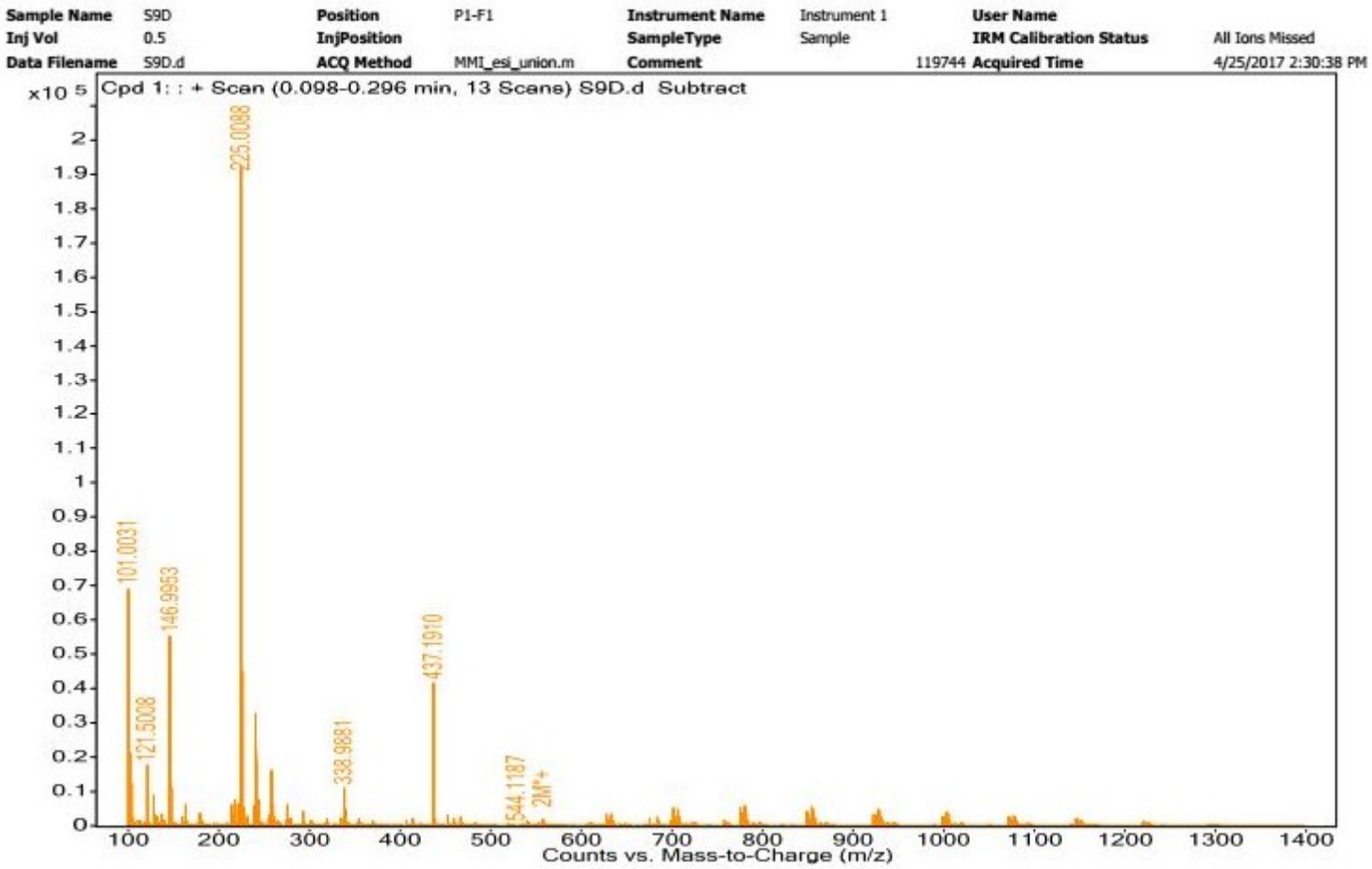
1-(Furan-2-carbonyl)1,2,3,4-tetrahydro-5H-benzo[e][1,4]diazepin-5-one ($C_{14}H_{12}N_2O_3$) **9c**

HRMS (ESI) m/z calcd for (M+H)+ 257.0921, found 257.0906



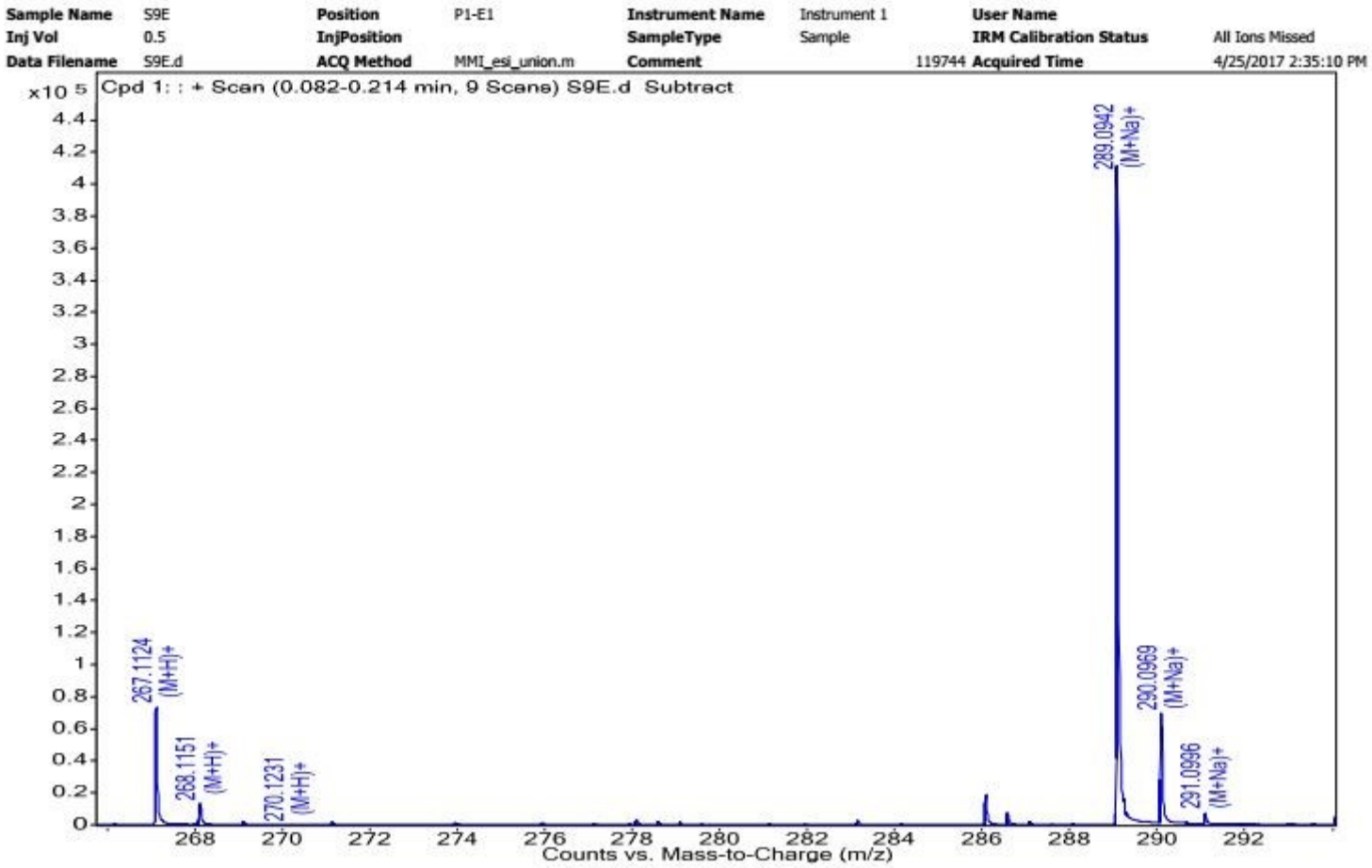
# 1-(Thiophene-2-carbonyl)1,2,3,4-tetrahydro-5H-benzo[e][1,4]diazepin-5-one ($C_{14}H_{12}N_2O_2S$) **9d**

HRMS (ESI) m/z calcd for 2M*+ 544.1233, found 544.1187



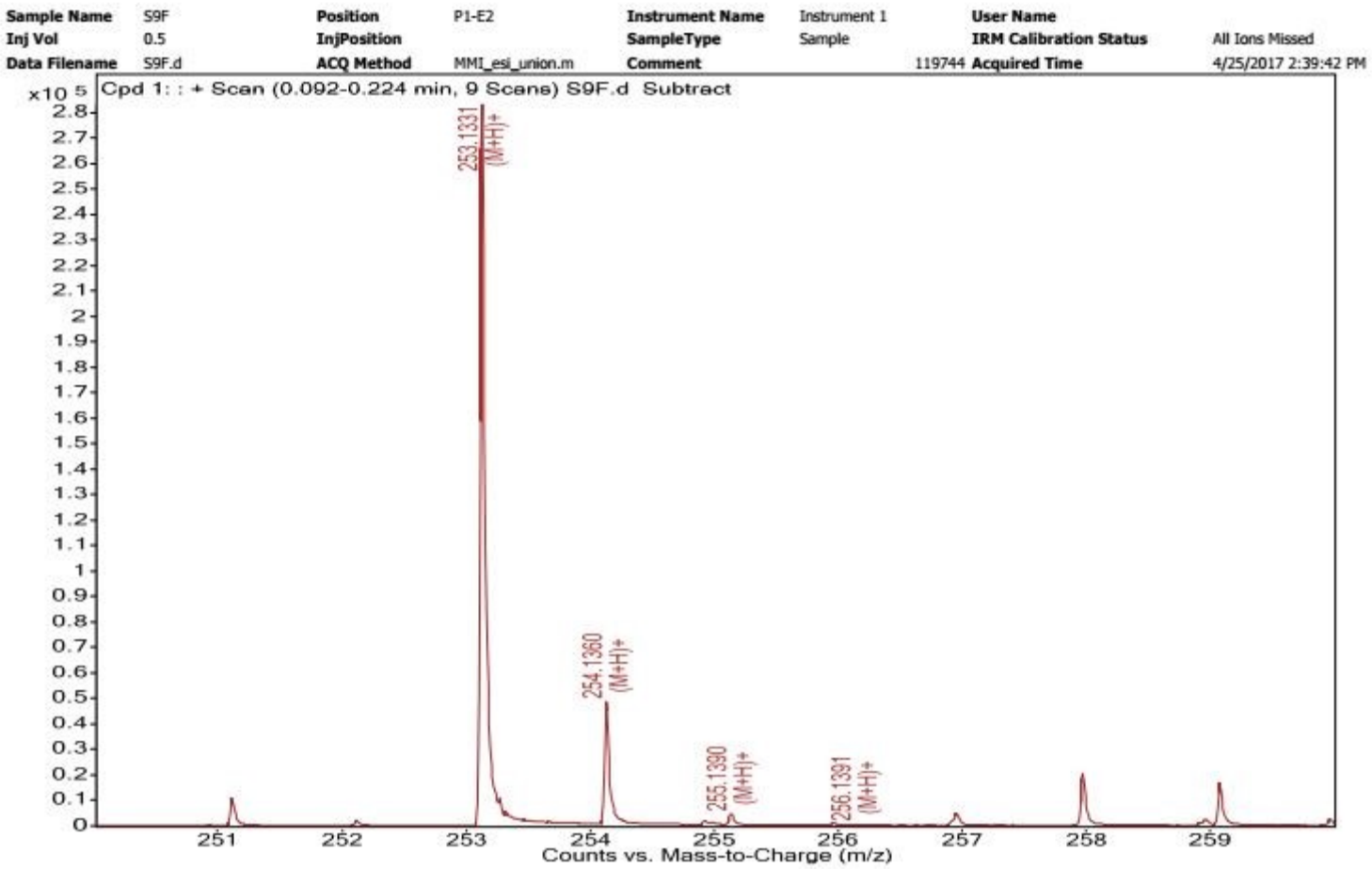
# 1-Benzoyl-1,2,3,4-tetrahydro-5H-benzo[e][1,4]diazepin-5-one ($C_{16}H_{14}N_2O_2$) **9e**

HRMS (ESI) m/z calcd for (M+H)+ 267.1128, found 267.1124



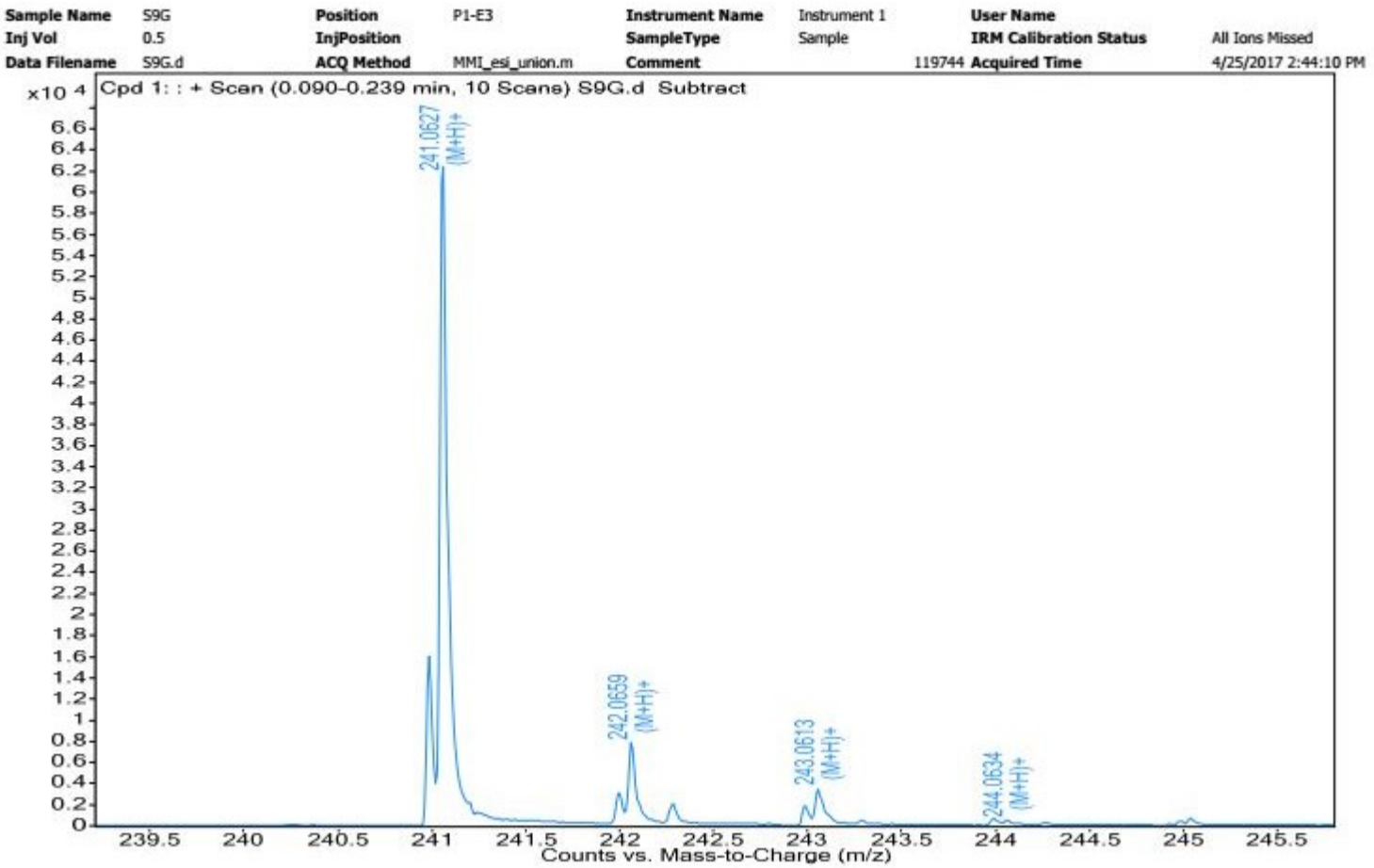
# 1-benzyl-1,2,3,4-tetrahydro-5H-benzo[e][1,4]diazepin-5-one ($C_{16}H_{16}N_2O$) **9f**

HRMS (ESI) m/z calcd for (M+H)+ 253.1335, found 253.1331



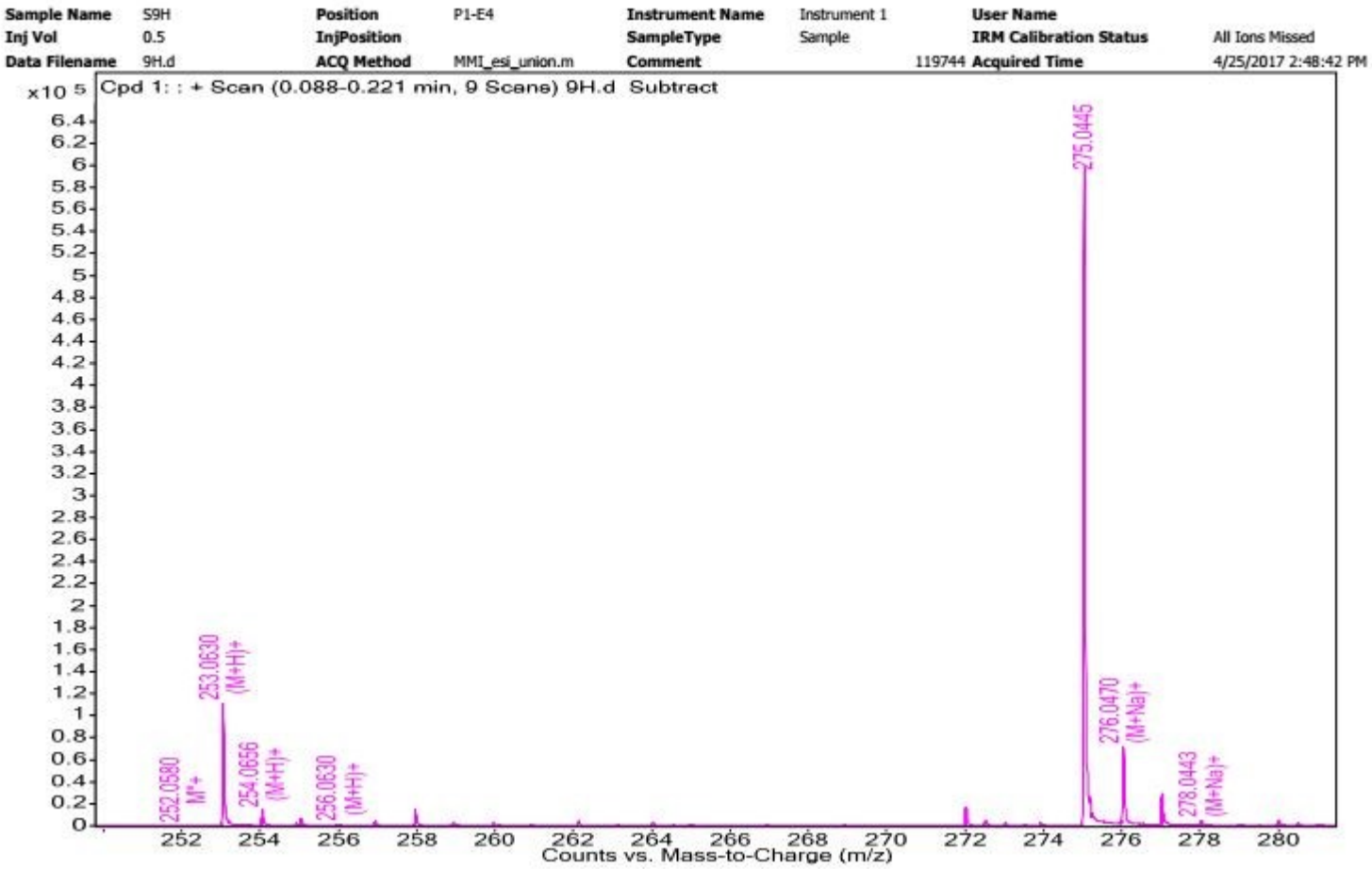
# 1-(Methylsulfonyl)-1,2,3,4tetrahydro-5H-benzo[e][1,4]diazepin-5-one ($C_{10}H_{12}N_2O_3S$) **9g**

HRMS (ESI) m/z calcd for (M+H)+ 241.0641, found 241.0627



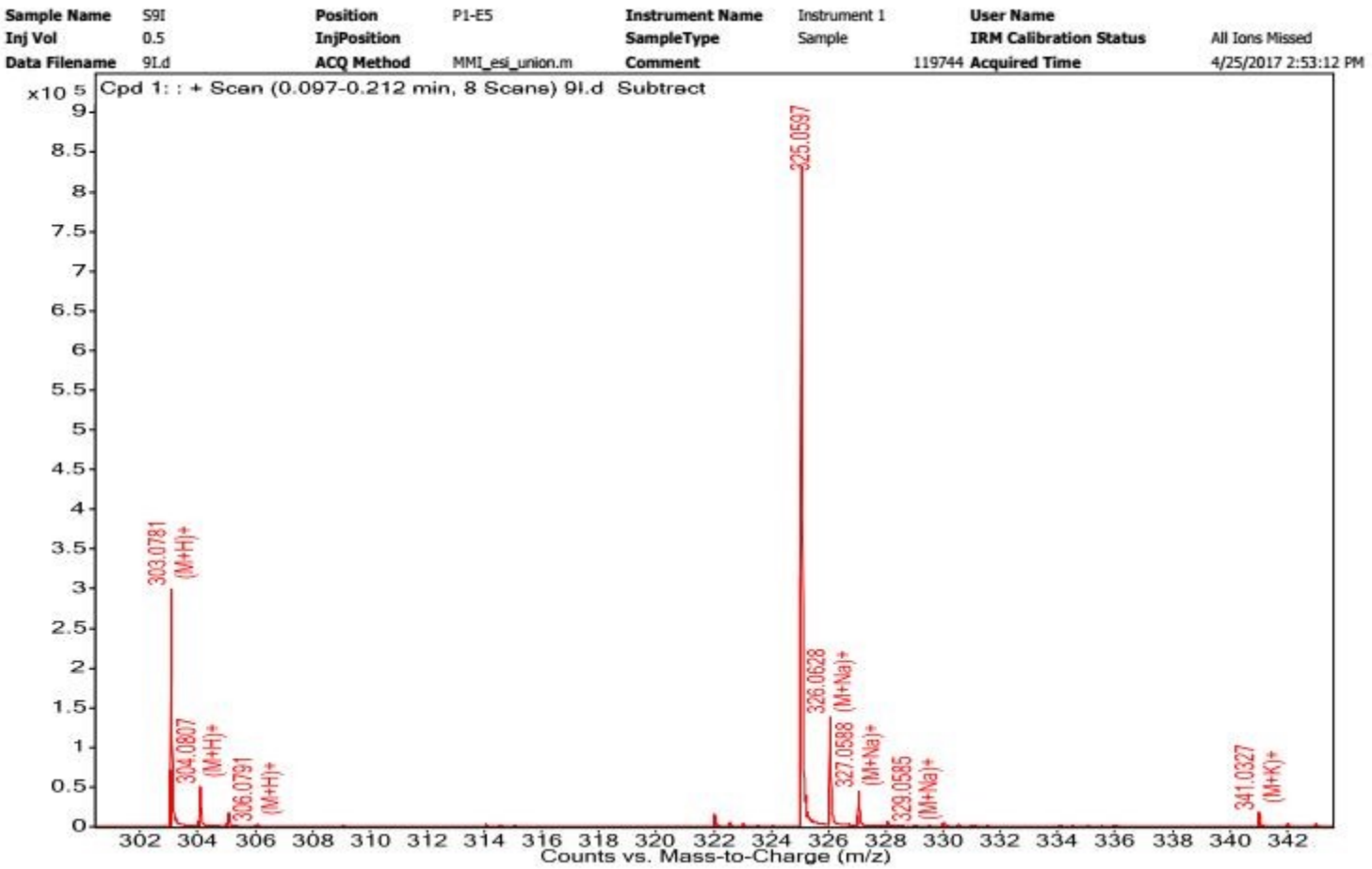
1-(vinylsulfonyl)-1,2,3,4-tetrahydro-5H-benzo[e][1,4]diazepin-5-one ($C_{11}H_{12}N_2O_3S$) **9h**

HRMS (ESI) m/z calcd for (M+H)+ 253.0641, found 253.0630



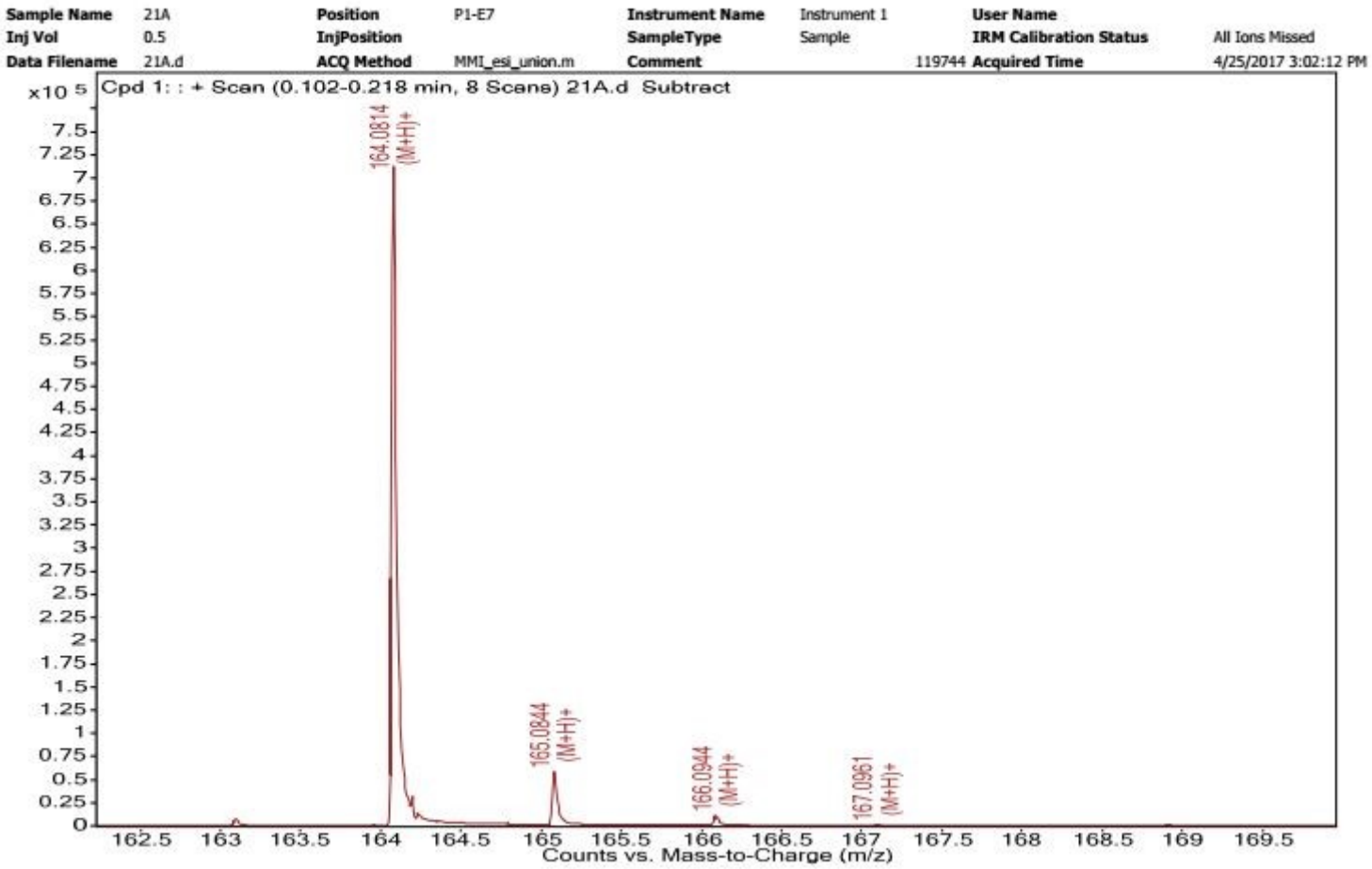
1-(Phenylsulfonyl)1,2,3,4-tetrahydro-5H-benzo[e][1,4]diazepin-5-one ($C_{15}H_{14}N_2O_3S$) **9i**

HRMS (ESI) m/z calcd for (M+H)+ 303.0798, found 303.0781



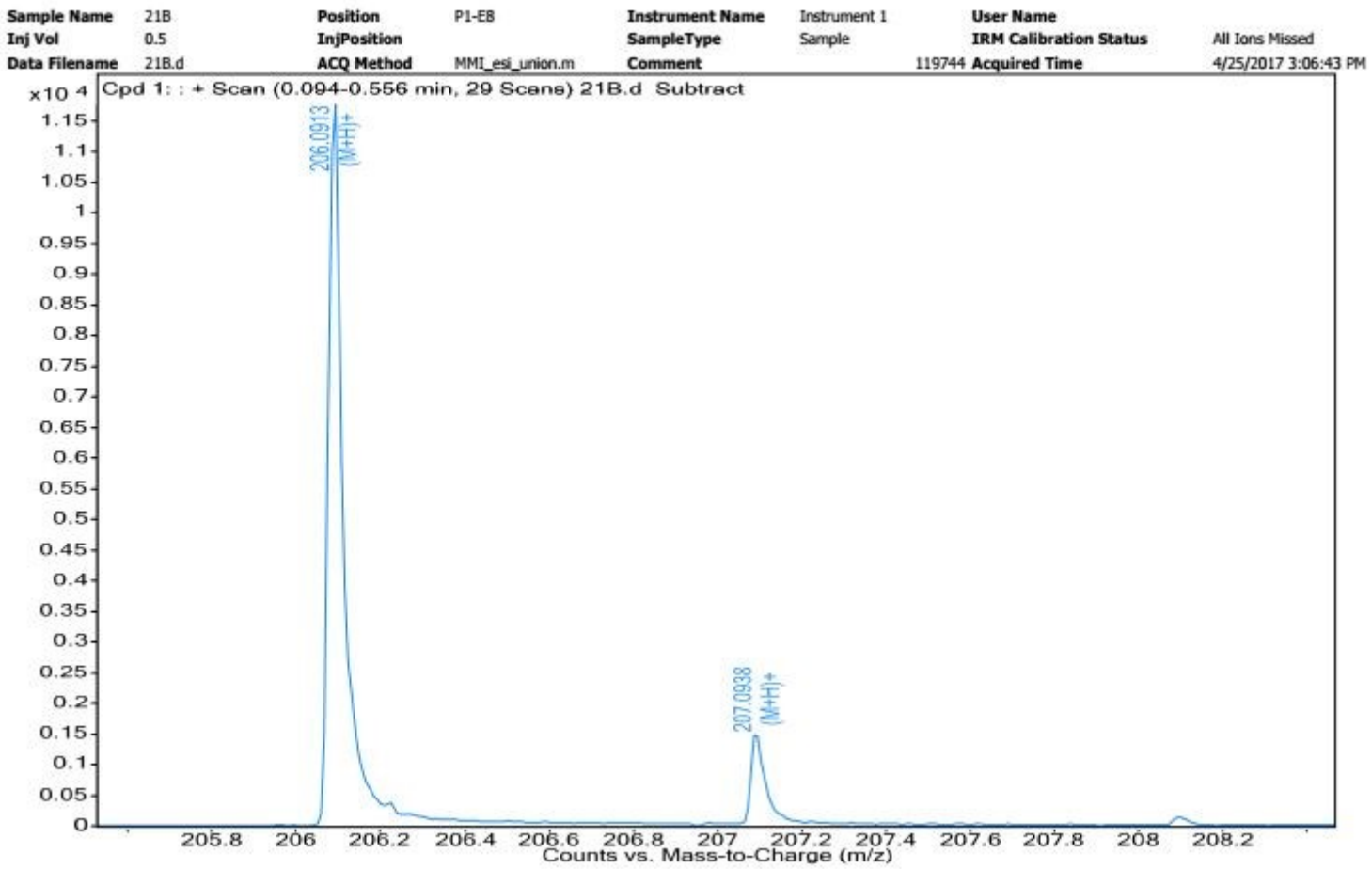
1,2,3,4-tetrahydro-5H-pyrido[2,3-e][1,4]diazepin-5-one ($C_8H_9N_3O$) **21a**

HRMS (ESI) m/z calcd for (M+H)+ 164.0818, found 164.0814



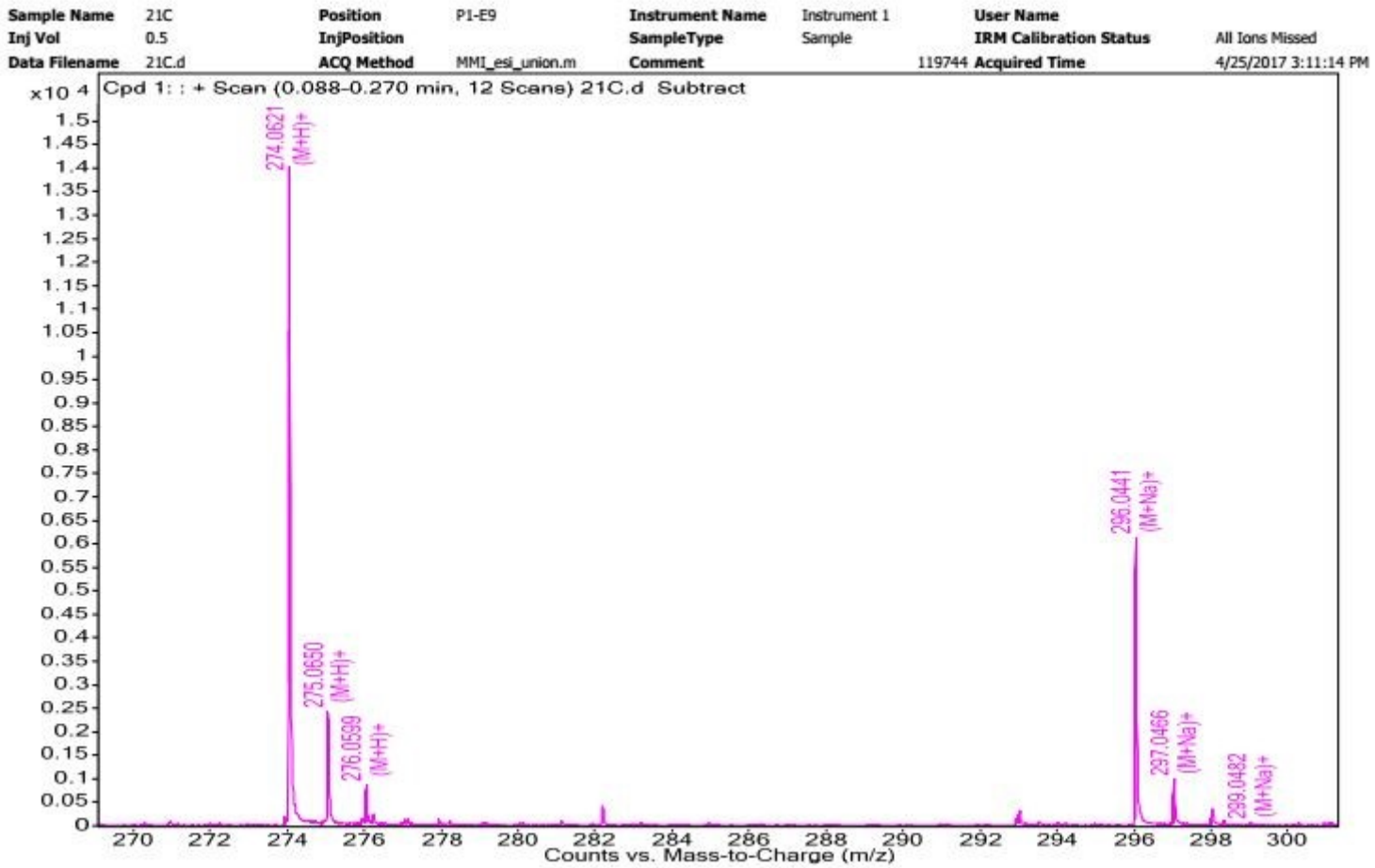
# 1-Acetyl1,2,3,4-tetrahydro-5H-pyrido[2,3-e][1,4]diazepin-5-one ($C_{10}H_{11}N_3O_2$) **21b**

HRMS (ESI) m/z calcd for (M+H)+ 206.0924, found 206.0913



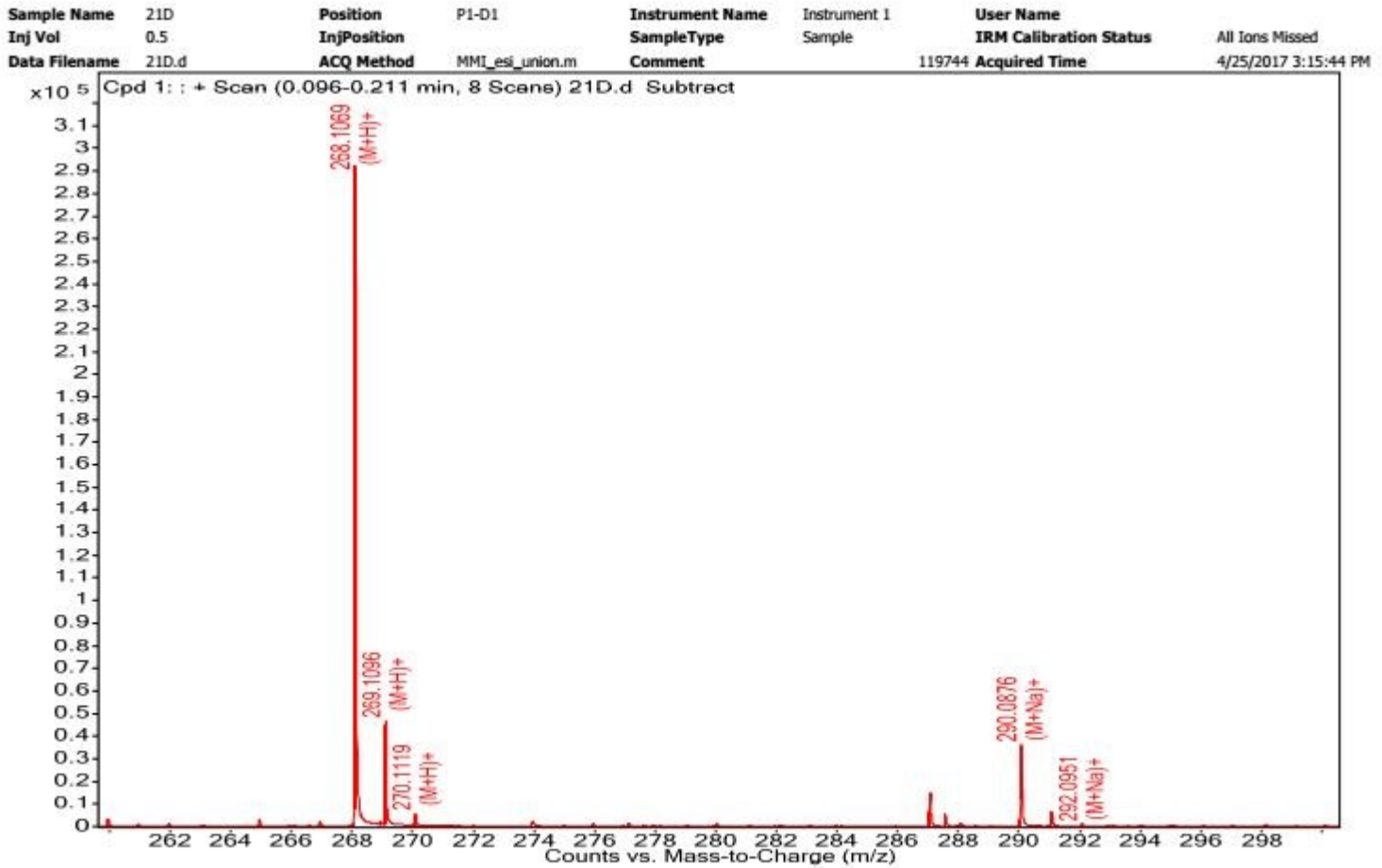
1-(Thiophene-2-carbonyl)-1,2,3,4-tetrahydro-5H-pyrido[2,3-e][1,4]diazepin-5-one ($C_{13}H_{11}N_3O_2S$) **21c**

HRMS (ESI) m/z calcd for (M+H)+ 274.0645, found 274.0621



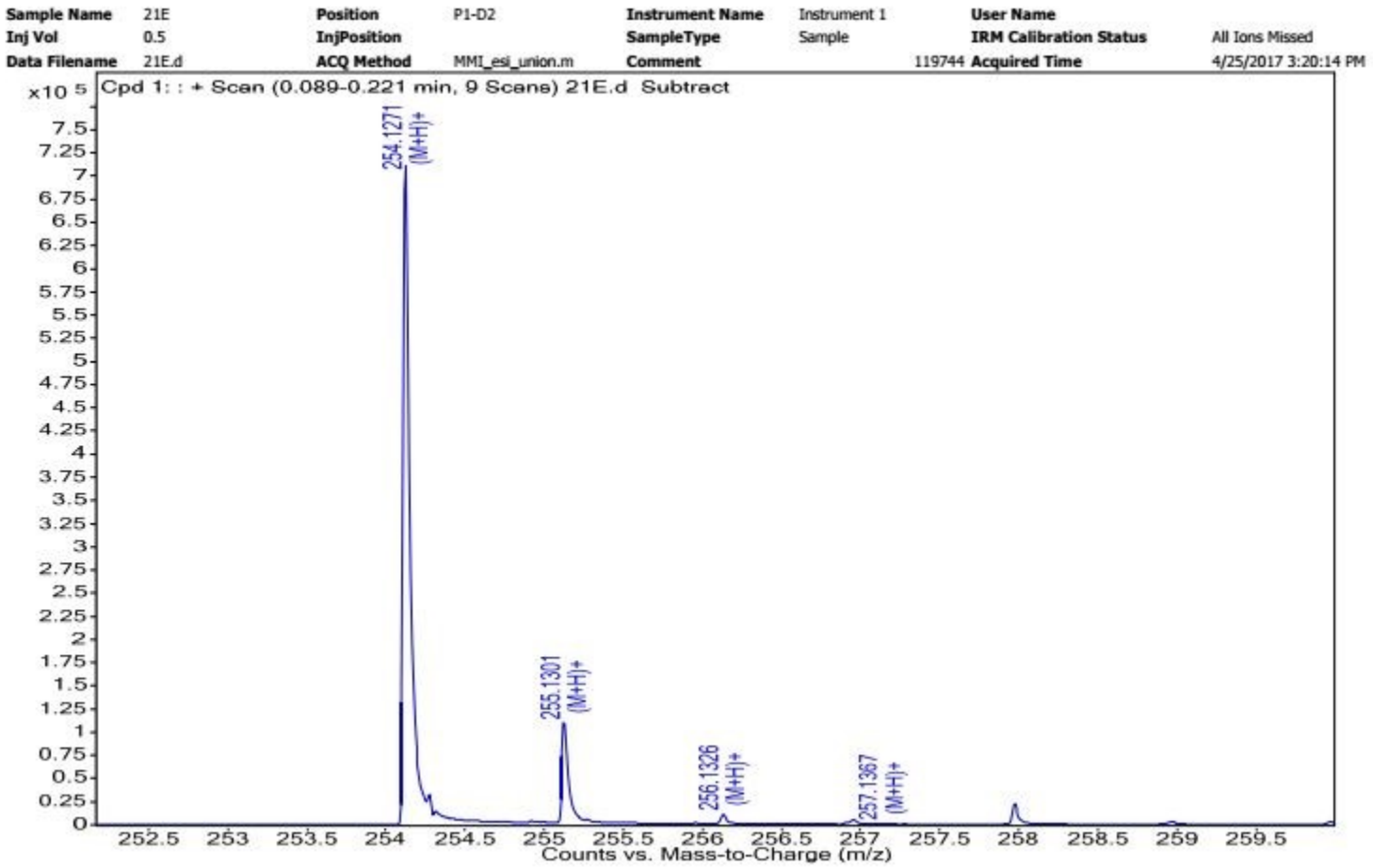
# 1-Benzoyl-1,2,3,4-tetrahydro-5H-pyrido[2,3-e][1,4]diazepin-5-one ($C_{15}H_{13}N_3O_2$) **21d**

HRMS (ESI) m/z calcd for (M+H)+ 268.1081, found 268.1069



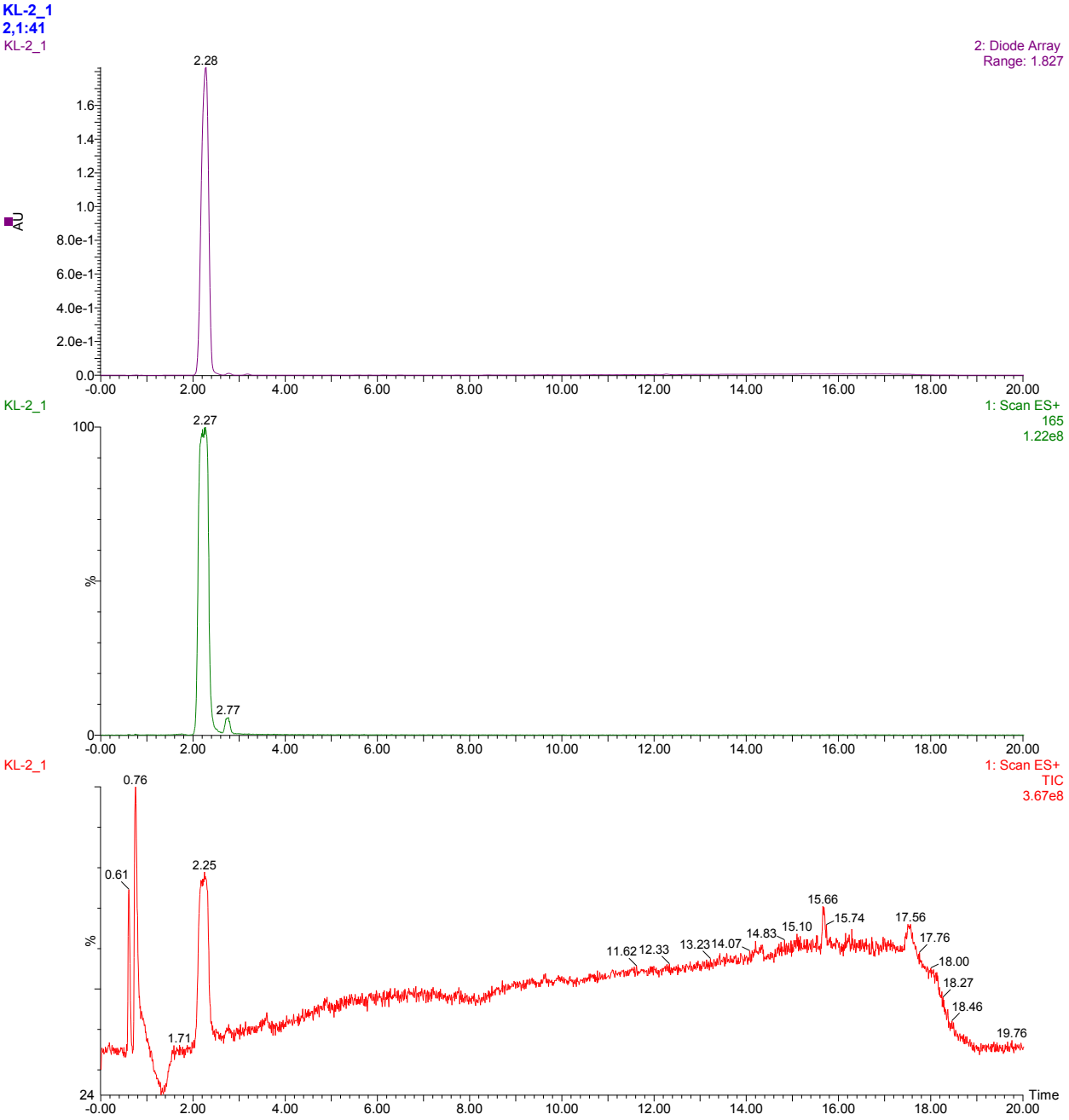
# 1-benzyl-1,2,3,4-tetrahydro-5H-pyrido[2,3-e][1,4]diazepin-5-one ($C_{15}H_{15}N_3O$) **21e**

HRMS (ESI) m/z calcd for (M+H)+ 254.1288, found 254.1271

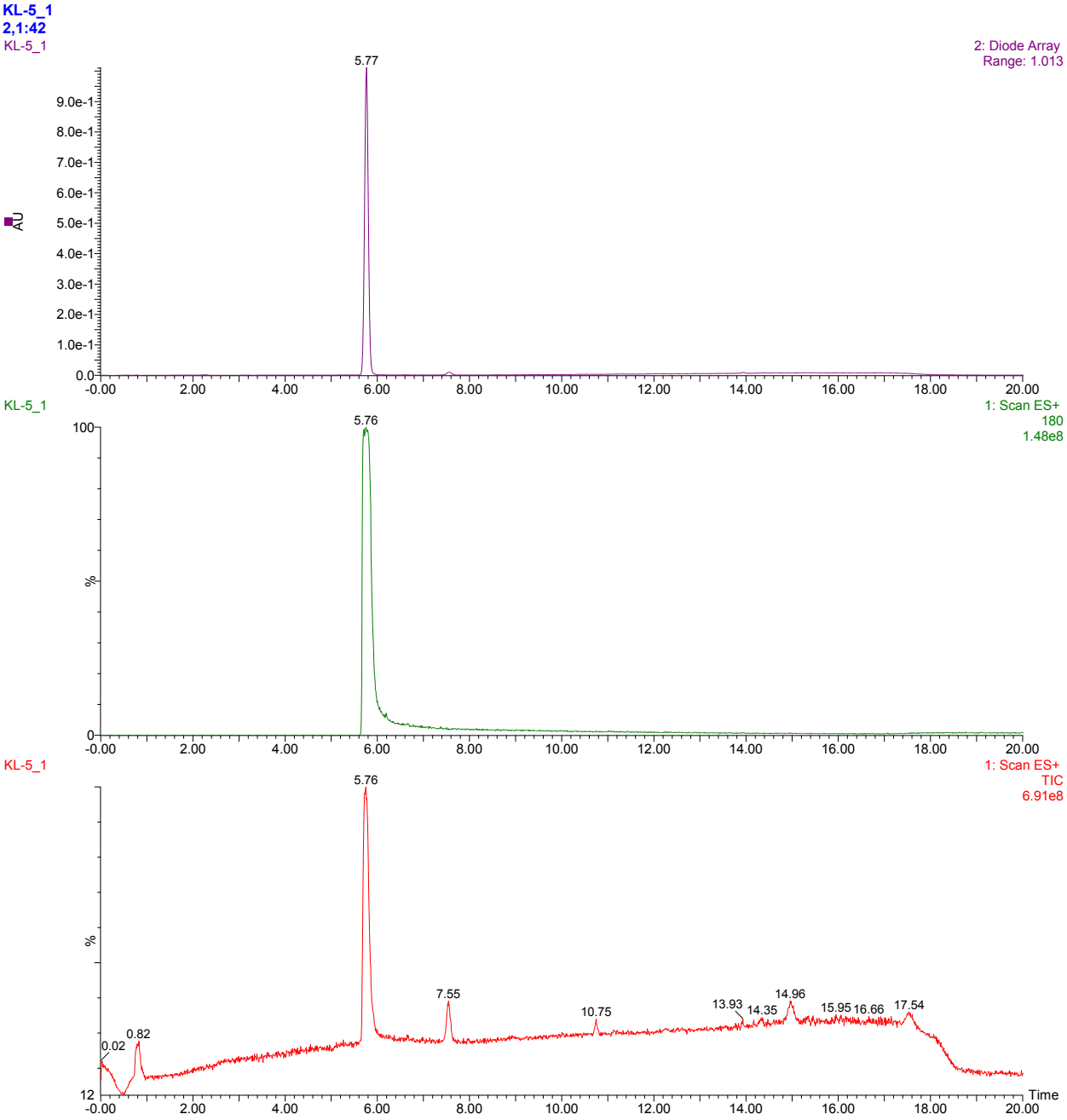


# APPENDIX F: HIGH PERFORMANCE LIQUID CHROMATOGRAPHY (HPLC)

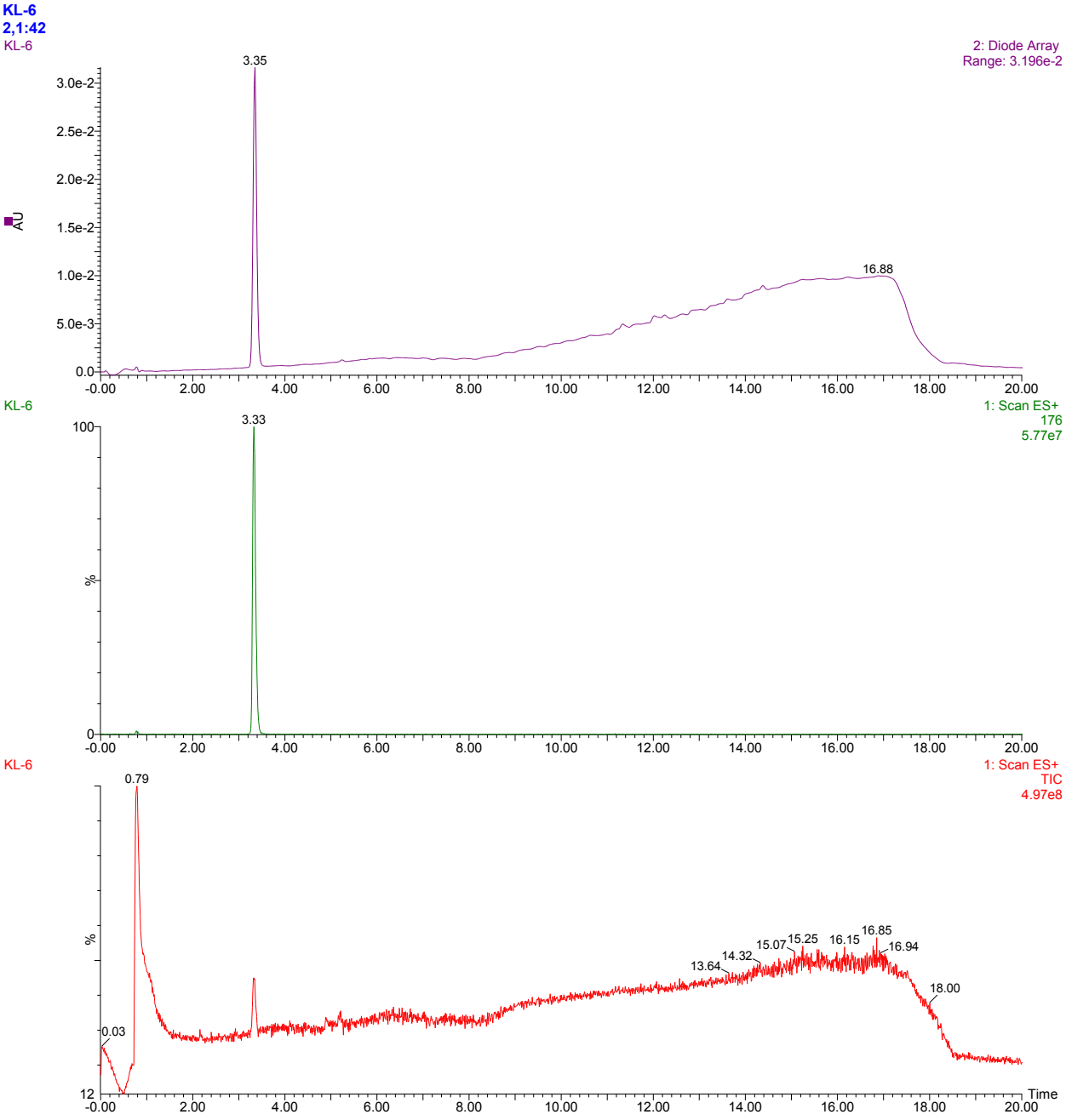
6,7-dihydropyrrolo[2,3-c]azepine-4,8(1H,5H)-dione (2)



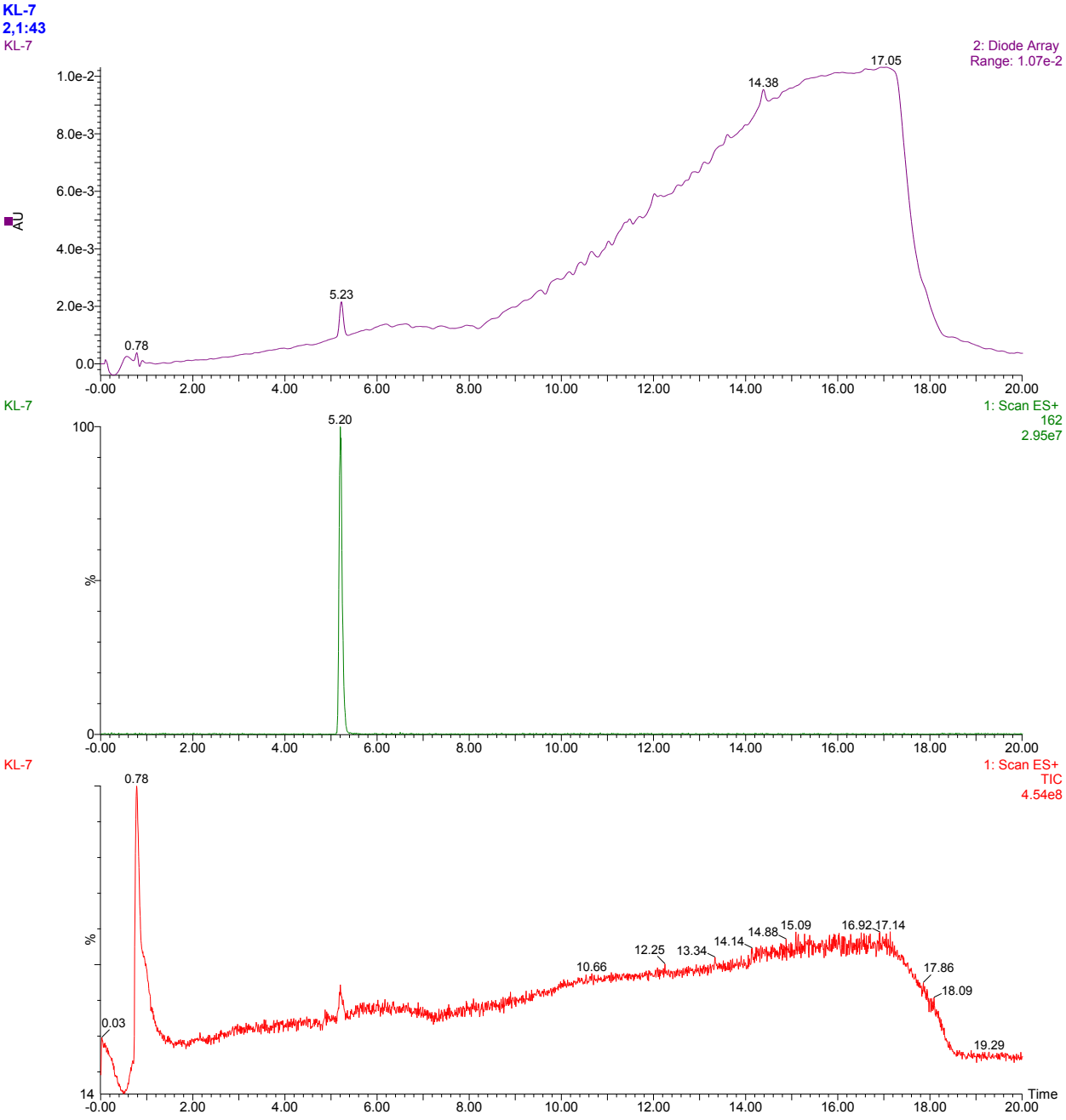
8-fluoro-2,3,4,5-tetrahydro-1H-benzo[c]azepin-1-one (5)



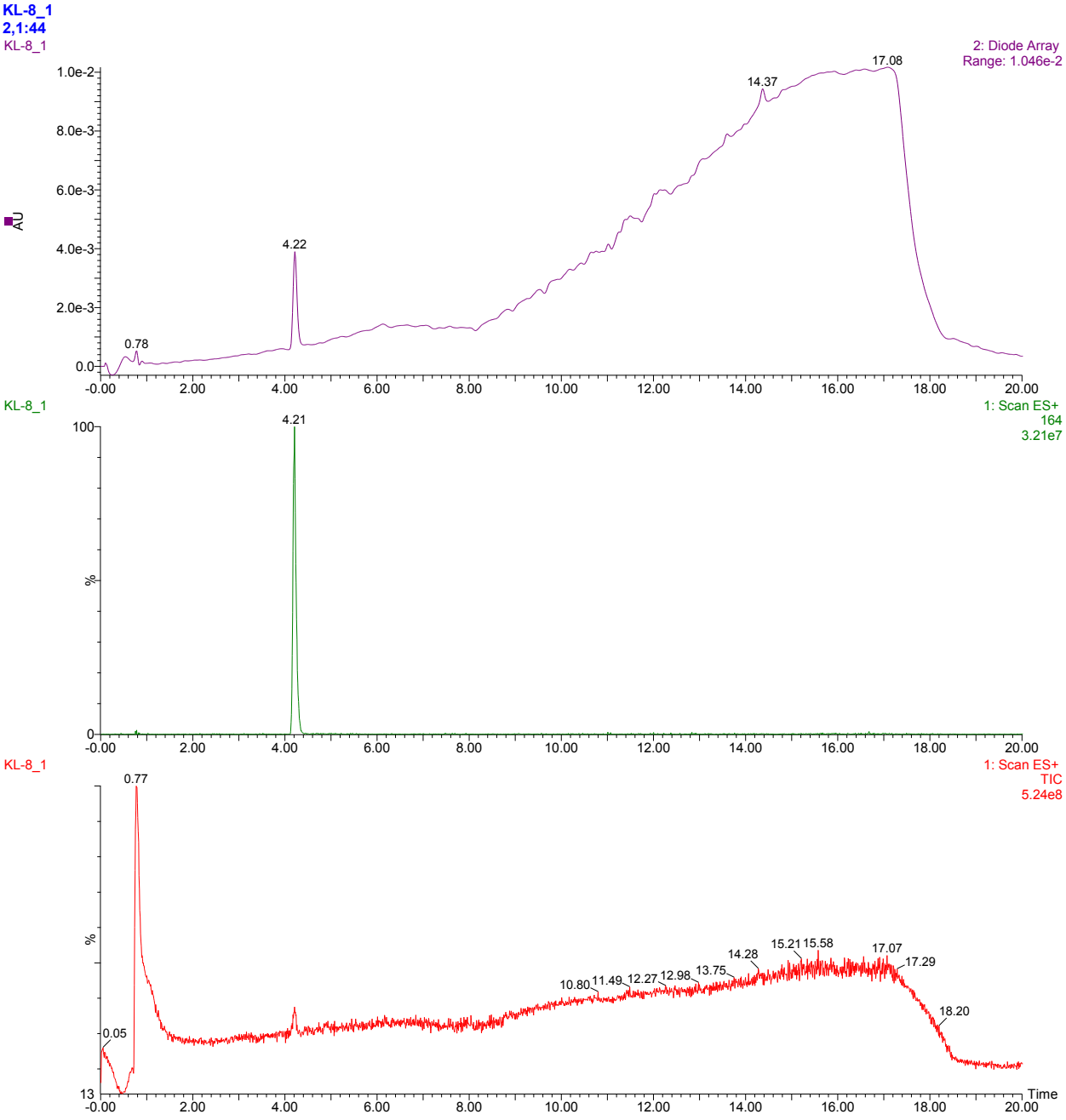
3,4-dihydro-1H-benzo[c]azepine-1,5(2H)-dione (6)



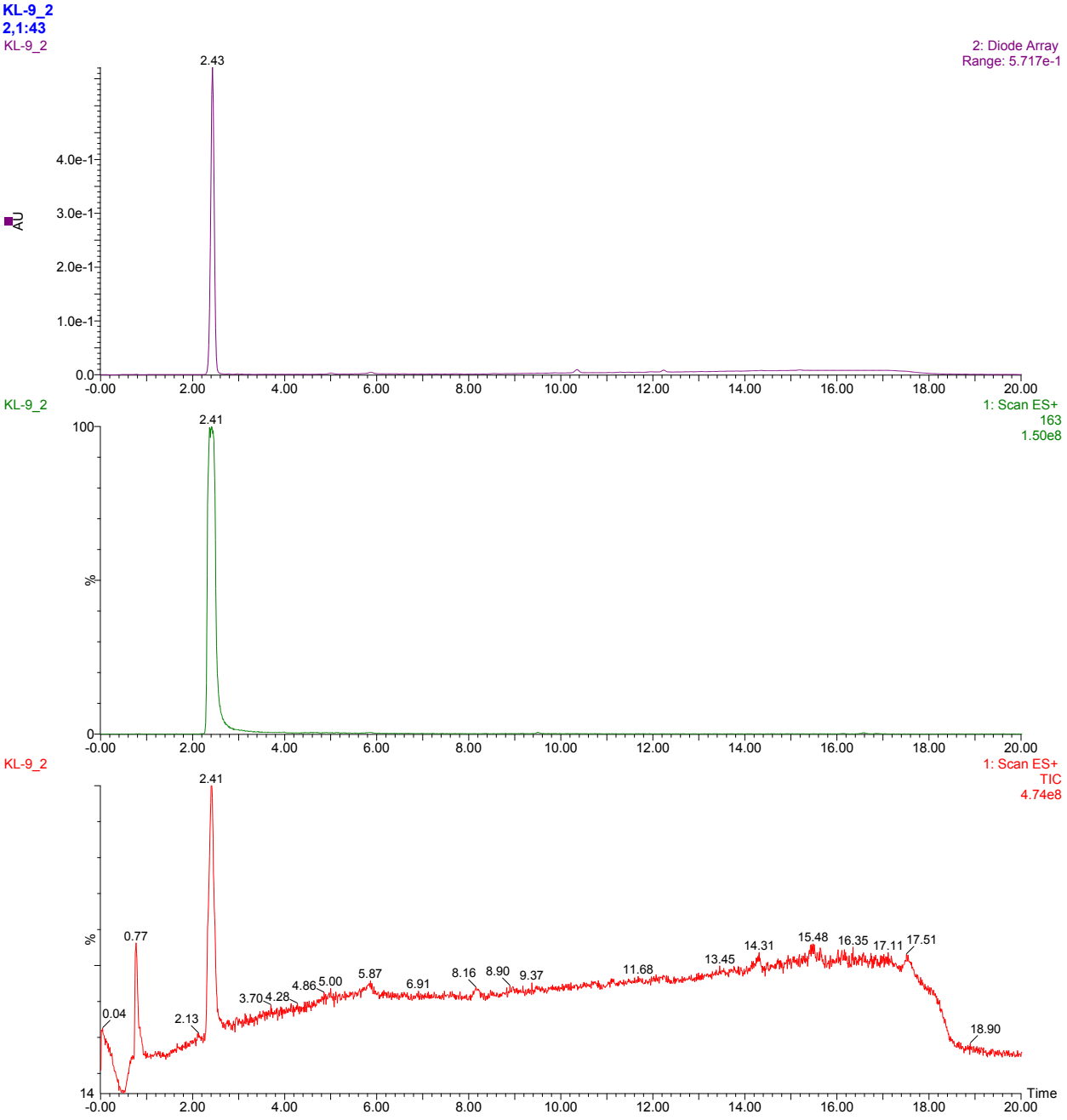
2,3,4,5-Tetrahydro-1H-benzo[c]azepin-1-one (7)



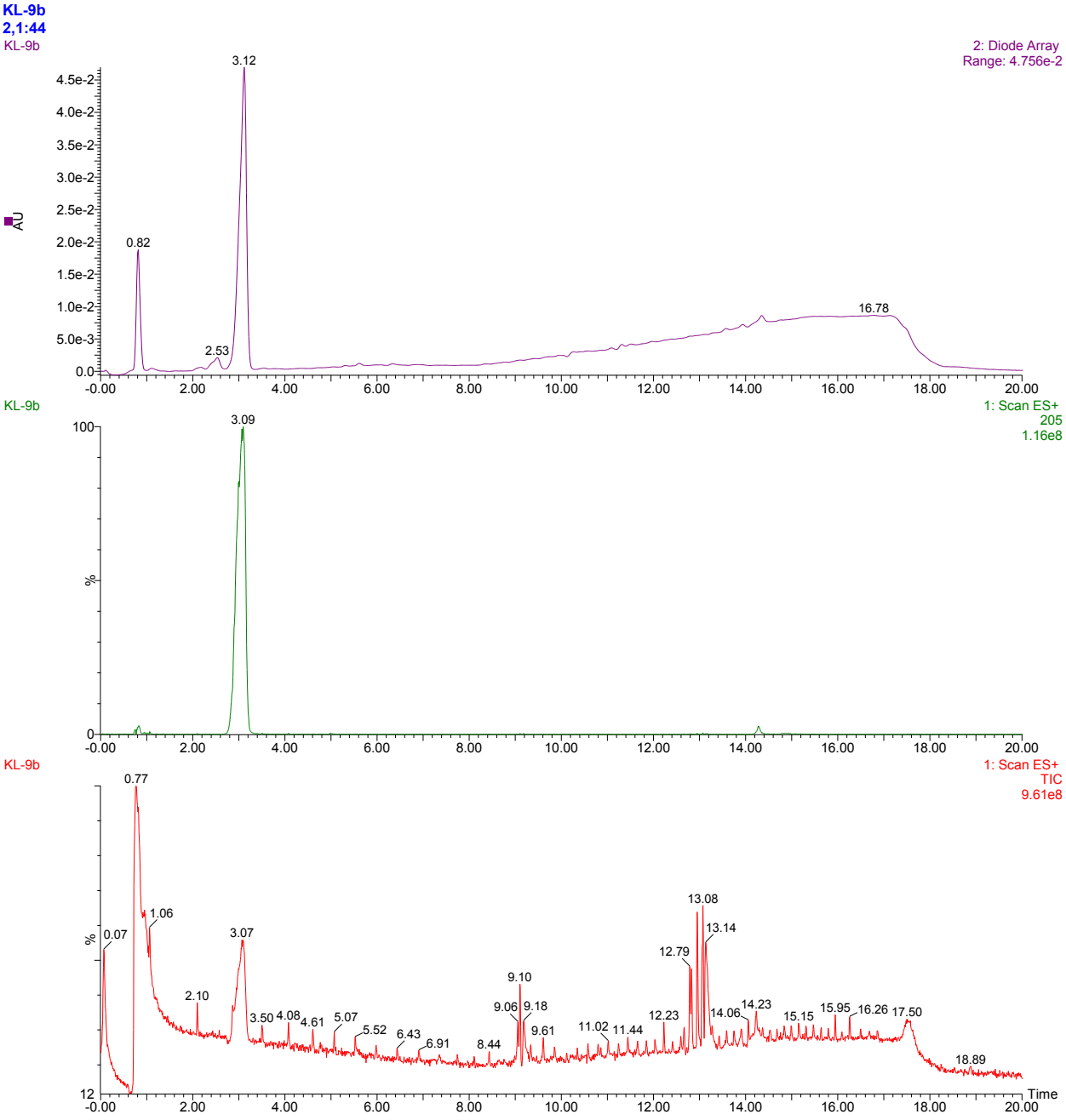
3,4-dihydrobenzo[f][1,4]oxazepin-5(2H)-one (8)



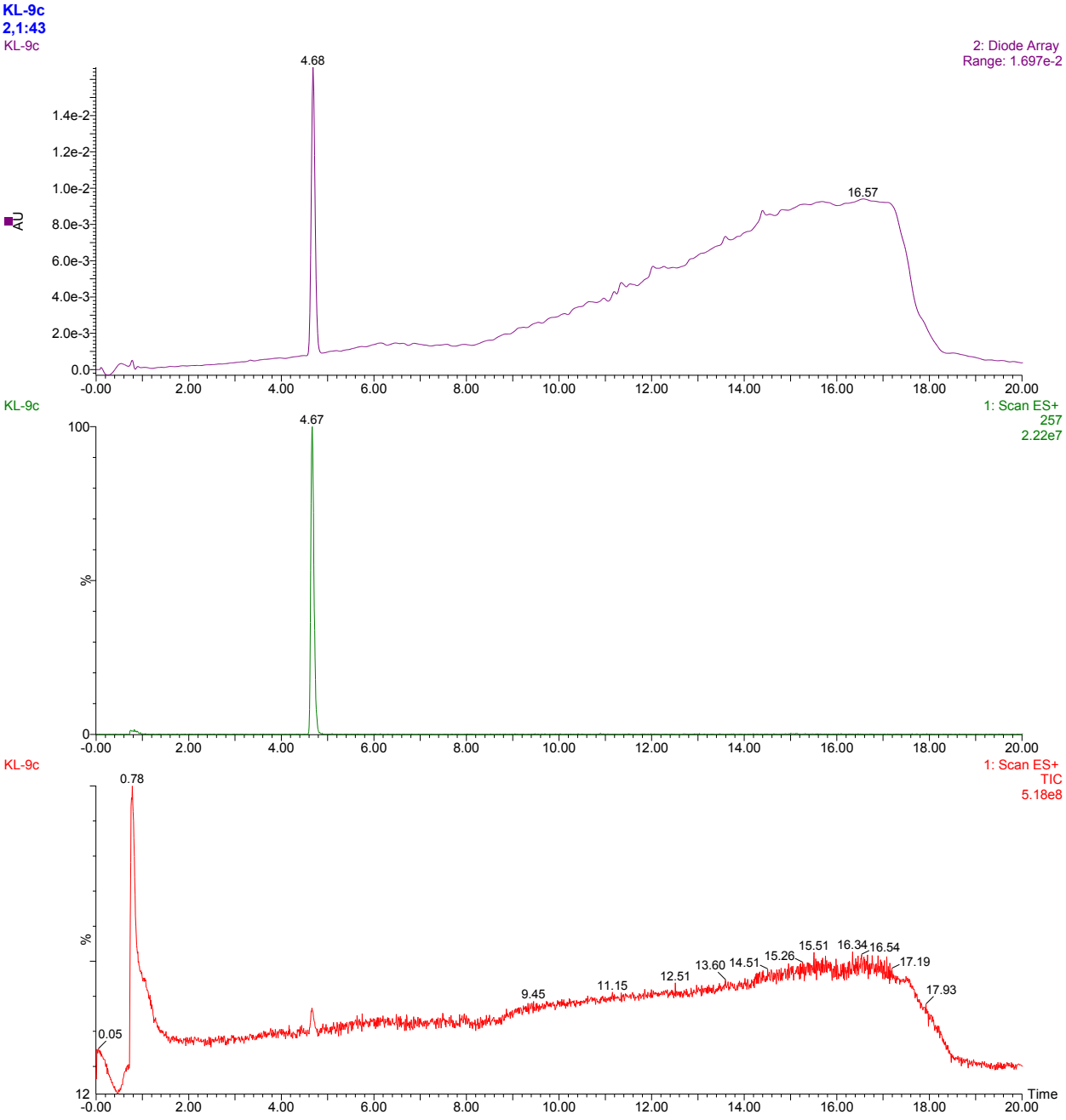
1,2,3,4-tetrahydro-5Hbenzo[e][1,4]diazepine-5-one (9a)



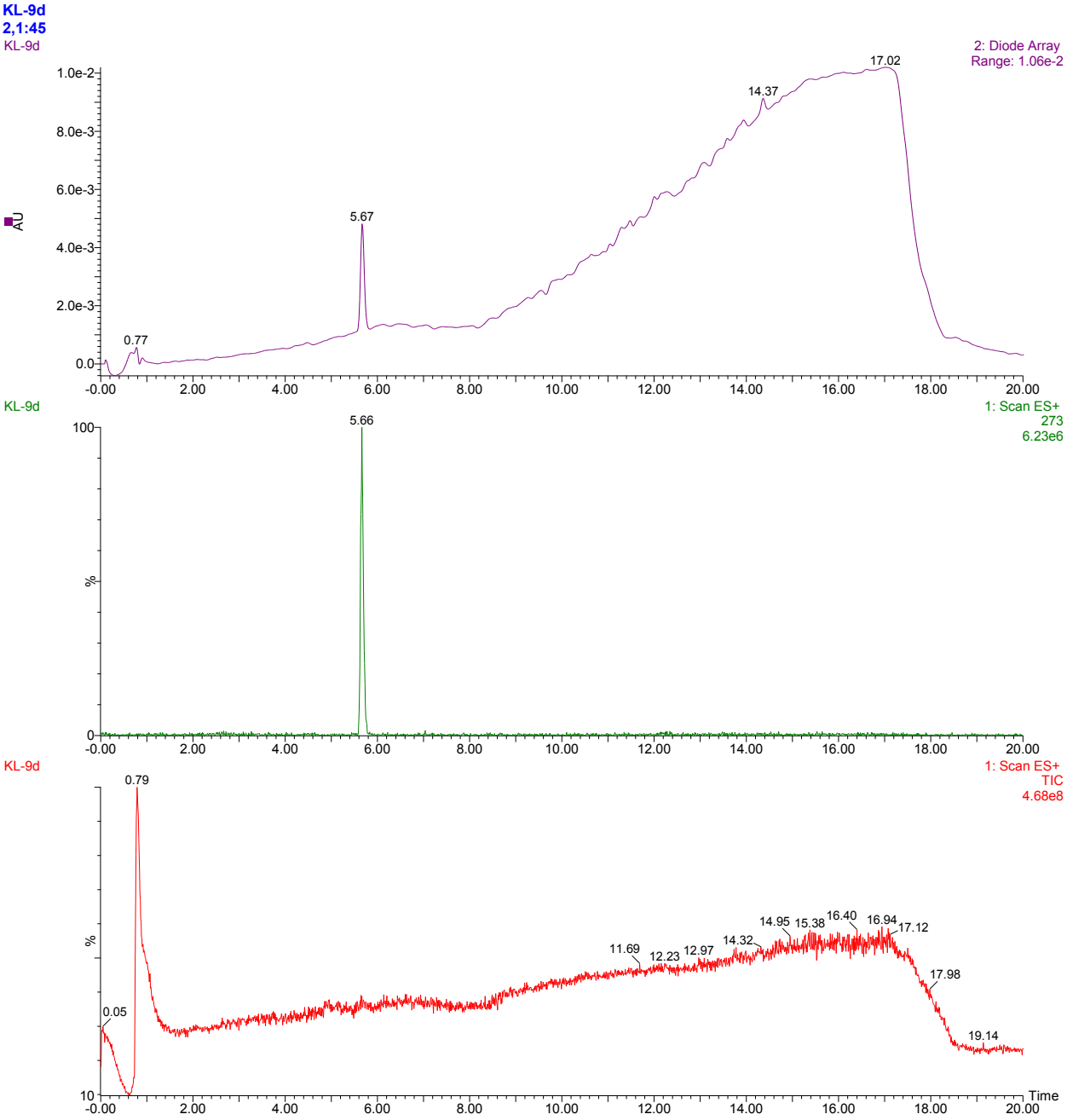
1-acetyl-1,2,3,4-tetrahydro-5H-benzo[e][1,4]diazepin-5-one (9b)



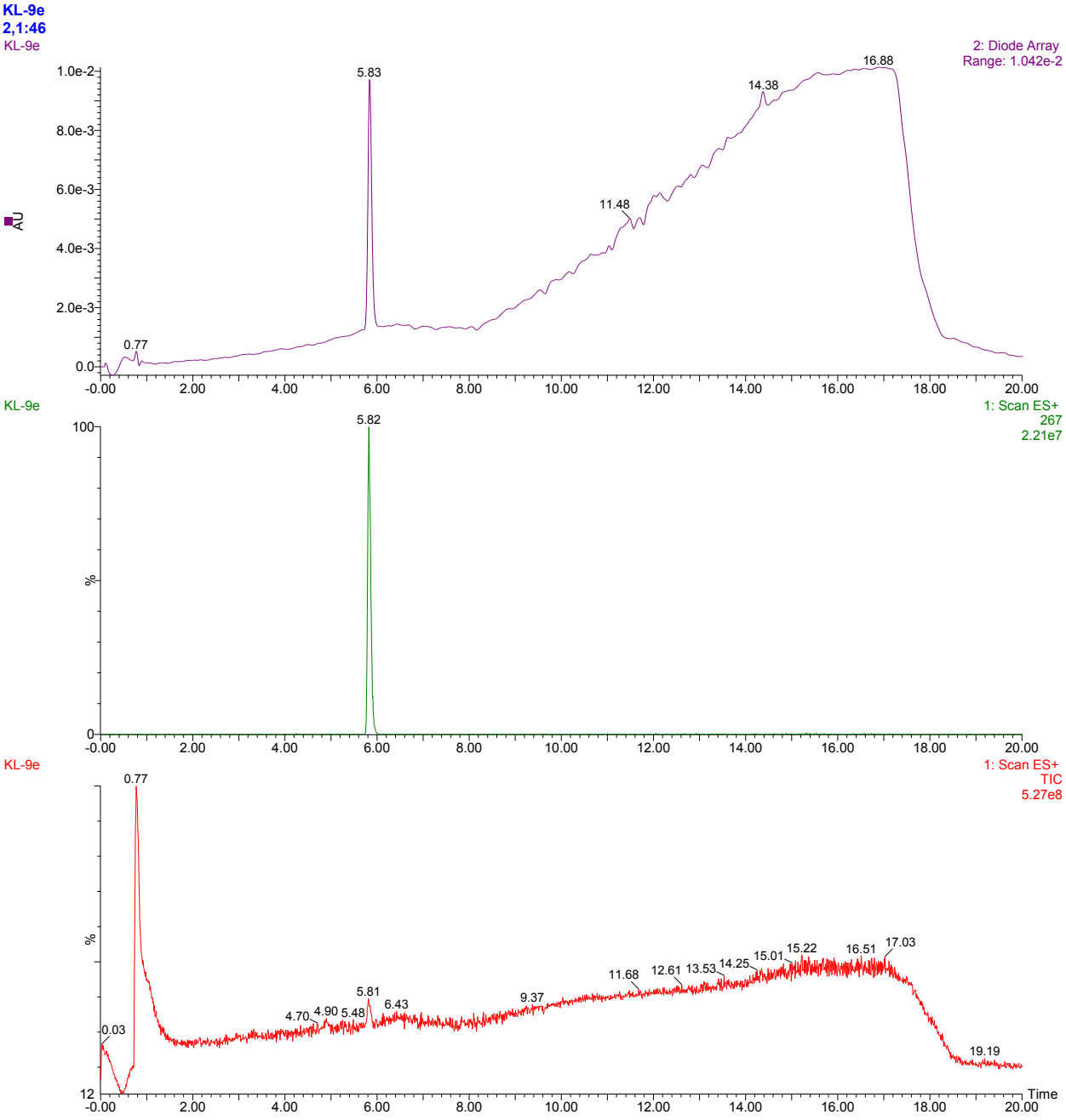
1-(Furan-2-carbonyl)1,2,3,4-tetrahydro-5H-benzo[e][1,4]diazepin-5-one (9c)



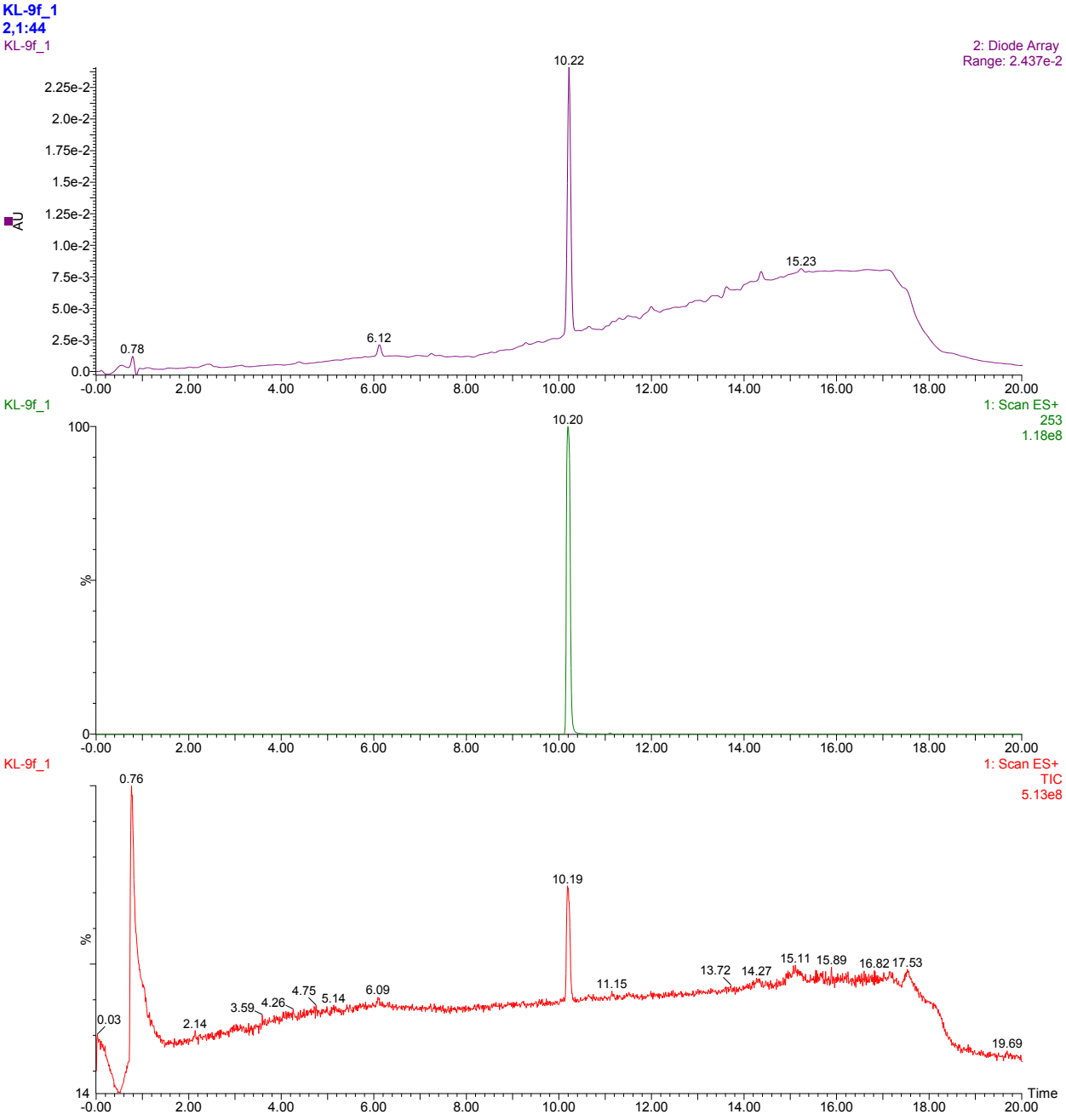
1-(Thiophene-2-carbonyl)1,2,3,4-tetrahydro-5H-benzo[e][1,4]diazepin5-one (9d)



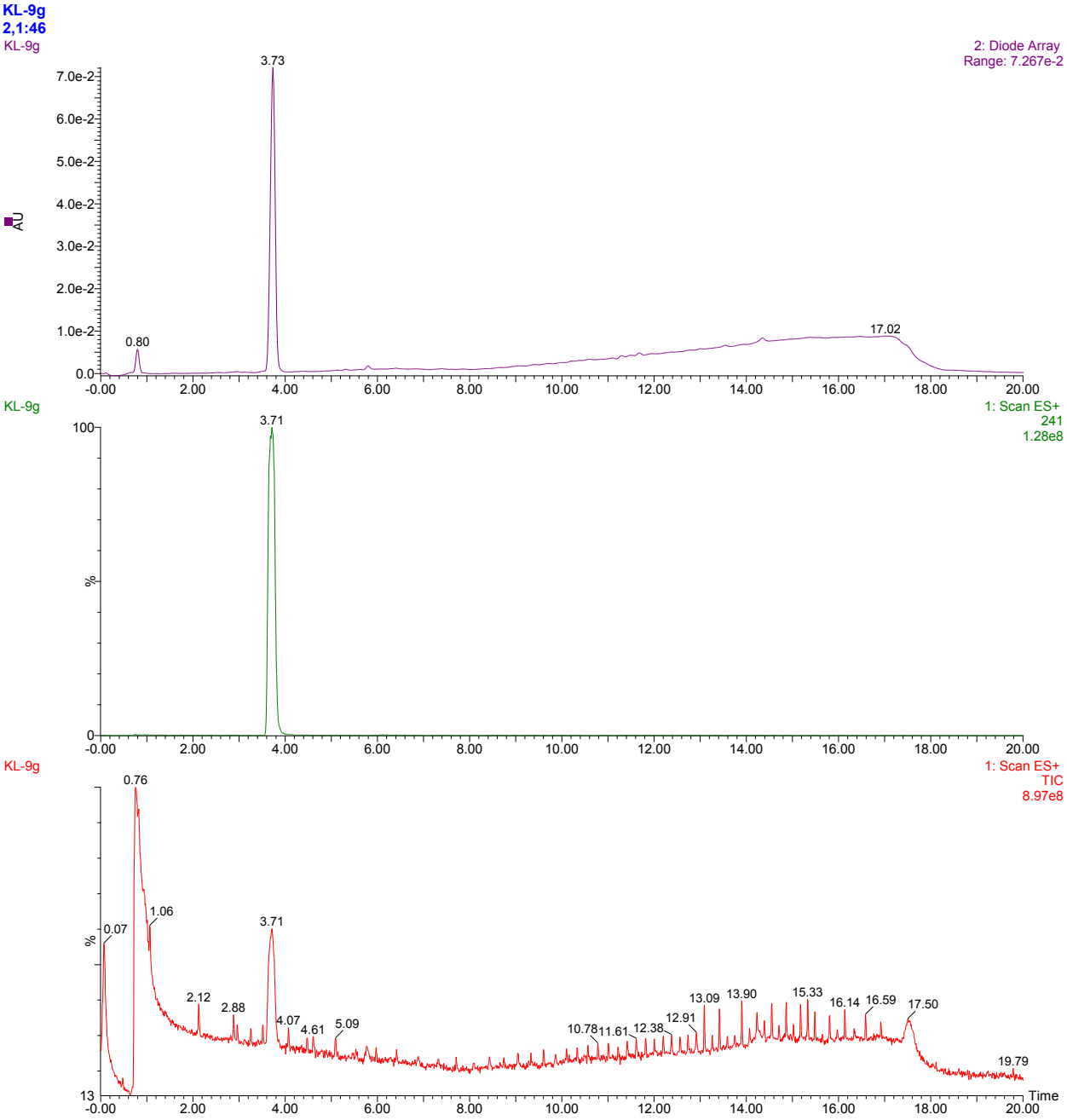
1-Benzoyl-1,2,3,4-tetrahydro-5H-benzo[e][1,4]diazepin-5-one (9e)



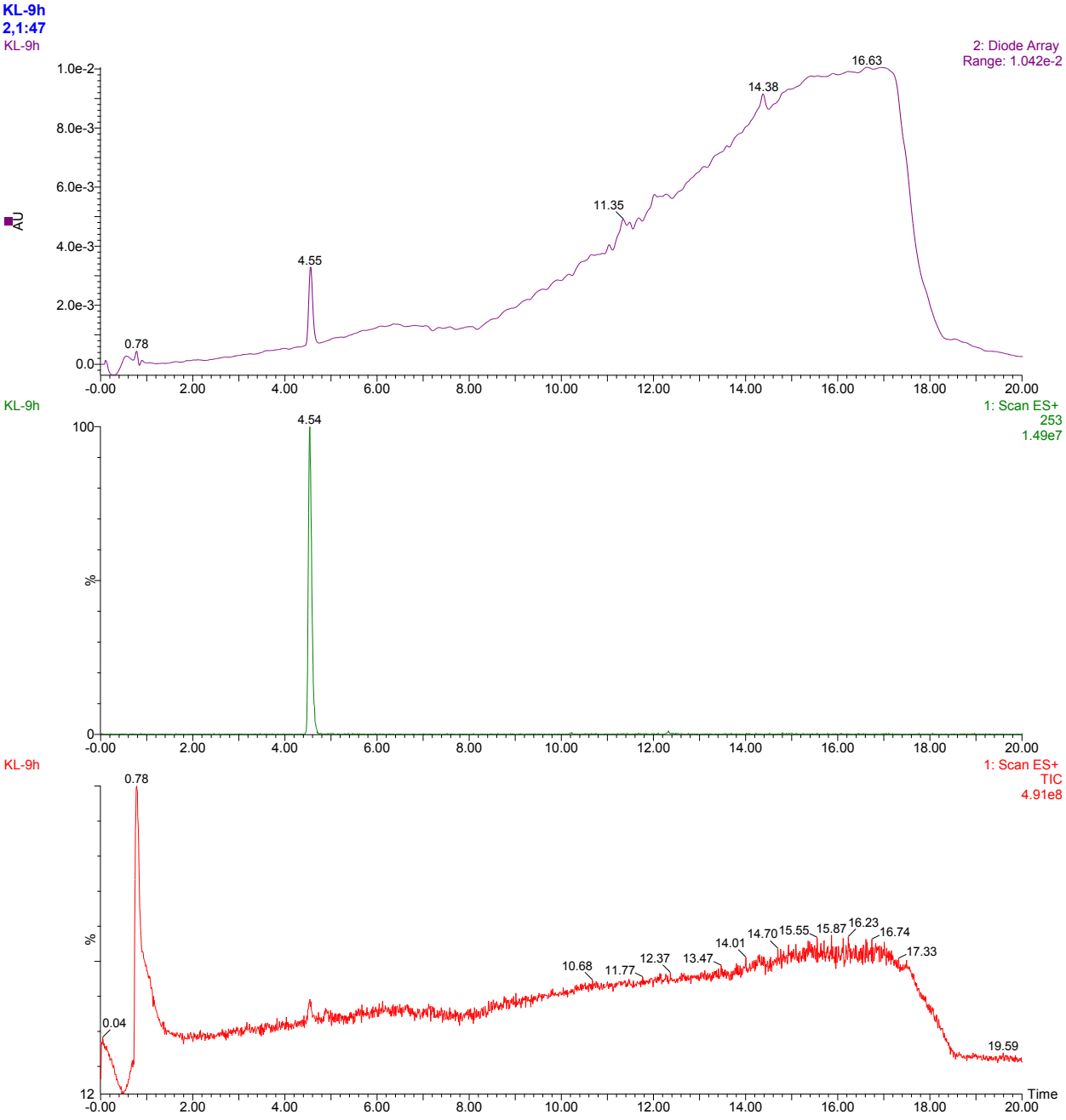
1-benzyl-1,2,3,4-tetrahydro-5H-benzo[e][1,4]diazepin-5-one (9f)



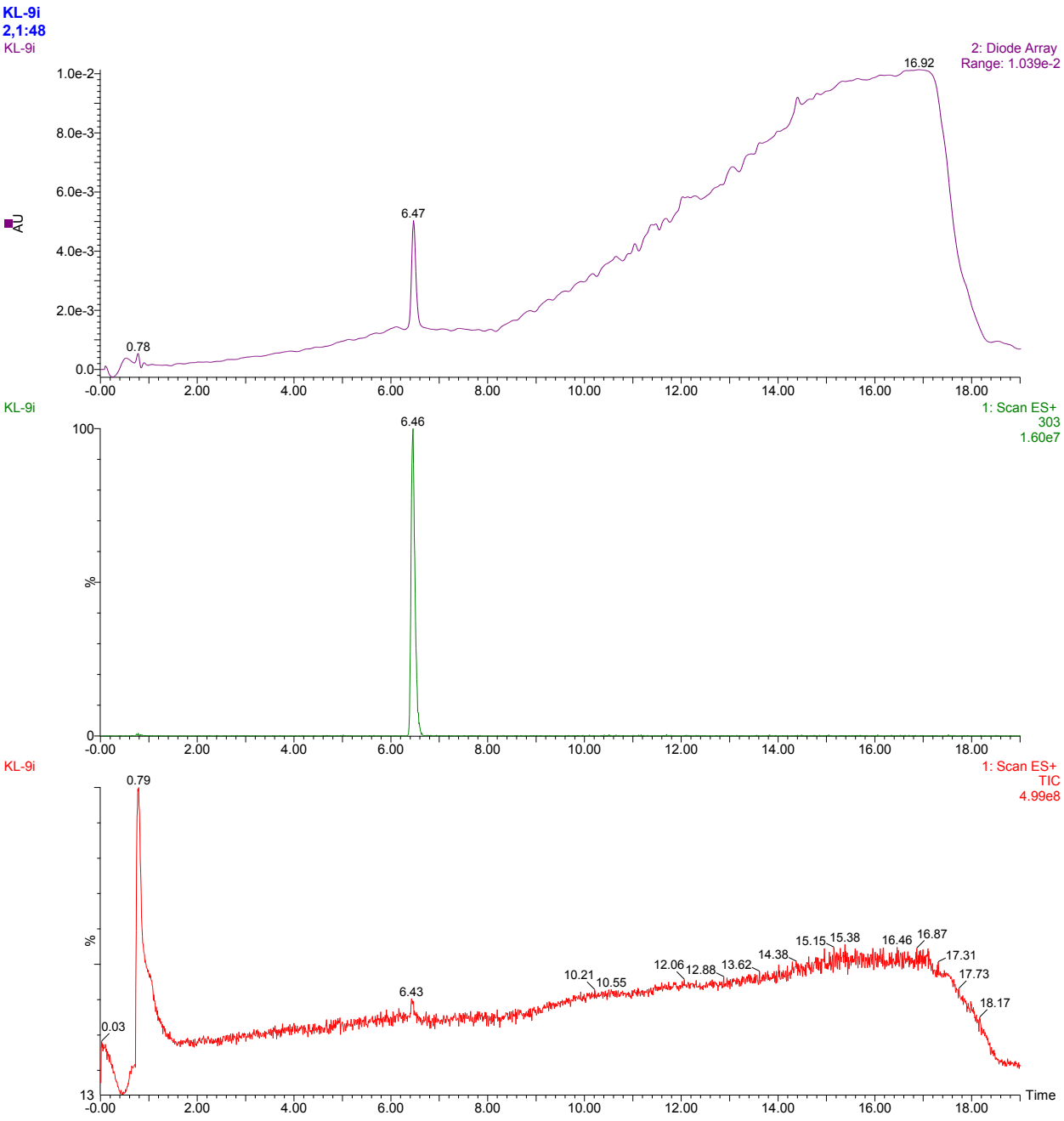
1-(Methylsulfonyl)-1,2,3,4tetrahydro-5H-benzo[e][1,4]diazepin-5-one (9g)



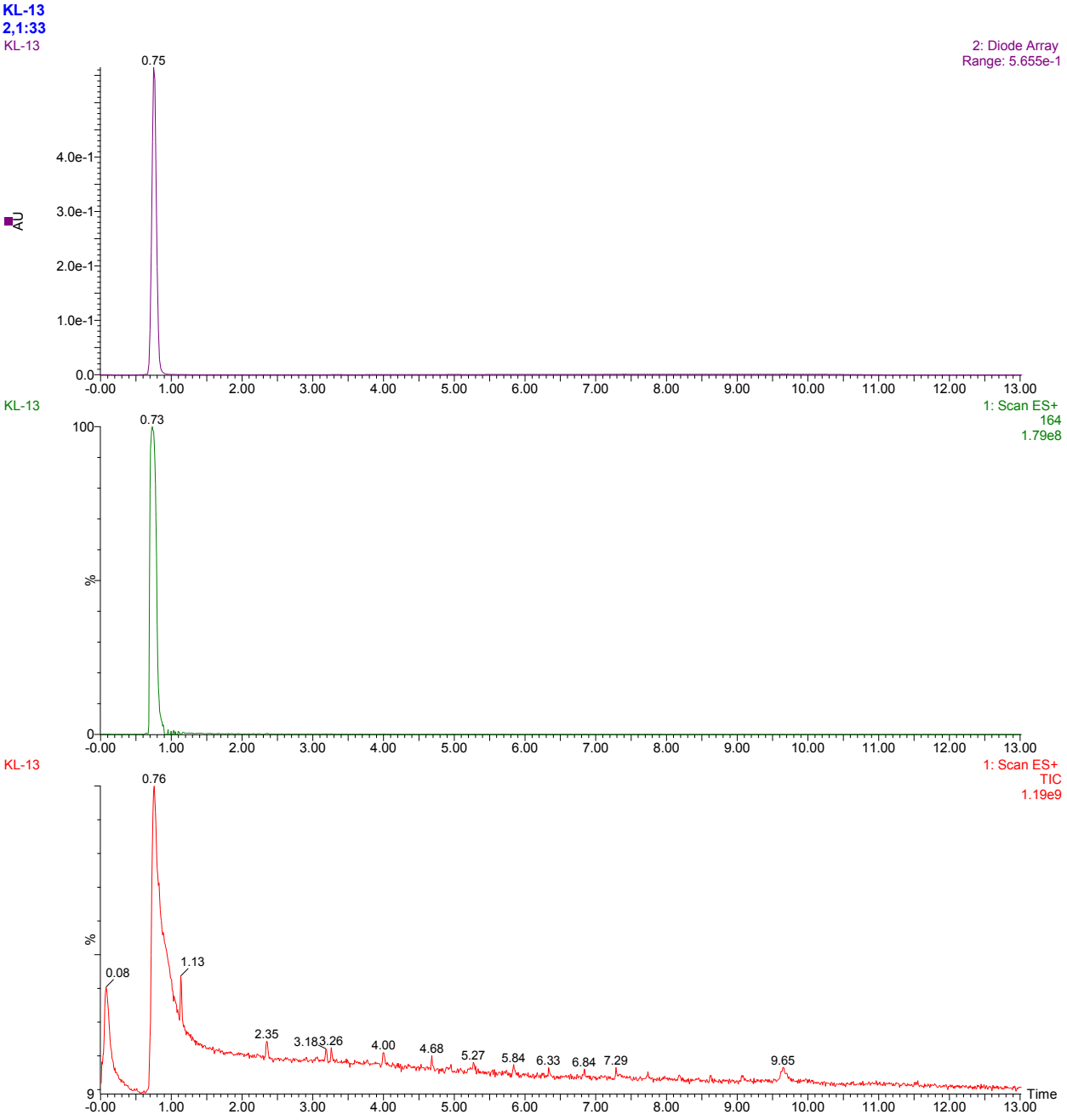
1-(vinylsulfonyl)-1,2,3,4-tetrahydro-5H-benzo[e][1,4]diazepin-5-one (9h)



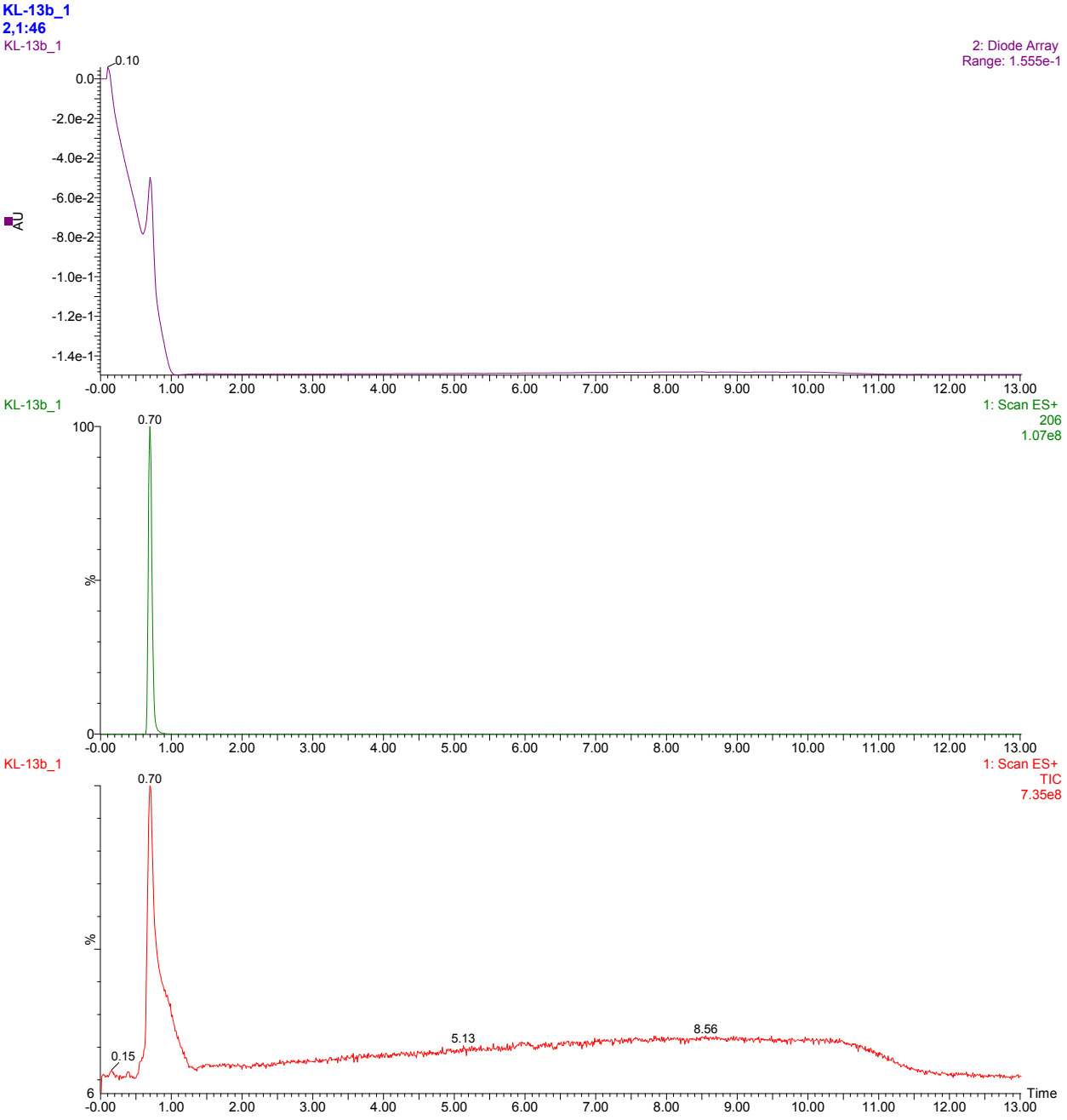
1-(Phenylsulfonyl)1,2,3,4-tetrahydro-5H-benzo[e][1,4]diazepin-5-one (9i)



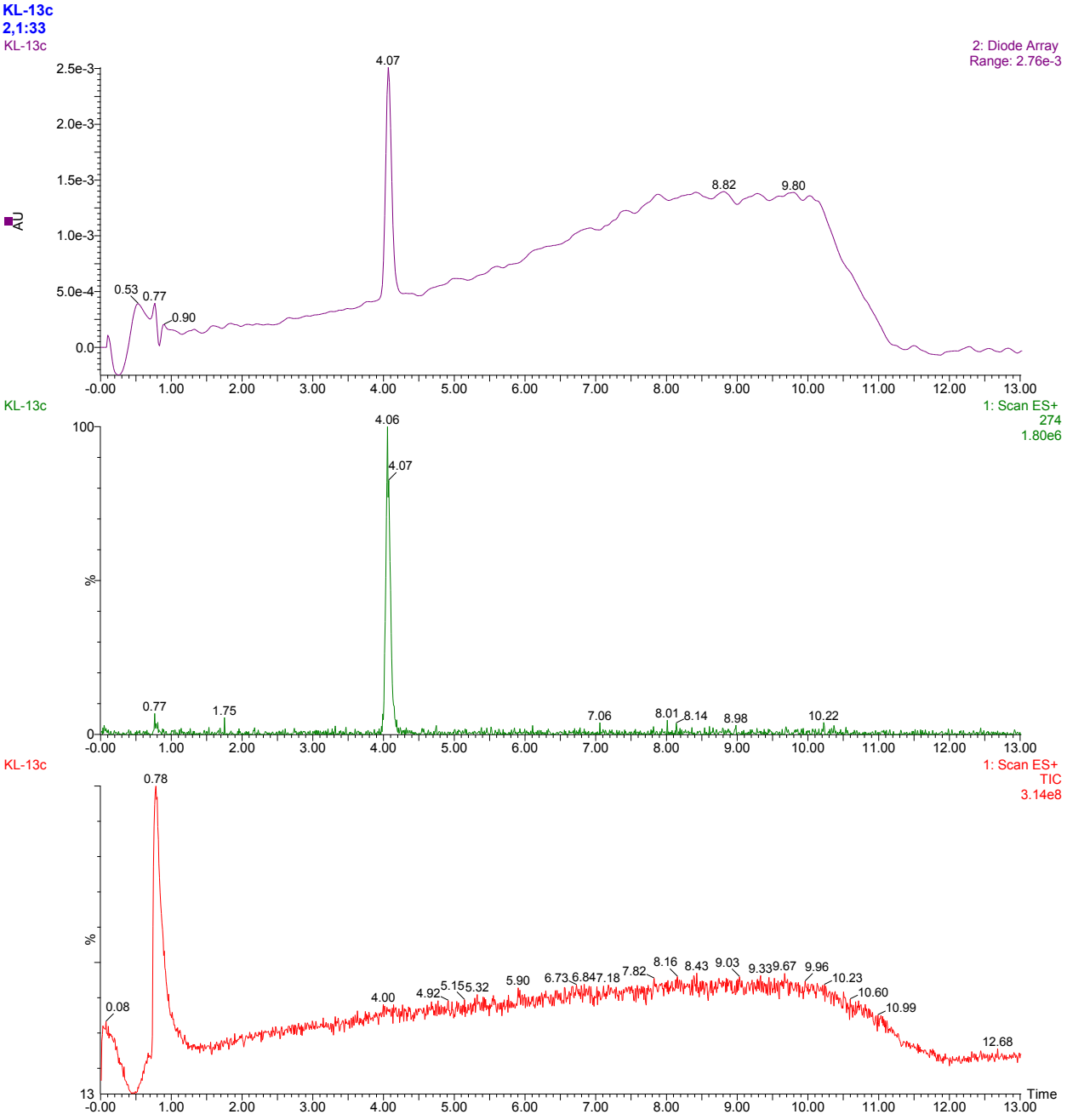
1,2,3,4-tetrahydro-5H-pyrido[2,3-e][1,4]diazepin-5-one (21a)



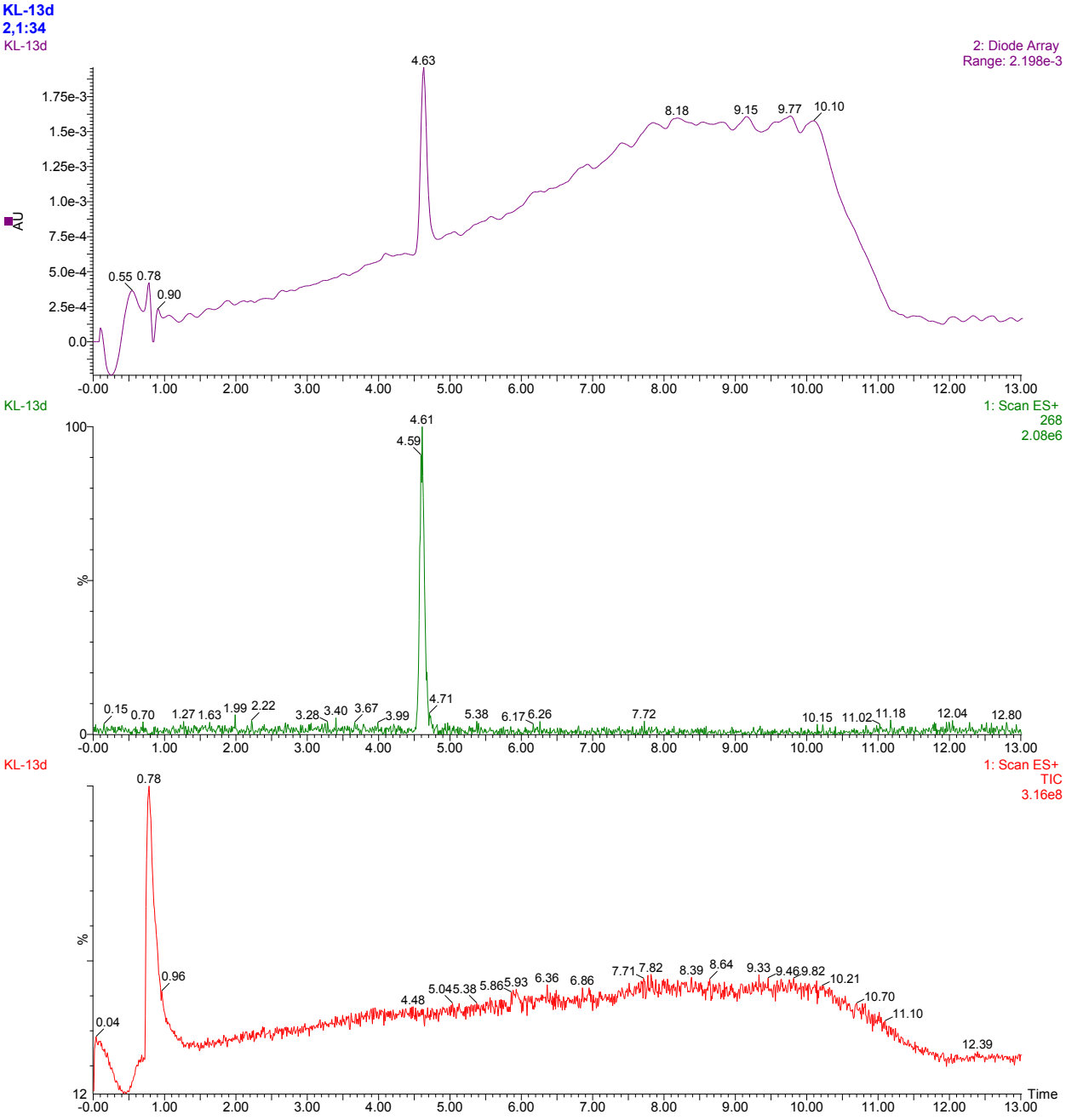
1-Acetyl-1,2,3,4-tetrahydro-5H-pyrido[2,3-e][1,4]diazepin-5-one (21b)



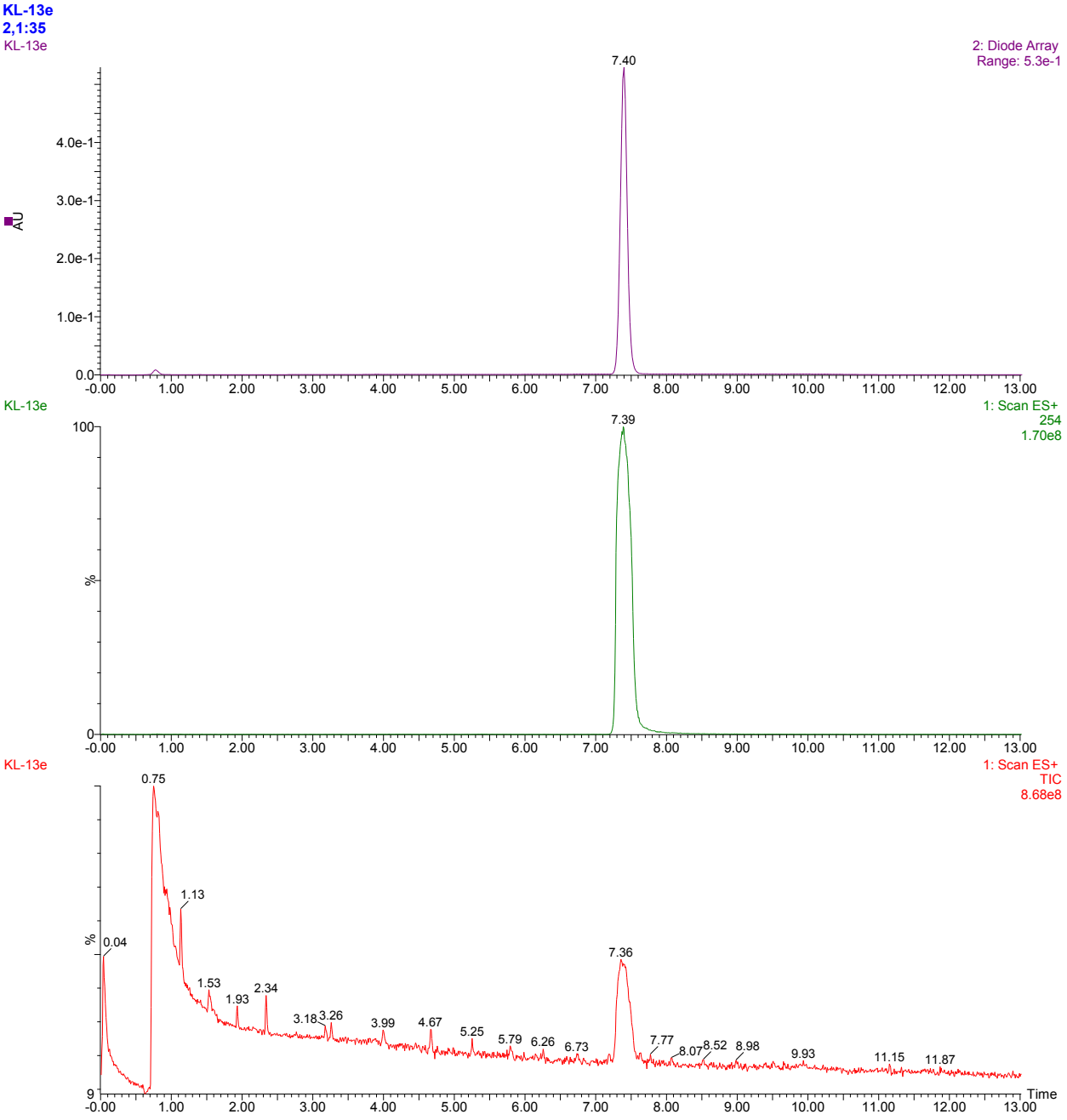
1-(Thiophene-2-carbonyl)-1,2,3,4-tetrahydro-5H-pyrido[2,3e][1,4]diazepin-5-one (21C)



1-Benzoyl-1,2,3,4-tetrahydro-5H-pyrido[2,3-e][1,4]diazepin-5-one (21d)



1-benzyl-1,2,3,4-tetrahydro-5H-pyrido[2,3-e][1,4]diazepin-5-one (21e)



# APPENDIX G: X-RAY CRYSTALLOGRAPHY

**Experimental**

A colorless plate was cut into an irregular shape (0.05 x 0.10 x 0.17 $mm^3$) and centered on the goniometer of a Rigaku Oxford Diffraction Gemini E Ultra diffractometer operating with CuKα radiation. The data collection routine, unit cell refinement, and data processing were carried out with the program CrysAlisPro.[1] The Laue symmetry and systematic absences were consistent with the monoclinic space group $P2_1/n$. The structure was solved using SHELXS-2014[2] and refined using SHELXL-2014[3] via Olex2.[4] The final refinement model involved anisotropic displacement parameters for non-hydrogen atoms. A riding model was used for the aromatic and alkyl hydrogens. The H-atom position and isotropic displacement parameter of the N-H group were refined independently.


(1) CrysAlisPro Software System, v1.171.38.43, Rigaku Oxford Diffraction, **2017**, Rigaku Corporation, Oxford, UK.
(2) Sheldrick, G. M. "A short history of SHELX." *Acta Cryst.* **2008**, *A64*, 112-122.
(3) Sheldrick, G. M. "Crystal structure refinement with SHELXL." *Acta Cryst.* **2015**, *C71*, 3-8.
(4) Dolomanov, O.V.; Bourhis, L. J.; Gildea, R. J.; Howard, J. A. K.; Puschmann, H. *J. Appl. Cryst.* **2009**, *42*, 339–341.

**Table 1**. Crystal data and structure refinement for cs2383.

| | | |
|---|---|---|
| Identification code | KL-III-171C | |
| Empirical formula | $C_{15}H_{14}N_2O_3S$ | |
| Formula weight | 302.34 | |
| Temperature | 101.1(8) K | |
| Wavelength | 1.54184 Å | |
| Crystal system | Monoclinic | |
| Space group | $P\ 1\ 2_1/n\ 1$ | |
| Unit cell dimensions | $a$ = 12.3970(4) Å | $\alpha$= 90°. |
| | $b$ = 6.7530(2) Å | $\beta$= 100.803(3)°. |
| | $c$ = 16.3651(5) Å | $\gamma$= 90°. |
| Volume | 1345.75(7) Å$^3$ | |
| Z | 4 | |
| Density (calculated) | 1.492 Mg/m$^3$ | |
| Absorption coefficient | 2.255 mm$^{-1}$ | |
| F(000) | 632 | |
| Crystal size | 0.17 x 0.102 x 0.05 mm$^3$ | |
| Theta range for data collection | 4.123 to 72.073°. | |
| Index ranges | -15<=h<=14, -8<=k<=8, -20<=l<=19 | |
| Reflections collected | 10201 | |
| Independent reflections | 2637 [R(int) = 0.0394] | |
| Completeness to theta = 67.684° | 100.0 % | |
| Absorption correction | Gaussian | |
| Max. and min. transmission | 0.914 and 0.766 | |
| Refinement method | Full-matrix least-squares on $F^2$ | |
| Data / restraints / parameters | 2637 / 0 / 194 | |
| Goodness-of-fit on $F^2$ | 1.040 | |
| Final R indices [I>2sigma(I)] | R1 = 0.0340, wR2 = 0.0851 | |
| R indices (all data) | R1 = 0.0384, wR2 = 0.0887 | |
| Extinction coefficient | n/a | |
| Largest diff. peak and hole | 0.331 and -0.407 e.Å$^{-3}$ | |

**Table 2**. Bond lengths [Å] and angles [°] for cs2383.

| | | | | | |
|---|---|---|---|---|---|
| N(1)-C(2) | 1.480(2) | C(6)-C(7) | 1.386(2) | C(12)-S(1) | 1.7663(16) |
| N(1)-C(10) | 1.4374(19) | C(6)-C(11) | 1.396(2) | C(13)-C(14) | 1.393(2) |
| N(1)-S(1) | 1.6438(13) | C(7)-C(8) | 1.394(2) | C(14)-C(15) | 1.383(3) |
| C(2)-C(3) | 1.519(2) | C(8)-C(9) | 1.392(2) | C(15)-C(16) | 1.385(2) |
| C(3)-N(4) | 1.4576(19) | C(9)-C(10) | 1.396(2) | C(16)-C(17) | 1.390(2) |
| N(4)-C(5) | 1.337(2) | C(10)-C(11) | 1.403(2) | S(1)-O(2) | 1.4329(13) |
| C(5)-C(11) | 1.5029(19) | C(12)-C(13) | 1.388(2) | S(1)-O(3) | 1.4345(13) |
| C(5)-O(1) | 1.2361(19) | C(12)-C(17) | 1.388(2) | | |

| | | | |
|---|---|---|---|
| C(2)-N(1)-S(1) | 118.73(10) | C(15)-C(16)-C(17) | 119.77(16) |
| C(10)-N(1)-C(2) | 119.61(12) | C(12)-C(17)-C(16) | 119.44(15) |
| C(10)-N(1)-S(1) | 118.84(10) | N(1)-S(1)-C(12) | 107.59(7) |
| N(1)-C(2)-C(3) | 111.52(12) | O(2)-S(1)-N(1) | 106.36(7) |
| N(4)-C(3)-C(2) | 112.78(13) | O(2)-S(1)-C(12) | 107.24(8) |
| C(5)-N(4)-C(3) | 122.60(13) | O(2)-S(1)-O(3) | 120.40(8) |
| N(4)-C(5)-C(11) | 117.31(13) | O(3)-S(1)-N(1) | 106.78(8) |
| O(1)-C(5)-N(4) | 123.57(13) | O(3)-S(1)-C(12) | 107.89(7) |
| O(1)-C(5)-C(11) | 119.11(13) | | |
| C(7)-C(6)-C(11) | 120.71(14) | | |
| C(6)-C(7)-C(8) | 119.78(14) | | |
| C(9)-C(8)-C(7) | 120.26(14) | | |
| C(8)-C(9)-C(10) | 119.97(14) | | |
| C(9)-C(10)-N(1) | 118.56(14) | | |
| C(9)-C(10)-C(11) | 119.91(14) | | |
| C(11)-C(10)-N(1) | 121.52(13) | | |
| C(6)-C(11)-C(5) | 118.49(13) | | |
| C(6)-C(11)-C(10) | 119.33(13) | | |
| C(10)-C(11)-C(5) | 122.03(13) | | |
| C(13)-C(12)-S(1) | 120.36(13) | | |
| C(17)-C(12)-C(13) | 121.25(15) | | |
| C(17)-C(12)-S(1) | 118.38(12) | | |
| C(12)-C(13)-C(14) | 118.61(15) | | |
| C(15)-C(14)-C(13) | 120.53(15) | | |
| C(14)-C(15)-C(16) | 120.40(16) | | |

**Table 3**. Hydrogen bonds for cs2383 [Å and °].

| D-H...A | d(D-H) | d(H...A) | d(D...A) | <(DHA) |
|---|---|---|---|---|
| N(4)-H(4)...O(1)#1 | 0.81(2) | 2.05(2) | 2.8552(17) | 170(2) |

Symmetry transformations used to generate equivalent atoms:

#1 -x+2,-y,-z+1

# APPENDIX H: GEOMETRY OPTIMIZATIONS[1]

All Chapter 2 derivatives (9b–i, 21b–e) were drawn with the previously optimized A/B ring core (9a or 21a) for all of the isomers and then optimized. We have included the Cartesian coordinates, energies, and vibrational frequencies for all the optimized geometries reported in Chapter 2 at the B3LYP/6-31G(d) level of theory with Gaussian 09. For the amide-based derivatives (9b–e, 21b–d), we have reported only one set of Cartesian coordinates, energies, and vibrational frequencies for one *cis*-enantiomer and *trans*-enantiomer. All of the isomers reported herein have the same relative stereochemistry.

**6,7-dihydropyrrolo[2,3-c]azepine-4,8(1H,5H)-dione (2)**
#N B3LYP/6-31G(d) OPT Geom=Connectivity
Cmpd 2
0,1

| | | | |
|---|---|---|---|
| C | -0.0899015345 | -0.0818942564 | 0.0491491859 |
| N | -0.037970479 | -0.0373537263 | 1.5098141851 |
| C | 1.0787584113 | 0.1253105813 | 2.2806901909 |
| C | 2.3953812763 | 0.1242955096 | 1.662820955 |
| N | 3.4824354792 | 0.2141552249 | 2.4161618278 |
| C | 4.6406334692 | 0.07449668 | 1.746155816 |
| C | 4.2998627901 | 0.6158931496 | 0.5261718079 |
| C | 2.8770779292 | 0.6579778228 | 0.4581790351 |
| C | 2.1220651135 | 1.2289400931 | -0.6671426235 |
| C | 0.5990491928 | 1.3028914837 | -0.5730299176 |
| H | 0.2361782964 | 1.4524162215 | -1.5945355684 |
| H | 0.3282338632 | 2.1984996812 | 0.003565238 |
| O | 2.6961080785 | 1.6695266381 | -1.6542403322 |
| H | 4.969206943 | 0.961522046 | -0.2479439115 |
| H | 5.6063455179 | 0.1260267408 | 2.1872951508 |
| H | 3.3684959266 | 0.593809283 | 3.3479934043 |
| O | 1.0111724214 | 0.4606295282 | 3.4665782951 |
| H | -0.8824719615 | 0.2305710913 | 1.9999370489 |
| H | -1.1507227171 | -0.1103045281 | -0.2134822196 |
| H | 0.3220385564 | 0.8418065316 | -0.3836076703 |

RB3LYP Energy = -569.6340851 Hartrees

| Mode | Frequency ($cm^{-1}$) | Mode | Frequency ($cm^{-1}$) | Mode | Frequency ($cm^{-1}$) |
|---|---|---|---|---|---|
| 1 | 66.0178 | 19 | 751.1312 | 37 | 1420.6171 |
| 2 | 122.1302 | 20 | 782.7361 | 38 | 1467.1932 |
| 3 | 174.6405 | 21 | 886.2937 | 39 | 1471.0896 |
| 4 | 190.7929 | 22 | 899.6437 | 40 | 1478.1292 |

| | | | | | |
|---|---|---|---|---|---|
| 5 | 262.2408 | 23 | 927.1127 | 41 | 1490.0829 |
| 6 | 266.0559 | 24 | 933.8824 | 42 | 1519.7611 |
| 7 | 330.2492 | 25 | 1014.0819 | 43 | 1532.0069 |
| 8 | 394.4123 | 26 | 1069.4485 | 44 | 1596.6504 |
| 9 | 411.6390 | 27 | 1088.9277 | 45 | 1747.7184 |
| 10 | 523.4260 | 28 | 1110.6468 | 46 | 1762.6665 |
| 11 | 544.6357 | 29 | 1135.8542 | 47 | 3025.0045 |
| 12 | 582.0374 | 30 | 1181.2340 | 48 | 3050.1771 |
| 13 | 602.3907 | 31 | 1234.5630 | 49 | 3113.2250 |
| 14 | 613.6631 | 32 | 1251.8896 | 50 | 3119.6043 |
| 15 | 638.1270 | 33 | 1290.7698 | 51 | 3276.7355 |
| 16 | 679.1888 | 34 | 1342.5082 | 52 | 3293.9968 |
| 17 | 686.7405 | 35 | 1381.3181 | 53 | 3599.9510 |
| 18 | 726.7540 | 36 | 1398.4349 | 54 | 3619.3912 |

**7-chloro-3,4-dihydro-1H-benzo[e][1,4]diazepine-2,5-dione (4)**

#N B3LYP/6-31G(d)OPT Geom=Connectivity

Cmpd 4

0,1

| | | | |
|---|---|---|---|
| C | -0.0343627276 | -0.0053957123 | 0.0030463283 |
| N | -0.0536676718 | 0.0239528496 | 1.4557132213 |
| C | 1.0392185031 | 0.0821527801 | 2.2772492787 |
| C | 2.3834328748 | -0.2161257464 | 1.6704215792 |
| C | 2.6326881418 | -1.1019449549 | 0.5985292694 |
| C | 3.9643016514 | -1.3715772454 | 0.2357076466 |
| C | 5.0311593592 | -0.7779422684 | 0.8945046081 |
| C | 4.7739450888 | 0.1079956801 | 1.9430986263 |
| C | 3.4710703667 | 0.3746828862 | 2.3327623104 |
| H | 3.2604123297 | 1.0222174735 | 3.175710182 |
| Cl | 6.1135241468 | 0.872780314 | 2.780847991 |
| H | 6.0513855154 | -0.9942865515 | 0.5964938037 |
| H | 4.1581914043 | -2.0570924783 | -0.5852620358 |
| N | 1.6306126457 | -1.8005597546 | -0.1053745217 |
| C | 0.3904449462 | -1.3669934751 | -0.5335351039 |
| O | -0.291410483 | -2.0375383395 | -1.2879857816 |
| H | 1.916067905 | -2.6637112654 | -0.5549768796 |
| O | 0.9287080326 | 0.3649114042 | 3.4650853692 |

| | | | |
|---|---|---|---|
| H | -0.928368785 | 0.2228777886 | 1.9243159816 |
| H | -1.0417774552 | 0.1828905546 | -0.3670561965 |
| H | 0.6296414176 | 0.7730938939 | -0.3997302236 |

RB3LYP Energy = -1067.3468206 Hartrees

| Mode | Frequency ($cm^{-1}$) | Mode | Frequency ($cm^{-1}$) | Mode | Frequency ($cm^{-1}$) |
|---|---|---|---|---|---|
| 1 | 59.3592 | 20 | 683.4808 | 39 | 1354.7152 |
| 2 | 71.3781 | 21 | 706.2326 | 40 | 1392.1036 |
| 3 | 129.0656 | 22 | 737.5285 | 41 | 1399.8485 |
| 4 | 147.8916 | 23 | 783.1484 | 42 | 1432.3875 |
| 5 | 181.9410 | 24 | 810.4104 | 43 | 1472.9436 |
| 6 | 212.8298 | 25 | 831.7941 | 44 | 1501.4022 |
| 7 | 301.7599 | 26 | 876.7010 | 45 | 1511.1215 |
| 8 | 322.6507 | 27 | 927.0589 | 46 | 1524.8394 |
| 9 | 342.9168 | 28 | 935.1080 | 47 | 1621.1362 |
| 10 | 370.0415 | 29 | 955.5341 | 48 | 1653.1008 |
| 11 | 393.5692 | 30 | 992.8483 | 49 | 1773.3168 |
| 12 | 441.6675 | 31 | 1089.9551 | 50 | 1814.5943 |
| 13 | 459.8424 | 32 | 1125.8563 | 51 | 3034.2676 |
| 14 | 514.7465 | 33 | 1146.3402 | 52 | 3169.3065 |
| 15 | 543.7324 | 34 | 1191.6033 | 53 | 3191.3067 |
| 16 | 556.1769 | 35 | 1246.5635 | 54 | 3228.2545 |
| 17 | 568.7334 | 36 | 1275.9170 | 55 | 3244.7365 |
| 18 | 591.9885 | 37 | 1291.7657 | 56 | 3576.9218 |
| 19 | 651.3227 | 38 | 1314.2876 | 57 | 3609.8272 |

**8-fluoro-2,3,4,5-tetrahydro-1H-benzo[c]azepin-1-one (5)**
#N B3LYP/6-31G(d) OPT Geom=Connectivity
Cmpd 5
0,1

| | | | |
|---|---|---|---|
| C | -0.3118448724 | -0.7383842709 | 0.1864981919 |
| N | -0.1082968529 | 0.2712368414 | 1.2238663833 |

| | | | |
|---|---|---|---|
| C | 0.944873989 | 0.751619447 | 1.963370156 |
| C | 2.3926613677 | 0.4664518797 | 1.6302351849 |
| C | 2.9070647523 | -0.0051785615 | 0.403396788 |
| C | 4.2967450035 | -0.1327703674 | 0.2680473013 |
| C | 5.1767201873 | 0.1868169369 | 1.2987902749 |
| C | 4.6408266677 | 0.6455752373 | 2.4949715249 |
| C | 3.2767474768 | 0.7958316564 | 2.6695828075 |
| H | 2.8776119207 | 1.1822632947 | 3.5992097518 |
| F | 5.4729995594 | 0.9567297371 | 3.511490002 |
| H | 6.251095231 | 0.0828986994 | 1.1874160501 |
| H | 4.6998587135 | -0.4945077849 | -0.6744963209 |
| C | 2.0279820506 | -0.4120179044 | -0.7565942023 |
| C | 0.9440270449 | -1.4188633967 | -0.3371791761 |
| H | 1.3519321411 | -2.1079314268 | 0.4116473684 |
| H | 0.6392150382 | -2.0290584242 | -1.1959573821 |
| H | 1.5491454168 | 0.4674563724 | -1.2111449249 |
| H | 2.6607711212 | -0.8511891174 | -1.5350564725 |
| O | 0.6865657623 | 1.4752929685 | 2.9263033323 |
| H | -0.9682240489 | 0.6319429797 | 1.6227839361 |
| H | -1.0011733118 | -1.5009376914 | 0.5756630586 |
| H | -0.8235147579 | -0.252984855 | -0.6575111745 |

RB3LYP Energy = -616.911166 Hartrees

| Mode | Frequency ($cm^{-1}$) | Mode | Frequency ($cm^{-1}$) | Mode | Frequency ($cm^{-1}$) |
|---|---|---|---|---|---|
| 1 | 27.4348 | 22 | 831.1835 | 43 | 1406.9839 |
| 2 | 61.3410 | 23 | 871.3547 | 44 | 1429.2914 |
| 3 | 120.1705 | 24 | 905.0375 | 45 | 1465.4984 |
| 4 | 159.7634 | 25 | 922.5458 | 46 | 1513.6200 |
| 5 | 230.9245 | 26 | 928.5538 | 47 | 1518.7721 |
| 6 | 258.0150 | 27 | 952.7380 | 48 | 1527.5313 |
| 7 | 307.8475 | 28 | 981.3305 | 49 | 1542.6598 |
| 8 | 367.8835 | 29 | 1021.9146 | 50 | 1556.0859 |
| 9 | 390.3561 | 30 | 1089.9679 | 51 | 1637.1567 |
| 10 | 425.6557 | 31 | 1109.8572 | 52 | 1667.1060 |
| 11 | 446.5628 | 32 | 1142.9000 | 53 | 1739.7631 |
| 12 | 498.9347 | 33 | 1178.2505 | 54 | 3013.8034 |

| | | | | | |
|---|---|---|---|---|---|
| 13 | 515.1319 | 34 | 1209.7250 | 55 | 3030.8988 |
| 14 | 544.7116 | 35 | 1220.7103 | 56 | 3039.7787 |
| 15 | 576.4747 | 36 | 1247.1406 | 57 | 3058.6023 |
| 16 | 641.3997 | 37 | 1275.0808 | 58 | 3091.3501 |
| 17 | 668.2804 | 38 | 1304.8847 | 59 | 3098.0324 |
| 18 | 707.7676 | 39 | 1316.7683 | 60 | 3187.2046 |
| 19 | 714.2204 | 40 | 1354.3151 | 61 | 3223.6750 |
| 20 | 773.6232 | 41 | 1366.9165 | 62 | 3252.4690 |
| 21 | 785.5067 | 42 | 1393.8565 | 63 | 3571.1100 |

**3,4-dihydro-1H-benzo[c]azepine-1,5(2H)-dione (6)**

#N B3LYP/6-31G(d) OPT Geom=Connectivity

Cmpd 6

0,1

| | | | |
|---|---|---|---|
| C | 0.0107293156 | 0.0484131555 | 0.0751412453 |
| N | -0.0399645078 | -0.1301674488 | 1.5165814139 |
| C | 1.0071055853 | -0.06285235 | 2.3889092564 |
| C | 2.3949232861 | 0.1829670912 | 1.838199211 |
| C | 2.9432160794 | -0.3122714483 | 0.6295977409 |
| C | 4.296939709 | -0.0536092248 | 0.3455127448 |
| C | 5.0893529101 | 0.7012053011 | 1.2006314425 |
| C | 4.5469508096 | 1.1862073871 | 2.3927531408 |
| C | 3.2223410348 | 0.9075726106 | 2.7102204482 |
| H | 2.7969574332 | 1.2346208403 | 3.6524427829 |
| H | 5.1569810179 | 1.7675414097 | 3.0786502362 |
| H | 6.1266535736 | 0.9002173393 | 0.9460045734 |
| H | 4.7074254898 | -0.4700442058 | -0.5678409837 |
| C | 2.2462090765 | -1.1661767542 | -0.3998511392 |
| C | 0.7365081365 | -1.0979250384 | -0.6208531502 |
| H | 0.3059411444 | -2.0564816301 | -0.3027230803 |
| H | 0.5984098496 | -1.0418921521 | -1.7072719012 |
| O | 2.9028994596 | -1.8977500075 | -1.1241016532 |
| O | 0.8260214534 | -0.1579517429 | 3.59 95567041 |
| H | -0.9334786018 | -0.2749282748 | 1.9686585908 |
| H | -1.022098431 | 0.1015155737 | -0.27989375 |
| H | 0.4819829554 | 1.0085978582 | -0.173215714 |

RB3LYP Energy =-591.6950807 Hartrees

| Mode | Frequency ($cm^{-1}$) | Mode | Frequency ($cm^{-1}$) | Mode | Frequency ($cm^{-1}$) |
|---|---|---|---|---|---|
| 1 | 41.7390 | 21 | 787.3282 | 41 | 1391.4588 |
| 2 | 75.3054 | 22 | 808.0196 | 42 | 1431.1101 |
| 3 | 111.4489 | 23 | 910.8251 | 43 | 1464.8784 |
| 4 | 164.2701 | 24 | 912.5603 | 44 | 1481.8211 |
| 5 | 269.0557 | 25 | 933.8968 | 45 | 1488.8559 |
| 6 | 279.5214 | 26 | 986.2582 | 46 | 1519.1142 |
| 7 | 341.2740 | 27 | 1007.3905 | 47 | 1524.8593 |
| 8 | 367.4147 | 28 | 1046.4803 | 48 | 1618.3760 |
| 9 | 407.4166 | 29 | 1069.0798 | 49 | 1650.6265 |
| 10 | 429.0204 | 30 | 1079.7442 | 50 | 1766.2933 |
| 11 | 445.0029 | 31 | 1119.3043 | 51 | 1767.1904 |
| 12 | 526.7332 | 32 | 1126.5575 | 52 | 3047.2257 |
| 13 | 530.3760 | 33 | 1179.3242 | 53 | 3056.1933 |
| 14 | 555.8981 | 34 | 1199.3008 | 54 | 3099.7494 |
| 15 | 583.3362 | 35 | 1239.5485 | 55 | 3117.9671 |
| 16 | 612.8309 | 36 | 1260.1580 | 56 | 3193.2357 |
| 17 | 661.8093 | 37 | 1301.6307 | 57 | 3208.5584 |
| 18 | 683.7561 | 38 | 1304.5108 | 58 | 3230.4522 |
| 19 | 719.4229 | 39 | 1352.6084 | 59 | 3234.1104 |
| 20 | 779.3694 | 40 | 1367.0718 | 60 | 3609.8298 |

**2,3,4,5-tetrahydro-1H-benzo[c]azepin-1-one (7)**

#N B3LYP/6-31G(d)
OPT Geom=Connectivity
Cmpd 7
0,1

| | | | |
|---|---|---|---|
| C | -0.3037183355 | -0.7620799375 | 0.2106294918 |
| N | -0.0964572435 | 0.3225905077 | 1.1701472446 |
| C | 0.9493893667 | 0.7682727761 | 1.9468999602 |
| C | 2.3932917398 | 0.4654236708 | 1.6296367997 |
| C | 2.9050244261 | 0.0131097191 | 0.3949956569 |
| C | 4.2927178058 | -0.1247652763 | 0.255743734 |

| | | | |
|---|---|---|---|
| C | 5.1673491717 | 0.1664080805 | 1.3002829109 |
| C | 4.6582112529 | 0.6071029644 | 2.5220273282 |
| C | 3.2849927901 | 0.7612354177 | 2.6741609612 |
| H | 2.8637852063 | 1.1295609716 | 3.6025404127 |
| H | 5.3259129887 | 0.8354334053 | 3.3481425169 |
| H | 6.2384770175 | 0.0464573039 | 1.159795491 |
| H | 4.690341697 | -0.4713677461 | -0.695387183 |
| C | 2.0161719676 | -0.3754181965 | -0.7640309503 |
| C | 0.9592525454 | -1.4105372418 | -0.3418556704 |
| H | 1.3958429408 | -2.0953273083 | 0.3942620348 |
| H | 0.6562001006 | -2.0221193778 | -1.2002227588 |
| H | 1.514017641 | 0.5069731767 | -1.1856444573 |
| H | 2.642261313 | -0.7859907945 | -1.5632237084 |
| O | 0.6826851735 | 1.4941257179 | 2.9061636641 |
| H | -0.9576834883 | 0.6972810007 | 1.5537910002 |
| H | -0.9363414496 | -1.5349264852 | 0.6714466914 |
| H | -0.8782455222 | -0.3443843428 | -0.6281485266 |

RB3LYP Energy =-517.6785041 Hartrees

| **Mode** | **Frequency ($cm^{-1}$)** | **Mode** | **Frequency ($cm^{-1}$)** | **Mode** | **Frequency ($cm^{-1}$)** |
|---|---|---|---|---|---|
| 1 | 45.6684 | 22 | 893.7416 | 43 | 1436.1773 |
| 2 | 73.3977 | 23 | 914.8911 | 44 | 1494.4438 |
| 3 | 131.4173 | 24 | 970.8212 | 45 | 1514.3390 |
| 4 | 187.4776 | 25 | 977.6472 | 46 | 1518.3022 |
| 5 | 270.2279 | 26 | 999.1863 | 47 | 1526.8995 |
| 6 | 307.7311 | 27 | 1006.7201 | 48 | 1535.0384 |
| 7 | 345.7258 | 28 | 1072.6294 | 49 | 1555.9561 |
| 8 | 384.5962 | 29 | 1101.7081 | 50 | 1630.2084 |
| 9 | 443.7466 | 30 | 1112.9192 | 51 | 1659.3783 |
| 10 | 484.7133 | 31 | 1137.2841 | 52 | 1739.6205 |
| 11 | 523.9102 | 32 | 1195.7857 | 53 | 3014.4563 |
| 12 | 559.1003 | 33 | 1196.9039 | 54 | 3035.3475 |
| 13 | 589.0103 | 34 | 1217.6096 | 55 | 3037.8240 |
| 14 | 633.0005 | 35 | 1224.4813 | 56 | 3058.3712 |
| 15 | 681.4986 | 36 | 1249.1777 | 57 | 3092.7802 |

| | | | | | |
|---|---|---|---|---|---|
| 16 | 706.8456 | 37 | 1303.6484 | 58 | 3098.2252 |
| 17 | 737.3319 | 38 | 1322.2738 | 59 | 3176.9202 |
| 18 | 764.0943 | 39 | 1354.2291 | 60 | 3191.7976 |
| 19 | 807.0672 | 40 | 1367.0695 | 61 | 3206.6254 |
| 20 | 820.5250 | 41 | 1392.3755 | 62 | 3237.4407 |
| 21 | 864.1550 | 42 | 1405.7918 | 63 | 3567.1222 |

**3,4-dihydrobenzo[f][1,4]oxazepin-5(2H)-one (8)**

#N B3LYP/6-31G(d) OPT Geom=Connectivity

Cmpd 8

0,1

| | | | |
|---|---|---|---|
| C | 0.0182607046 | -0.0088133839 | -0.0030907586 |
| N | -0.0149190202 | 0.056074057 | 1.4435295792 |
| C | 0.9970422364 | 0.0265060271 | 2.369070979 |
| C | 2.4473568655 | -0.1117983094 | 1.9645362063 |
| C | 3.0216529679 | -0.3107281051 | 0.6885266895 |
| C | 4.4182995327 | -0.324503389 | 0.5376946119 |
| C | 5.2598776988 | -0.1629635498 | 1.6268133129 |
| C | 4.7139570617 | 0.0045175029 | 2.90394552 |
| C | 3.3370808662 | 0.0266234384 | 3.0528462292 |
| H | 2.8839914501 | 0.1668207926 | 4.0272458621 |
| H | 5.3576181335 | 0.1224901846 | 3.7705235078 |
| H | 6.3369123183 | -0.1794324177 | 1.4825251592 |
| H | 4.8089766075 | -0.4776895035 | -0.4632356338 |
| O | 2.3633002831 | -0.4811452378 | -0.4995764461 |
| C | 1.044783265 | -1.0054458764 | -0.516082558 |
| H | 0.9924966834 | -1.9385118791 | 0.0613481193 |
| H | 0.8514519417 | -1.2284773182 | -1.5689612411 |
| O | 0.6973527622 | 0.1325238091 | 3.5580838133 |
| H | -0.9109842088 | 0.2050473489 | 1.8897042054 |
| H | -0.9768994132 | -0.3254381224 | -0.3350627525 |
| H | 0.2214418949 | 0.9697935673 | -0.4626182345 |

RB3LYP Energy = -553.5773062 Hartrees

| Mode | Frequency ($cm^{-1}$) | Mode | Frequency ($cm^{-1}$) | Mode | Frequency ($cm^{-1}$) |
|---|---|---|---|---|---|
| 1 | 38.8625 | 20 | 825.1635 | 39 | 1427.1300 |
| 2 | 98.6729 | 21 | 884.1440 | 40 | 1431.4552 |
| 3 | 134.8782 | 22 | 890.5914 | 41 | 1485.6654 |

| | | | | | |
|---|---|---|---|---|---|
| 4 | 237.9475 | 23 | 977.3438 | 42 | 1498.6342 |
| 5 | 299.2486 | 24 | 998.7936 | 43 | 1514.5003 |
| 6 | 321.3208 | 25 | 1008.7962 | 44 | 1530.6709 |
| 7 | 372.2225 | 26 | 1059.8238 | 45 | 1533.5843 |
| 8 | 404.1814 | 27 | 1073.8741 | 46 | 1622.1440 |
| 9 | 438.0992 | 28 | 1110.2031 | 47 | 1664.2764 |
| 10 | 514.9260 | 29 | 1120.7319 | 48 | 1747.0782 |
| 11 | 535.6783 | 30 | 1140.9881 | 49 | 3025.1660 |
| 12 | 568.9562 | 31 | 1183.4060 | 50 | 3046.4466 |
| 13 | 570.2722 | 32 | 1193.8059 | 51 | 3090.6545 |
| 14 | 597.6873 | 33 | 1252.5483 | 52 | 3124.7943 |
| 15 | 663.6239 | 34 | 1276.4923 | 53 | 3190.9114 |
| 16 | 689.2154 | 35 | 1295.5679 | 54 | 3207.7402 |
| 17 | 704.6467 | 36 | 1328.6294 | 55 | 3218.7921 |
| 18 | 768.1470 | 37 | 1359.9078 | 56 | 3240.1443 |
| 19 | 796.2337 | 38 | 1388.4118 | 57 | 3603.8563 |

**1,2,3,4-tetrahydro-5H-benzo[e][1,4]diazepin-5-one (9)**

#N B3LYP/6-31G(d) OPT Geom=Connectivity

Cmpd 9a

0,1

| | | | |
|---|---|---|---|
| C | 0. | 0. | 0. |
| N | 0. | 0. | 1.4490057 |
| C | 1.0248165839 | 0. | 2.3643503808 |
| C | 2.4758839774 | -0.1040162934 | 1.9614269735 |
| C | 3.0491998456 | -0.3456636749 | 0.6835488576 |
| C | 4.4596050459 | -0.3644157225 | 0.5716692344 |
| C | 5.2878628428 | -0.1622376899 | 1.6609996748 |
| C | 4.7322065498 | 0.0590367483 | 2.9257471894 |
| C | 3.3538745753 | 0.0808430108 | 3.0515900269 |
| H | 2.887829093 | 0.2486833038 | 4.0153301709 |
| H | 5.3658962606 | 0.213431107 | 3.7936901005 |
| H | 6.3661919494 | -0.1856845529 | 1.5253132186 |
| H | 4.8951258511 | -0.5468584697 | -0.4092774998 |
| N | 2.3483490311 | -0.5323666995 | -0.5029834553 |

| | | | |
|---|---|---|---|
| C | 0.9831178405 | -1.0105873436 | -0.5821738053 |
| H | 0.8408058538 | -1.9792596796 | -0.0757157897 |
| H | 0.7579686012 | -1.1496443625 | -1.6444991951 |
| H | 2.9385029945 | -0.8577786419 | -1.2565487386 |
| O | 0.7209185497 | 0.0936274125 | 3.5550865313 |
| H | -0.8898758611 | 0.118903317 | 1.9159221605 |
| H | -1.0140699948 | -0.2703688613 | -0.3131840494 |
| H | 0.2233440362 | 0.9920280861 | -0.4180802541 |

RB3LYP Energy = -533.7141493 Hartrees

| Mode | Frequency ($cm^{-1}$) | Mode | Frequency ($cm^{-1}$) | Mode | Frequency ($cm^{-1}$) |
|---|---|---|---|---|---|
| 1 | 41.1273 | 21 | 838.6336 | 41 | 1430.4019 |
| 2 | 87.6817 | 22 | 857.9520 | 42 | 1474.3933 |
| 3 | 137.0393 | 23 | 894.0333 | 43 | 1490.3853 |
| 4 | 233.6212 | 24 | 964.4089 | 44 | 1513.5248 |
| 5 | 285.8965 | 25 | 996.3641 | 45 | 1534.5031 |
| 6 | 325.4740 | 26 | 1014.4909 | 46 | 1542.1660 |
| 7 | 366.9121 | 27 | 1065.6331 | 47 | 1563.5398 |
| 8 | 411.0440 | 28 | 1077.3592 | 48 | 1630.1326 |
| 9 | 434.6811 | 29 | 1099.1550 | 49 | 1666.4713 |
| 10 | 467.4587 | 30 | 1131.3946 | 50 | 1738.9032 |
| 11 | 518.1240 | 31 | 1157.2696 | 51 | 2998.2376 |
| 12 | 538.8600 | 32 | 1192.7451 | 52 | 3030.3503 |
| 13 | 568.0265 | 33 | 1199.5529 | 53 | 3093.4722 |
| 14 | 571.9435 | 34 | 1260.0552 | 54 | 3101.5879 |
| 15 | 634.7419 | 35 | 1284.5795 | 55 | 3162.5128 |
| 16 | 665.3060 | 36 | 1292.0945 | 56 | 3191.3024 |
| 17 | 692.1114 | 37 | 1331.9234 | 57 | 3209.5136 |
| 18 | 706.3863 | 38 | 1362.3340 | 58 | 3240.5842 |
| 19 | 764.4126 | 39 | 1393.1232 | 59 | 3595.8125 |
| 20 | 788.4932 | 40 | 1415.5935 | 60 | 3602.7263 |

**1-acetyl-1,2,3,4-tetrahydro-5H-benzo[e][1,4]diazepin-5-one (*cis*-9b)**

#N B3LYP/6-31G(d) OPT Geom=Connectivity

Cmpd 9b_cis

0,1

| | | | |
|---|---|---|---|
| C | -0.0998977641 | -0.1185465167 | -0.0323963182 |
| N | -0.0724259475 | 0.0535167982 | 1.4084587319 |
| C | 0.9178717309 | 0.1499855763 | 2.3588558735 |
| C | 2.39042454 | -0.0137167441 | 2.0536787148 |
| C | 3.0502528252 | 0.0948020219 | 0.8113903817 |
| C | 4.4486369244 | 0.0004916906 | 0.7531820084 |
| C | 5.1983447355 | -0.2069544247 | 1.9036213887 |
| C | 4.5574207744 | -0.3334994199 | 3.1382200942 |
| C | 3.1755644874 | -0.2324445825 | 3.2021898934 |
| H | 2.6546200334 | -0.2989480561 | 4.1497595108 |
| H | 5.132195233 | -0.5023632213 | 4.0442625115 |
| H | 6.2802345271 | -0.2786512646 | 1.8328643317 |
| H | 4.9378887328 | 0.0993467263 | -0.207470468 |
| N | 2.3283453857 | 0.2396513614 | -0.4127290025 |
| C | 1.1984151917 | -0.6656084258 | -0.6059721422 |
| H | 1.4444319622 | -1.6218848244 | -0.1335227529 |
| H | 1.0574149307 | -0.8601119352 | -1.6709815508 |
| C | 2.6901885118 | 1.2149915682 | -1.3402701162 |
| O | 3.5995965589 | 2.002301512 | -1.132753963 |
| C | 1.9128980849 | 1.2511521262 | -2.6517017059 |
| H | 2.2838227238 | 2.1074104794 | -3.2156370138 |
| H | 2.0800870136 | 0.3428433175 | -3.2430661629 |
| H | 0.8334326499 | 1.3624013801 | -2.5057168257 |
| O | 0.5665845384 | 0.3478015031 | 3.5216171233 |
| H | -0.9710457803 | 0.2231708581 | 1.8451898155 |
| H | -0.9113192638 | -0.8177808583 | -0.2767559905 |
| H | -0.3370480843 | 0.8352446882 | -0.527519041 |

RB3LYP Energy = -686.3664377 Hartrees

| Mode | Frequency ($cm^{-1}$) | Mode | Frequency ($cm^{-1}$) | Mode | Frequency ($cm^{-1}$) |
|---|---|---|---|---|---|
| 1 | 50.5355 | 26 | 776.6258 | 51 | 1431.5094 |
| 2 | 69.0001 | 27 | 794.3836 | 52 | 1437.0401 |
| 3 | 89.1028 | 28 | 877.9003 | 53 | 1491.0369 |
| 4 | 98.2064 | 29 | 894.4906 | 54 | 1496.8359 |
| 5 | 144.2704 | 30 | 926.6144 | 55 | 1513.1796 |
| 6 | 171.3072 | 31 | 972.4745 | 56 | 1521.0938 |

| | | | | | |
|---|---|---|---|---|---|
| 7 | 202.4085 | 32 | 984.0871 | 57 | 1525.8074 |
| 8 | 273.8603 | 33 | 997.6226 | 58 | 1532.7613 |
| 9 | 290.9720 | 34 | 1030.2753 | 59 | 1546.6249 |
| 10 | 338.8692 | 35 | 1059.4987 | 60 | 1626.9797 |
| 11 | 350.5650 | 36 | 1061.4832 | 61 | 1658.0857 |
| 12 | 398.9499 | 37 | 1082.1481 | 62 | 1741.4337 |
| 13 | 409.0089 | 38 | 1122.4278 | 63 | 1781.7736 |
| 14 | 437.7903 | 39 | 1136.9625 | 64 | 3011.0443 |
| 15 | 518.4288 | 40 | 1166.5195 | 65 | 3050.6790 |
| 16 | 536.8920 | 41 | 1196.5521 | 66 | 3059.2141 |
| 17 | 551.4431 | 42 | 1198.1358 | 67 | 3088.2744 |
| 18 | 576.8539 | 43 | 1250.5693 | 68 | 3121.9954 |
| 19 | 597.1285 | 44 | 1269.0772 | 69 | 3142.1642 |
| 20 | 615.3870 | 45 | 1299.8088 | 70 | 3179.4998 |
| 21 | 625.9020 | 46 | 1321.3866 | 71 | 3192.6098 |
| 22 | 667.4345 | 47 | 1349.2367 | 72 | 3208.8692 |
| 23 | 684.9937 | 48 | 1369.9856 | 73 | 3242.7251 |
| 24 | 719.4105 | 49 | 1397.3301 | 74 | 3245.6008 |
| 25 | 754.1108 | 50 | 1418.7865 | 75 | 3583.9828 |

**1-acetyl-1,2,3,4-tetrahydro-5H-benzo[e][1,4]diazepin-5-one (*trans*-9b)**

#N B3LYP/6-31G(d) OPT Geom=Connectivity

Cmpd 9b_trans

0,1

| | | | |
|---|---|---|---|
| C | -0.0945772866 | -0.0458044092 | -0.0177528879 |
| N | -0.0838624977 | -0.0279766813 | 1.4413703075 |
| C | 0.8778896938 | 0.0165916886 | 2.4187145932 |
| C | 2.3645148964 | 0.0260718711 | 2.1277532472 |
| C | 3.005606431 | 0.3745589626 | 0.9202087995 |
| C | 4.4058123193 | 0.3801868646 | 0.8495405096 |
| C | 5.179902416 | 0.0739441524 | 1.9640287195 |
| C | 4.5561563293 | -0.2689263508 | 3.1650488503 |
| C | 3.1684076621 | -0.2899283719 | 3.2364910101 |
| H | 2.659763198 | -0.5342739308 | 4.1617227282 |

| | | | |
|---|---|---|---|
| H | 5.1481428984 | -0.520175811 | 4.0402912439 |
| H | 6.263696139 | 0.0848951528 | 1.8873711412 |
| H | 4.8781173684 | 0.6091106277 | -0.1003274324 |
| N | 2.2541993455 | 0.6533251991 | -0.2537419034 |
| C | 1.2572150265 | -0.3457990996 | -0.6405153424 |
| H | 1.6233169857 | -1.3306119574 | -0.3371515439 |
| H | 1.1557129198 | -0.3202370338 | -1.7269576123 |
| C | 2.2874693894 | 1.8365087727 | -0.9806782698 |
| C | 3.2020176167 | 2.9524736153 | -0.5044387403 |
| H | 4.2140682557 | 2.8186881078 | -0.902021756 |
| H | 2.8043566347 | 3.8864691467 | -0.905279196 |
| H | 3.2743563354 | 3.0125807229 | 0.584175 7108 |
| O | 1.5801973694 | 1.9728140798 | -1.9722219456 |
| O | 0.5084723685 | 0.0264004588 | 3.5940063273 |
| H | -0.9988110371 | -0.0025236604 | 1.8771770457 |
| H | -0.8128160107 | -0.8102088903 | -0.3431157443 |
| H | -0.4451309188 | 0.9193560116 | -0.405561514 |

RB3LYP Energy = -686.3726943 Hartrees

| **Mode** | **Frequency ($cm^{-1}$)** | **Mode** | **Frequency ($cm^{-1}$)** | **Mode** | **Frequency ($cm^{-1}$)** |
|---|---|---|---|---|---|
| 1 | 45.5836 | 26 | 782.2050 | 51 | 1430.0141 |
| 2 | 73.3036 | 27 | 799.9201 | 52 | 1434.0684 |
| 3 | 84.2332 | 28 | 898.8689 | 53 | 1492.7822 |
| 4 | 91.5879 | 29 | 912.0987 | 54 | 1498.0482 |
| 5 | 135.3798 | 30 | 927.0805 | 55 | 1503.2844 |
| 6 | 150.1244 | 31 | 976.9636 | 56 | 1512.5920 |
| 7 | 165.4393 | 32 | 987.5592 | 57 | 1514.0866 |
| 8 | 274.5679 | 33 | 1003.0883 | 58 | 1530.9905 |
| 9 | 289.1927 | 34 | 1020.0026 | 59 | 1551.3063 |
| 10 | 340.5368 | 35 | 1057.6135 | 60 | 1625.4128 |
| 11 | 355.0097 | 36 | 1066.0462 | 61 | 1656.4205 |
| 12 | 396.2725 | 37 | 1076.2837 | 62 | 1739.5060 |
| 13 | 429.0638 | 38 | 1128.5697 | 63 | 1761.0643 |
| 14 | 435.7565 | 39 | 1132.0319 | 64 | 3038.9583 |
| 15 | 460.6535 | 40 | 1141.8069 | 65 | 3069.8695 |

| | | | | | |
|---|---|---|---|---|---|
| 16 | 545.9005 | 41 | 1189.3972 | 66 | 3073.0056 |
| 17 | 556.1980 | 42 | 1196.3309 | 67 | 3097.8214 |
| 18 | 574.7936 | 43 | 1255.3416 | 68 | 3140.5625 |
| 19 | 614.7894 | 44 | 1282.4043 | 69 | 3155.7393 |
| 20 | 625.1463 | 45 | 1298.2993 | 70 | 3174.2722 |
| 21 | 634.7676 | 46 | 1338.2652 | 71 | 3192.6845 |
| 22 | 672.5475 | 47 | 1344.1170 | 72 | 3207.7037 |
| 23 | 688.5320 | 48 | 1373.5221 | 73 | 3217.9494 |
| 24 | 725.3627 | 49 | 1403.2949 | 74 | 3241.7736 |
| 25 | 758.9711 | 50 | 1421.7147 | 75 | 3580.0489 |

**1-(furan-2-carbonyl)-1,2,3,4-tetrahydro-5H-benzo[e][1,4]diazepin-5-one (*cis*-9c)**

#N B3LYP/6-31G(d) OPT Geom=Connectivity

Cmpd 9c_cis

0,1

| | | | |
|---|---|---|---|
| C | -0.0002485096 | -0.0005982443 | -0.0000305137 |
| N | 0.0001678751 | 0.0006528209 | 1.4519473905 |
| C | 0.9828914335 | -0.0006073925 | 2.4147625306 |
| C | 2.4419315385 | -0.2629371928 | 2.1138027266 |
| C | 3.134182646 | -0.1123059791 | 0.8934215653 |
| C | 4.5149840659 | -0.3561393667 | 0.8415722259 |
| C | 5.2149270942 | -0.7429688685 | 1.9771689292 |
| C | 4.5420770871 | -0.8991395074 | 3.190677419 |
| C | 3.177670418 | -0.6567124658 | 3.248189321 |
| H | 2.6334157515 | -0.7486506357 | 4.1803859662 |
| H | 5.0781195174 | -1.2032086888 | 4.0851078631 |
| H | 6.2834874456 | -0.9279500267 | 1.9099518135 |
| H | 5.0331749526 | -0.2288543862 | -0.0995878204 |
| N | 2.4499478494 | 0.2165201524 | -0.3203896816 |
| C | 1.2647424271 | -0.5843833455 | -0.6128835289 |
| H | 1.4345015212 | -1.5945584155 | -0.227154696 |
| H | 1.1427676374 | -0.6653557547 | -1.6941369191 |
| C | 2.97656199 | 1.1899062155 | -1.167091463 |
| O | 3.9959324141 | 1.8076985643 | -0.8931379991 |
| C | 2.2978267979 | 1.4790153536 | -2.4660888369 |
| O | 3.1580848778 | 2.0308515797 | -0.3804656453 |
| C | 2.4423987561 | 2.3489765382 | -4.4810 795876 |
| C | 1.1270798593 | 2.0338856086 | -4.311047512 |
| C | 1.0319499766 | 1.4676872938 | -3.0048546297 |
| H | 0.1224089829 | 1.1317145506 | -2.5320162139 |

| | | | |
|---|---|---|---|
| H | 0.3246990266 | 2.1848059051 | -5.0193315387 |
| H | 3.0040136372 | 2.7824089226 | -5.29499 17202 |
| O | 0.6319845579 | 0.1601943121 | 3.5831138871 |
| H | -0.8910029743 | 0.2125220572 | 1.8859930584 |
| H | -0.8591628632 | -0.5978072835 | -0.3355048344 |
| H | -0.1452295971 | 1.0214346699 | -0.37928571 |

RB3LYP Energy = -875.8719787 Hartrees

| **Mode** | **Frequency ($cm^{-1}$)** | **Mode** | **Frequency ($cm^{-1}$)** | **Mode** | **Frequency ($cm^{-1}$)** |
|---|---|---|---|---|---|
| 1 | 32.4667 | 30 | 768.9578 | 59 | 1349.5594 |
| 2 | 43.7289 | 31 | 778.6263 | 60 | 1371.1121 |
| 3 | 59.5160 | 32 | 795.4851 | 61 | 1400.8422 |
| 4 | 78.2071 | 33 | 827.9051 | 62 | 1427.5684 |
| 5 | 110.3693 | 34 | 835.7645 | 63 | 1434.5680 |
| 6 | 124.8013 | 35 | 875.8313 | 64 | 1438.1972 |
| 7 | 140.6810 | 36 | 893.1418 | 65 | 1490.9159 |
| 8 | 179.8603 | 37 | 903.4280 | 66 | 1509.3855 |
| 9 | 221.1319 | 38 | 924.0162 | 67 | 1512.8576 |
| 10 | 254.1269 | 39 | 935.6756 | 68 | 1523.3514 |
| 11 | 296.7762 | 40 | 974.4555 | 69 | 1532.5446 |
| 12 | 331.0059 | 41 | 986.1826 | 70 | 1546.8909 |
| 13 | 353.9172 | 42 | 997.7976 | 71 | 1613.6783 |
| 14 | 373.9076 | 43 | 1055.5142 | 72 | 1627.1282 |
| 15 | 406.3574 | 44 | 1064.1888 | 73 | 1657.3461 |
| 16 | 434.6848 | 45 | 1081.3210 | 74 | 1738.6543 |
| 17 | 463.6696 | 46 | 1092.7395 | 75 | 1747.8946 |
| 18 | 547.7505 | 47 | 1127.8802 | 76 | 3018.7758 |
| 19 | 549.9548 | 48 | 1133.4068 | 77 | 3053.9105 |
| 20 | 566.8026 | 49 | 1144.6426 | 78 | 3089.7478 |
| 21 | 594.0023 | 50 | 1187.6403 | 79 | 3148.7412 |

| | | | | | |
|---|---|---|---|---|---|
| 22 | 608.9878 | 51 | 1199.0735 | 80 | 3193.1753 |
| 23 | 617.3300 | 52 | 1200.1865 | 81 | 3209.4241 |
| 24 | 646.4217 | 53 | 1224.1506 | 82 | 3243.4835 |
| 25 | 674.5031 | 54 | 1256.9200 | 83 | 3253.4608 |
| 26 | 676.1248 | 55 | 1270.0618 | 84 | 3271.9010 |
| 27 | 713.5662 | 56 | 1286.1448 | 85 | 3295.3080 |
| 28 | 722.5273 | 57 | 1304.6488 | 86 | 3304.3144 |
| 29 | 751.6958 | 58 | 1321.0275 | 87 | 3581.0737 |

**1-(furan-2-carbonyl)-1,2,3,4-tetrahydro-5H-benzo[e][1,4]diazepin-5-one (*trans*-9c)**

#N B3LYP/6-31G(d) OPT Geom=Connectivity

Cmpd 9c_trans

0,1

| | | | |
|---|---|---|---|
| C | 0.3415933587 | -0.4516979221 | -0.1315038095 |
| N | 0.1863768637 | -0.8322556008 | 1.2661930766 |
| C | 1.1482750599 | -0.6588700899 | 2.2242032897 |
| C | 2.3304798328 | 0.1812736093 | 1.8207226234 |
| C | 2.2163139481 | 1.3577852298 | 1.0517141709 |
| C | 3.370734666 | 2.0838034909 | 0.7302545411 |
| C | 4.6188192216 | 1.6702789031 | 1.1904915331 |
| C | 4.7307852468 | 0.5209422651 | 1.9767160317 |
| C | 3.5896059105 | -0.212433831 | 2.2901178117 |
| H | 3.6470615083 | -1.0993465017 | 2.9131330253 |
| H | 5.7015994037 | 0.1996625352 | 2.3427742291 |
| H | 5.5032079375 | 2.2469540633 | 0.9341904012 |
| H | 3.2757531772 | 2.9824511258 | 0.1284615881 |
| N | 0.9381592035 | 1.8307954784 | 0.6230384188 |
| C | 0.1654317269 | 1.0509917576 | -0.3557206615 |
| H | 0.4608567387 | 1.3069223512 | -1.3837022205 |
| H | -0.8792728282 | 1.3441311143 | -0.237248947 |
| C | 0.4700492069 | 3.1192839766 | 0.8678035755 |
| O | -0.4159704402 | 3.6126285714 | 0.1796329313 |
| C | 1.0062575766 | 3.837435772 | 2.0462870649 |
| O | 0.8047513388 | 5.1928268563 | 2.0244776685 |
| C | 1.2293086451 | 5.6792681931 | 3.213261701 |
| C | 1.6911488329 | 4.6740153531 | 4.012850145 |
| C | 1.5485767169 | 3.4750725766 | 3.25393749 |
| H | 1.8038214325 | 2.4739799521 | 3.56886707 |
| H | 2.0824711515 | 4.7720015315 | 5.0157157767 |
| H | 1.1435551137 | 6.7482953394 | 3.338518506 |
| O | 1.0709095814 | -1.1738487799 | 3.3341867712 |

| | | | |
|---|---|---|---|
| H | -0.5848183566 | -1.4247279532 | 1.5450254155 |
| H | 1.3206210621 | -0.782699949 | -0.4979695172 |
| H | -0.4121336188 | -0.9841057548 | -0.7185344988 |

RB3LYP Energy = -875.8828158 Hartrees

| Mode | Frequency ($cm^{-1}$) | Mode | Frequency ($cm^{-1}$) | Mode | Frequency ($cm^{-1}$) |
|---|---|---|---|---|---|
| 1 | 34.4591 | 30 | 767.8926 | 59 | 1341.0233 |
| 2 | 42.2935 | 31 | 783.2234 | 60 | 1370.8423 |
| 3 | 57.8297 | 32 | 804.5402 | 61 | 1374.5592 |
| 4 | 78.4421 | 33 | 837.0602 | 62 | 1414.8509 |
| 5 | 100.0385 | 34 | 853.2702 | 63 | 1430.9710 |
| 6 | 129.5715 | 35 | 891.8839 | 64 | 1440.0443 |
| 7 | 147.2945 | 36 | 896.7033 | 65 | 1467.7266 |
| 8 | 189.8897 | 37 | 903.2286 | 66 | 1498.8093 |
| 9 | 221.2790 | 38 | 922.1182 | 67 | 1511.2620 |
| 10 | 275.5682 | 39 | 936.4538 | 68 | 1521.0862 |
| 11 | 281.2314 | 40 | 964.9880 | 69 | 1523.0720 |
| 12 | 306.9969 | 41 | 965.8862 | 70 | 1538.4192 |
| 13 | 341.8182 | 42 | 994.7345 | 71 | 1616.9888 |
| 14 | 365.0940 | 43 | 1044.2901 | 72 | 1625.4384 |
| 15 | 401.3239 | 44 | 1056.6480 | 73 | 1656.1149 |
| 16 | 429.7560 | 45 | 1066.2478 | 74 | 1743.8079 |
| 17 | 441.7443 | 46 | 1086.9116 | 75 | 1778.1229 |
| 18 | 497.5274 | 47 | 1125.9707 | 76 | 3031.9569 |
| 19 | 524.5236 | 48 | 1128.7638 | 77 | 3061.8164 |
| 20 | 540.3959 | 49 | 1149.9480 | 78 | 3119.6177 |
| 21 | 573.0568 | 50 | 1178.9915 | 79 | 3142.5395 |
| 22 | 608.1923 | 51 | 1190.6448 | 80 | 3192.8177 |
| 23 | 609.1942 | 52 | 1195.3503 | 81 | 3205.7442 |

| | | | | | |
|---|---|---|---|---|---|
| 24 | 637.3852 | 53 | 1229.0642 | 82 | 3215.0622 |
| 25 | 649.1257 | 54 | 1268.4530 | 83 | 3223.6881 |
| 26 | 686.0096 | 55 | 1272.1411 | 84 | 3270.4961 |
| 27 | 726.0328 | 56 | 1280.0624 | 85 | 3288.7973 |
| 28 | 755.5553 | 57 | 1306.5109 | 86 | 3301.7333 |
| 29 | 766.4647 | 58 | 1318.3790 | 87 | 3612.4577 |

**1-(thiophene-2-carbonyl)-1,2,3,4-tetrahydro-5H-benzo[e][1,4]diazepin-5-one (*cis*-9d)**

#N B3LYP/6-31G(d) OPT Geom=Connectivity

Cmpd 9d_cis

0,1

| | | | |
|---|---|---|---|
| C | 0. | 0. | 0. |
| N | 0. | 0. | 1.4525794 |
| C | 0.9745082055 | 0. | 2.4231533562 |
| C | 2.445935802 | -0.1838173063 | 2.1252955519 |
| C | 3.1350085346 | 0.0557962374 | 0.9185812594 |
| C | 4.5257638043 | -0.1158681553 | 0.8626441516 |
| C | 5.2389886433 | -0.5187418126 | 1.9845669931 |
| C | 4.5693724791 | -0.7629756127 | 3.1855221637 |
| C | 3.1942552682 | -0.5909661876 | 3.2462258534 |
| H | 2.6515352755 | -0.7502045823 | 4.1702911142 |
| H | 5.1167052284 | -1.080255305 | 4.0684651356 |
| H | 6.315769382 | -0.6471694548 | 1.9166999754 |
| H | 5.0401600877 | 0.0802150032 | -0.0689301619 |
| N | 2.4311607604 | 0.398326341 | -0.2817472481 |
| C | 1.3094919463 | -0.4764661578 | -0.6114699974 |
| H | 1.5489339243 | -1.4792927242 | -0.2448902304 |
| H | 1.2085060269 | -0.5475823452 | -1.6953191727 |
| C | 2.8831806547 | 1.4527260316 | -1.0668912258 |
| O | 3.8690485467 | 2.1100592052 | -0.7399992458 |
| C | 2.2190645119 | 1.7970279346 | -2.3598993781 |
| S | 3.2296712073 | 2.7923205302 | -3.3900789702 |
| C | 1.9984995687 | 2.8928922499 | -4.5913393339 |
| C | 0.8583434604 | 2.2293194319 | -4.2204521621 |
| C | 0.9835671723 | 1.606143404 | -2.9482164589 |
| H | 0.1610264219 | 1.070974301 | -2.4945935555 |
| H | -0.0412974964 | 2.1848134406 | -4.8246168194 |
| H | 2.1755239535 | 3.4435601557 | - 5.50623737 |
| O | 0.6100306699 | 0.1044405322 | 3.5937551928 |
| H | -0.9028075959 | 0.1557059428 | 1.886238262 |
| H | -0.8068441278 | -0.6637235762 | -0.34092836 |
| H | -0.2274518649 | 1.0084677261 | -0.3740155384 |

RB3LYP Energy = -1198.8536804 Hartrees

| Mode | Frequency ($cm^{-1}$) | Mode | Frequency ($cm^{-1}$) | Mode | Frequency ($cm^{-1}$) |
|---|---|---|---|---|---|
| 1 | 28.3862 | 30 | 728.1891 | 59 | 1350.3781 |
| 2 | 44.8946 | 31 | 738.4462 | 60 | 1371.8501 |
| 3 | 58.5164 | 32 | 755.8778 | 61 | 1396.5895 |
| 4 | 75.7164 | 33 | 778.9957 | 62 | 1401.4866 |
| 5 | 107.2902 | 34 | 795.1599 | 63 | 1433.9445 |
| 6 | 120.4940 | 35 | 821.5644 | 64 | 1434.9589 |
| 7 | 140.5657 | 36 | 852.9536 | 65 | 1476.1061 |
| 8 | 178.7813 | 37 | 873.4418 | 66 | 1491.4862 |
| 9 | 210.8588 | 38 | 893.2623 | 67 | 1514.8652 |
| 10 | 225.2131 | 39 | 916.4971 | 68 | 1528.3779 |
| 11 | 295.3455 | 40 | 928.3017 | 69 | 1533.0604 |
| 12 | 322.8875 | 41 | 960.0346 | 70 | 1547.9076 |
| 13 | 346.2027 | 42 | 974.1124 | 71 | 1580.8327 |
| 14 | 375.7730 | 43 | 997.7207 | 72 | 1627.6104 |
| 15 | 407.0219 | 44 | 1030.6098 | 73 | 1657.0533 |
| 16 | 426.8869 | 45 | 1060.8847 | 74 | 1710.0039 |
| 17 | 443.6178 | 46 | 1084.0262 | 75 | 1743.6694 |
| 18 | 477.5125 | 47 | 1100.3826 | 76 | 3021.0124 |
| 19 | 541.3666 | 48 | 1117.7010 | 77 | 3051.4847 |
| 20 | 549.4561 | 49 | 1129.2936 | 78 | 3093.4264 |
| 21 | 561.6423 | 50 | 1138.4113 | 79 | 3151.0257 |
| 22 | 577.4818 | 51 | 1179.6464 | 80 | 3193.1670 |
| 23 | 603.9690 | 52 | 1198.1212 | 81 | 3209.3442 |
| 24 | 617.5311 | 53 | 1199.2279 | 82 | 3224.7988 |
| 25 | 645.7462 | 54 | 1251.0973 | 83 | 3242.6168 |
| 26 | 674.2759 | 55 | 1269.2274 | 84 | 3251.1795 |

| | | | | | |
|---|---|---|---|---|---|
| 27 | 694.1511 | 56 | 1285.1016 | 85 | 3264.4724 |
| 28 | 712.0023 | 57 | 1302.8358 | 86 | 3268.2287 |
| 29 | 723.4813 | 58 | 1319.9315 | 87 | 3582.0447 |

**1-(thiophene-2-carbonyl)-1,2,3,4-tetrahydro-5H-benzo[e][1,4]diazepin-5-one (*trans*-9d)**

#N B3LYP/6-31G(d) OPT Geom=Connectivity

Cmpd 9d_trans

0,1

| | | | |
|---|---|---|---|
| C | 0. | 0. | 0. |
| N | 0. | 0. | 1.4591837 |
| C | 0.9567936674 | 0. | 2.4433686483 |
| C | 2.4431835984 | -0.0309525473 | 2.1591009948 |
| C | 3.0969614072 | 0.3432393026 | 0.9678779075 |
| C | 4.4969122391 | 0.3008075548 | 0.8912546682 |
| C | 5.2569071049 | -0.0803945002 | 1.9908555894 |
| C | 4.6214279761 | -0.4466161511 | 3.1804451264 |
| C | 3.2345497235 | -0.4188667192 | 3.2551985923 |
| H | 2.7173983792 | -0.6816736379 | 4.1706320487 |
| H | 5.2051350465 | -0.7545561184 | 4.0430646419 |
| H | 6.340298915 | -0.1069862275 | 1.9130715695 |
| H | 4.9761761088 | 0.5675209177 | -0.0449489169 |
| N | 2.3510955713 | 0.6827533137 | -0.1920032086 |
| C | 1.3536607051 | -0.3015783892 | -0.6180721401 |
| H | 1.7069003972 | -1.2961946242 | -0.3316695707 |
| H | 1.2702375026 | -0.2506771799 | -1.7046458766 |
| C | 2.5154469657 | 1.8081583758 | -0.9912441913 |
| O | 2.001016233 | 1.8599936915 | -2.1083974612 |
| C | 3.2661153046 | 2.9753099071 | -0.4721352429 |
| C | 3.5487168192 | 3.420797863 | 0.8015792273 |
| C | 4.1940654541 | 4.6871197448 | 0.8180891353 |
| C | 4.3933388129 | 5.1911436138 | -0.4419932691 |
| S | 3.7747565578 | 4.1465462049 | -1.668039973 |
| H | 4.8677557991 | 6.1249191564 | -0.7148146453 |
| H | 4.4951146457 | 5.1978752247 | 1.726176727 |
| H | 3.2958609292 | 2.8706301951 | 1.6989790353 |
| O | 0.5812708976 | 0.0010594313 | 3.6165812545 |
| H | -0.9171113359 | 0.04372514 | 1.8889928168 |
| H | -0.7225646167 | -0.7528876714 | -0.3428510223 |
| H | -0.3422325941 | 0.974575462 | -0.373873122 |

RB3LYP Energy = -1198.8629252 Hartrees

| Mode | Frequency ($cm^{-1}$) | Mode | Frequency ($cm^{-1}$) | Mode | Frequency ($cm^{-1}$) |
|---|---|---|---|---|---|

| | | | | | |
|---|---|---|---|---|---|
| 1 | 33.3394 | 30 | 745.2886 | 59 | 1344.0664 |
| 2 | 43.4250 | 31 | 749.8557 | 60 | 1373.3388 |
| 3 | 54.2643 | 32 | 755.3647 | 61 | 1398.6096 |
| 4 | 74.4784 | 33 | 782.4295 | 62 | 1402.5372 |
| 5 | 78.8489 | 34 | 798.5996 | 63 | 1424.8354 |
| 6 | 122.0803 | 35 | 834.7533 | 64 | 1432.6222 |
| 7 | 145.9214 | 36 | 862.8945 | 65 | 1475.3746 |
| 8 | 177.9094 | 37 | 875.9583 | 66 | 1492.8965 |
| 9 | 192.7673 | 38 | 897.1502 | 67 | 1504.2415 |
| 10 | 247.4882 | 39 | 925.9133 | 68 | 1514.4203 |
| 11 | 285.4730 | 40 | 931.2777 | 69 | 1529.9076 |
| 12 | 321.2631 | 41 | 950.8634 | 70 | 1549.9412 |
| 13 | 338.6492 | 42 | 976.8134 | 71 | 1582.1816 |
| 14 | 380.7797 | 43 | 1001.7822 | 72 | 1624.3182 |
| 15 | 403.4290 | 44 | 1034.1898 | 73 | 1655.6321 |
| 16 | 435.5865 | 45 | 1057.2091 | 74 | 1713.0964 |
| 17 | 448.6600 | 46 | 1075.2197 | 75 | 1739.9117 |
| 18 | 455.3209 | 47 | 1092.5949 | 76 | 3032.8190 |
| 19 | 505.9972 | 48 | 1117.3695 | 77 | 3062.7461 |
| 20 | 548.5887 | 49 | 1130.2810 | 78 | 3097.3727 |
| 21 | 568.7090 | 50 | 1131.6963 | 79 | 3161.3122 |
| 22 | 578.9255 | 51 | 1165.9155 | 80 | 3193.6703 |
| 23 | 593.9092 | 52 | 1190.5269 | 81 | 3208.6435 |
| 24 | 625.4610 | 53 | 1196.6576 | 82 | 3220.5404 |
| 25 | 654.7150 | 54 | 1254.3150 | 83 | 3227.0186 |
| 26 | 670.5271 | 55 | 1271.7916 | 84 | 3241.7231 |
| 27 | 688.7764 | 56 | 1288.9032 | 85 | 3255.1143 |
| 28 | 721.8646 | 57 | 1296.6485 | 86 | 3266.2058 |

| | | | | | |
|---|---|---|---|---|---|
| 29 | 726.5035 | 58 | 1337.9908 | 87 | 3580.3016 |

**1-benzoyl-1,2,3,4-tetrahydro-5H-benzo[e][1,4]diazepin-5-one (*cis*-9e)**

#N B3LYP/6-31G(d) OPT Geom=Connectivity

Cmpd 9e_cis

0,1

| | | | |
|---|---|---|---|
| C | -0.0008783316 | -0.0001371264 | 0.0013465585 |
| N | -0.0003630952 | -0.0010336309 | 1.4534675441 |
| C | 0.9714659978 | -0.001262949 | 2.4243957382 |
| C | 2.4542756446 | -0.0112883652 | 2.1224949293 |
| C | 3.1090575169 | 0.2847896781 | 0.9096453734 |
| C | 4.5101161406 | 0.3238428679 | 0.8636822184 |
| C | 5.2720503622 | 0.0624736351 | 1.9941191666 |
| C | 4.6371923737 | -0.2575048068 | 3.1969426162 |
| C | 3.2515453688 | -0.2865845024 | 3.2507125779 |
| H | 2.7332944496 | -0.502243045 | 4.1773709387 |
| H | 5.2196937702 | -0.474606738 | 4.0876487382 |
| H | 6.3562923211 | 0.0976481507 | 1.9329544036 |
| H | 4.9906289211 | 0.5632465801 | -0.0784990771 |
| N | 2.4097135784 | 0.4955678861 | -0.3189962701 |
| C | 1.3185875406 | -0.4327907779 | -0.6182676561 |
| H | 1.6087866269 | -1.4234632162 | -0.2550661713 |
| H | 1.1791145605 | -0.5009007422 | -1.6967075926 |
| C | 2.6013635943 | 1.6941749686 | -1.0075494115 |
| O | 3.2246920304 | 2.6281338718 | -0.523886079 |
| C | 2.041937881 | 1.809390558 | -2.4019315856 |
| C | 2.3223927916 | 0.8698356607 | -3.4042582543 |
| C | 1.8791835316 | 1.0806509652 | -4.7103000609 |
| C | 1.142477545 | 2.2246992025 | -5.0233241666 |
| C | 0.8697073953 | 3.1694427151 | -4.0311262234 |
| C | 1.3310071408 | 2.9711493818 | -2.7307900039 |
| H | 1.1565690379 | 3.7169343672 | -1.9612076447 |
| H | 0.3080367263 | 4.0674045572 | -4.2735316837 |
| H | 0.7913991284 | 2.3845554018 | -6.0391403017 |
| H | 2.1137520776 | 0.3541119664 | -5.4835182623 |
| H | 2.9101800344 | -0.0137165794 | -3.1681852478 |
| O | 0.6008390255 | -0.0081383884 | 3.5985709933 |
| H | -0.9125220719 | 0.0426287833 | 1.8925946721 |
| H | -0.7854992052 | -0.6906195513 | -0.3368428503 |
| H | -0.2596499078 | 0.9959846609 | -0.3876506308 |

RB3LYP Energy = -878.1004128 Hartrees

| Mode | Frequency ($cm^{-1}$) | Mode | Frequency ($cm^{-1}$) | Mode | Frequency ($cm^{-1}$) |
|---|---|---|---|---|---|
| 1 | 24.3013 | 33 | 777.6468 | 65 | 1364.8286 |

| | | | | | |
|---|---|---|---|---|---|
| 2 | 45.3355 | 34 | 794.9869 | 66 | 1373.4096 |
| 3 | 47.8458 | 35 | 800.4714 | 67 | 1401.9915 |
| 4 | 68.2153 | 36 | 851.4837 | 68 | 1426.0219 |
| 5 | 83.6392 | 37 | 867.8740 | 69 | 1438.0721 |
| 6 | 102.1049 | 38 | 892.9894 | 70 | 1490.1955 |
| 7 | 143.5319 | 39 | 928.5058 | 71 | 1491.0850 |
| 8 | 160.1816 | 40 | 942.8601 | 72 | 1509.0423 |
| 9 | 194.5296 | 41 | 970.8046 | 73 | 1516.5892 |
| 10 | 240.8632 | 42 | 973.4522 | 74 | 1530.8422 |
| 11 | 289.4393 | 43 | 977.1484 | 75 | 1540.7317 |
| 12 | 320.1094 | 44 | 998.9695 | 76 | 1548.9501 |
| 13 | 346.0173 | 45 | 1001.6059 | 77 | 1626.3827 |
| 14 | 354.8756 | 46 | 1018.4220 | 78 | 1637.2283 |
| 15 | 384.6740 | 47 | 1052.0589 | 79 | 1658.7649 |
| 16 | 412.8440 | 48 | 1060.0858 | 80 | 1660.1115 |
| 17 | 418.1621 | 49 | 1075.8914 | 81 | 1739.4984 |
| 18 | 439.4941 | 50 | 1087.2721 | 82 | 1755.8200 |
| 19 | 499.6215 | 51 | 1112.6212 | 83 | 3016.9476 |
| 20 | 537.2872 | 52 | 1130.8686 | 84 | 3053.7488 |
| 21 | 554.7236 | 53 | 1137.0894 | 85 | 3095.3176 |
| 22 | 577.2699 | 54 | 1187.4774 | 86 | 3165.9864 |
| 23 | 607.7682 | 55 | 1194.7375 | 87 | 3183.5137 |
| 24 | 612.6599 | 56 | 1196.9426 | 88 | 3191.3104 |
| 25 | 631.8733 | 57 | 1202.8957 | 89 | 3192.5109 |
| 26 | 643.1876 | 58 | 1212.3031 | 90 | 3200.6488 |
| 27 | 666.0096 | 59 | 1257.4687 | 91 | 3208.3401 |
| 28 | 689.2245 | 60 | 1271.3422 | 92 | 3210.3327 |
| 29 | 712.9304 | 61 | 1302.6945 | 93 | 3218.1458 |

| | | | | | |
|---|---|---|---|---|---|
| 30 | 718.4473 | 62 | 1316.4233 | 94 | 3225.9841 |
| 31 | 728.9532 | 63 | 1343.6318 | 95 | 3243.4520 |
| 32 | 742.6830 | 64 | 1349.4237 | 96 | 3585.7590 |

**1-benzoyl-1,2,3,4-tetrahydro-5H-benzo[e][1,4]diazepin-5-one (*trans*-9e)**

#N B3LYP/6-31G(d) OPT Geom=Connectivity

Cmpd 9d_trans

0,1

| | | | |
|---|---|---|---|
| C | -0.2647682267 | 0.0605211946 | -0.2770128511 |
| N | -0.2788650906 | -0.6045141659 | 1.0208013974 |
| C | 0.6214991385 | -0.7835777063 | 2.0416808157 |
| C | 1.999403229 | -0.1569866665 | 2.0578097267 |
| C | 2.4525273128 | 0.9460019117 | 1.3038945812 |
| C | 3.7481741441 | 1.4452422596 | 1.5031014676 |
| C | 4.5901252554 | 0.8802874151 | 2.454039479 |
| C | 4.1541163553 | -0.2133078922 | 3.2057483464 |
| C | 2.8753345131 | -0.7169886165 | 3.0045231519 |
| H | 2.5039999703 | -1.5507425235 | 3.5888536397 |
| H | 4.8074243661 | -0.6695998617 | 3.9437179618 |
| H | 5.5897424925 | 1.2826576411 | 2.5933866943 |
| H | 4.0863573679 | 2.2786789749 | 0.8966381553 |
| N | 1.6407040119 | 1.5060336282 | 0.281857864 |
| C | 1.1065803285 | 0.5556153835 | -0.6968916498 |
| H | 1.8121070521 | -0.2744299203 | -0.7961481454 |
| H | 1.0243202541 | 1.0712044552 | -1.6549274857 |
| C | 1.4300678459 | 2.8603719457 | 0.0397062114 |
| O | 0.9686506679 | 3.2358429748 | -1.0347642359 |
| C | 1.7139993437 | 3.8582468381 | 1.1257926296 |
| C | 1.4397657999 | 3.6218651752 | 2.480212967 |
| C | 1.6272736147 | 4.6349866139 | 3.420018336 |
| C | 2.101953499 | 5.8854878139 | 3.0198894368 |
| C | 2.3683223362 | 6.129420203 | 1.670348638 |
| C | 2.1596724371 | 5.1265029695 | 0.7265438963 |
| H | 2.3288886977 | 5.3116294352 | -0.3293277278 |
| H | 2.7275095064 | 7.1044367652 | 1.3525202669 |
| H | 2.2552954365 | 6.6701357155 | 3.7560181608 |
| H | 1.4008302309 | 4.4459508545 | 4.4656738886 |
| H | 1.0665553318 | 2.6554825888 | 2.8020841555 |
| O | 0.283918778 | -1.4926470318 | 2.9909819978 |
| H | -1.1376585827 | -1.093630883 | 1.2461606179 |
| H | -0.6333441583 | -0.6463857919 | -1.0330318239 |
| H | -0.9550819054 | 0.9149464992 | -0.2658603334 |

RB3LYP Energy = -878.1075043 Hartrees

| Mode | Frequency ($cm^{-1}$) | Mode | Frequency ($cm^{-1}$) | Mode | Frequency ($cm^{-1}$) |
|---|---|---|---|---|---|
| 1 | 39.5228 | 33 | 780.7200 | 65 | 1367.3651 |
| 2 | 42.1262 | 34 | 797.9701 | 66 | 1371.7616 |
| 3 | 49.4470 | 35 | 804.7610 | 67 | 1398.9366 |
| 4 | 69.8798 | 36 | 864.6416 | 68 | 1423.0812 |
| 5 | 73.4457 | 37 | 877.2317 | 69 | 1431.5378 |
| 6 | 106.5101 | 38 | 895.2280 | 70 | 1493.0965 |
| 7 | 141.0064 | 39 | 929.4573 | 71 | 1493.5031 |
| 8 | 169.7777 | 40 | 946.1686 | 72 | 1504.9038 |
| 9 | 208.2268 | 41 | 969.2994 | 73 | 1514.8654 |
| 10 | 249.4658 | 42 | 974.8659 | 74 | 1529.4925 |
| 11 | 298.6411 | 43 | 977.1319 | 75 | 1542.2134 |
| 12 | 316.3597 | 44 | 999.9897 | 76 | 1549.3543 |
| 13 | 336.7924 | 45 | 1002.2624 | 77 | 1624.9005 |
| 14 | 379.7175 | 46 | 1018.8785 | 78 | 1638.4295 |
| 15 | 397.5226 | 47 | 1044.2998 | 79 | 1655.8250 |
| 16 | 416.7704 | 48 | 1055.8140 | 80 | 1660.3278 |
| 17 | 430.9694 | 49 | 1067.6190 | 81 | 1732.8579 |
| 18 | 439.0245 | 50 | 1089.2311 | 82 | 1739.4293 |
| 19 | 456.2331 | 51 | 1116.0607 | 83 | 3030.4386 |
| 20 | 533.9552 | 52 | 1131.0414 | 84 | 3059.7016 |
| 21 | 550.4738 | 53 | 1131.9662 | 85 | 3094.3602 |
| 22 | 573.9903 | 54 | 1181.8123 | 86 | 3158.5940 |
| 23 | 601.1509 | 55 | 1191.2357 | 87 | 3186.4762 |
| 24 | 624.4968 | 56 | 1194.7577 | 88 | 3193.2366 |
| 25 | 632.3534 | 57 | 1197.0264 | 89 | 3197.7553 |
| 26 | 659.4936 | 58 | 1214.4915 | 90 | 3208.0370 |
| 27 | 669.8761 | 59 | 1253.7289 | 91 | 3208.5492 |

| | | | | | |
|---|---|---|---|---|---|
| 28 | 690.7172 | 60 | 1286.9748 | 92 | 3221.0476 |
| 29 | 709.1288 | 61 | 1295.5494 | 93 | 3221.6993 |
| 30 | 720.5697 | 62 | 1338.9491 | 94 | 3223.5111 |
| 31 | 730.3965 | 63 | 1343.5769 | 95 | 3240.2841 |
| 32 | 758.7515 | 64 | 1346.5295 | 96 | 3581.1079 |

**1-benzyl-1,2,3,4-tetrahydro-5H-benzo[e][1,4]diazepin-5-one (9f)**

#N B3LYP/6-31G(d) OPT Geom=Connectivity

Cmpd 9f

0,1

| | | | |
|---|---|---|---|
| C | 0.1410395811 | 0.3484782993 | -0.1782794334 |
| N | -0.0446184064 | -0.2836154626 | 1.1125501341 |
| C | 0.820702186 | -0.6269239677 | 2.1253967814 |
| C | 2.2657779687 | -0.1810337867 | 2.1778555564 |
| C | 3.0064541062 | 0.6097242462 | 1.2541793255 |
| C | 4.3078707931 | 1.0279969082 | 1.6206606279 |
| C | 4.8794930778 | 0.6693825683 | 2.8308205897 |
| C | 4.1773475437 | -0.1492408373 | 3.7200158546 |
| C | 2.8989411111 | -0.5599115537 | 3.3808025366 |
| H | 2.3143930329 | -1.1707626935 | 4.0582254526 |
| H | 4.6187952415 | -0.4535854628 | 4.6642784184 |
| H | 5.8856580594 | 1.0074097155 | 3.0660942105 |
| H | 4.8909032223 | 1.6045330718 | 0.9098806749 |
| N | 2.5380347815 | 0.9709909485 | -0.0091033306 |
| C | 1.5600246124 | 0.1580062381 | -0.7016787708 |
| H | 1.8345568211 | -0.9013841922 | -0.6203071742 |
| H | 1.5969272441 | 0.4221764516 | -1.7635050441 |
| C | 2.8731012459 | 2.2504708127 | -0.6167615737 |
| C | 3.8117317656 | 2.184061873 | -1.8170320927 |
| C | 3.8358365622 | 3.2457854361 | -2.7312255935 |
| C | 4.7122291583 | 3.2341252607 | -3.815577869 |
| C | 5.573670237 | 2.1510830741 | -4.0074684407 |
| C | 5.5498901625 | 1.0850905962 | -3.1080177648 |
| C | 4.6745404682 | 1.1018037196 | -2.019442352 |
| H | 4.654328657 | 0.2688237891 | -1.3225987783 |
| H | 6.2127997581 | 0.2358401453 | -3.2520476761 |
| H | 6.2537014752 | 2.1374227451 | -4.8549300638 |
| H | 4.7178789874 | 4.0661362059 | -4.5149549529 |
| H | 3.161724515 | 4.0891818929 | -2.5918175612 |
| H | 1.9426027547 | 2.7519433233 | -0.9269472903 |
| H | 3.3034618893 | 2.8921983628 | 0.1591602005 |
| O | 0.3557972856 | -1.2935752248 | 3.0531833285 |
| H | -0.9673520836 | -0.6469396981 | 1.3161930034 |

| | | | |
|---|---|---|---|
| H | -0.5710272527 | -0.1109067861 | -0.8757470854 |
| H | -0.0905612084 | 1.4245897724 | -0.1432433665 |

RB3LYP Energy = -804.0681465 Hartress

| Mode | Frequency ($cm^{-1}$) | Mode | Frequency ($cm^{-1}$) | Mode | Frequency ($cm^{-1}$) |
|---|---|---|---|---|---|
| 1 | 17.2747 | 34 | 814.9756 | 67 | 1402.8814 |
| 2 | 32.3112 | 35 | 864.4889 | 68 | 1420.0447 |
| 3 | 41.7710 | 36 | 877.6980 | 69 | 1431.2505 |
| 4 | 55.8399 | 37 | 888.6923 | 70 | 1444.2964 |
| 5 | 87.2538 | 38 | 922.0178 | 71 | 1492.2339 |
| 6 | 130.9927 | 39 | 960.2101 | 72 | 1499.3923 |
| 7 | 170.3865 | 40 | 971.3396 | 73 | 1501.4268 |
| 8 | 182.9238 | 41 | 975.8978 | 74 | 1504.8492 |
| 9 | 226.6481 | 42 | 995.5119 | 75 | 1519.7422 |
| 10 | 245.3777 | 43 | 998.9706 | 76 | 1540.5953 |
| 11 | 332.8318 | 44 | 1009.5123 | 77 | 1543.6880 |
| 12 | 345.0747 | 45 | 1017.7308 | 78 | 1546.2848 |
| 13 | 356.2626 | 46 | 1051.2950 | 79 | 1615.9701 |
| 14 | 395.6543 | 47 | 1058.9925 | 80 | 1645.2568 |
| 15 | 418.0784 | 48 | 1067.1180 | 81 | 1659.2103 |
| 16 | 440.2809 | 49 | 1089.9895 | 82 | 1664.8125 |
| 17 | 446.2130 | 50 | 1111.0884 | 83 | 1731.5287 |
| 18 | 473.2611 | 51 | 1119.3857 | 84 | 2998.3676 |
| 19 | 540.1858 | 52 | 1132.4227 | 85 | 3004.4560 |
| 20 | 543.2335 | 53 | 1187.7899 | 86 | 3050.4357 |
| 21 | 573.3276 | 54 | 1192.8189 | 87 | 3065.6100 |
| 22 | 577.2967 | 55 | 1196.5549 | 88 | 3090.3709 |
| 23 | 587.4061 | 56 | 1205.3648 | 89 | 3108.3074 |
| 24 | 626.1706 | 57 | 1210.3505 | 90 | 3168.6561 |

| | | | | | |
|---|---|---|---|---|---|
| 25 | 635.3229 | 58 | 1223.1545 | 91 | 3184.0819 |
| 26 | 667.0073 | 59 | 1258.5170 | 92 | 3185.0378 |
| 27 | 688.6770 | 60 | 1280.0514 | 93 | 3193.9219 |
| 28 | 712.5536 | 61 | 1293.0341 | 94 | 3204.2489 |
| 29 | 715.5951 | 62 | 1328.2591 | 95 | 3205.6870 |
| 30 | 746.8242 | 63 | 1339.6374 | 96 | 3211.6473 |
| 31 | 767.6951 | 64 | 1355.7835 | 97 | 3213.9178 |
| 32 | 792.6716 | 65 | 1361.3332 | 98 | 3242.0095 |
| 33 | 794.1407 | 66 | 1366.1047 | 99 | 3596.3123 |

**1-(methylsulfonyl)-1,2,3,4-tetrahydro-5H-benzo[e][1,4]diazepin-5-one (9g)**

#N B3LYP/6-31G(d) OPT Geom=Connectivity

Cmpd 9g

0,1

| | | | |
|---|---|---|---|
| C | 0. | 0. | 0. |
| N | 0. | 0. | 1.4578036 |
| C | 1.1429319248 | 0. | 2.220281943 |
| C | 2.4204492962 | -0.3786740617 | 1.5197317085 |
| C | 2.4997766314 | -1.3724639593 | 0.5190726687 |
| C | 3.7410347533 | -1.6916308817 | -0.0433287797 |
| C | 4.8950169602 | -1.033358426 | 0.3784795819 |
| C | 4.8213157975 | -0.0527465092 | 1.370241976 |
| C | 3.5913169636 | 0.2632937159 | 1.9410739187 |
| H | 3.5136248169 | 1.0021151308 | 2.7321809389 |
| H | 5.7205715932 | 0.4574897277 | 1.703297822 |
| H | 5.8522699085 | -1.2914360364 | -0.0655858149 |
| H | 3.7856136024 | -2.4743668971 | -0.7915457115 |
| N | 1.3315286699 | -2.0922719609 | 0.1057223372 |
| C | 0.2274984254 | -1.4024029655 | -0.5771825472 |
| H | -0.6654637173 | -2.0187959451 | -0.4659452792 |
| H | 0.4411882349 | -1.3198538475 | -1.6520565308 |
| S | 1.120006326 | -3.6858641057 | 0.6419069034 |
| O | 2.404321415 | -4.3761278856 | 0.5243248345 |
| O | -0.0796655254 | -4.1862913916 | -0.0345731455 |
| C | 0.7490453708 | -3.5462752669 | 2.40438189 |
| H | 0.6385934012 | -4.5633871851 | 2.7873171113 |
| H | 1.5758828567 | -3.0410985884 | 2.9066764846 |
| H | -0.1790173275 | -2.9858674922 | 2.5251715817 |
| O | 1.1250040541 | 0.2947662796 | 3.410198749 |
| H | -0.8136008913 | 0.3471508015 | 1.9502425306 |
| H | -0.9668260598 | 0.3765166861 | -0.3467371642 |

H 0.7650181636 0.6906081721 -0.3747933559

RB3LYP Energy = -1121.5970247 Hartrees

| Mode | Frequency ($cm^{-1}$) | Mode | Frequency ($cm^{-1}$) | Mode | Frequency ($cm^{-1}$) |
|---|---|---|---|---|---|
| 1 | 32.0061 | 27 | 738.1207 | 53 | 1370.7035 |
| 2 | 53.4197 | 28 | 761.0907 | 54 | 1377.7272 |
| 3 | 87.0448 | 29 | 782.5849 | 55 | 1410.4994 |
| 4 | 92.2494 | 30 | 805.0326 | 56 | 1428.0562 |
| 5 | 132.4390 | 31 | 888.5692 | 57 | 1464.1163 |
| 6 | 188.3157 | 32 | 911.3906 | 58 | 1482.9451 |
| 7 | 215.8361 | 33 | 924.7388 | 59 | 1487.4197 |
| 8 | 231.3558 | 34 | 932.7928 | 60 | 1498.0298 |
| 9 | 263.9012 | 35 | 971.6443 | 61 | 1519.7628 |
| 10 | 283.5305 | 36 | 993.0743 | 62 | 1526.4862 |
| 11 | 295.4537 | 37 | 998.7803 | 63 | 1538.5771 |
| 12 | 304.5283 | 38 | 999.7723 | 64 | 1624.1589 |
| 13 | 343.1562 | 39 | 1047.1020 | 65 | 1654.1136 |
| 14 | 360.0993 | 40 | 1067.0296 | 66 | 1774.2547 |
| 15 | 394.2265 | 41 | 1119.9440 | 67 | 3037.7460 |
| 16 | 420.4699 | 42 | 1126.2664 | 68 | 3060.6915 |
| 17 | 455.3823 | 43 | 1132.0855 | 69 | 3089.1611 |
| 18 | 483.9570 | 44 | 1161.8433 | 70 | 3118.0693 |
| 19 | 531.6276 | 45 | 1177.6618 | 71 | 3153.8833 |
| 20 | 535.9933 | 46 | 1196.4065 | 72 | 3187.1204 |
| 21 | 540.6973 | 47 | 1262.6032 | 73 | 3195.1218 |
| 22 | 572.6709 | 48 | 1292.0905 | 74 | 3197.5205 |
| 23 | 592.3458 | 49 | 1299.2252 | 75 | 3209.7294 |
| 24 | 643.6938 | 50 | 1315.1916 | 76 | 3224.7420 |
| 25 | 678.2786 | 51 | 1343.6367 | 77 | 3239.7436 |

| | | | | | |
|---|---|---|---|---|---|
| 26 | 726.7131 | 52 | 1344.6869 | 78 | 3602.4647 |

**1-(vinylsulfonyl)-1,2,3,4-tetrahydro-5H-benzo[e][1,4]diazepin-5-one (9h)**

#N Geom=AllCheck Guess=TCheck SCRF=Check GenChk RB3LYP/6-31G(d)Freq

Cmpd 9h

0,1

| | | | |
|---|---|---|---|
| C | 0.0004057953 | -0.0620612424 | 0.1922146283 |
| N | 0.1055048849 | -0.2706996557 | 1.6300320882 |
| C | 1.2949837349 | -0.2970572004 | 2.3152518198 |
| C | 2.5410745509 | -0.4083111149 | 1.4805057307 |
| C | 2.6375800602 | -1.2045854064 | 0.3167188846 |
| C | 3.8425700471 | -1.2355680053 | -0.3969562341 |
| C | 4.9449401097 | -0.5081736612 | 0.0515592643 |
| C | 4.8588604319 | 0.262671839 | 1.2114805561 |
| C | 3.6608704933 | 0.3065141411 | 1.9197090461 |
| H | 3.5699705523 | 0.8862972664 | 2.8326455106 |
| H | 5.7192609361 | 0.8248324361 | 1.5629299366 |
| H | 5.8729236315 | -0.5467402881 | -0.5121497625 |
| H | 3.9122132409 | -1.8515532599 | -1.2845348872 |
| N | 1.5098339555 | -1.9924210224 | -0.0935690718 |
| C | 0.2916733869 | -1.3364139413 | -0.6057289878 |
| H | -0.5283580193 | -2.047704128 | -0.5082850253 |
| H | 0.3948270853 | -1.0786789483 | -1.6697176731 |
| S | 1.6756459382 | -3.6618893044 | -0.3426674421 |
| O | 2.8869089856 | -3.9629033058 | -1.1132523807 |
| O | 0.3708997197 | -4.1117434609 | -0.8373241465 |
| C | 1.9780045282 | -4.3349357419 | 1.2874627302 |
| C | 1.4502365496 | -3.8491354332 | 2.4059404376 |
| H | 1.6544560428 | -4.3224059214 | 3.3623318027 |
| H | 0.8110533416 | -2.9728016337 | 2.4135762659 |
| H | 2.6236740428 | -5.2070605629 | 1.2408083992 |
| O | 1.3371662017 | -0.2181535573 | 3.5383237289 |
| H | -0.70364967 | -0.1087090835 | 2.2160866561 |
| H | -1.0167937583 | 0.2683092401 | -0.0370166971 |
| H | 0.6762728576 | 0.7431624779 | -0.1191056949 |

RB3LYP Energy = -1159.6661383 Hartrees

| Mode | Frequency ($cm^{-1}$) | Mode | Frequency ($cm^{-1}$) | Mode | Frequency ($cm^{-1}$) |
|---|---|---|---|---|---|
| 1 | 20.6557 | 28 | 726.1173 | 55 | 1328.8393 |
| 2 | 52.0080 | 29 | 735.3614 | 56 | 1342.9054 |
| 3 | 69.2190 | 30 | 764.8958 | 57 | 1370.2112 |
| 4 | 94.0159 | 31 | 782.0423 | 58 | 1412.2102 |

| | | | | | |
|---|---|---|---|---|---|
| 5 | 109.2887 | 32 | 806.1178 | 59 | 1429.5196 |
| 6 | 140.9105 | 33 | 891.7851 | 60 | 1438.9742 |
| 7 | 166.6541 | 34 | 912.4974 | 61 | 1465.1327 |
| 8 | 193.6870 | 35 | 935.9054 | 62 | 1497.2907 |
| 9 | 246.0961 | 36 | 938.4489 | 63 | 1521.3801 |
| 10 | 274.9262 | 37 | 974.3709 | 64 | 1524.4183 |
| 11 | 278.6540 | 38 | 978.7439 | 65 | 1540.6011 |
| 12 | 303.7734 | 39 | 998.7260 | 66 | 1625.8598 |
| 13 | 325.2249 | 40 | 1009.0839 | 67 | 1653.4247 |
| 14 | 344.2786 | 41 | 1038.6926 | 68 | 1695.4399 |
| 15 | 386.0321 | 42 | 1046.5994 | 69 | 1773.3816 |
| 16 | 393.5639 | 43 | 1069.7264 | 70 | 3031.3269 |
| 17 | 422.7733 | 44 | 1115.1031 | 71 | 3063.3775 |
| 18 | 456.1547 | 45 | 1119.4901 | 72 | 3120.6779 |
| 19 | 494.5263 | 46 | 1125.4491 | 73 | 3162.2637 |
| 20 | 528.1517 | 47 | 1157.6599 | 74 | 3183.3154 |
| 21 | 532.1110 | 48 | 1180.0243 | 75 | 3194.3564 |
| 22 | 550.1549 | 49 | 1197.9780 | 76 | 3209.2000 |
| 23 | 571.3809 | 50 | 1254.9560 | 77 | 3220.6451 |
| 24 | 586.3371 | 51 | 1287.0182 | 78 | 3223.8920 |
| 25 | 639.5988 | 52 | 1289.4601 | 79 | 3252.9562 |
| 26 | 651.3009 | 53 | 1297.9365 | 80 | 3273.9639 |
| 27 | 679.2500 | 54 | 1314.2847 | 81 | 3605.6097 |

**1-(phenylsulfonyl)-1,2,3,4-tetrahydro-5H-benzo[e][1,4]diazepin-5-one (9i)**

#N B3LYP/6-31G(d) OPT Geom=Connectivity

Cmpd 9i

0,1

| | | | |
|---|---|---|---|
| C | 1.2052118704 | -2.3573749335 | -0.2519034983 |
| N | 0.360823977 | -1.3025479603 | 0.2875891692 |
| C | 0.5602650781 | -0.0182599928 | 0.7308456384 |

| | | | |
|---|---|---|---|
| C | 1.9292641509 | 0.5960355771 | 0.9349029913 |
| C | 3.1653747432 | 0.2008576934 | 0.3759684156 |
| C | 4.3250134335 | 0.947179802 | 0.6403432464 |
| C | 4.2736898043 | 2.0841341849 | 1.4388588715 |
| C | 3.0610268909 | 2.4780923037 | 2.0079402265 |
| C | 1.9127673616 | 1.7393884049 | 1.7545570545 |
| H | 0.9558802591 | 2.0359835283, | 2.1673262888 |
| H | 3.0104520639 | 3.3557872168 | 2.6459755627 |
| H | 5.183030346 | 2.6470725867 | 1.6304168758 |
| H | 5.2590844805 | 0.6156343609 | 0.2048782492 |
| N | 3.2965426886 | -0.9805107505 | -0.4140206641 |
| C | 2.6802395071 | -2.2149307206 | 0.0809234309 |
| H | 2.8358273657 | -2.2237529035 | 1.1643890457 |
| H | 3.2206656739 | -3.0614044815 | -0.345714292 |
| S | 3.7652516132 | -0.888639003 | -2.0480007945 |
| O | 4.8939277832 | 0.0379122452 | -2.1284501585 |
| C | 2.4020294324 | -0.1291318736 | -2.9407949695 |
| C | 1.5761060129 | -0.9305972162 | -3.7322119237 |
| C | 0.515783477 | -0.338223004 | -4.4190299432 |
| C | 0.2893082077 | 1.0352937121 | -4.3091423166 |
| C | 1.1302804067 | 1.8269527659 | -3.5230868662 |
| C | 2.1990267819 | 1.2503159449 | -2.8379120346 |
| H | 2.8727865069 | 1.8600147998 | -2.2461586347 |
| H | 0.9586856737 | 2.896578683 | -3.4468050854 |
| H | -0.5393438141 | 1.4917666313 | -4.8431235558 |
| H | -0.128057331 | -0.9496459952 | -5.0448471474 |
| H | 1.7813570846 | -1.9921613176 | -3.8192830685 |
| O | 3.8768694934 | -2.2816695528 | -2.4905922387 |
| O | -0.435042457 | 0.6470720442 | 1.0199091677 |
| H | -0.6359111013 | -1.4757582107 | 0.2223788031 |
| H | 0.8539244409 | -3.3141252047 | 0.1573617531 |
| H | 1.0891596142 | -2.4151037394 | -1.3425204119 |

RB3LYP Energy = -1313.3269125 Hartrees

| Mode | Frequency ($cm^{-1}$) | Mode | Frequency ($cm^{-1}$) | Mode | Frequency ($cm^{-1}$) |
|---|---|---|---|---|---|
| 1 | 19.3261 | 34 | 723.4745 | 67 | 1336.4192 |
| 2 | 29.0129 | 35 | 735.2454 | 68 | 1345.1572 |
| 3 | 44.9417 | 36 | 765.3508 | 69 | 1351.8717 |
| 4 | 67.7595 | 37 | 777.3415 | 70 | 1365.5216 |
| 5 | 71.1621 | 38 | 800.2185 | 71 | 1386.0970 |
| 6 | 101.1275 | 39 | 860.7181 | 72 | 1416.6162 |

| | | | | | |
|---|---|---|---|---|---|
| 7 | 151.1032 | 40 | 867.0791 | 73 | 1436.7578 |
| 8 | 159.7261 | 41 | 904.9989 | 74 | 1489.1258 |
| 9 | 179.7277 | 42 | 919.3026 | 75 | 1492.1629 |
| 10 | 224.8608 | 43 | 942.8143 | 76 | 1502.8955 |
| 11 | 257.6112 | 44 | 981.4877 | 77 | 1516.6571 |
| 12 | 288.7815 | 45 | 982.6011 | 78 | 1524.9011 |
| 13 | 303.9517 | 46 | 989.1680 | 79 | 1526.3807 |
| 14 | 305.9927 | 47 | 1002.6296 | 80 | 1549.1248 |
| 15 | 334.4115 | 48 | 1007.9852 | 81 | 1622.3682 |
| 16 | 354.2435 | 49 | 1015.1698 | 82 | 1642.4245 |
| 17 | 390.9363 | 50 | 1049.5478 | 83 | 1643.7184 |
| 18 | 402.1999 | 51 | 1050.5447 | 84 | 1653.6653 |
| 19 | 414.3384 | 52 | 1074.5864 | 85 | 1739.3996 |
| 20 | 440.1142 | 53 | 1086.7832 | 86 | 3035.3030 |
| 21 | 462.5561 | 54 | 1111.7083 | 87 | 3061.8003 |
| 22 | 476.2793 | 55 | 1122.8799 | 88 | 3092.0399 |
| 23 | 531.4798 | 56 | 1127.6345 | 89 | 3156.1595 |
| 24 | 550.1641 | 57 | 1136.8803 | 90 | 3193.8125 |
| 25 | 567.8761 | 58 | 1142.0131 | 91 | 3194.2270 |
| 26 | 582.8280 | 59 | 1194.5506 | 92 | 3205.5721 |
| 27 | 598.4830 | 60 | 1196.5464 | 93 | 3209.6790 |
| 28 | 623.9416 | 61 | 1197.2911 | 94 | 3215.8198 |
| 29 | 627.0191 | 62 | 1212.7367 | 95 | 3230.4692 |
| 30 | 667.8986 | 63 | 1256.8146 | 96 | 3234.5198 |
| 31 | 673.4628 | 64 | 1286.1458 | 97 | 3242.4724 |
| 32 | 699.2901 | 65 | 1305.0013 | 98 | 3250.5438 |
| 33 | 716.2216 | 66 | 1332.0378 | 99 | 3579.1947 |

**1,2,3,4-tetrahydro-5H-pyrido[2,3-e][1,4]diazepin-5-one (21a)**

#N B3LYP/6-31G(d) OPT Geom=Connectivity
Cmpd 21a
0,1

| | | | |
|---|---|---|---|
| C | 0. | 0. | 0. |
| N | 0. | 0. | 1.4507473 |
| C | 1.037878675 | 0. | 2.3492781948 |
| C | 2.4677746453 | -0.1715335052 | 1.9121680344 |
| C | 3.0060220634 | -0.5163372076 | 0.6394525414 |
| N | 4.3388578525 | -0.608524789 | 0.4234613954 |
| C | 5.1771590426 | -0.376282997 | 1.4269688203 |
| C | 4.7643182963 | -0.0544825137 | 2.720781343 |
| C | 3.3993585895 | 0.0392673111 | 2.942528504 |
| H | 2.9975815656 | 0.2828066458 | 3.9197367939 |
| H | 5.4840106878 | 0.1157886632 | 3.514375663 |
| H | 6.2361758461 | -0.4589679867 | 1.184167784 |
| N | 2.2860626813 | -0.7685476859 | -0.5042032339 |
| C | 0.8824624348 | -1.1017310512 | -0.5847811699 |
| H | 0.6434822648 | -2.0518597897 | -0.0808503799 |
| H | 0.6463503255 | -1.218762391 | -1.6471288619 |
| H | 2.8880249455 | -1.094711229 | -1.2492596843 |
| O | 0.7725697029 | 0.1447658398 | 3.5436126879 |
| H | -0.8810122134 | 0.1671282491 | 1.9199013573 |
| H | -1.0349507314 | -0.1733161427 | -0.3114814847 |
| H | 0.3137752335 | 0.9676702156 | -0.4166664523 |

RB3LYP Energies = -549.7629368 Hartrees

| Mode | Frequency ($cm^{-1}$) | Mode | Frequency ($cm^{-1}$) | Mode | Frequency ($cm^{-1}$) |
|---|---|---|---|---|---|
| 1 | 43.2659 | 20 | 827.8101 | 39 | 1430.8254 |
| 2 | 86.9904 | 21 | 856.2945 | 40 | 1459.2115 |
| 3 | 130.7216 | 22 | 900.8917 | 41 | 1484.0839 |
| 4 | 239.2489 | 23 | 980.2513 | 42 | 1499.2683 |
| 5 | 276.1210 | 24 | 1007.8433 | 43 | 1521.1967 |
| 6 | 328.2121 | 25 | 1014.0046 | 44 | 1533.3050 |
| 7 | 373.1153 | 26 | 1065.6272 | 45 | 1570.9567 |
| 8 | 410.5039 | 27 | 1090.6820 | 46 | 1620.9263 |
| 9 | 434.8891 | 28 | 1097.0998 | 47 | 1650.8003 |
| 10 | 511.8764 | 29 | 1136.3765 | 48 | 1743.7014 |
| 11 | 527.2644 | 30 | 1162.7347 | 49 | 3004.1264 |

| | | | | | |
|---|---|---|---|---|---|
| 12 | 554.4908 | 31 | 1190.3968 | 50 | 3033.8097 |
| 13 | 572.0387 | 32 | 1247.0901 | 51 | 3100.4814 |
| 14 | 575.8184 | 33 | 1277.5725 | 52 | 3106.6085 |
| 15 | 630.5592 | 34 | 1288.2643 | 53 | 3166.2514 |
| 16 | 664.0876 | 35 | 1329.6266 | 54 | 3218.1133 |
| 17 | 695.8899 | 36 | 1355.4089 | 55 | 3238.4286 |
| 18 | 737.9894 | 37 | 1383.1163 | 56 | 3600.2330 |
| 19 | 782.2077 | 38 | 1414.7426 | 57 | 3602.8213 |

**1-acetyl-1,2,3,4-tetrahydro-5H-pyrido[2,3-e][1,4]diazepin-5-one (*cis*-21b)**

#N B3LYP/6-31G(d) OPT Geom=Connectivity

Cmpd 21b_cis

0,1

| | | | |
|---|---|---|---|
| C | -0.0925892416 | 0.0103471244 | -0.0219562266 |
| N | -0.0848952545 | -0.0501093539 | 1.4308437386 |
| C | 0.8871459968 | -0.001617192 | 2.3994406195 |
| C | 2.3645233704 | 0.0699702454 | 2.090555283 |
| C | 3.0087880806 | 0.4410841914 | 0.89188302 |
| N | 4.3366616719 | 0.5327560895 | 0.7700315184 |
| C | 5.0937970955 | 0.2786173847 | 1.8353158722 |
| C | 4.5730177457 | -0.1092934104 | 3.0711647307 |
| C | 3.1956340346 | -0.2116235941 | 3.1880304351 |
| H | 2.7186139341 | -0.4847678835 | 4.1222622948 |
| H | 5.2282307443 | -0.3200810071 | 3.910416612 |
| H | 6.1682804479 | 0.3755630225 | 1.6881366035 |
| N | 2.2773120048 | 0.6885665101 | -0.3007786801 |
| C | 1.2583351846 | -0.2926518698 | -0.6550594259 |
| H | 1.6079392967 | -1.2825732599 | -0.3441198641 |
| H | 1.1381310602 | -0.3227214722 | -1.7399069016 |
| C | 2.4874794239 | 1.8782457677 | -1.0103332549 |
| O | 3.1523884595 | 2.7892016648 | -0.5558363781 |
| C | 1.8412465116 | 1.9775709901 | -2.3871610719 |
| H | 0.7468640013 | 1.942300368 | -2.3399120384 |
| H | 2.1404643039 | 2.9365986643 | -2.8110565713 |
| H | 2.1766994004 | 1.1725849251 | -3.0512748517 |
| O | 0.5306923304 | -0.051570157 | 3.5766023889 |
| H | -0.9972536656 | -0.0700549317 | 1.87185691 |
| H | -0.8248105992 | -0.7229369014 | -0.3861258694 |
| H | -0.4312133265 | 1.0010852223 | -0.3600951033 |

RB3LYP Energy = -702.4041998 Hartrees

| Mode | Frequency ($cm^{-1}$) | Mode | Frequency ($cm^{-1}$) | Mode | Frequency ($cm^{-1}$) |
|---|---|---|---|---|---|
| 1 | 48.1843 | 25 | 775.8403 | 49 | 1428.9912 |
| 2 | 70.7914 | 26 | 799.0163 | 50 | 1435.7360 |
| 3 | 87.8557 | 27 | 839.5028 | 51 | 1471.7302 |
| 4 | 92.8155 | 28 | 897.6258 | 52 | 1494.7408 |
| 5 | 138.5682 | 29 | 921.2174 | 53 | 1496.9823 |
| 6 | 166.0717 | 30 | 979.4117 | 54 | 1513.1035 |
| 7 | 202.8469 | 31 | 984.6357 | 55 | 1520.2005 |
| 8 | 272.2963 | 32 | 1011.7181 | 56 | 1525.2057 |
| 9 | 279.0464 | 33 | 1028.8169 | 57 | 1545.9529 |
| 10 | 343.4968 | 34 | 1058.1934 | 58 | 1613.2812 |
| 11 | 358.1856 | 35 | 1061.0624 | 59 | 1643.1981 |
| 12 | 395.1730 | 36 | 1093.1084 | 60 | 1742.8044 |
| 13 | 406.2949 | 37 | 1121.6353 | 61 | 1801.9799 |
| 14 | 440.8692 | 38 | 1134.5288 | 62 | 3015.7121 |
| 15 | 517.0318 | 39 | 1192.5755 | 63 | 3054.9344 |
| 16 | 541.0908 | 40 | 1193.3390 | 64 | 3057.2763 |
| 17 | 553.3509 | 41 | 1243.2085 | 65 | 3086.1287 |
| 18 | 571.5859 | 42 | 1255.8052 | 66 | 3118.0269 |
| 19 | 599.9300 | 43 | 1297.7729 | 67 | 3141.7691 |
| 20 | 623.3431 | 44 | 1315.3069 | 68 | 3176.4432 |
| 21 | 631.0200 | 45 | 1326.2415 | 69 | 3178.4740 |
| 22 | 663.1895 | 46 | 1367.9165 | 70 | 3215.9125 |
| 23 | 678.9884 | 47 | 1396.8982 | 71 | 3242.6790 |
| 24 | 739.6972 | 48 | 1415.1356 | 72 | 3583.3635 |

**1-acetyl-1,2,3,4-tetrahydro-5H-pyrido[2,3-e][1,4]diazepin-5-one (*trans*-21b)**
#N B3LYP/6-31G(d) OPT Geom=Connectivity
Cmpd 21b_trans

0,1

| | | | |
|---|---|---|---|
| C | 0. | 0. | 0. |
| N | 0. | 0. | 1.4574771 |
| C | 0.9760740657 | 0. | 2.4169722167 |
| C | 2.4525859323 | 0.1306344895 | 2.1031040528 |
| C | 3.082320616 | 0.5523951681 | 0.9077144471 |
| N | 4.400957487 | 0.7685762408 | 0.8166244018 |
| C | 5.1629140538 | 0.56267353 | 1.8914356304 |
| C | 4.6623754653 | 0.0930289473 | 3.1044759281 |
| C | 3.2927208728 | -0.1099907329 | 3.2009096653 |
| H | 2.8255374066 | -0.4268354317 | 4.1263199706 |
| H | 5.3219520694 | -0.0895329753 | 3.9466559468 |
| H | 6.2248817953 | 0.7671938822 | 1.7656806609 |
| N | 2.3449266155 | 0.7184688593 | -0.2822065023 |
| C | 1.3574382228 | -0.3134336516 | -0.6000896941 |
| H | 1.7295755923 | -1.2782548873 | -0.2415314541 |
| H | 1.2644897017 | -0.3476151506 | -1.6861491258 |
| C | 2.5050988703 | 1.7561692774 | -1.2090374768 |
| O | 1.8631481181 | 1.7395384163 | -2.250454985 |
| C | 3.4344689824 | 2.9037422393 | -0.8723782314 |
| H | 3.1770146293 | 3.7297068298 | -1.5377269029 |
| H | 3.346660074 | 3.220309431 | 0.1707094119 |
| H | 4.4742246607 | 2.6102294987 | -1.0346755932 |
| O | 0.6369257372 | -0.0989658154 | 3.597460787 |
| H | -0.9104953944 | -0.0538516916 | 1.8994354762 |
| H | -0.7215358338 | -0.7552789689 | -0.3384025264 |
| H | -0.337780121 | 0.9711936733 | -0.3852225459 |

RB3LYP Energy = -702.4161117 Hartrees

| Mode | Frequency ($cm^{-1}$) | Mode | Frequency ($cm^{-1}$) | Mode | Frequency ($cm^{-1}$) |
|---|---|---|---|---|---|
| 1 | 46.5367 | 25 | 789.1648 | 49 | 1426.3803 |
| 2 | 72.6304 | 26 | 798.1254 | 50 | 1435.5223 |
| 3 | 78.5412 | 27 | 839.4522 | 51 | 1478.9013 |
| 4 | 98.0278 | 28 | 908.6001 | 52 | 1489.0406 |
| 5 | 146.9755 | 29 | 937.2686 | 53 | 1494.6160 |
| 6 | 153.6881 | 30 | 982.5999 | 54 | 1503.0997 |
| 7 | 181.8000 | 31 | 998.8147 | 55 | 1507.1274 |
| 8 | 275.6561 | 32 | 1012.8857 | 56 | 1513.9347 |
| 9 | 290.7314 | 33 | 1024.6845 | 57 | 1548.6609 |

| | | | | | |
|---|---|---|---|---|---|
| 10 | 346.4039 | 34 | 1062.3952 | 58 | 1613.4431 |
| 11 | 362.9165 | 35 | 1070.4603 | 59 | 1641.0793 |
| 12 | 397.2825 | 36 | 1090.7283 | 60 | 1741.3986 |
| 13 | 428.5385 | 37 | 1126.8614 | 61 | 1769.8181 |
| 14 | 440.2102 | 38 | 1136.4813 | 62 | 3037.7352 |
| 15 | 468.4815 | 39 | 1159.0990 | 63 | 3067.5780 |
| 16 | 553.9277 | 40 | 1189.7623 | 64 | 3081.9694 |
| 17 | 562.2849 | 41 | 1251.1722 | 65 | 3091.3089 |
| 18 | 574.1831 | 42 | 1267.0593 | 66 | 3154.1836 |
| 19 | 618.1316 | 43 | 1297.0006 | 67 | 3162.3534 |
| 20 | 626.3360 | 44 | 1315.9891 | 68 | 3175.1884 |
| 21 | 642.7814 | 45 | 1344.2851 | 69 | 3177.4038 |
| 22 | 665.7083 | 46 | 1365.3650 | 70 | 3218.5082 |
| 23 | 683.0065 | 47 | 1408.7834 | 71 | 3242.6148 |
| 24 | 739.5086 | 48 | 1421.4181 | 72 | 3584.3516 |

**1-(thiophene-2-carbonyl)-1,2,3,4-tetrahydro-5H-pyrido[2,3-e][1,4]diazepin-5-one (*cis*-21c)**

#N B3LYP/6-31G(d) OPT Geom=Connectivity

Cmpd 21c_cis

0,1

| | | | |
|---|---|---|---|
| C | 0. | 0. | 0. |
| N | 0. | 0. | 1.4559331 |
| C | 0.9677096058 | 0. | 2.4302750041 |
| C | 2.4436584755 | -0.1131702711 | 2.1293925737 |
| C | 3.126389019 | 0.1639849286 | 0.9286904279 |
| N | 4.4502734656 | 0.0620579979 | 0.7935952225 |
| C | 5.1718293138 | -0.2900237524 | 1.8563467688 |
| C | 4.6109896777 | -0.5806500943 | 3.1015755614 |
| C | 3.2332774772 | -0.4908766501 | 3.2279591223 |
| H | 2.7290737675 | -0.686610857 | 4.1674159378 |
| H | 5.237063828 | -0.8692698625 | 3.9399360723 |
| H | 6.2472263483 | -0.3553207553 | 1.6996852013 |
| N | 2.4089588413 | 0.5067098464 | -0.2556046978 |
| C | 1.332489715 | -0.4093022877 | -0.6122572299 |
| H | 1.6124188243 | -1.4091341459 | -0.2665157626 |
| H | 1.2430103862 | -0.4651751826 | -1.6979456583 |
| C | 2.7733560343 | 1.662960551 | -0.9456384316 |

| | | | |
|---|---|---|---|
| O | 3.613120573 | 2.4282268545 | -0.4898053054 |
| C | 2.1784789088 | 1.9769986786 | -2.2799452089 |
| S | 3.158367986 | 3.0870324295 | -3.2165407954 |
| C | 2.00540829 | 3.1082129633 | -4.4973591195 |
| C | 0.9081381743 | 2.3367896558 | -4.217918334 |
| C | 1.0059896351 | 1.6933736124 | -2.9528023123 |
| H | 0.2048944366 | 1.0798419455 | -2.5635130306 |
| H | 0.0576780732 | 2.2289547049 | -4.8823680853 |
| H | 2.1936792397 | 3.6934071364 | -5.3882164946 |
| O | 0.6064679487 | 0.050835888 | 3.6055857548 |
| H | -0.9108643163 | 0.1029473479 | 1.8887411715 |
| H | -0.7755185684 | -0.7002424944 | -0.339974279 |
| H | -0.2752618302 | 0.9975321841 | -0.3708544379 |

RB3LYP Energy = -1214.8906391 Hartrees

| **Mode** | **Frequency ($cm^{-1}$)** | **Mode** | **Frequency ($cm^{-1}$)** | **Mode** | **Frequency ($cm^{-1}$)** |
|---|---|---|---|---|---|
| 1 | 19.9031 | 29 | 726.0861 | 57 | 1323.2917 |
| 2 | 44.8408 | 30 | 735.5811 | 58 | 1372.2591 |
| 3 | 59.5363 | 31 | 742.9157 | 59 | 1394.3937 |
| 4 | 70.2947 | 32 | 757.1788 | 60 | 1399.5959 |
| 5 | 101.8707 | 33 | 801.4124 | 61 | 1431.2601 |
| 6 | 120.9329 | 34 | 838.3676 | 62 | 1435.7406 |
| 7 | 134.7760 | 35 | 843.5550 | 63 | 1469.6381 |
| 8 | 174.9674 | 36 | 849.3825 | 64 | 1478.7755 |
| 9 | 202.9651 | 37 | 875.3195 | 65 | 1495.7972 |
| 10 | 226.5564 | 38 | 913.1056 | 66 | 1515.4171 |
| 11 | 284.4495 | 39 | 925.8943 | 67 | 1530.2608 |
| 12 | 321.2443 | 40 | 957.4944 | 68 | 1547.4183 |
| 13 | 357.9741 | 41 | 983.5890 | 69 | 1580.6814 |
| 14 | 374.4142 | 42 | 1011.3394 | 70 | 1613.7232 |
| 15 | 404.5100 | 43 | 1031.4496 | 71 | 1643.0996 |
| 16 | 422.6132 | 44 | 1059.6729 | 72 | 1731.0625 |
| 17 | 443.8789 | 45 | 1093.3343 | 73 | 1746.0745 |

| | | | | | |
|---|---|---|---|---|---|
| 18 | 480.0854 | 46 | 1098.9925 | 74 | 3023.4398 |
| 19 | 541.6117 | 47 | 1116.9074 | 75 | 3054.6333 |
| 20 | 555.7386 | 48 | 1130.7067 | 76 | 3093.3034 |
| 21 | 563.3600 | 49 | 1138.7284 | 77 | 3152.2190 |
| 22 | 577.8936 | 50 | 1193.1910 | 78 | 3177.9002 |
| 23 | 615.3912 | 51 | 1202.0586 | 79 | 3215.8812 |
| 24 | 625.6715 | 52 | 1242.1609 | 80 | 3223.9362 |
| 25 | 643.1279 | 53 | 1260.6416 | 81 | 3241.7392 |
| 26 | 669.7347 | 54 | 1281.7177 | 82 | 3258.3029 |
| 27 | 693.4499 | 55 | 1298.7271 | 83 | 3266.5119 |
| 28 | 715.0668 | 56 | 1316.4367 | 84 | 3581.7129 |

**1-(thiophene-2-carbonyl)-1,2,3,4-tetrahydro-5H-pyrido[2,3-e][1,4]diazepin-5-one (*trans*-21c)**

#N B3LYP/6-31G(d) OPT Geom=Connectivity

Cmpd 13c_trans

0,1

| | | | |
|---|---|---|---|
| C | 0. | 0. | 0. |
| N | 0. | 0. | 1.4579896 |
| C | 0.9701581284 | 0. | 2.4250006926 |
| C | 2.4483553889 | 0.0748071853 | 2.1145788504 |
| C | 3.0858211404 | 0.4821638205 | 0.9209716042 |
| N | 4.4138724279 | 0.6064504454 | 0.8037095091 |
| C | 5.1762257555 | 0.3418069511 | 1.8640718948 |
| C | 4.6635754017 | -0.0948467342 | 3.0862794538 |
| C | 3.2864172436 | -0.2209245353 | 3.201168372 |
| H | 2.8148130356 | -0.5228531965 | 4.1294457979 |
| H | 5.3230782052 | -0.3210290856 | 3.9179013946 |
| H | 6.2478989958 | 0.4685149051 | 1.7200900399 |
| N | 2.3401718529 | 0.7218076295 | -0.2513933995 |
| C | 1.3556537227 | -0.3005502057 | -0.6126206498 |
| H | 1.7207638719 | -1.2814706097 | -0.2909724235 |
| H | 1.27284544 | -0.3002266989 | -1.7003195918 |
| C | 2.6901205414 | 1.6583873141 | -1.2381703082 |
| O | 2.3737005219 | 1.4803814063 | -2.4098441357 |
| C | 3.3340618812 | 2.9180026035 | -0.8172587973 |
| S | 4.0876241988 | 3.8792983148 | -2.0648476124 |
| C | 4.4504897985 | 5.1328732294 | -0.9352451237 |
| C | 3.9935476304 | 4.8430134955 | 0.3257003773 |

| | | | |
|---|---|---|---|
| C | 3.3543288021 | 3.5760834698 | 0.3923713116 |
| H | 2.9193205403 | 3.1723051529 | 1.2989099772 |
| H | 4.1077084976 | 5.5077769949 | 1.1749353701 |
| H | 4.9778900254 | 6.0196942937 | -1.2618389777 |
| O | 0.6216594685 | -0.0666047483 | 3.6048393608 |
| H | -0.9137958872 | -0.0247974244 | 1.8959345482 |
| H | -0.7169163502 | -0.7594591103 | -0.3396620174 |
| H | -0.3498936146 | 0.9710930774 | -0.376581897 |

RB3LYP Energy = -1214.9036257 Hartrees

| **Mode** | **Frequency ($cm^{-1}$)** | **Mode** | **Frequency ($cm^{-1}$)** | **Mode** | **Frequency ($cm^{-1}$)** |
|---|---|---|---|---|---|
| 1 | 29.0831 | 29 | 737.9733 | 57 | 1340.0653 |
| 2 | 39.7292 | 30 | 750.6846 | 58 | 1364.0162 |
| 3 | 47.0974 | 31 | 757.4620 | 59 | 1397.7046 |
| 4 | 73.4993 | 32 | 770.8480 | 60 | 1402.6355 |
| 5 | 76.9867 | 33 | 798.2084 | 61 | 1419.6366 |
| 6 | 118.3971 | 34 | 837.6810 | 62 | 1433.6517 |
| 7 | 138.9307 | 35 | 842.6519 | 63 | 1470.5307 |
| 8 | 179.2659 | 36 | 858.7304 | 64 | 1481.1339 |
| 9 | 193.6153 | 37 | 877.2970 | 65 | 1495.4279 |
| 10 | 244.1138 | 38 | 922.3719 | 66 | 1511.0706 |
| 11 | 287.6068 | 39 | 937.5276 | 67 | 1517.5703 |
| 12 | 316.7852 | 40 | 953.4821 | 68 | 1545.3511 |
| 13 | 343.6221 | 41 | 983.4311 | 69 | 1584.7277 |
| 14 | 379.5163 | 42 | 1011.1467 | 70 | 1612.5349 |
| 15 | 402.6433 | 43 | 1041.2773 | 71 | 1641.3268 |
| 16 | 436.1031 | 44 | 1060.7094 | 72 | 1732.6356 |
| 17 | 448.3434 | 45 | 1084.5134 | 73 | 1741.7254 |
| 18 | 459.8479 | 46 | 1093.1616 | 74 | 3031.0786 |
| 19 | 510.4372 | 47 | 1117.3548 | 75 | 3061.6839 |
| 20 | 554.6034 | 48 | 1129.0050 | 76 | 3086.0400 |

| | | | | | |
|---|---|---|---|---|---|
| 21 | 572.0155 | 49 | 1139.0029 | 77 | 3161.2206 |
| 22 | 577.7883 | 50 | 1173.2244 | 78 | 3178.7118 |
| 23 | 601.8082 | 51 | 1191.6596 | 79 | 3217.5479 |
| 24 | 626.4794 | 52 | 1247.3757 | 80 | 3225.2031 |
| 25 | 654.1850 | 53 | 1267.3261 | 81 | 3241.2738 |
| 26 | 666.7164 | 54 | 1279.5045 | 82 | 3243.3110 |
| 27 | 686.7820 | 55 | 1292.7173 | 83 | 3266.9448 |
| 28 | 723.8615 | 56 | 1314.9530 | 84 | 3583.0753 |

**1-benzoyl-1,2,3,4-tetrahydro-5H-pyrido[2,3-e][1,4]diazepin-5-one (*cis*-21d)**

#N B3LYP/6-31G(d) OPT Geom=Connectivity

Cmpd 21d_cis

0,1

| | | | |
|---|---|---|---|
| C | -0.4880559982 | -0.0742186343 | 1.0229136889 |
| N | 0.2202769375 | -0.647336822 | 2.1539669006 |
| C | 1.4654236457 | -0.4567643298 | 2.6942673054 |
| C | 2.4897769457 | 0.4882824972 | 2.1052778826 |
| C | 2.3433558628 | 1.4852930159 | 1.1160929283 |
| N | 3.3293030951 | 2.3242128428 | 0.7727096688 |
| C | 4.5052153995 | 2.2205895163 | 1.3848464218 |
| C | 4.7821951363 | 1.2495369537 | 2.3489671814 |
| C | 3.7586006244 | 0.3862901301 | 2.7036692339 |
| H | 3.8887728132 | -0.3719139389 | 3.4671198545 |
| H | 5.7632232292 | 1.1826630755 | 2.808402923 |
| H | 5.2658902674 | 2.9365459037 | 1.0773391279 |
| N | 1.1613530907 | 1.6593814356 | 0.3512338689 |
| C | 0.4319887114 | 0.4646754099 | -0.0645872606 |
| H | 1.1545707151 | -0.3010408186 | -0.3664396373 |
| H | -0.1781082032 | 0.7089032998 | -0.9343516863 |
| C | 0.5814583013 | 2.9430252023 | 0.3063378397 |
| O | 0.8168597356 | 3.785813307 | 1.1542350525 |
| C | -0.3322008109 | 3.2479931394 | -0.8466451618 |
| C | -1.4679302962 | 4.0309940579 | -0.6009777822 |
| C | -2.3039575123 | 4.4045356056 | -1.65129079 |
| C | -1.9963097909 | 4.0239808145 | -2.9600811226 |
| C | -0.848693442 | 3.2702429524 | -3.2157041386 |
| C | -0.021626575 | 2.878196328 | -2.163180793 |
| H | 0.8828661915 | 2.3094198309 | -2.3614027712 |
| H | -0.5942137819 | 2.992885987 | -4.2350202601 |
| H | -2.6438210298 | 4.3229355289 | -3.7800004132 |
| H | -3.1897550017 | 5.0012397064 | -1.4515241083 |

| | | | |
|---|---|---|---|
| H | -1.676478206 | 4.3464798678 | 0.4166674247 |
| O | 1.7633869859 | -1.1026123378 | 3.6995896424 |
| H | -0.3076059103 | -1.2907819682 | 2.7318087608 |
| H | -1.1126037031 | -0.8670384342 | 0.5914408685 |
| H | -1.1640974518 | 0.7318679319 | 1.3446211605 |

RB3LYP Energy = -894.1400921 Hartrees

| Mode | Frequency ($cm^{-1}$) | Mode | Frequency ($cm^{-1}$) | Mode | Frequency ($cm^{-1}$) |
|---|---|---|---|---|---|
| 1 | 20.4253 | 32 | 756.4278 | 63 | 1364.9521 |
| 2 | 48.5569 | 33 | 797.8297 | 64 | 1366.6770 |
| 3 | 50.1362 | 34 | 805.3625 | 65 | 1407.2568 |
| 4 | 76.8912 | 35 | 838.6678 | 66 | 1420.7277 |
| 5 | 84.6970 | 36 | 869.5723 | 67 | 1437.3063 |
| 6 | 110.9824 | 37 | 874.5891 | 68 | 1469.8783 |
| 7 | 134.7275 | 38 | 925.7399 | 69 | 1492.4537 |
| 8 | 164.2135 | 39 | 948.3381 | 70 | 1493.7029 |
| 9 | 194.6665 | 40 | 974.0923 | 71 | 1509.2362 |
| 10 | 246.1779 | 41 | 980.2846 | 72 | 1512.9243 |
| 11 | 280.3983 | 42 | 984.7235 | 73 | 1540.1578 |
| 12 | 329.7652 | 43 | 1003.2687 | 74 | 1545.1353 |
| 13 | 344.2039 | 44 | 1014.9024 | 75 | 1612.3845 |
| 14 | 364.3995 | 45 | 1018.8436 | 76 | 1638.4302 |
| 15 | 392.0584 | 46 | 1052.2109 | 77 | 1644.4186 |
| 16 | 412.9879 | 47 | 1061.6951 | 78 | 1659.7837 |
| 17 | 420.0387 | 48 | 1081.3126 | 79 | 1742.3276 |
| 18 | 441.8164 | 49 | 1092.8540 | 80 | 1770.4408 |
| 19 | 494.8309 | 50 | 1112.1314 | 81 | 3019.9666 |
| 20 | 536.6928 | 51 | 1129.6726 | 82 | 3063.5411 |
| 21 | 558.7561 | 52 | 1140.6405 | 83 | 3086.2263 |
| 22 | 586.5831 | 53 | 1190.1111 | 84 | 3161.1416 |

| | | | | | |
|---|---|---|---|---|---|
| 23 | 607.6857 | 54 | 1194.3784 | 85 | 3175.2703 |
| 24 | 613.5634 | 55 | 1206.2528 | 86 | 3185.8685 |
| 25 | 631.8727 | 56 | 1209.8779 | 87 | 3194.2626 |
| 26 | 641.7297 | 57 | 1246.6906 | 88 | 3202.7145 |
| 27 | 662.8763 | 58 | 1264.0723 | 89 | 3211.4196 |
| 28 | 685.3662 | 59 | 1298.4120 | 90 | 3215.8697 |
| 29 | 707.5552 | 60 | 1309.7491 | 91 | 3219.8385 |
| 30 | 725.3844 | 61 | 1329.9220 | 92 | 3243.7632 |
| 31 | 737.7812 | 62 | 1346.0478 | 93 | 3587.5557 |

**1-benzoyl-1,2,3,4-tetrahydro-5H-pyrido[2,3-e][1,4]diazepin-5-one (*trans*-21d)**

#N B3LYP/6-31G(d) OPT Geom=Connectivity

Cmpd 21d_trans

0,1

| | | | |
|---|---|---|---|
| C | 0. | 0. | 0. |
| N | 0. | 0. | 1.4578091 |
| C | 0.9723876693 | 0. | 2.4230661527 |
| C | 2.4468146298 | 0.1292159167 | 2.1130832491 |
| C | 3.0716317918 | 0.5579504542 | 0.9197746808 |
| N | 4.3933801918 | 0.7403496409 | 0.8087795145 |
| C | 5.1621368986 | 0.5139154745 | 1.8735528676 |
| C | 4.6642649445 | 0.0555030701 | 3.0933351274 |
| C | 3.2930592232 | -0.1296361289 | 3.2024042253 |
| H | 2.8307034538 | -0.4496321679 | 4.1292343212 |
| H | 5.3292653333 | -0.1406809188 | 3.9281622051 |
| H | 6.2273219177 | 0.6907074801 | 1.7344460997 |
| N | 2.3261137366 | 0.7653182795 | -0.2582769675 |
| C | 1.3609986377 | -0.2777971685 | -0.6105160517 |
| H | 1.7439829232 | -1.2501373259 | -0.2831499932 |
| H | 1.2784341515 | -0.2840461607 | -1.6982952541 |
| C | 2.678394146 | 1.6912766933 | -1.2549301623 |
| O | 2.351530941 | 1.5024234293 | -2.4195960013 |
| C | 3.3468113852 | 2.9680541956 | -0.848211836 |
| C | 3.0584767079 | 3.6241885842 | 0.3559479855 |
| C | 3.6259114293 | 4.8677325702 | 0.6298809537 |
| C | 4.4929587705 | 5.4603948349 | -0.2902208895 |
| C | 4.7760761123 | 4.8140155418 | -1.496104881 |
| C | 4.1940615718 | 3.5812101742 | -1.7804171494 |
| H | 4.3837846591 | 3.0789417186 | -2.7232873892 |
| H | 5.4439566143 | 5.2756483238 | -2.2182678033 |
| H | 4.9402979167 | 6.4264781461 | -0.0717763754 |

| | | | |
|---|---|---|---|
| H | 3.3887492956 | 5.3744159971 | 1.5613821672 |
| H | 2.3790671242 | 3.173604639 | 1.0728411335 |
| O | 0.6266532571 | -0.1018267996 | 3.6012490633 |
| H | -0.9115401827 | -0.0608587491 | 1.8968445799 |
| H | -0.7031159574 | -0.7720868805 | -0.3399868194 |
| H | -0.366367291 | 0.9645036903 | -0.3777354216 |

RB3LYP Energy = -894.1491247 Hartrees

| Mode | Frequency ($cm^{-1}$) | Mode | Frequency ($cm^{-1}$) | Mode | Frequency ($cm^{-1}$) |
|---|---|---|---|---|---|
| 1 | 37.9973 | 32 | 783.3648 | 63 | 1362.9534 |
| 2 | 41.9006 | 33 | 797.7870 | 64 | 1367.0105 |
| 3 | 45.4859 | 34 | 807.5579 | 65 | 1400.3609 |
| 4 | 71.3910 | 35 | 838.3671 | 66 | 1419.0354 |
| 5 | 76.1241 | 36 | 863.5496 | 67 | 1433.6007 |
| 6 | 108.2238 | 37 | 882.3858 | 68 | 1476.0979 |
| 7 | 136.1185 | 38 | 935.3175 | 69 | 1493.7992 |
| 8 | 175.7864 | 39 | 946.2887 | 70 | 1496.1055 |
| 9 | 209.7512 | 40 | 975.1738 | 71 | 1510.3733 |
| 10 | 247.6755 | 41 | 976.4138 | 72 | 1517.4515 |
| 11 | 299.0887 | 42 | 983.5398 | 73 | 1542.4612 |
| 12 | 316.0547 | 43 | 1000.7775 | 74 | 1545.4545 |
| 13 | 341.8833 | 44 | 1011.3219 | 75 | 1612.9514 |
| 14 | 379.5446 | 45 | 1018.9589 | 76 | 1639.6411 |
| 15 | 400.0618 | 46 | 1049.9799 | 77 | 1641.7041 |
| 16 | 417.7895 | 47 | 1057.0556 | 78 | 1661.3980 |
| 17 | 430.5625 | 48 | 1074.8482 | 79 | 1740.9312 |
| 18 | 439.3214 | 49 | 1095.0791 | 80 | 1750.6062 |
| 19 | 462.9151 | 50 | 1115.7342 | 81 | 3030.9561 |
| 20 | 533.2421 | 51 | 1129.3925 | 82 | 3061.2350 |
| 21 | 557.1083 | 52 | 1140.7233 | 83 | 3084.5931 |

| | | | | | |
|---|---|---|---|---|---|
| 22 | 579.8153 | 53 | 1183.3147 | 84 | 3159.4847 |
| 23 | 606.5688 | 54 | 1193.2609 | 85 | 3178.7156 |
| 24 | 626.0302 | 55 | 1194.2735 | 86 | 3184.9895 |
| 25 | 632.6847 | 56 | 1212.4642 | 87 | 3195.7478 |
| 26 | 658.9013 | 57 | 1248.3361 | 88 | 3205.5855 |
| 27 | 666.6461 | 58 | 1276.6708 | 89 | 3214.6288 |
| 28 | 686.9296 | 59 | 1292.4892 | 90 | 3218.0002 |
| 29 | 709.4256 | 60 | 1315.2884 | 91 | 3224.8822 |
| 30 | 732.4409 | 61 | 1341.0255 | 92 | 3242.2212 |
| 31 | 740.5594 | 62 | 1347.2235 | 93 | 3583.2240 |

**1-benzyl-1,2,3,4-tetrahydro-5H-pyrido[2,3-e][1,4]diazepin-5-one (21e)**

#N B3LYP/6-31G(d) OPT Geom=Connectivity

Cmpd 21e

0,1

| | | | |
|---|---|---|---|
| C | 1.1273965647 | 1.3843040638 | -0.0797011739 |
| N | 0.8154323122 | 1.4230051295 | 1.3350132507 |
| C | 1.3471822062 | 0.7442424633 | 2.3990634195 |
| C | 2.5961198823 | -0.099681317 | 2.2827637746 |
| C | 3.3973202505 | -0.456660952 | 1.1494028859 |
| N | 4.5909653195 | -1.0667769519 | 1.3068386967 |
| C | 5.0132376449 | -1.4110020125 | 2.5181821184 |
| C | 4.2704035781 | -1.2030400865 | 3.6771779227 |
| C | 3.0652745646 | -0.5320267306 | 3.5338300767 |
| H | 2.4492734412 | -0.2859087758 | 4.3911109692 |
| H | 4.6336331109 | -1.5247245472 | 4.6474092689 |
| H | 5.993676231 | -1.8850733709 | 2.5578820808 |
| N | 3.0345590192 | -0.2182022046 | -0.1645324897 |
| C | 1.6463817109 | 0.0192965516 | -0.5211368293 |
| H | 0.9956591246 | -0.7664909549 | -0.1081162019 |
| H | 1.5819638578 | -0.0327474757 | -1.6102664439 |
| C | 3.9275334381 | -0.5890555791 | -1.2703070059 |
| C | 4.1045492222 | 0.5267934892 | -2.2837394605 |
| C | 3.8577288159 | 0.3048057979 | -3.642726322 |
| C | 4.0546405597 | 1.320553787 | -4.5823299057 |
| C | 4.4972950067 | 2.5765936327 | -4.1695658402 |
| C | 4.7449479189 | 2.8105097141 | -2.813481314 |
| C | 4.5508734723 | 1.7940480191 | -1.8797699988 |
| H | 4.7471065352 | 1.977765731 | -0.8263453722 |
| H | 5.0941661319 | 3.7859743832 | -2.4848376298 |

| | | | |
|---|---|---|---|
| H | 4.6492209539 | 3.3693960298 | -4.8970827444 |
| H | 3.8577800343 | 1.1290294639 | -5.6339605049 |
| H | 3.5127674407 | -0.6739330089 | -3.9703732699 |
| H | 4.8834839097 | -0.8611990079 | -0.8229004658 |
| H | 3.5417719989 | -1.4875440659 | -1.7746897708 |
| O | 0.803128047 | 0.878815444 | 3.4976105946 |
| H | 0.0115817477 | 1.9657939191 | 1.6238746743 |
| H | 0.197871628 | 1.6009559522 | -0.6193333066 |
| H | 1.8589377139 | 2.152272455 | -0.3648142141 |

RB3LYP Energy = -820.1185143 Hartrees

| **Mode** | **Frequency ($cm^{-1}$)** | **Mode** | **Frequency ($cm^{-1}$)** | **Mode** | **Frequency ($cm^{-1}$)** |
|---|---|---|---|---|---|
| 1 | 11.6159 | 33 | 826.5263 | 65 | 1395.1127 |
| 2 | 22.0253 | 34 | 838.8360 | 66 | 1415.1505 |
| 3 | 34.9217 | 35 | 863.9201 | 67 | 1431.3688 |
| 4 | 61.5459 | 36 | 904.1224 | 68 | 1436.0323 |
| 5 | 85.5900 | 37 | 923.9368 | 69 | 1477.2038 |
| 6 | 112.9816 | 38 | 956.7441 | 70 | 1493.3563 |
| 7 | 166.8494 | 39 | 970.4698 | 71 | 1500.9297 |
| 8 | 212.6250 | 40 | 977.5517 | 72 | 1504.2222 |
| 9 | 230.3564 | 41 | 994.8377 | 73 | 1522.5521 |
| 10 | 245.8195 | 42 | 1000.3396 | 74 | 1533.9959 |
| 11 | 322.0407 | 43 | 1016.3433 | 75 | 1541.2528 |
| 12 | 336.7237 | 44 | 1018.3279 | 76 | 1547.0811 |
| 13 | 346.3466 | 45 | 1050.1213 | 77 | 1605.4471 |
| 14 | 400.5689 | 46 | 1058.5148 | 78 | 1644.4932 |
| 15 | 412.8719 | 47 | 1077.4870 | 79 | 1647.6882 |
| 16 | 418.0593 | 48 | 1098.6722 | 80 | 1664.3489 |
| 17 | 439.0542 | 49 | 1111.0738 | 81 | 1738.1583 |
| 18 | 483.5486 | 50 | 1118.5521 | 82 | 3016.0862 |
| 19 | 546.1850 | 51 | 1135.4774 | 83 | 3019.4477 |
| 20 | 549.3853 | 52 | 1182.7693 | 84 | 3040.6954 |

| | | | | | |
|---|---|---|---|---|---|
| 21 | 574.5574 | 53 | 1192.8126 | 85 | 3082.3583 |
| 22 | 580.9400 | 54 | 1204.9361 | 86 | 3129.6448 |
| 23 | 584.5449 | 55 | 1212.6582 | 87 | 3153.1529 |
| 24 | 630.1863 | 56 | 1230.4985 | 88 | 3163.5643 |
| 25 | 635.6778 | 57 | 1260.3592 | 89 | 3173.1743 |
| 26 | 663.7537 | 58 | 1266.6237 | 90 | 3182.4607 |
| 27 | 686.3603 | 59 | 1291.3935 | 91 | 3191.4766 |
| 28 | 716.7112 | 60 | 1316.3699 | 92 | 3199.6380 |
| 29 | 734.7776 | 61 | 1344.6577 | 93 | 3210.0568 |
| 30 | 759.6581 | 62 | 1347.4215 | 94 | 3218.6547 |
| 31 | 780.9057 | 63 | 1366.1190 | 95 | 3240.4267 |
| 32 | 817.8781 | 64 | 1367.7268 | 96 | 3601.6766 |

(1) Frisch, M. J.; Trucks, G. W.; Schlegel, H. B.; Scuseria, G. E.; Robb, M. A.; Cheeseman, J. R.; Scalmani, G.; Barone, V.; Mennucci, B.; Petersson, G. A.; Nakatsuji, H.; Caricato, M.; Li, X.; Hratchian, H. P.; Izmaylov, A. F.; Bloino, J.; Zheng, G.; Sonnenberg, J. L.; Hada, M.; Ehara, M.; Toyota, K.; Fukuda, R.; Hasegawa, J.; Ishida, M.; Nakajima, T.; Honda, Y.; Kitao, O.; Nakai, H.; Vreven, T.; J. A. Montgomery, J.; Peralta, J. E.; Ogliaro, F.; Bearpark, M.; Heyd, J. J.; Brothers, E.; Kudin, K. N.; Staroverov, V. N.; Kobayashi, R.; Normand, J.; Raghavachari, K.; Rendell, A.; Burant, J. C.; Iyengar, S. S.; Tomasi, J.; Cossi, M.; Rega, N.; Millam, J. M.; Klene, M.; Knox, J. E.; Cross, J. B.; Bakken, V.; Adamo, C.; Jaramillo, J.; Gomperts, R.; Stratmann, R. E.; Yazyev, O.; Austin, A. J.; Cammi, R.; Pomelli, C.; Ochterski, J. W.; Martin, R. L.; Morokuma, K.; Zakrzewski, V. G.; Voth, G. A.; Salvador, P.; Dannenberg, J. J.; Dapprich, S.; Daniels, A. D.; Farkas, O.; Foresman, J. B.; Ortiz, J. V.; Cioslowski, J.; Fox, D. J.; Revision A.02 ed.; Gaussian, Inc.: Wallingford CT, 2009.

# APPENDIX I: PARP1 ASSAY- Tips and Tricks

Our PARP1 assay procedure strongly resembles the manufacture's procedure (BPS Biosciences). In order to decrease expenses, serial dilutions were made with an "in-house" PARP buffer (50 mM Tris, 2.5 mM $MgCl_2 \cdot 6H_2O$, pH 8). There are a few tips and tricks to running the PARP1 assay.

- General remarks
  - Avoid the formation of bubbles while pipetting, especially for:
    - Solutions containing the blocking buffer
      - Blocking step (step 1, number 5)
      - Addition of strep-HRP (step 3, number 2)
    - The addition of the chemiluminescence substrates (step 3, number five)
  - Once the inhibitor solutions are added, the following steps are prone to contamination:
    - Washing the plate (step 2, number 5 and step 3, number 3)
    - The addition of the PARP enzyme to each well
  - Ensure the entire solution is added to the wells
    - No lingering droplets at the end of the pipette tips
    - No bubbles in the pipette tips during addition
  - Prepare PBST solutions prior to running the assays to ensure homogeneity
  - Plate brand: Greiner LUMITRAC 384 well plates
- Storage
  - The 1x histone mixture (BPS Biosciences) can be stored for future assays at −20°C for up to six months
  - Store the diluted PARP1 enzyme in appropriate volumes for future uses
    - **Important**: do not vortex diluted enzyme solutions
- Procedural advice
  - During the 90 minute blocking period in step 1, prepare the necessary solutions for step 2 to save time
    - **Important**: make the master mixture in slight excess
    - The inhibitor serial dilutions can be made prior to the assay
  - Ensure there are no droplets of solution on the edge of the wells after the addition of the enzyme (step 2, number 4) since the working volume at this step is small
  - Ensure the Strp-HRP is added to all the wells in a timely manner
  - For reproducibility, ensure that the time lapse between the addition of the chemiluminescence solution and the luminescence reading is the same each time
  - Running a full plate (384 wells) is error prone
    - If possible, avoid running full plate assays
    - For best results, run the plate with every other well to avoid contamination

For our customized procedure see below.

**384 well plate BPS procedure**

<u>Step 1: Histone Coating</u>

1) Dilute **5x histone mixture** 1:5 with PBS.
2) Add 25 µL of diluted histone solution to each well and incubate at 4°C overnight.

3) Wash the plate (three times) using 100 µL PBST buffer (1X PBS containing 0.05% Tween-20) per well.
4) Tap plate onto clean paper towel to remove liquid. Do not leave the plate without solution in the wells.
5) Block the wells by adding 100 µL of **Blocking buffer** to every well. Incubate at room temperature for 90 minutes.
**IMPORTANT: Prepare master mixture, inhibitor solutions, and diluted PARP1 enzyme during incubation period, see step 2**
6) Wash the plate (three times) using 100 µL PBST buffer per well.
7) Tap plate onto clean paper towel to remove liquid. Do not leave the plate without solution in the wells.

Step 2: Inhibitor and Enzyme Addition

1) Prepare the master mixture: N wells x (1.25 µL **10x PARP buffer** + 1.25 µL **10x PARP Assay mixture** + 2.5 µL **Activated DNA** + 7.5 µL distilled water). *Note: Make a slight excess of master mixture (approx. 10 wells).* Add 12.5 µL to every well.
2) Prepare inhibitor dilutions with in house PARP buffer, as necessary for single point or IC50, and add 2.5 µL to every well.

**Blanks**

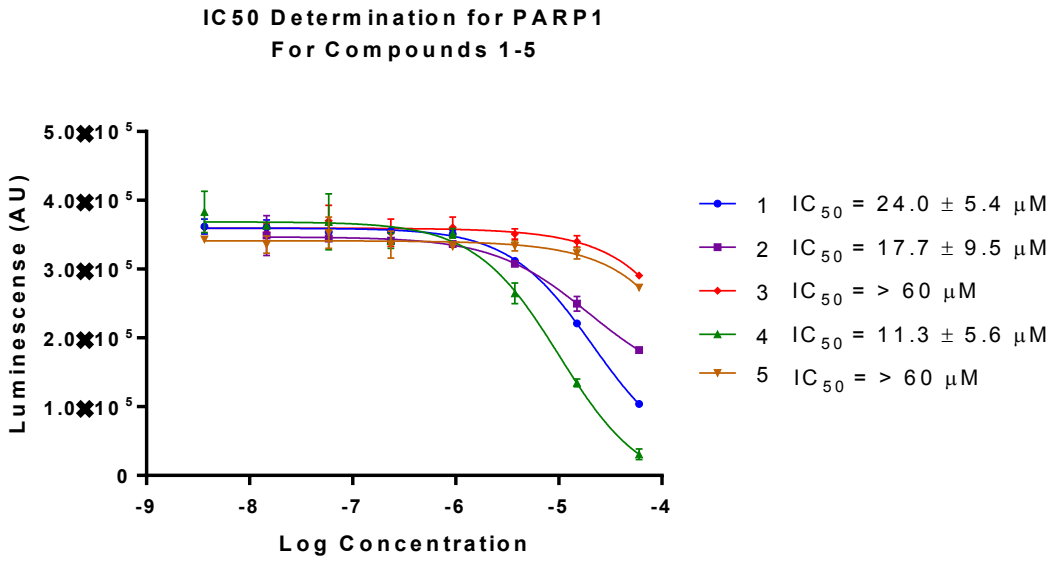
| | | |
|---|---|---|
| Blank 1 | No inhibitor | Sub DMSO |
| Blank 2 | No inhibitor, No protein | Sub DMSO, Sub buffer |
| Blank 3 | No inhibitor, No STRP-HRP | Sub DMSO, Sub water |

3) Prepare 1x PARP buffer by adding 1 part **10x PARP buffer (BPS)** to 9 parts distilled water.
4) Thaw **PARP1 enzyme (5 µg)** on ice. Dilute enzyme to 1.0 ng/µL with 1x PARP buffer (5 mL). Add 10 µL of **diluted PARP1 enzyme** to each well. Incubate at room temperature **for 60 minutes**. *Store **PARP1 enzyme** in aliquots to avoid multiple freeze/thaw cycles.*
5) Wash the plate (three times) using 100 µL PBST buffer per well.
6) Tap plate onto clean paper towel to remove liquid. Do not leave the plate without solution in the wells.

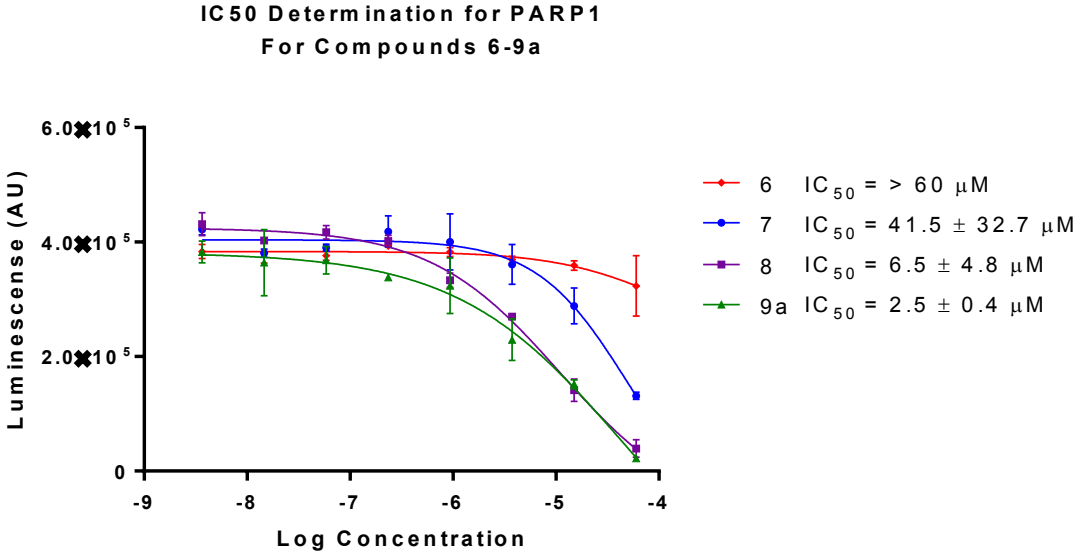
Step 3: Detection

1) Dilute **Streptavidin-HRP** in 1:50 in **Blocking buffer**.
2) Add 25 µL of diluted Streptavidin-HRP to each well. Incubate for 30 minutes at room temperature.
3) Wash the plate (three times) using 100 µL PBST buffer per well.
4) Tap plate onto clean paper towel to remove liquid. Do not leave the plate without solution in the wells.
5) Just before use, mix on ice 50% **HRP chemiluminescent substrate A** and 50% **HRP chemiluminescent substrate B**. Add 50 µL per well (approximately 20mL total for a full 384 well plate).
6) Immediately read the plate.
**IMPORTANT:** to **PROPERLY** read chemiluminescence, make sure the **plate reader is set for LUMINESCENCE**. Integration time: 1 second. **DO NOT USE A FILTER WHEN MEASURING LIGHT EMISSION.** Optics position: top. Read type: endpoint.

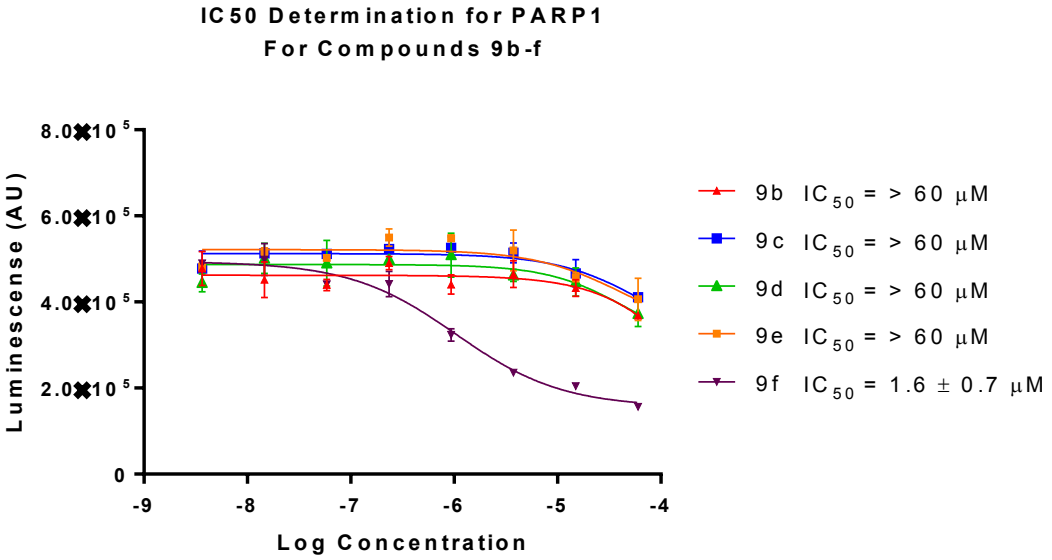
# APPENDIX J: DOSE-RESPONSE CURVES



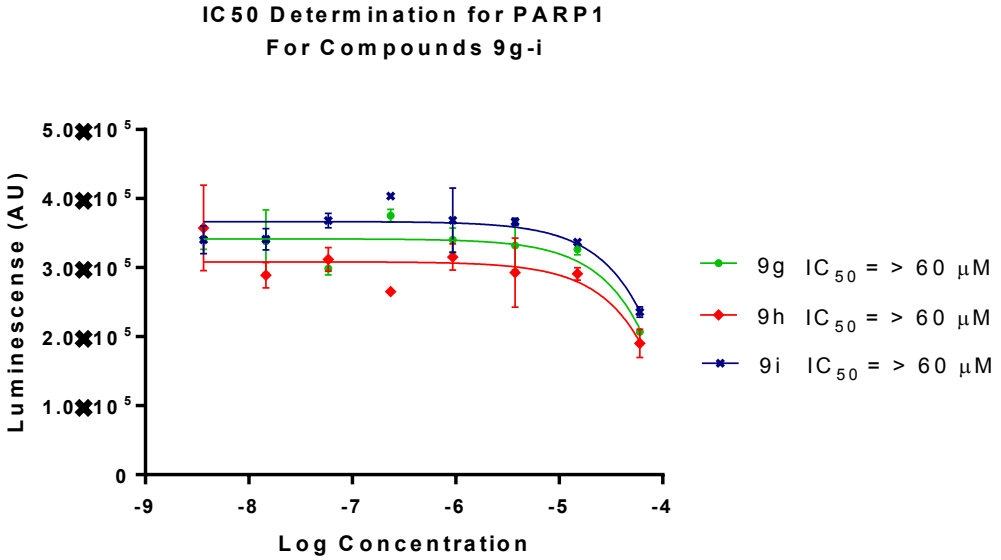

**1**: de-brominated hymenialdisine
**2**: 6,7-dihydropyrrolo[2,3-c]azepine-4,8(1H,5H)-dione
**3**: 7-chloro-1,2,3,4-tetrahydro-5H-benzo[b]azepin-5-one
**4**: 7-chloro-3,4-dihydro-1H-benzo[e][1,4]diazepine-2,5-dione
**5**: 8-fluoro-2,3,4,5-tetrahydro-1H-benzo[c]azepin-1-one



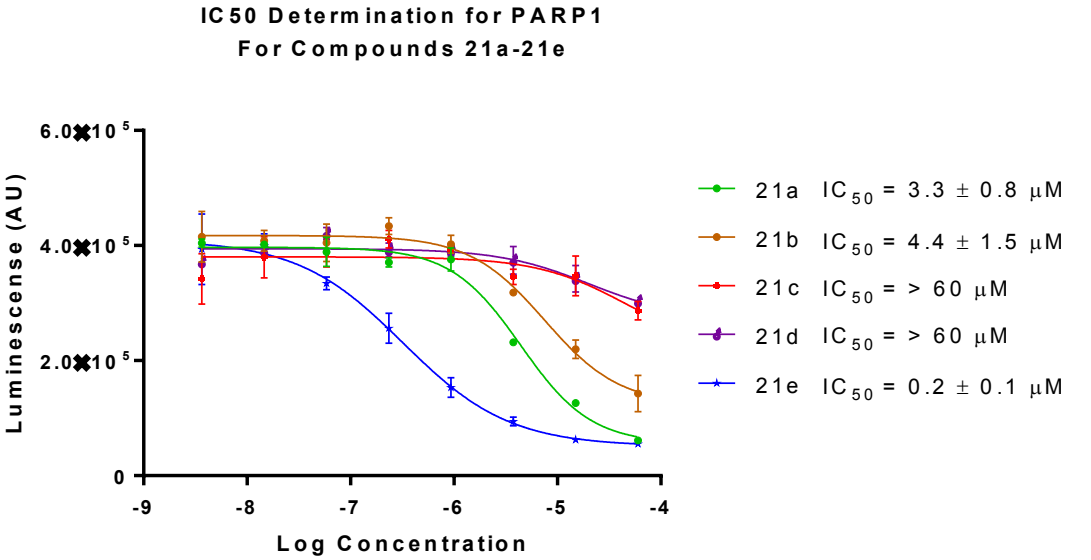

**6**: 3,4-dihydro-1H-benzo[c]azepine-1,5(2H)-dione
**7**: 2,3,4,5-tetrahydro-1H-benzo[c]azepin-1-one
**8**: 3,4-dihydrobenzo[f][1,4]oxazepin-5(2H)-one
**9**: 1,2,3,4-tetrahydro-5H-benzo[e][1,4]diazepin-5-one




**9b**: 1-acetyl-1,2,3,4-tetrahydro-5H-benzo[e][1,4]diazepin-5-one
**9c**: 1-(furan-2-carbonyl)-1,2,3,4-tetrahydro-5H-benzo[e][1,4]diazepin-5-one
**9d**: 1-(thiophene-2-carbonyl)-1,2,3,4-tetrahydro-5H-benzo[e][1,4]diazepin-5-one
**9e**: 1-benzoyl-1,2,3,4-tetrahydro-5H-benzo[e][1,4]diazepin-5-one
**9f**: 1-benzyl-1,2,3,4-tetrahydro-5H-benzo[e][1,4]diazepin-5-one




**9g**: 1-(methylsulfonyl)-1,2,3,4-tetrahydro-5H-benzo[e][1,4]diazepin-5-one
**9h**: 1-(vinylsulfonyl)-1,2,3,4-tetrahydro-5H-benzo[e][1,4]diazepin-5-one
**9i**: 1-(phenylsulfonyl)-1,2,3,4-tetrahydro-5H-benzo[e][1,4]diazepin-5-one




**21a**: 1,2,3,4-tetrahydro-5H-pyrido[2,3-e][1,4]diazepin-5-one
**21b**: 1-acetyl-1,2,3,4-tetrahydro-5H-pyrido[2,3-e][1,4]diazepin-5-one
**21c**: 1-(thiophene-2-carbonyl)-1,2,3,4-tetrahydro-5H-pyrido[2,3-e][1,4]diazepin-5-one
**21d**: 1-benzoyl-1,2,3,4-tetrahydro-5H-pyrido[2,3-e][1,4]diazepin-5-one
**21e**: 1-benzyl-1,2,3,4-tetrahydro-5H-pyrido[2,3-e][1,4]diazepin-5-one

# APPENDIX K: BPS BIOSCIENCES PROCEDURES AND DATA

Single Point Assay

**Assay Conditions**

In general, all assays were done by following the BPS PARP or TNKS assay kit protocols.

The enzymatic reactions were conducted in duplicate at room temperature for 1 hour in a 96 well plate coated with histone substrate.

50 µl of reaction buffer (Tris·HCl, pH 8.0) contains $NAD^+$, biotinylated $NAD^+$ (see **2.3.1**), activated DNA (see **2.3.1**), a PARP enzyme (see **2.3.1**) and the test compound (see **2.2**). After enzymatic reactions, 50µl of Streptavidin-horseradish peroxidase was added to each well and the plate was incubated at room temperature for an additional 30 min.

100 µl of developer reagents were added to wells and luminescence was measured using a BioTek Synergy™ 2 microplate reader.

**Data Analysis**

PARP or TNKS activity assays were performed in duplicates. The luminescence data were analyzed using the computer software, Graphpad Prism. In the absence of the compound, the luminescence ($L_t$) in each data set was defined as 100% activity. In the absence of the PARP or TNKS, the luminescence ($L_b$) in each data set was defined as 0% activity. The percent activity in the presence of each compound was calculated according to the following equation: % activity = $[(L- L_b)/(L_t - L_b)]\times100$, where L= the luminescence in the presence of the compound, $L_b$ = the luminescence in the absence of the PARP or TNKS, and $L_t$ = the luminescence in the absence of the compound. The percent inhibition was calculated according to the following equation:

% inhibition = 100 - % activity.

$IC_{50}$ Determination

**Assay Conditions**

In general, all assays were done by following the BPS PARP or TNKS assay kit protocols.

The enzymatic reactions were conducted in duplicate at room temperature for 1 hour in a 96 well plate coated with histone substrate.

50 µl of reaction buffer (Tris·HCl, pH 8.0) contains $NAD^+$, biotinylated $NAD^+$ (see **2.3.1**), activated DNA (see **2.3.1**), a PARP enzyme (see **2.3.1**) and the test compound (see **2.2**). After enzymatic reactions, 50µl of Streptavidin-horseradish peroxidase was added to each well and the plate was incubated at room temperature for an additional 30 min.

100 µl of developer reagents were added to wells and luminescence was measured using a BioTek Synergy$^{TM}$ 2 microplate reader.

## Data Analysis

PARP or TNKS activity assays were performed in duplicates. The luminescence data were analyzed using the computer software, Graphpad Prism. In the absence of the compound, the luminescence ($L_t$) in each data set was defined as 100% activity. In the absence of the PARP or TNKS, the luminescence ($L_b$) in each data set was defined as 0% activity. The percent activity in the presence of each compound was calculated according to the following equation: % activity = $[(L- L_b)/(L_t - L_b)]\times100$, where L= the luminescence in the presence of the compound, $L_b$ = the luminescence in the absence of the PARP or TNKS, and $L_t$ = the luminescence in the absence of the compound. The percent inhibition was calculated according to the following equation:
% inhibition = 100 - % activity.

The values of % activity versus a series of compound concentrations were then plotted using non-linear regression analysis of Sigmoidal dose-response curve generated with the equation $Y=B+(T-B)/1+10^{((LogEC50-X)\times Hill\ Slope)}$, where Y=percent activity, B=minimum percent activity, T=maximum percent activity, X= logarithm of compound and Hill Slope=slope factor or Hill coefficient. The IC50 value was determined by the concentration causing a half-maximal percent activity.

PARPtrapping

## Assay Conditions

In general, all assays were done by following the BPS PARPtrap assay kit protocols.

The enzymatic reactions were conducted in duplicate at room temperature in a 96 well plate.

45 µl of PARPtrap buffer contains 5 nM Alexa488 labeled Nicked DNA, PARP1 enzyme (see **2.3.1**) and the test compound (see **2.2**). After incubation for 30 min at room temperature, PARP1 enzymatic reaction was initiated by adding 5 µl NAD (see **2.3.1**), and incubated for 45 min at room temperature.

Fluorescence intensity was measured at an excitation of 485 nm and an emission of 528 nm using a Tecan Infinite M1000 microplate reader.

## Data Analysis

Fluorescence intensity is converted to fluorescence polarization using the Tecan Magellan6 software. The fluorescence polarization data were analyzed using the software, Graphpad Prism. The fluorescence polarization (FPo) in absence of the compound in each data set was defined as 0 % activity, while the fluorescence polarization in the absence of NAD and the compound was defined as 100% activity (FPt). In the absence of PARP and the compound, the value of fluorescent polarization ($FP_b$) in each data set was defined as background activity. The percent activity in the presence of the compound was calculated according to the following equation: % activity = $[(FP-FP_b)-(FPo-FPb)]/[(FP_t-FP_b)-(FPo-FPb)]\times 100\%$, where FP= the fluorescence polarization in the presence of the compound.

The values of % activity versus a series of compound concentrations were then plotted using non-linear regression analysis of Sigmoidal dose-response curve generated with the equation $Y=B+(T-B)/1+10^{((LogEC50-X)\times Hill\ Slope)}$, where Y=percent activity, B=minimum percent activity, T=maximum percent activity, X= logarithm of compound and Hill Slope=slope factor or Hill coefficient. The EC50 value was determined by the concentration causing a half-maximal percent activity.

6042 Cornerstone Court West, Suite B
San Diego, CA 92121
**Tel:** 1.858.829.3082
**Fax:** 1.858.481.8694
**Email:** info@bpsbioscience.com

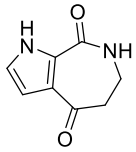
# Materials and Methods

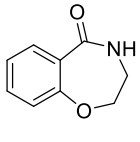
## 2.1 Materials

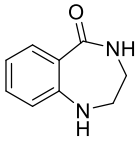
BPS PARP assay kits are used in the assay

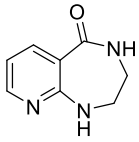
## 2.2 Compounds

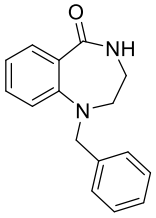
The test compound is supplied by Virginia Tech

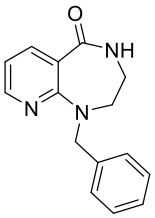

KL-2

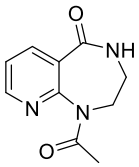

KL-8

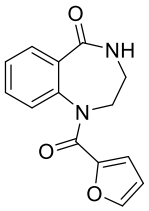

KL-9

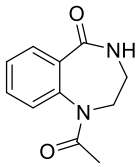

KL-13

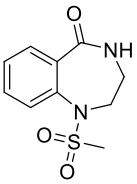

KL-9F

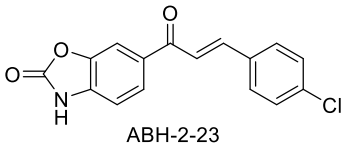

KL-13E

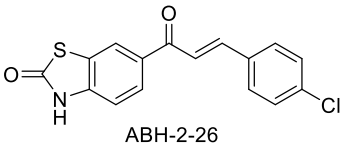

KL-13B

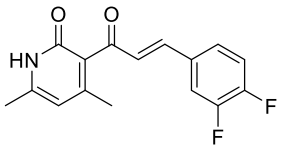

KL-9C

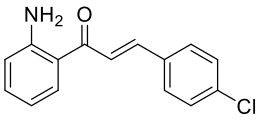

KL-9B

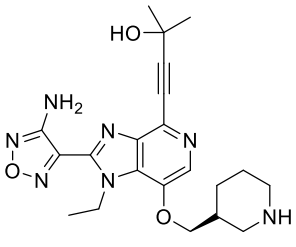

KL-9G


ABH-2-23


ABH-2-26


ABH-1-63


ABH-2-15


AKT

6042 Cornerstone Court West, Suite B
San Diego, CA 92121
**Tel:** 1.858.829.3082
**Fax:** 1.858.481.8694
**Email:** info@bpsbioscience.com

| Compound I.D. | Compound Supplied | Stock Concentration | Dissolving Solvent | Test Range | Intermediate Dilution |
|---|---|---|---|---|---|
| KL-2 | solution | 10 mM | DMSO | 10 µM | 10 % DMSO (aq) |
| KL-8 | solution | 10 mM | DMSO | 10 µM | 10 % DMSO (aq) |
| KL-9 | solution | 10 mM | DMSO | 10 µM | 10 % DMSO (aq) |
| KL-13 | solution | 10 mM | DMSO | 10 µM | 10 % DMSO (aq) |
| KL-9F | solution | 10 mM | DMSO | 10 µM | 10 % DMSO (aq) |
| KL-13E | solution | 10 mM | DMSO | 10 µM | 10 % DMSO (aq) |
| KL-13B | solution | 10 mM | DMSO | 10 µM | 10 % DMSO (aq) |
| KL-9C | solution | 10 mM | DMSO | 10 µM | 10 % DMSO (aq) |
| KL-9B | solution | 10 mM | DMSO | 10 µM | 10 % DMSO (aq) |
| KL-9BZI | solution | 10 mM | DMSO | 10 µM | 10 % DMSO (aq) |
| ABH-2-23 | solution | 10 mM | DMSO | 10 µM | 10 % DMSO (aq) |
| ABH-2-26 | solution | 10 mM | DMSO | 10 µM | 10 % DMSO (aq) |
| ABH-1-63 | solution | 10 mM | DMSO | 10 µM | 10 % DMSO (aq) |
| KL-9G | solution | 10 mM | DMSO | 10 µM | 10 % DMSO (aq) |
| ABH-2-15 | solution | 10 mM | DMSO | 10 µM | 10 % DMSO (aq) |
| AKT | solution | 1 mM | DMSO | 10 µM | 10 % DMSO (aq) |
| AZD2281 | powder | 10 mM | DMSO | 10 µM | 10 % DMSO (aq) |

## 2.3 Experimental Conditions

### 2.3.1 Enzymes and Substrates

| Assay | Catalog # (Lot #) | Enzyme Used/ Reaction | Substrate |
|---|---|---|---|
| | | | Activated DNA |
| PARP1 | 80501 (120206-1) | 10 ng | 2.5 µM $NAD^+$/2.5 µM $NAD^+$-Biotin |
| | | | 0.026 mg/ml |
| PARP2 | 80502 (140729-P4) | 25 ng | 2.5 µM $NAD^+$/2.5 µM $NAD^+$-Biotin |
| | | | 0.026 mg/ml |
| PARP3 | 80503 (130111G) | 80 ng | 25 µM $NAD^+$/2.5 µM $NAD^+$-Biotin |
| | | | 0.026 mg/ml |
| TNKS1 | 80504 (140116-1) | 30 ng | 25 µM $NAD^+$/2.5 µM $NAD^+$-Biotin |
| | | | N/A |
| TNKS2 | 80505 (130314G2) | 10 ng | 25 µM $NAD^+$/2.5 µM $NAD^+$-Biotin |
| | | | N/A |

6042 Cornerstone Court West, Suite B
San Diego, CA 92121
**Tel:** 1.858.829.3082
**Fax:** 1.858.481.8694
**Email:** info@bpsbioscience.com

| | | | |
|---|---|---|---|
| PARP6 | 80506 (160301-1) | 500 ng | 50 µM $NAD^+$/5 µM $NAD^+$-Biotin |
| | | | 0.026 mg/ml |
| PARP7 | (160229-1) | 150 ng | 50 µM $NAD^+$/5 µM $NAD^+$-Biotin |
| | | | N/A |
| PARP8 | (130301) | 300 ng | 50 µM $NAD^+$/5 µM $NAD^+$-Biotin |
| | | | N/A |
| PARP10 | 80510 (150813) | 50 ng | 25 µM $NAD^+$/2.5 µM $NAD^+$-Biotin |
| | | | N/A |
| PARP11 | 80511 (150820B) | 800 ng | 50 µM $NAD^+$/5 µM $NAD^+$-Biotin |
| | | | N/A |
| PARP12 | 80513 (151102A) | 400 ng | 50 µM $NAD^+$/5 µM $NAD^+$-Biotin |
| | | | N/A |
| PARP14 | 80514 (141121) | 150 ng | 50 µM $NAD^+$/5 µM $NAD^+$-Biotin |
| | | | N/A |
| PARP15 | 80517 (121211-1) | 70 ng | 25 µM $NAD^+$/2.5 µM $NAD^+$-Biotin |
| | | | N/A |

6042 Cornerstone Court West, Suite B
San Diego, CA 92121
**Tel:** 1.858.829.3082
**Fax:** 1.858.481.8694
**Email:** info@bpsbioscience.com

# 3. Assay Results

## 3.1. Summary of the effects of the compounds on PARP Activities

The % inhibition of the compounds against PARP are summarized in Table 3.1

**Table 3.1 Inhibitory Effects of the Compounds on PARP Activities**

| PARPs | % inhibition at 10 µM | | | | | | | | |
|---|---|---|---|---|---|---|---|---|---|
| | KL-2 | KL-8 | KL-9 | KL-13 | KL-9F | KL-13E | KL-13B | KL-9C | KL-9B |
| PARP1 | 22 | 55 | 74 | 82 | 92 | 99 | 12 | 0 | 2 |
| PARP2 | 35 | 94 | 99 | 100 | 100 | 100 | 36 | 20 | 31 |
| PARP3 | 12 | 7 | 18 | 23 | 17 | 42 | 9 | 6 | 0 |
| TNKS1 | 0 | 0 | 12 | 11 | 19 | 18 | 18 | 21 | 14 |
| TNKS2 | 5 | 10 | 25 | 15 | 16 | 42 | 16 | 19 | 12 |
| PARP6 | 10 | 15 | 14 | 16 | 18 | 25 | 25 | 29 | 28 |
| PARP7 | 7 | 15 | 25 | 38 | 47 | 56 | 20 | 19 | 17 |
| PARP8 | 3 | 0 | 4 | 5 | 15 | 15 | 12 | 14 | 17 |
| PARP10 | 3 | 12 | 16 | 18 | 11 | 12 | 6 | 6 | 4 |
| PARP11 | 0 | 27 | 13 | 21 | 54 | 80 | 7 | 13 | 8 |
| PARP12 | 0 | 37 | 0 | 2 | 12 | 6 | 0 | 0 | 1 |
| PARP14 | 0 | 0 | 4 | 6 | 8 | 5 | 2 | 5 | 0 |
| PARP15 | 0 | 13 | 14 | 20 | 21 | 15 | 20 | 19 | 17 |

6042 Cornerstone Court West, Suite B
San Diego, CA 92121
**Tel:** 1.858.829.3082
**Fax:** 1.858.481.8694
**Email:** info@bpsbioscience.com

| PARPs | % inhibition at 10 µM | | | | | | | | |
|---|---|---|---|---|---|---|---|---|---|
| | KL-9BZI | ABH-2-23 | ABH-2-26 | ABH-1-63 | KL-9G | ABH-2-15 | AKT | AZD 2281 | |
| **PARP1** | **15** | **34** | **4** | **4** | **9** | **2** | ***84*** | **100** | |
| **PARP2** | **62** | **13** | **16** | **19** | **22** | **18** | ***13*** | **100** | |
| **PARP3** | **6** | **9** | **0** | **8** | **5** | **0** | ***31*** | **100** | |
| **TNKS1** | **8** | **6** | **13** | **21** | **27** | **25** | ***31*** | **96** | |
| **TNKS2** | **6** | **26** | **26** | **7** | **3** | **17** | ***43*** | **97** | |
| **PARP6** | **33** | **1** | **13** | **15** | **17** | **6** | ***5*** | **94** | |
| **PARP7** | **18** | **6** | **11** | **12** | **17** | **14** | ***0*** | **91** | |
| **PARP8** | **24** | **22** | **0** | **10** | **15** | **14** | ***0*** | **61** | |
| **PARP10** | **4** | **12** | **10** | **12** | **9** | **9** | ***30*** | **92** | |
| **PARP11** | **8** | **20** | **20** | **3** | **17** | **20** | ***0*** | **67** | |
| **PARP12** | **0** | **27** | **7** | **8** | **8** | **15** | ***0*** | **62** | |
| **PARP14** | **0** | **34** | **12** | **7** | **8** | **9** | ***29*** | **0** | |
| **PARP15** | **17** | **40** | **12** | **21** | **13** | **20** | ***0*** | **51** | |

6042 Cornerstone Court West, Suite B
San Diego, CA 92121
**Tel:** 1.858.829.3082
**Fax:** 1.858.481.8694
**Email:** info@bpsbioscience.com

## 3.2. Results of effects of the compounds on PARPs

### 3.2.1 PARP1

**Table 3.2.1-1 Data for the Effect of the compounds on PARP Activity**

| Compound 10 μM | PARP Activity [(Luminescence Signal)] | | % Activity | |
|---|---|---|---|---|
| | Repeat1 | Repeat2 | Repeat1 | Repeat2 |
| No Compound | 18299 | 18415 | 100 | 100 |
| KL-2 | 14407 | 14170 | 78 | 77 |
| KL-8 | 8202 | 8272 | 45 | 45 |
| KL-9 | 4889 | 4710 | 27 | 26 |
| KL-13 | 3515 | 3191 | 19 | 17 |
| KL-9F | 1525 | 1249 | 8 | 7 |
| KL-13E | 241 | 149 | 1 | 1 |
| KL-13B | 16451 | 15731 | 90 | 86 |
| KL-9C | 18779 | 17915 | 102 | 98 |
| KL-9B | 17956 | 17881 | 98 | 97 |
| KL-9BZI | 15762 | 15567 | 86 | 85 |
| ABH-2-23 | 11835 | 12267 | 64 | 67 |
| ABH-2-26 | 17289 | 17806 | 94 | 97 |
| ABH-1-63 | 18137 | 17055 | 99 | 93 |
| KL-9G | 17142 | 16403 | 93 | 89 |
| ABH-2-15 | 17623 | 18200 | 96 | 99 |
| AKT | 8472 | 9312 | 46 | 51 |
| AZD2281 | 12 | 10 | 0 | 0 |
| Background | 10 | 8 | 0 | 0 |
| No Compound | 20141 | 19520 | 102 | 98 |
| AKT | 3317 | 3132 | 17 | 16 |
| Background | 3 | 3 | 0 | 0 |

6042 Cornerstone Court West, Suite B
San Diego, CA 92121
**Tel:** 1.858.829.3082
**Fax:** 1.858.481.8694
**Email:** info@bpsbioscience.com

### 3.2.2 PARP2

**Table 3.2.2-1 Data for the Effect of the compounds on PARP Activity**

| Compound 10 µM | PARP Activity [(Luminescence Signal)] | | % Activity | |
|---|---|---|---|---|
| | Repeat1 | Repeat2 | Repeat1 | Repeat2 |
| No Compound | 9070 | 9007 | 100 | 100 |
| KL-2 | 6677 | 5160 | 74 | 57 |
| KL-8 | 678 | 442 | 7 | 5 |
| KL-9 | 134 | 98 | 1 | 1 |
| KL-13 | 72 | 50 | 0 | 0 |
| KL-9F | 49 | 36 | 0 | 0 |
| KL-13E | 49 | 34 | 0 | 0 |
| KL-13B | 6321 | 5222 | 70 | 58 |
| KL-9C | 7603 | 6955 | 84 | 77 |
| KL-9B | 6018 | 6484 | 66 | 72 |
| KL-9BZI | 3671 | 3155 | 40 | 35 |
| ABH-2-23 | 8110 | 7682 | 90 | 85 |
| ABH-2-26 | 7157 | 8034 | 79 | 89 |
| ABH-1-63 | 6955 | 7748 | 77 | 86 |
| KL-9G | 6964 | 7225 | 77 | 80 |
| ABH-2-15 | 7323 | 7571 | 81 | 84 |
| AKT | 5927 | 7420 | 65 | 82 |
| AZD2281 | 31 | 34 | 0 | 0 |
| Background | 34 | 28 | 0 | 0 |
| No Compound | 11520 | 9353 | 110 | 90 |
| AKT | 9583 | 8680 | 92 | 83 |
| Background | 45 | 25 | 0 | 0 |

6042 Cornerstone Court West, Suite B
San Diego, CA 92121
**Tel:** 1.858.829.3082
**Fax:** 1.858.481.8694
**Email:** info@bpsbioscience.com

### 3.2.3 PARP3

**Table 3.2.3-1 Data for the Effect of the compounds on PARP Activity**

| Compound 10 µM | PARP Activity [(Luminescence Signal)] | | % Activity | |
|---|---|---|---|---|
| | Repeat1 | Repeat2 | Repeat1 | Repeat2 |
| No Compound | 8329 | 9448 | 94 | 106 |
| KL-2 | 7712 | 7960 | 87 | 90 |
| KL-8 | 8569 | 7909 | 96 | 89 |
| KL-9 | 7059 | 7493 | 79 | 84 |
| KL-13 | 6612 | 7003 | 74 | 79 |
| KL-9F | 7303 | 7481 | 82 | 84 |
| KL-13E | 5135 | 5240 | 58 | 59 |
| KL-13B | 7472 | 8768 | 84 | 99 |
| KL-9C | 7378 | 9384 | 83 | 106 |
| KL-9B | 8696 | 9305 | 98 | 105 |
| KL-9BZI | 8382 | 8268 | 94 | 93 |
| ABH-2-23 | 7979 | 8161 | 90 | 92 |
| ABH-2-26 | 9131 | 9168 | 103 | 103 |
| ABH-1-63 | 8645 | 7665 | 97 | 86 |
| KL-9G | 8563 | 8300 | 96 | 93 |
| ABH-2-15 | 9779 | 9687 | 110 | 109 |
| AKT | 9587 | 8635 | 108 | 97 |
| AZD2281 | 7 | 5 | 0 | 0 |
| Background | 6 | 4 | 0 | 0 |
| No Compound | 10988 | 9774 | 106 | 94 |
| AKT | 7059 | 7365 | 68 | 71 |
| Background | 9 | 10 | 0 | 0 |

6042 Cornerstone Court West, Suite B
San Diego, CA 92121
**Tel:** 1.858.829.3082
**Fax:** 1.858.481.8694
**Email:** info@bpsbioscience.com

### 3.2.4 TNKS1

**Table 3.2.4-1 Data for the Effect of the compounds on PARP Activity**

| Compound 10 μM | PARP Activity [(Luminescence Signal)] | | % Activity | |
|---|---|---|---|---|
| | Repeat1 | Repeat2 | Repeat1 | Repeat2 |
| No Compound | 9516 | 9634 | 99 | 101 |
| KL-2 | 10102 | 9542 | 106 | 100 |
| KL-8 | 9745 | 9323 | 102 | 97 |
| KL-9 | 8529 | 8358 | 89 | 87 |
| KL-13 | 8894 | 8223 | 93 | 86 |
| KL-9F | 7676 | 7870 | 80 | 82 |
| KL-13E | 756 | 7199 | 89 | 75 |
| KL-13B | 9399 | 6288 | 98 | 66 |
| KL-9C | 7890 | 7193 | 82 | 75 |
| KL-9B | 8556 | 7890 | 89 | 82 |
| KL-9BZI | 8492 | 9199 | 89 | 96 |
| ABH-2-23 | 9358 | 8673 | 98 | 91 |
| ABH-2-26 | 9068 | 7673 | 95 | 80 |
| ABH-1-63 | 8128 | 6991 | 85 | 73 |
| KL-9G | 7389 | 6518 | 77 | 68 |
| ABH-2-15 | 6790 | 7510 | 71 | 78 |
| AKT | 6848 | 6984 | 71 | 73 |
| AZD2281 | 337 | 500 | 3 | 5 |
| Background | 7 | 7 | 0 | 0 |

| | | | | |
|---|---|---|---|---|
| No Compound | 9877 | 9596 | 101 | 99 |
| AKT | 7244 | 6281 | 74 | 64 |
| Background | 3 | 3 | 0 | 0 |

6042 Cornerstone Court West, Suite B
San Diego, CA 92121
**Tel:** 1.858.829.3082
**Fax:** 1.858.481.8694
**Email:** info@bpsbioscience.com

### 3.2.5 TNKS2

**Table 3.2.5-1 Data for the Effect of the compounds on PARP Activity**

| Compound 10 μM | PARP Activity [(Luminescence Signal)] | | % Activity | |
|---|---|---|---|---|
| | Repeat1 | Repeat2 | Repeat1 | Repeat2 |
| No Compound | 8698 | 9392 | 96 | 104 |
| KL-2 | 8946 | 8253 | 99 | 91 |
| KL-8 | 7783 | 8497 | 86 | 94 |
| KL-9 | 6680 | 6829 | 74 | 75 |
| KL-13 | 6987 | 8371 | 77 | 93 |
| KL-9F | 7811 | 7396 | 86 | 82 |
| KL-13E | 5282 | 5135 | 58 | 57 |
| KL-13B | 7345 | 7930 | 81 | 88 |
| KL-9C | 7311 | 7349 | 81 | 81 |
| KL-9B | 7614 | 8336 | 84 | 92 |
| KL-9BZI | 8659 | 8258 | 96 | 91 |
| ABH-2-23 | 6283 | 7094 | 69 | 78 |
| ABH-2-26 | 6434 | 6880 | 71 | 76 |
| ABH-1-63 | 8888 | 7892 | 98 | 87 |
| KL-9G | 9045 | 8435 | 100 | 93 |
| ABH-2-15 | 6706 | 8329 | 74 | 92 |
| AKT | 7940 | 7717 | 88 | 85 |
| AZD2281 | 277 | 303 | 3 | 3 |
| Background | 9 | 10 | 0 | 0 |
| | | | | |
| No Compound | 9353 | 9695 | 98 | 102 |
| AKT | 5348 | 5429 | 56 | 57 |
| Background | 2 | 2 | 0 | 0 |

6042 Cornerstone Court West, Suite B
San Diego, CA 92121
**Tel:** 1.858.829.3082
**Fax:** 1.858.481.8694
**Email:** info@bpsbioscience.com

### 3.2.6 PARP6

**Table 3.2.6-1 Data for the Effect of the compounds on PARP Activity**

| Compound 10 µM | PARP Activity [(Luminescence Signal)] | | % Activity | |
|---|---|---|---|---|
| | Repeat1 | Repeat2 | Repeat1 | Repeat2 |
| No Compound | 4657 | 4313 | 104 | 96 |
| KL-2 | 4043 | 3995 | 90 | 89 |
| KL-8 | 3804 | 3862 | 85 | 86 |
| KL-9 | 3884 | 3801 | 87 | 85 |
| KL-13 | 3852 | 3732 | 86 | 83 |
| KL-9F | 3774 | 3580 | 84 | 80 |
| KL-13E | 3270 | 3477 | 73 | 77 |
| KL-13B | 3315 | 3434 | 74 | 76 |
| KL-9C | 3070 | 3309 | 68 | 74 |
| KL-9B | 3133 | 3301 | 70 | 74 |
| KL-9BZI | 2949 | 3099 | 66 | 69 |
| ABH-2-23 | 4075 | 4806 | 91 | 107 |
| ABH-2-26 | 3768 | 4041 | 84 | 90 |
| ABH-1-63 | 3658 | 3970 | 81 | 88 |
| KL-9G | 3576 | 3890 | 80 | 87 |
| ABH-2-15 | 4028 | 4411 | 90 | 98 |
| AKT | 3494 | 4033 | 78 | 90 |
| AZD2281 | 242 | 339 | 5 | 7 |
| Background | 17 | 16 | 0 | 0 |
| No Compound | 4694 | 4461 | 103 | 97 |
| AKT | 4391 | 4267 | 96 | 93 |
| Background | 13 | 24 | 0 | 0 |

6042 Cornerstone Court West, Suite B
San Diego, CA 92121
**Tel:** 1.858.829.3082
**Fax:** 1.858.481.8694
**Email:** info@bpsbioscience.com

### 3.2.7 PARP7

**Table 3.2.7-1 Data for the Effect of the compounds on PARP Activity**

| Compound 10 μM | PARP Activity [(Luminescence Signal)] | | % Activity | |
|---|---|---|---|---|
| | Repeat1 | Repeat2 | Repeat1 | Repeat2 |
| No Compound | 3873 | 3971 | 99 | 101 |
| KL-2 | 3659 | 3650 | 93 | 93 |
| KL-8 | 3414 | 3294 | 87 | 83 |
| KL-9 | 3043 | 2878 | 77 | 72 |
| KL-13 | 2442 | 2545 | 61 | 64 |
| KL-9F | 2137 | 2126 | 53 | 52 |
| KL-13E | 1853 | 1756 | 45 | 43 |
| KL-13B | 3070 | 3242 | 77 | 82 |
| KL-9C | 3186 | 3239 | 81 | 82 |
| KL-9B | 3218 | 3343 | 81 | 85 |
| KL-9BZI | 3157 | 3335 | 80 | 84 |
| ABH-2-23 | 3630 | 3740 | 92 | 95 |
| ABH-2-26 | 3475 | 3524 | 88 | 89 |
| ABH-1-63 | 3372 | 3553 | 85 | 90 |
| KL-9G | 3156 | 3442 | 80 | 87 |
| ABH-2-15 | 3310 | 3440 | 84 | 87 |
| AKT | 3436 | 3332 | 87 | 84 |
| AZD2281 | 369 | 592 | 6 | 12 |
| Background | 118 | 176 | -1 | 1 |
| | | | | |
| No Compound | 3921 | 3852 | 101 | 99 |
| AKT | 4177 | 4096 | 108 | 105 |
| Background | 25 | 19 | 0 | 0 |

6042 Cornerstone Court West, Suite B
San Diego, CA 92121
**Tel:** 1.858.829.3082
**Fax:** 1.858.481.8694
**Email:** info@bpsbioscience.com

### 3.2.8 PARP8

**Table 3.2.8-1 Data for the Effect of the compounds on PARP Activity**

| Compound 10 µM | PARP Activity [(Luminescence Signal)] | | % Activity | |
|---|---|---|---|---|
| | Repeat1 | Repeat2 | Repeat1 | Repeat2 |
| No Compound | 3779 | 3903 | 98 | 102 |
| KL-2 | 3845 | 3581 | 100 | 93 |
| KL-8 | 3825 | 3825 | 100 | 100 |
| KL-9 | 3601 | 3749 | 94 | 98 |
| KL-13 | 3504 | 3771 | 91 | 98 |
| KL-9F | 3134 | 3401 | 81 | 88 |
| KL-13E | 3248 | 3326 | 84 | 86 |
| KL-13B | 3415 | 3374 | 89 | 87 |
| KL-9C | 3343 | 3325 | 87 | 86 |
| KL-9B | 3098 | 3314 | 80 | 86 |
| KL-9BZI | 2923 | 2960 | 75 | 76 |
| ABH-2-23 | 3001 | 3012 | 77 | 78 |
| ABH-2-26 | 3464 | 4286 | 90 | 112 |
| ABH-1-63 | 3396 | 3522 | 88 | 91 |
| KL-9G | 2934 | 3610 | 76 | 94 |
| ABH-2-15 | 3170 | 3480 | 82 | 90 |
| AKT | 3389 | 3765 | 88 | 98 |
| AZD2281 | 1545 | 1622 | 38 | 40 |
| Background | 107 | 152 | -1 | 1 |
| No Compound | 4802 | 3847 | 111 | 89 |
| AKT | 5405 | 4077 | 125 | 94 |
| Background | 76 | 77 | 0 | 0 |

6042 Cornerstone Court West, Suite B
San Diego, CA 92121
**Tel:** 1.858.829.3082
**Fax:** 1.858.481.8694
**Email:** info@bpsbioscience.com

### 3.2.9 PARP10

**Table 3.2.9-1 Data for the Effect of the compounds on PARP Activity**

| Compound 10 µM | PARP Activity [(Luminescence Signal)] | | % Activity | |
|---|---|---|---|---|
| | Repeat1 | Repeat2 | Repeat1 | Repeat2 |
| No Compound | 10232 | 10371 | 99 | 101 |
| KL-2 | 10286 | 9772 | 100 | 95 |
| KL-8 | 9324 | 8907 | 90 | 86 |
| KL-9 | 8998 | 8307 | 87 | 81 |
| KL-13 | 8660 | 8174 | 84 | 79 |
| KL-9F | 9488 | 8888 | 92 | 86 |
| KL-13E | 9196 | 9031 | 89 | 88 |
| KL-13B | 9858 | 9522 | 96 | 92 |
| KL-9C | 9853 | 9423 | 96 | 91 |
| KL-9B | 10216 | 9634 | 99 | 93 |
| KL-9BZI | 10158 | 9630 | 99 | 93 |
| ABH-2-23 | 8978 | 9136 | 87 | 89 |
| ABH-2-26 | 9188 | 9400 | 89 | 91 |
| ABH-1-63 | 8920 | 9250 | 87 | 90 |
| KL-9G | 9435 | 9276 | 92 | 90 |
| ABH-2-15 | 9387 | 9384 | 91 | 91 |
| AKT | 8951 | 8719 | 87 | 85 |
| AZD2281 | 915 | 906 | 8 | 8 |
| Background | 44 | 46 | 0 | 0 |
| No Compound | 11602 | 9785 | 109 | 91 |
| AKT | 7627 | 7449 | 71 | 70 |
| Background | 13 | 13 | 0 | 0 |

6042 Cornerstone Court West, Suite B
San Diego, CA 92121
**Tel:** 1.858.829.3082
**Fax:** 1.858.481.8694
**Email:** info@bpsbioscience.com

### 3.2.10 PARP11

**Table 3.2.10-1 Data for the Effect of the compounds on PARP Activity**

| Compound 10 µM | PARP Activity [(Luminescence Signal)] | | % Activity | |
|---|---|---|---|---|
| | Repeat1 | Repeat2 | Repeat1 | Repeat2 |
| No Compound | 3037 | 2970 | 101 | 99 |
| KL-2 | 3186 | 3018 | 106 | 100 |
| KL-8 | 2362 | 2075 | 78 | 68 |
| KL-9 | 2708 | 2558 | 90 | 85 |
| KL-13 | 2393 | 2359 | 79 | 78 |
| KL-9F | 1524 | 1327 | 50 | 43 |
| KL-13E | 631 | 659 | 19 | 20 |
| KL-13B | 2937 | 2671 | 98 | 89 |
| KL-9C | 2683 | 2545 | 89 | 84 |
| KL-9B | 2826 | 2696 | 94 | 90 |
| KL-9BZI | 2815 | 2715 | 94 | 90 |
| ABH-2-23 | 2380 | 2471 | 79 | 82 |
| ABH-2-26 | 2367 | 2478 | 78 | 82 |
| ABH-1-63 | 2845 | 3007 | 95 | 100 |
| KL-9G | 2620 | 2390 | 87 | 79 |
| ABH-2-15 | 2342 | 2507 | 78 | 83 |
| AKT | 2823 | 2564 | 94 | 85 |
| AZD2281 | 1047 | 995 | 34 | 32 |
| Background | 71 | 45 | 0 | 0 |
| No Compound | 2489 | 2800 | 94 | 106 |
| AKT | 3617 | 3016 | 137 | 114 |
| Background | 52 | 42 | 0 | 0 |

6042 Cornerstone Court West, Suite B
San Diego, CA 92121
**Tel:** 1.858.829.3082
**Fax:** 1.858.481.8694
**Email:** info@bpsbioscience.com

### 3.2.11 PARP12

**Table 3.2.11-1 Data for the Effect of the compounds on PARP Activity**

| Compound 10 μM | PARP Activity [(Luminescence Signal)] | | % Activity | |
|---|---|---|---|---|
| | Repeat1 | Repeat2 | Repeat1 | Repeat2 |
| No Compound | 3038 | 2961 | 101 | 99 |
| KL-2 | 3020 | 2959 | 101 | 99 |
| KL-8 | 3113 | 669 | 104 | 21 |
| KL-9 | 2906 | 3090 | 97 | 103 |
| KL-13 | 2978 | 2919 | 99 | 97 |
| KL-9F | 2731 | 2584 | 91 | 86 |
| KL-13E | 2794 | 2872 | 93 | 96 |
| KL-13B | 3016 | 3250 | 101 | 108 |
| KL-9C | 3148 | 3249 | 105 | 108 |
| KL-9B | 2993 | 2936 | 100 | 98 |
| KL-9BZI | 2992 | 3077 | 100 | 103 |
| ABH-2-23 | 2188 | 2237 | 73 | 74 |
| ABH-2-26 | 2477 | 3133 | 82 | 105 |
| ABH-1-63 | 2753 | 988 | 92 | 93 |
| KL-9G | 2620 | 2890 | 87 | 96 |
| ABH-2-15 | 2331 | 2763 | 77 | 92 |
| AKT | 2682 | 3055 | 89 | 102 |
| AZD2281 | 1124 | 1192 | 37 | 39 |
| Background | 37 | 43 | 0 | 0 |
| No Compound | 2866 | 2887 | 100 | 100 |
| AKT | 2896 | 3060 | 101 | 106 |
| Background | 10 | 11 | 0 | 0 |

6042 Cornerstone Court West, Suite B
San Diego, CA 92121
**Tel:** 1.858.829.3082
**Fax:** 1.858.481.8694
**Email:** info@bpsbioscience.com

### 3.2.12 PARP14

**Table 3.2.1-1 Data for the Effect of the compounds on PARP Activity**

| Compound 10 µM | PARP Activity [(Luminescence Signal)] | | % Activity | |
|---|---|---|---|---|
| | Repeat1 | Repeat2 | Repeat1 | Repeat2 |
| No Compound | 3702 | 3645 | 101 | 99 |
| KL-2 | 3849 | 3655 | 105 | 99 |
| KL-8 | 3876 | 3558 | 106 | 97 |
| KL-9 | 3688 | 3381 | 100 | 92 |
| KL-13 | 3488 | 3393 | 95 | 92 |
| KL-9F | 3696 | 3102 | 101 | 84 |
| KL-13E | 3456 | 3508 | 94 | 95 |
| KL-13B | 3644 | 3524 | 99 | 96 |
| KL-9C | 3609 | 3346 | 98 | 91 |
| KL-9B | 3712 | 3644 | 101 | 99 |
| KL-9BZI | 3810 | 3781 | 104 | 103 |
| ABH-2-23 | 2539 | 2331 | 69 | 63 |
| ABH-2-26 | 3388 | 3119 | 92 | 85 |
| ABH-1-63 | 3492 | 3319 | 95 | 90 |
| KL-9G | 3478 | 3292 | 95 | 89 |
| ABH-2-15 | 3460 | 3221 | 94 | 88 |
| AKT | 3360 | 3134 | 91 | 85 |
| AZD2281 | 3757 | 3668 | 102 | 100 |
| Background | 45 | 39 | 0 | 0 |
| | | | | |
| No Compound | 3927 | 3808 | 102 | 98 |
| AKT | 2675 | 2827 | 69 | 73 |
| Background | 7 | 8 | 0 | 0 |

6042 Cornerstone Court West, Suite B
San Diego, CA 92121
**Tel:** 1.858.829.3082
**Fax:** 1.858.481.8694
**Email:** info@bpsbioscience.com

### 3.2.13 PARP15

**Table 3.2.1-1 Data for the Effect of the compounds on PARP Activity**

| Compound 10 µM | PARP Activity [(Luminescence Signal)] | | % Activity | |
|---|---|---|---|---|
| | Repeat1 | Repeat2 | Repeat1 | Repeat2 |
| No Compound | 9890 | 10292 | 98 | 102 |
| KL-2 | 10106 | 10104 | 100 | 100 |
| KL-8 | 8550 | 9001 | 85 | 89 |
| KL-9 | 8760 | 8609 | 87 | 85 |
| KL-13 | 8067 | 8063 | 80 | 80 |
| KL-9F | 8727 | 7273 | 86 | 72 |
| KL-13E | 8425 | 8754 | 83 | 87 |
| KL-13B | 7743 | 8492 | 77 | 84 |
| KL-9C | 8231 | 8131 | 82 | 81 |
| KL-9B | 8845 | 7970 | 88 | 79 |
| KL-9BZI | 8226 | 8526 | 81 | 84 |
| ABH-2-23 | 5713 | 6335 | 57 | 63 |
| ABH-2-26 | 8597 | 9104 | 85 | 90 |
| ABH-1-63 | 9491 | 6524 | 94 | 65 |
| KL-9G | 8688 | 8794 | 86 | 87 |
| ABH-2-15 | 7980 | 8180 | 79 | 81 |
| AKT | 8417 | 8433 | 83 | 84 |
| AZD2281 | 5117 | 4771 | 51 | 47 |
| Background | 11 | 10 | 0 | 0 |
| | | | | |
| No Compound | 9727 | 9394 | 102 | 98 |
| AKT | 9814 | 12107 | 103 | 127 |
| Background | 4 | 4 | 0 | 0 |

6042 Cornerstone Court West, Suite B
San Diego, CA 92121
**Tel:** 1.858.829.3082
**Fax:** 1.858.481.8694
**Email:** info@bpsbioscience.com

# Materials and Methods

## 2.1 Materials

BPS PARP assay kits are used in the assay

## 2.2 Compounds

The test compound is supplied by Virginia Tech

| Compound I.D. | Compound Supplied | Stock Concentration | Dissolving Solvent | Test Range | Intermediate Dilution |
|---|---|---|---|---|---|
| KL-8 | solution | 10 mM | DMSO | 1 nM - 100 µM | 10 % DMSO (aq) |
| KL-13E | solution | 10 mM | DMSO | 0.01 nM - 30 µM | 10 % DMSO (aq) |
| AZD2281 | powder | 10 mM | DMSO | 10 nM, 100 µM | 10 % DMSO (aq) |

## 2.3 Experimental Conditions

### 2.3.1 Enzymes and Substrates

| Assay | Catalog # (Lot #) | Enzyme Used/ Reaction | Substrate |
|---|---|---|---|
| | | | Activated DNA |
| PARP1 | 80501 (120206-1) | 10 ng | 2.5 µM $NAD^+$/2.5 µM $NAD^+$-Biotin |
| | | | 0.026 mg/ml |
| PARP2 | 80502 (140729-P4) | 25 ng | 2.5 µM $NAD^+$/2.5 µM $NAD^+$-Biotin |
| | | | 0.026 mg/ml |
| PARP11 | 80511 (150820B) | 800 ng | 50 µM $NAD^+$/5 µM $NAD^+$-Biotin |
| | | | N/A |

6042 Cornerstone Court West, Suite B
San Diego, CA 92121
**Tel:** 1.858.829.3082
**Fax:** 1.858.481.8694
**Email:** info@bpsbioscience.com

# 3. Assay Results

## 3.1. Summary of the effects of the compounds on PARP Activities

The % inhibition of the compounds against PARP are summarized in Table 3.1

**Table 3.1 Inhibitory Effects of the Compounds on PARP Activities**

| PARPs | IC50 (or % inhibition) | | |
|---|---|---|---|
| | KL-13E | KL-8 | AZD2281 |
| PARP1 | 178 nM | 8.7 µM | 93 % |
| PARP2 | 15.0 nM | 1.5 µM | 100 % |
| PARP11 | 3.1 µM | N/A | 93 % |

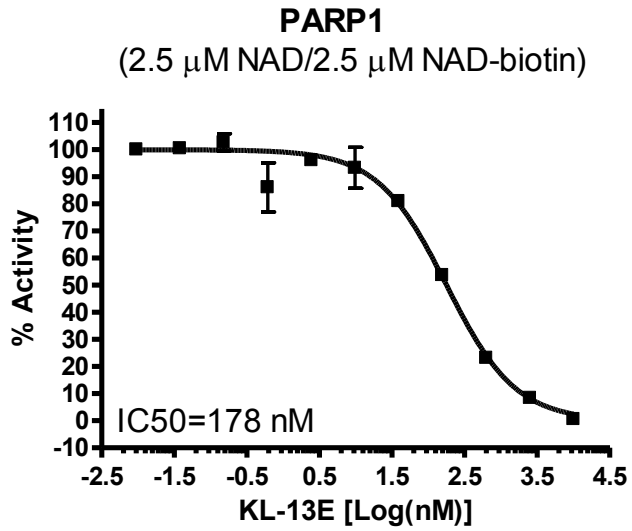
6042 Cornerstone Court West, Suite B
San Diego, CA 92121
**Tel:** 1.858.829.3082
**Fax:** 1.858.481.8694
**Email:** info@bpsbioscience.com

## 3.2. Results of effects of the compounds on PARPs

### 3.2.1 KL-13E

**Table 3.2.1-1 Data for the Effect of the compounds on PARP1 Activity**

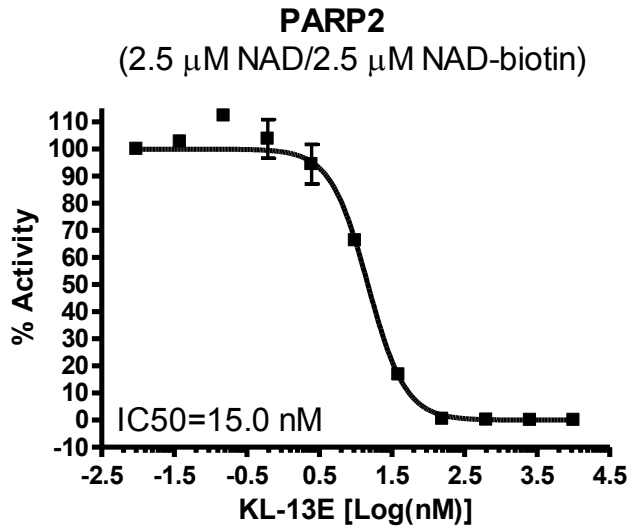
| KL-13E (Log [nM]) | PARP Activity [(Luminescence Signal)] | | % Activity | |
|---|---|---|---|---|
| | Repeat1 | Repeat2 | Repeat1 | Repeat2 |
| No Compound | 18830 | 18359 | 101 | 99 |
| -1.4 | 18809 | 18542 | 101 | 100 |
| -0.8 | 18502 | 19689 | 100 | 106 |
| -0.2 | 17699 | 14327 | 95 | 77 |
| 0.4 | 17778 | 17946 | 96 | 97 |
| 1.0 | 15947 | 18755 | 86 | 101 |
| 1.6 | 14647 | 15478 | 79 | 83 |
| 2.2 | 9892 | 10079 | 53 | 54 |
| 2.8 | 4270 | 4357 | 23 | 23 |
| 3.4 | 1586 | 1552 | 9 | 8 |
| 4.0 | 148 | 85 | 1 | 0 |
| AZD2281. 10 nM | 1074 | 1290 | 6 | 7 |
| Background | 3 | 3 | 0 | 0 |



6042 Cornerstone Court West, Suite B
San Diego, CA 92121
**Tel:** 1.858.829.3082
**Fax:** 1.858.481.8694
**Email:** info@bpsbioscience.com

**Table 3.2.1-2 Data for the Effect of the compounds on PARP2 Activity**

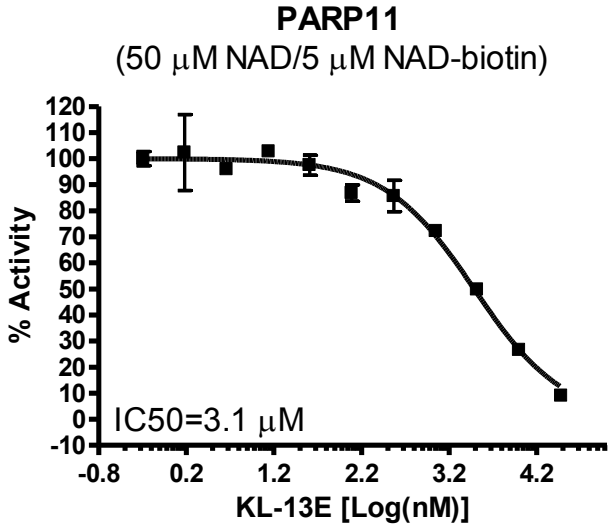
| **KL-13E** (Log [nM]) | PARP Activity [(Luminescence Signal)] | | % Activity | |
|---|---|---|---|---|
| | Repeat1 | Repeat2 | Repeat1 | Repeat2 |
| No Compound | 9815 | 9980 | 99 | 101 |
| -1.4 | 10175 | 10169 | 103 | 103 |
| -0.8 | 10981 | 11248 | 111 | 114 |
| -0.2 | 10976 | 9567 | 111 | 97 |
| 0.4 | 10072 | 8628 | 102 | 87 |
| 1.0 | 6388 | 6760 | 64 | 68 |
| 1.6 | 1574 | 1795 | 16 | 18 |
| 2.2 | 62 | 79 | 0 | 1 |
| 2.8 | 25 | 43 | 0 | 0 |
| 3.4 | 20 | 29 | 0 | 0 |
| 4.0 | 22 | 24 | 0 | 0 |
| AZD2281. 10 nM | 28 | 11 | 0 | 0 |
| Background | 21 | 25 | 0 | 0 |



6042 Cornerstone Court West, Suite B
San Diego, CA 92121
**Tel:** 1.858.829.3082
**Fax:** 1.858.481.8694
**Email:** info@bpsbioscience.com

**Table 3.2.1-3 Data for the Effect of the compounds on PARP11 Activity**

| **KL-13E** (Log [nM]) | PARP Activity [(Luminescence Signal)] | | % Activity | |
|---|---|---|---|---|
| | Repeat1 | Repeat2 | Repeat1 | Repeat2 |
| No Compound | 2548 | 2417 | 103 | 97 |
| 0.2 | 2887 | 2189 | 117 | 88 |
| 0.7 | 2377 | 2392 | 96 | 96 |
| 1.1 | 2489 | 2605 | 100 | 105 |
| 1.6 | 2513 | 2331 | 101 | 94 |
| 2.1 | 2091 | 2242 | 84 | 90 |
| 2.6 | 1996 | 2282 | 80 | 92 |
| 3.0 | 1792 | 1841 | 71 | 73 |
| 3.5 | 1294 | 1268 | 50 | 49 |
| 4.0 | 675 | 778 | 24 | 29 |
| 4.5 | 319 | 293 | 10 | 8 |
| AZD2281, 100 µM | 199 | 270 | 5 | 8 |
| Background | 109 | 71 | 1 | -1 |

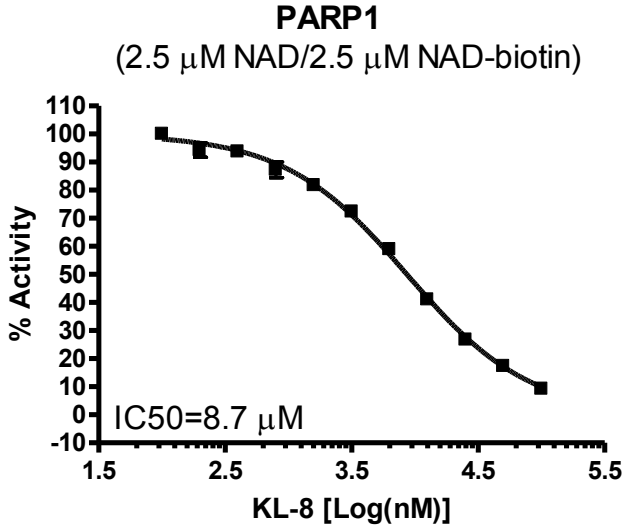


6042 Cornerstone Court West, Suite B
San Diego, CA 92121
**Tel:** 1.858.829.3082
**Fax:** 1.858.481.8694
**Email:** info@bpsbioscience.com

### 3.2.2 KL-8

**Table 3.2.2-1 Data for the Effect of the compounds on PARP1 Activity**

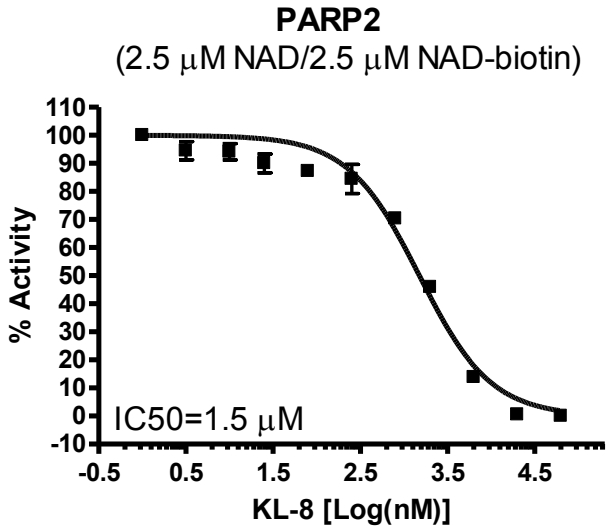
| KL-8 (Log [nM]) | PARP Activity [(Luminescence Signal)] | | % Activity | |
|---|---|---|---|---|
| | Repeat1 | Repeat2 | Repeat1 | Repeat2 |
| No Compound | 19177 | 19566 | 99 | 101 |
| 2.3 | 18763 | 17770 | 97 | 92 |
| 2.6 | 18108 | 18223 | 93 | 94 |
| 2.9 | 16359 | 17449 | 84 | 90 |
| 3.2 | 16088 | 15594 | 83 | 80 |
| 3.5 | 14371 | 13670 | 74 | 71 |
| 3.8 | 11139 | 11716 | 57 | 60 |
| 4.1 | 8037 | 7860 | 41 | 41 |
| 4.4 | 4937 | 5422 | 25 | 28 |
| 4.7 | 3384 | 3332 | 17 | 17 |
| 5.0 | 1757 | 1824 | 9 | 9 |
| Background | 3 | 3 | 0 | 0 |



6042 Cornerstone Court West, Suite B
San Diego, CA 92121
**Tel:** 1.858.829.3082
**Fax:** 1.858.481.8694
**Email:** info@bpsbioscience.com

**Table 3.2.2-2 Data for the Effect of the compounds on PARP2 Activity**

| **KL-8** (Log [nM]) | PARP Activity [(Luminescence Signal)] | | % Activity | |
|---|---|---|---|---|
| | Repeat1 | Repeat2 | Repeat1 | Repeat2 |
| No Compound | 9589 | 9755 | 99 | 101 |
| 0.5 | 8830 | 9459 | 91 | 98 |
| 1.0 | 9387 | 8824 | 97 | 91 |
| 1.4 | 8382 | 9032 | 87 | 93 |
| 1.9 | 8423 | 8456 | 87 | 87 |
| 2.4 | 7670 | 8673 | 79 | 90 |
| 2.9 | 6772 | 6845 | 70 | 71 |
| 3.3 | 4534 | 4374 | 47 | 45 |
| 3.8 | 1280 | 1432 | 13 | 15 |
| 4.3 | 71 | 72 | 1 | 1 |
| 4.8 | 23 | 24 | 0 | 0 |
| Background | 22 | 18 | 0 | 0 |



6042 Cornerstone Court West, Suite B
San Diego, CA 92121
**Tel:** 1.858.829.3082
**Fax:** 1.858.481.8694
**Email:** info@bpsbioscience.com

# Materials and Methods

## 2.1 Materials

BPS PARPtrap assay kits are used in the assay

## 2.2 Compounds

The test compound is supplied by Virginia Tech

| Compound I.D. | Compound Supplied | Stock Concentration | Dissolving Solvent | Test Range | Intermediate Dilution |
|---|---|---|---|---|---|
| KL-13E | Solution | 1 mM | DMSO | 1 nM – 10 µM | 10 % DMSO (aq) |
| Olaparib | solution | 10 mM | DMSO | 0.1 nM – 1 µM | 10 % DMSO (aq) |

## 2.3 Experimental Conditions

### 2.3.1 Enzymes and Substrates

| Assay | Catalog # (Lot #) | Enzyme Used/ Reaction | Substrate |
|---|---|---|---|
| | | | Activated DNA |
| PARP1 | 80501 (160526-G2) | 80 ng | 5 nM Alexa488 labeled Nicked DNA |
| | | | 1 mM NAD |

6042 Cornerstone Court West, Suite B
San Diego, CA 92121
**Tel:** 1.858.829.3082
**Fax:** 1.858.481.8694
**Email:** info@bpsbioscience.com

# 3. Assay Results

## 3.1. Summary of the effects of the compounds on PARP Activities

The % inhibition of the compounds against PARP are summarized in Table 3.1

**Table 3.1 Inhibitory Effects of the Compounds on PARP Activities**

| Compounds | EC50 |
|---|---|
| **KL-13E** | **>10 µM** (35% FP at 10 µM) |
| **Olaparib** | **12.0 nM** |

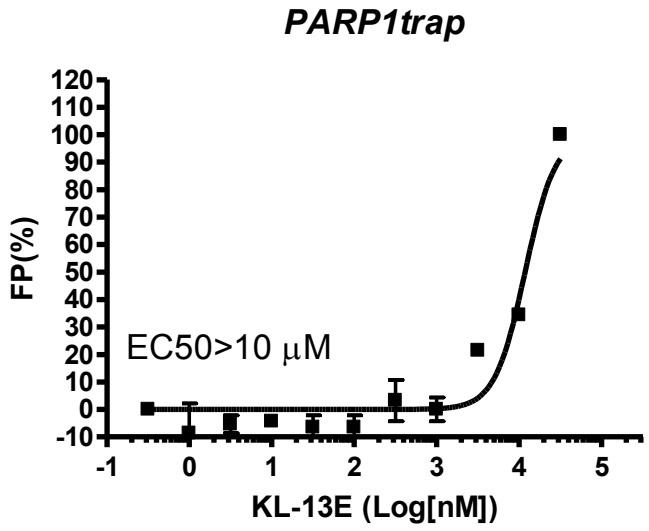
6042 Cornerstone Court West, Suite B
San Diego, CA 92121
**Tel:** 1.858.829.3082
**Fax:** 1.858.481.8694
**Email:** info@bpsbioscience.com

## 3.2. Results of effects of the compounds on PARPs

### 3.2.1 KL-13E

**Table 3.2.1-1 Data for the Effect of the compound on PARP1trap Activity**

| KL-13E (Log [nM]) | PARP1trap Activity [(Fluorescence Polarization)] | | % Activity | |
|---|---|---|---|---|
| | Repeat1 | Repeat2 | Repeat1 | Repeat2 |
| No Compound | 71 | 69 | 2 | -2 |
| 0 | 71 | 61 | 2 | -19 |
| 0.5 | 69 | 66 | -2 | -9 |
| 1.0 | 69 | 67 | -2 | -6 |
| 1.5 | 65 | 69 | -11 | -2 |
| 2.0 | 65 | 69 | -11 | -2 |
| 2.5 | 75 | 68 | 11 | -4 |
| 3.0 | 72 | 68 | 4 | -4 |
| 3.5 | 80 | 80 | 22 | 22 |
| 4.0 | 85 | 87 | 32 | 37 |
| No NAD | 116 | 117 | 99 | 101 |
| Background | 19 | 19 | | |



6042 Cornerstone Court West, Suite B
San Diego, CA 92121
**Tel:** 1.858.829.3082
**Fax:** 1.858.481.8694
**Email:** info@bpsbioscience.com

### 3.2.2 Olaparib

**Table 3.2.7-1 Data for the Effect of the compound on PARP1trap Activity**

| **Olaparib** (Log [nM]) | PARP1trap Activity [(Fluorescence Polarization)] | | % Activity | |
|---|---|---|---|---|
| | Repeat1 | Repeat2 | Repeat1 | Repeat2 |
| No Compound | 67 | 62 | 5 | -5 |
| -1.0 | 65 | 64 | 1 | -1 |
| -0.5 | 72 | 62 | 14 | -5 |
| 0 | 75 | 75 | 20 | 20 |
| 0.5 | 84 | 77 | 38 | 24 |
| 1.0 | 92 | 92 | 53 | 53 |
| 1.5 | 97 | 100 | 63 | 68 |
| 2.0 | 105 | 102 | 78 | 72 |
| 2.5 | 110 | 109 | 88 | 86 |
| 3.0 | 109 | 110 | 86 | 88 |
| No NAD | 116 | 117 | 99 | 101 |
| Background | 19 | 19 | | |

